

# **Fuel Cell Handbook**

**(Fifth Edition)**

**By**  
**EG&G Services**  
**Parsons, Inc.**  
**Science Applications International Corporation**

**Under Contract No. DE-AM26-99FT40575**

**U.S. Department of Energy**  
**Office of Fossil Energy**  
**National Energy Technology Laboratory**  
**P.O. Box 880**  
**Morgantown, West Virginia 26507-0880**

**October 2000**

## **DISCLAIMER**

This report was prepared as an account of work sponsored by an agency of the United States Government. Neither the United States Government nor any agency thereof, nor any of their employees, makes any warranty, express or implied, or assumes any legal liability or responsibility for the accuracy, completeness, or usefulness of any information, apparatus, product, or process disclosed, or represents that its use would not infringe privately owned rights. Reference herein to any specific commercial product, process, or service by trade name, trademark, manufacturer, or otherwise does not necessarily constitute or imply its endorsement, recommendation, or favoring by the United States Government or any agency thereof. The views and opinions of authors expressed herein do not necessarily state or reflect those of the United States Government or any agency thereof.

Available to DOE and DOE contractors from the Office of Scientific and Technical Information, P.O. Box 62, 175 Oak Ridge Turnpike, Oak Ridge, TN 37831; prices available at (423) 576-8401, fax C (423) 576-5725, E-mail C reports@adonis.osti.gov

Available to the public from the National Technical Information Service, U.S. Department of Commerce, 5285 Port Royal Road, Springfield, VA 22161; phone orders accepted at (703) 487-4650.

# TABLE OF CONTENTS

Section	Title	Page
<b>1.</b>	<b>TECHNOLOGY OVERVIEW.....</b>	<b>1-1</b>
1.1	FUEL CELL DESCRIPTION.....	1-1
1.2	CELL STACKING.....	1-7
1.3	FUEL CELL PLANT DESCRIPTION.....	1-8
1.4	CHARACTERISTICS.....	1-9
1.5	ADVANTAGES/DISADVANTAGES.....	1-11
1.6	APPLICATIONS, DEMONSTRATIONS, AND STATUS.....	1-13
1.6.1	Stationary Electric Power.....	1-13
1.6.2	Distributed Generation.....	1-21
1.6.3	Vehicle Motive Power.....	1-25
1.6.4	Space and Other Closed Environment Power.....	1-26
1.6.5	Fuel Cell Auxiliary Power Systems.....	1-26
1.6.6	Derivative Applications.....	1-35
1.7	REFERENCES.....	1-35
<b>2.</b>	<b>FUEL CELL PERFORMANCE.....</b>	<b>2-1</b>
2.1	PRACTICAL THERMODYNAMICS.....	2-1
2.1.1	Ideal Performance.....	2-1
2.1.2	Actual Performance.....	2-4
2.1.3	Fuel Cell Performance Variables.....	2-9
2.1.4	Cell Energy Balance.....	2-16
2.2	SUPPLEMENTAL THERMODYNAMICS.....	2-17
2.2.1	Cell Efficiency.....	2-17
2.2.2	Efficiency Comparison to Heat Engines.....	2-19
2.2.3	Gibbs Free Energy and Ideal Performance.....	2-19
2.2.4	Polarization: Activation (Tafel) and Concentration.....	2-23
2.3	REFERENCES.....	2-26
<b>3.</b>	<b>POLYMER ELECTROLYTE FUEL CELL.....</b>	<b>3-1</b>
3.1	CELL COMPONENTS.....	3-1
3.1.1	Water Management.....	3-2
3.1.2	State-of-the-Art Components.....	3-3
3.1.3	Development Components.....	3-6
3.2	PERFORMANCE.....	3-9
3.3	DIRECT METHANOL PROTON EXCHANGE FUEL CELL.....	3-12
3.4	REFERENCES.....	3-14
<b>4.</b>	<b>ALKALINE FUEL CELL.....</b>	<b>4-1</b>
4.1	CELL COMPONENTS.....	4-3
4.1.1	State-of-the-Art Components.....	4-3
4.1.2	Development Components.....	4-4
4.2	PERFORMANCE.....	4-5
4.2.1	Effect of Pressure.....	4-5
4.2.2	Effect of Temperature.....	4-7
4.2.3	Effect of Reactant Gas Composition.....	4-8
4.2.4	Effect of Impurities.....	4-8
4.2.5	Effects of Current Density.....	4-10

4.2.6	Effects of Cell Life.....	4-12
4.3	SUMMARY OF EQUATIONS FOR AFC .....	4-12
4.4	REFERENCES .....	4-12
<b>5.</b>	<b>PHOSPHORIC ACID FUEL CELL.....</b>	<b>5-1</b>
5.1	CELL COMPONENTS .....	5-2
5.1.1	State-of-the-Art Components .....	5-2
5.1.2	Development Components .....	5-5
5.2	PERFORMANCE.....	5-9
5.2.1	Effect of Pressure .....	5-10
5.2.2	Effect of Temperature .....	5-11
5.2.3	Effect of Reactant Gas Composition and Utilization .....	5-12
5.2.4	Effect of Impurities .....	5-14
5.2.5	Effects of Current Density.....	5-17
5.2.6	Effects of Cell Life.....	5-18
5.3	SUMMARY OF EQUATIONS FOR PAFC .....	5-18
5.4	REFERENCES .....	5-20
<b>6.</b>	<b>MOLTEN CARBONATE FUEL CELL .....</b>	<b>6-1</b>
6.1	CELL COMPONENTS .....	6-4
6.1.1	State-of-the-Art .....	6-4
6.1.2	Development Components .....	6-9
6.2	PERFORMANCE.....	6-12
6.2.1	Effect of Pressure .....	6-14
6.2.2	Effect of Temperature .....	6-17
6.2.3	Effect of Reactant Gas Composition and Utilization .....	6-19
6.2.4	Effect of Impurities .....	6-23
6.2.5	Effects of Current Density.....	6-28
6.2.6	Effects of Cell Life.....	6-28
6.2.7	Internal Reforming .....	6-29
6.3	SUMMARY OF EQUATIONS FOR MCFC .....	6-32
6.4	REFERENCES .....	6-36
<b>7.</b>	<b>INTERMEDIATE TEMPERATURE SOLID OXIDE FUEL CELL .....</b>	<b>7-1</b>
<b>8.</b>	<b>SOLID OXIDE FUEL CELL .....</b>	<b>8-1</b>
8.1	CELL COMPONENTS .....	8-3
8.1.1	State-of-the-Art .....	8-3
8.1.2	Cell Configuration Options .....	8-6
8.1.3	Development Components .....	8-11
8.2	PERFORMANCE.....	8-13
8.2.1	Effect of Pressure .....	8-13
8.2.2	Effect of Temperature .....	8-14
8.2.3	Effect of Reactant Gas Composition and Utilization .....	8-16
8.2.4	Effect of Impurities .....	8-19
8.2.5	Effects of Current Density.....	8-21
8.2.6	Effects of Cell Life.....	8-21
8.3	SUMMARY OF EQUATIONS FOR SOFC <sup>41</sup> .....	8-22
8.4	REFERENCES .....	8-22

<b>9.</b>	<b>FUEL CELL SYSTEMS.....</b>	<b>9-1</b>
9.1	SYSTEM PROCESSES.....	9-2
9.1.1	Fuel Processing .....	9-2
9.1.2	Rejected Heat Utilization .....	9-30
9.1.3	Power Conditioners and Grid Interconnection.....	9-30
9.1.4	System and Equipment Performance Guidelines .....	9-32
9.2	SYSTEM OPTIMIZATIONS.....	9-34
9.2.1	Pressurization .....	9-34
9.2.2	Temperature .....	9-36
9.2.3	Utilization.....	9-37
9.2.4	Heat Recovery .....	9-38
9.2.5	Miscellaneous.....	9-39
9.2.6	Concluding Remarks on System Optimization .....	9-39
9.3	FUEL CELL SYSTEM DESIGNS .....	9-40
9.3.1	Natural Gas Fueled PEFC System .....	9-40
9.3.2	Natural Gas Fueled PAFC System.....	9-41
9.3.3	Natural Gas Fueled Internally Reformed MCFC System .....	9-44
9.3.4	Natural Gas Fueled Pressurized SOFC System.....	9-45
9.3.5	Natural Gas Fueled Multi-Stage Solid State Power Plant System .....	9-50
9.3.6	Coal Fueled SOFC System (Vision 21) .....	9-54
9.3.7	Power Generation by Combined Fuel Cell and Gas Turbine Systems.....	9-57
9.3.8	Heat and Fuel Recovery Cycles .....	9-58
9.4	FUEL CELL NETWORKS.....	9-70
9.4.1	Molten Carbonate Fuel Cell Networks: Principles, Analysis and Performance .....	9-70
9.4.2	MCFC Network.....	9-74
9.4.3	Recycle Scheme .....	9-74
9.4.4	Reactant Conditioning Between Stacks in Series.....	9-74
9.4.5	Higher Total Reactant Utilization .....	9-75
9.4.6	Disadvantages of MCFC Networks.....	9-76
9.4.7	Comparison of Performance.....	9-76
9.4.8	Conclusions .....	9-77
9.5	HYBRIDS .....	9-77
9.5.1	Technology.....	9-77
9.5.2	Projects.....	9-79
9.5.3	World's First Hybrid Project.....	9-81
9.5.4	Hybrid Electric Vehicles (HEV) .....	9-81
9.6	REFERENCES .....	9-83
<b>10.</b>	<b>SAMPLE CALCULATIONS .....</b>	<b>10-1</b>
10.1	UNIT OPERATIONS .....	10-1
10.1.1	Fuel Cell Calculations.....	10-1
10.1.2	Fuel Processing Calculations .....	10-16
10.1.3	Power Conditioners.....	10-20
10.1.4	Others .....	10-20
10.2	SYSTEM ISSUES .....	10-21
10.2.1	Efficiency Calculations .....	10-21
10.2.2	Thermodynamic Considerations .....	10-23
10.3	SUPPORTING CALCULATIONS .....	10-27

10.4	COST CALCULATIONS .....	10-35
10.4.1	Cost of Electricity .....	10-35
10.4.2	Capital Cost Development .....	10-36
10.5	COMMON CONVERSION FACTORS.....	10-37
10.6	AUTOMOTIVE DESIGN CALCULATIONS .....	10-38
10.7	REFERENCES .....	10-39
<b>11.</b>	<b>APPENDIX .....</b>	<b>11-1</b>
11.1	EQUILIBRIUM CONSTANTS .....	11-1
11.2	CONTAMINANTS FROM COAL GASIFICATION .....	11-2
11.3	SELECTED MAJOR FUEL CELL REFERENCES, 1993 TO PRESENT.....	11-4
11.4	LIST OF SYMBOLS .....	11-7
11.5	FUEL CELL RELATED CODES AND STANDARDS .....	11-10
11.5.1	Introduction .....	11-10
11.5.2	Organizations .....	11-10
11.5.3	Codes & Standards.....	11-12
11.5.4	Application Permits.....	11-14
11.6	FUEL CELL FIELD SITES DATA.....	11-15
11.6.1	Worldwide Sites .....	11-15
11.6.2	PEFC .....	11-16
11.6.3	PAFC.....	11-16
11.6.4	AFC .....	11-16
11.6.5	MCFC.....	11-16
11.6.6	SOFC.....	11-17
11.6.7	DoD Field Sites .....	11-18
11.6.8	IFC Field Units.....	11-18
11.6.9	Fuel Cell Energy .....	11-18
11.6.10	Siemens Westinghouse.....	11-18
11.7	THERMAL-HYDRAULIC MODEL OF A MONOLITHIC SOLID OXIDE FUEL CELL.....	11-24
11.8	REFERENCES .....	11-24
<b>12.</b>	<b>INDEX.....</b>	<b>12-1</b>

## LIST OF FIGURES

<b>Figure</b>	<b>Title</b>	<b>Page</b>
Figure 1-1	Schematic of an Individual Fuel Cell .....	1-1
Figure 1-2	Simplified Fuel Cell Schematic.....	1-2
Figure 1-3	External Reforming and Internal Reforming MCFC System Comparison .....	1-6
Figure 1-4	Expanded View of a Basic Fuel Cell Repeated Unit in a Fuel Cell Stack .....	1-8
Figure 1-5	Fuel Cell Power Plant Major Processes.....	1-9
Figure 1-6	Relative Emissions of PAFC Fuel Cell Power Plants Compared to Stringent Los Angeles Basin Requirements .....	1-10
Figure 1-7	PC-25 Fuel Cell .....	1-14
Figure 1-8	Combining the TSOFC with a Gas Turbine Engine to Improve Efficiency .....	1-18
Figure 1-9	Overview of Fuel Cell Activities Aimed at APU Applications .....	1-27
Figure 1-10	Overview of APU Applications.....	1-27
Figure 1-11	Overview of typical system requirements .....	1-28
Figure 1-12	Stage of development for fuel cells for APU applications .....	1-29
Figure 1-13	Overview of subsystems and components for SOFC and PEM systems .....	1-31
Figure 1-14	Simplified System process flow diagram of pre-reformer/SOFC system.....	1-32
Figure 1-15	Multilevel system modeling approach.....	1-33
Figure 1-16	Projected cost structure of a 5kWnet APU SOFC system. Gasoline fueled POX reformer, Fuel cell operating at 300mW/cm <sup>2</sup> , 0.7 V, 90 % fuel utilization, 500,000 units per year production volume. ....	1-35
Figure 2-1	H <sub>2</sub> /O <sub>2</sub> Fuel Cell Ideal Potential as a Function of Temperature .....	2-4
Figure 2-2	Ideal and Actual Fuel Cell Voltage/Current Characteristic.....	2-5
Figure 2-3	Contribution to Polarization of Anode and Cathode .....	2-8
Figure 2-4	Flexibility of Operating Points According to Cell Parameters.....	2-9
Figure 2-5	Voltage/Power Relationship.....	2-10
Figure 2-6	Dependence of the Initial Operating Cell Voltage of Typical Fuel Cells on Temperature.....	2-12
Figure 2-7	The Variation in the Reversible Cell Voltage as a Function of Reactant Utilization.....	2-15
Figure 2-8	Example of a Tafel Plot.....	2-24
Figure 3-1	PEFC Schematic.....	3-4
Figure 3-2	Performance of Low Platinum Loading Electrodes .....	3-5
Figure 3-3	Multi-Cell Stack Performance on Dow Membrane.....	3-7
Figure 3-4	Effect on PEFC Performances of Bleeding Oxygen into the Anode Compartment.....	3-9
Figure 3-5	Evolutionary Changes in PEFCs Performance [(a) H <sub>2</sub> /O <sub>2</sub> , (b) Reformate Fuel/Air, (c) H <sub>2</sub> /Air)].....	3-10
Figure 3-6	Influence of O <sub>2</sub> Pressure on PEFCs Performance (93°C, Electrode Loadings of 2 mg/cm <sup>2</sup> Pt, H <sub>2</sub> Fuel at 3 Atmospheres) .....	3-11
Figure 3-7	Cell Performance with Carbon Monoxide in Reformed Fuel .....	3-12
Figure 3-8	Single Cell Direct Methanol Fuel Cell Data.....	3-13
Figure 4-1	Principles of Operation of Alkaline Fuel Cells (Siemens).....	4-2
Figure 4-2	Evolutionary Changes in the Performance of AFC's .....	4-5
Figure 4-3	Reversible Voltage of The Hydrogen-Oxygen Cell .....	4-6

Figure 4-4	Influence of Temperature on O <sub>2</sub> , (air) Reduction in 12 N KOH.....	4-7
Figure 4-5	Influence of Temperature on the AFC Cell Voltage .....	4-8
Figure 4-6	Degradation in AFC Electrode Potential with CO <sub>2</sub> Containing and CO <sub>2</sub> Free Air.....	4-9
Figure 4-7	iR Free Electrode Performance with O <sub>2</sub> and Air in 9 N KOH at 55 to 60°C Catalyzed (0.5 mg Pt/cm <sup>2</sup> Cathode, 0.5 mg Pt-Rh/cm <sup>2</sup> Anode) Carbon-based Porous Electrodes.....	4-10
Figure 4-8	iR Free Electrode Performance with O <sub>2</sub> and Air in 12 N KOH at 65°C. ....	4-11
Figure 5-1	Improvement in the Performance of H <sub>2</sub> -Rich Fuel/Air PAFCs.....	5-4
Figure 5-2	Advanced Water-Cooled PAFC Performance.....	5-6
Figure 5-3	Effect of Temperature: Ultra-High Surface Area Pt Catalyst. Fuel: H <sub>2</sub> , H <sub>2</sub> + 200 ppm H <sub>2</sub> S and Simulated Coal Gas.....	5-12
Figure 5-4	Polarization at Cathode (0.52 mg Pt/cm <sup>2</sup> ) as a Function of O <sub>2</sub> Utilization, which is Increased by Decreasing the Flow Rate of the Oxidant at Atmospheric Pressure 100% H <sub>3</sub> PO <sub>4</sub> , 191°C, 300 mA/cm <sup>2</sup> , 1 atm. ....	5-13
Figure 5-5	Influence of CO and Fuel Gas Composition on the Performance of Pt Anodes in 100% H <sub>3</sub> PO <sub>4</sub> at 180°C. 10% Pt Supported on Vulcan XC-72, 0.5 mg Pt/cm <sup>2</sup> . Dew Point, 57°. Curve 1, 100% H <sub>2</sub> ; Curves 2-6, 70% H <sub>2</sub> and CO <sub>2</sub> /CO Contents (mol%) Specified .....	5-16
Figure 5-6	Effect of H <sub>2</sub> S Concentration: Ultra-High Surface Area Pt Catalyst.....	5-17
Figure 5-7	Reference Performances at 8.2 atm and Ambient Pressure.....	5-20
Figure 6-1	Dynamic Equilibrium in Porous MCFC Cell Elements (Porous electrodes are depicted with pores covered by a thin film of electrolyte).....	6-3
Figure 6-2	Progress in the Generic Performance of MCFCs on Reformate Gas and Air.....	6-5
Figure 6-3	Effect of Oxidant Gas Composition on MCFC Cathode Performance at 650°C, (Curve 1, 12.6% O <sub>2</sub> /18.4% CO <sub>2</sub> /69.0% N <sub>2</sub> ; Curve 2, 33% O <sub>2</sub> / 67% CO <sub>2</sub> ) .....	6-13
Figure 6-4	Voltage and Power Output of a 1.0/m <sup>2</sup> 19 cell MCFC Stack after 960 Hours at 965°C and 1 atm, Fuel Utilization, 75% .....	6-13
Figure 6-5	Influence of Cell Pressure on the Performance of a 70.5 cm <sup>2</sup> MCFC at 650°C (anode gas, not specified; cathode gases, 23.2% O <sub>2</sub> /3.2% CO <sub>2</sub> /66.3% N <sub>2</sub> /7.3% H <sub>2</sub> O and 9.2% O <sub>2</sub> /18.2% CO <sub>2</sub> /65.3% N <sub>2</sub> /7.3% H <sub>2</sub> O; 50% CO <sub>2</sub> , utilization at 215 mA/cm <sup>2</sup> ).....	6-16
Figure 6-6	Influence of Pressure on Voltage Gain.....	6-17
Figure 6-7	Effect of CO <sub>2</sub> /O <sub>2</sub> Ratio on Cathode Performance in an MCFC, Oxygen Pressure is 0.15 atm.....	6-20
Figure 6-8	Influence of Reactant Gas Utilization on the Average Cell Voltage of an MCFC Stack.....	6-21
Figure 6-9	Dependence of Cell Voltage on Fuel Utilization .....	6-23
Figure 6-10	Influence of 5 ppm H <sub>2</sub> S on the Performance of a Bench Scale MCFC (10 cm x 10 cm) at 650°C, Fuel Gas (10% H <sub>2</sub> /5% CO <sub>2</sub> /10% H <sub>2</sub> O/75% He) at 25% H <sub>2</sub> Utilization .....	6-27
Figure 6-11	IIR/DIR Operating Concept, Molten Carbonate Fuel Cell Design .....	6-29



Figure 6-12	CH <sub>4</sub> Conversion as a Function of Fuel Utilization in a DIR Fuel Cell (MCFC at 650°C and 1 atm, steam/carbon ratio = 2.0, >99% methane conversion achieved with fuel utilization > 65%).....	6-31
Figure 6-13	Voltage Current Characteristics of a 3kW, Five Cell DIR Stack with 5,016 cm <sup>2</sup> Cells Operating on 80/20% H <sub>2</sub> /CO <sub>2</sub> and Methane .....	6-31
Figure 6-14	Performance Data of a 0.37m <sup>2</sup> 2 kW Internally Reformed MCFC Stack at 650°C and 1 atm .....	6-32
Figure 6-15	Average Cell Voltage of a 0.37m <sup>2</sup> 2 kW Internally Reformed MCFC Stack at 650°C and 1 atm. Fuel, 100% CH <sub>4</sub> , Oxidant, 12% CO <sub>2</sub> /9% O <sub>2</sub> /77% N <sub>2</sub> .....	6-33
Figure 6-16	Model Predicted and Constant Flow Polarization Data Comparison.....	6-35
Figure 8-1	Solid Oxide Fuel Cell Designs at the Cathode .....	8-1
Figure 8-2	Solid Oxide Fuel Cell Operating Principle.....	8-2
Figure 8-3	Cross Section (in the Axial Direction of the +) of an Early Tubular Configuration for SOFCs .....	8-8
Figure 8-4	Cross Section (in the Axial Direction of the Series-Connected Cells) of an Early "Bell and Spigot" Configuration for SOFCs .....	8-8
Figure 8-5	Cross Section of Present Tubular Configuration for SOFCs.....	8-9
Figure 8-6	Gas-Manifold Design for a Tubular SOFC .....	8-9
Figure 8-7	Cell-to-Cell Connections Among Tubular SOFCs.....	8-10
Figure 8-8	Effect of Pressure on AES Cell Performance at 1000°C.....	8-14
Figure 8-9	Two Cell Stack Performance with 67% H <sub>2</sub> + 22% CO + 11% H <sub>2</sub> O/Air.....	8-15
Figure 8-10	Two Cell Stack Performance with 97% H <sub>2</sub> and 3% H <sub>2</sub> O/Air .....	8-16
Figure 8-17	Cell Performance at 1000°C with Pure Oxygen (o) and Air (Δ) Both at 25% Utilization (Fuel (67% H <sub>2</sub> /22% CO/11%H <sub>2</sub> O) Utilization is 85%).....	8-17
Figure 8-12	Influence of Gas Composition of the Theoretical Open-Circuit Potential of SOFC at 1000°C.....	8-18
Figure 8-13	Variation in Cell Voltage as a Function of Fuel Utilization and Temperature (Oxidant (o - Pure O <sub>2</sub> ; Δ - Air) Utilization is 25%. Currently Density is 160 mA/cm <sup>2</sup> at 800, 900 and 1000°C and 79 mA/cm <sup>2</sup> at 700°C).....	8-19
Figure 8-14	SOFC Performance at 1000°C and 350 mA/cm, <sup>2</sup> 85% Fuel Utilization and 25% Air Utilization (Fuel = Simulated Air-Blown Coal Gas Containing 5000 ppm NH <sub>3</sub> , 1 ppm HCl and 1 ppm H <sub>2</sub> S) .....	8-20
Figure 8-15	Voltage-Current Characteristics of an AES Cell (1.56 cm Diameter, 50 cm Active Length).....	8-21
Figure 9-1	A Rudimentary Fuel Cell Power System Schematic .....	9-1
Figure 9-2	Representative Fuel Processor Major Components <sup>a</sup> & Temperatures .....	9-3
Figure 9-3	"Well-to Wheel" Efficiency for Various Vehicle Scenarios.....	9-8
Figure 9-4	Carbon Deposition Mapping of Methane (CH <sub>4</sub> ) (Carbon-Free Region to the Right and Above the Curve).....	9-23
Figure 9-5	Carbon Deposition Mapping of Octane (C <sub>8</sub> H <sub>18</sub> ) (Carbon-Free Region to the Right and Above the Curve).....	9-24
Figure 9-6	Optimization Flexibility in a Fuel Cell Power System.....	9-35
Figure 9-7	Natural Gas Fueled PEFC Power Plant.....	9-40
Figure 9-8	Natural Gas fueled PAFC Power System.....	9-42
Figure 9-9	Natural Gas Fueled MCFC Power System.....	9-44

Figure 9-10 Schematic for a 4.5 MW Pressurized SOFC .....	9-46
Figure 9-11 Schematic for a 4 MW Solid State Fuel Cell System.....	9-51
Figure 9-12 Schematic for a 500 MW Class Coal Fueled Pressurized SOFC .....	9-54
Figure 9-13 Regenerative Brayton Cycle Fuel Cell Power System.....	9-59
Figure 9-14 Combined Brayton-Rankine Cycle Fuel Cell Power Generation System.....	9-62
Figure 9-15 Combined Brayton-Rankine Cycle Thermodynamics.....	9-63
Figure 9-16 T-Q Plot for Heat Recovery Steam Generator (Brayton-Rankine) .....	9-64
Figure 9-17 Fuel Cell Rankine Cycle Arrangement.....	9-65
Figure 9-18 T-Q Plot of Heat Recovery from Hot Exhaust Gas .....	9-66
Figure 9-19 MCFC System Designs .....	9-71
Figure 9-20 Stacks in Series Approach Reversibility .....	9-72
Figure 9-21 MCFC Network .....	9-75
Figure 9-22 Estimated performance of Power Generation Systems .....	9-78
Figure 9-23 Diagram of a Proposed Siemens-Westinghouse Hybrid System .....	9-79
Figure 11-1 Equilibrium Constants (Partial Pressures in MPa) for (a) Water Gas Shift, (b) Methane Formation, (c) Carbon Deposition (Boudouard Reaction), and (d) Methane Decomposition (J.R. Rostrup-Nielsen, in Catalysis Science and Technology, Edited by J.R. Anderson and M. Boudart, Springer-Verlag, Berlin GDR, p.1, 1984.).....	11-2

## LIST OF TABLES AND EXAMPLES

<b>Table</b>	<b>Title</b>	<b>Page</b>
Table 1-1	Summary of Major Differences of the Fuel Cell Types .....	1-5
Table 1-2	Summary of Major Fuel Constituents Impact on PEFC, AFC, PAFC, MCFC, ITSOFC, and SOFC .....	1-11
Table 1-3	Attributes of Selected Distributed Generation Systems .....	1-22
Table 2-1	Electrochemical Reactions in Fuel Cells .....	2-2
Table 2-2	Fuel Cell Reactions and the Corresponding Nernst Equations.....	2-3
Table 2-3	Ideal Voltage as A Function of Cell Temperature.....	2-4
Table 2-4	Outlet Gas Composition as a Function of Utilization in MCFC at 650°C .....	2-16
Table 5-1	Evolution of Cell Component Technology for Phosphoric Acid Fuel Cells .....	5-3
Table 5-2	Advanced PAFC Performance.....	5-6
Table 5-3	Dependence of $k(T)$ on Temperature.....	5-15
Table 6-1	Evolution of Cell Component Technology for Molten Carbonate Fuel Cells.....	6-4
Table 6-2	Amount in Mol% of Additives to Provide Optimum Performance.....	6-11
Table 6-3	Qualitative Tolerance Levels for Individual Contaminants in Isothermal Bench-Scale Carbonate Fuel Cells.....	6-12
Table 6-4	Equilibrium Composition of Fuel Gas and Reversible Cell Potential as a Function of Temperature .....	6-18
Table 6-5	Influence of Fuel Gas Composition on Reversible Anode Potential at 650°C.....	6-22
Table 6-6	Contaminants from Coal-Derived Fuel Gas and Their Potential Effect on MCFCs .....	6-24
Table 6-7	Gas Composition and Contaminants from Air-Blown Coal Gasifier After Hot Gas Cleanup, and Tolerance Limit of MCFCs to Contaminants .....	6-25
Table 8-1	Evolution of Cell Component Technology for Tubular Solid Oxide Fuel Cells.....	8-3
Table 8-2	K Values for $\Delta V_T$ .....	8-15
Table 9-1	Calculated Thermoneutral Oxygen-to-Fuel Molar Ratios ( $x_o$ ) and Maximum Theoretical Efficiencies (at $x_o$ ) for Common Fuels.....	9-16
Table 9-2	Typical Steam Reformed Natural Gas Reformate .....	9-17
Table 9-3	Typical Partial Oxidation Reformed Fuel Oil Reformate.....	9-19
Table 9-4	Typical Coal Gas Compositions for Selected Oxygen-Blown Gasifiers .....	9-21
Table 9-5	Equipment Performance Assumptions.....	9-33
Table 9-6	Stream Properties for the Natural Gas Fueled Pressurized PAFC.....	9-42
Table 9-7	Operating/Design Parameters for the NG fueled PAFC .....	9-43
Table 9-8	Performance Summary for the NG fueled PAFC .....	9-43
Table 9-9	Operating/Design Parameters for the NG Fueled IR-MCFC.....	9-45
Table 9-10	Overall Performance Summary for the NG Fueled IR-MCFC.....	9-45
Table 9-11	Stream Properties for the Natural Gas Fueled Pressurized SOFC.....	9-47
Table 9-12	Operating/Design Parameters for the NG Fueled Pressurized SOFC.....	9-48
Table 9-13	Overall Performance Summary for the NG Fueled Pressurized SOFC.....	9-49
Table 9-14	Heron Gas Turbine Parameters.....	9-49
Table 9-15	Example Fuel Utilization in a Multi-Stage Fuel Cell Module.....	9-50

Table 9-16	Stream Properties for the Natural Gas Fueled Solid State Fuel Cell Power Plant System.....	9-51
Table 9-17	Operating/Design Parameters for the NG fueled Multi-Stage Fuel Cell System ...	9-53
Table 9-18	Overall Performance Summary for the NG fueled Multi-Stage Fuel Cell System .	9-53
Table 9-19	Stream Properties for the 500 MW Class Coal Gas Fueled Cascaded SOFC .....	9-55
Table 9-20	Coal Analysis.....	9-56
Table 9-21	Operating/Design Parameters for the Coal Fueled Pressurized SOFC.....	9-57
Table 9-22	Overall Performance Summary for the Coal Fueled Pressurized SOFC.....	9-57
Table 9-23	Performance Calculations for a Pressurized, High Temperature Fuel Cell (SOFC) with a Regenerative Brayton Bottoming Cycle; Approach Delta T=30F .....	9-60
Table 9-24	Performance Computations for Various High Temperature Fuel Cell (SOFC) Heat Recovery Arrangements.....	9-61
Table 10-1	Common Atomic Elements and Weights.....	10-28
Table 10-2	HHV Contribution of Common Gas Constituents.....	10-30
Table 10-3	Ideal Gas Heat Capacity Coefficients for Common Fuel Cell Gases .....	10-33
Table 10-4	Distributive Estimating Factors .....	10-36
Table 11-1	Typical Contaminant Levels Obtained from Selected Coal Gasification Processes .....	11-3
Table 11-2	Summary of Related Codes and Standards.....	11-12
Table 11-3	DoD Field Site .....	11-19
Table 11-4	IFC Field Units .....	11-21
Table 11-5	Fuel Cell Energy Field Sites .....	11-23
Table 11-6	Siemens Westinghouse SOFC Field Units .....	11-23

---

## FORWARD

---

Fuel cells are an important technology for a potentially wide variety of applications including micropower, auxiliary power, transportation power, stationary power for buildings and other distributed generation applications, and central power. These applications will be in a large number of industries worldwide.

This edition of the Fuel Cell Handbook is more comprehensive than previous versions in that it includes several changes. First, calculation examples for fuel cells are included for the wide variety of possible applications. This includes transportation and auxiliary power applications for the first time. In addition, the handbook includes a separate section on alkaline fuel cells. The intermediate temperature solid-state fuel cell section is being developed. In this edition, hybrids are also included as a separate section for the first time. Hybrids are some of the most efficient power plants ever conceived and are actually being demonstrated. Finally, an updated list of fuel cell URLs is included in the Appendix and an updated index assists the reader in locating specific information quickly.

It is an important task that NETL undertakes to provide you with this handbook. We realize it is an important educational and informational tool for a wide audience. We welcome suggestions to improve the handbook.

Mark C. Williams

Strategic Center for Natural Gas  
National Energy Technology Laboratory

---

## PREFACE

---

Progress continues in fuel cell technology since the previous edition of the Fuel Cell Handbook was published in November 1998. Uppermost, polymer electrolyte fuel cells, molten carbonate fuel cells, and solid oxide fuel cells have been demonstrated at commercial size in power plants. The previously demonstrated phosphoric acid fuel cells have entered the marketplace with more than 220 power plants delivered. Highlighting this commercial entry, the phosphoric acid power plant fleet has demonstrated 95+% availability and several units have passed 40,000 hours of operation. One unit has operated over 49,000 hours.

Early expectations of very low emissions and relatively high efficiencies have been met in power plants with each type of fuel cell. Fuel flexibility has been demonstrated using natural gas, propane, landfill gas, anaerobic digester gas, military logistic fuels, and coal gas, greatly expanding market opportunities. Transportation markets worldwide have shown remarkable interest in fuel cells; nearly every major vehicle manufacturer in the U.S., Europe, and the Far East is supporting development.

This Handbook provides a foundation in fuel cells for persons wanting a better understanding of the technology, its benefits, and the systems issues that influence its application. Trends in technology are discussed, including next-generation concepts that promise ultrahigh efficiency and low cost, while providing exceptionally clean power plant systems. Section 1 summarizes fuel cell progress since the last edition and includes existing power plant nameplate data. Section 2 addresses the thermodynamics of fuel cells to provide an understanding of fuel cell operation at two levels (basic and advanced). Sections 3 through 8 describe the six major fuel cell types and their performance based on cell operating conditions. Alkaline and intermediate solid state fuel cells were added to this edition of the Handbook. New information indicates that manufacturers have stayed with proven cell designs, focusing instead on advancing the system surrounding the fuel cell to lower life cycle costs. Section 9, Fuel Cell Systems, has been significantly revised to characterize near-term and next-generation fuel cell power plant systems at a conceptual level of detail. Section 10 provides examples of practical fuel cell system calculations. A list of fuel cell URLs is included in the Appendix. A new index assists the reader in locating specific information quickly.

---

## ACKNOWLEDGEMENTS

---

The authors of this edition of the Fuel Cell Handbook acknowledge the cooperation of the fuel cell community for their contributions to this Handbook. Many colleagues provided data, information, references, valuable suggestions, and constructive comments that were incorporated into the Handbook. In particular, we would like to acknowledge the contributions of the following individuals: C. Read and J. Thijssen of Arthur D. Little, Inc., M. Krumpelt, J. Ralph, S. Ahmed and R. Kumar of ANL, D. Harris of Ballard Power Systems, H. Maru of Fuel Cell Energy, H. Heady and J. Staniunas of International Fuel Cells Corporation, J. Pierre of Siemens Westinghouse and J. O'Sullivan.

C. Hitchings, SAIC, provided technical editing and final layout of the Handbook.

The authors wish to thank Dr. Mark C. Williams of the U.S. Department of Energy, National Energy Technology Laboratory, for his support and encouragement, and for providing the opportunity to write this Handbook.

This work was supported by the U.S. Department of Energy, National Energy Technology Laboratory, under Contract DE-AM26-99FT40575.

---

# 1. TECHNOLOGY OVERVIEW

---

## 1.1 Fuel Cell Description

Fuel cells are electrochemical devices that convert the chemical energy of a reaction directly into electrical energy. The basic physical structure or building block of a fuel cell consists of an electrolyte layer in contact with a porous anode and cathode on either side. A schematic representation of a fuel cell with the reactant/product gases and the ion conduction flow directions through the cell is shown in Figure 1-1.

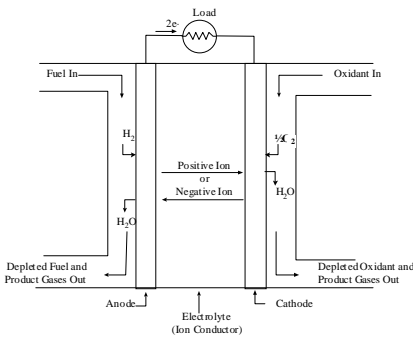


**Figure 1-1 Schematic of an Individual Fuel Cell**

In a typical fuel cell, gaseous fuels are fed continuously to the anode (negative electrode) compartment and an oxidant (i.e., oxygen from air) is fed continuously to the cathode (positive electrode) compartment; the electrochemical reactions take place at the electrodes to produce an electric current. A fuel cell, although having components and characteristics similar to those of a typical battery, differs in several respects. The battery is an energy storage device. The maximum energy available is determined by the amount of chemical reactant stored within the battery itself. The battery will cease to produce electrical energy when the chemical reactants are consumed (i.e., discharged). In a secondary battery, the reactants are regenerated by recharging, which involves putting energy into the battery from an external source. The fuel cell, on the other hand, is an energy conversion device that theoretically has the capability of producing electrical energy for as long as the fuel and oxidant are supplied to the electrodes. Figure 1-2 is a simplified diagram that demonstrates how the fuel cell works. In reality, degradation, primarily corrosion, or malfunction of components limits the practical operating life of fuel cells.

Note that the ion specie and its transport direction can differ, influencing the site of water production and removal, a system impact. The ion can be either a positive or a negative ion,



meaning that the ion carries either a positive or negative charge (surplus or deficit of electrons). The fuel or oxidant gases flow past the surface of the anode or cathode opposite the electrolyte and generate electrical energy by the electrochemical oxidation of fuel, usually hydrogen, and the electrochemical reduction of the oxidant, usually oxygen. Appleby and Foulkes (1) have

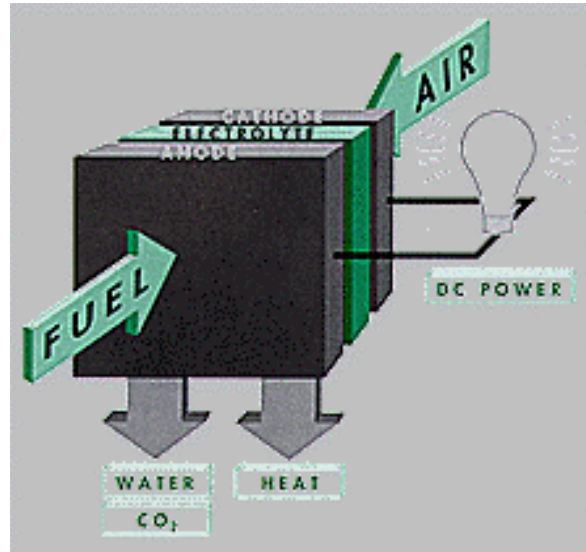


**Figure 1-2 Simplified Fuel Cell Schematic**

noted that in theory, any substance capable of chemical oxidation that can be supplied continuously (as a fluid) can be burned galvanically as the fuel at the anode of a fuel cell. Similarly, the oxidant can be any fluid that can be reduced at a sufficient rate. Gaseous hydrogen has become the fuel of choice for most applications, because of its high reactivity when suitable catalysts are used, its ability to be produced from hydrocarbons for terrestrial applications, and its high energy density when stored cryogenically for closed environment applications, such as in space. Similarly, the most common oxidant is gaseous oxygen, which is readily and economically available from air for terrestrial applications, and again easily stored in a closed environment. A three-phase interface is established among the reactants, electrolyte, and catalyst in the region of the porous electrode. The nature of this interface plays a critical role in the electrochemical performance of a fuel cell, particularly in those fuel cells with liquid electrolytes. In such fuel cells, the reactant gases diffuse through a thin electrolyte film that wets portions of the porous electrode and react electrochemically on their respective electrode surface. If the porous electrode contains an excessive amount of electrolyte, the electrode may "flood" and restrict the transport of gaseous species in the electrolyte phase to the reaction sites. The consequence is a reduction in the electrochemical performance of the porous electrode. Thus, a delicate balance must be maintained among the electrode, electrolyte, and gaseous phases in the porous electrode structure. Much of the recent effort in the development of fuel cell technology has been devoted to reducing the thickness of cell components while refining and improving the electrode structure and the electrolyte phase, with the aim of obtaining a higher and more stable electrochemical performance while lowering cost.

The electrolyte not only transports dissolved reactants to the electrode, but also conducts ionic charge between the electrodes and thereby completes the cell electric circuit, as illustrated in

Figure 1-1. It also provides a physical barrier to prevent the fuel and oxidant gas streams from directly mixing.

The functions of porous electrodes in fuel cells are: 1) to provide a surface site where gas/liquid ionization or de-ionization reactions can take place, 2) to conduct ions away from or into the three-phase interface once they are formed (so an electrode must be made of materials that have good electrical conductance), and 3) to provide a physical barrier that separates the bulk gas phase and the electrolyte. A corollary of Item 1 is that, in order to increase the rates of reactions, the electrode material should be catalytic as well as conductive, porous rather than solid. The catalytic function of electrodes is more important in lower temperature fuel cells and less so in high-temperature fuel cells because ionization reaction rates increase with temperature. It is also a corollary that the porous electrodes must be permeable to both electrolyte and gases, but not such that the media can be easily "flooded" by the electrolyte or "dried" by the gases in a one-sided manner (see latter part of next section).

A variety of fuel cells are in different stages of development. They can be classified by use of diverse categories, depending on the combination of type of fuel and oxidant, whether the fuel is processed outside (external reforming) or inside (internal reforming) the fuel cell, the type of electrolyte, the temperature of operation, whether the reactants are fed to the cell by internal or external manifolds, etc. The most common classification of fuel cells is by the type of electrolyte used in the cells and includes 1) polymer electrolyte fuel cell (PEFC), 2) alkaline fuel cell (AFC), 3) phosphoric acid fuel cell (PAFC), 4) molten carbonate fuel cell (MCFC), 5) intermediate temperature solid oxide fuel cell (ITSOFC), and 6) tubular solid oxide fuel cell (TSOFC). These fuel cells are listed in the order of approximate operating temperature, ranging from ~80°C for PEFC, ~100°C for AFC, ~200°C for PAFC, ~650°C for MCFC, ~800°C for ITSOFC, and 1000°C for TSOFC. The operating temperature and useful life of a fuel cell dictate the physicochemical and thermomechanical properties of materials used in the cell components (i.e., electrodes, electrolyte, interconnect, current collector, etc.). Aqueous electrolytes are limited to temperatures of about 200°C or lower because of their high water vapor pressure and/or rapid degradation at higher temperatures. The operating temperature also plays an important role in dictating the type of fuel that can be used in a fuel cell. The low-temperature fuel cells with aqueous electrolytes are, in most practical applications, restricted to hydrogen as a fuel. In high-temperature fuel cells, CO and even CH<sub>4</sub> can be used because of the inherently rapid electrode kinetics and the lesser need for high catalytic activity at high temperature. However, descriptions later in this section note that the higher temperature cells can favor the conversion of CO and CH<sub>4</sub> to hydrogen, then use the equivalent hydrogen as the actual fuel.

A brief description of various electrolyte cells of interest follows. A detailed description of these fuel cells may be found in References (1) and (2).

***Polymer Electrolyte Fuel Cell (PEFC):*** The electrolyte in this fuel cell is an ion exchange membrane (fluorinated sulfonic acid polymer or other similar polymer) that is an excellent proton conductor. The only liquid in this fuel cell is water; thus, corrosion problems are minimal. Water management in the membrane is critical for efficient performance; the fuel cell must operate under conditions where the byproduct water does not evaporate faster than it is produced because the membrane must be hydrated. Because of the limitation on the operating

temperature imposed by the polymer, usually less than 120°C, and because of problems with water balance, a H<sub>2</sub>-rich gas with minimal or no CO (a poison at low temperature) is used. Higher catalyst loading (Pt in most cases) than that used in PAFCs is required for both the anode and cathode.

***Alkaline Fuel Cell (AFC):*** The electrolyte in this fuel cell is concentrated (85 wt%) KOH in fuel cells operated at high temperature (~250°C), or less concentrated (35-50 wt%) KOH for lower temperature (<120°C) operation. The electrolyte is retained in a matrix (usually asbestos), and a wide range of electrocatalysts can be used (e.g., Ni, Ag, metal oxides, spinels, and noble metals). The fuel supply is limited to non-reactive constituents except for hydrogen. CO is a poison, and CO<sub>2</sub> will react with the KOH to form K<sub>2</sub>CO<sub>3</sub>, thus altering the electrolyte. Even the small amount of CO<sub>2</sub> in air must be considered with the alkaline cell.

***Phosphoric Acid Fuel Cell (PAFC):*** Phosphoric acid concentrated to 100% is used for the electrolyte in this fuel cell, which operates at 150 to 220°C. At lower temperatures, phosphoric acid is a poor ionic conductor, and CO poisoning of the Pt electrocatalyst in the anode becomes severe. The relative stability of concentrated phosphoric acid is high compared to other common acids; consequently the PAFC is capable of operating at the high end of the acid temperature range (100 to 220°C). In addition, the use of concentrated acid (100%) minimizes the water vapor pressure so water management in the cell is not difficult. The matrix universally used to retain the acid is silicon carbide (1), and the electrocatalyst in both the anode and cathode is Pt.

***Molten Carbonate Fuel Cell (MCFC):*** The electrolyte in this fuel cell is usually a combination of alkali carbonates, which is retained in a ceramic matrix of LiAlO<sub>2</sub>. The fuel cell operates at 600 to 700°C where the alkali carbonates form a highly conductive molten salt, with carbonate ions providing ionic conduction. At the high operating temperatures in MCFCs, Ni (anode) and nickel oxide (cathode) are adequate to promote reaction. Noble metals are not required.

***Intermediate Temperature Solid Oxide Fuel Cell (ITSOFC):*** The electrolyte and electrode materials in this fuel cell are basically the same as used in the TSOFC. The ITSOFC operates at a lower temperature, however, typically between 600 to 800°C. For this reason, thin film technology is being developed to promote ionic conduction; alternative electrolyte materials are also being developed.

***Tubular Solid Oxide Fuel Cell (TSOFC):*** The electrolyte in this fuel cell is a solid, nonporous metal oxide, usually Y<sub>2</sub>O<sub>3</sub>-stabilized ZrO<sub>2</sub>. The cell operates at 1000°C where ionic conduction by oxygen ions takes place. Typically, the anode is Co-ZrO<sub>2</sub> or Ni-ZrO<sub>2</sub> cermet, and the cathode is Sr-doped LaMnO<sub>3</sub>.

In low-temperature fuel cells (PEFC, AFC, PAFC), protons or hydroxyl ions are the major charge carriers in the electrolyte, whereas in the high-temperature fuel cells, MCFC, ITSOFC, and TSOFC, carbonate ions and oxygen ions are the charge carriers, respectively. A detailed discussion of these different types of fuel cells is presented in Sections 3 through 8. Major differences between the various cells are shown in Table 1-1.

**Table 1-1 Summary of Major Differences of the Fuel Cell Types**

	<b>PEFC</b>	<b>AFC</b>	<b>PAFC</b>	<b>MCFC</b>	<b>ITSOFC</b>	<b>TSOFC</b>
Electrolyte	Ion Exchange Membranes	Mobilized or Immobilized Potassium Hydroxide	Immobilized Liquid Phosphoric Acid	Immobilized Liquid Molten Carbonate	Ceramic	Ceramic
Operating Temperature	80°C	65°C - 220°C	205°C	650°	600-800°C	800-1000°C
Charge Carrier	H <sup>+</sup>	OH <sup>-</sup>	H <sup>+</sup>	CO <sub>3</sub> <sup>=</sup>	O <sup>=</sup>	O <sup>=</sup>
External Reformer for CH <sub>4</sub> (below)	Yes	Yes	Yes	No	No	No
Prime Cell Components	Carbon-based	Carbon-based	Graphite-based	Stainless-based	Ceramic	Ceramic
Catalyst	Platinum	Platinum	Platinum	Nickel	Perovskites	Perovskites
Product Water Management	Evaporative	Evaporative	Evaporative	Gaseous Product	Gaseous Product	Gaseous Product
Product Heat Management	Process Gas + Independent Cooling Medium	Process Gas + Electrolyte Calculation	Process Gas + Independent Cooling Medium	Internal Reforming + Process Gas	Internal Reforming + Process Gas	Internal Reforming + Process Gas

Even though the electrolyte has become the predominant means of characterizing a cell, another important distinction is the method used to produce hydrogen for the cell reaction. Hydrogen can be reformed from natural gas and steam in the presence of a catalyst starting at a temperature of ~760°C. The reaction is endothermic. MCFC, ITSOFC, and TSOFC operating temperatures are high enough that reforming reactions can occur within the cell, a process referred to as internal reforming. Figure 1-3 shows a comparison of internal reforming and external reforming MCFCs. The reforming reaction is driven by the decrease in hydrogen as the cell produces power. This internal reforming can be beneficial to system efficiency because there is an effective transfer of heat from the exothermic cell reaction to satisfy the endothermic reforming reaction. A reforming catalyst is needed adjacent to the anode gas chamber for the reaction to occur. The cost of an external reformer is eliminated and system efficiency is improved, but at the expense of a more complex cell configuration and increased maintenance issues. This provides developers of high-temperature cells a choice of an external reforming or internal reforming approach. Section 6 will show that the present internal reforming MCFC is limited to ambient pressure operation, whereas external reforming MCFC can operate at pressures up to 3 atmospheres. The slow rate of the reforming reaction makes internal reforming impractical in the lower temperature cells. Instead, a separate external reformer is used.

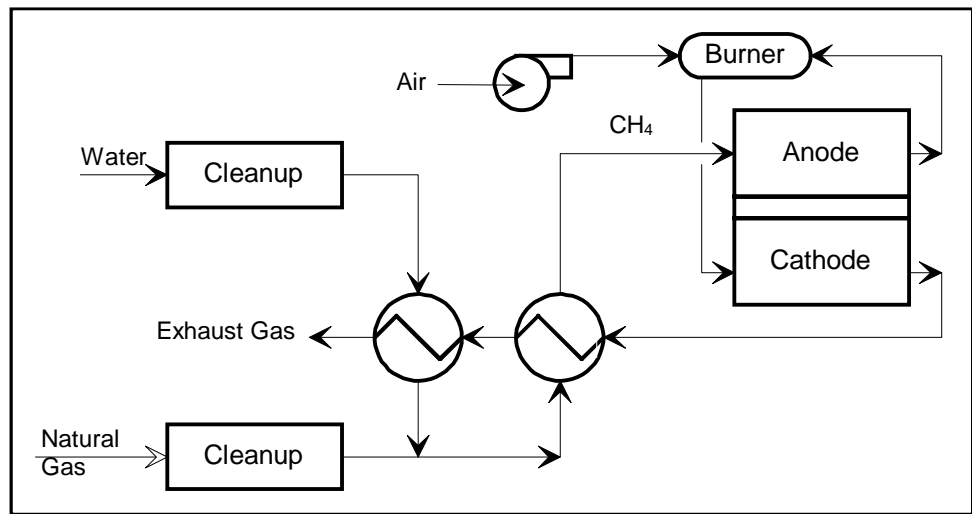
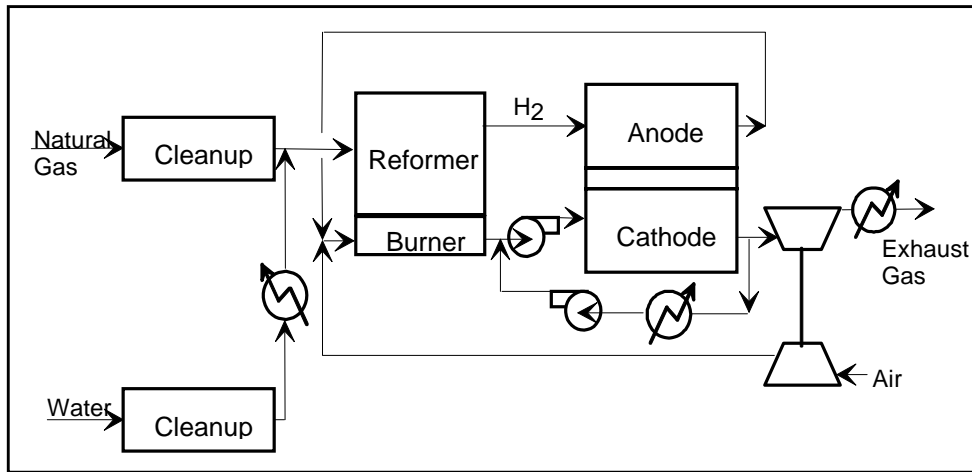


**Figure 1-3 External Reforming and Internal Reforming MCFC System Comparison**

Porous electrodes, mentioned several times above, are key to good electrode performance. The reason for this is that the current densities obtained from smooth electrodes are usually in the range of a single digit mA/cm<sup>2</sup> or less because of rate-limiting issues such as the available area of the reaction sites. Porous electrodes, used in fuel cells, achieve much higher current densities. These high current densities are possible because the electrode has a high surface area, relative to the geometric plate area that significantly increases the number of reaction sites, and the optimized electrode structure has favorable mass transport properties. In an idealized porous gas fuel cell electrode, high current densities at reasonable polarization are obtained when the liquid (electrolyte) layer on the electrode surface is sufficiently thin so that it does not significantly impede the transport of reactants to the electroactive sites, and a stable three-phase (gas/electrolyte/electrode surface) interface is established. When an excessive amount of electrolyte is present in the porous electrode structure, the electrode is considered to be "flooded" and the concentration polarization increases to a large value.

The porous electrodes used in low-temperature fuel cells consist of a composite structure that contains platinum (Pt) electrocatalyst on a high surface area carbon black and a PTFE (polytetrafluoroethylene) binder. Such electrodes for acid and alkaline fuel cells are described by Kordesch et al. (3). In these porous electrodes, PTFE is hydrophobic (acts as a wet proofing agent) and serves as the gas permeable phase, and carbon black is an electron conductor that provides a high surface area to support the electrocatalyst. Platinum serves as the electrocatalyst, which promotes the rate of electrochemical reactions (oxidation/reduction) for a given surface area. The carbon black is also somewhat hydrophobic, depending on the surface properties of the material. The composite structure of PTFE and carbon establishes an extensive three-phase interface in the porous electrode, which is the benchmark of PTFE bonded electrodes. Some interesting results have been reported by Japanese workers on higher performance gas diffusion electrodes for phosphoric acid fuel cells (see Section 5.1.2).

In MCFCs, which operate at relatively high temperature, no materials are known that wet-proof a porous structure against ingress by molten carbonates. Consequently, the technology used to obtain a stable three-phase interface in MCFC porous electrodes is different from that used in PAFCs. In the MCFC, the stable interface is achieved in the electrodes by carefully tailoring the pore structures of the electrodes and the electrolyte matrix ( $\text{LiAlO}_2$ ) so that the capillary forces establish a dynamic equilibrium in the different porous structures. Pigeaud et al. (4) provide a discussion of porous electrodes for MCFCs.

In a SOFC, there is no liquid electrolyte present that is susceptible to movement in the porous electrode structure, and electrode flooding is not a problem. Consequently, the three-phase interface that is necessary for efficient electrochemical reaction involves two solid phases (solid electrolyte/electrode) and a gas phase. A critical requirement of porous electrodes for SOFC is that they are sufficiently thin and porous to provide an extensive electrode/electrolyte interfacial region for electrochemical reaction.

## 1.2 Cell Stacking

Additional components of a cell are best described by using a typical cell schematic, Figure 1-4. This figure depicts a PAFC. As with batteries, individual fuel cells must be combined to produce appreciable voltage levels and so are joined by interconnects. Because of the configuration of a flat plate cell, Figure 1-4, the interconnect becomes a separator plate with two functions: 1) to provide an electrical series connection between adjacent cells, specifically for flat plate cells, and 2) to provide a gas barrier that separates the fuel and oxidant of adjacent cells. The interconnect of a tubular solid oxide fuel cell is a special case, and the reader is referred to Section 8 for its slightly altered function. All interconnects must be an electrical conductor and impermeable to gases. Other important parts of the cell are 1) the structure for distributing the reactant gases across the electrode surface and which serves as mechanical support, shown as ribs in Figure 1-4, 2) electrolyte reservoirs for liquid electrolyte cells to replenish electrolyte lost over life, and 3) current collectors (not shown) that provide a path for the current between the electrodes and the separator of flat plate cells. Other arrangements of gas flow and current flow are used in fuel cell stack designs, and are mentioned in Sections 3 through 8 for the various type cells.

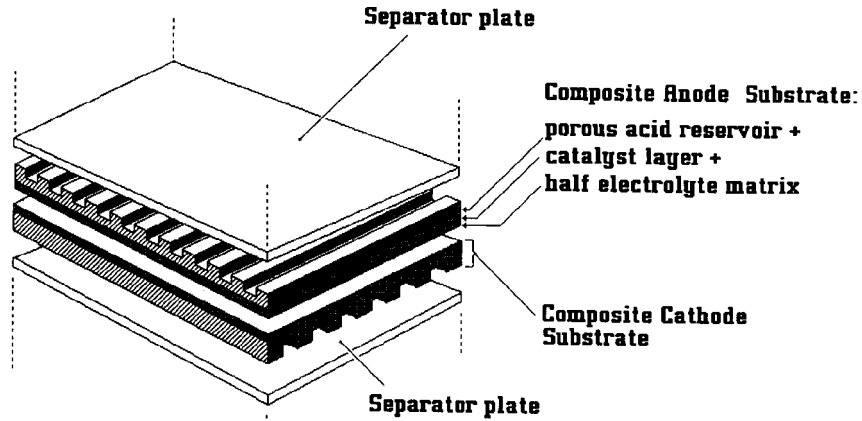


**Figure 1-4 Expanded View of a Basic Fuel Cell Repeated Unit in a Fuel Cell Stack (1)**

### **1.3 Fuel Cell Plant Description**

As shown in Figure 1-1, the fuel cell combines hydrogen produced from the fuel and oxygen from the air to produce dc power, water, and heat. In cases where CO and CH<sub>4</sub> are reacted in the cell to produce hydrogen, CO<sub>2</sub> is also a product. These reactions must be carried out at a suitable temperature and pressure for fuel cell operation. A system must be built around the fuel cells to supply air and clean fuel, convert the power to a more usable form such as grid quality ac power, and remove the depleted reactants and heat that are produced by the reactions in the cells.

Figure 1-5 shows a simple rendition of a fuel cell power plant. Beginning with fuel processing, a conventional fuel (natural gas, other gaseous hydrocarbons, methanol, naphtha, or coal) is cleaned, then converted into a gas containing hydrogen. Energy conversion occurs when dc electricity is generated by means of individual fuel cells combined in stacks or bundles. A varying number of cells or stacks can be matched to a particular power application. Finally, power conditioning converts the electric power from dc into regulated dc or ac for consumer use. Section 9.1 describes the processes of a fuel cell power plant system.

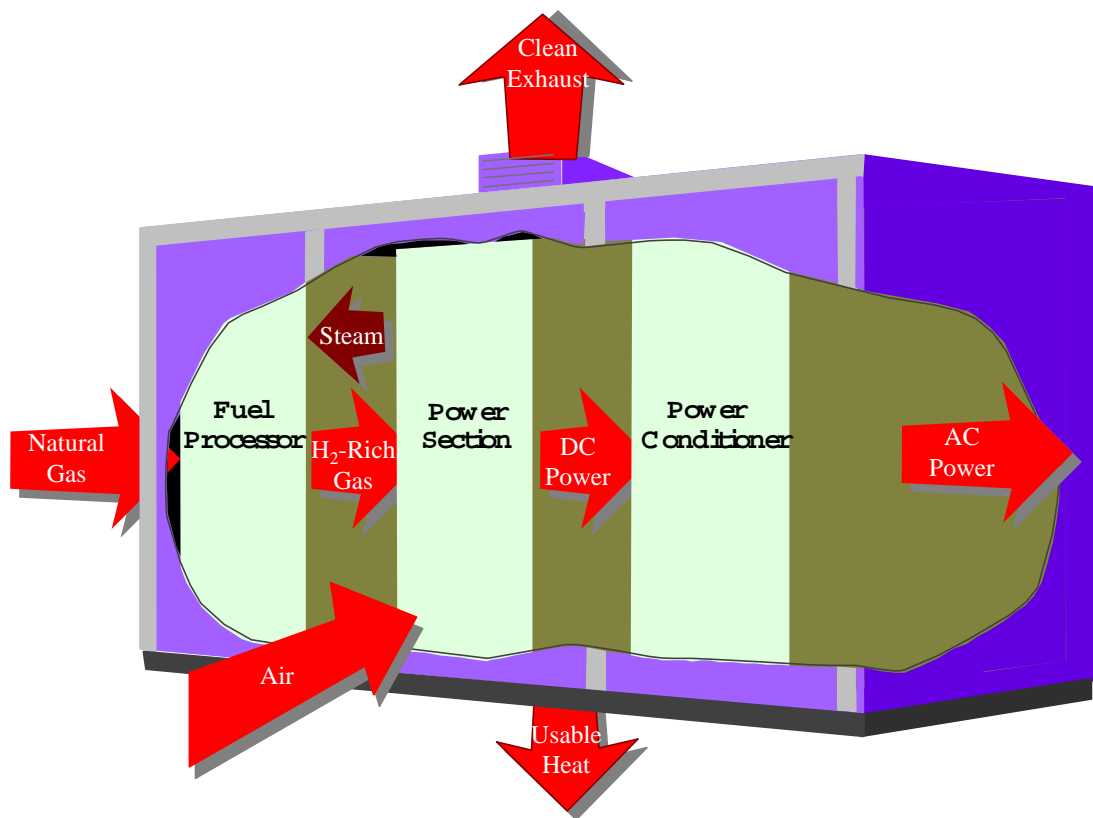


**Figure 1-5 Fuel Cell Power Plant Major Processes**

## 1.4 Characteristics

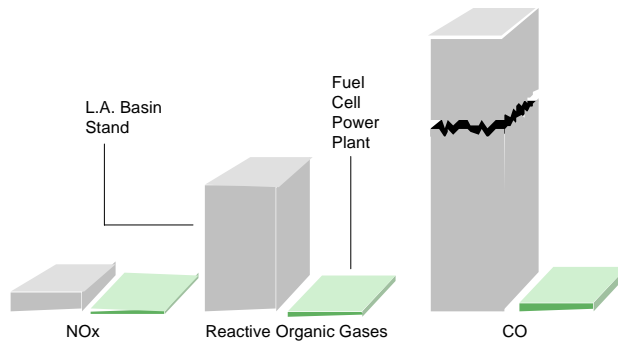
Fuel cells have many characteristics that make them favorable as energy conversion devices. Two that have been instrumental in driving the interest for terrestrial application of the technology are the combination of relatively high efficiency and very low environmental intrusion (virtually no acid gas or solid emissions). Efficiencies of present fuel cell plants are in the range of 40 to 55% based on the lower heating value (LHV) of the fuel. Hybrid fuel cell/reheat gas turbine cycles that offer efficiencies greater than 70% LHV, using demonstrated cell performance, have been proposed.

Figure 1-6 illustrates demonstrated low emissions of installed PAFC units compared to the Los Angeles Basin (South Coast Air Quality Management District) requirements, the strictest requirements in the US. Measured emissions from the PAFC unit are < 1 ppm of NO<sub>x</sub>, 4 ppm of CO, and <1 ppm of reactive organic gases (non-methane) (5). In addition, fuel cells operate at a constant temperature, and the heat from the electrochemical reaction is available for cogeneration applications. Because fuel cells operate at nearly constant efficiency, independent of size, small fuel cell plants operate nearly as efficiently as large ones.<sup>1</sup> Thus, fuel cell power plants can be configured in a wide range of electrical output, ranging from watts to megawatts. Fuel cells are quiet and even though fuel flexible, they are sensitive to certain fuel contaminants that must be minimized in the fuel gas. Table 1-2 summarizes the impact of the major constituents within fuel gases on the various fuel cells. The reader is referred to Sections 3 through 8 for detail on trace contaminants. The two major

1. The fuel processor efficiency is size dependent; therefore, small fuel cell power plants using externally reformed hydrocarbon fuels would have a lower overall system efficiency.



impediments to the widespread use of fuel cells are 1) high initial cost and 2) high-temperature cell endurance operation. These two aspects are the major focus of manufacturers' technological efforts.



**Figure 1-6 Relative Emissions of PAFC Fuel Cell Power Plants Compared to Stringent Los Angeles Basin Requirements**

Other characteristics that fuel cells and fuel cell plants offer are

- Direct energy conversion (no combustion).
- No moving parts in the energy converter.
- Quiet.
- Demonstrated high availability of lower temperature units.
- Siting ability.
- Fuel flexibility.
- Demonstrated endurance/reliability of lower temperature units.
- Good performance at off-design load operation.
- Modular installations to match load and increase reliability.
- Remote/unattended operation.
- Size flexibility.
- Rapid load following capability.

General negative features of fuel cells include

- Market entry cost high; N<sup>th</sup> cost goals not demonstrated.
- Unfamiliar technology to the power industry.
- No infrastructure.

**Table 1-2 Summary of Major Fuel Constituents Impact on PEFC, AFC, PAFC, MCFC, ITSOFC, and SOFC**

<b>Gas Species</b>	<b>PEFC</b>	<b>AFC</b>	<b>PAFC</b>	<b>MCFC</b>	<b>ITSOFC</b>	<b>TSOFC</b>
H <sub>2</sub>	Fuel	Fuel	Fuel	Fuel	Fuel	Fuel
CO	Poison (50 ppm per stack)	Poison	Poison (<0.5%)	Fuel <sup>a</sup>	Fuel	Fuel
CH <sub>4</sub>	Diluent	Poison	Diluent	Diluent <sup>b</sup>	Fuel <sup>a</sup>	Fuel <sup>a</sup>
CO <sub>2</sub> & H <sub>2</sub> O	Diluent	Poison	Diluent	Diluent	Diluent	Diluent
S as (H <sub>2</sub> S & COS)	No Studies to date (11)	Poison	Poison (<50 ppm)	Poison (<0.5 ppm)	Poison	Poison (<1.0 ppm)

<sup>a</sup> In reality, CO, with H<sub>2</sub>O, shifts to H<sub>2</sub> and CO<sub>2</sub>, and CH<sub>4</sub>, with H<sub>2</sub>O, reforms to H<sub>2</sub> and CO faster than reacting as a fuel at the electrode.

<sup>b</sup> A fuel in the internal reforming MCFC.

## 1.5 Advantages/Disadvantages

The fuel cell types addressed in this handbook have significantly different operating regimes. As a result, their materials of construction, fabrication techniques, and system requirements differ. These distinctions result in individual advantages and disadvantages that govern the potential of the various cells to be used for different applications.

**PEFC:** The PEFC, like the SOFC, has a solid electrolyte. As a result, this cell exhibits excellent resistance to gas crossover. In contrast to the SOFC, the cell operates at a low 80°C. This results in a capability to bring the cell to its operating temperature quickly, but the rejected heat cannot be used for cogeneration or additional power. Test results have shown that the cell can operate at very high current densities compared to the other cells. However, heat and water management issues may limit the operating power density of a practical system. The PEFC tolerance for CO is in the low ppm level.

**AFC:** The AFC was one of the first modern fuel cells to be developed, beginning in 1960. The application at that time was to provide on-board electric power for the Apollo space vehicle. Desirable attributes of the AFC include its excellent performance on hydrogen (H<sub>2</sub>) and oxygen (O<sub>2</sub>) compared to other candidate fuel cells due to its active O<sub>2</sub> electrode kinetics and its flexibility to use a wide range of electrocatalysts, an attribute that provides development flexibility. Once development was in progress for space application, terrestrial applications began to be investigated. Developers recognized that pure hydrogen would be required in the fuel stream, because CO<sub>2</sub> in any reformed fuel reacts with the KOH electrolyte to form a carbonate, reducing the electrolyte's ion mobility. Pure H<sub>2</sub> could be supplied to the anode by passing a reformed, H<sub>2</sub>-rich fuel stream by a precious metal (palladium/silver) membrane. The H<sub>2</sub> molecule is able to pass through the membrane by absorption and mass transfer, and into the fuel cell anode. However, a significant pressure differential is required across the membrane and the membrane is prohibitive in cost. Even the small amount of CO<sub>2</sub> in ambient air, the source of O<sub>2</sub> for the

reaction, would have to be scrubbed. At the time, U.S. investigations determined that scrubbing of the small amount of CO<sub>2</sub> within the air, coupled with purification of the hydrogen, was not cost effective and that terrestrial application of the AFC could be limited to special applications, such as closed environments, at best. Major R&D on AFC is no longer done in the U.S. but recent development in Europe has created renewed interest in this fuel cell type.

**PAFC:** The CO<sub>2</sub> in the reformed fuel gas stream and the air does not react with the electrolyte in a phosphoric acid electrolyte cell, but is a diluent. This attribute and the relatively low temperature of the PAFC made it a prime, early candidate for terrestrial application. Although its cell performance is somewhat lower than the alkaline cell because of the cathode's slow oxygen reaction rate, and although the cell still requires hydrocarbon fuels to be reformed into an H<sub>2</sub>-rich gas, the PAFC system efficiency improved because of its higher temperature environment and less complex fuel conversion (no membrane and attendant pressure drop). The need for scrubbing CO<sub>2</sub> from the process air is also eliminated. The rejected heat from the cell is high enough in temperature to heat water or air in a system operating at atmospheric pressure. Some steam is available in PAFCs, a key point in expanding cogeneration applications.

PAFC systems achieve about 37 to 42% electrical efficiency (based on the LHV of natural gas). This is at the low end of the efficiency goal for fuel cell power plants. PAFCs use high cost precious metal catalysts such as platinum. The fuel has to be reformed external to the cell, and CO has to be shifted by a water gas reaction to below 3 to 5 vol% at the inlet to the fuel cell anode or it will affect the catalyst. These limitations have prompted development of the alternate, higher temperature cells, MCFC, and SOFC.

**MCFC:** Many of the disadvantages of the lower temperature as well as higher temperature cells can be alleviated with the higher operating temperature MCFC (approximately 650°C). This temperature level results in several benefits: the cell can be made of commonly available sheet metals that can be stamped for less costly fabrication, the cell reactions occur with nickel catalysts rather than with expensive precious metal catalysts, reforming can take place within the cell provided a reforming catalyst is added (results in a large efficiency gain), CO is a directly usable fuel, and the rejected heat is of sufficiently high temperature to drive a gas turbine and/or produce a high pressure steam for use in a steam turbine or for cogeneration. Another advantage of the MCFC is that it operates efficiently with CO<sub>2</sub>-containing fuels such as bio-fuel derived gases. This benefit is derived from the cathode performance enhancement resulting from CO<sub>2</sub> enrichment.

The MCFC has some disadvantages, however: the electrolyte is very corrosive and mobile, and a source of CO<sub>2</sub> is required at the cathode (usually recycled from anode exhaust) to form the carbonate ion. Sulfur tolerance is controlled by the reforming catalyst and is low, which is the same for the reforming catalyst in all cells. Operation requires use of stainless steel as the cell hardware material. The higher temperatures promote material problems, particularly mechanical stability that impacts life.

**ITSOFC:** The intermediate temperature solid oxide fuel cell combines the best available attributes of fuel cell technology development with intermediate temperature (600-800°C) operation. Ceramic components are used for electrodes and electrolytes: carbon does not

deposit on these ceramic materials; therefore, this fuel cell may accept hydrocarbons and carbon monoxide in the fuel. Internal reforming is practical at temperatures above 650°C. Moreover, use of solid state components avoids design issues, such as corrosion and handling, inherent in liquid electrolyte fuel cells. The reduced temperature from the TSOFC allows stainless steel construction, which represents reduced manufacturing costs over more exotic metals. The disadvantages of ITSOFCs are that electrolyte conductivity and electrode kinetics drop significantly with lowered temperature. Present technology development is addressing these issues through thin-film electrolyte development and also a search for alternate materials.

**TSOFC:** The TSOFC is the fuel cell with the longest continuous development period, starting in the late 1950s, several years before the AFC. The solid ceramic construction of the cell alleviates cell hardware corrosion problems characterized by the liquid electrolyte cells and has the advantage of being impervious to gas cross-over from one electrode to the other. The absence of liquid also eliminates the problem of electrolyte movement or flooding in the electrodes. The kinetics of the cell are fast, and CO is a directly useable fuel as it is in the MCFC and ITSOFC. There is no requirement for CO<sub>2</sub> at the cathode as with the MCFC. At the temperature of presently operating TSOFCs (~1000°C), fuel can be reformed within the cell. The temperature of a TSOFC is significantly higher than that of the MCFC and ITSOFC. However, some of the rejected heat from a TSOFC is needed to preheat the incoming process air.

The high temperature of the TSOFC has its drawbacks. There are thermal expansion mismatches among materials, and sealing between cells is difficult in the flat plate configurations. The high operating temperature places severe constraints on materials selection and results in difficult fabrication processes. The TSOFC also exhibits a high electrical resistivity in the electrolyte, which results in a lower cell performance than the MCFC by approximately 100 mV.

Developers are assessing the advantages of each type of fuel cell to identify early applications and address research and development issues (see Sections 3 through 8).

## **1.6 Applications, Demonstrations, and Status**

The characteristics, advantages, and disadvantages summarized in the previous section form the basis for selection of the candidate fuel cell types to respond to a variety of application needs. The major applications for fuel cells are as stationary electric power plants, including cogeneration units; as motive power for vehicles; and as on-board electric power for space vehicles or other closed environments. Derivative applications will be summarized.

### **1.6.1 Stationary Electric Power**

One of the characteristics of fuel cell systems is that their efficiency is nearly unaffected by size. This means that small, relatively high efficient power plants can be developed, thus avoiding the higher cost exposure associated with large plant development. As a result, initial stationary plant development has been focused on several hundred kW to low MW capacity plants. Smaller plants (several hundred kW to 1 to 2 MW) can be sited at the user's facility and are suited for cogeneration operation, that is, the plants produce electricity and thermal energy. Larger, dispersed plants (1 to 10 MW) are likely to be used for distributed generation. The plants are fueled primarily with natural gas. Once these plants are commercialized and price improvements materialize, fuel cells will be considered for large base-load plants because of their high efficiency.

The base-load plants could be fueled by natural gas or coal. The fuel product from a coal gasifier, once cleaned, is compatible for use with fuel cells. Systems integration studies show that high temperature fuel cells closely match coal gasifier operation.

Operation of complete, self-contained, stationary plants has been demonstrated using PEFC, AFC, PAFC, MCFC, ITSOFC, and TSOFC technology. Demonstrations of these technologies that occurred before 1998 were addressed in previous editions of the Fuel Cell Handbook and in the literature of the period. Recent U.S. manufacturer experience with these various fuel cell technologies has produced timely information. A case in point is the 200 kW PAFC on-site plant, the PC-25, that is the first to enter the commercial market (see Figure 1-7). The plant was



**Figure 1-7 PC-25 Fuel Cell**

developed by International Fuel Cells Corporation (IFC), a division of United Technologies Corporation (UTC). The plants are built by IFC. The Toshiba Corporation of Japan and Ansaldo SpA of Italy are partners with UTC in IFC. The on-site plant is proving to be an economic and beneficial addition to the operating systems of commercial buildings and industrial facilities because it is superior to conventional technologies in reliability, efficiency, environmental impact, and ease of siting. Because the PC-25 is the first available commercial unit, it serves as a model for fuel cell application. Because of its attributes, the PC-25 is being installed in various applications, such as hospitals, hotels, large office buildings, manufacturing sites, wastewater treatment plants, and institutions, to meet the following requirements:

- On-site energy
- Continuous power – backup
- Uninterrupted power supply
- Premium power quality

- Independent power source

Characteristics of the plant are as follows:

- Power Capacity 0 to 200 kW with natural gas fuel (-30 to 45°C, up to 1500 m)
- Voltage and Phasing 480/277 volts at 60 Hz ; 400/230 volts at 50 Hz
- Thermal Energy 740,000 kJ/hour at 60°C (700,000 Btu/hour heat at 140°F);  
(Cogeneration) module provides 369,000 kJ/hour at 120°C (350,000 Btu/hour at 250°F) and 369,000 kJ/hour at 60°C
- Electric Connection Grid-connected for on-line service and grid-independent for on-site premium service
- Power Factor Adjustable between 0.85 to 1.0
- Transient Overload None
- Grid Voltage Unbalance 1%
- Grid Frequency Range +/-3%
- Voltage Harmonic Limits <3%
- Plant Dimensions 3 m (10 ft) wide by 3 m (10 ft) high by 5.5 m (18 ft) long, not including a small fan cooling module (5)
- Plant Weight 17,230 kg (38,000 lb)

Results from the operating units as of August, 2000 are as follows: total fleet operation stands at more than 3.5 million hours. The plants achieve 40% LHV electric efficiency, and overall use of the fuel energy approaches 80% for cogeneration applications (8). Operations confirm that rejected heat from the initial PAFC plants can be used for heating water, space heating, and low pressure steam. One plant has completed over 50,000 hours of operation, and a number of plants have operated over 40,000 hours (6). Fourteen additional plants have operated over 35,000 hours. The longest continuous run stands at 9,500 hours for a unit purchased by Tokyo Gas for use in a Japanese office building (9). This plant ended its duration record because it had to be shut down because of mandated maintenance. It is estimated at this time that cell stacks can achieve a life of 5 to 7 years. The fleet has attained an average of over 95% availability. The latest model, the PC-25C, is expected to achieve over 96%. The plants have operated on natural gas, propane, butane, landfill gas (10,11), hydrogen (12), and gas from anaerobic digestors (13). Emissions are so low (see Figure 1-6) that the plant is exempt from air permitting in the South Coast and Bay Area (California) Air Quality Management Districts, which have the most stringent limits in the U.S. The sound pressure level is 62 dBA at 9 meters (30 feet) from the unit. The PC-25 has been subjected to ambient conditions varying from -32°C to +49°C and altitudes from sea level to 1600 meters (~1 mile). Impressive ramp rates result from the solid state electronics. The PC-25 can be ramped at 10 kW/sec up or down in the grid connected mode. The ramp rate for the grid independent mode is idle to full power in ~one cycle or essentially one-step instantaneous from idle to 200 kW. Following the initial ramp to full power, the unit can adjust at an 80 kW/sec ramp up or down in one cycle.

IFC recently (spring, 2000) delivered a 1 megawatt PAFC power plant to a utility in Anchorage, Alaska. The unit consists of 5-200 kilowatt PC-25 units integrated with a supervisory dispatching controller. The system was installed and is being operated by Chugach Electric. Operation began in June, 2000.

Recent customers have obtained a Federal Grant rebate of \$1,000/kW as the result of the Climate Change Fuel Cell Program. The PC-25 program also has received the support of the U.S. military, which installed 30 units at government facilities.

The fuel cell stacks are made and assembled into units at an 80,000 ft<sup>2</sup> facility located in South Windsor, Connecticut, U.S. Low cost/high volume production depends on directly insertable sub-assemblies as complete units and highly automatic processes such as robotic component handling and assembly. The stack assembly is grouped in a modified spoke arrangement to allow for individual manufacturing requirements of each of the cell components while bringing them in a continuous flow to a central stacking elevator (14).

Ballard Generation Systems, a subsidiary of Ballard Power Systems, has produced a PEFC stationary on-site plant. It has these characteristics:

- Power Capacity 250 kW with natural gas fuel
- Electric Efficiency 40% LHV
- Thermal Energy 854,600 kJ/hour at 74°C (810,000 Btu/hour at 165°F)
- Plant Dimensions 2.4 m (8 ft) wide by 2.4 m (8 ft) high by 5.7 m (18.5 ft) long
- Plant Weight 12,100 kg (26,700 lb)

One plant demonstration, which began operation in August 1997, has been completed. The plant achieved an electric efficiency of 40% LHV. Ballard is in the process of securing plant orders to field test additional plants. Ballard expects field trials from 1998 to 2001 and commercial production of the plant with the characteristics listed above in 2002. Partners are GPU International, GEC Alstom, and EBARA Corporation (15).

Fuel Cell Energy (FCE), formerly Energy Research Corporation (ERC) completed successful testing in June 2000 of a near-commercial molten carbonate fuel cell system at their corporate site in Danbury, Connecticut. The power plant was rated at 250 kilowatts and achieved a maximum of 263 kilowatts. Power was produced by a single stack having 340 cells. The fuel delivered to the stack was internally reformed. Over the 16 month run, the system operated for more than 11,800 hours, providing 1.8 million kilowatt-hours to FCE's facility and the grid. Electric efficiency was 45% (LHV). For most of this time, it operated unattended. Acid gas emissions during the test were negligible. Post-operation analysis will be performed on the fuel cell module after disassembly.

FCE's German partner, MTU Friedrichshafen, is operating a 250 kilowatt molten carbonate fuel cell system in Bielefeld, Germany. The power plant is located on the campus of the University of Bielefeld and provides electric power and byproduct heat. The fuel cells were manufactured by FCE. MTU developed a new power plant configuration for this unit termed a "Hot Module" that simplifies the balance of plant. The system began operation in November 1999 and logged over 4,200 hours by August, 2000. Electric efficiency is 45% (LHV).

The focus of the utility demonstrations and FCE's fuel cell development program is the commercialization of 300 kilowatt, 1.5 megawatt, and 3 megawatt MCFC plants. Characteristics of the FCE 3 megawatt internal reforming commercial MCFC plant are as follows (17):

- Power Capacity                    3.0 MW net AC
- Electric efficiency                57% (LHV) on natural gas
- Voltage and Phasing              Voltage is site dependent, 3 phase 60 Hz
- Thermal energy                    ~4.2 million kJ/hour (~4 million Btu/hour)
- Availability                        95%

Field trials employing FCE's commercial MCFC design are being planned at a number of sites. Some are discussed below.

FCE plans to demonstrate a molten carbonate fuel cell/turbine hybrid system in late 2000. The balance of plant equipment employed in the 250 kilowatt test at ERC's facility will be modified to accommodate a fuel cell and a gas turbine. The turbine is to be powered by waste heat from the fuel cell. The goal of the test is to demonstrate that the hybrid system will realize high efficiencies. This activity is a part of the U.S. DOE Office of Fossil Energy Vision 21 Program.

A demonstration of a MCFC power plant at an automobile manufacturing plant site in Tuscaloosa, Alabama is planned for the first quarter of 2001. The 250 kilowatt system will feed the production facility power distribution grid. Four companies are teaming up to support the program: Southern Company, Alabama Municipal Electric Authority (AMEA), Fuel Cell Energy, and Mercedes Benz U.S. International, Inc. (MBUSI). The system will employ FCE's stack and MTU's power plant design, called the "Hot Module."

FCE plans to build a 1 megawatt power plant for a King County site near Renton, Washington. The molten carbonate fuel cell system will be installed as part of a municipal waste water treatment system. The power plant will use fuel produced by a digester in the form of a methane rich gas. The fuel cell system will provide power to the water treatment facility and provide a means to control methane and carbon dioxide emissions. Delivery is expected in 2001. The U.S. Environmental Protection Agency and the King County Washington Department of Natural Resources are supporting this program.

FCE and the Los Angeles Department of Water and Power (LADWP) plan to install a MCFC power plant at their downtown Los Angeles headquarters building. The 250 kilowatt system is expected to be operational in 2001 (16, 17).

Siemens Westinghouse Power Corporation (SWPC) has three TSOFC systems employing tubular cell technology operating on user sites. All were produced in their Pittsburgh, Pennsylvania facility. The capacities of the systems are 220 kilowatts, 100 kilowatts, and 25 kilowatts.

The most recent system is a 220 kilowatt fuel cell/gas turbine power plant operating at the University of California's National Fuel Cell Research Center located in Irvine, California. The first-of-a-kind hybrid power plant consists of a 200 kilowatt fuel cell generator pressurized at about 3.5 atmospheres in combination with a 20 kilowatt two-shaft gas turbine. The system was first run at the Pittsburgh facility and started operating at Irvine in June, 2000. Total run time until July, 2000 was 264 hours. Electric energy delivered was 42 megawatt-hours. Electric efficiency was 51% (LHV). An electric power feed-through mounted on the pressure vessel devel-



oped a problem. Although the fuel cells were intact, it was necessary that the fuel cell generator be shipped back to Pittsburgh for repair. Operation is expected to resume by October, 2000.

The 25 kilowatt system is back on test at the National Fuel Cell Research Center. The unit typically operates at 21.7 kW DC and 173 amperes. The unit has operated at two facilities on various fuels for a combined time of more than 9,500 hours. Support for this test is provided by Wright Patterson Air Force Base.

The nominal 100 kW 50 Hz unit is presently operating at the NUON District Heating site in Westvoort, The Netherlands. The unit is sponsored by EDB/ELSAM, a consortium of Dutch and Danish Energy distribution companies. Site acceptance was completed by February 6, 1998. Since then, this system has operated unattended, delivering 105 kW ac to the grid for over 14,000 hours. The electric only efficiency is 45%, plus the plant supplies 85 kW of hot water at 110°C to the local district heating system. The plant, which consists of three major systems, measures 8.42 m long by 2.75 m wide by 3.58 m high. The unit is scheduled to operate until autumn 2000

The Siemens Westinghouse TSOFC commercialization plan is focused on an initial offering of a hybrid fuel cell/gas turbine plant. The fuel cell module replaces the combustion chamber of the gas turbine engine. Figure 1-8 shows the benefit behind this combined plant approach. Additional details are provided in Section 8. As a result of the hybrid approach, the 1 MW early commercial unit is expected to attain ~60% efficiency LHV when operating on natural gas.

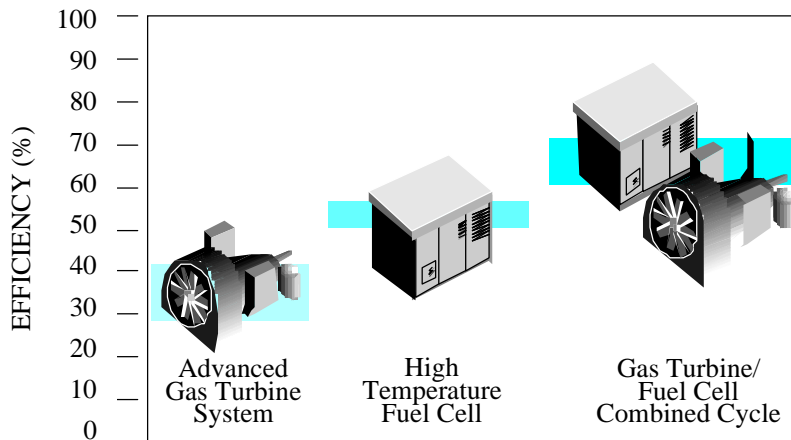


**Figure 1-8 Combining the TSOFC with a Gas Turbine Engine to Improve Efficiency**

Siemens Westinghouse is planning a number of tests on power plants that are prototypes of future products. All systems employ the tubular SOFC concept and most are combined with gas turbines in a hybrid configuration. Capacities of these systems are 250 kilowatts atmospheric, 300 kilowatt class hybrid, and 1 megawatt class hybrid. They are to operate at various sites in the U.S., Canada, and Europe. Some of them are discussed below.

A 250 kilowatt atmospheric system is planned for a Toronto, Ontario, Canada site. The system will be operated by Ontario Power Technologies (formerly Ontario Hydro). The unit will supply 145 kilowatts of heat to the site heating system. Electric efficiency is expected to be about 47% (LHV). Operation of the combined heat and power system is expected in late 2001.

Operation of a 300 kilowatt class hybrid system is planned for Essen, Germany. The utility RWE will operate the system. Efficiency of the system will be about 57% (LHV). Operation is expected in late 2001 to early 2002.

A 300 kilowatt class hybrid system is planned to operate near Milan, Italy. The power plant will be operated by Edison SpA. Efficiency will be about 57% (LHV). Operation is expected to begin in mid 2002.

Plans are underway for a field test of a megawatt class fuel cell/gas turbine hybrid system on an Environmental Protection Agency site at Ft. Mead, Maryland. This system is expected to exhibit an efficiency of about 60 % (LHV) depending on the turbine and the inverter selected. Operation is expected in the second half of 2002.

A 250 kilowatt system is planned for a site in Norway. The system will be operated by Norske Shell to demonstrate that CO<sub>2</sub> can be economically recovered. The CO<sub>2</sub> recovery technology is being developed by Shell Hydrogen. The CO<sub>2</sub> could be sequestered in underground reservoirs or could be used for special applications such as fish farms or agricultural greenhouses. The test system will be sited at a fish hatchery. The system is expected to begin operation in early 2003.

A megawatt class hybrid system is planned for a site in Stuttgart, Germany. The system will be operated by ENBW. Efficiency of the system will be about 60 %. Partial support for the operation will be provided by the European Union. Operation is expected in the second half of 2003.

The military finds certain characteristics of fuel cell power plants desirable for field duty. Foremost, a fuel cell unit is quiet so can be close to the front line. It has a low heat trace, and can be scaled to various sizes, from a few kW backpack to larger mobile power plant. The main drawback for the military is that the existing infrastructure is limited to logistic fuels. Logistic fuels (defined as easily transportable and stored, and compatible with military uses) are difficult to convert to hydrogen for fuel cell use. The burden of changing the fuel infrastructure to accommodate lighter fuels, normally used in fuel cells, is far greater than the benefits fuel cells offer the military. The Advanced Research Projects Agency of DOD funded several projects to investigate adapting logistics fuels to fuel cell use.

IFC conducted testing of a 100 kW mobile electric power plant (MEP) with the logistic fuels of JP-8 and DF-2. An auto-thermal reformer that achieved 98% conversion was used to convert the logistic fuel to a methane rich fuel.

FCE tested a lab-scale carbonate fuel cell stack on a model diesel-like fuel (Exxsol) using an adiabatic pre-reformer to convert the liquid fuel to methane in 1991 to 1993. In 1995 and 1996, FCE verified a 32 kW MCFC stack operation on jet fuel (JP-8) and diesel (DF-2) in system inte-

grated tests using the diesel-to-methane adiabatic pre-reformer approach. Test results showed that there was a 5% power derating compared to natural gas operation.

The 25 kW TSOFC power unit (see Siemens Westinghouse, above) was fitted with a pre-reformer similar to the FCE and operated with JP-8 (766 hours) and DF-2 (1555 hours) while the unit was installed at FCE's Highgrove Station.

SOFCo, a limited partnership of Babcock and Wilcox (a McDermott International Company) and Ceramatec (an Elkem company), has tested a planar SOFC unit for the MEP program that will operate on logistic fuels. Honeywell tested their MEP unit on logistic fuel.

All demonstrations showed that fuel cell units can be operated with military logistic fuels (18).

An eventual market for fuel cells is the large (100 to 300 MW), base-loaded, stationary plants operating on coal or natural gas. Another related, early opportunity may be in repowering older, existing plants with high-temperature fuel cells (19). MCFCs and SOFCs coupled with coal gasifiers have the best attributes to compete for the large, base load market. The rejected heat from the fuel cell system can be used to produce steam for the existing plant's turbines. Studies showing the potential of high-temperature fuel cells for plants of this size have been performed (see Section 9). These plants are expected to attain from 50 to 60% efficiency based on the HHV of the fuel. Coal gasifiers produce a fuel gas product requiring cleaning to the stringent requirements of the fuel cells' electrochemical environment, a costly process. The trend of environmental regulations has also been towards more stringent cleanup. If this trend continues, coal-fired technologies will be subject to increased cleanup costs that may worsen process economics. This will improve the competitive position of plants based on the fuel cell approach. Fuel cell systems will emit less than target emissions limits. U.S. developers have begun investigating the viability of coal gas fuel to MCFCs and SOFCs (20,21,22). An FCE 20 kW MCFC stack was tested for a total of 4,000 hours, of which 3,900 hours was conducted at the Plaquemine, LA, site on coal gas as well as pipeline gas. The test included 1,500 hours of operation using 9,142 kJ/m<sup>3</sup> syngas from a slip stream of a 2,180 tonne/day Destec entrained gasifier. The fuel processing system incorporated cold gas cleanup for bulk removal of H<sub>2</sub>S and other contaminants, allowing the 21 kW MCFC stack to demonstrate that the FCE technology can operate on either natural gas or coal gas.

User groups have organized together with the manufacturers in stationary plant development programs. The groups are listed below:

- PAFC, IFC   The North American Fuel Cell Owners Group
- MCFC, FCE   The Fuel Cell Commercialization Group
- SOFC, Siemens Westinghouse                        SOFC Commercialization Association (SOCA)

These groups provide invaluable information from a user viewpoint about fuel cell technology for stationary power plant application. They can be contacted through the manufacturers.

A series of standards is being developed to facilitate the application of stationary fuel cell technology power plants. Standard development activities presently underway are

- Design and Manufacturing Standard                ANSI Z21.83/CGA 12.10
- Interconnect Standards for Interfacing        Revive/Revise ANSI/IEEE Std 1001-1988
- Performance Test                                       ASME PTC50, Fuel Cell Performance Code Committee
- Emergency Generator Standards                  NFPA 70,110
- Installation Standard                                Review NFPA TC 850

**MILITARY APPLICATIONS**

The utility applications for DOD refers to power plants that serve the load of a particular population and range in size from a few megawatts for distributed power generation to 100+ MW. Electricity purchased from local utilities is expensive. Master metering and large air-conditioning loads can cause the demand portion of the electric bill to be more than 50 % of the total bill. There is significant potential for improving the security of electrical power supplied by using onsite power generation. The increased concern of environmental issues has made producing clean power desirable and mandatory. In addition, most central heat plants on U.S. military installations are nearing the end of their useful life, there are opportunities to replace outdated existing equipment with modern technologies.

**1.6.2 Distributed Generation**

Distributed generation is small, modular power systems that are sited at or near their point of use. The typical system is less than 30 MW, used for generation or storage, and extremely clean. Examples of technologies used in distributed generation include proven gas turbines and reciprocating engines, biomass-based generators, concentrating solar power and photovoltaic systems, fuel cells, wind turbines, micro-turbines, and flywheel storage devices. See Table 1-3 for size and efficiencies of selected systems.

**Table 1-3 Attributes of Selected Distributed Generation Systems**

<b>Type</b>	<b>Size</b>	<b>Efficiency, %</b>
Reciprocating Engines	50 kW – 6 MW	33 – 37
Micro turbines	10 kW – 300 kW	20 – 30
Phosphoric Acid Fuel Cell (PAFC)	50 kW – 1 MW	40
Solid Oxide Fuel Cell (SOFC)	5 kW – 3 MW	45 – 65
Proton Exchange Membrane Fuel Cell (PEM)	<1 kW – 1 MW	34 – 36
Photovoltaics (PV)	1 kW – 1 MW	NA
Wind Turbines	150 kW – 500 kW	NA
Hybrid Renewable	<1 kW – 1 MW	40 – 50

The market for distributed generation is aimed at customers dependent on reliable energy, such as hospitals, manufacturing plants, grocery stores, restaurants, and banking facilities. There is currently over 15 GW of distributed power generation operating in the U.S. Over the next decade, the domestic market for distributed generation, in terms of installed capacity to meet the demand, is estimated to be 5-6 GW per year. The projected global market capacity increases are estimated to be 20 GW per year (23). Several factors have played a role in the rise in demand for distributed generation. Utility restructuring is one of the factors. Energy suppliers must now take on the financial risk of capacity additions. This leads to less capital intensive projects and shorter construction periods. Also, energy suppliers are increasing capacity factors on existing plants rather than installing new capacity, which places pressure on reserve margins. This increases the possibility of forced outages, thereby increasing the concern for reliable service. There is also a demand for capacity additions that offer high efficiency and use of renewables as the pressure for enhanced environmental performance increases (23).

There are many applications for distributed generation systems. They include:

- Peak shaving - Power costs fluctuate hour by hour depending upon demand and generation, therefore customers would select to use distributed generation during relatively high-cost on-peak periods.
- Combined heat and power (CHP) (Cogeneration) –The thermal energy created while converting fuel to electricity would be utilized for heat in addition to electricity in remote areas and electricity and heat for sites that have a 24 hour thermal/electric demand.
- Grid support – Strategic placement of distributed generation can provide system benefits and preclude the need for expensive upgrades and provide electricity in regions where small increments of new baseload capacity is needed.
- Standby power – Power during system outages is provided by a distributed generation system until service can be restored. This is used for customers that require reliable back-up power for health or safety reasons, companies with voltage sensitive equipment, or where outage costs are unacceptably high.
- Remote/Stand alone – The user is isolated from the grid either by choice or circumstance. The purpose is for remote applications and mobile units to supply electricity where needed.

**Benefits and Obstacles:**

Distributed generation systems have small footprints, are modular and mobile making them very flexible in use. The systems provide benefits at the customer level, the supplier level as well as the national level. Benefits to the customer include high power quality, improved reliability, and flexibility to react to electricity price spikes. Supplier benefits include avoiding investments in transmission and distribution (T&D) capacity upgrades by locating power where it is most needed and opening new markets in remote areas. At the national level, the market for distributed generation establishes a new industry, boosting the economy. The improved efficiencies also reduce greenhouse gas emissions.

However, there are also a number of barriers and obstacles to overcome before distributed generation can become a mainstream service. These barriers include technical, economic, institutional and regulatory issues. Many of the proposed technologies have not yet entered the market and will need to meet performance and pricing targets before entry. Questions have also risen on requirements for connection to the grid. Lack of standardized procedures creates delays and discourages customer-owned projects. Siting, permitting and environmental regulations can also delay and increase the costs of distributed generation projects.

In 1998, the Department of Energy created a Distributed Power Program to focus on market barriers and other issues, which are prohibiting the growth of distributed generation systems. Under the leadership of the National Renewable Energy Laboratory (NREL), a collaboration of national laboratories and industry partners have been creating new standards and identifying and removing regulatory barriers. The goals of the program include 1) Strategic research, 2) System Integration, and 3) Mitigation of regulatory and institutional barriers (24).

**Fuel Cells:**

Fuel cells, one of the emerging technologies in distributed generation, have been hindered by high initial costs. However, costs are expected to decline as manufacturing capacity and capability increase and designs and integration improve. The fuel cell systems offer many potential benefits as a distributed generation system. They are small and modular and capital costs are relatively insensitive to scale. This makes them ideal candidates for a diverse amount of applications where they can be matched to meet specific load requirements. The systems are unobtrusive with very low noise levels and have negligible air emissions. These qualities enable them to be placed close to the source of power demand. Fuel cells also offer higher efficiencies than conventional plants. The efficiencies can be enhanced by utilizing the quality waste heat derived from the fuel cell reactions for combined heat and power and combined-cycle applications.

Phosphoric acid fuel cells have successfully been commercialized. Second generation fuel cells, including solid oxide fuel cells and molten carbonate fuel cells, are expected to make market entry by 2002. Research is ongoing in areas such as fuel options and new ceramic materials. Different manufacturing techniques are also being sought to help reduce capital costs. Proton exchange membrane fuel cells are currently still in the development and testing phase.

**Projects:**

There are currently several projects in the distributed generation market underway with various fuel cell developers and utility companies. These projects are helping to drive costs down and bring the fuel cells closer to commercialization. Below is a summary of some of the projects, taken from reference (25).

IdaTech LLC (formerly Northwest Power Systems), of Bend, Oregon, an Idacorp subsidiary, delivered the first of 110 planned fuel cell systems to the Bonneville Power Administration (BPA), Portland, Oregon in June 2000. The BPA program is part of a fuel cell test and development phase intended to commercialize fuel cell systems for home and small commercial applications by 2003.

Avista Labs, an affiliate of Avista Corp., of Spokane, Washington, received a US patent in March 2000 that covers 162 claims for its modular, cartridge-based proton exchange membrane (PEM) fuel cell. The fuel cell cartridges can be removed and replaced while the power system continues to operate. Additional elements of the patented system include proprietary designs that simplify the humidifying and cooling systems, resulting in lower manufacturing costs and higher efficiency. Currently, Avista has 30 fuel cells installed around the U.S. The second-generation fuel cell is planned to begin field demonstration in 2001.

Bewag AG's Treptow heating plant, located in Berlin, Germany received a 250 kW PEM fuel cell unit in April 2000 from Ballard Generation Systems, a subsidiary of Ballard Power System, of Burnaby, BC, Canada.

Plug Power, Inc, of Latham, NY manufactured six alpha fuel cells to be field tested as part of the Clean Energy Initiative, the Long Island Power Authority (LIPA), Uniondale, NY. Hofstra University was the site of the first tests, which began in February 2000. By the 60-day mark, the fuel cells had generated approximately 1900 kWh and operated in parallel with LIPA's T&D system.

Energy USA, a subsidiary of NiSource Inc, of Merrillville, Ind formed a joint venture with Institute of Gas Technology called Mosiac Energy LLC. They designed fuel cells for the core of the home's energy-generating system to be used in a Chesterton, Indiana housing development. Space heating and other household needs will be provided by the byproduct heat production.

IFC Corp, of South Windsor, Connecticut, has the most commercially advanced fuel cell for electricity generation, the PC25, a 200-kW phosphoric acid fuel cell (PAFC). IFC has over 200 fuel cells delivered around the world.

Siemens Westinghouse, of Pittsburgh, PA has manufactured the largest tubular solid oxide fuel cell (TSOFC) system. The Dutch/Danish consortium EDB/Elsam operates the system, which supplies 110 kW of electricity to the grid and 64 kW to the city of Westervoort, Netherlands district heating system. The efficiency is about 46% with exhaust gas values for NO<sub>x</sub>, SO<sub>x</sub>, CO and VHC under 1 ppm each. Commercial units ranging in size from 250 to 1000 kW are expected in 2004. Siemens Westinghouse installed a 250 kW unit at the National Fuel Cell Center.

The Los Angeles Department of Water and Power (LADWP) is investing \$1.5 million to develop and install a 250 kW molten carbonate fuel cell (MCFC) powerplant. FCE, of Danbury, Connecticut will supply the fuel cell. The goals of the project include testing and demonstrating the feasibility of the technology to generate electricity for the LADWP system.

In early 2000, FCE's Direct Fuel Cell (DFC) went into a joint public/private development with NETL. This system uses internal conversion of the natural-gas fuel to hydrogen, as opposed to an external unit. This reduces costs and creates efficient use of excess heat. The DFC system has already passed 8600 hours and a one-year milestone at FCE's headquarters.

## **MILITARY APPLICATIONS**

The Navy is studying the concept of all electric ships. These new ships will not have a central engine room and long drive shafts. The ships will depend on redundancy of generator capacity for combat survival, rather than protection of a centralized engine room.

### **1.6.3 Vehicle Motive Power**

Since the late 1980s, there has been a strong push to develop fuel cells for use in light-duty and heavy-duty vehicle propulsion. A major drive for this development is the need for clean, efficient cars, trucks, and buses that can operate on conventional fuels (gasoline, diesel), as well as renewable and alternative fuels (hydrogen, methanol, ethanol, natural gas, and other hydrocarbons). With hydrogen as the on-board fuel, such vehicles would be zero emission vehicles. With on-board fuels other than hydrogen, the fuel cell systems would use an appropriate fuel processor to convert the fuel to hydrogen, yielding vehicle power trains with very low acid gas emissions and high efficiencies. Further, such vehicles offer the advantages of electric drive and low maintenance because of the few critical moving parts. This development is being sponsored by various governments in North America, Europe, and Japan, as well as by major automobile manufacturers worldwide. As of May 1998, several fuel cell-powered cars, vans, and buses operating on hydrogen and methanol have been demonstrated.

In the early 1970s, K. Kordesch modified a 1961 Austin A-40 two-door, four-passenger sedan to an air-hydrogen fuel cell/battery hybrid car (23). This vehicle used a 6-kW alkaline fuel cell in conjunction with lead acid batteries, and operated on hydrogen carried in compressed gas cylinders mounted on the roof. The car was operated on public roads for three years and about 21,000 km.

In 1994 and 1995, H-Power (Belleville, New Jersey) headed a team that built three PAFC/battery hybrid transit buses (24,25). These 9 meter (30 foot), 25 seat (with space for two wheel chairs) buses used a 50 kW fuel cell and a 100 kW, 180 amp-hour nickel cadmium battery.

Recently, the major activity in transportation fuel cell development has focused on the polymer electrolyte fuel cell (PEFC). In 1993, Ballard Power Systems (Burnaby, British Columbia, Canada) demonstrated a 10 m (32 foot) light-duty transit bus with a 120 kW fuel cell system, followed by a 200 kW, 12 meter (40 foot) heavy-duty transit bus in 1995 (26). These buses use no traction batteries. They operate on compressed hydrogen as the on-board fuel. In 1997, Ballard provided 205 kW (275 HP) PEFC units for a small fleet of hydrogen-fueled, full-size transit buses for demonstrations in Chicago, Illinois, and Vancouver, British Columbia. Working



in collaboration with Ballard, Daimler-Benz built a series of PEFC-powered vehicles, ranging from passenger cars to buses (27). The first such vehicles were hydrogen-fueled. A methanol-fueled PEFC A-class car unveiled by Daimler-Benz in 1997 has a 640 km (400 mile) range. Plans are to offer a commercial vehicle by 2004. A hydrogen-fueled (metal hydride for hydrogen storage), fuel cell/battery hybrid passenger car was built by Toyota in 1996, followed in 1997 by a methanol-fueled car built on the same (RAV4) platform (28).

Other major automobile manufacturers, including General Motors, Volkswagen, Volvo, Honda, Chrysler, Nissan, Toyota, and Ford, have also announced plans to build prototype polymer electrolyte fuel cell vehicles operating on hydrogen, methanol, or gasoline (29). IFC and Plug Power in the U.S., and Ballard Power Systems of Canada (15), are involved in separate programs to build 50 to 100 kW fuel cell systems for vehicle motive power. Other fuel cell manufacturers are involved in similar vehicle programs. Some are developing fuel cell-powered utility vehicles, golf carts, etc. (30,31).

## **MILITARY APPLICATIONS**

The U.S. Army plans to reduce battlefield fuel consumption 75% by the year 2020. This will make supplying combat units easier, while also making it easier to protect supply lines. The future Army must reduce its vehicle exhaust emissions during peacetime. The Army owns a large number of vehicles equipped with non-emission controlled diesel engines, and will still own a significant number of these engines in 2020. One example of military-sponsored research is the all-electric tank with an electromagnetic rail gun. The gun would use a powerful magnetic field to propel a small armor-piercing projectile to hypersonic speeds. Such a vehicle would be fast, quiet, and capable of firing flurries of rounds at multiple targets.

### **1.6.4 Space and Other Closed Environment Power**

The application of fuel cells in the space program (1 kW PEFC in the Gemini program and 1.5 kW AFC in the Apollo program) was demonstrated in the 1960s. More recently, three 12 kW AFC units have been used for at least 87 missions with 65,000 hours flight time in the Space Shuttle Orbiter. In these space applications, the fuel cells use pure reactant gases. IFC has produced a H<sub>2</sub>/O<sub>2</sub> 30 kW unit for the Navy's Lockheed Deep Quest vehicle. It operates at depths of 1500 meters (5000 feet). Ballard Power Systems has produced an 80 kW PEFC fuel cell unit for submarine use (methanol fueled) and for portable power systems.

### **1.6.5 Fuel Cell Auxiliary Power Systems**

In addition to high-profile fuel cell applications such as automotive propulsion and distributed power generation, the use of fuel cells as auxiliary power units (APUs) for vehicles has received considerable attention (see Figure 1-9). APU applications may be an attractive market because it offers a true mass-market opportunity that does not require the challenging performance and low cost required for propulsion systems for vehicles. In this section, a discussion of the technical performance requirements for such fuel cell APUs, as well as the current status of the technology and the implications for fuel cell system configuration and cost is given.

<i>Participants</i>	<i>Application</i>	<i>Size range</i>	<i>Fuel /Fuel Cell type</i>	<i>Nature of Activity</i>
BMW, International Fuel Cells <sup>2</sup>	passenger car, BMW 7-series	5kW net	Hydrogen, Atmospheric PEM	Demonstration
Ballard, Daimler-Chrysler <sup>3</sup>	Class 8 Freightliner heavy-duty Century Class S/T truck cab	1.4 kW net for 8000 BTU/h A/C unit	Hydrogen, PEM	Demonstration
BMW, Delphi, Global Thermoelectric <sup>4</sup>	passenger car	1-5kW net	Gasoline, SOFC	Technology development program

**Figure 1-9 Overview of Fuel Cell Activities Aimed at APU Applications**

Auxiliary power units are devices that can provide all or part of the non-propulsion power for vehicles. Such units are already in widespread use in a range of vehicle types and for a variety of applications, in which they provide a number of potential benefits (see Figure 1-10). Although each of these applications could provide attractive future markets for fuel cells, this section will focus on application to on-road vehicles (specifically trucks).

<i>Vehicles Types</i>	<i>Loads Served</i>	<i>Potential Benefits</i>
<ul style="list-style-type: none"> <li>• Heavy-duty &amp; utility trucks</li> <li>• Airplanes</li> <li>• Trains</li> <li>• Yachts &amp; Ships</li> <li>• Recreational vehicles</li> <li>• Automobiles &amp; light trucks (not commercial yet)</li> </ul>	<ul style="list-style-type: none"> <li>• Space conditioning</li> <li>• Refrigeration</li> <li>• Lighting and other cabin amenities</li> <li>• Communication and information equipment</li> <li>• Entertainment (TV, radio)</li> </ul>	<ul style="list-style-type: none"> <li>• Can operate when main engine unavailable</li> <li>• Reduce emissions and noise while parked</li> <li>• Extend life of main engine</li> <li>• Improve power generation efficiency when parked</li> </ul>

**Figure 1-10 Overview of APU Applications**

In 1997, the Office of Naval Research initiated an advanced development program to demonstrate a ship service fuel cell power generation module. The ship service generator supplies the electrical power requirements of the ship. This program will provide the basis for a new fuel cell-based design that will be an attractive option for the future Navy surface ships. This program will provide the Navy with a ship service that is more efficient and incorporates a distributive power system that will remain operating even if the engine is destroyed.

Fuel cells can serve as a generator, battery charger, battery replacements and heat supply. They can adapt to most environments, even locations in Arctic and Antarctic regions. One effort, being run in collaboration with the Army Research Office, has demonstrated a prototype fuel cell designed to replace in many applications a popular military standard battery. The target application is the Army's BA-5590 primary (i.e., use-once-and-dispose) lithium battery. The Army purchases approximately 350,000 of these batteries every year at a cost of approximately \$100 per battery, including almost \$30 per battery for disposal. Fuel cells, on the

other hand, are not thrown away after each use but can be reused hundreds of times. Mission weight savings of factors of 10 or more are projected. The prototype fuel cell, which has the same size and delivers the same power as a battery, has been tested in all orientations and under simulated adverse weather conditions, and was enthusiastically received by Army senior management.

### System Performance Requirements

A key reason for interest in fuel cell APU applications is that there may be a good fit between APU requirements and fuel cell system characteristics. Fuel cells could be efficient and quiet, and APUs do have the load following requirements and physical size and weight constraints associated with propulsion applications. However, in order to understand the system requirements for fuel cell APUs, it is critical to understand the required functionality (refer to Figure 1-10) as well as competing technologies. To provide the functionality of interest, and to be competitive with internal combustion engine (ICE) driven APUs, fuel cell APUs must meet various requirements; an overview is provided in Figure 1-11.

<i>Key Parameter</i>	<i>Typical Requirements</i>	<i>Expected fuel cell performance</i>
Power output	12 – 42 V DC is acceptable for most applications, 110 / 220 V AC may be desirable for powering power tools etc.	DC power output simplifies the power conditioning and control for fuel cells
System Capacity	1 – 5 kW for light duty vehicles and truck cabins  up to 15 kW for truck refrigeration	Fits expected range for PEFCs and probably also advanced SOFCs
System Efficiency	More than 15-25% based on LHV	Efficiency target should be achievable, even in smallest capacity range
Operating life and reliability	Greater than about 5,000 hours stack life, with regular service intervals less than once every 1,000 hours	Insufficient data available to assess whether this is a challenge or not

**Figure 1-11 Overview of typical system requirements**

Fuel cell APUs will likely have to operate on gasoline, and for trucks preferably on diesel fuel, in order to match the infrastructure available, and preferably to be able to share on-board storage tanks with the main engine. The small amount of fuel involved in fueling APUs would likely not justify the establishment of a specialized infrastructure (e.g. a hydrogen infrastructure) for APUs alone. Similarly, fuel cell APUs should be water self-sufficient, as the need to carry water for the APU would be a major inconvenience to the operator, and would require additional space and associated equipment.

In addition to the requirement for stationary operation mentioned in Figure 3, fuel cell APUs must be able to provide power rapidly after start-up, and must be able to follow loads. While the

use of batteries to accomplish this is almost a given, a system start-up time of about ten minutes or less will likely be required to arrive at a reasonable overall package.

Finally, fuel cell APUs are and clean. These attributes may well be the key competitive advantage that fuel cell APUs have over conventional APUs, and hence their performance must more than match that of internal combustion engines APUs.

### Technology Status

Active technology development efforts in both PEFC and planar SOFC technology, driven primarily by the interest in distributed generation and automotive propulsion markets, have achieved significant progress in the development of these technologies. For distributed power applications refined and even early commercial prototypes are being constructed. However, in the case of planar SOFC a distinction must be made between different types of SOFC technologies. Neither the tubular nor the electrolyte supported SOFC technology is suitable for APU applications due to their very high operating temperature, large size and weight. Only the electrode supported planar SOFC technology may be applicable to APU applications. Since it has only been developed over the past nine years, as opposed to several decades for PEFC and other SOFC technologies, it is not developed as far, although it appears to be catching up quickly (See figure 1-12).

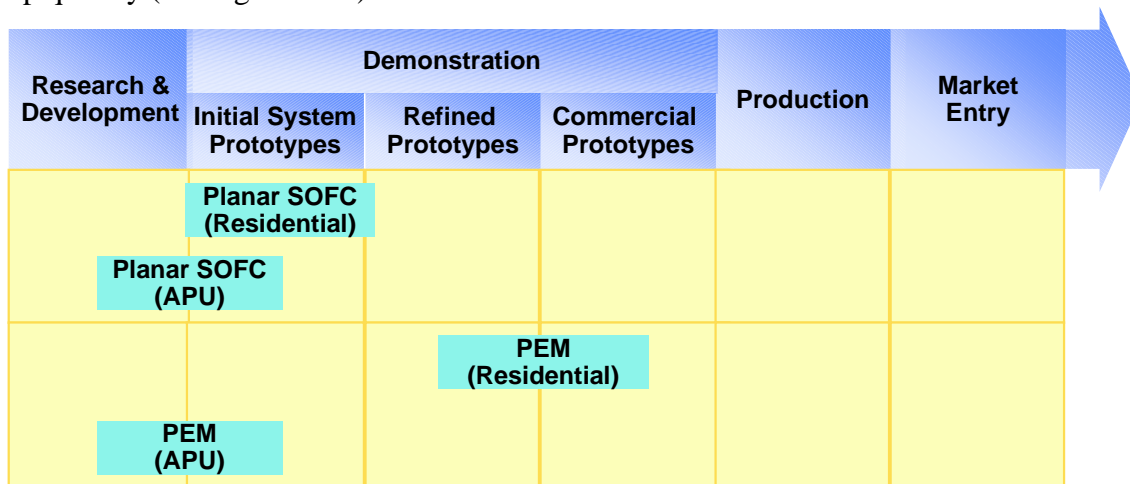


**Figure 1-12 Stage of development for fuel cells for APU applications**

Fuel cell APU applications could benefit significantly from the development of distributed generation systems, especially from residential scale systems, because of the similarity in scale and duty cycle. However, distributed generation systems are designed mostly for operation on natural gas, and do not face as stringent weight and volume requirements as APU applications. As a result, fuel cell APUs are in the early initial system prototype stage.

Several developers, including Nuvera, Honeywell, and Plug Power are active in the development for residential PEFC power systems. Most of the PEM system technology can be adapted for APU application, except that a fuel processor capable of handling transportation fuels is required. However, most of the players in the residential PEFC field are also engaged in the

development of PEFC systems for automotive propulsion applications, which are targeting the ability to utilize transportation fuels for PEFC systems.

Relatively few developers of SOFC technology have paid attention to non-stationary markets. All are focused on small to medium sized distributed generation and on-site generation markets. Only Global Thermoelectric (Calgary, Canada) has been active in the application of its technology to APUs. A recently conducted a detailed conceptual design and cost estimate of a 5-kW<sub>net</sub> SOFC-based truck APU conclude that, provided continued improvement in several technology areas, planar SOFCs could ultimately become a realistic option for this mass-market application.

### **System Configuration and Technology Issues**

Based on the system requirements discussed above, fuel cell APUs will consist of a fuel processor, a stack system and the balance of plant. Figure 1-13 lists the components required in SOFC and PEM based systems. The components needed in a PEM system for APU applications are similar to that needed in residential power. The main issue for components for PEM-based systems is the minimization or elimination of the use of external supplied water. For both PEM and SOFC systems, start-up batteries (either existing or dedicated units) will be needed since external electric power is not available.

Detailed cost and design studies for both PEFC and SOFC systems at sizes ranging from 5kW to 1 MW were made that point to the fundamental differences between PEFC and SOFC technology that impact the system design and by implication the cost structure. These differences will be discussed in the following paragraphs.

The main components in a SOFC APU are the fuel cell stack, the fuel processor, and the thermal management system. In addition there are several balance of plant components, which are listed in Figure 5. The relatively simple reformer design is possible because the SOFC stack operates at high temperatures (around 800°C) and is capable of utilizing both carbon monoxide and certain hydrocarbons as fuel. Since both the anode and cathode exhaust at temperatures of 600-850°C, high temperature recuperators are required to maintain system efficiency. These recuperators are of expensive materials (high temperature reducing and oxidizing atmosphere), making it an expensive component in the system. However, if hydrocarbons are converted inside the stack, this leads to a less exothermic overall reaction so that the stack cooling requirements are reduced.

Further system simplification would occur if a sulfur-free fuel was used or if the fuel cell were sulfur tolerant, in that case, the fuel can be provided directly from the reformer to the fuel cell. In order to minimize system volume, (and minimize the associated system weight and start-up time) integration of the system components is a key design issue. By recycling the entire anode tailgas to provide steam, a water management system can be avoided, though a hot gas recirculation system is required.

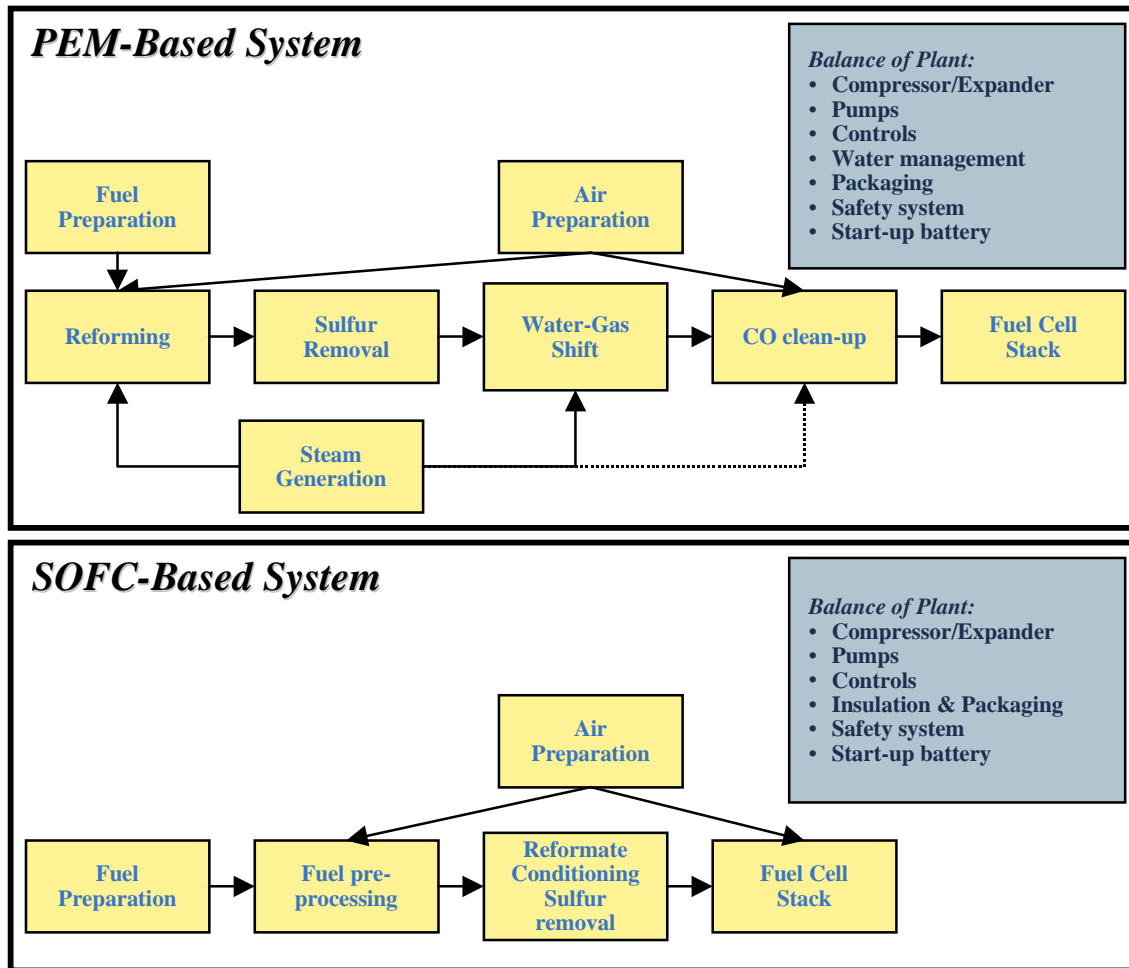


**Figure 1-13. Overview of subsystems and components for SOFC and PEM systems**

Figure 1-14 shows a simplified layout for an SOFC-based APU. The air for reformer operation and cathode requirements is compressed in a single compressor and then split between the unit operations. The external water supply shown in figure 1-14 will most likely not be needed; the anode recycle stream provides water. Unreacted anode tail gas is recuperated in a tail gas burner. Additional energy is available in a SOFC system from enthalpy recovery from tail gas effluent streams that are typically 400-600°C. Current thinking is that reformers for transportation fuel based SOFC APUs will be of the exothermic type (i.e. partial oxidation or autothermal reforming), as no viable steam reformers are available for such fuels.

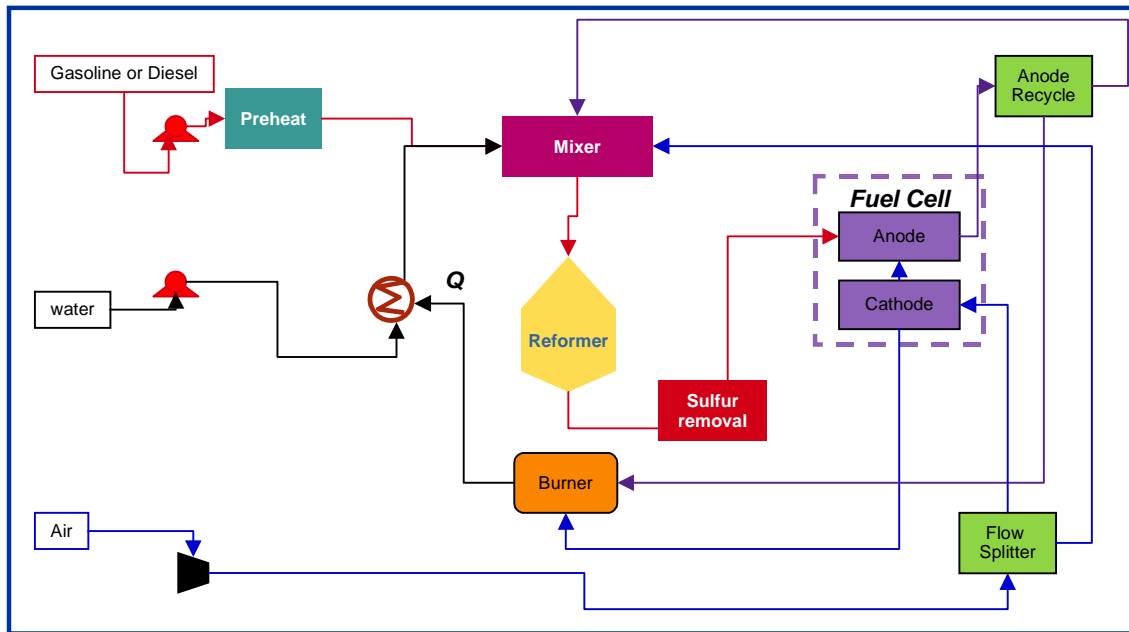


**Figure 1-14. Simplified System process flow diagram of pre-reformer/SOFC system**

Due to the operating requirements of PEM stack technology, shift reactors and a carbon monoxide removal step are required to produce reformat of sufficient quality. Similarly, the stack operating temperature and its humidity requirements require a water management system as well as radiators for heat rejection. Some developers are developing pressurized systems to the benefit from higher reactant partial pressures on both anode and cathode. Fuel processing for PEM APU systems is identical to that needed in residential power or propulsion applications. The additional issue for PEM is the minimization of steam needed for the fuel processor system. Since an APU is a mobile and/or remote unit, the need for external sources of water should be minimized. The reformat stream is further diluted by additional steam, if that water is not removed prior to the fuel cell stack.

Another design integration issue in PEM systems is water management for hydrating the electrolyte and providing the necessary steam for reforming and water-gas shift operations. Additional steam may be required for the CO clean-up device. Some reformat-based PEM systems are run under pressure to increase the partial pressure of reactants for the PEM anode and cathode, increasing efficiency. Pressure operation also aids in heat integration for the internal generation of steam at pressures greater than atmospheric (i.e. steam generated at temperatures greater than 100°C). PEM system integration involves the integration of a reformer (either exothermic or endothermic overall, ~850-1000°C), shift reactors (exothermic, 150-500°C), CO-cleanup (primarily exothermic, 50-200°C), and the fuel cell stack (exothermic, 80°C). Each reaction zone operates at a significantly different temperature thus providing a challenge for system integration and heat rejection. To alleviate some of these drawbacks, and further reduce the cost of the PEFC systems, developers are now investigating the possibility of using higher temperature membranes (e.g. operating slightly above 100°C). This would increase the carbon monoxide tolerance, potentially simplifying the fuel processor design, and simplify the heat rejection.

The power requirements for auxiliary power applications require smaller fuel cell stack duties. The heat losses for a SOFC stack operating at a smaller power duty are a larger proportion of the gross rating than in a stationary power application. Insulation required for specified system skin temperatures requirements could conceivably result in large proportion of the total system volume. Integration of the high temperature components is important in order to reduce the system volume and insulation requirements. SOFC APU systems will require inexpensive high performance insulation materials to decrease both system volume and cost.

### System Cost Considerations

As for any new class of product, total cost of ownership and operation of fuel cells will be a critical factor in their commercialization, along with the offered functionality and performance. This total cost of ownership typically has several components for power systems such as fuel cells. These components include fuel cost, other operating costs such as maintenance cost, and the first cost of the equipment. This first cost has a significant impact on fuel cells' competitiveness.

The main component of a fuel cell's first cost is the manufacturing cost, which is strongly related to the physical configuration and embodiment of the system, as well as to the manufacturing methods used. System configuration and design in turn are directly related to the desired system functionality and performance, while the manufacturing methods used are strongly linked to the anticipated production volume.

Arthur D. Little has carried out cost structure studies for a variety of fuel cell technologies for a wide range of applications, including SOFC tubular, planar and PEM technologies. Because phenomena at many levels of abstraction have a significant impact on performance and cost, they have developed a multi-level system performance and cost modeling approach (see Figure 1-15). At the most elementary level, it includes fundamental chemical reaction/reactor models for the fuel processor and fuel cell as one-dimensional systems.

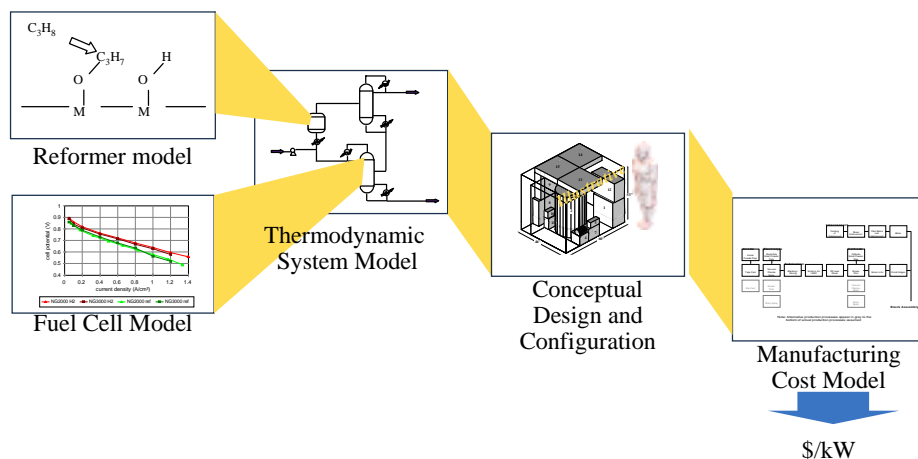


**Figure 1-15 Multilevel system modeling approach.**

Each of the detailed sub-models feed into the thermodynamic system model, and provides sizing information directly to the conceptual design and configuration. The thermodynamic system



model provides a technical hub for the multi-level approach. It provides inputs on the required flow rates and heat duties in the system. Sizing information, together with information from the thermodynamic model then flows to the conceptual design.

### **SOFC System Cost Structure**

The main difference in SOFC stack cost structure as compared to PEFC cost relates to the simpler system configuration of the SOFC-based system. This is mainly due to the fact that SOFC stacks do not contain the type of high-cost precious metals that PEFCs contain. This is off-set in part by the relatively complex manufacturing process required for the manufacture of the SOFC electrode electrolyte plates and by the somewhat lower power density in SOFC systems. Low temperature operation (enabled with electrode supported planar configuration) enables the use of low cost metallic interconnects which can be manufactured with conventional metal forming operations.

The balance of plant contains all the direct stack support systems, reformer, compressors, pumps, and the recuperating heat exchangers. Its cost is low by comparison to the PEFC because of the simplicity of the reformer. However, the cost of the recuperating heat exchangers partially offsets that.

To provide some perspective on the viability of SOFCs in APU applications from a cost perspective, NETL sponsored an estimate of the cost structure of small-scale (5 kW), simple-cycle SOFC anode-supported system, operated on gasoline. The estimated manufacturing cost for such systems (see Figure 1-16) could well be close to that estimated for comparable PEM systems, while providing somewhat higher system efficiency.

While the stack, insulation and stack balance in this simple-cycle system is a key component; the balance of plant is also an important factor. The stack cost again mainly depends on the achievable power density. Small systems like these will likely not be operated under high pressure. While this simplifies the design and reduces cost for compressors and expanders (which are not readily available at low cost for this size range in any case) it might also negatively affect the power density achievable.

One of the key challenges with small-scale SOFC systems is to overcome heat losses. The higher the heat losses are, the more recuperation is required to maintain the fuel cell within an acceptable operating temperature range and hence to ensure good performance.

The large fraction of cost related to balance of plant issues is mainly due to the very small scale of this system, which results in a significant reverse economy of scale. While design work is still ongoing, it is anticipated that the cost structure of this system will change rapidly to reduce the cost of balance of plant further, and further improve the competitiveness of these systems.

**SOFC System  
Cost Structure:**  
**Manufacturing Costs:  
\$350-550/kW**

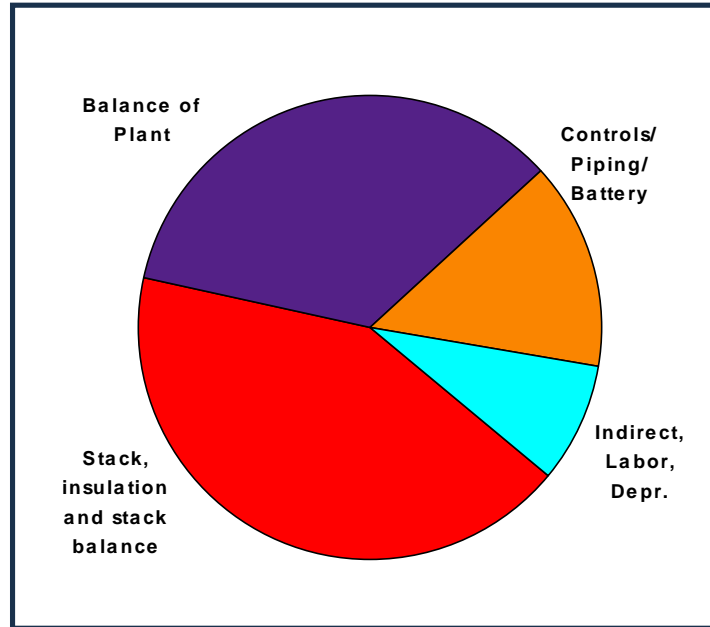


**Figure 1-16. Projected cost structure of a 5kWnet APU SOFC system. Gasoline fueled POX reformer, Fuel cell operating at 300mW/cm<sup>2</sup>, 0.7 V, 90 % fuel utilization, 500,000 units per year production volume.**

## **Outlook and Conclusions**

In conclusion, both PEM and SOFC have the potential to meet the allowable cost targets, provided successful demonstrations prove the technology. It is critical however, that for the current technologies to be commercially successful, especially in small-capacity markets, high production volumes will have to be reached. APU applications might provide such markets. It is similarly critical that the technologies be demonstrated to perform and achieve the projected performance targets, and demonstrate long life. These are the challenges ahead for the fuel cell industry in the APU market segment.

### **1.6.6 Derivative Applications**

Because of the modular nature of fuel cells, they are attractive for use in small portable units, ranging in size from 5 W or smaller to 100 W power levels. Examples of uses include the Ballard fuel cell, demonstrating 20 hour operation of a portable power unit (32), and an IFC military backpack. There has also been technology transfer from fuel cell system components. The best example is a joint IFC and Praxair, Inc., venture to develop a unit that converts natural gas to 99.999% pure hydrogen based on using fuel cell reformer technology and pressure swing adsorption process.

## **1.7 References**

1. A.J. Appleby, F.R. Foulkes, *Fuel Cell Handbook*, Van Nostrand Reinhold, New York, NY, 1989.
2. *Report of the DOE Advanced Fuel-Cell Commercialization Working Group*, Edited by S.S.

- Penner, DOE/ER/0643, prepared by the DOE Advanced Fuel Cell Working Group (AFC2WG) or the United States Department of Energy under Contract No. DEFG03-93ER30213, March 1995.
3. K. Kordesch, J. Gsellmann, S. Jahangir, M. Schautz, in *Proceedings of the Symposium on Porous Electrodes: Theory and Practice*, Edited by H.C. Maru, T. Katan, M.G. Klein, The Electrochemical Society, Inc., Pennington, NJ, p. 163, 1984.
  4. A. Pigeaud, H.C. Maru, L. Paetsch, J. Doyon, R. Bernard, in *Proceedings of the Symposium on Porous Electrodes: Theory and Practice*, Edited by H.C. Maru, T. Katan, M.G. Klein, The Electrochemical Society, Inc., Pennington, NJ, p. 234, 1984.
  5. J.M. King, N. Ishikawa, "Phosphoric Acid Fuel Cell Power Plant Improvements and Commercial Fleet Experience," Nov. 96 Fuel Cell Seminar.
  6. [www.internationalfuelcells.com](http://www.internationalfuelcells.com).
  7. Communications with IFC, August 24, 2000.
  8. K. Yokota, et al., "GOI 11 MW FC Plant Operation Interim Report," in *Fuel Cell Program and Abstracts*, 1992 Fuel Cell Seminar, Tucson, AZ, November 29-December 2, 1992.
  9. ONSI Press Release, "Fuel Cell Sets World Record; Runs 9,500 Hours Nonstop," May 20, 1997.
  10. Northeast Utilities System Press Release, "Converting Landfill Gas into Electricity is an Environmental Plus," June 24, 1996.
  11. "Groton's Tidy Machine," Public Power, March-April 1997.
  12. ONSI Press Release, "World's First Hydrogen Fueled Fuel Cell Begins Operation in Hamburg, Germany," November 7, 1997.
  13. "Anaerobic Gas Fuel Cell Shows Promise," Modern Power Systems, June 1997.
  14. E.W. Hall, W.C. Riley, G.J. Sandelli, "PC25™ Product and Manufacturing Experience," IFC, Fuel Cell Seminar, November 1996.
  15. [www.ballard.com](http://www.ballard.com), 1998.
  16. [www.fuelcellenergy.com](http://www.fuelcellenergy.com).
  17. Information supplied by ERC for the Fuel Cell Handbook.
  18. M.M. Piwetz, J.S. Larsen, T.S. Christensen, "Hydrodesulfurization and Pre-reforming of Logistic Fuels for Use in Fuel Cell Applications," *Fuel Cell Seminar Program and Abstracts*, Courtesy Associates, Inc., November 1996.
  19. Westinghouse Electric Corporation, Bechtel Group, Inc., "Solid Oxide Fuel Cell Repowering of Highgrove Station Unit 1, Final Report," prepared for Southern California Edison Research Center, March 1992.
  20. ERC, "Effects of Coal-Derived Trace Species on the Performance of Molten Carbonate Fuel Cells," topical report prepared for U.S. DOE/METC, DOE/MC/25009-T26, October 1991.
  21. N. Maskalick, "Contaminant Effects in Solid Oxide Fuel Cells," in *Agenda and Abstracts*, Joint Contractors Meeting, *Fuel Cells and Coal-Fired Heat Engines Conference*, U.S. DOE/METC, August 3-5, 1993.
  22. D.M. Rastler, C. Keeler, C.V. Chang, "Demonstration of a Carbonate on Coal Derived Gas," Report 15, in *An EPRI/GRI Fuel Cell Workshop on Technology Research and Development*. Stonehart Associates, Madison, CT, 1993.
  23. Distributed Generation, Securing America's Future with Reliable, Flexible Power," U.S. Department of Energy, Office of Fossil Energy, National Energy Technology Center, October 1999.
  24. U. S. Department of Energy's Office of Energy Efficiency and Renewable Energy webpage,

- <http://www.eren.doe.gov/distributedpower> Giovando, CarolAnn, "Distributed resources carve out a niche in competitive markets," *Power*, July/August 2000, pp. 46 – 57.
25. K.V. Kordesch, "City Car with H<sub>2</sub>-Air Fuel Cell and Lead Battery," *6<sup>th</sup> Intersociety Energy Conversion Engineering Conference*, SAE Paper No. 719015, 1971.
  26. A. Kaufman, "Phosphoric Acid Fuel Cell Bus Development," *Proceedings of the Annual Automotive Technology Development Contractors' Coordination Meeting*, Dearborn, MI, October 24-27, 1994, SAE Proceedings Volume P-289, pp. 289-293, 1995.
  27. R.R. Wimmer, "Fuel Cell Transit Bus Testing & Development at Georgetown University," *Proceedings of the Thirty Second Intersociety Energy Conversion Engineering Conference*, July 27-August 1, 1997, Honolulu, HI, pp. 825-830, 1997.
  28. N.C. Otto, P.F. Howard, "Transportation Engine Commercialization at Ballard Power Systems," *Program and Abstracts 1996 Fuel Cell Seminar*, November 17-20, 1996, Orlando, FL, pp. 559-562.
  29. F. Panik, "Fuel Cells for Vehicle Application in Cars - Bringing the Future Closer," *J. Power Sources*, 71, 36-38, 1998.
  30. S. Kawatsu, "Advanced PEFC Development for Fuel Cell Powered Vehicles," *J. Power Sources*, 71, 150-155, 1998.
  31. *Fuel-Cell Technology: Powering the Future*, Electric Line, November/December 1996.
  32. M. Graham, F. Barbir, F. Marken, M. Nadal, "Fuel Cell Power System for Utility Vehicle," *Program and Abstracts 1996 Fuel Cell Seminar*, November 17-20, 1996, Orlando, FL, pp. 571-574.
  33. P.A. Lehman, C.E. Chamberlin, "Design and Performance of a Prototype Fuel Cell Powered Vehicle," *Program and Abstracts 1996 Fuel Cell Seminar*, November 17-20, 1996, Orlando, FL, pp. 567-570.
  34. J. Leslie, "Dawn of the Hydrogen Age," *Wired* (magazine), October 1997.

---

## 2. FUEL CELL PERFORMANCE

---

The purpose of this section is to provide the framework to understand the chemical and thermodynamic operation of fuel cells, i.e., how operating conditions affect the performance of fuel cells. The impact of variables, such as temperature, pressure, and gas constituents, on fuel cell performance needs to be assessed to predict how the cells interact with the power plant system supporting it. Understanding the impact of these variables allows system analysis studies to "engineer" a specific fuel cell application. The first part of this section is intended for those who need to understand the practical thermodynamics that lead to a description of cell operation and performance. Practical cell thermodynamics is the link between fuel cell design, Section 1, and cell performance variables, Section 3 through Section 8. The second part of the section, Supplemental Thermodynamics, is a limited expansion of the Practical Thermodynamics to apprise interested readers and students of additional fundamentals. Neither of these topics is intended to provide a rigorous or detailed explanation of fuel cell thermodynamics. Numerous fuel cell books and scientific papers are available to provide additional details, (see General Fuel Cell References, Section 11.3).

Readers interested only in understanding systems incorporating fuel cells should proceed directly to the systems section, Section 9.

### 2.1 Practical Thermodynamics

A logical first step in understanding the operation of a fuel cell is to define its ideal performance. Once the ideal performance is determined, losses can be calculated and then deducted from the ideal performance to describe the actual operation. Section 2.1.1 is a description of the thermodynamics that characterize ideal performance. Actual performance is addressed in Section 2.1.2. Section 2.1.3 provides a lead-in to the development of equations in Section 3 through Section 8 that quantify the actual cell performance as a function of operating conditions for PEM, PAFC, AFC, ITSOFC, MCFC, and SOFC, respectively.

#### 2.1.1 Ideal Performance

The ideal performance of a fuel cell depends on the electrochemical reactions that occur with different fuels and oxygen as summarized in Table 2-1. Low-temperature fuel cells (PEFC, AFC, and PAFC) require noble metal electrocatalysts to achieve practical reaction rates at the anode and cathode, and H<sub>2</sub> is the only acceptable fuel. With high-temperature fuel cells (MCFC, ITSOFC, and SOFC), the requirements for catalysis are relaxed, and the number of potential fuels expands. Carbon monoxide "poisons" a noble metal anode catalyst such as platinum (Pt) in low-temperature

fuel cells, but it serves as a potential source of H<sub>2</sub> in high-temperature fuel cells where non-noble metal catalysts such as nickel (Ni) are used.

Note that H<sub>2</sub>, CO, and CH<sub>4</sub> are shown in Table 2-1 as undergoing anodic oxidation. In actuality, insignificant direct oxidation of the CO and CH<sub>4</sub> may occur. It is common system analysis practice to assume that H<sub>2</sub>, the more readily oxidized fuel, is produced by CO and CH<sub>4</sub> reacting, at equilibrium, with H<sub>2</sub>O through the water gas shift and steam reforming reactions, respectively. The H<sub>2</sub> calculated to be produced from CO and CH<sub>4</sub>, along with any H<sub>2</sub> in the fuel supply stream, is referred to as equivalent H<sub>2</sub>. The temperature and catalyst of present MCFCs provide the proper environment for the water gas shift reaction to produce H<sub>2</sub> and CO<sub>2</sub> from CO and H<sub>2</sub>O. An MCFC that reacts only H<sub>2</sub> and CO is known as an external reforming (ER) MCFC. In an internal reforming (IR) MCFC, the reforming reaction to produce H<sub>2</sub> and CO<sub>2</sub> from CH<sub>4</sub> and H<sub>2</sub>O can occur if a reforming catalyst is placed in proximity to the anode to promote the reaction. The direct oxidation of CO and CH<sub>4</sub> in a high-temperature SOFC is feasible without the catalyst, but again the direct oxidation of these fuels is favored less than the water gas shift of CO to H<sub>2</sub> and reforming of CH<sub>4</sub> to H<sub>2</sub>. These are critical arguments in determining the equations needed to describe the electrical characteristics and the energy balance of the various type cells. It is fortunate that converting CO and CH<sub>4</sub> to equivalent H<sub>2</sub>, then reacting within the cell simplifies analysis while accurately predicting the electrochemical behavior of the fuel cell.

**Table 2-1 Electrochemical Reactions in Fuel Cells**

Fuel Cell	Anode Reaction	Cathode Reaction
Proton Exchange Membrane and Phosphoric Acid	$H_2 \rightarrow 2H^+ + 2e^-$	$\frac{1}{2} O_2 + 2H^+ + 2e^- \rightarrow H_2O$
Alkaline	$H_2 + 2(OH)^- \rightarrow 2H_2O + 2e^-$	$\frac{1}{2} O_2 + H_2O + 2e^- \rightarrow 2(OH)^-$
Molten Carbonate	$H_2 + CO_3^- \rightarrow H_2O + CO_2 + 2e^-$ $CO + CO_3^- \rightarrow 2CO_2 + 2e^-$	$\frac{1}{2} O_2 + CO_2 + 2e^- \rightarrow CO_3^-$
Solid Oxide	$H_2 + O^- \rightarrow H_2O + 2e^-$ $CO + O^- \rightarrow CO_2 + 2e^-$ $CH_4 + 4O^- \rightarrow 2H_2O + CO_2 + 8e^-$	$\frac{1}{2} O_2 + 2e^- \rightarrow O^-$

CO - carbon monoxide

e<sup>-</sup> - electron

H<sub>2</sub>O - water

CO<sub>2</sub> - carbon dioxide

H<sup>+</sup> - hydrogen ion

O<sub>2</sub> - oxygen

CO<sub>3</sub><sup>-</sup> - carbonate ion

H<sub>2</sub> - hydrogen

OH<sup>-</sup> - hydroxyl ion

The ideal performance of a fuel cell is defined by its Nernst potential represented as cell voltage. The overall cell reactions corresponding to the individual electrode reactions listed in Table 2-1 are given in Table 2-2, along with the corresponding form of the Nernst equation. The Nernst

equation provides a relationship between the ideal standard<sup>2</sup> potential<sup>3</sup> ( $E^\circ$ ) for the cell reaction and the ideal equilibrium potential ( $E$ ) at other temperatures and partial pressures of reactants and products. Once the ideal potential at standard conditions is known, the ideal voltage can be determined at other temperatures and pressures through the use of these equations. According to the Nernst equation for hydrogen reaction, the ideal cell potential at a given temperature can be increased by operating at higher reactant pressures, and improvements in fuel cell performance have, in fact, been observed at higher pressures (see Sections 3 through 8).

The reaction of  $H_2$  and  $O_2$  produces  $H_2O$ . When a carbon-containing fuel is involved in the anode reaction,  $CO_2$  is also produced. For MCFCs,  $CO_2$  is required in the cathode reaction to maintain an invariant carbonate concentration in the electrolyte. Because  $CO_2$  is produced at the anode and consumed at the cathode in MCFCs, and because the concentrations in the anode and cathode feed streams are not necessarily equal, the Nernst equation in Table 2-2 includes the  $CO_2$  partial pressure for both electrode reactions.

**Table 2-2 Fuel Cell Reactions and the Corresponding Nernst Equations**

Cell Reactions <sup>a</sup>	Nernst Equation
$H_2 + \frac{1}{2}O_2 \rightarrow H_2O$	$E = E^\circ + (RT/2F) \ln [P_{H_2} / P_{H_2O}] + (RT/2F) \ln [P_{O_2}^{1/2}]$
$H_2 + \frac{1}{2}O_2 + CO_2(c) \rightarrow H_2O + CO_2(a)$	$E = E^\circ + (RT/2F) \ln [P_{H_2} / P_{H_2O} (P_{CO_2})_{(a)}] + (RT/2F) \ln [P_{O_2}^{1/2} (P_{CO_2})_{(c)}]$
$CO + \frac{1}{2}O_2 \rightarrow CO_2$	$E = E^\circ + (RT/2F) \ln [P_{CO} / P_{CO_2}] + (RT/2F) \ln [P_{O_2}^{1/2}]$
$CH_4 + 2O_2 \rightarrow 2H_2O + CO_2$	$E = E^\circ + (RT/8F) \ln [P_{CH_4} / P_{H_2O}^2 P_{CO_2}] + (RT/8F) \ln [P_{O_2}^2]$

(a) - anode                      P - gas pressure  
(c) - cathode                    R - universal gas constant  
E - equilibrium potential    T - temperature (absolute)

a - The cell reactions are obtained from the anode and cathode reactions listed in Table2-1.

The ideal standard potential of an  $H_2/O_2$  fuel cell ( $E^\circ$ ) is 1.229 volts with liquid water product and 1.18 water with gaseous product. This value is shown in numerous chemistry texts (1) as the oxidation potential of  $H_2$ . The potential force also can be expressed as a change in Gibbs free energy (Section 2.2.2) for the reaction of hydrogen and oxygen. It will be shown later in this section that the change in Gibbs free energy increases as cell temperature decreases and that the ideal potential of a cell, is proportional to the change in the standard Gibbs free energy.

- Standard conditions are one atmosphere and 25°C (77°F).
- The standard Nernst potential ( $E^\circ$ ) is the ideal cell voltage at standard conditions. It does not include losses that are found in an operating fuel cell. Thus, it can be thought of as the open circuit voltage.

Figure 2-1 shows the relation of  $E^\circ$  to cell temperature. Because the figure shows the potential of higher temperature cells, the ideal potential corresponds to a reaction where the water product is in a gaseous state. Hence,  $E^\circ$  is less than 1.229 at standard conditions when considering gaseous water product.

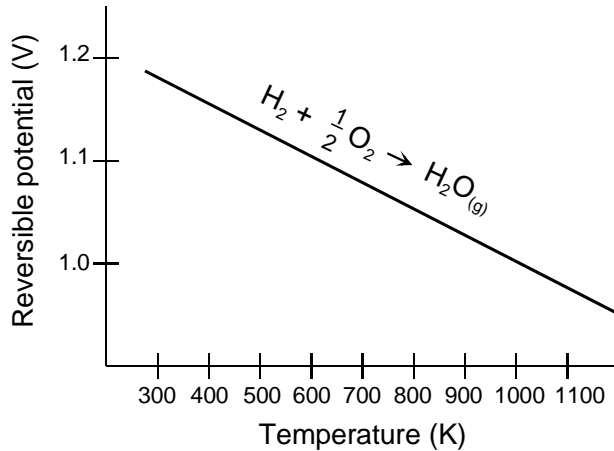


**Figure 2-1 H<sub>2</sub>/O<sub>2</sub> Fuel Cell Ideal Potential as a Function of Temperature**

The impact of temperature on the ideal voltage,  $E$ , for the oxidation of hydrogen is shown in Table 2-3.

**Table 2-3 Ideal Voltage as A Function of Cell Temperature**

Temperature	25°C (298K)	80°C (353K)	100°C (273K)	205°C (478K)	650°C (923K)	800°C (1073K)	1100°C (1373K)
Cell Type		PEFC	AFC	PAFC	MCFC	ITSOFC	SOFC
Ideal Voltage	1.18	1.17		1.14	1.03		0.91

### 2.1.2 Actual Performance

Large, complex computer models are used to characterize the actual operation of fuel cells based on minute details of cell component design (physical dimensions, materials, etc.) along with physical considerations (transport phenomena, electrochemistry, etc.). These codes, often proprietary, are needed in the design and development of fuel cells, but would be cumbersome and time consuming for use in system analysis models. Simpler approaches are normally used for system studies. One approach, for example, would be to conduct tests at every condition expected to be analyzed in the system; this would, however, be very costly. Instead, it is prudent to develop correlations based on thermodynamic modeling that depict cell performance as various cell operating conditions are changed, such as temperature, pressure, and gas constituents. Thermodynamic modeling is used to depict the equations so that only a limited number of tests are needed to define design constants within the equation. Adjustments can be



applied to a reference performance at known operating conditions to achieve the performance at the desired operating conditions.

Useful work (electrical energy) is obtained from a fuel cell only when a reasonable current is drawn, but the actual cell potential is decreased from its equilibrium potential because of irreversible losses as shown in Figure 2-2<sup>4</sup>. Several sources contribute to irreversible losses in a practical fuel cell. The losses, which are often called polarization, overpotential, or overvoltage ( $\eta$ ), originate primarily from three sources: (1) activation polarization ( $\eta_{act}$ ), (2) ohmic polarization ( $\eta_{ohm}$ ), and (3) concentration polarization ( $\eta_{conc}$ ). These losses result in a cell voltage ( $V$ ) for a fuel cell that is less than its ideal potential,  $E$  ( $V = E - \text{Losses}$ ).

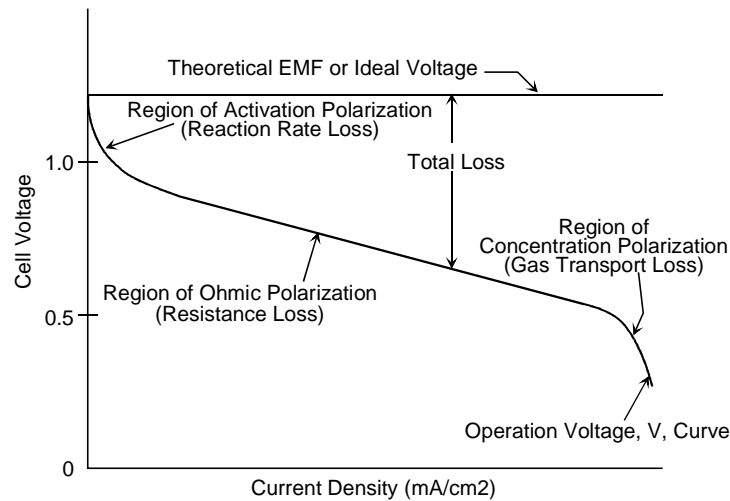


**Figure 2-2 Ideal and Actual Fuel Cell Voltage/Current Characteristic**

The activation polarization loss is dominant at low current density. At this point, electronic barriers have to be overcome prior to current and ion flow. Activation losses show some increase as current increases. Ohmic polarization (loss) varies directly with current, increasing over the whole range of current because cell resistance remains essentially constant. Gas transport losses occur over the entire range of current density, but these losses become prominent at high limiting currents where it becomes difficult to provide enough reactant flow to the cell reaction sites.

**Activation Polarization:** Activation polarization is present when the rate of an electrochemical reaction at an electrode surface is controlled by sluggish electrode kinetics. In other words, activation polarization is directly related to the rates of electrochemical reactions. There is a close similarity between electrochemical and chemical reactions in that both involve an activation barrier that must be overcome by the reacting species. In the case of an electrochemical reaction with  $\eta_{act} \geq 50\text{-}100\text{ mV}$ ,  $\eta_{act}$  is described by the general form of the Tafel equation (see Section 2.2.4):

<sup>4</sup> Activation region and concentration region more representative of low-temperature fuel cells.

$$\eta_{\text{act}} = \frac{RT}{\alpha n \mathbf{F}} \ln \frac{i}{i_0} \quad (2-1)$$

where  $\alpha$  is the electron transfer coefficient of the reaction at the electrode being addressed, and  $i_0$  is the exchange current density (see Section 2.2.4).

**Ohmic Polarization:** Ohmic losses occur because of resistance to the flow of ions in the electrolyte and resistance to flow of electrons through the electrode materials. The dominant ohmic losses, through the electrolyte, are reduced by decreasing the electrode separation and enhancing the ionic conductivity of the electrolyte. Because both the electrolyte and fuel cell electrodes obey Ohm's law, the ohmic losses can be expressed by the equation

$$\eta_{\text{ohm}} = iR \quad (2-2)$$

where  $i$  is the current flowing through the cell, and  $R$  is the total cell resistance, which includes electronic, ionic, and contact resistance.

**Concentration Polarization:** As a reactant is consumed at the electrode by electrochemical reaction, there is a loss of potential due to the inability of the surrounding material to maintain the initial concentration of the bulk fluid. That is, a concentration gradient is formed. Several processes may contribute to concentration polarization: slow diffusion in the gas phase in the electrode pores, solution/dissolution of reactants/products into/out of the electrolyte, or diffusion of reactants/products through the electrolyte to/from the electrochemical reaction site. At practical current densities, slow transport of reactants/products to/from the electrochemical reaction site is a major contributor to concentration polarization:

$$\eta_{\text{conc}} = \frac{RT}{n \mathbf{F}} \ln \left( 1 - \frac{i}{i_L} \right) \quad (2-3)$$

where  $i_L$  is the limiting current (see Section 2.2.4).

**Summing of Electrode Polarization:** Activation and concentration polarization can exist at both the positive (cathode) and negative (anode) electrodes in fuel cells. The total polarization at these electrodes is the sum of  $\eta_{act}$  and  $\eta_{conc}$ , or

$$\eta_{anode} = \eta_{act,a} + \eta_{conc,a} \quad (2-4)$$

and

$$\eta_{cathode} = \eta_{act,c} + \eta_{conc,c} \quad (2-5)$$

The effect of polarization is to shift the potential of the electrode ( $E_{electrode}$ ) to a new value ( $V_{electrode}$ ):

$$V_{electrode} = E_{electrode} \pm |\eta_{electrode}| \quad (2-6)$$

For the anode,

$$V_{anode} = E_{anode} + |\eta_{anode}| \quad (2-7)$$

and for the cathode,

$$V_{cathode} = E_{cathode} - |\eta_{cathode}| \quad (2-8)$$

The net result of current flow in a fuel cell is to increase the anode potential and to decrease the cathode potential, thereby reducing the cell voltage. Figure 2-3 illustrates the contribution to polarization of the two half cells for a PAFC. The reference point (zero polarization) is hydrogen. These shapes of the polarization curves are typical of other types of fuel cells.

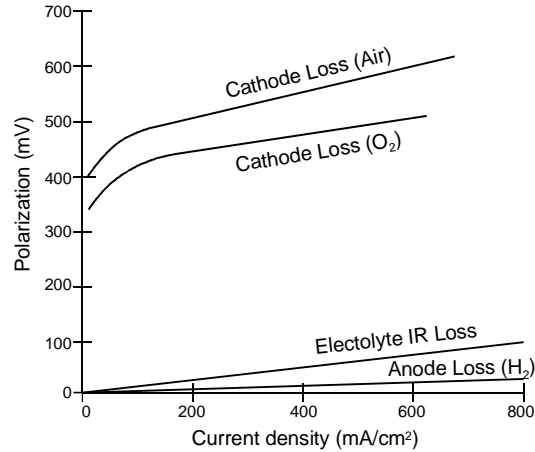


**Figure 2-3 Contribution to Polarization of Anode and Cathode**

**Summing of Cell Voltage:** The cell voltage includes the contribution of the anode and cathode potentials and ohmic polarization:

$$V_{\text{cell}} = V_{\text{cathode}} - V_{\text{anode}} - iR \quad (2-9)$$

When Equations (2-7) and (2-8) are substituted in Equation (2-9)

$$V_{\text{cell}} = E_{\text{cathode}} - |\eta_{\text{cathode}}| - (E_{\text{anode}} + |\eta_{\text{anode}}|) - iR \quad (2-10)$$

or

$$V_{\text{cell}} = \Delta E_e - |\eta_{\text{cathode}}| - |\eta_{\text{anode}}| - iR \quad (2-11)$$

where  $\Delta E_e = E_{\text{cathode}} - E_{\text{anode}}$ . Equation (2-11) shows that current flow in a fuel cell results in a decrease in the cell voltage because of losses by electrode and ohmic polarizations. The goal of fuel cell developers is to minimize the polarization so that  $V_{\text{cell}}$  approaches  $\Delta E_e$ . This goal is approached by modifications to fuel cell design (improvement in electrode structures, better electrocatalysts, more conductive electrolyte, thinner cell components, etc.). For a given cell design, it is possible to improve the cell performance by modifying the operating conditions (e.g., higher gas pressure, higher temperature, change in gas composition to lower the gas impurity concentration). However, for any fuel cell, compromises exist between achieving higher performance by operating at higher temperature or pressure and the problems associated with the stability/durability of cell components encountered at the more severe conditions.

### 2.1.3 Fuel Cell Performance Variables

The performance of fuel cells is affected by operating variables (e.g., temperature, pressure, gas composition, reactant utilizations, current density) and other factors (impurities, cell life) that influence the ideal cell potential and the magnitude of the voltage losses described above. Any number of operating points can be selected for application of a fuel cell in a practical system, as illustrated by Figure 2-4.

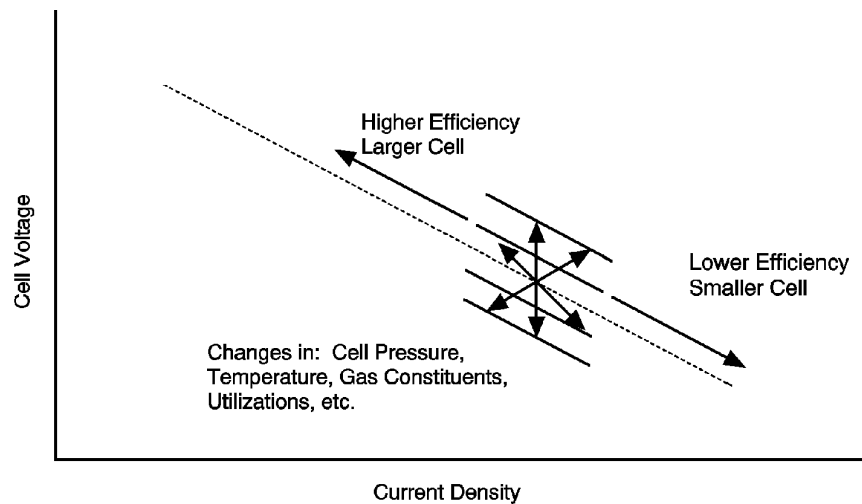


**Figure 2-4 Flexibility of Operating Points According to Cell Parameters**

Figure 2-4 represents the characteristics of a fuel cell once its physical design is set. Changing the cell operating parameters (temperature and pressure) can have either a beneficial or a detrimental impact on fuel cell performance and on the performance of other system components. These effects may be offsetting. Changes in operating conditions may lower the cost of the cell, but increase the cost of the surrounding system. Usually, compromises in the operating parameters are necessary to meet the application requirements, obtain lowest system cost, and achieve acceptable cell life. Operating conditions are based on defining specific system requirements, such as power level, voltage, or system weight. From this and through interrelated cycle studies, the power, voltage, and current requirements of the fuel cell stack and individual cells are determined. It is a matter of selecting a cell operating point (cell voltage and related current density) as shown by Figure 2-4 until the system requirements are satisfied (such as lowest cost, lightest unit, highest power density). For example, a design point at high current density will allow a smaller cell size at lower capital cost to be used for the stack, but a lower system efficiency results (because of the lower cell voltage) and attendant higher operating cost. This type of operating point would be typified by a vehicle application where light weight and small volume, as well as efficiency, are important drivers for cost effectiveness. Cells capable of higher current density operation would be of prime interest. Operating at a lower current density, but higher voltage (higher efficiency, lower operating cost) would be more suitable for stationary power plant operation. Operating at a higher pressure will increase cell performance and lower cost. However, there will be a higher parasitic power to compress the reactants, and the cell stack pressure vessel and piping will have to withstand the greater pressure. This adds

cost. It is evident that the selection of the cell design point interacts with the system design (see Section 9).

Figure 2-5 presents the same information as Figure 2-4, but in a way to highlight another aspect of determining the cell design point. It would seem logical to design the cell to operate at the maximum power density that peaks at a higher current density (right of the figure). However, operation at the higher power densities will mean operation at lower cell voltages or lower cell efficiency. Setting operation at the peak power density can cause instability in control because the system will have a tendency to oscillate between higher and lower current densities around the peak. It is usual practice to operate the cell to the left side of the power density peak and at a point that yields a compromise between low operating cost (high cell efficiency that occurs at high voltage/low current density) and low capital cost (less cell area that occurs at low voltage/high current density).

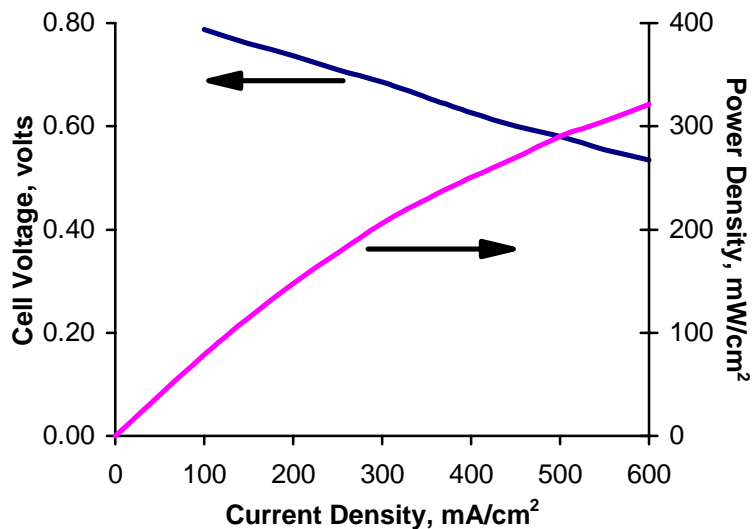


**Figure 2-5 Voltage/Power Relationship**

The equations describing performance variables, developed in Sections 3 through 8, address changes in cell performance as a function of major operating conditions to allow the reader to perform quantitative parametric analysis. The following discussion establishes the generic equations of performance variables.

**Temperature and Pressure:** The effect of temperature and pressure on the ideal potential (E) of a fuel cell can be analyzed on the basis of changes in the Gibbs free energy with temperature and pressure.

$$\left(\frac{\partial E}{\partial T}\right)_P = \frac{\Delta S}{nF} \quad (2-12)$$

or

$$\left(\frac{\partial E}{\partial P}\right)_T = \frac{-\Delta V}{nF} \quad (2-13)$$

Because the entropy change for the H<sub>2</sub>/O<sub>2</sub> reaction is negative, the reversible potential of the H<sub>2</sub>/O<sub>2</sub> fuel cell decreases with an increase in temperature by 0.84 mV/°C (assuming reaction product is liquid water). For the same reaction, the volume change is negative; therefore, the reversible potential increases with an increase in pressure.

The practical effect of temperature on the voltage of fuel cells is represented schematically in Figure 2-6, which presents initial (i.e., early in life) performance data from typical operating cells and the dependence of the reversible potential of H<sub>2</sub>/O<sub>2</sub> fuel cells on temperature (3). The cell voltages of PEFCs, PAFCs, and MCFCs show a strong dependence on temperature.<sup>5</sup> The reversible potential decreases with increasing temperature, but the operating voltages of these fuel cells actually increase with an increase in operating temperature. PEFCs, however, exhibit a maximum in operating voltage,<sup>6</sup> as in Figure 2-6. The lower operating temperature of state-of-the-art TSOFCs is limited to about 1000°C (1832°F) because the ohmic resistance of the solid electrolyte increases rapidly as the temperature decreases. The cell is limited by material concerns and fabrication processes at temperatures above 1000°C. Section 7 describes efforts to develop ITSOFC, which operate at lower temperatures than TSOFCs – between approximately 650-800°C. The other types of fuel cells typically operate at voltages considerably below the reversible cell voltage. The increase in performance is due to changes in the types of primary polarizations affecting the cell as temperature varies. An increase in the operating temperature is beneficial to fuel cell performance because of the increase in reaction rate, higher mass transfer rate, and usually lower cell resistance arising from the higher ionic conductivity of the electrolyte. In addition, the CO tolerance of electrocatalysts in low-temperature fuel cells improves as the operating temperature increases. These factors combine to reduce the polarization at higher temperatures.

---

5. The cell voltages are not taken at equal current densities. Absolute cell voltage should not be compared.

6. The cell voltage of PEFCs goes through a maximum as a function of temperature because of the difficulties with water management at higher temperature. It may be possible to adjust operating conditions so that the PEFC voltage will increase up to a temperature of ~140°C, the point at which the membrane degrades rapidly.

On the negative side, materials problems related to corrosion, electrode degradation, electrocatalyst sintering and recrystallization, and electrolyte loss by evaporation are all accelerated at higher temperatures.

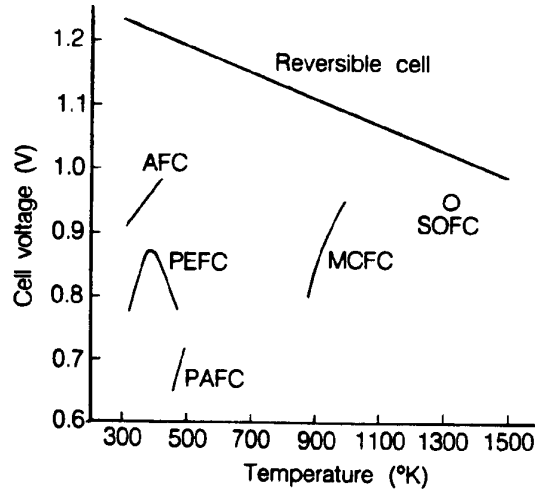


**Figure 2-6 Dependence of the Initial Operating Cell Voltage of Typical Fuel Cells on Temperature (1)**

An increase in operating pressure has several beneficial effects on fuel cell performance because the reactant partial pressure, gas solubility, and mass transfer rates are higher. In addition, electrolyte loss by evaporation is reduced at higher operating pressures. Increased pressure also tends to increase system efficiencies. However, there are compromises such as thicker piping and additional expense for the compression process. Section 9.2.1 addresses system aspects of pressurization. The benefits of increased pressure must be balanced against hardware and materials problems, as well as parasitic power costs. In particular, higher pressures increase material problems in MCFCs (see Section 6.1), pressure differentials must be minimized to prevent reactant gas leakage through the electrolyte and seals, and high pressure favors carbon deposition and methane formation in the fuel gas.

**Reactant Utilization and Gas Composition:** Reactant utilization and gas composition have major impacts on fuel cell efficiency. It is apparent from the Nernst equations in Table 2-2 that fuel and oxidant gases containing higher partial pressures of electrochemical reactants produce a higher cell voltage.



Utilization (U) refers to the fraction of the total fuel or oxidant introduced into a fuel cell that reacts electrochemically. In low-temperature fuel cells, determining the fuel utilization is relatively straightforward when H<sub>2</sub> is the fuel, because it is the only reactant involved in the electrochemical reaction,<sup>7</sup> i.e.

$$U_f = \frac{H_{2,in} - H_{2,out}}{H_{2,in}} = \frac{H_{2, \text{consumed}}}{H_{2,in}} \quad (2-14)$$

where H<sub>2,in</sub> and H<sub>2,out</sub> are the mass flow rates of H<sub>2</sub> at the inlet and outlet of the fuel cell, respectively. However, hydrogen can be consumed by various other pathways, such as by chemical reaction (i.e., with O<sub>2</sub> and cell components) and loss via leakage out of the cell. These pathways increase the apparent utilization of hydrogen without contributing to the electrical energy produced by the fuel cell. A similar type of calculation is used to determine the oxidant utilization. For the cathode in MCFCs, two reactant gases, O<sub>2</sub> and CO<sub>2</sub>, are utilized in the electrochemical reaction. The oxidant utilization should be based on the limiting reactant. Frequently O<sub>2</sub>, which is readily available from make-up air, is present in excess, and CO<sub>2</sub> is the limiting reactant.

A significant advantage of high-temperature fuel cells such as MCFCs is their ability to use CO as a fuel. The anodic oxidation of CO in an operating MCFC is slow compared to the anodic oxidation of H<sub>2</sub>; thus, the direct oxidation of CO is not favored. However, the water gas shift reaction



reaches equilibrium rapidly in MCFCs at temperatures as low as 650°C (1200°F) to produce H<sub>2</sub>.<sup>8</sup> As H<sub>2</sub> is consumed, the reaction is driven to the right because both H<sub>2</sub>O and CO<sub>2</sub> are produced in equal quantities in the anodic reaction. Because of the shift reaction, fuel utilization in MCFCs can exceed the value for H<sub>2</sub> utilization, based on the inlet H<sub>2</sub> concentration. For example, for an anode gas composition of 34% H<sub>2</sub>/22% H<sub>2</sub>O/13% CO/18% CO<sub>2</sub>/12% N<sub>2</sub>, a fuel utilization of 80% (i.e., equivalent to 110% H<sub>2</sub> utilization) can be achieved even though this would require 10% more H<sub>2</sub> (total of 37.6%) than is available in the original fuel. The high fuel utilization is possible because the shift reaction provides the necessary additional H<sub>2</sub> that is oxidized at the anode. In this case, the fuel utilization is defined by

$$U_f = \frac{H_{2, \text{consumed}}}{H_{2,in} + \text{CO}_{in}} \quad (2-16)$$

---

7. Assumes no gas cross-over or leakage out of the cell.

8. Example 10-5 in Section 10 illustrates how to determine the amount of H<sub>2</sub> produced by the shift reaction.

where the  $H_2$  consumed originates from the  $H_2$  present at the fuel cell inlet ( $H_{2,in}$ ) and any  $H_2$  produced in the cell by the water gas shift reaction ( $CO_{in}$ ).

Gas composition changes between the inlet and outlet of a fuel cell, caused by the electrochemical reaction, lead to reduced cell voltages. This voltage reduction arises because the cell voltage adjusts to the lowest electrode potential given by the Nernst equation for the various gas compositions at the exit of the anode and cathode chambers. Because electrodes are usually good electronic conductors and isopotential surfaces, the cell voltage can not exceed the minimum (local) value of the Nernst potential. In the case of a fuel cell with the flow of fuel and oxidant in the same direction (i.e., coflow), the minimum Nernst potential occurs at the cell outlet. When the gas flows are counterflow or crossflow, determining the location of the minimum potential is not straightforward.

The MCFC provides a good example to illustrate the influence of the extent of reactant utilization on the electrode potential. An analysis of the gas composition at the fuel cell outlet as a function of utilization at the anode and cathode is presented in Example 10-5. The Nernst equation can be expressed in terms of the mole fraction of the gases ( $X_i$ ) at the fuel cell outlet:

$$E = E^{\circ} + \frac{RT}{2F} \ln \frac{X_{H_2} X_{O_2}^{1/2} X_{CO_2,cathode} P^{1/2}}{X_{H_2O,anode} X_{CO_2,anode}} \quad (2-17)$$

where  $P$  is the cell gas pressure. The second term on the right side of Equation (2-17), the so-called Nernst term, reflects the change in the reversible potential as a function of reactant utilization, gas composition, and pressure. Figure 2-7 illustrates the change in reversible cell potential calculated as a function of utilization using Equation (2-17).

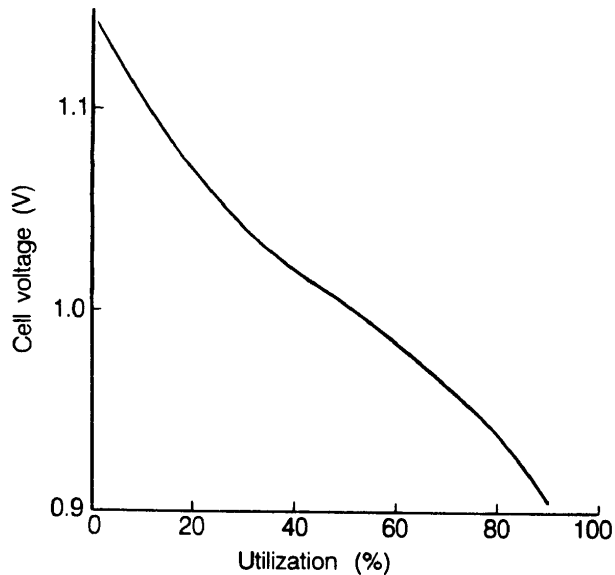


**Figure 2-7 The Variation in the Reversible Cell Voltage as a Function of Reactant Utilization**

(Fuel and oxidant utilizations equal) in a MCFC at 650°C and 1 atm. Fuel gas: 80% H<sub>2</sub>/20% CO<sub>2</sub> saturated with H<sub>2</sub>O at 25°C; oxidant gas: 60% CO<sub>2</sub>/30% O<sub>2</sub>/10% inert)

The reversible potential at 650°C (1200°F) and 1 atmosphere pressure is plotted as a function of reactant utilization (fuel and oxidant utilizations are equal) for inlet gas compositions of 80% H<sub>2</sub>/20% CO<sub>2</sub> saturated with H<sub>2</sub>O at 25°C (77°F) (fuel gas<sup>9</sup>) and 60% CO<sub>2</sub>/30% O<sub>2</sub>/10% inerts (oxidant gas); gas compositions and utilizations are listed in Table 2-4. Note that the oxidant composition is based on a gas of 2/1 CO<sub>2</sub> to O<sub>2</sub>. The gas is not representative of the cathode inlet gas of a modern system, but is used for illustrative purposes only. The mole fractions of H<sub>2</sub> and CO in the fuel gas decrease as the utilization increases and the mole fractions of H<sub>2</sub>O and CO<sub>2</sub> show the opposite trend. At the cathode, the mole fractions of O<sub>2</sub> and CO<sub>2</sub> decrease with an increase in utilization because they are both consumed in the electrochemical reaction. The reversible cell potential plotted in Figure 2-7 is calculated from the equilibrium compositions for the water gas shift reaction at the cell outlet. An analysis of the data in the figure indicates that a change in the utilization from 20 to 80% will cause a decrease in the reversible potential of about 0.158 V, or roughly 0.0026 V/% utilization. These results show that MCFCs operating at high utilization will suffer a large voltage loss because of the magnitude of the Nernst term.

An analysis by Cairns and Liebhafsky (3) for a H<sub>2</sub>/air fuel cell shows that a change in the gas composition that produces a 60 mV change in the reversible cell potential near room temperature corresponds to a 300 mV change at 1200°C (2192°F). Thus, gas composition changes are more significant in high temperature fuel cells.

9. Anode inlet composition is 64.5% H<sub>2</sub>/6.4% CO<sub>2</sub>/13% CO/16.1% H<sub>2</sub>O after equilibration by water gas shift reaction.

**Current Density:** Figure 2-4 depicts the impact of current density on the voltage (performance) of a fuel cell. The effects on performance of increasing current density were addressed in Section 2.1.2. That section described how activation, ohmic, and concentration losses occur as the current is changed. Figure 2-2 is a simplified depiction of how these losses affect the shape of the cell voltage-current characteristic. As current is initially drawn, sluggish kinetics (activation losses) causes a decrease in cell voltage. At high current densities, there is an inability to diffuse enough reactants to the reaction sites (concentration losses) so the cell experiences a sharp performance decrease through reactant starvation. There also may be an associated problem of diffusing the reaction products from the cell.

**Table 2-4 Outlet Gas Composition as a Function of Utilization in MCFC at 650°C**

Gas	Utilization <sup>a</sup> (%)				
	0	25	50	75	90
<b>Anode<sup>b</sup></b>					
X <sub>H2</sub>	0.645	0.410	0.216	0.089	0.033
X <sub>CO2</sub>	0.064	0.139	0.262	0.375	0.436
X <sub>CO</sub>	0.130	0.078	0.063	0.033	0.013
X <sub>H2O</sub>	0.161	0.378	0.458	0.502	0.519
<b>Cathode<sup>c</sup></b>					
X <sub>CO2</sub>	0.600	0.581	0.545	0.461	0.316
X <sub>O2</sub>	0.300	0.290	0.273	0.231	0.158

- a - Same utilization for fuel and oxidant. Gas compositions are given in mole fractions.
- b - 80% H<sub>2</sub>/20% CO<sub>2</sub> saturated with H<sub>2</sub>O at 25°C. Fuel gas compositions are based on compositions for water-gas shift equilibrium.
- c - 30% O<sub>2</sub>/60% CO<sub>2</sub>/10% inert gas. Gas is not representative of a modern system cathode inlet gas, but used for illustrative purposes only.

Ohmic losses predominate in the range of normal fuel cell operation. These losses can be expressed as  $iR$  losses where  $i$  is the current and  $R$  is the summation of internal resistances within the cell, Equation (2-2). As is readily evident from the equation, the ohmic loss and hence voltage change is a direct function of current (current density multiplied by cell area).

### 2.1.4 Cell Energy Balance

The information in the previous sections can be used to determine a mass balance around a fuel cell and describe its electrical performance. System analysis requires an energy or heat balance to fully understand the system. The energy balance around the fuel cell is based on the energy absorbing/releasing processes (e.g., power produced, reactions, heat loss) that occur in the cell. As a result, the energy balance varies for the different types of cells because of the differences in reactions that occur according to cell type.

In general, the cell energy balance states that the enthalpy flow of the reactants entering the cell will equal the enthalpy flow of the products leaving the cell plus the sum of three terms: (1) the net heat generated by physical and chemical processes within the cell, (2) the dc power output from the cell, and the rate of heat loss from the cell to its surroundings.

Component enthalpies are readily available on a per mass basis from data such as JANAF (4). Product enthalpy usually includes the heat of formation in published tables. A typical energy balance calculation is the determination of the cell exit temperature knowing the reactant composition, the temperatures, H<sub>2</sub> and O<sub>2</sub> utilization, the expected power produced, and a percent heat loss. The exit constituents are calculated from the fuel cell reactions as illustrated in Example 10-3, Section 10.

## 2.2 Supplemental Thermodynamics

These supplemental thermodynamics are provided to support the performance trends developed in Sections 2.1.2 and 2.1.3. The descriptions are not intended to be a detailed explanation.

### 2.2.1 Cell Efficiency

The thermal efficiency of an energy conversion device is defined as the amount of useful energy produced relative to the change in stored chemical energy (commonly referred to as thermal energy) that is released when a fuel is reacted with an oxidant.

$$\eta = \frac{\text{Useful Energy}}{\Delta H} \quad (2-18)$$

Hydrogen (a fuel) and oxygen (an oxidant) can exist in each other's presence at room temperature, but if heated to 580°C, they explode violently. The combustion reaction can be forced for gases lower than 580°C by providing a flame, such as in a heat engine. A catalyst and an electrolyte, such as in a fuel cell, can increase the rate of reaction of H<sub>2</sub> and O<sub>2</sub> at temperatures lower than 580°C. Note that a non-combustible reaction can occur in fuel cells at temperatures over 580°C because of controlled separation of the fuel and oxidant. The heat engine process is thermal; the fuel cell process is electrochemical. Differences in these two methods of producing useful energy are the root of efficiency comparison issues.

In the ideal case of an electrochemical converter, such as a fuel cell, the change in Gibbs free energy,  $\Delta G$ , (Section 2.2.3) of the reaction is available as useful electric energy at the temperature of the conversion. The ideal efficiency of a fuel cell, operating irreversibly, is then

$$\eta = \frac{\Delta G}{\Delta H} \quad (2-19)$$

The most widely used efficiency of a fuel cell is based on the change in the standard free energy for the cell reaction,



given by

$$\Delta G_r^o = G_{\text{H}_2\text{O}(l)}^o - G_{\text{H}_2}^o - \frac{1}{2} G_{\text{O}_2}^o$$

where the product water is in liquid form. At standard conditions of 25°C (298K) and 1 atmosphere, the chemical energy ( $\Delta H = \Delta H_o$ ) in the hydrogen/oxygen reaction is 285.8 kJ/mole, and the free energy available for useful work is 237.1 kJ/mole. Thus, the thermal efficiency of an ideal fuel cell operating reversibly on pure hydrogen and oxygen at standard conditions would be:

$$\eta_{ideal} = \frac{237.1}{285.8} = 0.83$$

The efficiency of an actual fuel cell can be expressed in terms of the ratio of the operating cell voltage to the ideal cell voltage. The actual cell voltage is less than the ideal cell voltage because of the losses associated with cell polarization and the  $iR$  loss, as discussed in Section 2.1.2. The thermal efficiency of the fuel cell can then be written in terms of the actual cell voltage,

$$\eta = \frac{\text{Useful Energy}}{\Delta H} = \frac{\text{Useful Power}}{(\Delta G/0.83)} = \frac{\text{Volts}_{actual} \times \text{Current}}{\text{Volts}_{ideal} \times \text{Current} / 0.83} = \frac{(0.83)(V_{actual})}{V_{ideal}} \quad (2-21)$$

As mentioned in Section 2.1.1, the ideal voltage of a cell operating reversibly on pure hydrogen and oxygen at 1 atm pressure and 25°C is 1.229 V. Thus, the thermal efficiency of an actual fuel cell operating at a voltage of  $V_{cell}$ , based on the higher heating value of hydrogen, is given by

$$\eta_{ideal} = 0.83 \times V_{cell} / V_{ideal} = 0.83 \times V_{cell} / 1.229 = 0.675 \times V_{cell} \quad (2-22)$$

A fuel cell can be operated at different current densities, expressed as mA/cm<sup>2</sup> or A/ft<sup>2</sup>. The corresponding cell voltage then determines the fuel cell efficiency. Decreasing the current density increases the cell voltage, thereby increasing the fuel cell efficiency. The trade-off is that as the current density is decreased, the active cell area must be increased to obtain the requisite amount of power. Thus, designing the fuel cell for higher efficiency increases the capital cost, but decreases the operating cost.

Two additional aspects of efficiency are of interest: 1) the effects of integrating a fuel cell into a complete system that accepts readily available fuels like natural gas and produces grid quality ac power (see Section 9), and 2) issues arising when comparing fuel cell efficiency with heat engine efficiency (see below).

It is interesting to observe that the resulting characteristic provides the fuel cell with a benefit compared to other energy conversion technologies. The fuel cell increases its efficiency at part load conditions.<sup>10</sup> Other components within the fuel cell system operate at lower component efficiencies as the system's load is reduced. The combination of increased fuel cell efficiency and lower supporting component efficiencies can result in a rather flat trace of total system efficiency as the load is reduced. Most competing energy conversion techniques experience a loss of efficiency as the design point load is reduced. This loss, coupled with the same supporting component losses of efficiency that the fuel cell system experiences, causes lower total efficiencies as the load is reduced. This gives the fuel cell system an operating cost advantage for applications where part load operation is important.

### 2.2.2 Efficiency Comparison to Heat Engines

It is commonly expressed that a fuel cell is more efficient than a heat engine because it is not subject to Carnot Cycle limitations, or a fuel cell is more efficient because it is not subject to the second law of thermodynamics. These statements are misleading. A more suitable statement for understanding differences between the theoretical efficiencies of fuel cells and heat engines<sup>11</sup> is that if a fuel cell is compared to an equivalent efficiency heat engine, the fuel cell is not limited by temperature as is the heat engine (5). The freedom from temperature limits of the fuel cell provides a great benefit because it relaxes material temperature problems when trying to achieve high efficiency.

### 2.2.3 Gibbs Free Energy and Ideal Performance

The maximum electrical work ( $W_{el}$ ) obtainable in a fuel cell operating at constant temperature and pressure is given by the change in Gibbs free energy ( $\Delta G$ )<sup>12</sup> of the electrochemical reaction,

$$W_{el} = \Delta G = -nFE \quad (2-23)$$

where  $n$  is the number of electrons participating in the reaction,  $F$  is Faraday's constant (96,487 coulombs/g-mole electron), and  $E$  is the ideal potential of the cell. If we consider the case of reactants and products being in the standard state, then

$$\Delta G^\circ = -nFE^\circ \quad (2-24)$$

---

10. Constraints can limit the degree of part load operation of a fuel cell. For example, a PAFC is limited to operation below approximately 0.85 volts because of entering into a corrosion region.

11. It should be remembered that the actual efficiencies of heat engines and fuel cells are substantially below their theoretical values.

12. Total energy is composed of two types of energy: 1) free energy,  $G$ , and unavailable energy,  $TS$ . Free energy earns its name because it is the energy that is available or free for conversion into usable work. The unavailable energy is unavailable for work because of the disorder or entropy of the system. Thus,  $G = H - TS$ . For changes in free energy at constant  $T$  and  $P$ , the equation can be written as  $\Delta G = \Delta H - T\Delta S$ . This is an important equation for chemical and physical reactions, for these reactions only occur spontaneously with a decrease in free energy,  $G$ , of the total system of reactants and products.

where the superscript stands for standard state conditions (25°C or 298K and 1 atm).

The overall reactions given in Table 2-2 can be used to produce both electrical energy and heat. The maximum work available from a fuel source is related to the free energy of reaction in the case of a fuel cell, whereas the enthalpy (heat) of reaction is the pertinent quantity for a heat engine, i.e.,

$$\Delta G_r = \Delta H_r - T\Delta S_r \quad (2-25)$$

where the difference between  $\Delta G_r$  and  $\Delta H_r$  is proportional to the change in entropy ( $\Delta S_r$ ). This entropy change is manifested in changes in the degrees of freedom for the chemical system being considered. The maximum amount of electrical energy available is  $\Delta G_r$ , as mentioned above, and the total thermal energy available is  $\Delta H_r$ . The amount of heat that is produced by a fuel cell operating reversibly is  $T\Delta S_r$ . Reactions in fuel cells that have negative entropy change generate heat, while those with positive entropy change may extract heat from their surroundings, if the irreversible generation of heat is smaller than the reversible absorption of heat.

Differentiating Equation (2-25) with respect to temperature or pressure, and substituting into Equation (2-23), yields

$$\left(\frac{\partial E}{\partial T}\right)_p = \frac{\Delta S}{nF} \quad (2-26)$$

or

$$\left(\frac{\partial E}{\partial P}\right)_T = \frac{-\Delta \text{Volume}}{nF} \quad (2-27)$$

which are shown earlier in this section.

The reversible potential of a fuel cell at temperature T is calculated from  $\Delta G$  for the cell reaction at that temperature. This potential can be computed from the heat capacities ( $C_p$ ) of the species involved as a function of T and from values of both  $\Delta S^\circ$  and  $\Delta H^\circ$  at one particular temperature, usually 298K. Empirically, the heat capacity of a species, as a function of T, can be expressed as

$$C_p = a + bT + cT^2 \quad (2-28)$$



where a, b, and c are empirical constants. The difference in the heat capacities for the products and reactants involved in the stoichiometric reaction is given by

$$\Delta(C_p) = \Delta(a) + \Delta(bT) + \Delta(cT^2) \quad (2-29)$$

Because

$$\Delta H_T = \Delta H^\circ + \int_{298}^T \Delta C_p dT \quad (2-30)$$

and, at constant pressure

$$\Delta S_T = \Delta S^\circ + \int_{298}^T \frac{\Delta C_p}{T} dT \quad (2-31)$$

then it follows that

$$\Delta H_T = \Delta H^\circ + \Delta a(T - 298) + 1/2 \Delta b(T^2 - 298^2) + 1/3 \Delta c(T^3 - 298^3) \quad (2-32)$$

and

$$\Delta S_T = \Delta S^\circ + \Delta a \ln \left( \frac{T}{298} \right) + \Delta b(T - 298) + 1/2 \Delta c(T^2 - 298^2) \quad (2-33)$$

The coefficients a, b, and c (see Table 10-3), as well as  $\Delta S^\circ$  and  $\Delta H^\circ$ , are available from standard reference tables, and may be used to calculate  $\Delta H_T$  and  $\Delta S_T$ . From these values it is then possible to calculate  $\Delta G_T$  and E.

Instead of using the coefficients a, b, and c, it is modern practice to rely on tables, such as JANAF Thermochemical Tables (4) to provide  $C_p$ ,  $\Delta H_T$ ,  $\Delta S_T$ , and  $\Delta G_T$  for a range of temperatures of various reactants and products.

For the general cell reaction,



the free energy change can be expressed by the equation:

$$\Delta G = \Delta G^\circ + RT \ln \frac{[C]^c [D]^\delta}{[A]^\alpha [B]^\beta} \quad (2-35)$$

When Equations (2-23) and (2-24) are substituted in Equation (2-35),

$$E = E^\circ + \frac{RT}{nF} \ln \frac{[A]^\alpha [B]^\beta}{[C]^c [D]^\delta} \quad (2-36)$$

or

$$E = E^\circ + \frac{RT}{nF} \ln \frac{\prod [\text{reactant activity}]}{\prod [\text{product activity}]} \quad (2-37)$$

which is the general form of the Nernst equation. For the overall cell reaction, the cell potential increases with an increase in the activity (concentration) of reactants and a decrease in the activity of products. Changes in temperature also influence the reversible cell potential, and the dependence of potential on temperature varies with the cell reaction. Figure 2-1 illustrates the change in the reversible standard potential for the reaction:



The Nernst equations for this reaction, as well as for CO and CH<sub>4</sub> reacting with O<sub>2</sub>, that can occur in various fuel cells, are listed in Table 2-2.

## 2.2.4 Polarization: Activation (Tafel) and Concentration

To determine actual cell performance, three losses must be deducted from the Nernst potential: activation polarization, ohmic polarization, and concentration polarization. Definition of the ohmic polarization is simply the product of cell current and cell resistance. Both activation polarization and concentration polarization required additional description for basic understanding.

**Activation Polarization:** It is customary to express the voltage drop due to activation polarization by a semi-empirical equation, called the Tafel equation (2). The equation for activation polarization is shown by Equation (2-38):

$$\eta_{\text{act}} = \frac{RT}{\alpha n F} \ln \frac{i}{i_0} \quad (2-1)$$

where  $\alpha$  is the electron transfer coefficient of the reaction at the electrode being addressed, and  $i_0$  is the exchange current density. Tafel plots provide a visual understanding of the activation polarization of a fuel cell. They are used to measure the exchange current density [given by the extrapolated intercept at  $\eta_{\text{act}} = 0$  which is a measure of the maximum current that can be extracted at negligible polarization (5)] and the transfer coefficient (from the slope).

The usual form of the Tafel equation that can be easily expressed by a Tafel Plot is

$$\eta_{\text{act}} = a + b \log i \quad (2-39)$$

where  $a = (-2.3RT/\alpha nF) \log i_0$  and  $b = 2.3RT/\alpha nF$ . The term  $b$  is called the Tafel slope, and is obtained from the slope of a plot of  $\eta_{\text{act}}$  as a function of  $\log i$ . The Tafel slope for an electrochemical reaction is about 100 mV/decade (log current density) at room temperature. Thus, a tenfold increase in current density causes a 100 mV increase in the activation polarization. Conversely, if the Tafel slope is only 50 mV/decade, then the same increase in current density produces a 50 mV increase in activation polarization. Clearly, there exists a strong incentive to develop electrocatalysts that yield a lower Tafel slope for electrochemical reactions.

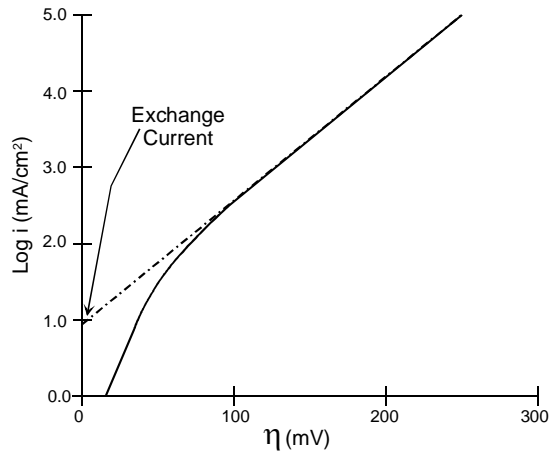


**Figure 2-8 Example of a Tafel Plot**

The simplified description presented here did not consider the processes that give rise to activation polarization, except for attributing it to sluggish electrode kinetics. A detailed discussion of the subject is outside the scope of this presentation, but processes involving absorption of reactant species, transfer of electrons across the double layer, desorption of product species, and the nature of the electrode surface can all contribute to activation polarization.

**Concentration Polarization:** The rate of mass transport to an electrode surface in many cases can be described by Fick's first law of diffusion:

$$i = \frac{nFD(C_B - C_S)}{\delta} \quad (2-40)$$

where  $D$  is the diffusion coefficient of the reacting species,  $C_B$  is its bulk concentration,  $C_S$  is its surface concentration, and  $\delta$  is the thickness of the diffusion layer. The limiting current ( $i_L$ ) is a measure of the maximum rate at which a reactant can be supplied to an electrode, and occurs when  $C_S = 0$ , i.e.,

$$i_L = \frac{nFD C_B}{\delta} \quad (2-41)$$

By appropriate manipulation of Equations (2-40) and (2-41),

$$\frac{C_S}{C_B} = 1 - \frac{i}{i_L} \quad (2-42)$$

The Nernst equation for the reactant species at equilibrium conditions, or when no current is flowing, is

$$E_{i=0} = E^\circ + \frac{RT}{nF} \ln C_B \quad (2-43)$$

When current is flowing, the surface concentration becomes less than the bulk concentration, and the Nernst equation becomes

$$E = E^\circ + \frac{RT}{nF} \ln C_S \quad (2-44)$$

The potential difference ( $\Delta E$ ) produced by a concentration change at the electrode is called the concentration polarization:

$$\Delta E = \eta_{\text{conc}} = \frac{RT}{nF} \ln \frac{C_S}{C_B} \quad (2-45)$$

Upon substituting Equations (2-42) in (2-45), the concentration polarization is given by the equation

$$\eta_{\text{conc}} = \frac{RT}{nF} \ln \left( 1 - \frac{i}{i_L} \right) \quad (2-46)$$

In this analysis of concentration polarization, the activation polarization is assumed to be negligible. The charge transfer reaction has such a high exchange current density that the activation polarization is negligible in comparison with the concentration polarization (most appropriate for the high temperature cells).

## 2.3 References

1. P.W. Atkins, "Physical Chemistry," 3<sup>rd</sup> Edition, W.H. Freeman and Company, New York, NY, 1986.
2. S.N. Simons, R.B. King and P.R. Prokopius, in *Symposium Proceedings Fuel Cells Technology Status and Applications*, Figure 1, p. 46, Edited by E.H. Camara, Institute of Gas Technology, Chicago, IL, 45, 1982.
3. E.J. Cairns and H.A. Liebhafsky, *Energy Conversion*, p. 9, 63, 1969.
4. M.W. Chase, et al., "JANAF Thermochemical Tables," Third Edition, American Chemical Society and the American Institute of Physics for the National Bureau of Standards (now National Institute of Standards and Technology), 1985.
5. "Fuel Cell Handbook," J. Appleby and F. Foulkes, Texas A&M University, Van Nostrand Reinhold, New York (out of print), republished by Krieger Publishing Co., Melbourne, FL, 1989.
6. W. Stanley Angrist, "Direct Energy Conversion," Third Edition, Allyn and Bacon, Inc. Boston, MA, date of publication unknown.

---

## 3. POLYMER ELECTROLYTE FUEL CELL

---

Polymer electrolyte fuel cells (PEFC) deliver high power density, which offers low weight, cost, and volume. The immobilized electrolyte membrane simplifies sealing in the production process, reduces corrosion, and provides for longer cell and stack life. PEFCs operate at low temperature, allowing for faster startups and immediate response to changes in the demand for power. The PEFC system is seen as the system of choice for vehicular power applications, but is also being developed for smaller scale stationary power. For more detailed technical information, there are excellent overviews of the PEFC (1, 2).

### 3.1 Cell Components

The use of organic cation exchange membrane polymers in fuel cells was originally conceived by William T. Grubbs (3) in 1959. The desired function of the ion membrane was to provide an ion conductive gas barrier. Strong acids were used to provide a contact between the adjacent membrane and catalytic surfaces. During further development, it was recognized that the cell functioned well without adding acid. As a result, present PEFCs do not use any electrolyte other than the hydrated membrane itself (4). The basic cell consists of a proton conducting membrane, such as a perfluorinated sulfonic acid polymer, sandwiched between two platinum impregnated porous electrodes. The back of the electrodes is made hydrophobic by coating with an appropriate compound, such as Teflon<sup>®</sup>. This wet proof coating provides a path for gas diffusion to the catalyst layer.

The electrochemical reactions of the PEFC are similar to those of the PAFC: hydrogen at the anode provides a proton, freeing an electron in the process that must pass through an external circuit to reach the cathode. The proton, which remains solvated with a certain number of water molecules, diffuses through the membrane to the cathode to react with oxygen and the returning electron (5). Water is subsequently produced at the cathode.

Because of the intrinsic nature of the materials used, low-temperature operation of approximately 80°C is possible. The cell also is able to sustain operation at very high current densities. These attributes lead to a fast start capability and the ability to make a compact and lightweight cell (5). Other beneficial attributes of the cell include no corrosive fluid hazard and lower sensitivity to orientation. As a result, the PEFC is particularly suited for vehicular power application. Transportation applications mean that the fuel of choice will probably be methanol (6), although hydrogen storage on-board in the form of pressurized gas and the partial oxidation of gasoline (1) is being considered. The cell also is being considered for stationary power application, which will use natural gas or other hydrogen-rich gases.

The lower operating temperature of a PEFC results in both advantages and disadvantages. Low temperature operation is advantageous because the cell can start from ambient conditions quickly, especially when pure hydrogen fuel is available. It is a disadvantage in that platinum catalysts are required to promote the electrochemical reaction. Carbon monoxide (CO) binds strongly to platinum sites at temperatures below 150°C, which reduces the sites available for hydrogen chemisorption and electro-oxidation. Due to CO affecting the anode, only a few ppm of CO can be tolerated with the platinum catalysis at 80°C. Because reformed and shifted hydrocarbons contain about one percent of CO, a mechanism to reduce the level of CO in the fuel gas is needed. The low temperature of operation also means that little if any heat is available from the fuel cell for any endothermic reforming process (2, 3).

Both temperature and pressure have a significant influence on cell performance; the impact of these parameters will be described later. Present cells operate at 80°C, nominally, 0.285 MPa (30 psig) (5), and a range of 0.10 to 1.0 MPa (10 to 100 psig). Using appropriate current collectors and supporting structure, polymer electrolyte fuel cells and electrolysis cells should be capable of operating at pressures up to 3000 psi and differential pressures up to 500 psi (4).

### **3.1.1 Water Management**

Water is produced not as steam, but as liquid in a PEFC. A critical requirement of these cells is maintaining a high water content in the electrolyte to ensure high ionic conductivity. The ionic conductivity of the electrolyte is higher when the membrane is fully saturated, and this offers a low resistance to current flow and increases overall efficiency. Water content in the cell is determined by the balance of water or its transport during the reactive mode of operation. Contributing factors to water transport are the water drag through the cell, back diffusion from the cathode, and the diffusion of any water in the fuel stream through the anode. Water transport is a function of cell current and the characteristics of the membrane and the electrodes. Water drag refers to the amount of water that is pulled by osmotic action along with the proton (5). Between 1 and 2.5 molecules are dragged with each proton (6). As a result, the ion exchanged can be envisioned as a hydrated proton,  $H(H_2O)_n^+$ . The water drag increases at high current density, and this makes the water balance a potential concern. During actual operation, however, back diffusion of water from the cathode to the anode through the thin membrane results in a net water transport of nearly zero (12, 7). Detailed modeling of the reactions and water balance is beyond the scope of this handbook; References (8) and (9) should be reviewed for specific modeling information.

Water management has a significant impact on cell performance, because at high current densities mass transport issues associated with water formation and distribution limit cell output. Without adequate water management, an imbalance will occur between water production and evaporation within the cell. Adverse effects include dilution of reactant gases by water vapor, flooding of the electrodes, and dehydration of the solid polymer membrane. The adherence of the membrane to the electrode also will be adversely affected if dehydration occurs. Intimate contact between the electrodes and the electrolyte membrane is important because there is no free liquid electrolyte to form a conducting bridge. If more water is exhausted than produced, then it is important to humidify the incoming anode gas. If there is too much humidification, however, the electrode floods, which causes problems with diffusing the gas to the electrode. A smaller current, larger reactant flow, lower humidity, higher temperature, or lower pressure will



result in a water deficit. A higher current, smaller reactant flow, higher humidity, lower temperature, or higher pressure will lead to a water surplus. There have been attempts to control the water in the cell by using external wicking connected to the membrane to either drain or supply water by capillary action. Another alternative is to control the cell water content by humidifying the incoming reactant gases (14). More reliable forms of water management also are being developed based on continuous flow field design and appropriate operating adjustments. A temperature rise can be used between the inlet and outlet of the flow field to increase the water vapor carrying capacity of the gas streams. At least one manufacturer, Ballard Power Systems of Canada, has demonstrated stack designs and automated systems that manage water balances successfully.

### **3.1.2 State-of-the-Art Components**

There has been an accelerated interest in polymer electrolyte fuel cells within the last few years, which has led to improvements in both cost and performance. Development has reached the point where motive power applications appear achievable at an acceptable cost for commercial markets. Noticeable accomplishments in the technology, which have been published, have been made at Ballard Power Systems. PEFC operation at ambient pressure has been validated for over 25,000 hours with a six-cell stack without forced air flow, humidification, or active cooling (17). Complete fuel cell systems have been demonstrated for a number of transportation applications including public transit buses and passenger automobiles. Recent development has focused on cost reduction and high volume manufacture for the catalyst, membranes, and bipolar plates. This coincides with ongoing research to increase power density, improve water management, operate at ambient conditions, tolerate reformed fuel, and extend stack life. In the descriptions that follow, Ballard Power Systems fuel cells are considered representative of the state-of-the-art.

Manufacturing details of the Ballard Power Systems cell and stack design are proprietary (18), but the literature provides some information on the cell and stack design. An example schematic of a manufacturer's cell is shown in Figure 3-1.

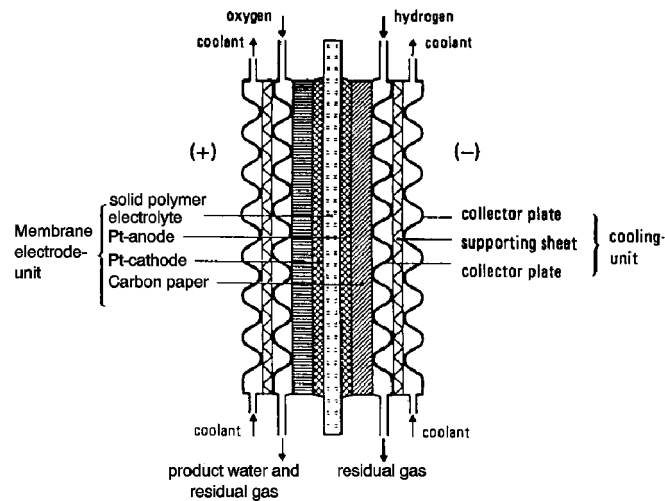


**Figure 3-1 PEFC Schematic (19)**

The standard electrolyte material presently used in PEFCs is a fully fluorinated Teflon-based material produced by E.I. DuPont de Nemours for space application in the mid-1960s. The DuPont electrolytes have the generic brand name Nafion<sup>®</sup>, and the specific type used most often in present PEFCs is membrane No. 117 (20). The Nafion membranes, which are fully fluorinated polymers, exhibit exceptionally high chemical and thermal stability and are stable against chemical attack in strong bases, strong oxidizing and reducing acids, H<sub>2</sub>O<sub>2</sub>, Cl<sub>2</sub>, H<sub>2</sub>, and O<sub>2</sub> at temperatures up to 125°C (21). Nafion consists of a fluoropolymer backbone, similar to Teflon, upon which sulfonic acid groups are chemically bonded (22). DuPont fluorinated electrolytes exhibited a substantial improvement in life over previous electrolytes and have achieved over 50,000 hours of operation. The Dow Chemical Company has produced an electrolyte membrane, the XUS 13204.10, which exhibits lower electrical resistance and permits higher current densities than the Nafion membrane, particularly when used in thinner form (18). These membranes exhibit good performance and stability, but their current price is deemed too high for transportation markets. This has led to ongoing research into alternative materials.

The present electrodes are cast as thin films and bonded to the membrane. Low platinum loading electrodes ( $\leq 0.60$  mg Pt/cm<sup>2</sup> cathode and  $\leq 0.25$  mg Pt/cm<sup>2</sup>, 0.12 mg Ru/cm<sup>2</sup> anode) tested in the Ballard Mark V stack have performed as well as current high platinum loading electrodes (4.0 to 8.0 mg Pt/cm<sup>2</sup>). These electrodes, which have been produced using a high-volume manufacturing process, have achieved 600 mA/cm<sup>2</sup> at 0.7 V. The equivalent platinum loading of these electrodes is 1.5 g Pt/kW (23). To improve utilization of the platinum, a soluble form of the polymer is incorporated into the porosity of the carbon support structure. This increases the interface between the electrocatalyst and the solid polymer electrolyte. Two methods are used to incorporate the polymer solution within the catalyst. In Type A, the polymer is introduced after fabrication of the electrode; in Type B, it is introduced before fabrication. Performance of low platinum loading electrodes (Type B) is shown in Figure 3-2.

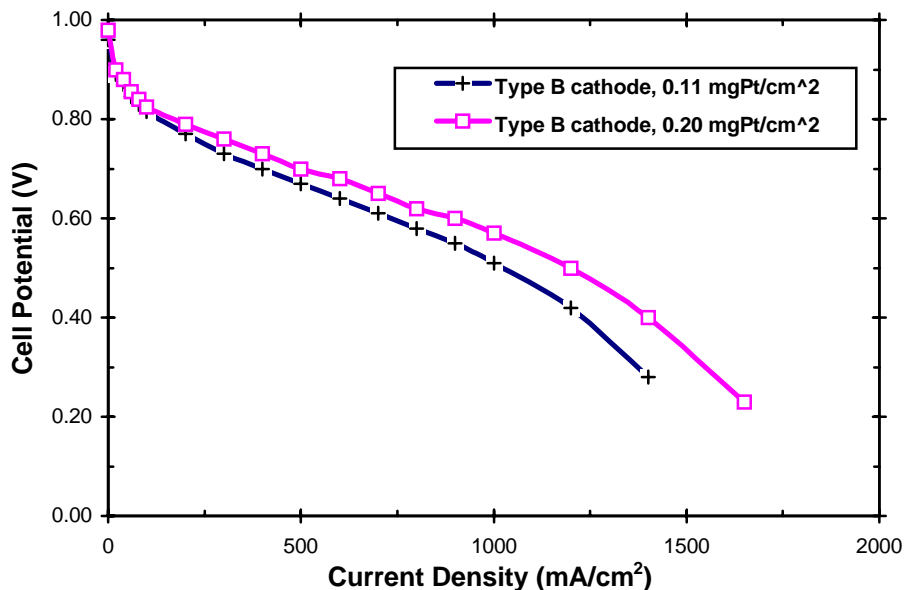


**Figure 3-2 Performance of Low Platinum Loading Electrodes (23)**

Most PEFCs currently use machined graphite plates for current collection and distribution, gas distribution, and thermal management. Cooling is accomplished by using a heat transfer fluid, usually water, which is pumped through integrated coolers within the stack. The temperature rise across the cell is kept to less than 10°C. Water-cooling and humidification are in series, which results in a need for high quality water. The cooling unit of a cell can be integrated to supply reactants to the membrane electrode assembly (MEA), remove reaction products from the cell, and seal off the various media against each other and the outside (Figure 3-1). The conducting parts of the frames are titanium; non-conducting parts are polysulfone (24).

The primary contaminants of a PEFC are carbon monoxide (CO), carbon dioxide (CO<sub>2</sub>), and the hydrocarbon fuel. Reformed hydrocarbon fuels typically contain at least 1% CO. Even small amounts of CO in the gas stream, however, will preferentially adsorb on the platinum catalyst surface and block access of the hydrogen to the catalyst sites. Tests indicate that approximately 10 ppm of CO in the gas stream begins to impact cell performance (6, 25). Fuel processing can reduce CO content to several ppm, but there are system costs associated with increased fuel purification. Platinum/ruthenium catalysts that have intrinsic tolerance to CO are being developed. These electrodes have been shown in controlled laboratory experiments to be CO tolerant up to 200 ppm (26). Although much less significant than CO poisoning, CO<sub>2</sub> affects anode performance through the reaction of CO<sub>2</sub> with adsorbed hydrides on platinum. This reaction is the electrochemical equivalent of the water gas shift reaction.

A number of system approaches can be used to clean up the fuel feed. These include pressure swing adsorption, membrane separation, methanation, and selective oxidation. Although selective oxidation does not remove CO<sub>2</sub>, it is usually the preferred method for CO removal because of the parasitic system loads and energy required by the other methods. In selective

oxidation, the reformed fuel is mixed with air or oxygen either before the fuel is fed into the cell or within the stack itself. Current selective oxidation technology can reduce CO levels to <10 ppm, but this is difficult to maintain under actual operating conditions (26). Another approach involves the use of a selective oxidation catalyst that is placed between the fuel stream inlet and the anode catalyst. Introducing an air bleed to the fuel stream, however, appears to be the most effective way to reduce CO to an acceptable level. Work is continuing to find approaches and materials that are more tolerant of impurities in the fuel feed.

A number of technical and cost issues facing polymer electrolyte fuel cells at the present stage of development have been recognized by managers and researchers (6, 27, 28, 29). These issues concern the cell membrane, cathode performance, and cell heating limits.

The membranes used in the present cells are expensive and available only in limited ranges of thickness and specific ionic conductivity. There is a need to lower the cost of the present membranes and to investigate lower cost membranes that exhibit low resistivity. This is particularly important for transportation applications where high current density operation is needed. Cheaper membranes promote lower cost PEFCs and thinner membranes with lower resistivities could contribute to power density improvement (29). It is estimated that the cost of current membranes could fall (by one order of magnitude) if the market increased significantly (by two orders of magnitude) (22).

There is some question of whether higher utilization of the catalyst is needed even though new research has resulted in the loading being reduced to less than 1 mg/cm<sup>2</sup>. Some researchers cite a need for higher utilization of catalysts, while others state that because only 10% of the cell materials cost is tied up in catalyst, it is better to concentrate on the design of an effective membrane and electrode assembly at this time (27).

Improved performance of the cathode when operating on air at high current densities is needed. At higher current densities, there is a limiting gas permeability and/or ionic conductivity within the catalyst layer. A nitrogen blanket forming on the gas supply side of the cathode is suspected of creating additional limitations (6). There is a need to develop a cathode that lessens the impact of the nitrogen blanket, increases the pressurization of the cell, or increases the ionic conductivity of the cathode catalyst.

Local heating problems limit stack operation with air to a current density of approximately 2 A/cm<sup>2</sup>. Single cells have shown the capability to operate at higher current densities on pure oxygen. It may be possible to increase current density and power density with better cooling.

### **3.1.3 Development Components**

The primary focus of ongoing research is to improve the performance of the cell and lower its cost. The principal areas of development are improving cell membranes, handling the CO in the fuel stream, and refining electrode design. There has been an effort to incorporate system requirements into the fuel cell stack in order to simplify the overall system. This work has included a move toward operation with zero humidification at ambient pressure and direct fuel use.

The Dow Chemical Company has developed the XUS 13204.10 membrane, which has been reported to achieve higher performance than that obtained with Nafion membranes (Figure 3-3). The Dow membrane, also a perfluorinated sulfonic acid, has a lower equivalent weight than Nafion and is prepared with shorter anion-anion distances. Because of these characteristics, the membrane has a slight increase in conductivity and water retention capability. Most of the improvement in performance can be attributed to the Dow membrane being supplied at a thickness of 2 mils, while the Nafion membrane is supplied at 7 mils thickness. DuPont is now producing a membrane of 2 mils thickness that achieves the same performance as the top curve in Figure 3-3 (30). Both the Nafion 117 and the Dow XUS 13204.10 membranes are, at present, expensive and available only in limited ranges of thickness and specific ionic conductivity. There is ongoing work to investigate alternative membranes that not only exhibit durability and high performance, but also can be manufactured inexpensively at high volume. Work at Ballard Advanced Materials Corporation has concentrated on developing low-cost membranes using trifluorostyrene and substituted trifluorostyrene copolymeric compositions (17).

Cells were originally made with an unimpregnated electrode/Nafion electrolyte interface. This was later replaced by a method where the proton conductor was impregnated into the active layer of the electrode. This allowed reduced loading to  $0.4 \text{ mg/cm}^2$  while obtaining high power density (16). The standard "Prototech" electrodes contained 10% Pt on carbon supports. Using higher surface area carbon supported catalysts, researchers have tested electrodes with even lower platinum loading, but having performance comparable to conventional electrodes. Los Alamos National Laboratory has tested a cathode with a  $0.12 \text{ mg Pt/cm}^2$  loading, and Texas A&M University has tested a cathode with a  $0.05 \text{ mg Pt/cm}^2$  loading. PSI Technology has developed its own fabrication method that has achieved platinum loading also as low as  $0.05 \text{ mg/cm}^2$  (22). These laboratory scale tests have used electrodes produced manually. Work continues to develop high-volume manufacturing techniques.

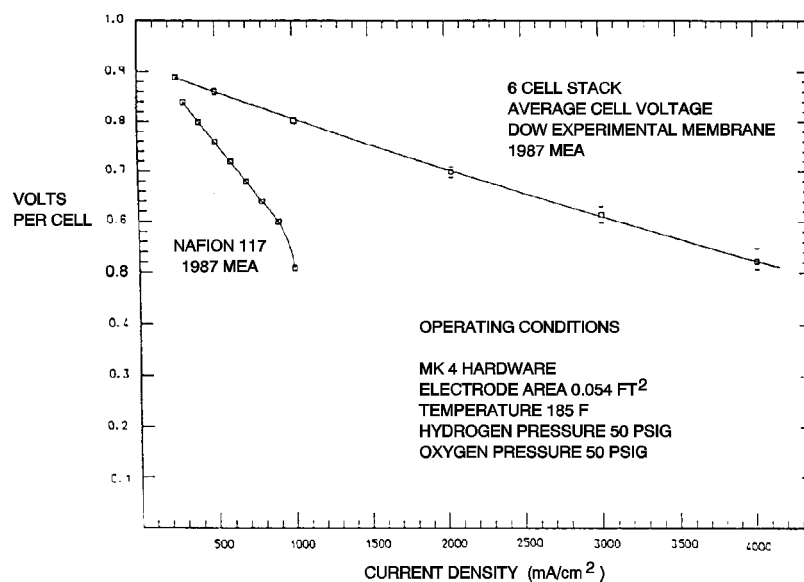


**Figure 3-3 Multi-Cell Stack Performance on Dow Membrane (31)**

Another approach has been developed to fabricate electrodes with loading as low as  $0.1 \text{ mg Pt/cm}^2$  (32). The electrode structure was improved by increasing the contact area between the electrolyte and the platinum clusters. The advantages of this approach are that a thinner catalyst layer of 2 to 3 microns and a uniform mix of catalyst and ionomer are produced. For example, a cell with a Pt loading of  $0.17$  to  $0.13 \text{ mg/cm}^2$  has been fabricated. The cell generated  $3 \text{ A/cm}^2$  at  $> 0.4 \text{ V}$  on pressurized  $\text{O}_2$  and  $0.65 \text{ V}$  at  $1 \text{ A/cm}^2$  on pressurized air (32, 33).

Stable performance was demonstrated to 4,000 hours with Nafion membrane cells having  $0.13 \text{ mg Pt/cm}^2$  and cell conditions of 2.4/5.1 atmospheres,  $\text{H}_2/\text{air}$ , and  $80^\circ\text{C}$  (4000 hour performance was  $0.5 \text{ V}$  at  $600 \text{ mA/cm}^2$ ). These results mean that the previous problem of water management is not severe, particularly after thinner membranes of somewhat lower equivalent weight have become available. Some losses may be caused by slow anode catalyst deactivation, but it has been concluded that the platinum catalyst "ripening" phenomenon does not contribute significantly to the long-term performance losses observed in PEFCs (5).

Research also has focused on developing low-cost, lightweight graphite materials that can be used in place of expensive high purity graphite bipolar plates. Conductive plastics and plated metals, such as aluminum and stainless steel, also are under consideration for this application, but these materials are typically inferior to graphite plates because of contact resistance and durability concerns (17). Stack operation has demonstrated the capability to decrease CO in a methanol reformed gas (anode fuel supply stream) from 1% to approximately 10 ppm by a selective oxidation process based on a platinum/alumina catalyst. But the performance of the anode catalyst, though satisfactory, is impacted even by this low amount of CO. Research at Los Alamos National Laboratory has demonstrated an approach to remedy this problem by bleeding a small amount of air or oxygen into the anode compartment. Figure 3-4 shows that performance equivalent to that obtained on pure hydrogen can be achieved with this approach. It is assumed that this approach also would apply to a reformed natural gas fuel that incorporates water gas shift to obtain CO levels of 1% into the fuel cell. This approach results in a loss of fuel, which should not exceed 4%, provided that the reformed fuel gas can be limited to 1% CO (6). Another approach is to develop a CO tolerant anode catalyst such as the platinum/ruthenium electrodes currently under consideration. Platinum/ruthenium anodes have allowed the cells to operate, with a low level air bleed, for over 3,000 continuous hours on reformat fuel containing 10 ppm CO (23).

There is considerable interest in extending PEFC technology to the direct methanol and formaldehyde electro-oxidation (34, 35). This requires Pt-based bi-metallic catalysts. Tests have been conducted with gas diffusion type Vulcan XC-72/Toray support electrodes with Pt/Sn ( $0.5 \text{ mg/cm}^2$ , 8% Sn) and Pt/Ru ( $0.5 \text{ mg/cm}^2$ , 50% Ru). The electrodes have Teflon content of 20% in the catalyst layer.

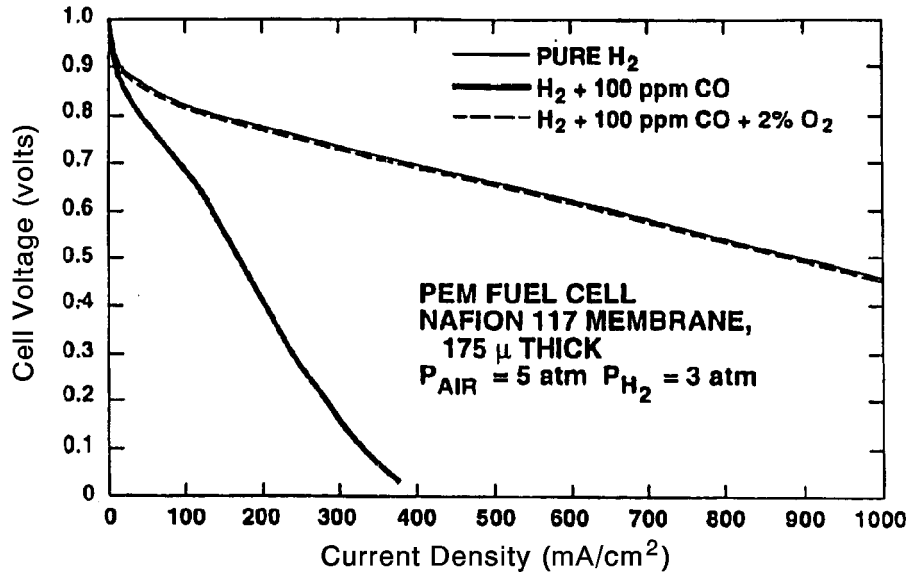
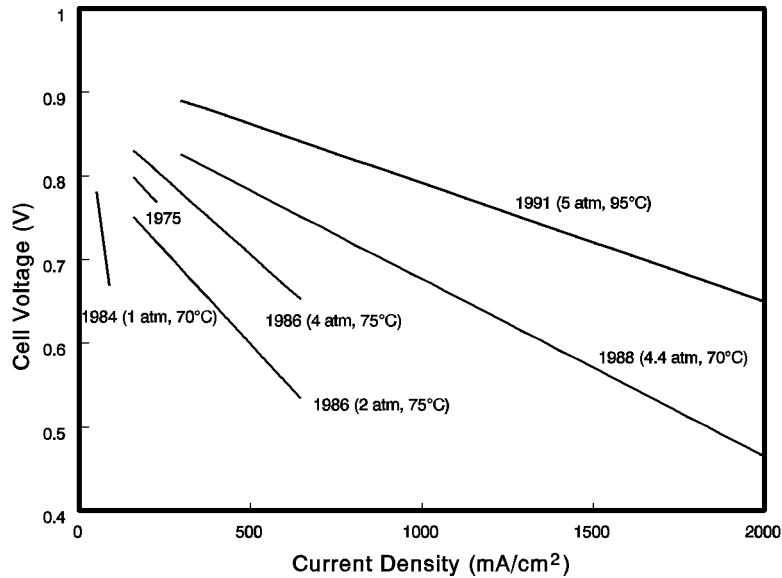


Figure 3-4 Effect on PEFC Performances of Bleeding Oxygen into the Anode Compartment (5)

### 3.2 Performance

A summary of the performance levels achieved with PEFCs since the mid-1960s is presented in Figure 3-5. Because of the changes in operating conditions involving pressure, temperature, reactant gases, and other parameters, a wide range of performance levels can be obtained. The performance of the PEFC in the U.S. Gemini Space Program was 37 mA/cm<sup>2</sup> at 0.78 V in a 32-cell stack that typically operated at 50°C and 2 atmospheres (1). Current technology yields performance levels that are vastly superior. Results from Los Alamos National Laboratory show that a performance of 0.78 V at about 200 mA/cm<sup>2</sup> (3 atmospheres H<sub>2</sub> and 5 atmospheres air) can be obtained at 80°C in PEFCs containing a Nafion membrane and electrodes with a platinum loading of 0.4 mg/cm<sup>2</sup>. Further details on PEFC performance developments with Nafion membranes are presented by Watkins et al. (36).



**Figure 3-5 Evolutionary Changes in PEFCs Performance [(a) H<sub>2</sub>/O<sub>2</sub>, (b) Reformate Fuel/Air, (c) H<sub>2</sub>/Air] [14, 37, 38]**

Operating temperature has a significant influence on PEFC performance. An increase in temperature lowers the internal resistance of the cell, mainly by decreasing the ohmic resistance of the electrolyte. In addition, mass transport limitations are reduced at higher temperatures. The overall result is an improvement in cell performance. Experimental data (39, 40) suggest a voltage gain in the range of 1.1 mV to 2.5 mV for each degree (°C) of temperature increase. Operating at higher temperatures also reduces the chemisorption of CO because this reaction is exothermic. Improving the cell performance through an increase in temperature, however, is limited by the high vapor pressure of water in the ion exchange membrane. This is due to the membrane's susceptibility to dehydration and the subsequent loss of ionic conductivity.

Operating pressure also impacts cell performance. The influence of oxygen pressure on the performance of a PEFC at 93°C is illustrated in Figure 3-6 (42). An increase in the oxygen pressure from 30 to 135 psig (3 to 10.2 atmospheres) produces an increase of 42 mV in the cell voltage at 215 mA/cm<sup>2</sup>. According to the Nernst equation, the increase in the reversible cathode potential that is expected for this increase in oxygen pressure is about 12 mV, which is considerably less than the measured value. When the temperature of the cell is increased to 104°C, the cell voltage increases by 0.054 V for the same increase in oxygen pressure. Additional data suggest an even greater pressure effect. A PEFC at 50°C and 500 mA/cm<sup>2</sup> (41) exhibited a voltage gain of 83 mV for an increase in pressure from 1 to 5 atmospheres. Another PEFC at 80°C and 431 mA/cm<sup>2</sup> (38) showed a voltage gain of 22 mV for a small pressure increase from 2.4 to 3.4 atmospheres. These results demonstrate that an increase in the pressure of oxygen results in a significant reduction in polarization at the cathode. Performance improvements due to increased pressure must be balanced against the energy required to pressurize the reactant gases. The overall system must be optimized according to output, efficiency, cost, and size. Operating at pressure above ambient conditions would most likely be reserved for stationary power applications.



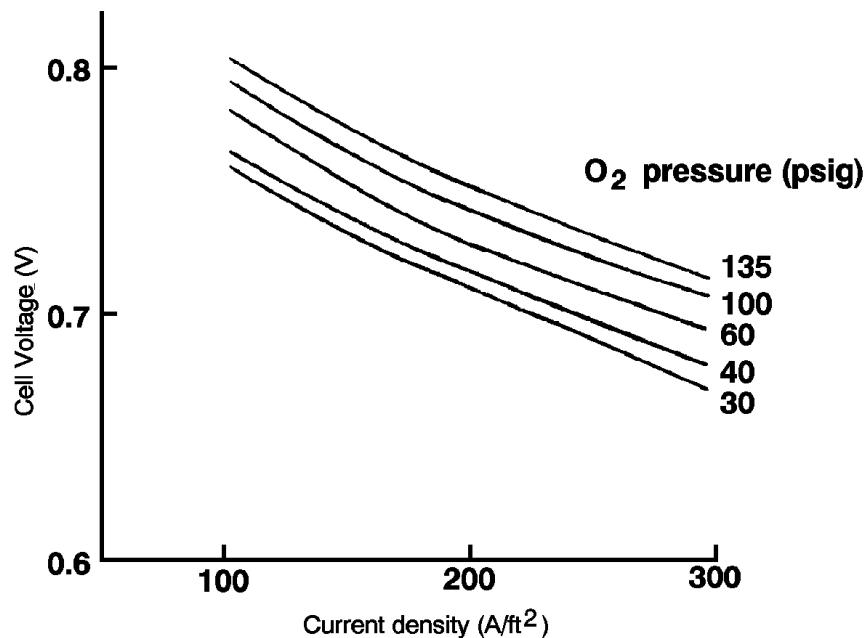


**Figure 3-6 Influence of O<sub>2</sub> Pressure on PEFCs Performance (93°C, Electrode Loadings of 2 mg/cm<sup>2</sup> Pt, H<sub>2</sub> Fuel at 3 Atmospheres) [(42) Figure 29, p. 49]**

Lifetime performance degradation is a key performance parameter in a fuel cell system, but the causes of this degradation are not fully understood. The sources of voltage decay are kinetic or activation loss, ohmic or resistive loss, loss of mass transport, or loss of reformate tolerance (17).

Currently, the major focus of R&D on PEFC technology is to develop a fuel cell system for terrestrial transportation applications, which requires the development of low-cost cell components. Reformed methanol is expected to be a major fuel source for PEFCs in transportation applications. Because the operating temperature of PEFCs is much lower than that of PAFCs, poisoning of the anode electrocatalyst by CO from steam reformed methanol is a concern. The performance achieved with a proprietary anode in a PEFC with four different concentrations of CO in the fuel gas are shown in Figure 3-7. The graph also shows that at higher current densities, the poisoning effect of CO is increased. At these higher current densities, the presence of CO in the fuel causes the cell voltage to become unstable and cycle over a wide range. Additional data (43) have suggested that the CO tolerance of a platinum electrocatalyst can be enhanced by increasing either the temperature or the pressure. As mentioned in Section 3.1.3, developers have designed systems to operate with reformed fuels containing CO, but these system "fixes" reduce efficiency.

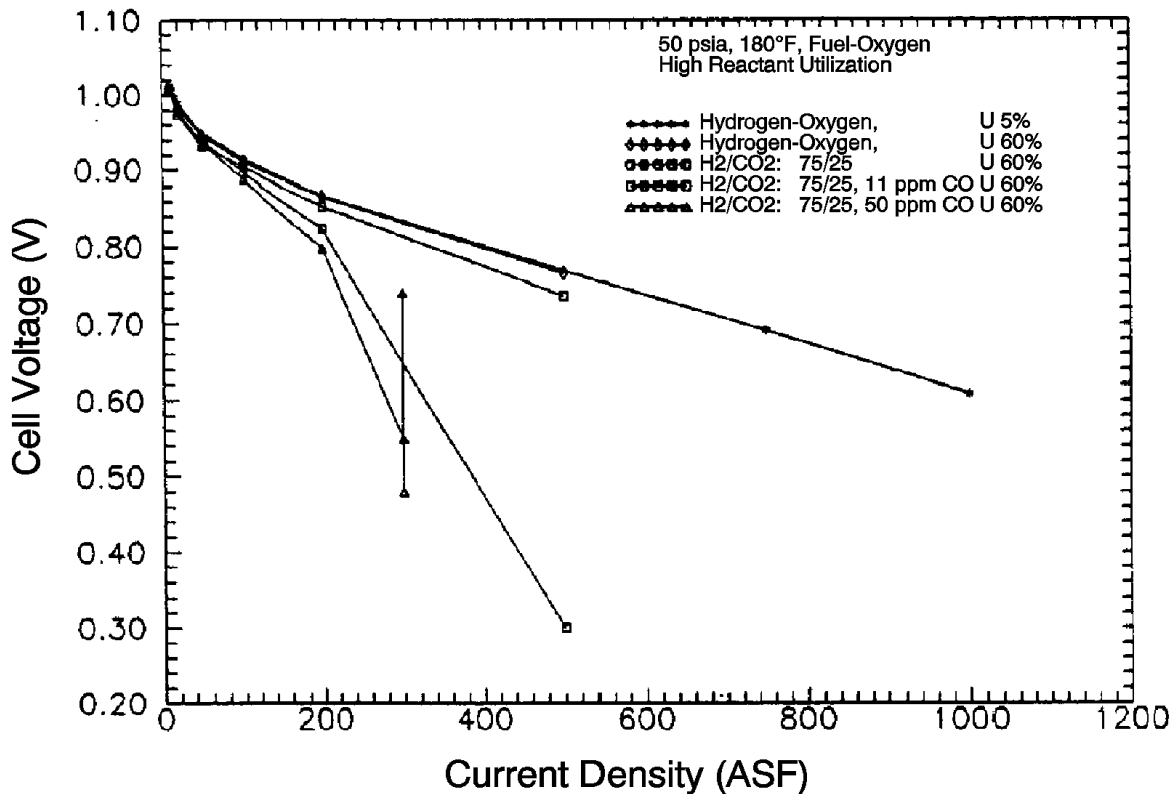


Figure 3-7 Cell Performance with Carbon Monoxide in Reformed Fuel (44)

### 3.3 Direct Methanol Proton Exchange Fuel Cell

The large potential market for fuel cell vehicle applications has generated a strong interest in a fuel cell that can run directly on methanol. Operation on liquid fuel would assist in rapid introduction of fuel cell technology into commercial markets, because it would greatly simplify the on-board system as well as reduce the infrastructure needed to supply fuel to passenger cars and commercial fleets. Performance levels achieved with a direct methanol PEFC using air are now in the range of 180 mA/cm<sup>2</sup> to 250 mA/cm<sup>2</sup> (17). Problems with methanol crossover and high overpotentials still inhibit performance. Research has focused on finding more advanced electrolyte materials to combat fuel crossover and more active anode catalysts to promote methanol oxidation. Significant progress has been made over the past few years in both of these key areas.

Improvements in solid polymer electrolyte materials have extended the operating temperatures of direct methanol PEFCs from 60°C to almost 100°C. Electrocatalyst developments have focused on materials that have higher intrinsic activity. Researchers at the University of Newcastle upon Tyne have reported over 200 mA/cm<sup>2</sup> at 0.3 V at 80°C with platinum/ruthenium electrodes having platinum loading of 3.0 mg/cm<sup>2</sup>. The Jet Propulsion Laboratory in the U.S. has reported over 100 mA/cm<sup>2</sup> at 0.4 V at 60°C with platinum loading of 0.5 mg/cm<sup>2</sup>. Recent work at Johnson Matthey has clearly shown that platinum/ruthenium materials possess substantially higher intrinsic activity than platinum alone (45).

All fuel cells exhibit kinetic losses that cause the electrode reactions to deviate from their theoretical ideal. This is particularly true for a direct methanol PEFC. Eliminating the need for a fuel reformer, however, makes methanol and air PEFCs an attractive alternative to PEFCs that require pure hydrogen as a fuel. The minimum performance goal for direct methanol PEFC commercialization is approximately 200 mW/cm<sup>2</sup> at 0.5 to 0.6 V.

Figure 3-8 summarizes the performance recently achieved by developers.

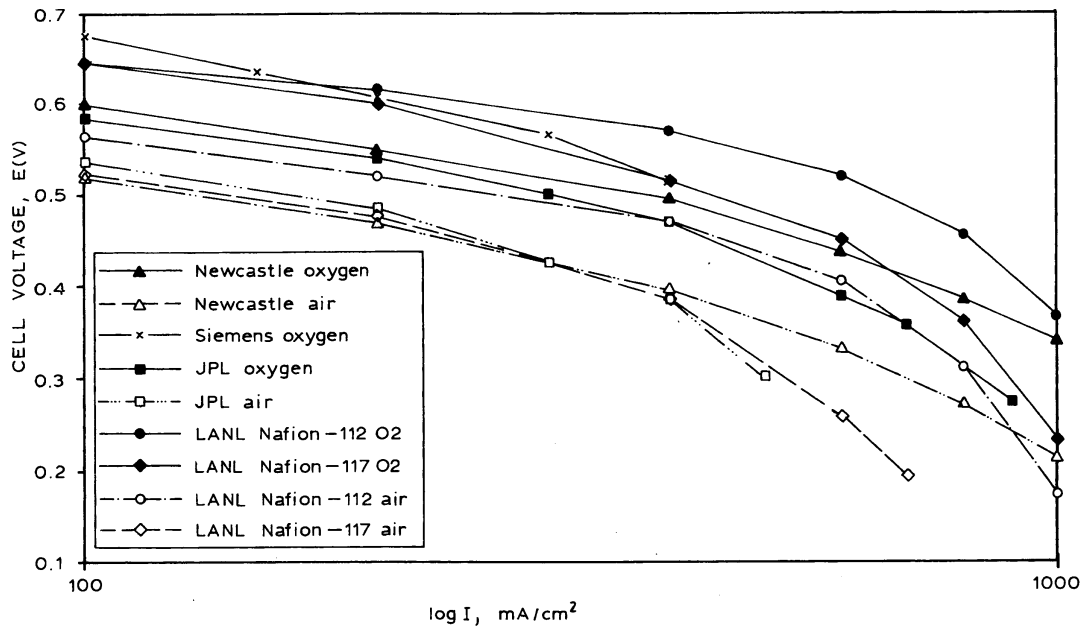


**Figure 3-8 Single Cell Direct Methanol Fuel Cell Data (45)**

### 3.4 References

1. A.J. Appleby, E.B. Yeager, *Energy*, pg. 11, 137, 1986.
2. S. Gottesfeld, T. Zawodzinski, PEFC Chapter in Advances in Electrochemical Science and Engineering, Volume 5, edited by R. Alkire, H. Gerischer, D. Kolb, C. Tobias, pp. 197-301, 1998.
3. W.T. Grubb, *Proceedings of the 11th Annual Battery Research and Development Conference*, PSC Publications Committee, Red Bank, NJ, p. 5, 1957; U.S. Patent No. 2,913,511, 1959.
4. H. Grune, *1992 Fuel Cell Seminar Program and Abstracts*, The Fuel Cell Seminar Organizing Committee, November 29 - December 2, 1992, Tucson, Arizona, p. 161, 1992.
5. J. C. Amphlett, M. Farahani, R. F. Mann, B. A. Peppley, P. R. Roberge, in *Proceedings of the 26th Intersociety Energy Conversion Engineering Conference*, August 4-9, 1991, Volume 3, Conversion Technologies/Electrochemical Conversion, American Nuclear Society, La Grange, Illinois, p. 624, 1991.
6. S. Gottesfeld, "Polymer Electrolyte Fuel Cells: Potential Transportation and Stationary Applications," No. 10, An EPRI/GRI Fuel Cell Workshop on Technology Research and Development, Stonehart Associates, Madison, Connecticut, 1993.
7. W. Teagan, J. Bentley, "Status: ADL/EPYX Fuel Processing Technology," joint DOE/EPRI/GRI Workshop on Fuel Cell Technology, San Francisco, CA, May 18-20, 1998.
8. M. Krumpelt, K. M. Myles, No. 8, An EPRI/GRI Fuel Cell Workshop on Technology Research and Development, April 13-14, 1993, Stonehart Associates, Madison, Connecticut, 1993.
9. M. Krumpelt, R. Kumar, J. Miller, C. Christianson, in *1992 Fuel Cell Seminar Program and Abstracts*, The Fuel Cell Seminar Organizing Committee, November 29 - December 2, 1992, Tucson, Arizona, p. 35, 1992.
10. T.G. Coker, A.B. LaConti, L.J. Nuttall, in *Proceedings of the Symposium on Membranes and Ionic and Electronic Conducting Polymers*, edited by E.G. Yeager, B. Schumm, K. Mauritz, K. Abbey, D. Blankenship, J. Akridge, The Electrochemical Society, Inc., Pennington, NJ, p. 191, 1983.
11. N. Giordano et al., in *Proceedings 26th Intersociety Energy Conversion Engineering Conference*, August 4-9, 1991, Volume 3, Conversion Technologies/Electrochemical Conversion, American Nuclear Society, La Grange, Illinois, p. 624, 1991.
12. T.A. Zawodzinski et al., *Journal of Electrochemical Society*, p. 140, 1042, 1993.
13. T.E. Springer et al., *Journal of Electrochemical Society*, p. 138, 2335, 1991.
14. D.M. Bernardi, *Journal of Electrochemical Society*, p. 137, 3344, 1990.
15. T.E. Springer, M. S. Wilson, S. Gottesfeld, "Modeling and Experimental Diagnostics in Polymer Electrolyte Fuel Cells," submitted to J. ElectroChem. Soc., LA-UR-93-1469 Los Alamos National Laboratory, New Mexico, 1993.
16. T.G. Coker, A.B. LaConti, L.J. Nuttall, in *Proceedings of the Symposium on Membranes and Ionic and Electronic Conducting Polymers*, edited by E.G. Yeager, B. Schumm, K. Mauritz, K. Abbey, D. Blankenship, J. Akridge, The Electrochemical Society, Inc., Pennington, NJ, p. 191, 1983.
17. D. Wilkinson, A. Steck, "General Progress in the Research of Solid Polymer Fuel Cell Technology at Ballard," *Proceedings of the Second International Symposium on New Materials for Fuel Cell and Modern Battery Systems*, Montreal, Quebec, Canada, July 6-10, 1997.
18. N.E. Vanderborgh, M.C. Kimble, J.R. Huff, J.C. Hedstrom, in *27th Intersociety Energy*

- Conversion Engineering Conference Proceedings*, Volume 3, Conversion Technologies/Electrochemical Conversions, San Diego, CA August 3-7, 1992, published by Society of Automotive Engineers, Inc., Warrendale, PA, 407, 1992.
19. K. Strasser, in *26th Intersociety Energy Conversion Engineering Conference Proceedings*, Volume 3, Conversion Technologies/Electrochemical Conversion, Boston, Massachusetts, August 4-9, 1991, published by Society of Automotive Engineers, Inc., Warrendale, PA, 1991.
  20. Ballard, J. of Power Sources, pp. 29 239-250, 1990.
  21. W.G.F. Grot, G.E. Munn, P.N. Walmsley, paper presented at the 141st National Meeting of the Electrochemical Society, Inc., Houston, TX, May 7-11, 1972; Abstract No. 154.
  22. T. Ralph, "Proton Exchange Membrane Fuel Cells: Progress in Cost Reduction of the Key Components," *Platinum Metals Review*, 41, pp. 102-113, 1997.
  23. T. Ralph, G. Hards, J. Keating, S. Campbell, D. Wilkinson, M. Davis, J. St. Pierre, M. Johnson, "Low Cost Electrodes for Proton Exchange Membrane Fuel Cells: Performance in Single Cells and Ballard Stacks," *J. Electrochemical Society*, Volume 144, No. 11, November 1997.
  24. V. Peinecke, K. Ledjeff, A. Heinzl, in *1992 Fuel Cell Seminar Program and Abstracts*, Tucson, Arizona, November 29 - December 2, 1992, sponsored by Fuel Cell Seminar Organizing Committee, p. 171, 1992.
  25. "Investigation of Design and Manufacturing Methods for Low-Cost Fabrication of High Efficiency, High Power Density PEM Fuel Cell Power Plant," prepared by International Fuel Cells, Final Report FCR-11320A, June 10, 1991.
  26. D. Wilkinson, D. Thompsett, "Materials and Approaches for CO and CO<sub>2</sub> Tolerance for Polymer Electrolyte Membrane Fuel Cells," *Proceedings of the Second International Symposium on New Materials for Fuel Cell and Modern Battery Systems*, pp. 266-285, (Montreal, Quebec, Canada, July 6-10, 1997).
  27. K. Sikairi, K. Tsurumi, S. Kawaguchi, M. Watanabe, P. Stonehart, in *1992 Fuel Cell Seminar Program and Abstracts*, Tucson, AZ, November 29 - December 2, 1992, sponsored by Fuel Cell Organizing Committee, p. 153, 1992.
  28. S. Srinivasan, O.A. Velez, A. Parthasarathy, A.C. Ferriera, S. Mukerjee, M. Wakizoe, Y.W. Rho, Y.T. Kho, A.J. Appleby, in *1992 Fuel Cell Seminar Program and Abstracts*, Tucson, Arizona November 29 - December 2, 1992, sponsored by Fuel Cell Organizing Committee, p. 619, 1992.
  29. F.N. Buchi, B. Gupta, M. Rouilly, P.C. Hauser, A. Chapiro, G.G. Scherer, in *27th Intersociety Energy Conversion Engineering Conference Proceedings*, Volume 3, Conversion Technologies/Electrochemical Conversions, San Diego, CA, August 3-7, 1992, published by Society of Automotive Engineers, Inc., Warrendale, PA, 419, 1992.
  30. T.A. Zawodzinski, T.A. Springer, F. Uribe, S. Gottesfeld, "Characterization of Polymer Electrolytes for Fuel Cell Applications," *Solid State Ionics* 60, pp. 199-211, North-Holland, 1993.
  31. K. Prater, "The Renaissance of the Solid Polymer Fuel Cell," Ballard Power Systems, Inc., *Journal of Power Sources*, p. 29, 1990.
  32. M.S. Wilson, T.E. Springer, T.A. Zawodzinski, S. Gottesfeld, in *26th Intersociety Energy Conversion Engineering Conference Proceedings*, Volume 3, Conversion Technologies/Electrochemical Conversion, Boston, Massachusetts, August 4-9, 1991, published by Society of Automotive Engineers, Inc., Warrendale, PA, 1991.

33. C. Derouin, T. Springer, F. Uribe, J. Valerio, M. Wilson, T. Zawodzinski, S. Gottesfeld, in *1992 Fuel Cell Seminar Program and Abstracts*, Tucson AZ, November 29 - December 2, 1992, sponsored by Fuel Cell Organizing Committee, p. 615, 1992.
34. P.D. Naylor, P.J. Mitchell, P.L. Adcock, in *1992 Fuel Cell Seminar Program and Abstracts*, Tucson, AZ, November 29 - December 2, 1992, sponsored by Fuel Cell Organizing Committee, 575, 1992.
35. S.R. Narayanan, E. Vamos, H. Frank, S. Surampudi, G. Halpert, in *1992 Fuel Cell Seminar Program and Abstracts*, Tucson, AZ, November 29 - December 2, 1992, sponsored by Fuel Cell Organizing Committee, p. 233, 1992.
36. D. Watkins, K. Dircks, E. Epp, A. Harkness, *Proceedings of the 32nd International Power Sources Symposium*, The Electrochemical Society, Inc., Pennington, NJ, p. 590, 1986.
37. J. R. Huff, "Status of Fuel Cell Technologies," *Fuel Cell Seminar Abstracts, Fuel Cell Seminar*, October 26-29, 1986, Tucson, AZ.
38. D. Watkins, K. Dircks, E. Epp, A. Harkness, *Proceedings of the 32nd International Power Sources Symposium*, The Electrochemical Society, Inc., Pennington, NJ, p. 590, 1986.
39. J.C. Amphlett, et al., "The Operation of a Solid Polymer Fuel Cell: A Parametric Model," Royal Military College of Canada.
40. K. Ledjeff, et al., "Low Cost Membrane Fuel Cell for Low Power Applications," Fraunhofer-Institute for Solar Energy Systems, *Program and Abstracts, 1992 Fuel Cell Seminar*.
41. J. Srmivason, et al., "High Energy Efficiency and High Power Density Proton Exchange Membrane Fuel Cells - Electrode Kinetics and Mass Transport," *Journal of Power Sources*, p. 36, 1991.
42. A. LaConti, G. Smarz, F. Sribnik, "New Membrane-Catalyst for Solid Polymer Electrolyte Systems," Final Report prepared by Electro-Chem Products, Hamilton Standard for Los Alamos National Laboratory under Contract No. 9-X53-D6272-1, 1986.
43. "Investigation of Design and Manufacturing Methods for Low-Cost Fabrication of High Efficiency, High Power Density PEM Fuel Cell Power Plant," IFC/LANL, Final Report FCR-11320A, 1991.
44. A. LaConti, G. Smarz, F. Sribnik, "New Membrane-Catalyst for Solid Polymer Electrolyte Systems," Final Report prepared by Electro-Chem Products, Hamilton Standard for Los Alamos National Laboratory under Contract No. 9-X53-D6272-1, 1986.
45. M. Hogarth, G. Hards, "Direct Methanol Fuel Cells: Technological Advances and Further Requirements," *Platinum Metals Review*, 40, pp. 150-159, 1996.

---

## 4. ALKALINE FUEL CELL

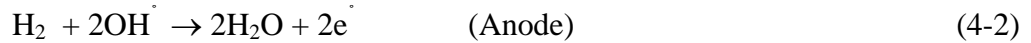
---

The Alkaline Fuel Cell (AFC) was one of the first modern fuel cells to be developed, beginning in 1960. The application at that time was to provide on-board electric power for the Apollo space vehicle. Desirable attributes of the AFC include its excellent performance on hydrogen ( $H_2$ ) and oxygen ( $O_2$ ) compared to other candidate fuel cells due to its active  $O_2$  electrode kinetics and its flexibility to use a wide range of electrocatalysts, an attribute which provides development flexibility.

The AFC fuel cell developed for space application was based, in large part, on work initiated by F.T. Bacon (1) in the 1930s. By 1952 construction and performance testing of a 5-kW alkaline fuel cell, operations on  $H_2$  and  $O_2$ , was completed. The fuel cell developed by Bacon operated at 200 to 240°C with 45% KOH, and the pressure was maintained at 40 to 55 atm to prevent the electrolyte from boiling. At these relatively high temperature and pressure operating conditions, performance of the Bacon cell was quite good (0.78 volts at 800 mA/cm<sup>2</sup>). The anode consisted of a dual-porosity Ni electrode (two layer structure with porous Ni of 16 . m maximum pore diameter on the electrolyte side and 30 . m pore diameter on the gas side), and the cathode consisted of a porous structure of lithiated NiO. The three phase boundary in the porous electrodes was maintained by a differential gas pressure across the electrode since a wetproofing agent was not available at that time, i.e., PTFE as a wetproofing material did not exist, and it would not be stable in the high temperature alkaline solution (2).

The kinetics of  $O_2$  reduction in alkaline electrolytes are more favorable than in  $H_3PO_4$ . Consider a Pt cathode (0.25 mg/cm<sup>2</sup>) in 30% KOH at 70°C and in 96%  $H_3PO_4$  at 165°C. The cathode potentials (vs RHE) at 100 mA/cm<sup>2</sup> in these two electrolytes are 0.868 and 0.730 mV, respectively, according to data reported by Appleby (Figure 2.15-1 in Reference 3). Various explanations have been advanced for the higher  $O_2$  reduction rates in alkaline electrolytes (4), these explanations are outside the scope of the present discussions. The practical consequence of the higher performance of Pt cathodes in alkaline electrolytes is that AFC's are capable of higher efficiencies than PAFC's at a given current density, or higher power densities at the same efficiency. It is estimated (2) that the efficiency of AFC's on pure  $H_2$  is about 60% and that of PAFC's is about 50%, based on the HHV of  $H_2$ .

Fig 4-1 is a schematic depicting the operating configuration of the alkaline fuel cell (Siemens). The half-cell reactions are:



Hydroxyl ions are the conducting species in the electrolyte and the net cell reaction is:

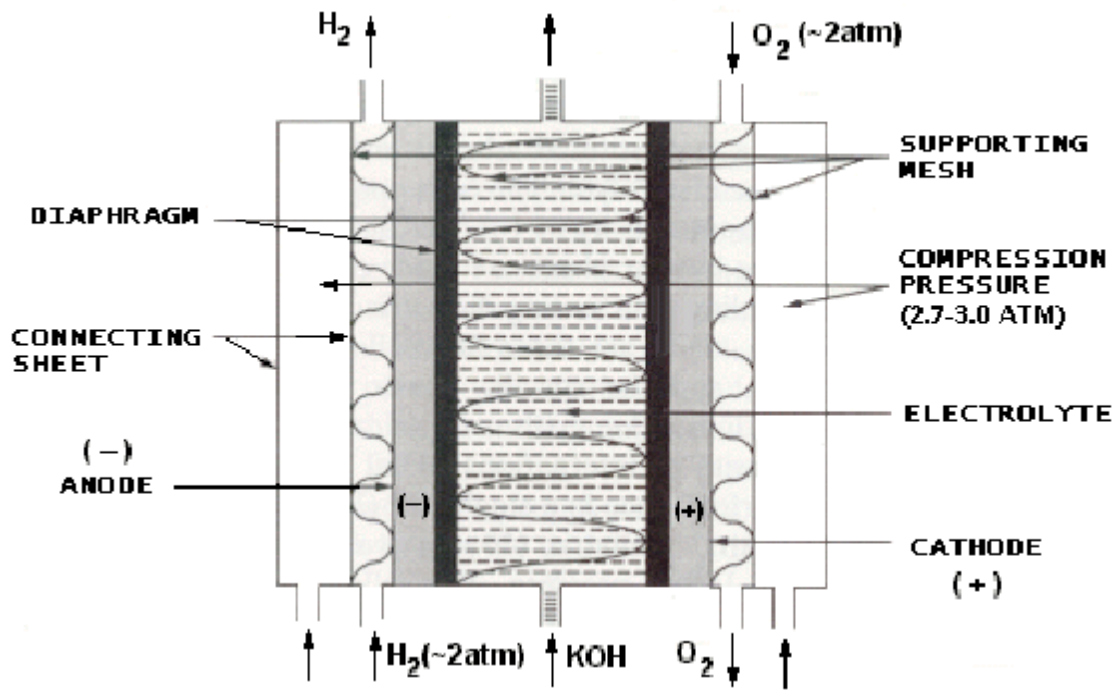
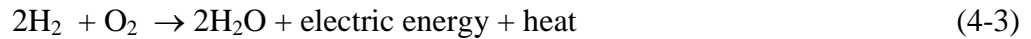


**Figure 4-1 Principles of Operation of Alkaline Fuel Cells (Siemens)**

In many cell designs, the electrolyte is circulated (mobile electrolyte) so that heat can be removed and water eliminated by evaporation (6). Since KOH has the highest conductance among the alkaline hydroxides, it is the preferred electrolyte. Approximately of the water formed at the anode migrates across the electrolyte and exits in the cathode.



## 4.1 Cell Components

### 4.1.1 State-of-the-Art Components

The electrolyte in the AFC is concentrated (85 wt%) KOH in cells designed for operation at high temperature (~260°C), or less concentrated (35-50 wt%) KOH for lower temperature (<120°C) operation. The electrolyte is retained in a matrix (usually asbestos), and a wide range of electrocatalysts can be used (e.g., Ni, Ag, metal oxides, spinels and noble metals).

The AFC modules used in the U.S. Apollo Space Program were cylindrical and had a 57 cm diameter, a 112 cm height, weighed about 110 kg, produced a peak power of 1.42 kW at 27-31 V, and were operated at an average power of 0.6 kW. These cells utilized pure H<sub>2</sub> and O<sub>2</sub> and concentrated electrolyte (85% KOH) to permit cell operation at a lower pressure (! 60 psia reactant gas pressure) without electrolyte boiling. With this concentrated electrolyte, the cell performance was not as high as in the less concentrated electrolyte, consequently the operating temperature was increased to 260°C. The typical performance of this AFC cell was 0.85 V at 150 mA/cm<sup>2</sup>, comparing favorably to the performance of the Bacon cell operating at about 10 times higher pressure.

The alkaline fuel cells in the Space Shuttle Orbiter are rectangular in cross-section with a width of 38 cm, a length of 101 cm, and a height of 35 cm. They weigh 91 kg produce a peak power of 12 kW at 27.5 V, and operate at an average power of 7 kW. They operate in the same pressure range as the Apollo program cells, but at a lower temperature (80 to 90°C) and a higher current density (470 mA/cm<sup>2</sup> at 0.86 V). The electrodes contained high loadings of noble metals. 80% Pt - 20% Pd anodes were loaded at 10 mg/cm<sup>2</sup> on Ag-plated Ni screen. 90% Au - 10% Pt cathodes were loaded at 20 mg/cm<sup>2</sup> on Ag-plated Ni screen. Both were bonded with PTFE to achieve high performance at the lower temperature of 80 to 90°C. A wide variety of materials (e.g., potassium titanate, ceria, asbestos, zirconium phosphate gel) have been used in the microporous separators for AFC's. The electrolyte is 35% KOH and is replenished via a reservoir on the anode side. Gold-plated magnesium is used for the bipolar plates. A brief survey of the advanced technology components in AFC's for space applications is given by Sheibley and Martin (7).

One manufacturer reported cell power densities of 4.3 w/cm<sup>2</sup> at a cell voltage of 0.8 V with an advanced space application cell configuration incorporating a 50 μm thick electrolyte matrix.

AFC's for remote applications (i.e., space, undersea, military) are not strongly constrained by cost. On the other hand, the consumer and industrial markets require the development of low cost components if the AFC is to successfully compete with alternative technologies. Much of the recent interest in AFC's for mobile and stationary terrestrial applications has addressed the development of low cost cell components. In this regard, carbon based porous electrodes play a prominent role.

An advanced cell configuration for underwater application has been developed using high-surface-area Raney nickel anodes loaded at 120 mg/cm<sup>2</sup> (1-2% Ti) and Raney silver cathodes loaded at 60 mg/cm<sup>2</sup> containing small amounts of Ni, Bi, and Ti (6).

### 4.1.2 Development Components

Once development of alkaline cells was underway for space application, terrestrial applications began to be investigated. Developers recognized that pure hydrogen would be required in the fuel stream. This is because the CO<sub>2</sub> in any reformed fuel reacts with the potassium hydroxide (KOH) electrolyte to form a solid carbonate, destroying the electrolyte's ion mobility. Pure H<sub>2</sub> could be supplied to the anode by passing a reformed, H<sub>2</sub>-rich fuel stream through a precious metal (palladium/silver) membrane. The H<sub>2</sub> molecule is able to pass through the membrane by absorption and mass transfer, and into the fuel cell anode. However, a significant pressure differential is required across the membrane and the membrane is prohibitive in cost. Even the small amount of CO<sub>2</sub> in ambient air, the source of O<sub>2</sub> for the reaction, would have to be scrubbed with an immobile electrolyte cell. Investigations soon showed that scrubbing the small amount of CO<sub>2</sub> in the air, coupled with purification of the hydrogen, is not cost effective, thus limiting practical use of AFC's to special terrestrial applications.

A significant cost advantage of alkaline fuel cells is that both anode and cathode reactions can be effectively catalyzed with nonprecious, relatively inexpensive metals. To date, most low cost catalyst development work has been directed towards Raney nickel powders for anodes and silver-based powders for cathodes. The essential characteristics of the catalyst structure are high electronic conductivity and stability (mechanical, chemical, and electrochemical).

Electrode development is concentrated on multi-layered structures with porosity characteristics optimized for flow of liquid electrolytes and gases (H<sub>2</sub> and O<sub>2</sub>). Both metallic (typically hydrophobic) and carbon-based (typically hydrophilic) electrode structures are being investigated. Development of low cost manufacturing processes including powder mixing and pressing of carbon-based electrodes, sedimentation and spraying and high-temperature sintering operations continues. Detailed information on these processes can be found in references 8, 9, 10 and 11.

AFC electrolyte development has been restricted to KOH water solutions with normalities ranging from 6 to 8. The two variants are pumped electrolytes (primarily for cooling) and immobile electrolytes contained in a matrix layer similar to the PAFC. Use of less expensive NaOH has been considered, but minimal cost advantages appear to be far outweighed by performance and lifetime characteristics of KOH.

The focus on AFC stack development is directed toward reducing space, weight and cost. Epoxy resins, polysulfone and ABS (acrylonitril-butadiene-styrene) have been under investigation. Framing techniques under continuing development include injection molding, filter pressing or welding. More detailed information on fuel cell stack development can be found in references 10 and 12.

## 4.2 Performance

Performance of AFC's since 1960 has undergone many changes, as evident in the performance data in Figure 4-2 (13). The early AFC's were operated at relatively high temperatures and pressures to meet the requirements for space applications, as discussed above. More recently, a major focus of the technology is for terrestrial applications where low cost components operating at near-ambient temperature and pressure with air as the oxidant are desirable. This shift in the fuel cell operating parameters has resulted in the lower performance shown in Figure 4-2.

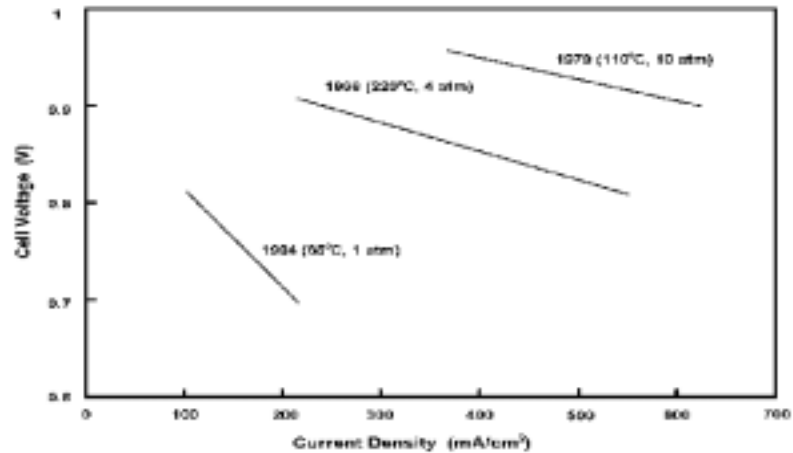
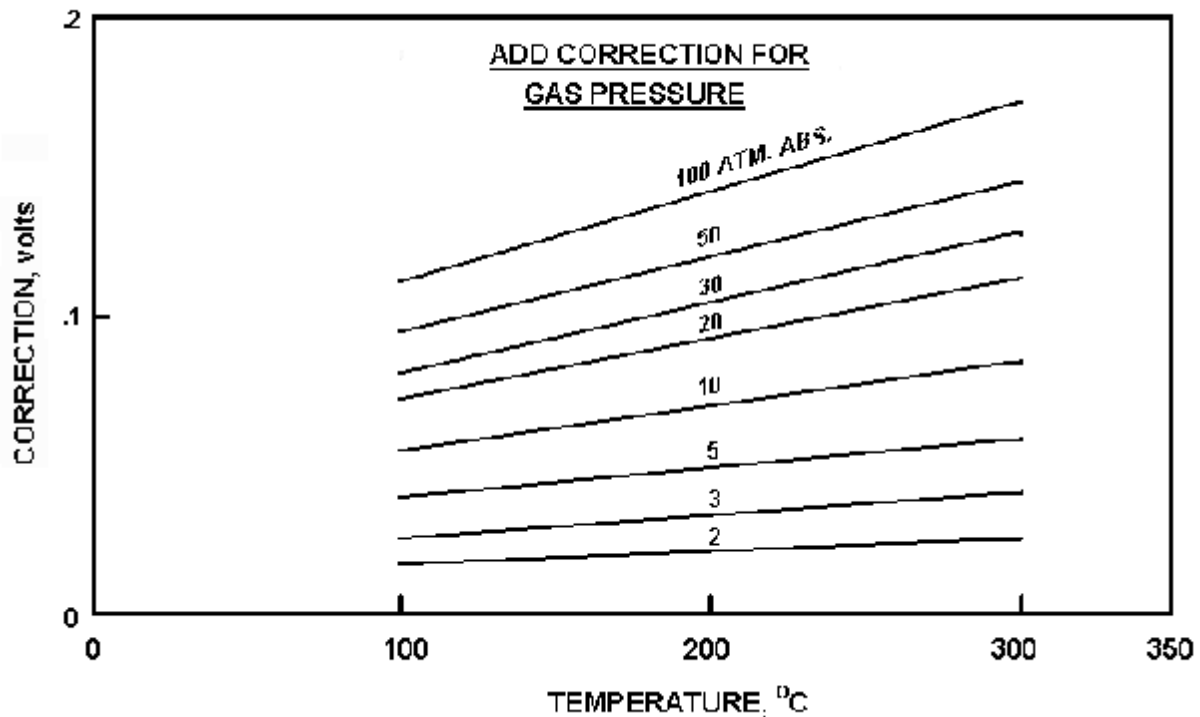


Figure 4-2 Evolutionary Changes in the Performance of AFC's (13)

### 4.2.1 Effect of Pressure

As in the case of PAFC discussed in the previous section, an increase in cell operating pressure enhances performance of AFC's. Figure 4-3 presents a plot of the increase in the reversible e.m.f. of alkaline cells with pressure over a wide range of temperatures (14). The increase in cell open circuit voltage will be somewhat less because of the greater gas solubility at increasing pressure which produces higher lost currents.



**Figure 4-3 Reversible Voltage of The Hydrogen-Oxygen Cell (14)**

At an operating temperature ( $T$ ), the change in voltage ( $\Delta V_p$ ) as a function of pressure ( $P$ ) can be expressed fairly accurately using the expression:

$$\Delta V_p \text{ (mV)} = .15 T \text{ (}^\circ\text{K)} \log (P_2/P_1) \quad (4-4)$$

over the entire range of pressures and temperatures shown in Fig. 4-3. In this expression  $P_2$  and  $P_1$  are different pressures.

In order to achieve faster kinetics, operating temperatures higher than  $100^\circ\text{C}$  accompanied by higher pressures are used. Spacecraft fuel cells have been operated for over 5,000 hours at  $200^\circ\text{C}$  at 50 atm achieving HHV efficiencies exceeding 60% (15, 16). It should be noted that a pressure increase beyond about 5 atm produces improvements which are usually outweighed by a significant weight increase required to sustain the higher operating pressure. For space applications, weight is critical.

### 4.2.2 Effect of Temperature

Figure 2-1 shows that the reversible cell potential for a fuel cell consuming H<sub>2</sub> and O<sub>2</sub> decreases by 0.27 mV/°C under standard conditions where the reaction product is water vapor. However, as is the case in PAFC's, an increase in temperature improves cell performance because activation polarization, mass transfer polarization, and ohmic losses are reduced.

The improvement in air performance of catalyzed carbon based (0.5 mg Pt/cm<sup>2</sup>) porous cathodes with cell temperature is illustrated in Figure 4-4 (17). As expected, the electrode potential at a given current density decreases at lower temperatures, and the decrease is more significant at higher current densities. In the temperature range of 60 to 90°C, the cathode performance increases by about 0.5 mV/°C at 50 to 150 mA/cm<sup>2</sup>.

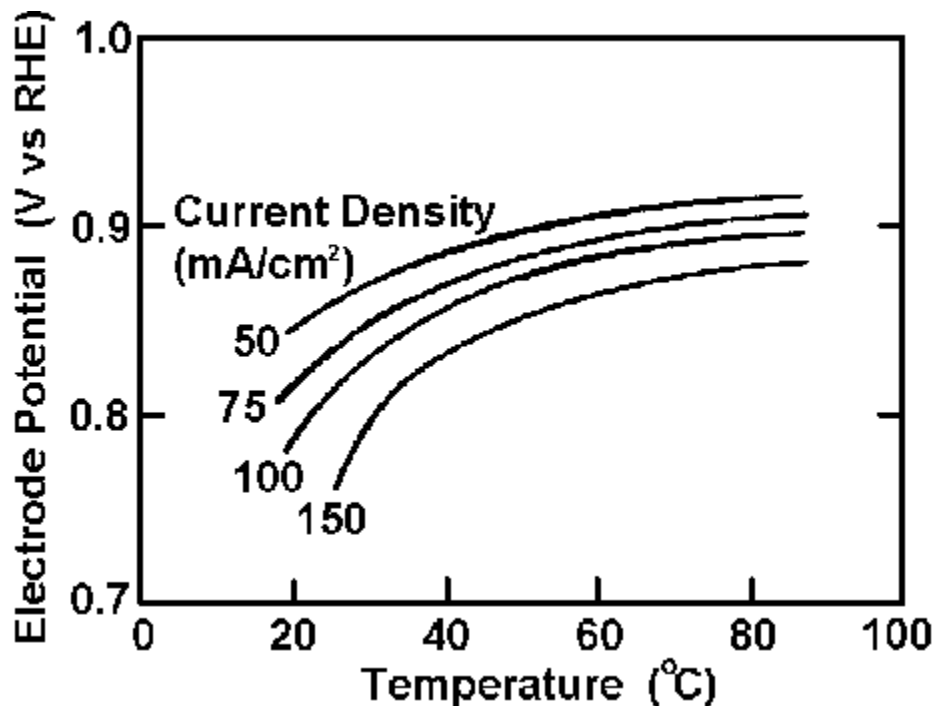


**Figure 4-4 Influence of Temperature on O<sub>2</sub>, (air) Reduction in 12 N KOH.**  
Source: Fig. 10, p. 324, reference (17).

Early data by Clark et al. (18) indicated a temperature coefficient for AFC's at 50-70°C of about 3 mV/°C at 50 mA/cm<sup>2</sup>, and cells with higher polarization had higher temperature coefficients under load. Later measurements by McBreen et al. (19) on H<sub>2</sub>/air single cells (289 cm<sup>2</sup> active area, carbon based Pd anode and Pt cathode) with 50% KOH showed that the temperature coefficient above 60°C was considerably lower than that obtained at lower temperatures as shown in Figure 4-5. The McBreen data suggest the following expression for evaluating the change in voltage ( $\Delta V_T$ ) as a function of temperature (T) at 100 mA/cm<sup>2</sup>:

$$\Delta V_T \text{ (mV)} = 4.0 (T_2 - T_1) \quad \text{for } T > 63^\circ\text{C} \quad (4-5)$$

or

$$\pm V_t \text{ (mV)} = 0.7 (T_2 - T_1) \quad \text{for } T > 63^\circ\text{C} \quad (4-6)$$

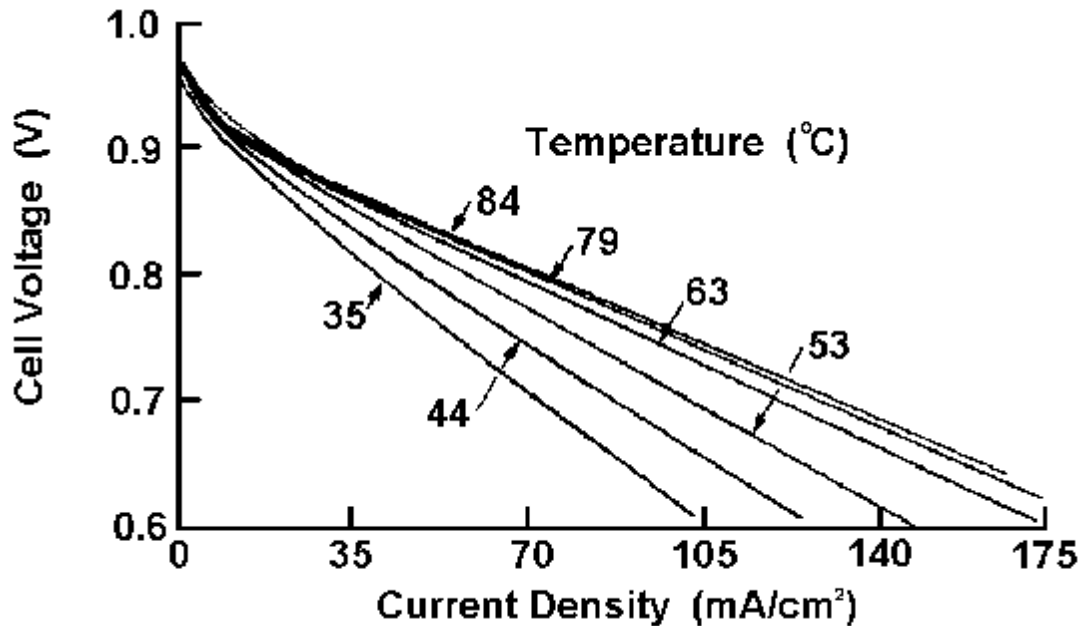


**Figure 4-5 Influence of Temperature on the AFC Cell Voltage**  
 Source: Figure 6, p. 889, reference (19).

Reasonable performance is exhibited by alkaline cells operated at low temperatures (room temperature up to about 70°C). This is because the conductivity of KOH solutions is relatively high at low temperatures. For instance an alkaline fuel cell designed to operate at 70°C will reduce to only half power level when its operating temperature is reduced to room temperature (20).

### 4.2.3 Effect of Reactant Gas Composition

Pure hydrogen and oxygen are required to operate an AFC. Reformed H<sub>2</sub> or air containing even trace amounts of CO<sub>2</sub> will dramatically affect performance and lifetime as described in the following section.

### 4.2.4 Effect of Impurities

AFCs suffer a drastic performance loss with fuels containing CO<sub>2</sub> from reformed fuels, and from the presence of CO<sub>2</sub> in air (approximately 350 ppm CO<sub>2</sub> in ambient air). The negative impact of CO<sub>2</sub> arises from its reaction with OH<sup>-</sup> ;



producing the following effects: 1) reduced  $\text{OH}^-$  concentration interfering with kinetics, 2) electrolyte viscosity increase resulting in lower diffusion rate and lower limiting currents, 3) precipitation of carbonate salts in the pores of the porous electrode, 4) reduced oxygen solubility, and 5) reduced electrolyte conductivity. The influence of  $\text{CO}_2$  on air cathodes ( $0.2 \text{ mg Pt/cm}^2$  supported on carbon black) in 6 N KOH at  $50^\circ\text{C}$  can be ascertained by analysis of the performance data presented in Figure 4-6 (21). To obtain these data, the air electrodes were operated continuously at  $32 \text{ mA/cm}^2$ , and current-voltage performance curves were periodically measured. Performance in both  $\text{CO}_2$  free air and  $\text{CO}_2$  containing air show evidence of degradation with time. However, with  $\text{CO}_2$  free air the performance remains much more nearly constant with 2000 to 3000 hour operation.

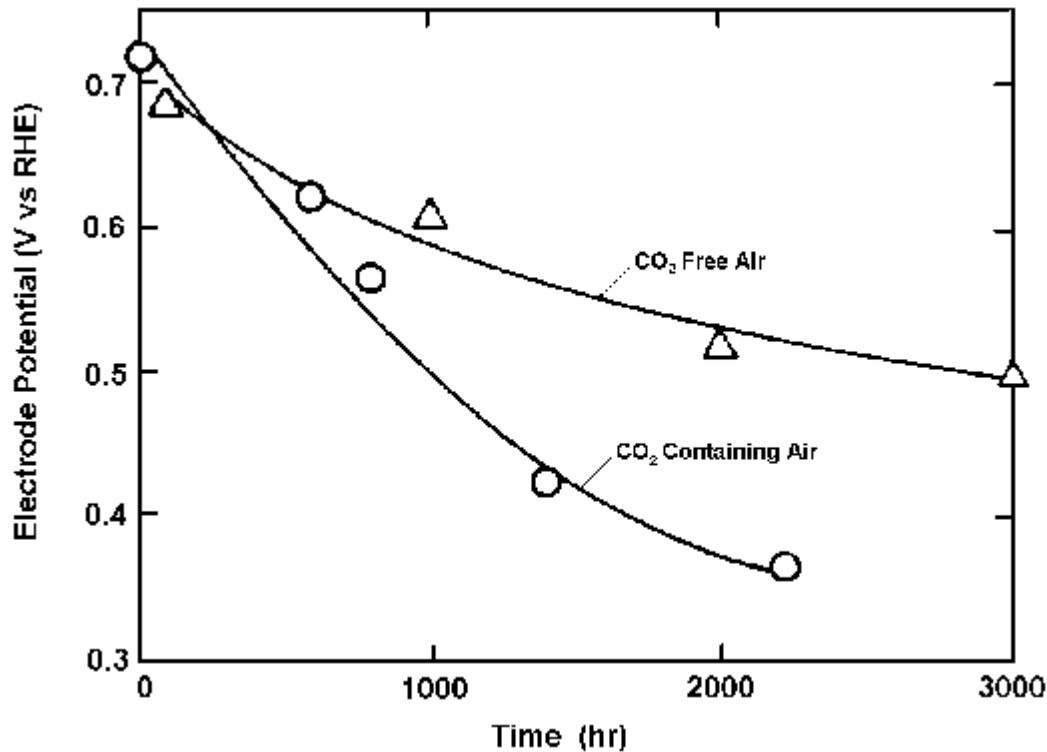


**Figure 4-6 Degradation in AFC Electrode Potential with  $\text{CO}_2$  Containing and  $\text{CO}_2$  Free Air**  
**Source: Figure 2, p. 381, reference (21)**

Higher concentrations of KOH are also detrimental to the life of  $\text{O}_2$  electrodes operating with  $\text{CO}_2$  containing air, but operating the electrode at higher temperature is beneficial because it increases the solubility of  $\text{CO}_2$  in the electrolyte. Modifying the operating conditions can prolong electrode life, but it is clear from the results in Figure 4-6 that the life expectancy of air cathodes is lowered by the presence of  $\text{CO}_2$ . Extensive studies by Kordesch et al. (21) indicate that the operational life of air electrodes (PTFE-bonded carbon electrodes on porous nickel substrates) with  $\text{CO}_2$  containing air in 9 N KOH at  $65^\circ\text{C}$  ranges from 1600 to 3400 hours at a

current density of  $65 \text{ mA/cm}^2$ . The life of these electrodes with  $\text{CO}_2$  free air tested under similar conditions ranged from 4000 to 5500 hours. It has been reported (2) that a lifetime of 15,000 hours has been achieved with AFC's, and failure at this time is by attack of the cell frames.

#### 4.2.5 Effects of Current Density

As in the case with PAFC's, voltage obtained from an AFC is affected by ohmic, activation, and concentration losses. Figure 4-7 presents data obtained in the 1960's (18) which summarizes these effects, excluding ohmic losses, for a catalyzed reaction ( $0.5\text{-}2.0 \text{ mg noble metal/cm}^2$ ) with carbon-based porous electrodes for  $\text{H}_2$  oxidation and  $\text{O}_2$  reduction in  $9 \text{ N KOH}$  at  $55\text{-}60^\circ\text{C}$ . The electrode technology was similar to that employed in the fabrication of PAFC electrodes. Performance of AFC's with carbon-based electrodes has not changed dramatically since these early results were obtained.

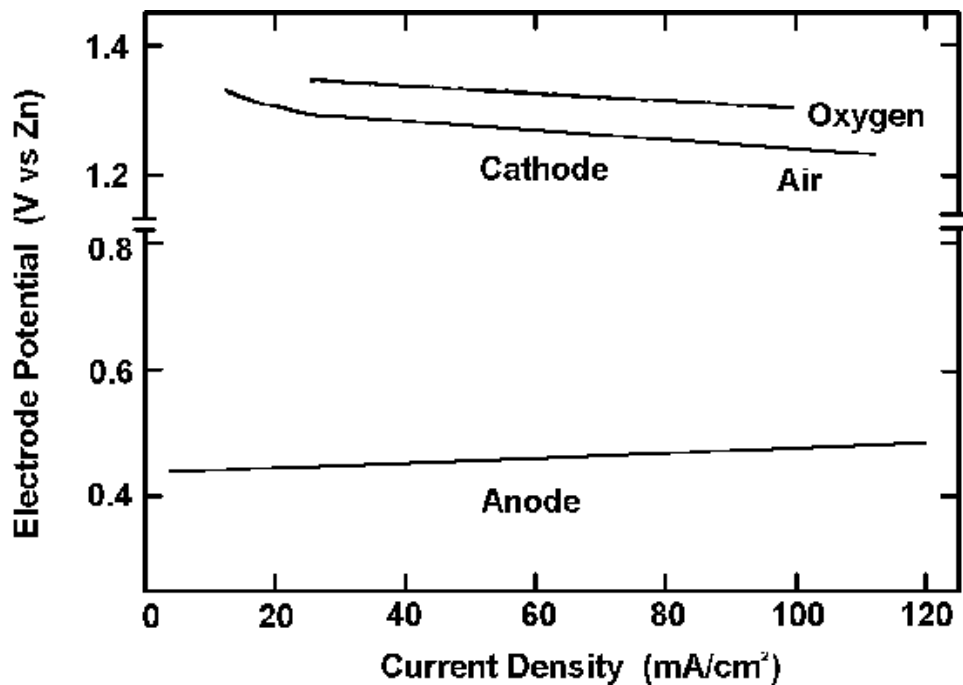


Figure 4-7 iR Free Electrode Performance with  $\text{O}_2$  and Air in  $9 \text{ N KOH}$  at  $55$  to  $60^\circ\text{C}$ . Catalyzed ( $0.5 \text{ mg Pt/cm}^2$  Cathode,  $0.5 \text{ mg Pt-Rh/cm}^2$  Anode) Carbon-based Porous Electrodes (18)



The results in Figure 4-7 yield the following current density equations for cells operating in 9 N KOH at 55-60°C:

$$E_{V_j} \text{ (mV)} = 1.18 - E_j \quad \text{for } J = 40 - 100 \text{ mA/cm}^2 \text{ operating in O}_2 \quad (4-8)$$

or

$$E_{V_j} \text{ (mV)} = 1.31 - E_j \quad \text{for } J = 40 - 100 \text{ mA/cm}^2 \text{ operating in air.} \quad (4-9)$$

The performance of a single cell with supported noble metal electrocatalysts (0.5 mg Pt-Rh/cm<sup>2</sup> anode, 0.5 mg Pt/cm<sup>2</sup> cathode) in 12 N KOH at 65°C is shown in Figure 4-8 (17). These results reported in 1986 are comparable to those obtained in 1965. The iR free electrode potentials (vs RHE) at 100 mA/cm<sup>2</sup> in Figure 4-8 are 0.9 V with O<sub>2</sub> and 0.85 V with air. One major difference between the early cathodes and the cathodes in current use is the limiting current for O<sub>2</sub> reduction from air has been improved (i.e., 100-200 mA/cm<sup>2</sup> improved to >250 mA/cm<sup>2</sup>).

These results yield the following equations for cells operating in 12 N KOH at 65°C:

$$E_{V_j} \text{ (mV)} = 1.025 - E_j \quad \text{for } J = 50 - 200 \text{ mA/cm}^2 \text{ operating in O}_2 \quad (4-10)$$

or

$$E_{V_j} \text{ (mV)} = 1.047 - E_j \quad \text{for } J = 50 - 200 \text{ mA/cm}^2 \text{ operating in air.} \quad (4-11)$$

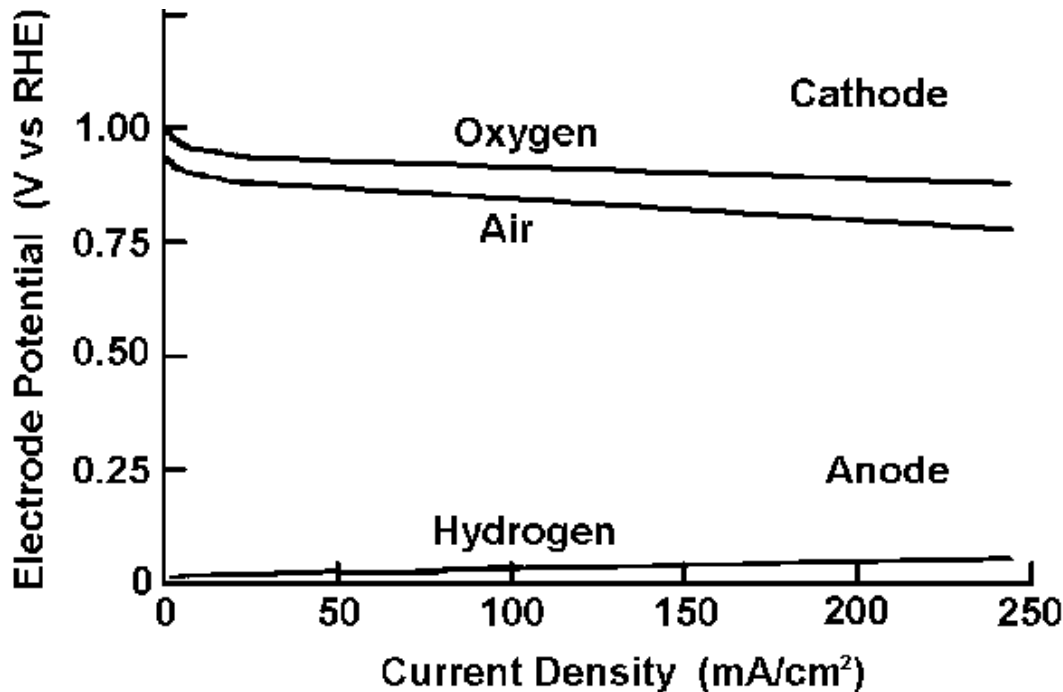


Figure 4-8 iR Free Electrode Performance with O<sub>2</sub> and Air in 12 N KOH at 65°C. Catalyzed (0.5 mg Pt/cm<sup>2</sup> Cathode, 0.5 mg Pt-Rh/cm<sup>2</sup> Anode), Carbon-based Porous Electrodes 17),

### 4.2.6 Effects of Cell Life

AFC cell stacks have demonstrated sufficiently stable operation for at least 5000 hours, with degradation rates of 20 . V per hour or less (20). Siemens has reported a total of >8000 operating hours with approximately 20 units (22). For large scale utility applications, economics demand operating times exceeding 40,000 hours which presents perhaps the most significant obstacle to commercialization of AFC devices in the realm of interest to the DOE Stationary Electric Power Program.

### 4.3 Summary of Equations for AFC

The preceding sections described parametric performance based on various referenced data at differing cell conditions. It is suggested that the following set of equations be used unless the reader prefers other data or rationale.

<u>Parameter</u>	<u>Equation</u>	<u>Comments</u>	
Pressure	$\xi V_P \text{ (mV)} = .15 T \text{ (}^\circ\text{K)} \log (P_2/P_1)$	1 atm $\xi$ P $\xi$ 100 atm 100 $^\circ\text{C}$ $\xi$ T $\xi$ 300 $^\circ\text{C}$	(4-4)
Temperature	$\xi V_T \text{ (mV)} = 4.0 (T_2-T_1)$	for T $\xi$ 63 $^\circ\text{C}$ , at 100 mA/cm <sup>2</sup>	(4-5)
Temperature	$\xi V_T \text{ (mV)} = 0.7 (T_2-T_1)$	for T > 63 $^\circ\text{C}$ , at 100 mA/cm <sup>2</sup>	(4-6)
Current Density	$\xi V_J \text{ (mV)} = \text{ }^\circ .18 \xi J$	for J = 40-100 mA/cm <sup>2</sup> operating in O <sub>2</sub> with 9 N KOH at 55-60 $^\circ\text{C}$ .	(4-8)
	$\xi V_J \text{ (mV)} = \text{ }^\circ .31 \xi J$	for J = 40-100 mA/cm <sup>2</sup> operating in air with 9 N KOH at 55-60 $^\circ\text{C}$ .	(4-9)
	$\xi V_J \text{ (mV)} = \text{ }^\circ .025 \xi J$	for J = 40-100 mA/cm <sup>2</sup> operating in O <sub>2</sub> with 12 N KOH at 65 $^\circ\text{C}$ .	(4-10)
	$\xi V_J \text{ (mV)} = \text{ }^\circ .047 \xi J$	for J = 40-100 mA/cm <sup>2</sup> operating in air with 12 N KOH at 65 $^\circ\text{C}$ .	(4-11)
Life Effects	$\xi V_{\text{Lifetime}} \text{ (mV)} = 20 \text{ . V per hour or less}$		(4-12)

### 4.4 References

1. F.T. Bacon, *Electrochim. Acta*, **14**, 569, 1969.
2. J. O'M Bockris and A.J. Appleby, *Energy*, **11**, 95, 1986.
3. A.J. Appleby, *Energy*, **11**, 13, 1986.
4. K.F. Blurton and E. McMullin, *Energy Conversion*, **9**, 141, 1969.
5. Courtesy of Siemens Corp.
6. K. Strasser, *J. Power Sources* **29**, 152-153, 1990.
7. D.W. Sheibley and R.A. Martin, *Prog. Batteries Solar Cells*, **6**, 155, 1987.
8. K. V. Kordesch, *J. Electrochem. Soc.* **125**, 77C-91C, 1978.
9. G. Sanstede, ed., *From Electrocatalysis to Fuel Cells*, The University of Washington Press, Seattle and London, 1972.
10. K. Strasser, *J. Electrochem. Soc.* **127**, 2173-2177, 1980.

11. K.V. Kordesch, *Brennstoffbatterien*, Springer-Verlag, New York, 1984.
12. H. van den Broeck, G. van Bogaert, G. Vennekens, L. Vermeeren, F. Vlasselaer, J. Lichtenberg, W. Schlösser, A. Blanchart, *Proc. 22<sup>nd</sup> IECEC Meeting*, 1005, Philadelphia, 1987.
13. J. Huff, paper presented at the 1986 "Status of Fuel Cell Technologies", *Fuel Cell Seminar Abstracts, Fuel Cell Seminar*, Tucson, AZ, October 26-29, 1986.
14. A.M. Adams, F.T. Bacon and R.G.H. Watson, *Fuel Cells* (W. Mitchell, ed.), Academic Press, New York, 138, 1963.
15. S.S. Penner, ed., *Assessment of Research Needs for Advanced Fuel Cells*, DOE/ER/300.60-T1, US DOE, 1985.
16. Fuel Cell Seminar Abstracts, Long Beach, CA; sponsored by the National Fuel Cell Coordinating Group, October 23-26, 1988.
17. K. Tomantschger, F. McClusky, L. Oporto, A. Reid and K. Kordesch, *J. Power Sources*, **18**, 317, 1986.
18. M.B. Clark, W.G. Darland and K.V. Kordesch, *Electrochem. Tech.*, **3**, 166, 1965.
19. J. McBreen, G. Kissel, K.V. Kordesch, F. Kulesa, E.J. Taylor, E. Gannon and S. Srinivasan, in *Proceedings of the 15th Intersociety Energy Conversion Engineering Conference*, Volume 2, American Institute of Aeronautics and Astronautics, New York, NY, 886, 1980.
20. J.M.J. Blomen and M.N. Mugerwa ed., *Fuel Cell Systems*, Plenum Press, New York and London, 251, 1993.
21. K. Kordesch, J. Gsellmann and B. Kraetschmer, in *Power Sources*, **9**, Edited by J. Thompson, Academic Press, New York, NY, 379, 1983.
22. K. Strasser, L. Blume and W. Stuhler, *Fuel Cell Seminar Program and Abstracts*, Long Beach, CA; sponsored by the National Fuel Cell Coordinating Group, October 23-26, 1988.

---

## 5. PHOSPHORIC ACID FUEL CELL

---

Discussions with the only U.S. PAFC manufacturer justified the direct use of the PAFC performance information from the 1994 edition of the *Fuel Cell Handbook*. There have been only minor changes in cell performance, mostly due to changing the operating conditions of the cell. These are considered within the performance trends shown in this section. The manufacturer has concentrated on improving cell stability and life, and in improving the system components to improve reliability and lower cost. It should be noted that the performance shown in this section is based on information from contracts that the manufacturer had with the Department of Energy or outside institutions. Any new PAFC performance has been accomplished with company funding and is considered proprietary by the manufacturer (1).

The phosphoric acid fuel cell (PAFC) is the only fuel cell technology that is in commercialization. There are over 75 MW of demonstrators, worldwide, that have been tested, are being tested, or are being fabricated. Most of the plants are in the 50 to 200 kW capacity range, but large plants of 1 MW and 5 MW have been built. The largest plant operated to date achieved 11 MW of grid quality ac power (2, 3). Major efforts in the U.S. are concentrated on the improvement of PAFCs for stationary dispersed power plants and on-site cogeneration power plants. The major industrial participants are International Fuel Cells Corporation in the U.S. and Fuji Electric Corporation, Toshiba Corporation, and Mitsubishi Electric Corporation in Japan. In this section, the status of the cell components and the performance of PAFCs are discussed.

The electrochemical reactions occurring in PAFCs are



at the anode, and



at the cathode. The overall cell reaction is



The electrochemical reactions occur on highly dispersed electrocatalyst particles supported on carbon black. Platinum (Pt) or Pt alloys are used as the catalyst at both electrodes.

## 5.1 Cell Components

### 5.1.1 State-of-the-Art Components

The evolution from 1965 to the present day in the development of cell components for PAFCs is summarized in Table 5-1. In the mid-1960s, the conventional porous electrodes were polytetrafluoroethylene (PTFE)-bonded Pt black, and the loadings were about 9 mg Pt/cm<sup>2</sup>. During the past two decades, Pt supported on carbon black has replaced Pt black in porous PTFE-bonded electrode structures as the electrocatalyst. A dramatic reduction in Pt loading has also occurred; the loadings<sup>13</sup> are currently about 0.10 mg Pt/cm<sup>2</sup> in the anode and about 0.50 mg Pt/cm<sup>2</sup> in the cathode. The operating temperatures and acid concentrations of PAFCs have increased to achieve higher cell performance; temperatures of about 200°C (392°F) and acid concentrations of 100% H<sub>3</sub>PO<sub>4</sub> are commonly used today. In addition, the operating pressure of PAFCs surpassed 8 atm in the 11 MW electric utility demonstration plant.

One of the major breakthroughs in PAFC technology that occurred in the late 1960s was the development of carbon black and graphite for cell construction materials; these developments are reviewed by Appleby (4) and Kordesch (5). It was shown at that time that carbon black and graphite were sufficiently stable to replace the more expensive gold-plated tantalum cell hardware. The use of high-surface-area carbon black to support Pt permitted a dramatic reduction in Pt loading, without sacrificing electrode performance. It has been reported (4) that "without carbon, a reasonably inexpensive acid fuel cell would be impossible, since no other material combines the necessary properties of electronic conductivity, good corrosion resistance, low density, surface properties (especially in high area form) and, above all, low cost." However, carbon corrosion and Pt dissolution become problematic at cell voltages above ~0.8 V; consequently, low current densities with cell voltage above 0.8 and hot idle at open circuit potential are to be avoided.

The porous electrodes used in PAFCs are described extensively in the patent literature (6); see also the review by Kordesch (5). These electrodes contain a mixture of the electrocatalyst supported on carbon black and a polymeric binder, usually PTFE (about 30 to 50 wt%). The PTFE binds the carbon black particles together to form an integral (but porous) structure, which is supported on a porous carbon paper substrate. The carbon paper serves as a structural support for the electrocatalyst layer, as well as the current collector. A typical carbon paper used in PAFCs has an

---

13. Assuming a cell voltage of 750 mV at 205 mA/cm<sup>2</sup> (approximate 11 MW design) and the current Pt loadings at the anode and cathode, ~54 g Pt is required per kilowatt of power generated.

**Table 5-1 Evolution of Cell Component Technology for Phosphoric Acid Fuel Cells**

Component	ca. 1965	ca. 1975	Current Status
<b>Anode</b>	PTFE-bonded Pt black	PTFE-bonded Pt/C	PTFE-bonded Pt/C
		Vulcan XC-72 <sup>a</sup>	Vulcan XC-72 <sup>a</sup>
	9 mg/cm <sup>2</sup>	0.25 mg Pt/cm <sup>2</sup>	0.1 mg Pt/cm <sup>2</sup>
<b>Cathode</b>	PTFE-bonded Pt black	PTFE-bonded Pt/C	PTFE-bonded Pt/C
		Vulcan XC-72 <sup>a</sup>	Vulcan XC-72 <sup>a</sup>
	9 mg/cm <sup>2</sup>	0.5 mg Pt/cm <sup>2</sup>	0.5 mg Pt/cm <sup>2</sup>
<b>Electrode Support</b>	• Ta mesh screen	• Carbon paper	• Carbon paper
<b>Electrolyte Support</b>	• glass fiber paper	• PTFE-bonded SiC	• PTFE-bonded SiC
<b>Electrolyte</b>	• 85% H <sub>3</sub> PO <sub>4</sub>	• 95% H <sub>3</sub> PO <sub>4</sub>	• 100% H <sub>3</sub> PO <sub>4</sub>

a - Conductive oil furnace black, product of Cabot Corp. Typical properties: 002 d-spacing of 3.6 Å by X-ray diffraction, surface area of 220 m<sup>2</sup>/g by nitrogen adsorption, and average particle size of 30 μm by electron microscopy.

initial porosity of about 90%, which is reduced to about 60% by impregnation with 40 wt% PTFE. This wet proof carbon paper contains macropores of 3 to 50 μm diameter (median pore diameter of about 12.5 μm) and micropores with a median pore diameter of about 34 Å for gas permeability. The composite structure consisting of a carbon black/PTFE layer on carbon paper substrate forms a stable, three-phase interface in the fuel cell, with H<sub>3</sub>PO<sub>4</sub> electrolyte on one side (electrocatalyst side) and the reactant gas environment on the other side of the carbon paper.

A bipolar plate serves to separate the individual cells and electrically connect them in series in a fuel cell stack (Figure 1-4). In some designs, the bipolar plate also contains the gas channels for introducing the reactant gases to the porous electrodes and removing the products and inerts. Bipolar plates made from graphite resin mixtures that are carbonized at low temperature (~900°C/1652°F) are not suitable because of their rapid degradation in PAFC operating environments (7 and 8). However, corrosion stability is improved by heat treatment to 2700°C (4892°F) (8), i.e., the corrosion current is reduced by two orders of magnitude at 0.8 V in 97% H<sub>3</sub>PO<sub>4</sub> at 190°C (374°F) and 4.8 atm (70.5 psi). The all-graphite bipolar plates are sufficiently corrosion resistant for a projected life of 40,000 hours in PAFCs, but they are still relatively costly to produce.

Several designs for the bipolar plate and ancillary stack components are used by fuel cell developers, and these are described in detail (9, 10, 11, and 12). A typical PAFC stack contains

cells connected in (electrical) series to obtain the practical voltage level desired for delivery to the load. In such an arrangement, individual cells are stacked with bipolar plates between the cells. The bipolar plates used in early PAFCs consisted of a single piece of graphite with gas channels machined on either side to direct the flow of fuel and oxidant gases in adjacent cells. Currently, both bipolar plates of the previous design and new designs consisting of several components are being considered. In the multi-component bipolar plates, a thin impervious plate separates the reactant gases in adjacent cells in the stack, and separate porous plates with ribbed channels are used to direct gas flow. In a cell stack, the impervious plate is subdivided into two parts, and each joins one of the porous plates. The porous structure, which allows rapid gas permeability, is also used to store additional acid to replenish the supply lost by evaporation during the cell operating life.

In PAFC stacks, provisions must be included to remove heat generated during cell operation. Heat has been removed by either liquid (two-phase water or a dielectric fluid) or gas (air) coolants that are routed through cooling channels located (usually about every fifth cell) in the cell stack. Liquid cooling requires complex manifolds and connections, but better heat removal is achieved than with air cooling. The advantage of gas cooling is its simplicity, reliability, and relatively low cost. However, the size of the cell is limited, and the air-cooling passages are much larger than the liquid-cooling passages.

Improvements in the state-of-the-art of phosphoric acid cells are illustrated by Figure 5-1. The performance by the  $\sim 1 \text{ m}^2$  (10 ft<sup>2</sup>) short stack, (f), results in a power density of nearly  $0.31 \text{ W/cm}^2$ .

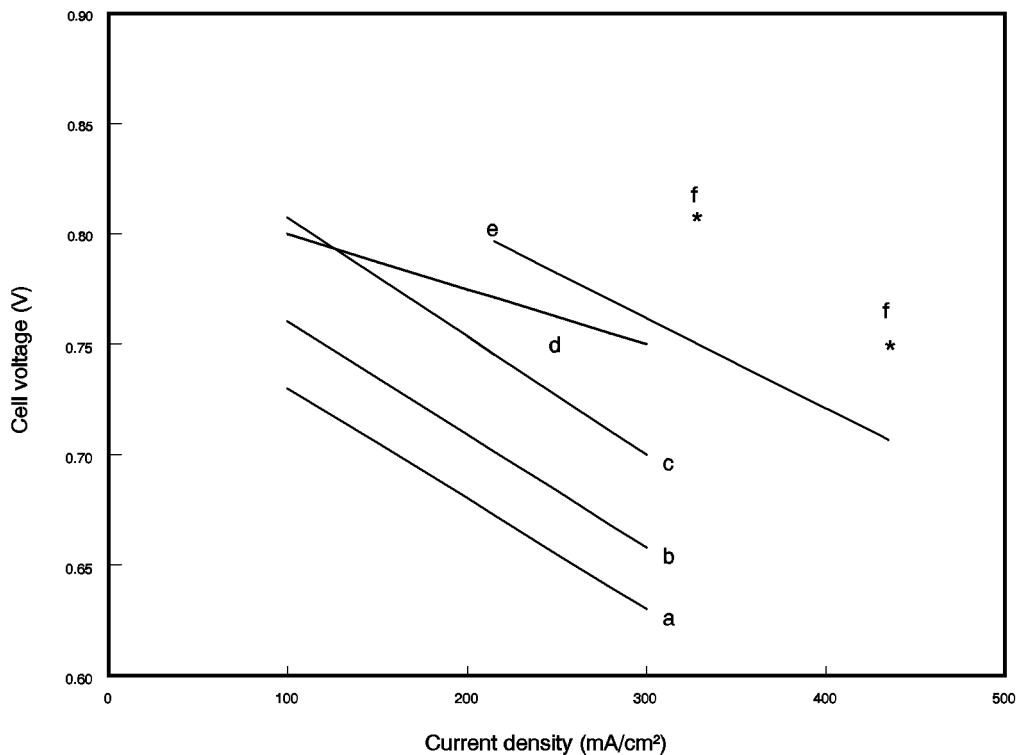


**Figure 5-1 Improvement in the Performance of H<sub>2</sub>-Rich Fuel/Air PAFCs**

- a - 1977: 190°C, 3 atm, Pt loading of 0.75 mg/cm<sup>2</sup> on each electrode (13)
- b - 1981: 190°C, 3.4 atm, cathode Pt loading of 0.5 mg/cm<sup>2</sup> (14)
- c - 1981: 205°C, 6.3 atm, cathode Pt loading of 0.5 mg/cm<sup>2</sup> (14)
- d - 1984: 205°C, 8 atm, electrocatalyst loading was not specified (15)
- e - 1992: 205°C, 8 atm, 10 ft<sup>2</sup> short stack, 200 hrs, electrocatalyst loading not specified (16)
- f - 1992: 205°C, 8 atm, subscale cells, electrocatalyst loading not specified (16)

### 5.1.2 Development Components

Phosphoric acid electrode/electrolyte technology has reached a level of maturity where developers and users commit resources to commercial capacity, multi-unit demonstrations and pre-prototype installations. Cell components are being manufactured at scale and in large quantities with confidence of meeting predicted performance. However, for the technology to achieve economic competitiveness with other energy technologies, there is a need to further increase the power density of the cells and reduce costs (17 and 18), which are interrelated. Fuel cell developers continue to address these issues. A thorough description of development components is beyond the scope of this handbook. The interested reader is referred to full texts such as the Fuel Cell Handbook (12), which describes many research activities and is well referenced.

In 1992, the International Fuel Cells Corporation completed a government-sponsored, advanced water-cooled PAFC development project to improve the performance and lower the cost of its atmospheric and pressurized technology for on-site and utility applications (16). The project focused on five major activities: 1) produce a conceptual design of a large stack with a goal of 175 WSF (0.188 W/cm<sup>2</sup>), 40,000 hour useful life, and a stack cost of less than \$400/kW; 2) test pressurized Configuration "B" single cells developed in a previous program, but improved with proprietary design advances in substrates, electrolyte reservoir plates, catalysts, seals, and electrolyte matrix to demonstrate the 175 WSF (0.188 W/cm<sup>2</sup>) power density goal; 3) test a pressurized short stack with subscale size, improved component cells and additional improvements in the integral separators and coolers to confirm the stack design; 4) test a pressurized short stack of improved full-size cell components, nominal 10 ft<sup>2</sup> size (approximately 1 m<sup>2</sup>), to demonstrate the 175 WSF (0.188 W/cm<sup>2</sup>) power density goal; and 5) test an advanced atmospheric "on-site" power unit stack with the improved components.

A conceptual design of an improved technology stack operating at 120 psi (8.2 atm) and 405°F (207°C) was produced based on cell and stack development and tests. The stack was designed for 355 10 ft<sup>2</sup> (approximately 1 m<sup>2</sup>) cells to produce over 1 MW dc power in the same physical envelope as the 670 kW stack used in the 11 MW PAFC plant built for Tokyo Electric Power. The improvements made to the design were tested in single cells, and in subscale and full size short stacks.

Table 5-2 summarizes the results. Single cells achieved an initial performance of 0.75 volts/cell at a current density of 400 ASF (431 mA/cm<sup>2</sup>), 8.2 atm and 207°C condition which was 300 WSF (0.323 W/cm<sup>2</sup>), well above the project goal. Several cells were operated to 600 ASF (645 mA/cm<sup>2</sup>), achieving up to 0.66 volts/cell. The flat plate component designs were verified in a subscale stack prior to fabricating the full size short stack. The pressurized short stack of 10 ft<sup>2</sup>



cells achieved a performance of 285 WSF (0.307 W/cm<sup>2</sup>). Although the average cell performance, 0.71 volts/cell at 400 ASF (431 mA/cm<sup>2</sup>), was not as high as the single cell tests, the performance was 65% over the project goal. Figure 5-2 presents single cell and stack performance data for pressurized operation. The stack was tested for over 3,000 hours. For reference purposes, Tokyo Electric Power Company's 11 MW power plant, operational in 1991, had an average cell performance of approximately 0.75 volts/cell at 190 mA/cm<sup>2</sup> or 0.142 W/cm<sup>2</sup> (19).

**Table 5-2 Advanced PAFC Performance**

	Average Cell Voltage, V	Current Density mA/cm <sup>2</sup>	Power Density W/cm <sup>2</sup>
<b>IFC Pressurized:</b>			
<b>Project Goal</b>			0.188
<b>Single Cells</b>	0.75 to 0.66	431 to 645	0.323
<b>Full Size Short Stack</b>	0.71	431	0.307
<b>11 MW Reference</b>	0.75	190	0.142
<b>IFC Atmospheric:</b>			
<b>Single Cells</b>	0.75	242	0.182
<b>Full Size Short Stack</b>	0.65	215	0.139
<b>Mitsubishi Electric Atmospheric</b>			
<b>Single Cells</b>	0.65	300	0.195

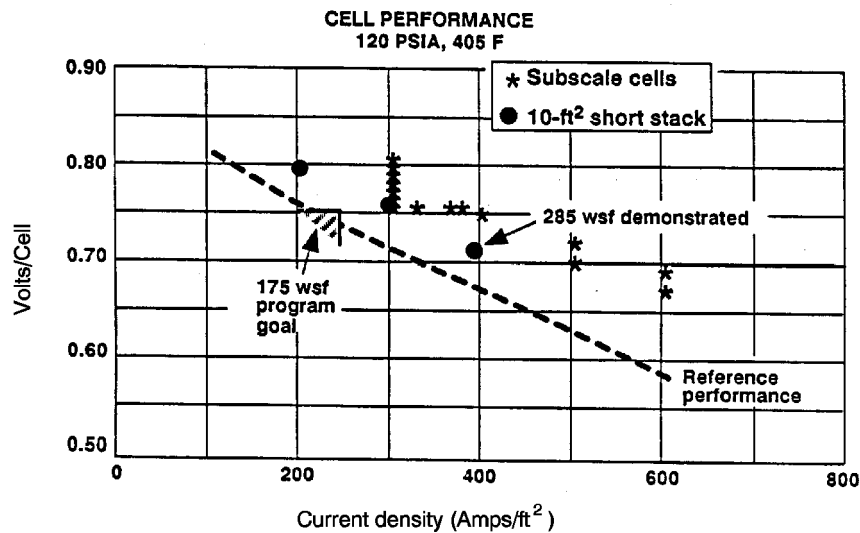


**Figure 5-2 Advanced Water-Cooled PAFC Performance (16)**

The atmospheric pressure on-site short stack consisting of 32 cells obtained an initial performance of 0.65 volts/cell at 200 ASF (215 mA/cm<sup>2</sup>) or 0.139 W/cm<sup>2</sup>. The performance degradation rate was less than 4 mV/1000 hours during the 4500 hour test. Single cells tested at atmospheric conditions achieved a 500 hour performance of approximately 0.75 volts/cell at 225 ASF

(242 mA/cm<sup>2</sup>) or 0.182 W/cm<sup>2</sup>. The results from this program represent the highest performance of full-size phosphoric acid cells and short stacks published to date.

Mitsubishi Electric Corporation investigated alloyed catalysts, processes to produce thinner electrolytes, and increases in utilization of the catalyst layer (20). These improvements resulted in an initial atmospheric performance of 0.65 mV at 300 mA/cm<sup>2</sup> or 0.195 W/cm<sup>2</sup>, which is higher than the IFC performance mentioned above (presented in Table 5-2 for comparison). Note that this performance was obtained on small 100 cm<sup>2</sup> cells and may not yet have been demonstrated with full-scale cells in stacks. Approaches to increase life are to use series fuel gas flow in the stack to alleviate corrosion, provide well-balanced micro-pore size reservoirs to avoid electrolyte flooding, and use a high corrosion resistant carbon support for the cathode catalyst. These improvements have resulted in the lowest PAFC degradation rate publicly acknowledged, 2 mV/1000 hours for 10,000 hours at 200 to 250 mA/cm<sup>2</sup> in a short stack with 3600 cm<sup>2</sup> area cells.

Several important technology development efforts for which details have been published are catalyst improvements, advanced gas diffusion electrode development, and tests on materials that offer better carbon corrosion protection. Transition metal (e.g., iron, cobalt) organic macrocycles<sup>14</sup> from the families of tetramethoxyphenylporphyrins (TMPP), phthalocyanines (PC), tetraazaannulenes (TAA) and tetraphenylporphyrins (TPP) have been evaluated as O<sub>2</sub>-reduction electrocatalysts in PAFCs. One major problem with these organic macrocycles is their limited chemical stability in hot concentrated phosphoric acid. However, after heat treatment of the organic macrocycle (i.e., CoTAA, CoPC, CoTMPP, FePC, FeTMPP) on carbon at about 500 to 800°C (932 to 1472°F), the pyrolyzed residue exhibits electrocatalytic activity that, in some instances, is comparable to that of Pt and has promising stability, at least up to about 100°C/212°F (21). Another approach that has been successful for enhancing the electrocatalysis of O<sub>2</sub> reduction is to alloy Pt with transition metals such as Ti (22), Cr (23), V(24), Zr, and Ta (24). The enhancement in electrocatalytic activity has been explained by a correlation between the optimum nearest-neighbor distance of the elements in the alloy and the bond length in O<sub>2</sub> (25).

Conventional cathode catalysts comprise either platinum or platinum alloys supported on conducting carbon black at 10 wt% platinum. Present platinum loadings on the anode and cathode are 0.1 mg/cm<sup>2</sup> and 0.5 mg/cm<sup>2</sup>, respectively (12,16). It has been suggested by Ito et.al. that the amount of platinum may have been reduced to the extent that it might be cost effective to increase the amount of platinum loading on the cathode (26). However, a problem exists in that fuel cell stack developers have not experienced satisfactory performance improvements when increasing the platinum loading. Johnson Matthey Technology Centre (J-M) presented data that resulted in a performance improvement nearly in direct proportion to that expected based on the increase in platinum (27). Initial tests by J-M confirmed previous results that using platinum alloy catalysts with a 10 wt% net platinum loading improves performance. Platinum/nickel alloy catalysts yielded a 49 wt% increase in specific activity over pure platinum. This translates into a 39 mV improvement in the air electrode performance at 200 mA/cm<sup>2</sup>.

Johnson Matthey then determined that the platinum loading in the alloyed catalyst could be increased up to 30 wt% while retaining the same amount of platinum without any decrease in

---

14. See Reference 21 for literature survey.

specific activity or performance. Note that the amount of nickel, hence the total amount of alloyed catalyst, decreased. Next, J-M researchers increased the amount of platinum from 10 to 30 wt% while keeping the same amount of nickel catalyst loading. The total amount of alloyed catalyst increased in this case. Results showed an additional 36 wt% increase in specific activity, which provided another 41 mV increase at 200 mA/cm<sup>2</sup>. The ideal voltage increase would be 46 mV for this increase in platinum. Thus, the performance increase obtained experimentally was nearly in direct proportion to the theoretical amount expected. The type of carbon support did not seem to be a major factor based on using several typical supports during the tests.

The anode of a phosphoric acid fuel cell is sensitive to catalytic poisoning by even low amounts of contaminants. Yet, hydrogen-rich fuel gases, other than pure hydrogen, are produced with contaminant levels well in excess of the anode's tolerance limit. Of particular concern are CO, COS, and H<sub>2</sub>S. The fuel stream in a current practice PAFC anode, operating at approximately 200°C (392°F), must contain 1 vol % or less of CO (12), less than 50 ppmv of COS plus H<sub>2</sub>S, or less than 20 ppmv of H<sub>2</sub>S (28). Current practice is to place COS and H<sub>2</sub>S cleanup systems and CO shift converters prior to the cell to reduce the fuel stream contaminant levels to the required amounts. Giner, Inc. performed experimental work to develop a contaminant tolerant anode catalyst with the purpose of reducing or eliminating the cleanup equipment (29). An anode catalyst, G87A-17-2, was identified which resulted in only a 24 mV loss from reference when exposed to a 75% H<sub>2</sub>, 1% CO, 24% CO<sub>2</sub>, 80 ppm H<sub>2</sub>S gas mixture at 190°C (374°F), 85% fuel utilization, and 200 mA/cm<sup>2</sup>. A baseline anode experienced a 36 mV loss from the reference at the same conditions. At 9.2 atm (120 psi) pressurization, the anode loss was only 19 mV at 190°C (374°) and 17 mV at 210°C (410°F) (compared with pure H<sub>2</sub>) with a gas of 71% H<sub>2</sub>, 5% CO, 24% CO<sub>2</sub>, and 200 ppm H<sub>2</sub>S. Economic studies comparing the loss of the cell performance with the savings in cost of selected plant components showed no increase when the new anode catalyst was used with gas containing 1% CO/200 ppm H<sub>2</sub>S. A \$7/kW increase resulted with the 5% CO gas (compared to a 1% CO gas) at a 50 MW size. Some savings would result with the elimination of the low temperature shift converter. The real value for the catalyst may be its ability to tolerate excessive CO and H<sub>2</sub>S concentrations during upsets and to simplify the system by the elimination of equipment.

As previously mentioned, state-of-the-art gas diffusion electrodes are configured to provide an electrolyte network and a gas network formed with the mixture of carbon black and PTFE. In the electrodes, carbon black agglomerates consisting of small primary particles, 0.02-0.04 μm, are mixed with much larger PTFE particles, ca. 0.3 μm. The carbon black surface may not be covered completely by the PTFE, because of the large size of conventional PTFE particles. The space in the agglomerates or that between the agglomerates and PTFE may act as gas networks at the initial stage of operation, but fill with electrolyte eventually because of the small contact angle of carbon black, uncovered with PTFE, to electrolyte (<90°), resulting in the degradation of cell performance. Attempts to solve this flooding problem by increasing the PTFE content have not been successful because of the offset of the performance resulting from the reduction of catalyst utilization. Higher performance and longer lifetime of electrodes are intrinsically at odds, and there is a limit to the improvement in performance over life by optimizing PTFE content in the current practice electrode structures. Watanabe et al. (30) proposed preparation of an electrode working at 100% utilization of catalyst clusters, where the functions of gas diffusion electrodes are allotted completely to a hydrophilic, catalyzed carbon black and a wet-proofed carbon black. The

former works as a fine electrolyte network, and the latter works as a gas-supplying network in a reaction layer. Higher utilization of catalyst clusters and longer life at the reaction layer are expected compared to state-of-the-art electrodes consisting of the uniform mixture of catalyzed carbon black and PTFE particles. The *i*R free electrode potentials for the reduction of oxygen and air at 200 mA/cm<sup>2</sup> on the advanced electrode are 10 mV higher than those of the conventional electrode.

As mentioned above, there is a trade-off between high power density and cell life performance. One of the major causes of declining cell performance over its life is that electrode flooding and drying, caused by the migration of phosphoric acid between the matrix and the electrodes, occurs during cell load cycling. Researchers at Fuji Electric addressed two approaches to improve cell life performance while keeping power density high (31). In one, the wettability of the cathode and anode were optimized, and in the other a heat treatment was applied to the carbon support for the cathode catalyst. During tests, it was observed that a cell with low cathode wettability and high anode wettability was over 50 mV higher than a cell with the reverse wetting conditions after 40 start-stop cycles.

The use of carbon blacks with large surface area to improve platinum dispersion on supports was investigated as one way to increase the power density of a cell (32). However, some large surface area carbon blacks are fairly corrosive in hot potassium acid, resulting in a loss of catalytic activity. The corrosivity of the carbon support for a cathode catalyst affects both the rate of loss and of electrode flooding and, in turn, the life performance of a cell. Furnace black has been heat treated at high temperatures by Fuji Electric to increase its resistance to corrosion. It was found that corrosivity can be increased and cell life performance improved by heat treating carbon supports at high temperatures, at least to around 3000°C (5432°F).

## 5.2 Performance

Cell performance for any fuel cell is a function of pressure, temperature, reactant gas composition and fuel utilization. In addition, performance can be adversely affected by impurities in both the fuel and oxidant gases.

The sources of polarization in PAFCs (with cathode and anode Pt loadings of 0.5 mg Pt/cm<sup>2</sup>, 180°C, 1 atm, 100% H<sub>3</sub>PO<sub>4</sub>) have been discussed in Section 2 and were illustrated as half cell performances in Figure 2-3. From Figure 2-3, it is clear that the major polarization occurs at the cathode, and furthermore, the polarization is greater with air (560 mV at 300 mA/cm<sup>2</sup>) than with pure oxygen (480 mV at 300 mA/cm<sup>2</sup>) because of dilution of the reactant. The anode exhibits very low polarization (-4 mV/100 mA/cm<sup>2</sup>) on pure H<sub>2</sub>, and increases when CO is present in the fuel gas. The ohmic (*i*R) loss in PAFCs is also relatively small, amounting to about 12 m at 100 mA/cm<sup>2</sup>.

Typical PAFCs will generally operate in the range of 100 to 400 mA/cm<sup>2</sup> at 600 to 800 mV/cell. Voltage and power constraints arise from increased corrosion of platinum and carbon components at cell potentials above approximately 800 mV.

### 5.2.1 Effect of Pressure

It is well known that an increase in the cell operating pressure enhances the performance of PAFCs (11, 33, 34). The theoretical change in voltage ( $\Delta V_P$ ) as a function of pressure (P) is expressed as

$$\Delta V_P(\text{mV}) = \frac{(3)(2.3RT)}{2F} \log \frac{P_2}{P_1} \quad (5-4)$$

where  $\frac{3(2.3RT)}{2F} = 138 \text{ mV}$  at  $190^\circ\text{C}$  ( $374^\circ\text{F}$ ). Experimental data (35) reported that the effect of pressure on cell performance at  $190^\circ\text{C}$  ( $374^\circ\text{F}$ ) and  $323 \text{ mA/cm}^2$  is correlated by the equation:

$$\Delta V_P (\text{mV}) = 146 \log \frac{P_2}{P_1} \quad (5-5)$$

where  $P_1$  and  $P_2$  are different cell pressures. The experimental data (35) also suggest that Equation (5-5) is a reasonable approximation for a temperature range of  $177^\circ\text{C} \leq T \leq 218^\circ\text{C}$  ( $351^\circ\text{F} \leq T \leq 424^\circ\text{F}$ ) and a pressure range of  $1 \text{ atm} \leq P \leq 10 \text{ atm}$  ( $14.7 \text{ psi} \leq P \leq 147.0 \text{ psi}$ ). Data from Appleby (14) in Figure 5-1 indicate that the voltage gain observed by increasing the pressure from 3.4 atm ( $190^\circ\text{C}$ ) to 6.3 atm ( $205^\circ\text{C}$ ) is about 44 mV. According to Equation (5-5), the voltage gain calculated for this increase in pressure at  $190^\circ\text{C}$  ( $374^\circ\text{F}$ ) is  $39 \text{ mV}^{15}$ , which is in reasonable agreement with experimental data in Figure 5-1. Measurements (33) of  $\Delta V_P$  for an increase in pressure from 4.7 to 9.2 atm (69.1 to 135.2 psia) in a cell at  $190^\circ\text{C}$  ( $374^\circ\text{F}$ ) show that  $\Delta V_P$  is a function of current density, increasing from 35 mV at  $100 \text{ mA/cm}^2$  to 42 mV at  $400 \text{ mA/cm}^2$  (50%  $\text{O}_2$  utilization with air oxidant, 85%  $\text{H}_2$  utilization with pure  $\text{H}_2$  fuel). From Equation (5-4),  $\Delta V_P$  is 43 mV for an increase in pressure from 4.7 to 9.2 atm (69.1 to 135.2 psia) at  $190^\circ\text{C}$  ( $374^\circ\text{F}$ ), which is very close to the experimental value obtained at  $400 \text{ mA/cm}^2$ . Other measurements (36) for the same increase in pressure from 4.7 to 9.2 atm (69.1 to 135.2 psia), but at a temperature of  $210^\circ\text{C}$  ( $410^\circ\text{F}$ ) show less agreement between the experimental data and Equation (5-4).

The improvement in cell performance at higher pressure and high current density can be attributed to a lower diffusion polarization at the cathode and an increase in the reversible cell potential. In addition, pressurization decreases activation polarization at the cathode because of the increased oxygen and water partial pressures. If the partial pressure of water is allowed to increase, a lower acid concentration will result. This will increase ionic conductivity and bring about a higher exchange current density. The net outcome is a reduction in ohmic losses. It was reported (33) that an increase in cell pressure (100%  $\text{H}_3\text{PO}_4$ ,  $169^\circ\text{C}$  ( $336^\circ\text{F}$ )) from 1 to 4.4 atm (14.7 to 64.7 psia) produces a reduction in acid concentration to 97%, and a decrease of about 0.001 ohm in the resistance of a small six cell stack ( $350 \text{ cm}^2$  electrode area).

---

15. The difference in temperature between 190 and  $205^\circ\text{C}$  is disregarded so Equation (5-5) is assumed to be valid at both temperatures.

### 5.2.2 Effect of Temperature

Figure 2-1 shows that the reversible cell potential for PAFCs consuming H<sub>2</sub> and O<sub>2</sub> decreases as the temperature increases by 0.27 mV/°C under standard conditions (product is water vapor). However, as discussed in Section 2, an increase in temperature has a beneficial effect on cell performance because activation polarization, mass transfer polarization, and ohmic losses are reduced.

The kinetics for the reduction of oxygen on Pt improves<sup>16</sup> as the cell temperature increases. At a mid-range operating load (~250 mA/cm<sup>2</sup>), the voltage gain ( $\Delta V_T$ ) with increasing temperature of pure H<sub>2</sub> and air is correlated by

$$\Delta V_T \text{ (mV)} = 1.15 (T_2 - T_1) \text{ (}^\circ\text{C)} \quad (5-6)$$

Data suggest that Equation (5-6) is reasonably valid for a temperature range of  $180^\circ\text{C} \leq T \leq 250^\circ\text{C}$  ( $356^\circ\text{F} \leq T \leq 482^\circ\text{F}$ ). It is apparent from this equation that each degree increase in cell temperature should increase performance by 1.15 mV. Other data indicate that the coefficient for Equation (5-6) may be in the range of 0.55 to 0.75, rather than 1.15. Although temperature has only a minimal effect on the H<sub>2</sub> oxidation reaction at the anode, it is important in terms of anode poisoning. Figure 5-3 shows that increasing the cell temperature results in increased anode tolerance to CO poisoning. This increased tolerance is a result of reduced CO adsorption. A strong temperature effect is also seen for simulated coal gas. Below 200°C (392°F), the cell voltage drop is significant. Experimental data suggest that the effect of contaminants is not additive, indicating that there is an interaction between CO and H<sub>2</sub>S (37). Increasing temperature increases performance, but elevated temperature also increases catalyst sintering, component corrosion, and electrolyte degradation, evaporation, and concentration.

---

16. The anode shows no significant performance improvement from 140 to 180° on pure H<sub>2</sub>, but in the presence of CO, increasing the temperature results in a marked improvement in performance (see discussion in Section 5.2.4).

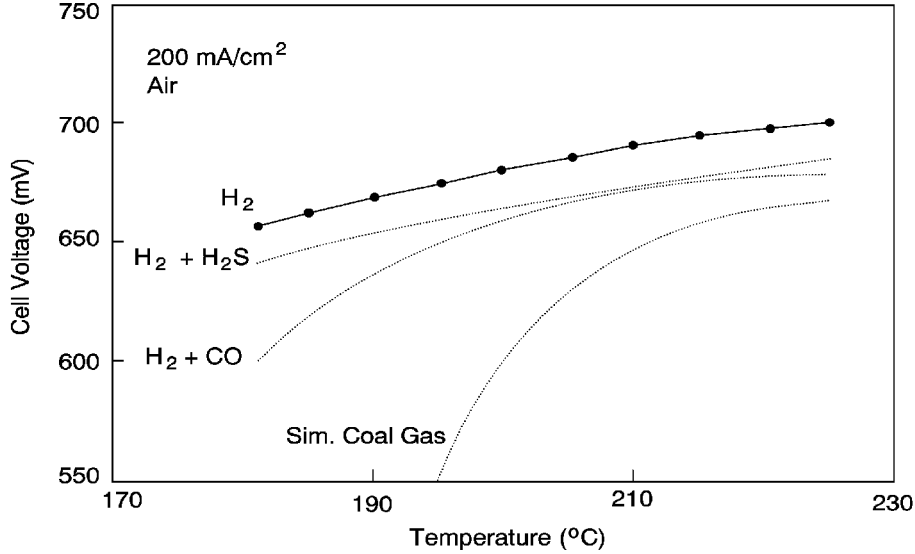


**Figure 5-3 Effect of Temperature: Ultra-High Surface Area Pt Catalyst. Fuel: H<sub>2</sub>, H<sub>2</sub> + 200 ppm H<sub>2</sub>S and Simulated Coal Gas (37)**

### 5.2.3 Effect of Reactant Gas Composition and Utilization

Increasing reactant gas utilization or decreasing inlet concentration results in decreased cell performance due to increased concentration polarization and Nernst losses. These effects are related to the partial pressures of reactant gases and are considered below.

**Oxidant:** The oxidant composition and utilization are parameters that affect the cathode performance, as evident in Figure 2-3. Air, which contains ~21% O<sub>2</sub>, is the oxidant of choice for PAFCs. The use of air with ~21% O<sub>2</sub> instead of pure O<sub>2</sub> results in a decrease in the current density of about a factor of three at constant electrode potential. The polarization at the cathode increases with an increase in O<sub>2</sub> utilization. Experimental measurements (38) of the change in overpotential ( $\Delta\eta_c$ ) at a PTFE-bonded porous electrode in 100% H<sub>3</sub>PO<sub>4</sub> (191°C, atmospheric pressure) as a function of O<sub>2</sub> utilization is plotted in Figure 5-4 in accordance with Equation (5-7):

$$\Delta\eta_c = \eta_c - \eta_{c,\infty} \quad (5-7)$$

where  $\eta_c$  and  $\eta_{c,\infty}$  are the cathode polarizations at finite and infinite (i.e., high flow rate, close to 0% utilization) flow rates, respectively. The additional polarization attributed to O<sub>2</sub> utilization is reflected in the results, and the magnitude of this loss increases rapidly as the utilization increases. At a nominal O<sub>2</sub> utilization of 50% for prototype PAFC power plants, the additional polarization estimated from the results in Figure 4-4 is 19 mV. Based on experimental data (16,38, and 39), the voltage loss due to a change in oxidant utilization can be described by Equations (5-8) and (5-9):

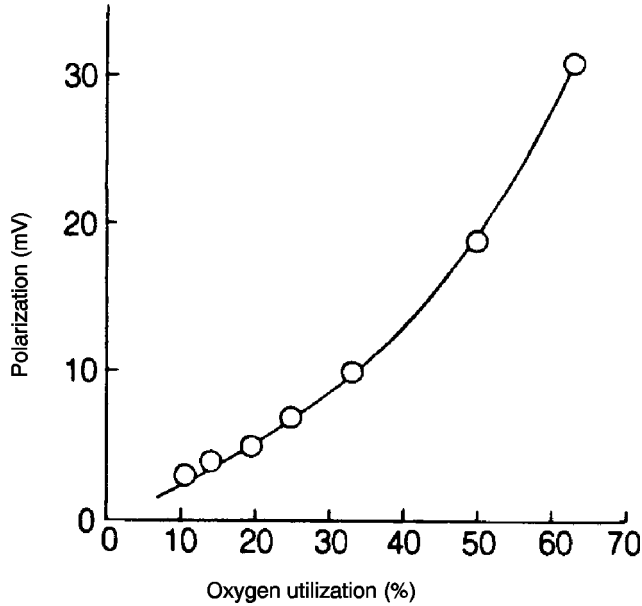


**Figure 5-4 Polarization at Cathode (0.52 mg Pt/cm<sup>2</sup>) as a Function of O<sub>2</sub> Utilization, which is Increased by Decreasing the Flow Rate of the Oxidant at Atmospheric Pressure 100% H<sub>3</sub>PO<sub>4</sub>, 191°C, 300 mA/cm<sup>2</sup>, 1 atm. (38)**

$$\Delta V_{\text{Cathode}} \text{ (mV)} = 148 \log \frac{(\bar{P}_{\text{O}_2})_2}{(\bar{P}_{\text{O}_2})_1} \quad 0.04 \leq \frac{\bar{P}_{\text{O}_2}}{\bar{P}_{\text{Total}}} \leq 0.20 \quad (5-8)$$

$$\Delta V_{\text{Cathode}} \text{ (mV)} = 96 \log \frac{(\bar{P}_{\text{O}_2})_2}{(\bar{P}_{\text{O}_2})_1} \quad 0.20 < \frac{\bar{P}_{\text{O}_2}}{\bar{P}_{\text{Total}}} < 1.00 \quad (5-9)$$

where

$\bar{P}$

$\bar{P}_{\text{O}_2}$  is the average partial pressure of O<sub>2</sub>. Using two equations more accurately correlates actual fuel cell operation. Equation (5-8) will generally apply to fuel cells using air as the oxidant and Equation (5-9) for fuel cells using an O<sub>2</sub>-enriched oxidant.

**Fuel:** Hydrogen for PAFC power plants will typically be produced from conversion of a wide variety of primary fuels such as CH<sub>4</sub> (e.g., natural gas), petroleum products (e.g., naphtha), coal liquids (e.g., CH<sub>3</sub>OH) or coal gases. Besides H<sub>2</sub>, CO and CO<sub>2</sub> are also produced during conversion of these fuels (unreacted hydrocarbons are also present). These reformed fuels contain low levels of CO (after steam reforming and shift conversion reactions in the fuel processor) which cause anode poisoning in PAFCs. The CO<sub>2</sub> and unreacted hydrocarbons (e.g., CH<sub>4</sub>) are electrochemically inert and act as diluents. Because the anode reaction is nearly reversible, the fuel



composition and hydrogen utilization generally do not strongly influence cell performance. The voltage change due to a change in the partial pressure of hydrogen (which can result from a change in either the fuel composition or utilization) can be described by Equation (5-10) (16,36,37):

$$\Delta V_{\text{Anode}}(\text{mV}) = 55 \log \frac{(\bar{P}_{\text{H}_2})_2}{(\bar{P}_{\text{H}_2})_1} \quad (5-10)$$

where

$\bar{P}$

$\bar{P}_{\text{H}_2}$  is the average partial pressure of  $\text{H}_2$  in the system. At  $190^\circ\text{C}$  ( $374^\circ\text{F}$ ), the presence of 10%  $\text{CO}_2$  in  $\text{H}_2$  should cause a voltage loss of about 2 mV. Thus, diluents in low concentrations are not expected to have a major effect on electrode performance; however, relative to the total anode polarization (i.e.,  $3 \text{ mV}/100 \text{ mA}/\text{cm}^2$ ), the effects are large. It has been reported (16) that with pure  $\text{H}_2$ , the cell voltage at  $215 \text{ mA}/\text{cm}^2$  remains nearly constant at  $\text{H}_2$  utilizations up to 90%, and then it decreases sharply at  $\text{H}_2$  utilizations above this value.

Low utilizations, particularly oxygen utilization, yield high performance. Low utilizations, however, result in poor fuel use. Optimization of this parameter is required. State-of-the-art utilizations are on the order of 85% and 50% for the fuel and oxidant, respectively.

#### 5.2.4 Effect of Impurities

The concentrations of impurities entering the PAFC are very low relative to diluents and reactant gases, but their impact on performance is significant. Some impurities (e.g., sulfur compounds) originate from fuel gas entering the fuel processor and are carried into the fuel cell with the reformed fuel, whereas others (e.g., CO) are produced in the fuel processor.

**Carbon Monoxide:** The presence of CO in a  $\text{H}_2$ -rich fuel has a significant effect on anode performance because CO affects Pt electrodes catalysts. The poisoning is reported to arise from the dual site replacement of one  $\text{H}_2$  molecule by two CO molecules on the Pt surface (40, 41). According to this model, the anodic oxidation current at a fixed overpotential, with ( $i_{\text{CO}}$ ) and without ( $i_{\text{H}_2}$ ) CO present, is given as a function of CO coverage ( $\theta_{\text{CO}}$ ) by Equation (5-11):

$$\frac{i_{\text{CO}}}{i_{\text{H}_2}} = (1 - \theta_{\text{CO}})^2 \quad (5-11)$$

For  $[\text{CO}]/[\text{H}_2] = 0.025$ ,  $\theta_{\text{CO}} = 0.31$  at  $190^\circ\text{C}$  (35); therefore,  $i_{\text{CO}}$  is about 50% of  $i_{\text{H}_2}$ .

As discussed previously, both temperature and CO concentration have a major influence on the oxidation of  $\text{H}_2$  on Pt in CO containing fuel gases. Benjamin et al. (35) derived Equation (5-12) for the voltage loss resulting from CO poisoning as a function of temperature

$$\Delta V_{CO} = k(T) ([CO]_2 - [CO]_1) \quad (5-12)$$

where  $k(T)$  is a function of temperature, and  $[CO]_1$  and  $[CO]_2$  are the mole fractions CO in the fuel gas. The values of  $k(T)$  at various temperatures are listed in Table 5-3. Using Equation (5-12) and the data in Table 5-3, it is apparent that for a given change in CO content,  $\Delta V_{CO}$  is about 8.5 times larger at 163°C (325°F) than at 218°C (424°F). The correlation provided by Equation (5-12) was obtained at 269 mA/cm<sup>2</sup>; thus, its use at significantly different current densities may not be appropriate. In addition, other more recent data (37) suggest a value for  $k(T)$  of -2.12 at a temperature of 190°C (374°F) rather than -3.54.

**Table 5-3 Dependence of  $k(T)$  on Temperature**

T	T	$k(T)^a$
(°C)	(°F)	(mV/%)
163	325	-11.1
177	351	-6.14
190	374	-3.54
204	399	-2.05
218	424	-1.30

a - Based on electrode with 0.35 mg Pt/cm<sup>2</sup>, and at 269 mA/cm<sup>2</sup> (35)

The data in Figure 5-5 illustrate the influence of H<sub>2</sub> partial pressure and CO content on the performance of Pt anodes (10% Pt supported on Vulcan XC-72, 0.5 mg Pt/cm<sup>2</sup>) in 100% H<sub>3</sub>PO<sub>4</sub> at 180°C (356°F) (11). Diluting the H<sub>2</sub> fuel gas with 30% CO<sub>2</sub> produces an additional polarization of about 11 mV at 300 mA/cm<sup>2</sup>. The results show that the anode polarization with fuel gases of composition 70% H<sub>2</sub>/(30-x)% CO<sub>2</sub>/x% CO (x = 0, 0.3, 1, 3 and 5) increases considerably as the CO content increases to 5%.

**Sulfur Containing Compounds:** Hydrogen sulfide and carbonyl sulfide (COS) are impurities<sup>17</sup> in fuel gases from fuel processors and coal gasifiers in PAFC power plants. The concentration levels of H<sub>2</sub>S in an operating PAFC (190 to 210°C (374 to 410°F), 9.2 atm (120 psig), 80% H<sub>2</sub> utilization, <325 mA/cm<sup>2</sup>) that can be tolerated by Pt anodes without suffering a destructive loss in performance are <50 ppm (H<sub>2</sub>S + COS) or <20 ppm (H<sub>2</sub>S) (42). Rapid cell failure occurs with fuel gas containing more than 50 ppm H<sub>2</sub>S. Sulfur poisoning does not affect the cathode, and poisoned anodes can be re-activated by polarization at high potentials (i.e., operating cathode potentials). As mentioned previously, there is a synergistic effect between H<sub>2</sub>S and CO that can negatively impact cell performance. Figure 5-6 (37) shows the effect of H<sub>2</sub>S concentration on  $\Delta V$  with and without 10% CO present in H<sub>2</sub>. The  $\Delta V$  is referenced to performance on pure H<sub>2</sub> in the case of H<sub>2</sub>S alone and to performance on H<sub>2</sub> with 10% CO for H<sub>2</sub>S and CO. In both cases, at higher H<sub>2</sub>S

17. Anode gases from coal gasifiers may contain total sulfur of 100 to 200 ppm.

concentrations, the  $\Delta V$  rises abruptly. This drop in performance occurs above 240 ppm for  $H_2S$  alone and above 160 ppm for  $H_2S$  with 10% CO.

Experimental studies by Chin and Howard (43) indicate that  $H_2S$  adsorbs on Pt and blocks the active sites for  $H_2$  oxidation. The following electrochemical reactions, Equations (5-13), (5-14), and (5-15) involving  $H_2S$  are postulated to occur on Pt electrodes:

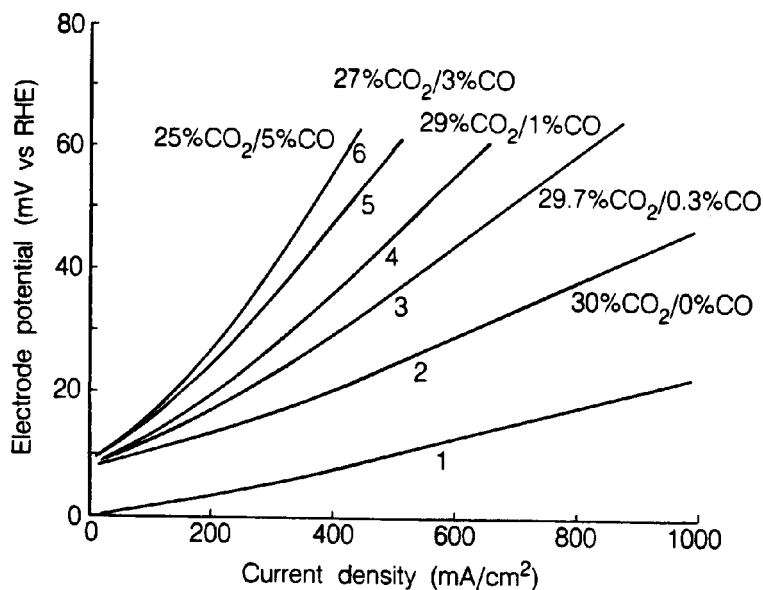


**Figure 5-5 Influence of CO and Fuel Gas Composition on the Performance of Pt Anodes in 100%  $H_3PO_4$  at 180°C. 10% Pt Supported on Vulcan XC-72, 0.5 mg Pt/cm<sup>2</sup>. Dew Point, 57°. Curve 1, 100%  $H_2$ ; Curves 2-6, 70%  $H_2$  and  $CO_2/CO$  Contents (mol%) Specified (21)**

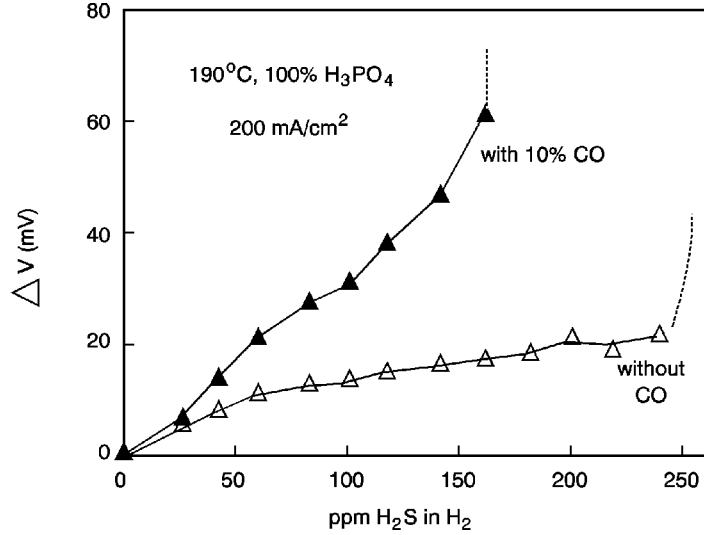


**Figure 5-6 Effect of H<sub>2</sub>S Concentration: Ultra-High Surface Area Pt Catalyst (37)**

Elemental sulfur (in Equation (5-15) is expected on Pt electrodes only at high anodic potentials, and at sufficiently high potentials, sulfur is oxidized to SO<sub>2</sub>. The extent of poisoning by H<sub>2</sub>S increases with increasing H<sub>2</sub>S concentration, electrode potential, and exposure time. H<sub>2</sub>S poisoning, however, decreases with increasing cell temperature.

**Other Compounds:** The effect of other compounds (such as those containing nitrogen) on PAFC performance has been adequately reviewed by Benjamin et al. (35). Molecular nitrogen acts as a diluent but other nitrogen compounds (e.g., NH<sub>3</sub>, HCN, NO<sub>x</sub>) may not be as innocuous. NH<sub>3</sub> in the fuel or oxidant gases reacts with H<sub>3</sub>PO<sub>4</sub> to form a phosphate salt, (NH<sub>4</sub>)H<sub>2</sub>PO<sub>4</sub>,



which decreases the rate of O<sub>2</sub> reduction. A concentration of less than 0.2 mol% (NH<sub>4</sub>)H<sub>2</sub>PO<sub>4</sub> must be maintained to avoid unacceptable performance losses (44). The effects of HCN and NO<sub>x</sub> on fuel cell performance have not been clearly established.

### 5.2.5 Effects of Current Density

The voltage that can be obtained from a PAFC is reduced by ohmic, activation, and concentration losses that increase with increasing current density. The magnitude of this loss can be approximated by the following equations:

$$\Delta V_J \text{ (mV)} = -0.53 \Delta J \quad \text{for } J = 100 - 200 \text{ mA/cm}^2 \quad (5-17)$$

$$\Delta V_J \text{ (mV)} = -0.39 \Delta J \quad \text{for } J = 200 - 650 \text{ mA/cm}^2 \quad (5-18)$$

The coefficients in these equations were correlated from performance data for cells (45) operating at 120 psia (8.2 atm), 405°F (207°C) (16) with fuel and oxidant utilizations of 85% and 70%, respectively<sup>18</sup>, an air fed cathode, and an anode inlet composition of 75% H<sub>2</sub>, and 0.5% CO. Similarly, at atmospheric conditions, the magnitude of this loss can be approximated by

$$\Delta V_J \text{ (mV)} = -0.74 \Delta J \quad \text{for } J = 50 - 120 \text{ mA/cm}^2 \quad (5-19)$$

$$\Delta V_J \text{ (mV)} = -0.45 \Delta J \quad \text{for } J = 120 - 215 \text{ mA/cm}^2 \quad (5-20)$$

The coefficients in the atmospheric condition equations have been derived from performance data for cells (45) operating at 14.7 psia (1 atm) and 400°F (204°C), fuel and oxidant utilizations of 80% and 60%, respectively<sup>18</sup>, an air fed cathode, and an anode inlet composition of 75% H<sub>2</sub> and 0.5% CO.

### 5.2.6 Effects of Cell Life

One of the primary areas of research is in extending cell life. The goal is to maintain the performance of the cell stack during a standard utility application (~40,000 hours). Current state-of-the-art PAFCs (46, 47, and 48) show the following degradation over time:

$$\Delta V_{\text{lifetime}} \text{ (mV)} = -3 \text{ mV/1,000 hours} \quad (5-21)$$

## 5.3 Summary of Equations for PAFC

The preceding sections provide parametric performance based on various referenced data at differing cell conditions. It is suggested that the following set of equations be used unless the reader prefers other data or rationale. Figure 5-7 is provided as reference PAFC performances at 8.2 atm and ambient pressure.

---

18. Assumes graph operating conditions (not provided) are the same as associated text of Ref. 15.

<u>Parameter</u>	<u>Equation</u>	<u>Comments</u>
Pressure	$\Delta V_p \text{ (mV)} = 146 \log \frac{P_2}{P_1}$	$1 \text{ atm} \leq P \leq 10 \text{ atm}$ $177^\circ\text{C} \leq T \leq 218^\circ\text{C}$ (5-5)
Temperature	$\Delta V_T \text{ (mV)} = 1.15 (T_2 - T_1)$	$180^\circ\text{C} \leq T \leq 250^\circ\text{C}$ (5-6)
Oxidant	$\Delta V_{\text{cathode}} \text{ (mV)} = 148 \log \frac{(\bar{P}_{O_2})_2}{(\bar{P}_{O_2})_1}$	$0.04 \leq \frac{\bar{P}_{O_2}}{P_{\text{Total}}} \leq 0.20$ (5-8)
	$\Delta V_{\text{cathode}} \text{ (mV)} = 96 \log \frac{(\bar{P}_{O_2})_2}{(\bar{P}_{O_2})_1}$	$0.20 \leq \frac{\bar{P}_{O_2}}{P_{\text{Total}}} < 1.0$ (5-9)
Fuel	$\Delta V_{\text{anode}} \text{ (mV)} = 55 \log \frac{(\bar{P}_{H_2})_2}{(\bar{P}_{H_2})_1}$	(5-10)
CO Poisoning	$\Delta V_{\text{CO}} \text{ (mV)} = -11.1 ([\text{CO}]_2 - [\text{CO}]_1)$ 163°C $\Delta V_{\text{CO}} \text{ (mV)} = -6.14 ([\text{CO}]_2 - [\text{CO}]_1)$ 177°C $\Delta V_{\text{CO}} \text{ (mV)} = -3.54 ([\text{CO}]_2 - [\text{CO}]_1)$ 190°C $\Delta V_{\text{CO}} \text{ (mV)} = -2.05 ([\text{CO}]_2 - [\text{CO}]_1)$ 204°C $\Delta V_{\text{CO}} \text{ (mV)} = -1.30 ([\text{CO}]_2 - [\text{CO}]_1)$ 218°C	(5-12)
Current Density	$\Delta V_J \text{ (mV)} = -0.53 \Delta J$ for $J = 100 - 200 \text{ mA/cm}^2$ , $P = 8.2 \text{ atm}$	(5-17)
	$\Delta V_J \text{ (mV)} = -0.39 \Delta J$ for $J = 200 - 650 \text{ mA/cm}^2$ , $P = 8.2 \text{ atm}$	(5-18)
	$\Delta V_J \text{ (mV)} = -0.74 \Delta J$ for $J = 50 - 120 \text{ mA/cm}^2$ , $P = 1 \text{ atm}$	(5-19)
	$\Delta V_J \text{ (mV)} = -0.45 \Delta J$ for $J = 120 - 215 \text{ mA/cm}^2$ , $P = 1 \text{ atm}$	(5-20)
Life Effects	$\Delta V_{\text{lifetime}} \text{ (mV)} = -3\text{mV}/1,000 \text{ hrs.}$	(5-21)

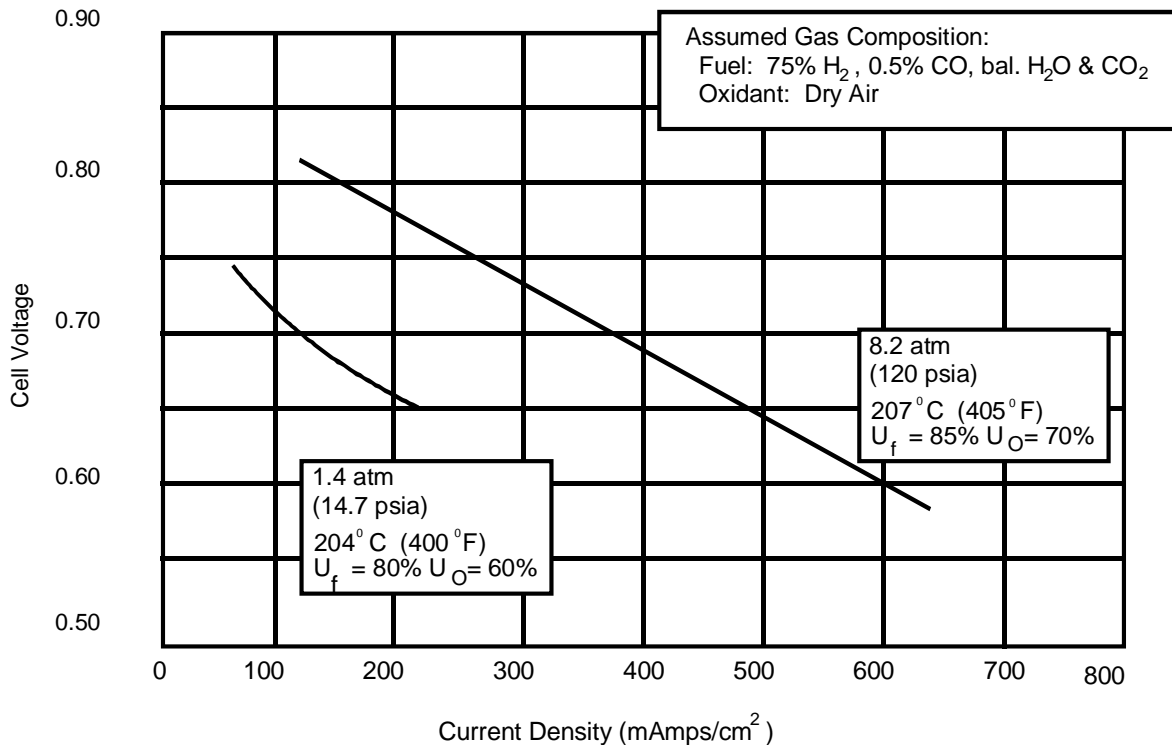


**Figure 5-7 Reference Performances at 8.2 atm and Ambient Pressure (16)**

## 5.4 References

1. Communications with IFC, September 21, 1998.
2. J. Hirschenhofer, "Latest Progress in Fuel Cell Technology," *IEEE-Aerospace and Electronic Systems Magazine*, 7, November 1992.
3. J. Hirschenhofer, "Status of Fuel Cell Commercialization Efforts," *American Power Conference*, Chicago, IL, April 1993.
4. J. Appleby, in *Proceedings of the Workshop on the Electrochemistry of Carbon*, Edited by S. Sarangapani, J.R. Akridge and B. Schumm, The Electrochemical Society, Inc., Pennington, NJ, p. 251, 1984.
5. K.V. Kordesch, "Survey of Carbon and Its Role in Phosphoric Acid Fuel Cells," BNL 51418, prepared for Brookhaven National Laboratory, December 1979.
6. K. Kinoshita, *Carbon: Electrochemical and Physicochemical Properties*, Wiley Interscience, New York, NY, 1988.
7. L. Christner, J. Ahmad, M. Farooque, in *Proceedings of the Symposium on Corrosion in Batteries and Fuel Cells and Corrosion in Solar Energy Systems*, Edited by C. J. Johnson and S.L. Pohlman, The Electrochemical Society, Inc., Pennington, NJ, p. 140, 1983.
8. P.W.T. Lu, L.L. France, in *Extended Abstracts*, Fall Meeting of The Electrochemical Society, Inc., Volume 84-2, Abstract No. 573, The Electrochemical Society, Inc., Pennington, NJ, p. 837, 1984.
9. M. Warshay, in *The Science and Technology of Coal and Coal Utilization*, Edited by B.R. Cooper, W.A. Ellingson, Plenum Press, New York, NY, p. 339, 1984.

10. P.R. Prokopius, M. Warshay, S.N. Simons, R.B. King, in *Proceedings of the 14th Intersociety Energy Conversion Engineering Conference*, Volume 2, American Chemical Society, Washington, D. C., p. 538, 1979.
11. S.N. Simons, R.B. King, P.R. Prokopius, in *Symposium Proceedings Fuel Cells Technology Status and Applications*, Edited by E. H. Camara, Institute of Gas Technology, Chicago, IL, p. 45, 1982.
12. Communications with IFC, September 2000.
13. A.P. Fickett, in *Proceedings of the Symposium on Electrode Materials and Processes for Energy Conversion and Storage*, Edited by J.D.E. McIntyre, S. Srinivasan and F.G. Will, The Electrochemical Society, Inc. Pennington, NJ, p. 546, 1977.
14. A.J. Appleby, *J. Electroanal. Chem.*, 118, 31, 1981.
15. J. Huff, "Status of Fuel Cell Technologies," in *Fuel Cell Seminar Abstracts*, 1986 National Fuel Cell Seminar, Tucson, AZ, October 1986.
16. "Advanced Water-Cooled Phosphoric Acid Fuel Cell Development, Final Report," Report No. DE/MC/24221-3130, International Fuel Cells Corporation for U.S. DOE under Contract DE-AC21-88MC24221, South Windsor, CT, September 1992.
17. N. Giordano, E. Passalacqua, L. Pino, V. Alderucci, P.L. Antonucci, "Catalyst and Electrochemistry in PAFC: A Unifying Approach," in *The International Fuel Cell Conference Proceedings*, NEDO/MITI, Tokyo, Japan, 1992.
18. B. Roland, J. Scholta, H. Wendt, "Phosphoric Acid Fuel Cells - Materials Problems, Process Techniques and Limits of the Technology," in *The International Fuel Cell Conference Proceedings*, NEDO/MITI, Tokyo, Japan, 1992.
19. "Overview of 11 MW Fuel Cell Power Plant," Non-published information from Tokyo Electric Power Company, September 1989.
20. M. Matsumoto, K. Usami, "PAFC Commercialization and Recent Progress of Technology in Mitsubishi Electric," in *The International Fuel Cell Conference Proceedings*, NEDO/MITI, Tokyo, Japan, 1992.
21. J.A.S. Bett, H.R. Kunz, S.W. Smith and L.L. Van Dine, "Investigation of Alloy Catalysts and Redox Catalysts for Phosphoric Acid Electrochemical Systems," FCR-7157F, prepared by International Fuel Cells for Los Alamos National Laboratory under Contract No. 9-X13-D6271-1, 1985.
22. B.C. Beard, P.N. Ross, *J. Electrochem. Soc.*, 133, 1839, 1986.
23. J.T. Glass, G.L. Cahen, G.E. Stoner, E.J. Taylor, *J. Electrochem. Soc.*, 134, 58, 1987.
24. P.N. Ross, "Oxygen Reduction on Supported Pt Alloys and Intermetallic Compounds in Phosphoric Acid," Final Report, EM-1553, prepared under Contract 1200-5 for the Electric Power Research Institute, Palo Alto, CA, September 1980.
25. V. Jalan, J. Giner, in *DECHEMA Monographs*, Volume 102, Edited by J.W. Schultze, VCH Verlagsgesellschaft, Weinheim, West Germany, p. 315, 1986.
26. T. Ito, K. Kato, S. Kamitomi, M. Kamiya, "Organization of Platinum Loading Amount of Carbon-Supported Alloy Cathode for Advanced Phosphoric Acid Fuel Cell," in *Fuel Cell Seminar Abstracts*, 1990 Fuel Cell Seminar, Phoenix, AZ, November 25-28, 1990.
27. J.S. Buchanan, G.A. Hards, L. Keck, R.J. Potter, "Investigation into the Superior Oxygen Reduction Activity of Platinum Alloy Phosphoric Acid Fuel Cell Catalysts," in *Fuel Cell Seminar Abstracts*, Tucson, AZ, November 29-December 2, 1992.



28. K. Kinoshita, F.R. McLarnon, E.J. Cairns, *Fuel Cells, A Handbook*, prepared by Lawrence Berkeley Laboratory for the U.S. Department of Energy under Contract DE-AC03-76F00098, May 1988.
29. N.D. Kackley, S.A. McCatty, J.A. Kosek, "Improved Anode Catalysts for Coal Gas-Fueled Phosphoric Acid Fuel Cells," Final Report DOE/MC/25170-2861, prepared for U.S. Department of Energy under Contract DE-AC21-88MC25170, July 1990.
30. M. Watanabe, C. Shirmura, N. Hara, K. Tsurumi, "An Advanced Gas-Diffusion Electrode for Long-Life and High Performance PAFC," in *The International Fuel Cell Conference Proceedings*, NEDO/MITI, Tokyo, Japan, 1992.
31. M. Aoki, Y. Ueki, H. Enomoto, K. Harashima, "Some Approaches to Improve the Life Performance of Phosphoric Acid Fuel Cell," paper provided to the authors by Fuji Electric Corporate Research and Development, 1992, date of preparation unknown.
32. M. Watanabe, H. Sei, P. Stonehart, *Journal of Electroanalytical Chemistry*. 261, 375, 1989.
33. M. Farooque, "Evaluation of Gas-Cooled Pressurized Phosphoric Acid Fuel Cells for Electric Utility Power Generation," Final Technical Report, NASA CR-168298 prepared by Energy Research Corp. under Contract No. DEN 3-201 for NASA Lewis Research Center, September 1983.
34. J. McBreen, W.E. O'Grady, R. Richter, *J. Electrochem. Soc.*, 131, 1215, 1984.
35. T.G. Benjamin, E.H. Camara, L.G. Marianowski, *Handbook of Fuel Cell Performance*, prepared by the Institute of Gas Technology for the United States Department of Energy under Contract No. EC-77-C-03-1545, May 1980.
36. J.M. Feret, "Gas Cooled Fuel Cell Systems Technology Development," Final Report, NASA CR-175047, prepared by Westinghouse Electric Corp. under Contract No. DEN 3-290 for NASA Lewis Research Center, August 1985.
37. V. Jalan, J. Poirier, M. Desai, B. Morrisean, "Development of CO and H<sub>2</sub>S Tolerant PAFC Anode Catalysts," in *Proceedings of the Second Annual Fuel Cell Contractors Review Meeting*, 1990.
38. P.W.T. Lu and L. L. France, in *Proceedings of the Symposium on Transport Processes in Electrochemical Systems*, R. S. Yeo, K. Katan and D. T. Chin, The Electrochemical Society, Inc., Pennington, NJ, p. 77, 1982.
39. P.N. Ross, "Anomalous Current Ratios in Phosphoric Acid Fuel Cell Cathodes," LBL-13955; submitted to *J. Electrochem. Soc.*, March 1986.
40. P. Ross, P. Stonehart, *Electrochim. Acta*, 21, 441, 1976.
41. W. Vogel, J. Lundquist, P. Ross, P. Stonehart, *Electrochim. Acta*, 20, 79, 1975.
42. H.R. Kunz, in *Proceedings of the Symposium on Electrode Materials and Processes for Energy Conversion and Storage*, Edited by J. D. E. McIntyre, S. Srinivasan and F. G. Will, The Electrochemical Society, Inc., Pennington, NJ, p. 607, 1977.
43. D.T. Chin, P.D. Howard, *J. Electrochem. Soc.*, 133, 2447, 1986.
44. S.T. Szymanski, G.A. Gruver, M. Katz, H.R. Kunz, *J. Electrochem. Soc.*, 127, 1440, 1980.
45. F.S. Kemp, IFC, "Status of Development of Water - Cooled Phosphoric Acid Fuel Cells," in *Proceedings of the Second Annual Fuel Cell Contractors Review Meeting*, U.S. DOE/METC, 1990.
46. N. Giordano, "Fuel Cells Activity at CNR, TAE Institute," CNR/TAE, Italy, 1992.
47. "Gas Cooled Fuel Cell Systems Technology Development," Westinghouse/DOE, WAES-TR-92-001, March 1992.
48. K. Harasawa, I. Kanno, I. Masuda, "Fuel Cell R&D and Demonstration Programs at Electric Utilities in Japan," in *Fuel Cell Seminar Abstracts*, Tucson, AZ, November 29-December 2, 1992.

---

## 6. MOLTEN CARBONATE FUEL CELL

---

The molten carbonate fuel cell operates at approximately 650°C (1200°F). The high operating temperature is needed to achieve sufficient conductivity of its carbonate electrolyte yet allow the use low cost metal cell components. Aneffect associated with this high temperature is that noble metal catalysts are not required for the cell electrochemical oxidation and reduction processes. Molten carbonate fuel cells are being developed for natural gas and coal-based power plants for industrial, electrical utility, and military applications. Currently, one industrial corporation is actively pursuing the commercialization of MCFCs in the U.S.: Fuel Cell Energy (FCE). Europe and Japan each have at least three developers pursuing the technology: Brandstofel Nederland B.V. (BCN), MTU Friedrichshafen, Ansaldo (Italy), Hitachi, Ishikawajima-Harima Heavy Industries, Mitsubishi Electric Corporation, and Toshiba Corporation.

The electrochemical reactions occurring in MCFCs are



at the anode, and



at the cathode. The overall cell reaction<sup>19</sup> is



---

<sup>19</sup>. CO is not directly used by electrochemical oxidation, but produces additional H<sub>2</sub> when combined with water in the water gas shift reaction.

Besides the reaction involving H<sub>2</sub> and O<sub>2</sub> to produce H<sub>2</sub>O, the equation shows a transfer of CO<sub>2</sub> from the cathode gas stream to the anode gas stream, with 1 mole CO<sub>2</sub> transferred along with two Faradays of charge or 2 gram moles of electrons. The reversible potential for an MCFC, taking into account the transfer of CO<sub>2</sub>, is given by the equation

$$E = E^\circ + \frac{RT}{2F} \ln \frac{P_{H_2} P_{O_2}^{1/2}}{P_{H_2O}} + \frac{RT}{2F} \ln \frac{P_{CO_2,c}}{P_{CO_2,a}} \quad (6-4)$$

where the subscripts a and c refer to the anode and cathode gas compartments, respectively. When the partial pressures of CO<sub>2</sub> are identical at the anode and cathode, and the electrolyte is invariant, the cell potential depends only on the partial pressures of H<sub>2</sub>, O<sub>2</sub>, and H<sub>2</sub>O. Typically, the CO<sub>2</sub> partial pressures are different in the two electrode compartments and the cell potential is affected accordingly, as shown in Equation (6-4).

It is usual practice in an MCFC system that the CO<sub>2</sub> generated at the anode be routed to the cathode where it is consumed. This will require some scheme that will either 1) transfer the CO<sub>2</sub> from the anode exit gas to the cathode inlet gas ("CO<sub>2</sub> transfer device"), 2) produce CO<sub>2</sub> by combustion of the anode exhaust gas, which is mixed directly with the cathode inlet gas, or 3) supply CO<sub>2</sub> from an alternate source.

MCFCs differ in many respects from PAFCs because of their higher operating temperature (650 vs 200°C) and the nature of the electrolyte. The higher operating temperature of MCFCs provides the opportunity for achieving higher overall system efficiencies (potential for heat rates below 7500 Btu/kWh) and greater flexibility in the use of available fuels.<sup>20</sup> On the other hand, the higher operating temperature places severe demands on the corrosion stability and life of cell components, particularly in the aggressive environment of the molten carbonate electrolyte. Another difference between PAFCs and MCFCs lies in the method used for electrolyte management in the respective cells. In a PAFC, PTFE serves as a binder and wet-proofing agent to maintain the integrity of the electrode structure and to establish a stable electrolyte/gas interface in the porous electrode. The phosphoric acid is retained in a matrix of PTFE and SiC between the anode and cathode. There are no materials available for use in MCFCs that are comparable to PTFE. Thus, a different approach is required to establish a stable electrolyte/gas interface in MCFC porous electrodes, and this is illustrated schematically in Figure 6-1. The MCFC relies on a balance in capillary pressures to establish the electrolyte interfacial boundaries in the porous electrodes (1,2,3). At thermodynamic equilibrium, the diameters of the largest flooded pores in the porous components are related by the equation

$$\frac{\gamma_c \cos \theta_c}{D_c} = \frac{\gamma_e \cos \theta_e}{D_e} = \frac{\gamma_a \cos \theta_a}{D_a} \quad (6-5)$$

<sup>20</sup>. *In situ* reforming of fuels in MCFCs is possible as discussed later in the section.

where  $\gamma$  is the interfacial surface tension,  $\theta$  is the contact angle of the electrolyte,  $D$  is the pore diameter, and the subscripts a, c, and e refer to the anode, cathode and electrolyte matrix, respectively. By properly coordinating the pore diameters in the electrodes with those of the electrolyte matrix, which contains the smallest pores, the electrolyte distribution depicted in Figure 6-1 is established. This arrangement permits the electrolyte matrix to remain completely filled with molten carbonate, while the porous electrodes are partially filled, depending on their pore size distributions. According to the model illustrated in Figure 6-1 and described by Equation (6-5), the electrolyte content in each of the porous components will be determined by the equilibrium pore size ( $\langle D \rangle$ ) in that component; pores smaller than  $\langle D \rangle$  will be filled with electrolyte, and pores larger than  $\langle D \rangle$  will remain empty. A reasonable estimate of the volume distribution of electrolyte in the various cell components is obtained from the measured pore-volume-distribution curves and the above relationship for  $D$  (2, 3).

Electrolyte management, that is, the control over the optimum distribution of molten carbonate electrolyte in the different cell components, is critical for achieving high performance and endurance with MCFCs. Various processes (i.e., consumption by corrosion reactions, potential driven migration, creepage of salt and salt vaporization) occur, all of which contribute to the redistribution of molten carbonate in MCFCs; these aspects are discussed by Maru et al. (4) and Kunz (5).

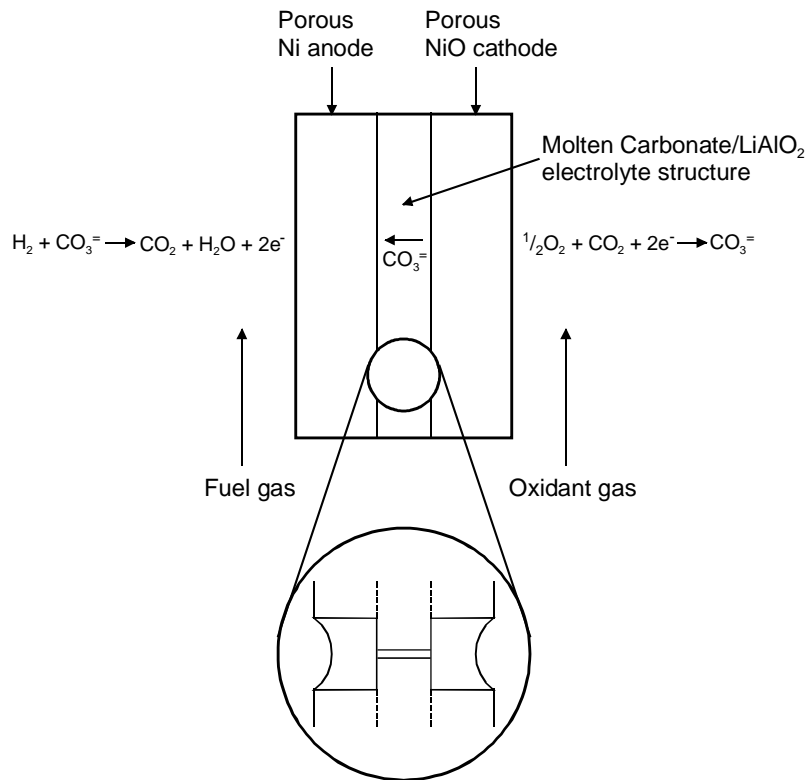


**Figure 6-1 Dynamic Equilibrium in Porous MCFC Cell Elements (Porous electrodes are depicted with pores covered by a thin film of electrolyte)**

## 6.1 Cell Components

### 6.1.1 State-of-the-Art

The data in Table 6-1 provide a chronology of the evolution in cell component technology for MCFCs. In the mid-1960s, electrode materials were, in many cases, precious metals, but the technology soon evolved to the use of Ni-based alloys at the anode and oxides at the cathode. Since the mid-1970s, the materials for the electrodes and electrolyte structure (molten carbonate/LiAlO<sub>2</sub>) have remained essentially unchanged. A major development in the 1980s was the evolution in the technology for fabrication of electrolyte structures. Developments in cell components for MCFCs have been reviewed by Maru et al. (6, 7), Petri and Benjamin (8), and Selman (9). Over the past 20 years, the performance of single cells has improved from about 10 mW/cm<sup>2</sup> to >150 mW/cm<sup>2</sup>. During the 1980s, both the performance and endurance of MCFC stacks showed dramatic improvements. The data in Figure 6-2 illustrate the progress that has been made in the performance of single cells, and in the cell voltage at 172 mA/cm<sup>2</sup> (160 A/ft<sup>2</sup>) of small stacks at 650°C, with low-Btu fuel [17% (H<sub>2</sub> + CO)] at 65 psia. Several MCFC stack developers have produced cell stacks with cell areas up to 1 m<sup>2</sup> cells. Tall, full-scale U.S. stacks fabricated to date include an FCE stack with 246 5600 cm<sup>2</sup> cells producing 125 kW, and an FCE stack with 253 7800 cm<sup>2</sup> cells producing 253 kW.

**Table 6-1 Evolution of Cell Component Technology for Molten Carbonate Fuel Cells**

Component	ca. 1965	ca. 1975	Current Status
Anode	<ul style="list-style-type: none"> <li>• Pt, Pd, or Ni</li> </ul>	<ul style="list-style-type: none"> <li>• Ni-10 wt% Cr</li> </ul>	<ul style="list-style-type: none"> <li>• Ni-Cr/Ni-Al</li> <li>• 3-6 μm pore size</li> <li>• 45-70% initial porosity</li> <li>• 0.20-1.5 mm thickness</li> <li>• 0.1-1 m<sup>2</sup>/g</li> </ul>
Cathode	<ul style="list-style-type: none"> <li>• Ag<sub>2</sub>O or lithiated NiO</li> </ul>	<ul style="list-style-type: none"> <li>• lithiated NiO</li> </ul>	<ul style="list-style-type: none"> <li>• lithiated NiO</li> <li>• 7-15 μm pore size</li> <li>• 70-80% initial porosity</li> <li>• 60-65% after lithiation and oxidation</li> <li>• 0.5-1 mm thickness</li> <li>• 0.5 m<sup>2</sup>/g</li> </ul>
Electrolyte Support	<ul style="list-style-type: none"> <li>• MgO</li> </ul>	<ul style="list-style-type: none"> <li>• mixture of α-, β-, and γ-LiAlO<sub>2</sub></li> <li>• 10-20 m<sup>2</sup>/g</li> </ul>	<ul style="list-style-type: none"> <li>• γ-LiAlO<sub>2</sub>, α-LiAlO<sub>2</sub></li> <li>• 0.1-12 m<sup>2</sup>/g</li> <li>• 0.5-1 mm thickness</li> </ul>

Component	ca. 1965	ca. 1975	Current Status
Electrolyte <sup>a</sup>	<ul style="list-style-type: none"> <li>• 52 Li-48 Na</li> <li>• 43.5 Li-31.5 Na-25 K</li> </ul>	<ul style="list-style-type: none"> <li>• 62 Li-38 K</li> <li>• ~60-65 wt%</li> </ul>	<ul style="list-style-type: none"> <li>• 62 Li-38 K</li> <li>• 50 Li-50 Na</li> <li>• ~50 wt%</li> </ul>
	<ul style="list-style-type: none"> <li>• "paste"</li> </ul>	<ul style="list-style-type: none"> <li>• hot press "tile"</li> <li>• 1.8 mm thickness</li> </ul>	<ul style="list-style-type: none"> <li>• tape cast</li> <li>• 0.5-1 mm thickness</li> </ul>

a - Mole percent of alkali carbonate salt

Specifications for the anode and cathode were obtained from (6), (10), and FCE correspondence, March 1998.

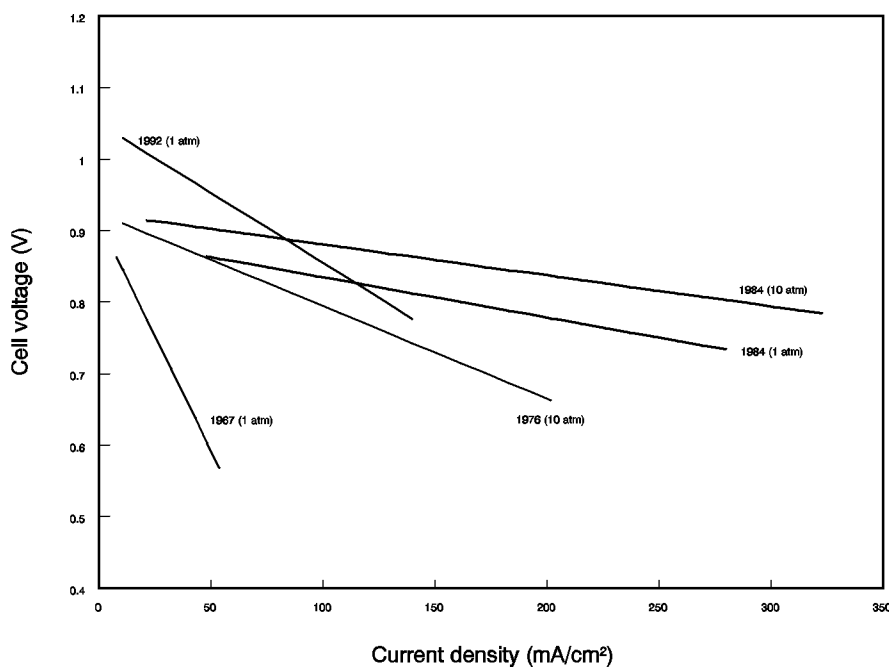


**Figure 6-2 Progress in the Generic Performance of MCFCs on Reformate Gas and Air (11, 12)**

The conventional process used to fabricate electrolyte structures until about 1980 involved hot pressing (about 5000 psi) mixtures of  $\text{LiAlO}_2$  and alkali carbonates (typically >50 vol% in liquid state) at temperatures slightly below the melting point of the carbonate salts (e.g., 490°C for electrolyte containing 62 mol%  $\text{Li}_2\text{CO}_3$ -38 mol%  $\text{K}_2\text{CO}_3$ ). These electrolyte structures (also called "electrolyte tiles") were relatively thick (1-2 mm) and difficult to produce in large sizes<sup>21</sup> because large tooling and presses were required. The electrolyte structures produced by hot pressing are often characterized by 1) void spaces (<5% porosity), 2) poor uniformity of microstructure,

<sup>21</sup>. The largest electrolyte tile produced by hot pressing was about 1.5 m<sup>2</sup> in area (7).

3) generally poor mechanical strength, and 4) high iR drop. To overcome these shortcomings of hot pressed electrolyte structures, alternative processes such as tape casting (7) and electrophoretic deposition (13) for fabricating thin electrolyte structures were developed. The greatest success to date with an alternative process has been reported with tape casting, which is a common processing technique used by the ceramics industry. This process involves dispersing the ceramic powder in a solvent,<sup>22</sup> which contains dissolved binders (usually an organic compound), plasticizers, and additives to yield the proper slip rheology. The slip is cast over a moving smooth substrate, and the desired thickness is established with a doctor blade device. After drying the slip, the "green" structure is assembled into the fuel cell where the organic binder is removed by thermal decomposition, and the absorption of alkali carbonate into the ceramic structure occurs during cell startup. Deposition (13) for fabricating thin electrolyte structures was developed.

The tape casting and electrophoretic deposition processes are amenable to scaleup, and thin electrolyte structures (0.25-0.5 mm) can be produced. The ohmic resistance of an electrolyte structure<sup>23</sup> and the resulting ohmic polarization have a large influence on the operating voltage of MCFCs (14). FCE has stated that the electrolyte matrix encompasses 70% of the ohmic loss (15). At a current density of 160 mA/cm<sup>2</sup>, the voltage drop ( $\Delta V_{\text{ohm}}$ ) of an 0.18 cm thick electrolyte structure, with a specific conductivity of  $-0.3 \text{ ohm}^{-1}\text{cm}^{-1}$  at 650°C, was found to obey the relationship (13).

$$\Delta V_{\text{ohm}} (\text{V}) = 0.533t \tag{6-6}$$

where t is the thickness in cm. Later data confirm this result (15). With this equation, it is apparent that a fuel cell with an electrolyte structure of 0.025 cm thickness would operate at a cell voltage that is 82 mV higher than that of an identical cell with an electrolyte structure of 0.18 cm thickness because of the lower ohmic loss. Thus, there is a strong incentive for making thinner electrolyte structures to improve cell performance.

The electrolyte composition affects the performance and endurance of MCFCs in several ways. Higher ionic conductivities, and hence lower ohmic polarization, are achieved with Li-rich electrolytes because of the relative high ionic conductivity of Li<sub>2</sub>CO<sub>3</sub> compared to that of Na<sub>2</sub>CO<sub>3</sub> and K<sub>2</sub>CO<sub>3</sub>. However, gas solubility and diffusivity are lower, and corrosion is more rapid in Li<sub>2</sub>CO<sub>3</sub>.

The major problems with Ni-based anodes and NiO cathodes are structural stability and NiO dissolution, respectively (9). Sintering and mechanical deformation of the porous Ni-based anode under compressive load lead to severe performance decay by redistribution of electrolyte in a MCFC stack. The dissolution of NiO in molten carbonate electrolyte became evident when thin electrolyte structures were used. Despite the low solubility of NiO in carbonate electrolytes (~10 ppm), Ni ions diffuse in the electrolyte towards the anode, and metallic Ni can precipitate in regions where a H<sub>2</sub> reducing environment is encountered. The precipitation of Ni provides a sink for Ni ions, and thus promotes the diffusion of dissolved Ni from the cathode. This phenomenon

<sup>22</sup>. An organic solvent is used because LiAlO<sub>2</sub> in the slip reacts with H<sub>2</sub>O.

<sup>23</sup>. Electrolyte structures containing 45 wt% LiAlO<sub>2</sub> and 55 wt% molten carbonate (62 mol% Li<sub>2</sub>CO<sub>3</sub>-38 mol% K<sub>2</sub>CO<sub>3</sub>) have a specific conductivity at 650°C of about 1/3 that of the pure carbonate phase (14).

becomes worse at high CO<sub>2</sub> partial pressures (16,17) because dissolution may involve the following mechanism:



The dissolution of NiO has been correlated to the acid/base properties of the molten carbonate. The basicity of the molten carbonate is defined as equal to  $-\log(\text{activity of O}^-)$  or  $-\log a_{\text{M}_2\text{O}}$ , where  $a$  is the activity of the alkali metal oxide M<sub>2</sub>O. Based on this definition, acidic oxides are associated with carbonates (e.g., K<sub>2</sub>CO<sub>3</sub>) that do not dissociate to M<sub>2</sub>O, and basic oxides are formed with highly dissociated carbonate salts (e.g., Li<sub>2</sub>CO<sub>3</sub>). The solubility of NiO in binary carbonate melts shows a clear dependence on the acidity/basicity of the melt (18,19). In relatively acidic melts, NiO dissolution can be expressed by



In basic melts, NiO reacts with O<sup>-</sup> to produce one of two forms of nickelate ions:



A distinct minimum in NiO solubility is observed in plots of log (NiO solubility) versus basicity ( $-\log a_{\text{M}_2\text{O}}$ ), which can be demarcated into two branches corresponding to acidic and basic dissolution. Acidic dissolution is represented by a straight line with a slope of +1, and a NiO solubility that decreases with an increase in  $a_{\text{M}_2\text{O}}$ . Basic dissolution is represented by a straight line with a slope of to either -1 or -1/2, corresponding to Equations (6-9) and (6-10), respectively. The CO<sub>2</sub> partial pressure is an important parameter in the dissolution of NiO in carbonate melts because the basicity is directly proportional to  $\log P_{\text{CO}_2}$ . An MCFC usually operates with a molten carbonate electrolyte that is acidic.

The goal of 40,000 hours for the lifetime of MCFCs appears achievable with cell operation at atmospheric pressure, but at 10 atm cell pressure, only about 5,000 to 10,000 hours may be possible with currently available NiO cathodes (20). The solubility of NiO in molten carbonates is complicated by its dependence on several parameters: carbonate composition, H<sub>2</sub>O partial pressure, CO<sub>2</sub> partial pressure, and temperature. For example, measurements of NiO dissolution by Kaun (21) indicate that the solubility is affected by changing the electrolyte composition; a lower solubility is obtained in a Li<sub>2</sub>CO<sub>3</sub>-K<sub>2</sub>CO<sub>3</sub> electrolyte that contains less Li<sub>2</sub>CO<sub>3</sub> (i.e., lower solubility in 38 mol% Li<sub>2</sub>CO<sub>3</sub>-62 mol% K<sub>2</sub>CO<sub>3</sub> than in 62 mol% Li<sub>2</sub>CO<sub>3</sub>-38 mol% K<sub>2</sub>CO<sub>3</sub> at



650°C). However, the solubility of Ni increases in the electrolyte with 38 mol%  $\text{Li}_2\text{CO}_3$  when the temperature decreases, whereas the opposite trend is observed in the electrolyte with 62 mol%  $\text{Li}_2\text{CO}_3$ . Another study reported by Appleby (22) indicates that the solubility of Ni decreases from 9 to 2 ppm by increasing the Li concentration in  $\text{Li}_2\text{CO}_3$ - $\text{K}_3\text{CO}_3$  from 62 to 75 wt%, and a lower solubility is obtained in 60 mol%  $\text{Li}_2\text{CO}_3$ -40 mol%  $\text{Na}_2\text{CO}_3$  at 650°C. The total loss of Ni from the cathode by dissolution in 40,000 hours is expected to correspond to only about 10% of the total cathode thickness. However, FCE estimated a 30 to 40 % loss of the baseline NiO cathode over 40,000 hours of operation (23). The loss of NiO from the cathode can be a critical problem if the possibility of a short circuit exists in the cell. The loss of NiO also facilitates compaction of the cathode. However, FCE endurance testing (7,000 to 10,000 hours) shows that the NiO loss is tolerable from the cathode performance point of view. The compaction of cathodes became evident in MCFC stacks once the anode creep was eliminated when strengthened by oxide dispersion [i.e., oxide dispersion strengthened (ODS) anode].

The bipolar plates used in MCFC stacks are usually fabricated from thin (~15 mil) sheets of an alloy (e.g., Incoloy 825, 310S or 316L stainless steel) that are coated on one side (i.e., the side exposed to fuel gases in the anode compartment) with a Ni layer. The Ni layer is stable in the reducing gas environment of the anode compartment, and it provides a conductive surface coating with low contact resistance. Approaches to circumvent the problems associated with gas leaks and corrosion of bipolar plates are described by Pigeaud et al. (24). Corrosion is largely overcome by application of a coating (about 50  $\mu\text{m}$  thickness) at the vulnerable locations on the bipolar plate. For example, the wet-seal<sup>24</sup> area on the anode side is subject to a high chemical potential gradient because of the fuel gas inside the cell and the ambient environment (usually air) on the outside of the cell, which promotes corrosion (about two orders of magnitude greater than in the cathode wet-seal area (25)). A general discussion on corrosion in the wet-seal area of MCFCs is presented by Donado et al. (26). A thin Al coating in the wet-seal area of a bipolar plate provides corrosion protection by forming a protective layer of  $\text{LiAlO}_2$  after reaction of Al with  $\text{Li}_2\text{CO}_3$  (27). Such a protective layer would not be useful in areas of the bipolar plate that must permit electronic conduction because  $\text{LiAlO}_2$  is an insulating material.

A dense and electronically insulating layer of  $\text{LiAlO}_2$  is not suitable for providing corrosion resistance to the cell current collectors because these components must remain electrically conductive. The typical materials used for this application are 316 stainless steel and chromium plated stainless steels. However, materials with better corrosion resistance are required for long-term operation of MCFCs. Research is continuing to understand the corrosion processes of chromium in molten carbonate salts under both fuel gas and oxidizing gas environments (23,25) and to identify improved alloys (29) for MCFCs. Stainless steels such as Type 310 and 446 have demonstrated better corrosion resistance than Type 316 in corrosion tests (29).

---

<sup>24</sup>. The area of contact between the outer edge of the bipolar plate and the electrolyte structure prevents gas from leaking out of the anode and cathode compartments. The gas seal is formed by compressing the contact area between the electrolyte structure and the bipolar plate so that the liquid film of molten carbonate at operating temperature does not allow gas to permeate through.

### 6.1.2 Development Components

MCFC components are limited by several technical problems (30), particularly those described in Section 6.1.1. A review of the literature from 1994 to the present shows that research efforts described in a previous issue of this handbook (31) essentially continue. It should be noted that MCFC component designs and operational approaches exist on an individual basis that would result in operation for a 40,000-hour lifetime at atmospheric pressure and with natural gas fuel. The coupling of these improvements needs to be proven to meet endurance goals; operation at pressure will definitely require design changes. The studies described in the recent literature provide updated information on promising development of the electrodes, the electrolyte matrix, and the capability of the cell to tolerate trace constituents in the fuel supply. The objectives of these works are to increase the life of the cells, improve cell performance, and lower cell component costs. Descriptions of some of this work follow.

**Anode:** As stated in Section 6.1.1 and Reference 32, present state-of-the-art anodes are made of a Ni-Cr/Ni-Al alloy. The Cr was added to eliminate the problem of anode sintering. However, Ni-Cr anodes are susceptible to creep when placed under the torquing load required in the stack to minimize contact resistance between components. The Cr in the anode is also lithiated by the electrolyte; then it consumes carbonate. Developers are trying lesser amounts of Cr (8%) to reduce the loss of electrolyte, but some have found that reducing the Cr by 2 percentage points increased creep (33). Several developers have begun testing with Ni-Al alloy anodes that provide creep resistance with minimum electrolyte loss (33,34,35). The low creep rate with this alloy is attributed to the formation of  $\text{LiAlO}_2$  dispersed in Ni (34).

Even though the above work is providing a stable, non-sintering, creep-resistant anode, electrodes made with Ni are relatively high in cost. Work is in progress to determine whether a cheaper material, particularly Cu, can be substituted for Ni to lower the cost while retaining stability. A complete substitution of Cu for Ni is not feasible because Cu would exhibit more creep than Ni. It has been found that anodes made of a Cu - 50% Ni - 5% Al alloy will provide long-term creep resistance (36). Another approach tested at IGT showed that an "IGT" stabilized Cu anode had a lower percent creep than a 10% Cr - Ni anode. Its performance was about 40 to 50 mV lower than the standard cell at  $160 \text{ mA/cm}^2$ . An analysis hypothesized that the polarization difference could be reduced to 32 mV at most by pore structure optimization (37).

There is a need to provide better tolerance to sulfur poisoning gases in systems using MCFCs, especially when considering coal operation. The strong incentive for sulfur tolerant cells is to eliminate cleanup equipment that impacts system efficiency. This is especially true if low temperature cleanup is required, because the system efficiency and capital cost suffer when the fuel gas temperature is first reduced, then increased to the cell temperature level. Tests are being conducted on ceramic anodes to alleviate the problems, including sulfur poisoning, being experienced with anodes (30). Anodes are being tested with undoped  $\text{LiFeO}_2$  and  $\text{LiFeO}_2$  doped with Mn and Nb. Preliminary testing where several parameters were not strictly controlled showed that the alternative electrodes exhibited poor performance and would not operate over  $80 \text{ mA/cm}^2$ . At the present time, no alternative anodes have been identified. Instead, future work will focus on performing tests to better understand material behavior and to develop other alternative materials with emphasis on sulfur tolerance.

**Cathode:** An acceptable candidate material for cathodes must have adequate electrical conductivity, structural strength, and a low dissolution rate in molten alkali carbonates to avoid precipitation of metal in the electrolyte structure. State-of-the-art cathodes are made of lithiated NiO (31,32), which has acceptable conductivity and structural strength. However, in early testing, the predecessor of International Fuel Cells Corporation found that the nickel dissolved, then precipitated and reformed as dendrites across the electrolyte matrix. This caused a loss of performance and eventual shorting of the cell (see Section 6.1.1). The dissolution of the cathode has turned out to be the primary life-limiting constraint of MCFCs, particularly in pressurized operation (34). Developers are investigating approaches to resolving the NiO dissolution problem: developing alternative materials for the cathodes, increasing the matrix thickness, using additives in the electrolyte to increase its basicity, and increasing the fraction of Li in the baseline electrolyte.

Initial work on  $\text{LiFeO}_2$  cathodes showed that electrodes made with this material were very stable chemically; cathode environment; there was essentially no dissolution (30). However, these electrodes have poor performance compound relative to the state-of-the-art NiO cathode at atmospheric pressure because of slow kinetics. The electrode shows promise at pressurized operation, so it is still being investigated. Higher performance improvements are expected with Co-doped  $\text{LiFeO}_2$ ; these cathodes will be tested in future work. It also has been shown that 5 mol% lithium doped NiO with a thickness of 0.02 cm provided a 43 mV overpotential (higher performance) at  $160 \text{ mA/cm}^2$  compared to the state-of-the-art NiO cathode. It is assumed that further performance improvements could be made by reconfiguring the structure, such as decreasing the agglomerate size.

Life is shortened by a decrease in the electrolyte matrix thickness (38). Concurrently, an increase in matrix thickness brings about an increase in life. This is due to an increase in the  $\text{Ni}^{++}$  diffusion path, which lowers the transport rate and shifts the Ni desposition zone. Developers found that an increase in electrolyte thickness from 0.5 mm to 1.0 mm increased the time to shorting from 1000 hours to 10,000 hours. Along with this, data showed that if the  $\text{P}_{\text{CO}_2}$  was reduced one-third, then the Ni dissolution decreased by a third. U.S. developers concluded that a two-fold improvement in the time-to-short can be achieved using a 60% increase in matrix thickness and an additive of  $\text{CaCO}_3$ . However, this combined approach caused an approximately 20 mV reduction in performance at  $160 \text{ mA/cm}^2$  (23).

Another idea for resolving the cathode dissolution problem is to formulate a milder cell environment. This leads to the approach of using additives in the electrolyte to increase its basicity. Small amounts of additives provide similar voltages to those without additives, but larger amounts adversely affect performance (39). Table 6-2 quantifies the limiting amounts of additives.

Another approach to having a milder cell environment is to increase the fraction of Li in the baseline electrolyte or change the electrolyte to Li/Na rather than the baseline 62/38 Li/K melt (23,39,40). Within the past 10 years, a lower cost stabilized cathode was developed with a base material cost comparable to the unstabilized cathode (41). A  $100 \text{ cm}^2$  cell test of the lower cost stabilized cathode with a Li/Na electrolyte system completed 10,000 hours of operation.

**Table 6-2 Amount in Mol% of Additives to Provide Optimum Performance (39)**

	<b>62 MOL% Li<sub>2</sub>CO<sub>3</sub>/K<sub>2</sub>CO<sub>2</sub></b>	<b>52 MOL% Li<sub>2</sub>CO<sub>3</sub>/NA<sub>2</sub>CO<sub>3</sub></b>
CaCO <sub>3</sub>	0 – 15	0 - 5
SrCO <sub>3</sub>	0 – 5	0 - 5
BaCO <sub>3</sub>	0 - 10	0 - 5

**Electrolyte Structure:** Ohmic losses contribute about 65 mV loss at the beginning of life and may increase to as much as 145 mV by 40,000 hours (15). The majority of the voltage loss is in the electrolyte and the cathode components. The electrolyte offers the highest potential for reduction because 70% of the total cell ohmic loss occurs there. FCE investigated increasing the porosity of the electrolyte 5% to reduce the matrix resistance by 15%, and change the melt to Li/Na from Li/K to reduce the matrix resistivity by 40%. Work is continuing on the interaction of the electrolyte with the cathode components. At the present time, an electrolyte loss of 25% of the initial inventory can be projected with a low surface area cathode current collector and with the proper selection of material.

Another area for electrolyte structure improvement is the ability of the matrix to prevent gas crossover from one electrode to the other. FCE produced an improved matrix fabrication process providing low temperature binder burnout. This process resulted in frequently achieving a 1% gas leakage, well below the goal of 2% (42). FCE reported in 1997 that it had developed a high performance rugged matrix that increases the gas sealing efficiency by approximately a factor of ten better than the design goal (43).

**Electrolyte Migration:** Cell performance suffers because of leakage of the electrolyte from the cell. There is a tendency for the electrolyte to migrate from the positive end of the stack to the negative end of the stack. The leakage is through the gasket used to couple the external manifolds to the cell stack. The baseline gasket material presently used is highly porous and provides a ready circuit for electrolyte transfer. A new gasket design having lower porosity plus end cell inventory capability offers the potential for reaching 40,000 hours, if only this mode of failure is considered (6). Stacks with internal manifolding do not require a gasket and do not experience this problem (44).

**Coal Gas Trace Species:** MCFCs to date have been operated on reformed or simulated natural gas and simulated coal gas. Testing is being conducted with simulated coal gas has involved the expected individual and multi-trace constituents to better understand coal operation (45).

Table 6-3 shows the contaminants and their impact on MCFC operation. The table denotes the species of concern and what cleanup of the fuel gas is required to operate on coal gas. Confidence in operation with coal will require the use of an actual gasifier product. An FCE MCFC stack was installed (fall of 1993) using a slipstream of an actual coal gasifier to further clarify the issues of operation with trace gases (46).

**Table 6-3 Qualitative Tolerance Levels for Individual Contaminants in Isothermal Bench-Scale Carbonate Fuel Cells (46, 47, and 48)**  
**(Only 4 out of the 10 contaminants studied appear to have a significant effect)**

CONTAMINANTS (typical ppm in raw coal gas)	REACTION MECHANISM	QUALITATIVE TOLERANCES	CONCLUSIONS
NO NOTICEABLE EFFECTS			
NH <sub>3</sub> (10,000) Cd (5) Hg (1) Sn (3)	$2\text{NH}_3 \rightarrow \text{N}_2 + 3\text{H}_2$ $\text{Cd} + \text{H}_2\text{O} \rightarrow \text{CdO(s)} + \text{H}_2$ (Hg Vapor Not Reactive) (Sn(l) Not Volatile)	~1 vol% NH <sub>3</sub> ~30 ppm Cd 35 ppm Hg No Vapor @ 650°C	No Effects No Cell Deposits No TGA Effects No Cell Deposits
MINOR EFFECTS			
Zn (100) Pb (15)	$\text{Zn} + \text{H}_2\text{O} \rightarrow \text{ZnO(s)} + \text{H}_2$ $\text{Pb} + \text{H}_2\text{O} \rightarrow \text{PbS(s)} + \text{H}_2$	<15 ppm Zn 1.0 ppm Pb sat'd vapor	No Cell Deposits at 75% Utilization Cell Deposits Possible in Presence of High H <sub>2</sub> Se
SIGNIFICANT EFFECTS			
H <sub>2</sub> S (15,000) HCl (500) H <sub>2</sub> Se (5) As (10)	$x\text{H}_2\text{S} + \text{Ni} \rightarrow \text{NiS}_x + x\text{H}_2$ $2\text{HCl} + \text{K}_2\text{CO}_3 \rightarrow 2\text{KCl(v)} + \text{H}_2\text{O/CO}_2$ $x\text{H}_2\text{Se} + \text{Ni} \rightarrow \text{NiSe}_x + x\text{H}_2$ $\text{AsH}_3 + \text{Ni} \rightarrow \text{NiAs(s)} + 3/2\text{H}_2$	<0.5 ppm H <sub>2</sub> S <0.1 ppm HCl <0.2 ppm H <sub>2</sub> Se <0.1 ppm As	Recoverable Effect Long Term Effects Possible Recoverable Effect Cumulative Long Term Effect

## 6.2 Performance

Factors affecting the selection of operating conditions are stack size, heat transfer rate, voltage level, load requirement, and cost. The performance curve is defined by cell pressure, temperature, gas composition, and utilization. Typical MCFCs will generally operate in the range of 100 to 200 mA/cm<sup>2</sup> at 750 to 900 mV/cell.

Typical cathode performance curves obtained at 650°C with an oxidant composition (12.6% O<sub>2</sub>/18.4% CO<sub>2</sub>/69% N<sub>2</sub>) that is anticipated for use in MCFCs, and a common baseline composition (33% O<sub>2</sub>/67% CO<sub>2</sub>) are presented in Figure 6-3 (20,49). The baseline composition contains O<sub>2</sub> and CO<sub>2</sub> in the stoichiometric ratio that is needed in the electrochemical reaction at the cathode (Equation (6-2)). With this gas composition, little or no diffusion limitations occur in the cathode because the reactants are provided primarily by bulk flow. The other gas composition, which contains a substantial fraction of N<sub>2</sub>, yields a cathode performance that is limited by gas phase diffusion from dilution by an inert gas.

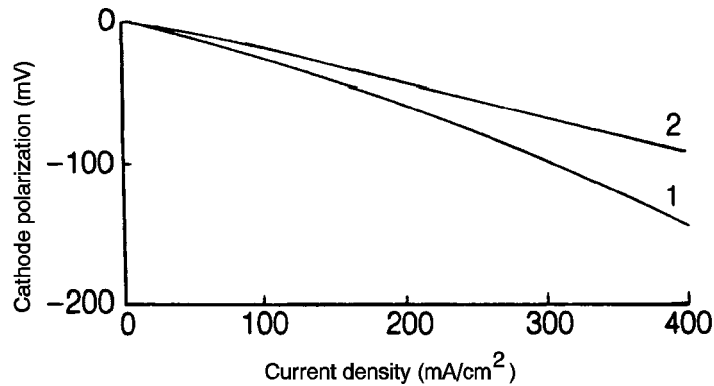


**Figure 6-3 Effect of Oxidant Gas Composition on MCFC Cathode Performance at 650°C, (Curve 1, 12.6% O<sub>2</sub>/18.4% CO<sub>2</sub>/69.0% N<sub>2</sub>; Curve 2, 33% O<sub>2</sub>/67% CO<sub>2</sub>) (49, Figure 3, Pg. 2712)**

In the 1980s, the performance of MCFC stacks increased dramatically. During the 1990s, cells as large as 1.0 m<sup>2</sup> are being tested in stacks. Most recently, the focus has been on achieving performance in a stack equivalent to single cell performance. Cells with an electrode area of 0.3 m<sup>2</sup> were routinely tested at ambient and above ambient pressures with improved electrolyte structures made by tape-casting processes (20). Several stacks underwent endurance testing in the range of 7,000 to 10,000 hours. The voltage and power as a function of current density after 960 hours for a 1.0 m<sup>2</sup> stack consisting of 19 cells are shown in Figure 6-4. The data were obtained with the cell stack at 650°C and 1 atmosphere.

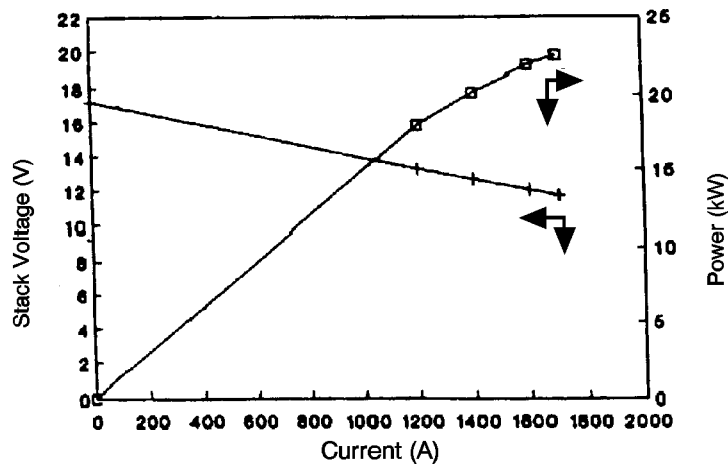


**Figure 6-4 Voltage and Power Output of a 1.0/m<sup>2</sup> 19 cell MCFC Stack after 960 Hours at 965°C and 1 atm, Fuel Utilization, 75% (50)**

The remainder of this section will review operating parameters that affect MCFC performance. Supporting data will be presented as well as equations derived from empirical analysis.

### 6.2.1 Effect of Pressure

The dependence of reversible cell potential on pressure is evident from the Nernst equation. For a change in pressure from  $P_1$  to  $P_2$ , the change in reversible potential ( $\Delta V_p$ ) is given by

$$\Delta V_p = \frac{RT}{2F} \ln \frac{P_{1,a}}{P_{2,a}} + \frac{RT}{2F} \ln \frac{P_{2,c}^{3/2}}{P_{1,c}^{3/2}} \quad (6-11)$$

where the subscripts a and c refer to the anode and cathode, respectively. In an MCFC with the anode and cathode compartments at the same pressure (i.e.,  $P_1=P_{1,a}=P_{1,c}$  and  $P_2=P_{2,a}=P_{2,c}$ ):

$$\Delta V_p = \frac{RT}{2F} \ln \frac{P_1}{P_2} + \frac{RT}{2F} \ln \frac{P_2^{3/2}}{P_1^{3/2}} = \frac{RT}{4F} \ln \frac{P_2}{P_1} \quad (6-12)$$

At 650°C

$$\Delta V_p \text{ (mV)} = 20 \ln \frac{P_2}{P_1} = \left( 46 \log \frac{P_2}{P_1} \right) \quad (6-13)$$

Thus, a tenfold increase in cell pressure corresponds to an increase of 46 mV in the reversible cell potential at 650°C.

Increasing the operating pressure of MCFCs results in enhanced cell voltages because of the increase in the partial pressure of the reactants, increase in gas solubilities, and increase in mass transport rates. Opposing the benefits of increased pressure are the effects of pressure on undesirable side reactions such as carbon deposition (Boudouard reaction):



and methane formation (methanation)



In addition, decomposition of  $\text{CH}_4$  to carbon and  $\text{H}_2$  is possible



but this reaction is suppressed at higher pressure. According to the Le Chatelier principle, an increase in pressure will favor carbon deposition by Equation (6-14) (<sup>25</sup>) and methane formation by Equations (6-15) and (6-16) (51). The water-gas shift reaction (52)<sup>26</sup>



is not expected to be affected significantly by an increase in pressure because the number of moles of gaseous reactants and products in the reaction is identical. Carbon deposition in an MCFC is to be avoided because it can lead to plugging of the gas passages in the anode. Methane formation is detrimental to cell performance because the formation of each mole consumes three moles of H<sub>2</sub>, which represents a considerable loss of reactant and would reduce power plant efficiency.

The addition of H<sub>2</sub>O and CO<sub>2</sub> to the fuel gas modifies the equilibrium gas composition so that the formation of CH<sub>4</sub> is not favored. Carbon deposition can be reduced by increasing the partial pressure of H<sub>2</sub>O in the gas stream. The measurements (20) on 10 cm x 10 cm cells at 650°C using simulated gasified coal GF-1 (38% H<sub>2</sub>/56% CO/6% CO<sub>2</sub>) at 10 atm showed that only a small amount of CH<sub>4</sub> is formed. At open circuit, 1.4 vol% CH<sub>4</sub> (dry gas basis) was detected, and at fuel utilizations of 50 to 85%, 1.2 to 0.5% CH<sub>4</sub> was measured. The experiments with a high CO fuel gas (GF-1) at 10 atmospheres and humidified at 163°C showed no indication of carbon deposition in a subscale MCFC. These studies indicated that CH<sub>4</sub> formation and carbon deposition at the anodes in an MCFC operating on coal-derived fuels can be controlled, and under these conditions, the side reactions would have little influence on power plant efficiency.

Figure 6-5 shows the effect of pressure (3, 5, and 10 atmospheres) and oxidant composition (3.2% CO<sub>2</sub>/23.2% O<sub>2</sub>/66.3% N<sub>2</sub>/7.3% H<sub>2</sub>O and 18.2% CO<sub>2</sub>/9.2% O<sub>2</sub>/65.3% N<sub>2</sub>/7.3% H<sub>2</sub>O) on the performance of 70.5 cm<sup>2</sup> MCFCs at 650°C (53). The major difference occurs as the CO<sub>2</sub> pressure changes is the change in open circuit potential, which increases with in cell pressure and CO<sub>2</sub> content (see Equation (6-11)). At 160 mA/cm<sup>2</sup>, ΔV<sub>p</sub> is -44 mV for a pressure change from 3 to 10 atmospheres for both oxidant compositions.

Because ΔV<sub>p</sub> is a function of the total gas pressure, the gas compositions in Figure 6-5 have little influence on ΔV<sub>p</sub>. Based on these results, the effect of cell voltage from a change in pressure can be expressed by the equation

$$\Delta V_p \text{ (mV)} = 84 \log \frac{P_2}{P_1} \quad (6-18)$$

<sup>25</sup>. Data from translation of Russian literature (51) indicate the equilibrium constant is almost independent of pressure.

<sup>26</sup>. Data from translation of Russian literature (52) indicate the equilibrium constant K is a function of pressure. In relative terms, if K (627°C) = 1 at 1 atm, it decreases to 0.74K at 500 atm and 0.60K at 1000 atmospheres. At the operating pressures of the MCFC, the equilibrium constant can be considered invariant with pressure.



where  $P_1$  and  $P_2$  are different cell pressures. Another analysis by Benjamin et al. (54) suggests that a coefficient less than 84 may be more applicable. The change in voltage as a function of pressure change was expressed as

$$V_p \text{ (mV)} = 76.5 \log \frac{P_2}{P_1} \quad (6-19)$$

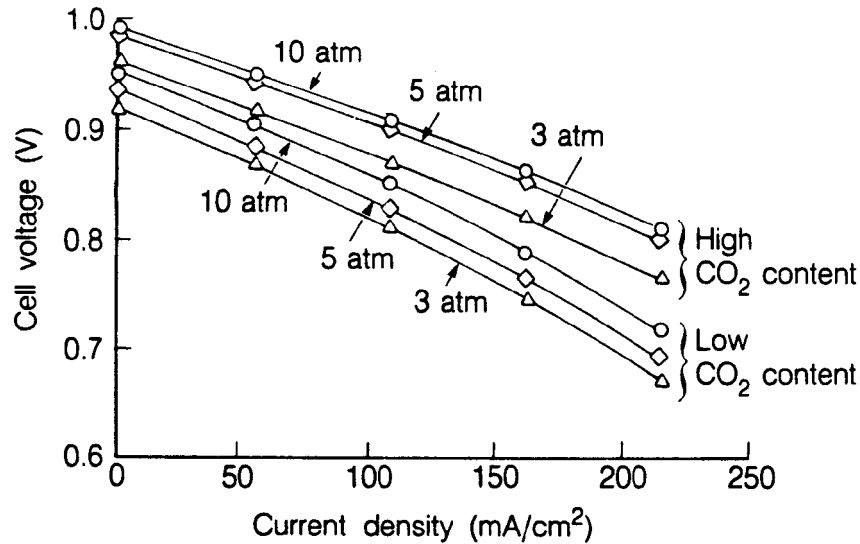


**Figure 6-5 Influence of Cell Pressure on the Performance of a 70.5 cm<sup>2</sup> MCFC at 650°C (anode gas, not specified; cathode gases, 23.2% O<sub>2</sub>/3.2% CO<sub>2</sub>/66.3% N<sub>2</sub>/7.3% H<sub>2</sub>O and 9.2% O<sub>2</sub>/18.2% CO<sub>2</sub>/65.3% N<sub>2</sub>/7.3% H<sub>2</sub>O; 50% CO<sub>2</sub>, utilization at 215 mA/cm<sup>2</sup>) (53, Figure 4, Pg. 395)**

Equation (6-19) was based on a load of 160 mA/cm<sup>2</sup> at a temperature of 650°C. It was also found to be valid for a wide range of fuels and for a pressure range of 1 atmosphere ≤ P ≤ 10 atmospheres. Other results (55) support this coefficient. Figure 6-6 shows the influence of pressure change on voltage gain for three different stack sizes. These values are for a temperature of 650°C and a constant current density of 150 mA/cm<sup>2</sup> at a fuel utilization of 70%. The line that corresponds to a coefficient of 76.5 falls approximately in the middle of these values. Further improvements in cell performance will lead to changes in the logarithmic coefficient. Additional data (56,57,58) indicate that the coefficient may indeed be less than 76.5, but Equation (6-19) appears to represent the effect of pressure change on performance.

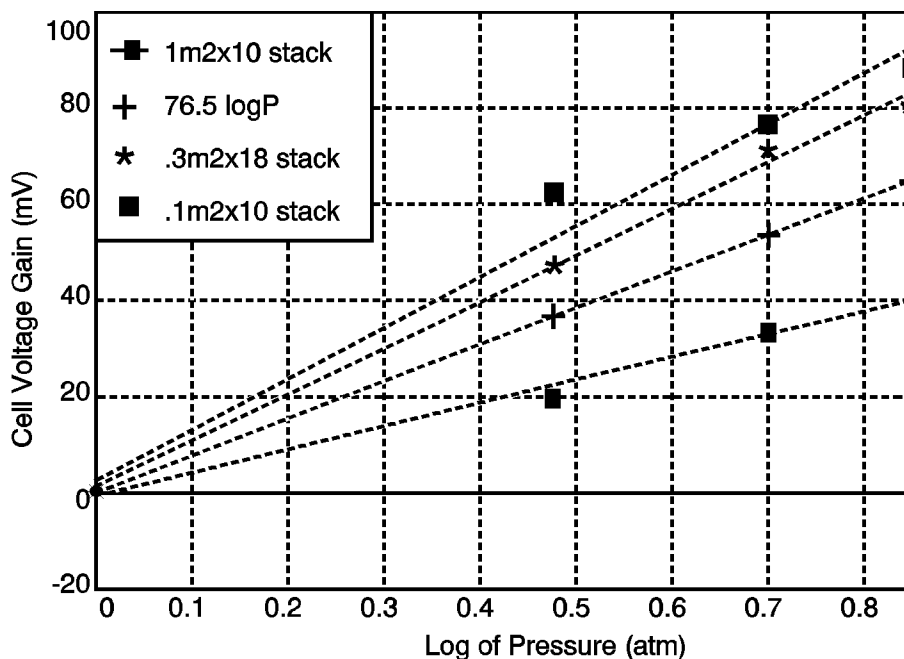


Figure 6-6 Influence of Pressure on Voltage Gain (55)

### 6.2.2 Effect of Temperature

The influence of temperature on the reversible potential of MCFCs depends on several factors, one of which involves the equilibrium composition of the fuel gas (20,59,60,61).<sup>27</sup> The water gas shift reaction achieves rapid equilibrium<sup>28</sup> at the anode in MCFCs, and consequently CO serves as an indirect source of H<sub>2</sub>. The equilibrium constant (K)

$$K = \frac{P_{CO} P_{H_2O}}{P_{H_2} P_{CO_2}} \quad (6-20)$$

increases with temperature (see Table 6-4 and Appendix 11.1), and the equilibrium composition changes with temperature and utilization to affect the cell voltage.

The influence of temperature on the voltage of MCFCs is illustrated by the following example. Consider a cell with an oxidant gas mixture of 30% O<sub>2</sub>/60% CO<sub>2</sub>/10% N<sub>2</sub>, and a fuel gas mixture of 80% H<sub>2</sub>/20% CO<sub>2</sub>. When the fuel gas is saturated with H<sub>2</sub>O vapor at 25°C, its composition becomes 77.5% H<sub>2</sub>/19.4% CO<sub>2</sub>/3.1% H<sub>2</sub>O. After considering the equilibrium established by the

<sup>27</sup>. For a fixed gas composition of H<sub>2</sub>, H<sub>2</sub>O, CO, CO<sub>2</sub>, and CH<sub>4</sub> there is a temperature, T<sub>b</sub>, below which the exothermic Boudouard reaction is thermodynamically favored, and a temperature, T<sub>m</sub>, above which carbon formation by the endothermic decomposition of CH<sub>4</sub> is thermodynamically favored; more extensive details on carbon deposition are found elsewhere (20,59,60,61).

<sup>28</sup>. The dependence of equilibrium constant on temperature for carbon deposition, methanation, and water gas shift reactions is presented in Appendix 11.1.

water gas shift reaction (Equation (6-17), the equilibrium concentrations can be calculated (see Example 10-5 in Section 10) using Equation (6-20) and the equilibrium constant; see for instance, Broers and Treijtel (62). The equilibrium concentrations are substituted into Equation (6-4) to determine E as a function of T.

**Table 6-4 Equilibrium Composition of Fuel Gas and Reversible Cell Potential as a Function of Temperature**

Parameter <sup>a</sup>	Temperature (°K)		
	800	900	1000
P <sub>H<sub>2</sub></sub>	0.669	0.649	0.643
P <sub>CO<sub>2</sub></sub>	0.088	0.068	0.053
P <sub>CO</sub>	0.106	0.126	0.141
P <sub>H<sub>2</sub>O</sub>	0.137	0.157	0.172
E <sup>b</sup> (V)	1.155	1.143	1.133
K <sup>c</sup>	0.2474	0.4538	0.7273

- a - P is the partial pressure computed from the water gas shift equilibrium of inlet gas with composition 77.5% H<sub>2</sub>/19.4% CO<sub>2</sub>/3.1% H<sub>2</sub>O at 1 atmosphere.  
 b - Cell potential calculated using Nernst equation and cathode gas composition of 30% O<sub>2</sub>/60% CO<sub>2</sub>/10% N<sub>2</sub>.  
 c - Equilibrium constant for water gas shift reaction from Reference (59).

The results of these calculations are presented in Table 6-4. Inspection of the results shows a change in the equilibrium gas composition with temperature. The partial pressures of CO and H<sub>2</sub>O increase at higher T because of the dependence of K on T. The result of the change in gas composition, and the decrease in E<sup>o</sup> with increasing T, is that E decreases with an increase in T. In an operating cell, the polarization is lower at higher temperatures, and the net result is that a higher cell voltage is obtained at elevated temperatures. The electrode potential measurements (9) in a 3 cm<sup>2</sup> cell<sup>29</sup> show that the polarization at the cathode is greater than at the anode, and that the polarization is reduced more significantly at the cathode with an increase in temperature. At a current density of 160 mA/cm<sup>2</sup>, cathode polarization is reduced by about 160 mV when the temperature increases from 550 to 650°C, whereas the corresponding reduction in anode polarization is only about 9 mV (between 600 and 650°C, no significant difference in polarization is observed at the anode).

Baker et al. (63) investigated the effect of temperature (575 to 650°C) on the initial performance of small cells (8.5 cm<sup>2</sup>). With steam-reformed natural gas as the fuel and 30% CO<sub>2</sub>/70% air as

<sup>29</sup>. Electrolyte is 55 wt% carbonate eutectic (57 wt% Li<sub>2</sub>CO<sub>3</sub>, 31 wt% Na<sub>2</sub>CO<sub>3</sub>, 12 wt% K<sub>2</sub>CO<sub>3</sub>) and 45 wt% LiAlO<sub>2</sub>, anode is Co + 10% Cr, cathode is NiO, fuel is 80% H<sub>2</sub>/20% CO<sub>2</sub> and oxidant is 30% CO<sub>2</sub>/70% air.

the oxidant, the cell voltage<sup>30</sup> at 200 mA/cm<sup>2</sup> decreased by 1.4 mV/° for a reduction in temperature from 650 to 600°C, and 2.16 mV/°C for a decrease from 600 to 575°C. In the temperature range 650 to 700°C, data analysis (58) indicates a relationship of 0.25 mV/°C. The following equations summarize these results.

$$\Delta V_T \text{ (mV)} = 2.16 (T_2 - T_1) \quad 575^\circ\text{C} \leq T < 600^\circ\text{C} \quad (6-21)$$

$$\Delta V_T \text{ (mV)} = 1.40 (T_2 - T_1) \quad 600^\circ\text{C} \leq T < 650^\circ\text{C} \quad (6-22)$$

$$\Delta V_T \text{ (mV)} = 0.25 (T_2 - T_1) \quad 650^\circ\text{C} < T \leq 700^\circ\text{C} \quad (6-23)$$

The two major contributors responsible for the change in cell voltage with temperature are the ohmic polarization and electrode polarization. It appears that in the temperature range of 575 to 650°C, about 1/3 of the total change in cell voltage with decreasing temperature is due to an increase in ohmic polarization, and the remainder from electrode polarization at the anode and cathode. Most MCFC stacks currently operate at an average temperature of 650°C. Most carbonates do not remain molten below 520°C, and as seen by the previous equations, cell performance is enhanced by increasing temperature. Beyond 650°C, however, there are diminishing gains with increased temperature. In addition, there is increased electrolyte loss from evaporation and increased material corrosion. An operating temperature of 650°C thus offers a compromise between high performance and stack life.

### 6.2.3 Effect of Reactant Gas Composition and Utilization

The voltage of MCFCs varies with the composition of the reactant gases. The effect of reactant gas partial pressure, however, is somewhat difficult to analyze. One reason involves the water gas shift reaction at the anode due to the presence of CO. The other reason is related to the consumption of both CO<sub>2</sub> and O<sub>2</sub> at the cathode. Data (55,64,65,66) show that increasing the reactant gas utilization generally decreases cell performance.

As reactant gases are consumed in an operating cell, the cell voltage decreases in response to the polarization (i.e., activation, concentration) and to the changing gas composition (see discussion in Section 2). These effects are related to the partial pressures of the reactant gases.

**Oxidant:** The electrochemical reaction at the cathode involves the consumption of two moles CO<sub>2</sub> per mole O<sub>2</sub> (see Equation (6-2)), and this ratio provides the optimum cathode performance. The influence of the [CO<sub>2</sub>]/[O<sub>2</sub>] ratio on cathode performance is illustrated in Figure 6-7 (46). As this ratio decreases, the cathode performance decreases, and a limiting current is discernible. In the limit where no CO<sub>2</sub> is present in the oxidant feed, the equilibrium involving the dissociation of carbonate ions becomes important.

---

<sup>30</sup>. Cell was operated at constant flow rate; thus, the utilization changes with current density.



(6-24)

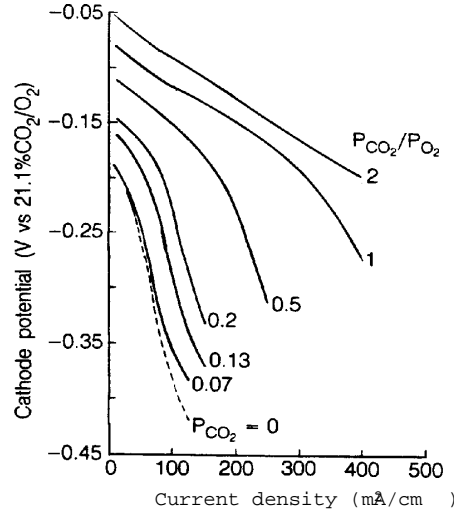


**Figure 6-7 Effect of CO<sub>2</sub>/O<sub>2</sub> Ratio on Cathode Performance in an MCFC, Oxygen Pressure is 0.15 atm (20, Figure 5-10, Pgs. 5-20)**

Under these conditions the cathode performance shows the greatest polarization because of the composition changes that occur in the electrolyte. The change in the average cell voltage of a ten-cell stack as a function of oxidant utilization is illustrated Figure 6-8. In this stack, the average cell voltage at 172 mA/cm<sup>2</sup> decreases by about 30 mV for a 30 percentage points increase in oxidant (20 to 50%) utilization. Based on this additional data (55,64,65), the voltage loss due to a change in oxidant utilization can be described by the following equations:

$$\Delta V_{\text{cathode}} \text{ (mV)} = 250 \log \frac{\left( \bar{P}_{\text{CO}_2} \bar{P}_{\text{O}_2}^{\frac{1}{2}} \right)}{\left( \bar{P}_{\text{CO}_2} \bar{P}_{\text{O}_2}^{\frac{1}{2}} \right)_1} \quad \text{for } 0.04 \leq \left( \bar{P}_{\text{CO}_2} \bar{P}_{\text{O}_2}^{\frac{1}{2}} \right) \leq 0.11 \quad (6-25)$$

$$V_{\text{cathode}} \text{ (mV)} = 99 \log \frac{\left( \bar{P}_{\text{CO}_2} \bar{P}_{\text{O}_2}^{\frac{1}{2}} \right)}{\left( \bar{P}_{\text{CO}_2} \bar{P}_{\text{O}_2}^{\frac{1}{2}} \right)_1} \quad \text{for } 0.11 < \left( \bar{P}_{\text{CO}_2} \bar{P}_{\text{O}_2}^{\frac{1}{2}} \right) \leq 0.38 \quad (6-26)$$

where the  $\bar{P}_{\text{CO}_2}$  and  $\bar{P}_{\text{O}_2}$  are the average partial pressures of  $\text{CO}_2$  and  $\text{O}_2$  in the system.

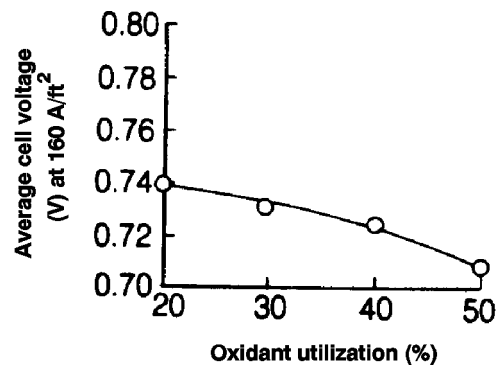


**Figure 6-8 Influence of Reactant Gas Utilization on the Average Cell Voltage of an MCFC Stack (67, Figure 4-21, Pgs. 4-24)**

**Fuel:** The data in Table 6-5 from Lu and Selman (68) illustrate the dependence of the anode potential on the composition of five typical fuel gases and two chemical equilibria occurring in the anode compartment.<sup>31</sup> The calculations show the gas compositions and open circuit anode potentials obtained after equilibria by the water gas shift and  $\text{CH}_4$  steam reforming reactions are considered. The open circuit anode potential calculated for the gas compositions after equilibration, and experimentally measured, is presented in Table 6-5. The equilibrium gas compositions obtained by the shift and steam reforming reactions clearly show that, in general, the  $\text{H}_2$  and  $\text{CO}_2$  contents in the dry gas decrease, and  $\text{CH}_4$  and  $\text{CO}$  are present in the equilibrated gases. The anode potential varies as a function of the  $[\text{H}_2]/[\text{H}_2\text{O}][\text{CO}_2]$  ratio; a higher potential is obtained when this ratio is higher. The results show that the measured potentials agree with the values calculated, assuming that simultaneous equilibria of the shift and the steam reforming reactions reach equilibrium rapidly in the anode compartments of MCFCs.

<sup>31</sup>. No gas phase equilibrium exists between  $\text{O}_2$  and  $\text{CO}_2$  in the oxidant gas that could alter the composition or cathode potential.

**Table 6-5 Influence of Fuel Gas Composition on Reversible Anode Potential at 650°C  
(68, Table 1, Pg. 385)**

Typical Fuel Gas <sup>a</sup>	Gas Composition (mole fraction)						-E <sup>b</sup> (mV)
	H <sub>2</sub>	H <sub>2</sub> O	CO	CO <sub>2</sub>	CH <sub>4</sub>	N <sub>2</sub>	
<i>Dry gas</i>							
High Btu (53°C)	0.80	-	-	0.20	-	-	1116±3 <sup>c</sup>
Intermed. Btu (71°C)	0.74	-	-	0.26	-	-	1071±2 <sup>c</sup>
Low Btu 1 (71°C)	0.213	-	0.193	0.104	0.011	0.479	1062±3 <sup>c</sup>
Low Btu 2 (60°C)	0.402	-	-	0.399	-	0.199	1030± <sup>c</sup>
Very low Btu (60°C)	0.202	-	-	0.196	-	0.602	1040± <sup>c</sup>
<i>Shift equilibrium</i>							
High Btu (53°)	0.591	0.237	0.096	0.076	-	-	1122 <sup>d</sup>
Intermed. Btu (71°C)	0.439	0.385	0.065	0.112	-	-	1075 <sup>d</sup>
Low Btu 1 (71°C)	0.215	0.250	0.062	0.141	0.008	0.326	1054 <sup>d</sup>
Low Btu 2 (60°C)	0.231	0.288	0.093	0.228	-	0.160	1032 <sup>d</sup>
Very low Btu (60°C)	0.128	0.230	0.035	0.123	-	0.484	1042 <sup>d</sup>
<i>Shift and Steam-reforming</i>							
High Btu (53°C)	0.555	0.267	0.082	0.077	0.020	-	1113 <sup>d</sup>
Intermed. Btu (71°C)	0.428	0.394	0.062	0.112	0.005	-	1073 <sup>d</sup>
Low Btu 1 (71°C)	0.230	0.241	0.067	0.138	0.001	0.322	1059 <sup>d</sup>
Low Btu 2 (60°C)	0.227	0.290	0.092	0.229	0.001	0.161	1031 <sup>d</sup>
Very low Btu (60°C)	0.127	0.230	0.035	0.123	0.0001	0.485	1042 <sup>d</sup>

a - Temperature in parenthesis is the humidification temperature

b - Anode potential with respect to 33% O<sub>2</sub>/67% CO<sub>2</sub> reference electrode

c - Measured anode potential

d - Calculated anode potential, taking into account the equilibrated gas composition

Further considering the Nernst equation, an analysis shows that the maximum cell potential for a given fuel gas composition is obtained when  $[CO_2]/[O_2] = 2$ . Furthermore, the addition of inert gases to the cathode, for a given  $[CO_2]/[O_2]$  ratio, causes a decrease in the reversible potential. On the other hand, the addition of inert gases to the anode increases the reversible potential for a given  $[H_2]/[H_2O][CO_2]$  ratio and oxidant composition. This latter result occurs because two moles of products are diluted for every mole of H<sub>2</sub> reactant. However, the addition of inert gases to either gas stream in an operating cell can lead to an increase in concentration polarization.

Figure 6-9 depicts an average voltage loss for the stack of about 30 mV for a 30% increase in fuel utilization (30 to 60%). This and other data (66) suggest that the voltage loss due to a change in fuel utilization can be described by the following equation:

$$\Delta V_{\text{anode}} \text{ (mV)} = 173 \log \frac{\left(\bar{P}_{\text{H}_2} / \bar{P}_{\text{CO}_2} \bar{P}_{\text{H}_2\text{O}}\right)_2}{\left(\bar{P}_{\text{H}_2} / \bar{P}_{\text{CO}_2} \bar{P}_{\text{H}_2\text{O}}\right)_1} \quad (6-27)$$

where  $\bar{P}_{\text{H}_2}$ ,  $\bar{P}_{\text{CO}_2}$ , and  $\bar{P}_{\text{H}_2\text{O}}$  are the average partial pressures of  $\text{H}_2$ ,  $\text{CO}_2$ , and  $\text{O}_2$  in the system.

The above discussion implies that MCFCs should be operated at low reactant gas utilizations to maintain voltage levels, but doing this means inefficient fuel use. As with other fuel cell types, a compromise must be made to optimize overall performance. Typical utilizations are 75 to 85% of the fuel.

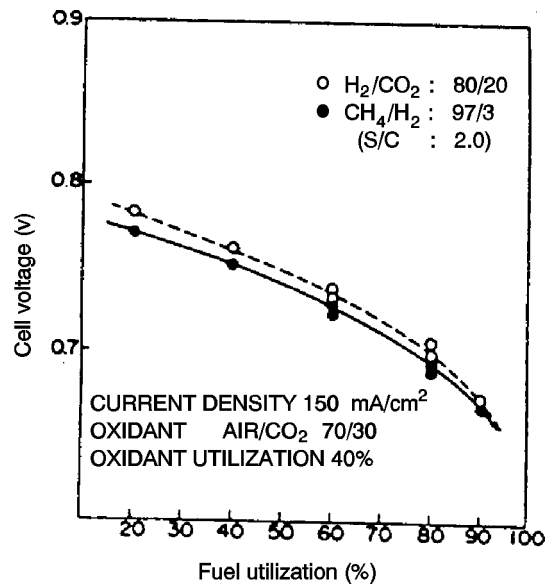


Figure 6-9 Dependence of Cell Voltage on Fuel Utilization (69)

#### 6.2.4 Effect of Impurities

Gasified coal is expected to be the major source of fuel gas for MCFCs, but because coal contains many contaminants in a wide range of concentrations, fuel derived from this source also contains a considerable number of contaminants.<sup>32</sup> A critical concern with these contaminants is the concentration levels that can be tolerated by MCFCs without suffering significant degradation in

<sup>32</sup>. See Table 11.1 for contaminant levels found in fuel gases from various coal gasification processes.



performance or reduction in cell life. A list of possible effects of contaminants from coal-derived fuel gases on MCFCs is summarized in Table 6-6 (70).

**Table 6-6 Contaminants from Coal-Derived Fuel Gas and Their Potential Effect on MCFCs (70, Table 1, Pg. 299)**

Class	Contaminant	Potential Effect
Particulates	Coal fines, ash	<ul style="list-style-type: none"> <li>• Plugging of gas passages</li> </ul>
Sulfur compounds	H <sub>2</sub> S, COS, CS <sub>2</sub> , C <sub>4</sub> H <sub>4</sub> S	<ul style="list-style-type: none"> <li>• Voltage losses</li> <li>• Reaction with electrolyte via SO<sub>2</sub></li> </ul>
Halides	HCl, HF, HBr, SnCl <sub>2</sub>	<ul style="list-style-type: none"> <li>• Corrosion</li> <li>• Reaction with electrolyte</li> </ul>
Nitrogen compounds	NH <sub>3</sub> , HCN, N <sub>2</sub>	<ul style="list-style-type: none"> <li>• Reaction with electrolyte via NO<sub>x</sub></li> </ul>
Trace metals	As, Pb, Hg, Cd, Sn Zn, H <sub>2</sub> Se, H <sub>2</sub> Te, AsH <sub>3</sub>	<ul style="list-style-type: none"> <li>• Deposits on electrode</li> <li>• Reaction with electrolyte</li> </ul>
Hydrocarbons	C <sub>6</sub> H <sub>6</sub> , C <sub>10</sub> H <sub>8</sub> , C <sub>14</sub> H <sub>10</sub>	<ul style="list-style-type: none"> <li>• Carbon deposition</li> </ul>

The typical fuel gas composition and contaminants from an air-blown gasifier that enter the MCFC at 650°C after hot gas cleanup, and the tolerance level of MCFCs to these contaminants are listed in Table 6-7 (58,71,72). It is apparent from this example that a wide spectrum of contaminants is present in coal-derived fuel gas. The removal of these contaminants can add considerably to the efficiency. A review of various options for gas cleanup is presented by Anderson and Garrigan (70) and Jalan et al. (73).

**Sulfur:** It is now well established that sulfur compounds in low ppm (parts per million) concentrations in fuel gas are detrimental to MCFCs (74,75,76,77,78). The tolerance of MCFCs to sulfur compounds (74) is strongly dependent on temperature, pressure, gas composition, cell components, and system operation (i.e., recycle, venting, gas cleanup). The principal sulfur compound that has an adverse effect on cell performance is H<sub>2</sub>S. At atmospheric pressure and high gas utilization (~75%), <10 ppm H<sub>2</sub>S in the fuel can be tolerated at the anode (tolerance level depends on anode gas composition and partial pressure of H<sub>2</sub>), and <1 ppm SO<sub>2</sub> is acceptable in the oxidant (74). These concentration limits increase when the temperature increases, but they decrease at increasing pressures.

**Table 6-7 Gas Composition and Contaminants from Air-Blown Coal Gasifier After Hot Gas Cleanup, and Tolerance Limit of MCFCs to Contaminants**

<b>Fuel Gas<sup>a</sup> (mol%)</b>	<b>Contaminants<sup>b,c</sup></b>	<b>Content<sup>b,c</sup></b>	<b>Remarks<sup>b</sup></b>	<b>Tolerance<sup>c,d</sup> Limit</b>
19.2 CO	Particulates	<0.5 mg/l	Also includes ZnO from H <sub>2</sub> S cleanup stage	<0.1 g/l for large particulates >0.3 :m
13.3 H <sub>2</sub>	NH <sub>3</sub>	2600 ppm		<10,000 ppm
2.6 CH <sub>4</sub>	AsH <sub>3</sub>	<5 ppm		< 1 ppm
6.1 CO <sub>2</sub>	H <sub>2</sub> S	<10 ppm	After first-stage cleanup	<0.5 ppm
12.9 H <sub>2</sub> O	HCl	500 ppm	Also includes other halides	<10 ppm
45.8 N <sub>2</sub>	Trace Metals	<2 ppm	Pb	<1 ppm
		<2 ppm	Cd	30+ ppm
		<2 ppm	Hg	35+ ppm
		<2 ppm	Sn	NA
	Zn	<50 ppm	From H <sub>2</sub> S hot cleanup	<20 ppm
	Tar	4000 ppm	Formed during desulfurization cleanup stage	<2000 ppm <sup>e</sup>

a - Humidified fuel gas enters MCFC at 650°C

b - (71, Table 1, Pg. 177)

c - (79)

d - (72)

e - Benzene

The mechanisms by which H<sub>2</sub>S affects cell performance have been investigated extensively (75,76,77,78). The adverse effects of H<sub>2</sub>S occur because of

- Chemisorption on Ni surfaces to block active electrochemical sites,
- Poisoning of catalytic reaction sites for the water gas shift reaction, and
- Oxidation to SO<sub>2</sub> in a combustion reaction, and subsequent reaction with carbonate ions in the electrolyte.

The adverse effect of H<sub>2</sub>S on the performance of MCFCs is illustrated in Figure 6-10. The cell voltage of a 10 cm x 10 cm cell at 650°C decreases when 5 ppm H<sub>2</sub>S is added to the fuel gas (10% H<sub>2</sub>/5% CO<sub>2</sub>/10% H<sub>2</sub>O/75% He), and current is drawn from the cell. The measurements indicate that low concentrations of H<sub>2</sub>S do not affect the open circuit potential, but they have a major impact on the cell voltage as the current density is progressively increased. The decrease in cell voltage is not permanent;<sup>33</sup> when fuel gas without H<sub>2</sub>S is introduced into the cell, the cell voltage returns to the level for a cell with clean fuel. These results can be explained by the chemical and electrochemical reactions that occur involving H<sub>2</sub>S and S<sup>=</sup>. A nickel anode at anodic potentials reacts with H<sub>2</sub>S to form nickel sulfide:



followed by



When the sulfided anode returns to open circuit, the NiS<sub>x</sub> is reduced by H<sub>2</sub>:



Similarly, when a fuel gas without H<sub>2</sub>S is introduced to a sulfided anode, reduction of NiS<sub>x</sub> to Ni can also occur. Detailed discussions on the effect of H<sub>2</sub>S on cell performance are presented by Vogel and co-workers (75,76) and Remick (77,78).

The rapid equilibration of the water gas shift reaction in the anode compartment provides an indirect source of H<sub>2</sub> by the reaction of CO and H<sub>2</sub>O. If H<sub>2</sub>S poisons the active sites for the shift reaction, this equilibrium might not be established in the cell, and a lower H<sub>2</sub> content than predicted would be expected. Fortunately, the evidence (77,78) indicates that the shift reaction is not significantly poisoned by H<sub>2</sub>S. In fact, Cr used in stabilized-Ni anodes appears to act as a sulfur tolerant catalyst for the water gas shift reaction (78).

The CO<sub>2</sub> required for the cathode reaction is expected to be supplied by recycling the anode gas exhaust (after combustion of the residual H<sub>2</sub>) to the cathode. Therefore, any sulfur in the anode effluent will be present at the cathode inlet unless provisions are made for sulfur removal. In the absence of sulfur removal, sulfur enters the cathode inlet as SO<sub>2</sub>, which reacts quantitatively (equilibrium constant is 10<sup>15</sup> to 10<sup>17</sup>) with carbonate ions to produce alkali sulfates. These sulfate

---

<sup>33</sup>. The effects of H<sub>2</sub>S on cell voltage are reversible if H<sub>2</sub>S concentrations are present at levels below that required to form nickel sulfide.

ions are transported through the electrolyte structure to the anode during cell operation. At the anode,  $\text{SO}_4^-$  is reduced to  $\text{S}^-$ , thus increasing the concentration of  $\text{S}^-$  there.

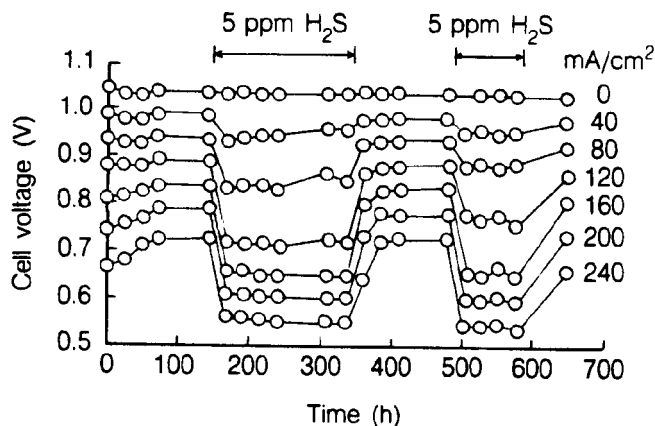


**Figure 6-10 Influence of 5 ppm H<sub>2</sub>S on the Performance of a Bench Scale MCFC (10 cm x 10 cm) at 650°C, Fuel Gas (10% H<sub>2</sub>/5% CO<sub>2</sub>/10% H<sub>2</sub>O/75% He) at 25% H<sub>2</sub> Utilization (78, Figure 4, Pg. 443)**

Based on the present understanding of the effect of sulfur on MCFCs, and with the available cell components, it is projected that long-term operation (40,000 hr) of MCFCs may require fuel gases with sulfur<sup>34</sup> levels of the order 0.01 ppm or less, unless the system is purged of sulfur at periodic intervals or sulfur is scrubbed from the cell burner loop (76). Sulfur tolerance would be approximately 0.5 ppm (see Table 6-3) in the latter case. Considerable effort has been devoted to develop low-cost techniques for sulfur removal, and research and development are continuing (80,81). The effects of H<sub>2</sub>S on cell voltage are reversible if H<sub>2</sub>S concentrations are present at levels below which nickel sulfide forms.

**Halides:** Halogen-containing compounds are destructive to MCFCs because they can lead to severe corrosion of cathode hardware. Thermodynamic calculations (82) show that HCl and HF react with molten carbonates (Li<sub>2</sub>CO<sub>3</sub> and K<sub>2</sub>CO<sub>3</sub>) to form CO<sub>2</sub>, H<sub>2</sub>O, and the respective alkali halides. Furthermore, the rate of electrolyte loss in the cell is expected to increase because of the high vapor pressure of LiCl and KCl. The concentration of Cl<sup>-</sup> species in coal-derived fuels is typically in the range 1 to 500 ppm. It has been suggested (83) that the level of HCl should be kept below 1 ppm in the fuel gas, perhaps below the level of 0.5 ppm (47), but the tolerable level for long-term operation has not been established.

**Nitrogen Compounds:** Compounds such as NH<sub>3</sub> and HCN do not appear to harm to MCFCs (70,79) in small amounts. However, if NO<sub>x</sub> is produced by combustion of the anode effluent in the cell burner loop, it could react irreversibly with the electrolyte in the cathode compartment to form nitrate salts. The projection by Gillis (84) for the NH<sub>3</sub> tolerance level of MCFCs was 0.1 ppm, but Table 6-3 indicates that the level could be increased to 1 vol% (47).

<sup>34</sup>. Both COS and CS<sub>2</sub> appear to be equivalent to H<sub>2</sub>S in their effect on MCFCs (76).

**Solid Particulates:** These contaminants can originate from a variety of sources, and their presence is a major concern because they can block gas passages and/or the anode surface. Carbon deposition and conditions that can be used to control its formation have been discussed earlier in this section. Solid particles such as ZnO, which is used for sulfur removal, can be entrained in the fuel gas leaving the desulfurizer. The results by Pigeaud (72) indicate that the tolerance limit of MCFCs to particulates larger than 3  $\mu\text{m}$  diameter is  $<0.1 \text{ g/l}$ .

**Other Compounds:** Experimental studies indicate that 1 ppm As from gaseous  $\text{AsH}_3$  in fuel gas does not affect cell performance, but when the level is increased to 9 ppm As, the cell voltage drops rapidly by about 120 mV at  $160 \text{ mA/cm}^2$  (71). Trace metals, such as Pb, Cd, Hg, and Sn in the fuel gas, are of concern because they can deposit on the electrode surface or react with the electrolyte (15). Table 6-3 addresses limits of these trace metals.

### 6.2.5 Effects of Current Density

The voltage output from an MCFC is reduced by ohmic, activation, and concentration losses that increase with increasing current density. The major loss over the range of current densities of interest is the linear  $iR$  loss. The magnitude of this loss ( $iR$ ) can be described by the following equations (64,85,86):

$$\Delta V_J(\text{mV}) = -1.21\Delta J \quad \text{for } 50 \leq J \leq 150 \quad (6-31)$$

$$\Delta V_J(\text{mV}) = -1.76\Delta J \quad \text{for } 150 \leq J \leq 200 \quad (6-32)$$

where  $J$  is the current density ( $\text{mA/cm}^2$ ) at which the cell is operating.

### 6.2.6 Effects of Cell Life

Endurance of the cell stack is a critical issue in the commercialization of MCFCs. Adequate cell performance must be maintained over the desired length of service, quoted by one MCFC developer as being an average potential degradation no greater than  $2\text{mV}/1000$  hours over a cell stack lifetime of 40,000 hours (42). Current state-of-the-art MCFCs (55,64,66,87,88) depict an average degradation over time of

$$\Delta V_{\text{lifetime}}(\text{mV}) = -5\text{mV}/1000 \text{ hours} \quad (6-33)$$

## 6.2.7 Internal Reforming

In a conventional fuel cell system, a carbonaceous fuel is fed to a fuel processor where it is steam reformed to produce  $H_2$  (as well as other products,  $CO$  and  $CO_2$ , for example), which is then introduced into the fuel cell and electrochemically oxidized. The internal reforming molten carbonate fuel cell, however, eliminates the need for a separate fuel processor for reforming carbonaceous fuels. This concept is practical in high-temperature fuel cells where the steam reforming reaction<sup>35</sup> can be sustained with catalysts. By closely coupling the reforming reaction and the electrochemical oxidation reaction within the fuel cell, the concept of the internal reforming MCFC is realized. The internal reforming MCFC eliminates the need for the external fuel reactor. It was recognized early that the internal reforming MCFC approach provides a highly efficient, simple, reliable, and cost effective alternative to the conventional MCFC system (89). Development to date in the U.S. and Japan continues to support this expectation (85,90).

There are two alternate approaches to internal reforming molten carbonate cells: indirect internal reforming (IIR) and direct internal reforming (DIR). In the first approach, the reformer section is separate, but adjacent to the fuel cell anode. This cell takes advantage of the close-coupled thermal benefit where the exothermic heat of the cell reaction can be used for the endothermic reforming reaction. Another advantage is that the reformer and the cell environments do not have a direct physical effect on each other. A disadvantage is that the conversion of methane to hydrogen is not promoted as well as in the direct approach. In the DIR cell, hydrogen consumption reduces its

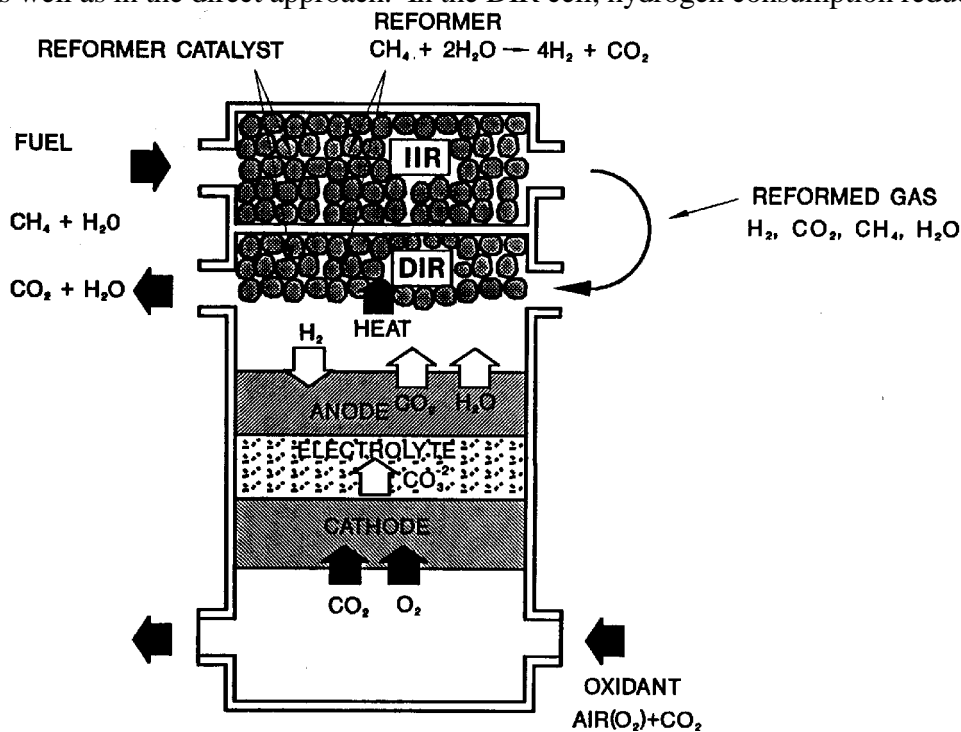


Figure 6-11 IIR/DIR Operating Concept, Molten Carbonate Fuel Cell Design (42)

<sup>35</sup>. Steam reforming of  $CH_4$  is typically performed at 750 to 900°C; thus, at the lower operating temperature of MCFCs, a high activity catalyst is required. Methanol is also a suitable fuel for internal reforming. It does not require an additional catalyst because the Ni-based anode is sufficiently active.

partial pressure, thus driving the methane reforming reaction, Equation (6-34), to the right. Figure 6-11 depicts one developer's approach where IIR and DIR have been combined.

Methane is a common fuel utilized in internal reforming MCFCs, where the steam reforming reaction



occurs simultaneously with the electrochemical oxidation of hydrogen (see reaction, Equation (6-1)) in the anode compartment. The steam reforming reaction is endothermic, with  $\Delta H_{650^\circ\text{C}} = 53.87 \text{ kcal/mol}$  (89), whereas the overall fuel cell reaction is exothermic. In an internal reforming MCFC, the heat required for the reaction in Equation (6-34) is supplied by heat from the fuel cell reaction, thus eliminating the need for external heat exchange that is required by a conventional fuel processor. In addition, the product steam from the reaction in Equation (6-1) can be used to enhance the reforming reaction and the water gas shift reaction (Equation (6-17)) to produce additional  $\text{H}_2$ . The forward direction of the reforming reaction (Equation (6-34)) is favored by high temperature and low pressure; thus, an internal reforming MCFC is best suited to operate near atmospheric pressure.

A supported Ni catalyst (e.g., Ni supported on  $\text{MgO}$  or  $\text{LiAlO}_2$ ) sustains the steam reforming reaction at  $650^\circ\text{C}$  to produce sufficient  $\text{H}_2$  to meet the needs of the fuel cell. The interrelationship between the conversion of  $\text{CH}_4$  to  $\text{H}_2$  and its utilization in an internal reforming MCFC at  $650^\circ\text{C}$  is illustrated in Figure 6-12. At open circuit, about 83% of the  $\text{CH}_4$  was converted to  $\text{H}_2$ , which corresponds closely to the equilibrium concentration at  $650^\circ\text{C}$ . When current is drawn from the cell,  $\text{H}_2$  is consumed and  $\text{H}_2\text{O}$  is produced, and the conversion of  $\text{CH}_4$  increases and approaches 100% at fuel utilizations greater than about 50%. Thus, by appropriate thermal management and adjustment of  $\text{H}_2$  utilization with the rate of  $\text{CH}_4$  reforming, a similar performance can be obtained in internal reforming MCFC stacks with natural gas and with synthesized reformat gas containing  $\text{H}_2$  and  $\text{CO}_2$ , Figure 6-13. The concept of internal reforming has been successfully demonstrated for 10,000 hours in 2 to 3 kW stacks and for 250 hours in a 100 kW stack (91). The performance of the 2 kW stack over time can be seen in Figure 6-14 (64).

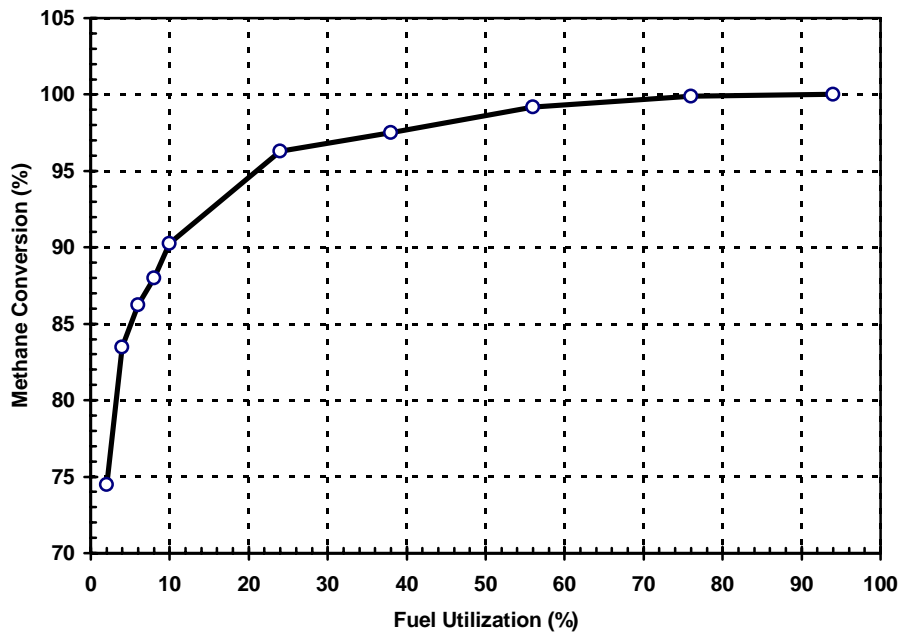


**Figure 6-12 CH<sub>4</sub> Conversion as a Function of Fuel Utilization in a DIR Fuel Cell (MCFC at 650°C and 1 atm, steam/carbon ratio = 2.0, >99% methane conversion achieved with fuel utilization > 65% (92))**

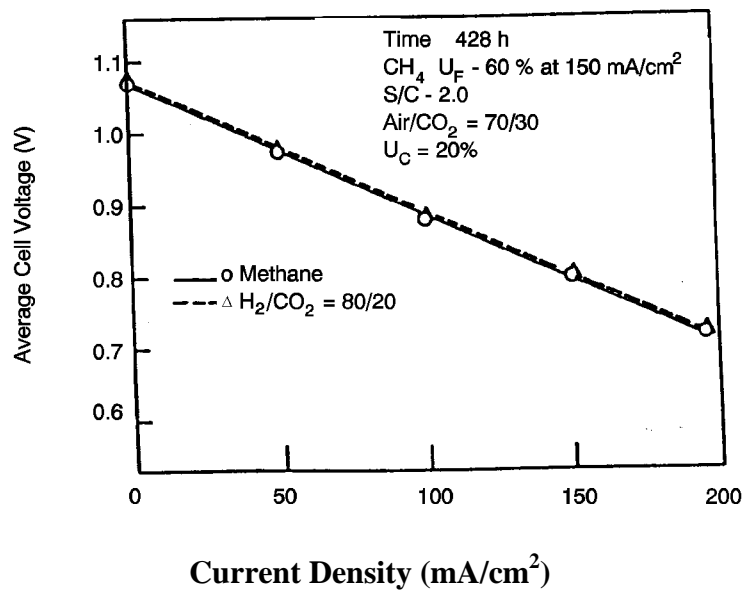


**Figure 6-13 Voltage Current Characteristics of a 3kW, Five Cell DIR Stack with 5,016 cm<sup>2</sup> Cells Operating on 80/20% H<sub>2</sub>/CO<sub>2</sub> and Methane (85)**



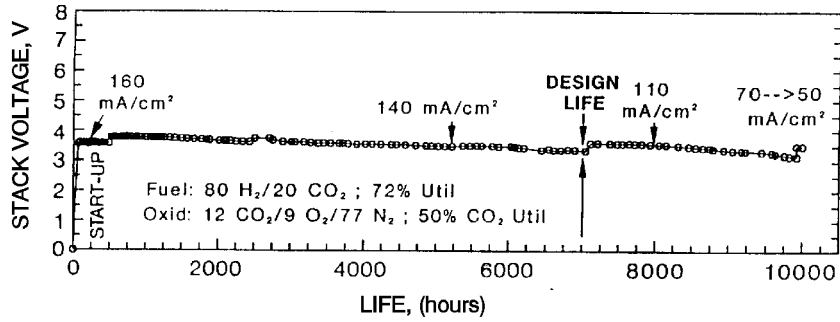


**Figure 6-14 Performance Data of a 0.37m<sup>2</sup> 2 kW Internally Reformed MCFC Stack at 650°C and 1 atm (12)**

### 6.3 Summary of Equations for MCFC

The preceding sections provide parametric performance based on various referenced data at different operating conditions. It is suggested that the following set of equations could be used for performance adjustments unless the reader prefers other data or correlations. Figure 6-15 is provided as reference MCFC performance.

<u>Parameter</u>	<u>Equation</u>	<u>Comments</u>	
Pressure	$\Delta V_p(\text{mV}) = 76.5 \log \frac{P_2}{P_1}$	$1 \text{ atm} \leq P \leq 10 \text{ atm}$	(6-19)
Temperature	$\Delta V_T(\text{mV}) = 2.16(T_2 - T_1)$	$575^\circ\text{C} \leq T < 600^\circ\text{C}$	(6-21)
	$\Delta V_T(\text{mV}) = 1.40(T_2 - T_1)$	$600^\circ\text{C} \leq T \leq 650^\circ\text{C}$	(6-22)
	$\Delta V_T(\text{mV}) = 0.25(T_2 - T_1)$	$650^\circ\text{C} < T \leq 700^\circ\text{C}$	(6-23)
Oxidant	$\Delta V_{\text{cathode}}(\text{mV}) = 250 \log \frac{(\bar{P}_{\text{CO}_2} \bar{P}_{\text{O}_2}^{1/2})_2}{(\bar{P}_{\text{CO}_2} \bar{P}_{\text{O}_2}^{1/2})_1}$	$0.04 \leq (\bar{P}_{\text{CO}_2} \bar{P}_{\text{O}_2}^{1/2}) \leq 0.11$	(6-25)
	$\Delta V_{\text{cathode}}(\text{mV}) = 99 \log \frac{(\bar{P}_{\text{CO}_2} \bar{P}_{\text{O}_2}^{1/2})_2}{(\bar{P}_{\text{CO}_2} \bar{P}_{\text{O}_2}^{1/2})_1}$	$0.11 \leq (\bar{P}_{\text{CO}_2} \bar{P}_{\text{O}_2}^{1/2}) \leq 0.38$	(6-26)
Fuel	$\Delta V_{\text{anode}}(\text{mV}) = 173 \log \frac{(\bar{P}_{\text{H}_2} / \bar{P}_{\text{CO}_2} \bar{P}_{\text{H}_2\text{O}}^{1/2})_2}{(\bar{P}_{\text{H}_2} / \bar{P}_{\text{CO}_2} \bar{P}_{\text{O}_2}^{1/2})_1}$		(6-27)
Current	$\Delta V_J(\text{mV}) = -1.21 \Delta J$	$50 \leq J \leq 150 \text{ mA/cm}^2$	(6-31)
Density	$\Delta V_J(\text{mV}) = -1.76 \Delta J$	$150 < J \leq 200 \text{ mA/cm}^2$	(6-32)
Life Effects	$\Delta V_{\text{lifetime}}(\text{mV}) = -5 \text{ mV}/1000 \text{ hours}$		(6-33)

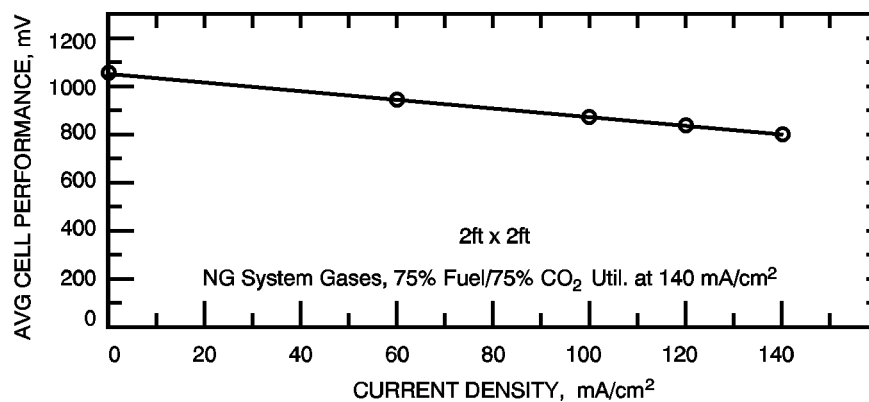


**Figure 6-15 Average Cell Voltage of a 0.37m<sup>2</sup> 2 kW Internally Reformed MCFC Stack at 650°C and 1 atm. Fuel, 100% CH<sub>4</sub>, Oxidant, 12% CO<sub>2</sub>/9% O<sub>2</sub>/77% N<sub>2</sub> (12)**

Fuel Cell Energy presented a computer model for predicting carbonate fuel cell performance at different operating conditions. The model was described in detail at the Fourth International Symposium on Carbonate Fuel Cell Technology, Montreal, Canada, 1997 (93). The model equations are listed as follows:

The general voltage versus current density relation is:

$$V = E_{\text{Nernst}} - (\eta_a + \eta_c) - \eta_{\text{conc}} - iz_r \quad (6-41)$$

where

$$V_0 = E_0 + \frac{RT}{2F} \ln \left( \frac{P_{\text{H}_2, a}}{P_{\text{CO}_2, a} P_{\text{H}_2\text{O}, a}} P_{\text{CO}_2, c} P_{\text{O}_2, c}^{1/2} \right) \quad (6-42)$$

At low current density ( $i < 0.04 \text{ A/cm}^2$ )

$$\eta_a = \frac{iRT}{2F} \frac{1}{K_a^0} e^{E_a/T} P_{\text{H}_2}^{\beta-0.5} P_{\text{CO}_2}^{-\beta} P_{\text{H}_2\text{O}}^{-\beta} \quad (6-43)$$

$$\eta_c = \frac{iRT}{2F} \frac{1}{K_a^0} e^{E_c/T} P_{\text{CO}_2}^{-b_1'} P_{\text{O}_2}^{-b_2'} \quad (6-44)$$

At high current density ( $i < 0.04 \text{ A/cm}^2$ )

$$\eta_a = \frac{RT}{2F} (a_0 + a_1 \ln P_{\text{H}_2} + a_2 \ln P_{\text{CO}_2, a} + a_3 \ln P_{\text{H}_2\text{O}} + a_4/T + a_5 \ln(i)) \quad (6-45)$$

$$\eta_c = \frac{RT}{2F} (b_0 + b_1 \ln P_{\text{CO}_2, c} + b_2 \ln P_{\text{O}_2} + b_3 / T + b_4 \ln i) \quad (6-46)$$

and

$$\eta = c_6 \ln(1 - i/i_L) \quad (6-47)$$

cell resistance

$$Z_r = Z_0 \exp\left[c\left(\frac{1}{T_0} - \frac{1}{T}\right)\right] \quad (6-48)$$

A description of the parameters in the model follows:

- V = Cell voltage, V
- $E^\circ$  = Standard E.M.F., V
- R = Universal gas constant (8.314 joule/deg-mole)
- T = Temperature, K
- P = Partial pressure of gas compositions at anode (a) or cathode (c), atm.
- $\eta$  = Polarization, V
- i = Current density, A/cm<sup>2</sup>
- z = Cell impedance,  $\Omega$ -cm<sup>2</sup>
- F = Faraday's Constant (96,487 joule/volt - gram equivalent)
- a,b,c = Parameters determined for experiments

The parameters in the above equations were calibrated from 400 sets of FCE's laboratory-scale test data and were further verified by several large-scale stack experiments. These parameter values may be dependent on the FCE cell design and characteristics and may not be directly applicable to other carbonate technologies. Figure 6-16 is a comparison of the measured data match with the model prediction.

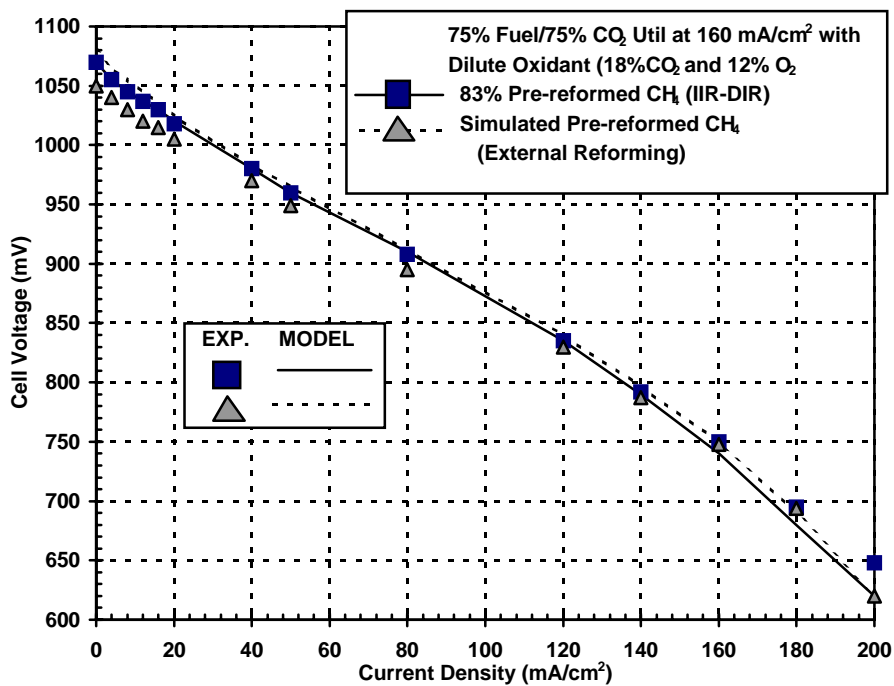


Figure 6-16 Model Predicted and Constant Flow Polarization Data Comparison (94)

## 6.4 References

1. R.H. Arendt, *J. Electrochem. Soc.*, 129, 942, 1982.
2. H.C. Maru, L.G. Marianowski, *Extended Abstracts*, Abstract #31, Fall Meeting of the Electrochemical Society, October 17-22, 1976, Las Vegas, NV, Pg. 82, 1976.
3. J. Mitteldorf, G. Wilemski, *J. Electrochem. Soc.*, 131, 1784, 1984.
4. H.C. Maru, A. Pigeaud, R. Chamberlin, G. Wilemski, in *Proceedings of the Symposium on Electrochemical Modeling of Battery, Fuel Cell, and Photoenergy Conversion Systems*, edited by J.R. Selman and H.C. Maru, The Electrochemical Society, Inc., Pennington, NJ, Pg. 398, 1986.
5. H.R. Kunz, *J. Electrochem. Soc.*, 134, 105, 1987.
6. A. Pigeaud, H.C. Maru, L. Paetsch, J. Doyon, R. Bernard, in *Proceedings of the Symposium on Porous Electrodes: Theory and Practices*, edited by H.C. Maru, T. Katan and M.G. Klein, The Electrochemical Society, Inc., Pennington, NJ, Pg. 234, 1984.
7. H.C. Maru, L. Paetsch, A. Pigeaud, in *Proceedings of the Symposium on Molten Carbonate Fuel Cell Technology*, edited by R.J. Selman and T.D. Claar, The Electrochemical Society, Inc., Pennington, NJ, Pg. 20, 1984.
8. R.J. Petri, T.G. Benjamin, in *Proceedings of the 21st Intersociety Energy Conversion Engineering Conference*, Volume 2, American Chemical Society, Washington, DC, Pg. 1156, 1986.
9. R.J. Selman, *Energy*, 11, 153, 1986.
10. M. Farooque, ERC, "Development on Internal Reforming Carbonate Fuel Cell Technology, Final Report," prepared for U.S. DOE/METC, DOE/MC/23274-2941, October, 1990, Pgs. 4-19 - 4-29.
11. R. Huff, "Status of Fuel Cell Technologies," 1986 Fuel Cell Seminar, October 26-29, 1986, Tucson, AZ, 1986.
12. M. Farooque, data from ERC testing, 1992.
13. C.E. Baumgartner, V.J. DeCarlo, P.G. Glugla, J.J. Grimaldi, *J. Electrochem. Soc.*, 132, 57, 1985.
14. P.G. Glugla, V.J. DeCarlo, *J. Electrochem. Soc.*, 129, 1745, 1982.
15. C. Yuh, M. Farooque, R. Johnsen, ERC, "Understanding of Carbonate Fuel Cell Resistances in MCFCs," in *Proceedings of the Fourth Annual Fuel Cells Contractors Review Meeting*, U.S. DOE/METC, Pgs. 53 - 57, July, 1992.
16. C. Baumgartner, *J. Electrochem. Soc.*, 131, 1850, 1984.
17. W.M. Vogel, L.J. Bregoli, H.R. Kunz, S.W. Smith, in *Proceedings of the Symposium on Molten Carbonate Fuel Cell Technology*, edited by R.J. Selman and T.D. Claar, The Electrochemical Society, Inc., Pennington, NJ, Pg. 443, 1984.
18. M.L. Orfield, D.A. Shores, in *Corrosion 86*, Paper No. 88, National Association of Corrosion Engineers, Houston, TX, 1986.
19. D.A. Shores, in *Proceedings of the 22nd Intersociety Energy Conversion Engineering Conference*, Volume 2, American Institute of Aeronautics & Astronautics, New York, NY, Pg. 1023, 1987.
20. "Development of Improved Molten Carbonate Fuel Cell Technology," Final Report prepared by United Technologies Corp. for the Electric Power Research Institute, Palo Alto, CA, under Contract #RP1085-4, July 1983.
21. T.D. Kaun, in *Proceedings of the Fourth International Symposium on Molten Salts*, edited by M. Blander, D.S. Newman, M.L. Saboungi, G. Mamantov, K. Johnson, The Electrochemical

- Society, Inc., Pennington, NJ, Pg. 489, 1984.
22. A.J. Appleby, "Advanced Fuel Cells and Their Future Market," to be published in *Energy Conservation Strategies*, Progress Series, edited by W.E. Murphy, L.H. Fletcher, American Society of Aeronautics and Astronautics, New York, NY.
  23. M. Farooque, ERC, "Development on Internal Reforming Carbonate Fuel Cell Technology, Final Report," prepared for U.S. DOE/METC, DOE/MC/23274-2941, Pgs. 3 - 18, October, 1990.
  24. A. Pigeaud, A.J. Skok, P.S. Patel, H.C. Maru, *Thin Solid Films*, 83, 1449, 1981.
  25. R.A. Donado, L.G. Marianowski, H.C. Maru, J.R. Selman, *J. Electrochem. Soc.*, 131, 2541, 1984.
  26. R.A. Donado, L.G. Marianowski, H.C. Maru, J.R. Selman, *J. Electrochem. Soc.*, 131, 2535, 1984.
  27. R.B. Swaroop, J.W. Sim, K. Kinoshita, *J. Electrochem. Soc.*, 125, 1799, 1978.
  28. H.S. Hsu, J.H. DeVan, *J. Electrochem. Soc.*, 133, 2077, 1986.
  29. D.A. Shores, P. Singh, in *Proceedings of the Symposium on Molten Carbonate Fuel Cell Technology*, edited by R.J. Selman and T. D. Claar, The Electrochemical Society, Inc., Pennington, NJ, Pg. 271, 1984.
  30. G. Kucera, K. Myles, A. Brown, M. Roche, D. Chu, E. Indacochea, "ANL's Research and Development of Alternate Components for MCFCs," in *Proceedings of the Fourth Annual Fuel Cells Contractors Review Meeting*, U.S. DOE/METC, July 1992, Pgs. 31 - 41.
  31. J. Hirschenhofer, D. Stauffer, R. Engleman, *Fuel Cells A Handbook (Revision 3)* prepared by Gilbert/Commonwealth, Inc. for the U.S. Department of Energy under Contract No. DE-ACO1-88FE61684, January 1994.
  32. N. Minh, "High Temperature Fuel Cells," in *CHEMTECH*, journal published by the American Chemical Society, Vol. 21, No. 1, January, Pgs. 32-37, 1991.
  33. Y. Yamamasu, T. Kakihara, E. Kasai, T. Morita, IHI, "Component Development and Durability Test of MCFC," in *The International Fuel Cell Conference Proceedings*, NEDO/MITI, Tokyo, Japan, Pgs. 161-164, 1992.
  34. H. Urushibata, T. Murahashi, MELCO, "Life Issues of Molten Carbonate Fuel Cell," in *The International Fuel Cell Conference Proceedings*, NEDO/MITI, Tokyo, Japan, Pgs. 223-226, 1992.
  35. S. Takashima, K. Ohtsuka, T. Kara, M. Takeuchi, Y. Fukui, H. Fujimura, Hitachi, "MCFC Stack Technology at Hitachi," in *The International Fuel Cell Conference Proceedings*, NEDO/MITI, Tokyo, Japan, Pgs. 265-268, 1992.
  36. K. Hoshino, T. Kohno, Central Research Institute, Mitsubishi Material Co., "Development of Copper Base Anodes for Molten Carbonate Fuel Cells," in *The International Fuel Cell Conference Proceedings*, NEDO/MITI, Tokyo, Japan, Pgs. 169-172, 1992.
  37. E.T. Ong, R.A. Donado, K.E. Hrdina, IGT, "Copper-Based Anode," in *Fuel Cell Program and Abstracts*, 1990 Fuel Cell Seminar, November 25-28, 1990, Phoenix, AR, Pgs. 314-317.
  38. Y. Mugikura, Y. Izaki, T. Watanabe, H. Kinoshita, E. Kouda, T. Abe, Central Research Institute of Electric Power Industry, and H. Urushibata, S. Yoshioka, H. Maeda, T. Murahashi, MELCO, "Evaluation of MCFC Performance at Elevated Pressure," in *The International Fuel Cell Conference Proceedings*, NEDO/MITI, Tokyo, Japan, Pgs. 215-218, 1992.
  39. K. Tanimoto, Y. Miyazaki, M. Yanagida, S. Tanase, T. Kojima, N. Ohtori, H. Okuyama, T. Kodama, Government Industrial Research Institute, Osaka, "Cell Performance of Molten Carbonate Fuel Cell with Alkali and Alkaline Earth Carbonate Mixtures," in *The International*

- Fuel Cell Conference Proceedings*, NEDO/MITI, Tokyo, Japan, Pgs. 185-188, 1992.
40. K. Ota, S. Mitsushima, K Kato, N. Kamiya, Yokahama National University, "Solubilities of Metal Oxides in Molten Carbonate, " in *Proceedings of the Second Symposium on Molten Carbonate Fuel Cell Technology*, Volume 90 - 16, The Electrochemical Society, Inc. Pennington, NJ, Pgs. 318-327, 1990.
  41. T. Benjamin et al., "Status of the M-C Power MCFC Commercialization Program," IECEC-97, Honolulu, Hawaii, July 27 - August 1, 1997.
  42. M. Farooque, ERC, "Development on Internal Reforming Carbonate Fuel Cell Technology, Final Report," Pgs. 3-6 to 3-11, prepared for U.S. DOE/METC, DOE/MC/23274-2941, October 1991.
  43. H. Maru et al., "ERC Direct Carbonate Fuel Cell Program Overview," DOE Contractor's Review Meeting, Morgantown, WV, August 26-28, 1997.
  44. R.O.Petkus, "Successful Test of a 250 kW Molten Carbonate Fuel Cell Power Generator at Miramar," POWER-GEN International '97, Dallas, TX, December 1997.
  45. A. Pigeaud, ERC, and G. Wilemski, Physical Sciences, "Effects of Coal-Derived Trace Species on the Performance of Carbonate Fuel Cells," in *Proceedings of the Fourth Annual Fuel Cells Contractors Review Meeting*, U.S. DOE/METC, Pgs. 42-45, July 1992.
  46. D. Rastler, EPRI, G. Devore, Destec Engineering, R. Castle, Haldor Topsoe, C. Chi, ERC, "Demonstration of a Carbonate Fuel Cell Stack on Coal-Derived Gas," in *Fuel Cell Seminar*.
  47. "Effects of Coal-Derived Trace Species on the Performance of Molten Carbonate Fuel Cells," Topical Report prepared by Energy Research Corporation for US DOE/METC, DOE/MC/25009-T26, October, 1991.
  48. A. Pigeaud et al., "Trace Contaminant Effects and Emissions with Integrated Coal Gasification and Cleanup," 1994 Fuel Cell Seminar, Pgs. 539-542 (1994).
  49. L.J. Bregoli and H.R. Kunz, *J. Electrochem. Soc.*, 129, 2711, 1982.
  50. Benjamin et al., "Status of MCFC Technology at M-C Power-1992," 1992 Fuel Cell Seminar Program and Abstracts, 1992.
  51. M.G. Gonikberg, *Chemical Equilibria and Reaction Rates at High Pressures*, Translated from Russian by M. Artment, edited by S. Monson, published for the National Science Foundation, Washington, D.C., by the Israel Program for Scientific Translations Jerusalem, Israel, Pg. 58, 1963.
  52. M.G. Gonikberg, *Chemical Equilibria and Reaction Rates at High Pressures*, Translated from Russian by M. Artment, edited by S. Monson, published for the National Science Foundation, Washington, DC, by the Israel Program for Scientific Translations, Jerusalem, Israel, Pg. 133, 1963.
  53. H.R. Kunz, L.A. Murphy, in *Proceedings of the Symposium on Electrochemical Modeling of Battery, Fuel Cell, and Photoenergy Conversion Systems*, edited by J.R. Selman and H.C. Maru, The Electrochemical Society, Inc., Pennington, NJ, Pg. 379, 1986.
  54. T.G. Benjamin, E.H. Camara, L.G. Marianowski, *Handbook of Fuel Cell Performance*, prepared by the Institute of Gas Technology for the United States Department of Energy under Contract No. EC-77-C-03-1545, May 1980.
  55. Research and Development on Fuel Cell Power Generation Technology FY1990 Annual Report, NEDO, April 1991.
  56. M. Hosalaetal, "IHI Large Site Molten Carbonate Fuel Cell Advancements," *Fuel Cell Program and Abstracts* 1990 Fuel Cell Seminar, Phoenix, AR, November 25-28, 1990.

57. W.H. Johnson, "Molten Carbonate Fuel Cell Technology Improvement," Quarterly Technical Progress Report No. 23 for the Period Ending May, 1990, prepared for US DOE/METC, DOE/MC/23270-2923, September 1990.
58. D.B. Stauffer et al., "An Aspen/SP MCFC Performance User Block," G/C Report No. 2906, July 1991.
59. J.R. Rostrup-Nielsen, in *Catalysis Science and Technology*, edited by J.R. Anderson and M. Boudart, Springer-Verlag, Berlin, German Democratic Republic, Pg. 1, 1984.
60. H.A. Leibhafsky, E.J. Cairns, *Fuel Cells and Fuel Batteries*, John Wiley and Sons, Inc., New York, NY, Pg. 654, 1968.
61. T.D. Tawari, E. Pigeaud, H.C. Maru, in *Proceedings of the Fifth Annual Contractors Meeting on Contaminant Control in Coal-Derived Gas Streams*, DOE/METC-85/6025, edited by D.C. Cicero and K.E. Markel, U.S. Department of Energy, Morgantown, WV, Pg. 425, January 1986.
62. G.H.J. Broers, B.W. Trierjtel, *Advanced Energy Conversion*, 5, 365, 1965.
63. B. Baker, S. Gionfriddo, A. Leonida, H. Maru, P. Patel, "Internal Reforming Natural Gas Fueled Carbonate Fuel Cell Stack," Final Report prepared by Energy Research Corporation for the Gas Research Institute, Chicago, IL, under Contract No. 5081-244-0545, March, 1984.
64. M. Farooque, Data from ERC testing, 1992.
65. S. Kaneko et al., "Research on On-Site Internal Reforming Molten Carbonate Fuel Cell," 1989 International Gas Research Conference, 1989.
66. M. Farooque, "Development of Internal Reforming Carbonate Fuel Cell Stack Technology," Final Report, DOE/MC/23274-2941, October 1991.
67. J.M. King, A.P. Meyer, C.A. Reiser, C.R. Schroll, "Molten Carbonate Fuel Cell System Verification and Scale-up," EM-4129, final report prepared by United Technologies Corp. for the Electric Power Research Institute, Research Project 1273-1, July 1985.
68. S.H. Lu, J.R. Selman, in *Proceedings of the Symposium on Molten Carbonate Fuel Cell Technology*, edited by R.J. Selman, T.D. Claar, The Electrochemical Society, Inc., Pennington, NJ, Pg. 372, 1984.
69. T. Tanaka et al., "Research on On-Site Internal-Reforming Molten Carbonate Fuel Cell," 1989 International Gas Research Conference, Pg. 252, 1989.
70. G.L. Anderson, P.C. Garrigan, in *Proceedings of the Symposium on Molten Carbonate Fuel Cell Technology*, edited by R.J. Selman, T.D. Claar, The Electrochemical Society, Inc., Pennington, NJ, Pg. 297, 1984.
71. A. Pigeaud, in *Proceedings of the Sixth Annual Contractors Meeting on Containment Control in Coal-Derived Gas Streams*, DOE/METC-86/6042, edited by K.E. Markel and D.C. Cicero, U.S. Department of Energy, Morgantown, WV, Pg. 176, July 1986.
72. A. Pigeaud, "Study of the Effects of Soot, Particulate and Other Contaminants on Molten Carbonate Fuel Cells Fueled by Coal Gas," Progress Report prepared by Energy Research Corporation for U.S. Department of Energy, Morgantown, WV, under Contract No. DE-AC21-84MC21154, June 1987.
73. V. Jalan, M. Desai, C. Brooks, in *Proceedings of the Symposium on Molten Carbonate Fuel Cell Technology*, edited by R. J. Selman, T. D. Claar, The Electrochemical Society, Inc., Pennington, NJ, Pg. 506, 1984.
74. L.J. Marianowski, *Prog. Batteries & Solar Cells*, 5, 283, 1984.
75. W.V. Vogel and S.W. Smith, *J. Electrochem. Soc.*, 129, 1441, 1982.
76. S.W. Smith, H.R. Kunz, W.M. Vogel and S.J. Szymanski, in *Proceedings of the Symposium*



- on *Molten Carbonate Fuel Cell Technology*, edited by R.J. Selman and T.D. Claar, The Electrochemical Society, Inc., Pennington, NJ, Pg. 246, 1984.
77. R.J. Remick, E.H. Camara, paper presented at the Fall Meeting for The Electrochemical Society, Inc., New Orleans, LA, October 7-12, 1984.
  78. R.J. Remick, in *Proceedings of the Fourth Annual Contractors Meeting on Contaminant Control in Hot Coal-Derived Gas Streams*, DOE/METC-85/3, edited by K. E. Markel, U.S. Department of Energy, Morgantown, WV, Pg. 440, May 1984.
  79. M.C. Williams, D.A. Berry, "Overview of the DOE-Funded Fuel Cell Contaminants R&D Program," Fuel Cell Seminar Program and Abstracts, 1990 Fuel Cell Seminar, Phoenix, AR, November 25-28, 1990.
  80. P.S. Patel, S.M. Rich, H.C. Maru, in *Proceedings of the Fourth Annual Contractors Meeting on Contaminant Control in Hot Coal-Derived Gas Streams*, DOE/METC-85/3, edited by K. E. Markel, U.S. Department of Energy, Morgantown, WV, Pg. 425, May 1984.
  81. G.L. Anderson, F.O. Berry, G.D. Harmon, R.M. Laurens, R. Biljetina, in *Proceedings of the Fifth Annual Contractors Meeting on Contaminant Control in Coal-Derived Gas Streams*, DOE/METC-85/6025, edited by D.C. Cicero, K.E. Markel, U.S. Department of Energy, Morgantown, WV, Pg. 87, January 1986.
  82. T.P. Magee, H.R. Kunz, M. Krasij, H.A. Cole, "The Effects of Halides on the Performance of Coal Gas-Fueled Molten Carbonate Fuel Cell," Semi-Annual Report, October 1986 - March 1987, prepared by International Fuel Cells for the U.S. Department of Energy, Morgantown, WV, under Contract No. DE-AC21-86MC23136, May 1987.
  83. G.N. Krishnan, B.J. Wood, G.T. Tong, M.A. Quinlan, in *Proceedings of the Fifth Annual Contractors Meeting on Contaminant Control in Coal-Derived Gas Streams*, DOE/METC-85/6025, edited by D.C. Cicero and K.E. Markel, U.S. Department of Energy, Morgantown, WV, Pg. 448, January 1986.
  84. E.A. Gillis, *Chem. Eng. Prog.*, 88, October 1980.
  85. T. Tanaka, et al., "Development of Internal Reforming Molten Carbonate Fuel Cell Technology," in *Proceedings of the 25th IECEC*, American Institute of Chemical Engineers, New York, NY, August 1990.
  86. M. Miyazaki, T. Okada, H. Ide, S. Matsumoto, T. Shinoki, J. Ohtsuki, "Development of an Indirect Internal Reforming Molten Carbonate Fuel Cell Stack," in the 27th Intersociety Energy Conversion Engineering Conference Proceedings, San Diego, CA, August 3-7, 1992, Pg. 290, 1992.
  87. W.H. Johnson, "International Fuel Cells MCFC Technical Accomplishment," in *Proceedings of the Second Annual Fuel Cells Contractor's Review Meeting*, US DOE/METC, May 1990.
  88. T. Benjamin, G. Rezniko, R. Donelson, D. Burmeister, "IMHEX<sup>R</sup> MCFC Stack Scale-Up," in the *Proceedings of the 27th Intersociety Energy Conversion Engineering Conference*, Vol. 3, San Diego, CA, Aug. 3-7, 1992, Pg. 290, 1992.
  89. H.C. Maru, B.S. Baker, *Prog. Batteries & Solar Cells*, 5, 264, 1984.
  90. M. Farooque, G. Steinfield, H. Maru, "Comparative Assessment of Coal-Fueled Carbonate Fuel Cell and Competing Technologies," in *Proceedings of the 25th IECEC*, Vol. 3, American Institute of Chemical Engineers, New York, NY, 1990.
  91. M. Farooque, "MCFC Power Plant System Verification," presentation at *FE Fuel Cells and Coal-Fired Heat Engines Conference*, US DOE/METC, August 3-5, 1993.
  92. ERC correspondence, laboratory data, March 1998.

93. J. Ding et al., "A Computer Model for Direct Carbonate Fuel Cells," Proceedings of the Fourth International Symposium on Carbonate Fuel Cells, 191<sup>st</sup> Electrochemical Society Meeting, Montreal, May 1997.
94. J. Ding, P. S. Patel, M. Farooque, H. C. Maru, in Carbonate Fuel Cell Technology IV, (eds. J. R. Selman et al.), The Electrochemical Society, Inc., New Jersey, Pg. 127-138, 1997.

---

## 7. INTERMEDIATE TEMPERATURE SOLID OXIDE FUEL CELL

---

The intermediate temperature range for a Solid Oxide Fuel Cell (SOFC) can be arbitrarily defined as 550°C to 800°C. Reducing the operating temperature of the SOFC stack is one of the significant directions being pursued to reduce the cost of SOFC stacks and balance of plant. There are both beneficial effects of reducing stack temperature and detrimental effects. In-the-balance, in most situations, the net effect is beneficial particularly in regard to cost. The most significant obstacle is that a set of fully compatible materials have not been developed for operation in this temperature range.

Beneficial effects:

- Reforming and Sulfur Removal - A better thermal match exists with existing reforming and sulfur removal processes. However, it should be noted the optimal nominal reformer temperature depends on the composition of the fuel.
- Sintering and Creep - Less sintering and creep of the stack materials. This helps maintain geometrical tolerances and high surface area of reaction.
- Thermal Stress - Lower operating temperature can in general improve material properties allowing greater geometrical flexibility and use of less material which in turn can improve overall area-specific-resistance and allow a wider range of sealing options.
- Material Flexibility - The type and range of materials is greater at lower temperatures. In particular metallics may be incorporated into SOFC stack designs.
- Balance of Plant - The balance of plant in general should cost less if the stack fuel and oxidant exit temperature is less than 800°C for the same reasons the stack should cost less.
- Heat Loss - Less heat loss from the stack for similar levels of insulation. In particular radiation losses can be significantly less since these are a function of  $T^4$ . This can have a significant effect on the self-sustainability of the stack.

- Time to Reach Operating Temperature - Lower nominal operating temperature is obviously a benefit. Potential use of metallics can also impact this in a beneficial way.
- Thermally Activated Processes - Any detrimental thermally activated processes can be affected beneficially such as chromium vaporization, elemental interdiffusion and migration, metallic corrosion affects and some ceramic aging affects.

There are some negative affects from lowering the nominal operating temperature of the SOFC.

- Cell Voltage - For an identical stack the overall cell voltage will be lower as temperature decreases due to the decreased kinetics, diffusion, and ionic conductivity versus the improved electrical conductivity which typically does not dominate the cell polarizations. This is partially but not fully offset by the increased theoretical open circuit voltage of the electrochemical reaction at the lower temperature.
- Stack Materials - The only proven stack material set is functional between approximately 800°C and 1100°C. A proven material set in the intermediate temperature range does not yet exist.

Given the large number of potential beneficial effects of lowering the nominal operating temperature of the SOFC stack and their corollary affect on system cost, intermediate temperature SOFC concepts are being pursued by many organizations throughout the U.S. and the World.

In closure it is well recognized that significant research has occurred in this important technology area. To accurately present this research efforts will continue to compile and summarize all relevant information. This information will be presented as an addendum to this handbook or in the next addition.

---

## 8. SOLID OXIDE FUEL CELL

---

Solid oxide fuel cells<sup>36</sup> (SOFCs) have grown in recognition as a viable high temperature fuel cell technology. There is no liquid electrolyte with its attendant material corrosion and electrolyte management problems. The operating temperature of  $>800^{\circ}\text{C}$  allows internal reforming, promotes rapid kinetics with nonprecious materials, and produces high quality byproduct heat for cogeneration or for use in a bottoming cycle, similar to the MCFC. The high temperature of the SOFC, however, places stringent requirements on its materials. The development of suitable low cost materials and the low cost fabrication of ceramic structures are presently the key technical challenges facing SOFCs (1).

The solid state character of all SOFC components means that, in principle, there is no restriction on the cell configuration. Instead, it is possible to shape the cell according to criteria such as overcoming design or application issues. Cells are being developed in two different configurations, as shown in Figure 8-1. One of these approaches, the tubular cell, has undergone development at Siemens Westinghouse Corporation and its predecessor since the late 1950s. During recent years, Siemens Westinghouse developed the tubular concept to the status where it is now being demonstrated at user sites in a complete, operating fuel cell power unit of nominal 100 kW (net AC) capacity.

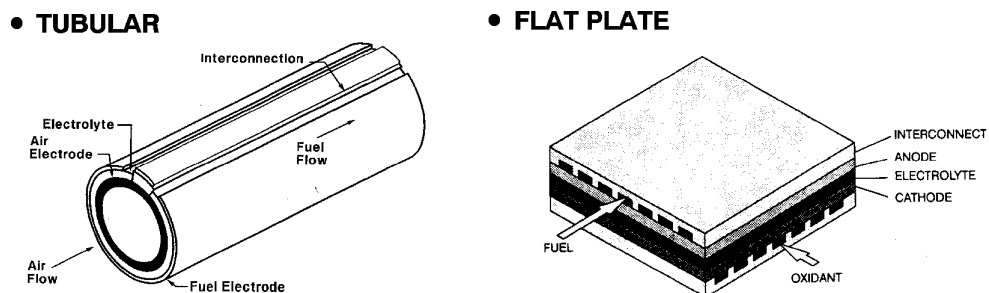


**Figure 8-1 Solid Oxide Fuel Cell Designs at the Cathode**

---

<sup>36</sup>. A broader, more generic name for fuel cells operating at the temperatures described in this section would be "ceramic" fuel cells. The electrolyte of these cells is made primarily from solid ceramic material to survive the high temperature environment. The electrolyte of present SOFCs is oxygen ion conducting. Ceramic cells could also be proton conducting.

The electrochemical reactions (Figure 8-2) occurring in SOFCs utilizing H<sub>2</sub> and O<sub>2</sub> are based on Equations (8-1) and (8-2):



at the anode, and



at the cathode. The overall cell reaction is

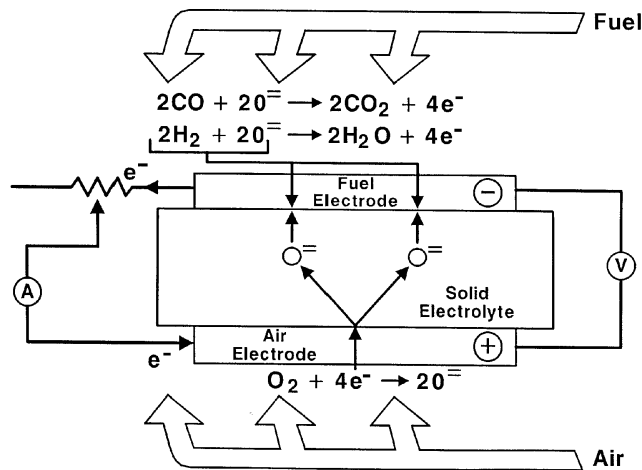


**Figure 8-2 Solid Oxide Fuel Cell Operating Principle (2)**

The corresponding Nernst equation, Equation (8-4), for the reaction in Equation (8-3) is

$$E = E^{\circ} + \frac{RT}{2F} \ln \frac{P_{\text{H}_2} P_{\text{O}_2}^{\frac{1}{2}}}{P_{\text{H}_2\text{O}}} \quad (8-4)$$

Carbon monoxide (CO) and hydrocarbons such as methane (CH<sub>4</sub>) can be used as fuels in SOFCs. It is feasible that the water gas shift involving CO (CO + H<sub>2</sub>O → H<sub>2</sub> + CO<sub>2</sub>) and the steam reforming of CH<sub>4</sub> (CH<sub>4</sub> + H<sub>2</sub>O → 3H<sub>2</sub> + CO) occur at the high temperature environment of SOFCs to produce H<sub>2</sub> that is easily oxidized at the anode. The direct oxidation of CO in fuel cells also is well established. It appears that the reforming of CH<sub>4</sub> to hydrogen predominates in

the present SOFCs. SOFC designs for the direct oxidation of CH<sub>4</sub> have not been thoroughly investigated in SOFCs in the past (3,4) nor lately (no significant work was found). For reasons of simplicity in this handbook, the reaction of CO is considered as a water gas shift rather than an oxidation. Similarly, the favored reaction of H<sub>2</sub> production from steam reforming is retained. Hydrogen produced by the water gas shift and the reforming of methane is included in the amount of hydrogen subject to reaction in Equations (8-1), (8-3), and (8-4).

## 8.1 Cell Components

### 8.1.1 State-of-the-Art

Table 8-1 provides a brief description of the materials currently used in the various cell components of the more developed tubular SOFC, and those that were considered earlier. Because of the high operating temperatures of present SOFCs (approximately 1000°C), the materials used in the cell components are limited by chemical stability in oxidizing and reducing environments, chemical stability of contacting materials, conductivity, and thermomechanical compatibility. These limitations have prompted investigations of developing cells with compositions of oxide and metals that operate at intermediate temperatures in the range of 600-800°C (see Section 7.1.3).

**Table 8-1 Evolution of Cell Component Technology for Tubular Solid Oxide Fuel Cells**

Component	ca. 1965	ca. 1975	Current Status <sup>a</sup>
Anode	<ul style="list-style-type: none"> <li>• Porous Pt</li> </ul>	<ul style="list-style-type: none"> <li>• Ni/ZrO<sub>2</sub> cermet<sup>a</sup></li> </ul>	<ul style="list-style-type: none"> <li>• Ni/ZrO<sub>2</sub> cermet<sup>b</sup></li> <li>• Deposit slurry, EVD fixed<sup>c</sup></li> <li>• 12.5 x 10<sup>-6</sup> cm/cm°C</li> <li>• ~150 μm thickness</li> <li>• 20-40% porosity</li> </ul>
Cathode	<ul style="list-style-type: none"> <li>• Porous Pt</li> </ul>	<ul style="list-style-type: none"> <li>• Stabilized ZrO<sub>2</sub> impregnated with praeosodymium oxide and covered with SnO doped In<sub>2</sub>O<sub>3</sub></li> </ul>	<ul style="list-style-type: none"> <li>• Doped lanthanum manganite</li> <li>• Extrusion, sintering</li> <li>• ~2 mm thickness</li> <li>• 11 x 10<sup>-6</sup> cm/cm°C expansion from room temperature to 1000°C</li> <li>• 30-40% porosity</li> </ul>

Component	ca. 1965	ca. 1975	Current Status <sup>a</sup>
Electrolyte	<ul style="list-style-type: none"> <li>• Yttria stabilized ZrO<sub>2</sub></li> <li>• 0.5-mm thickness</li> </ul>	<ul style="list-style-type: none"> <li>• Yttria stabilized ZrO<sub>2</sub></li> </ul>	<ul style="list-style-type: none"> <li>• Yttria stabilized ZrO<sub>2</sub> (8 mol% Y<sub>2</sub>O<sub>3</sub>)</li> <li>• EVD<sup>d</sup></li> <li>• 10.5 x 10<sup>-6</sup> cm/cm °C expansion from room temperature to 1000°C</li> <li>• 30-40-μm thickness</li> </ul>
Cell Interconnect	<ul style="list-style-type: none"> <li>• Pt</li> </ul>	<ul style="list-style-type: none"> <li>• Mn doped cobalt chromite</li> </ul>	<ul style="list-style-type: none"> <li>• Doped lanthanum chromite</li> <li>• Plasma spray 10 x 10<sup>-6</sup> cm/cm °C</li> <li>• ~100 μm thickness</li> </ul>

a - Specifications for Siemens Westinghouse SOFC.

b - Y<sub>2</sub>O<sub>3</sub> stabilized ZrO<sub>2</sub>

c - Fixed EVD" means additional ZrO<sub>2</sub> is grown by EVD to fix (attach) the nickel anode to the electrolyte. This process is expected to be replaced by anode sintering.

d - EVD = electrochemical vapor deposition

Present SOFC designs make use of thin film concepts where films of electrode, electrolyte, and interconnect material are deposited one on another and sintered, forming a cell structure. The fabrication techniques differ according to the type of cell configuration and developer. For example, an "electrochemical vapor deposition" (EVD) technique has been developed to produce thin layers of refractory oxides suitable for the electrolyte, anode, and interconnection in the Siemens Westinghouse tubular SOFC design (5). However, by the end of 1998, Siemens Westinghouse expects to be using EVD only for electrolyte deposition. In this technique, the appropriate metal chloride vapor is introduced on one side of the tube surface, and O<sub>2</sub>/H<sub>2</sub>O is introduced on the other side. The gas environments on both sides of the tube act to form two galvanic couples, as demonstrated in Equations (8-5) and (8-6).





The net result is the formation of a dense and uniform metal oxide layer in which the deposition rate is controlled by the diffusion rate of ionic species and the concentration of electronic charge carriers. This procedure is used to fabricate the solid electrolyte yttria stabilized zirconia (YSZ).

The anode consists of metallic Ni and a  $Y_2O_3$  stabilized  $ZrO_2$  skeleton. The latter serves to inhibit sintering of the metal particles and to provide a thermal expansion coefficient comparable to those of the other cell materials. The anode structure is fabricated with a porosity of 20 to 40% to facilitate mass transport of reactant and product gases. Doped lanthanum manganite is most commonly used for the cathode material. Similar to the anode, the cathode is a porous structure that must permit rapid mass transport of reactant and product gases. The cell interconnection material (doped lanthanum chromite), however, must be impervious to fuel and oxidant gases and must possess good electronic conductivity. In addition, the cell interconnection is exposed to both the cathode and anode environments thus, it must be chemically stable under  $O_2$  partial pressures of about  $\sim 1$  to  $10^{-18}$  atmospheres at  $1000^\circ C$  ( $1832^\circ F$ ).

The solid oxide electrolyte must be free of porosity that permits gas to permeate from one side of the electrolyte layer to the other, and it should be thin to minimize ohmic loss. In addition, the electrolyte must have a transport number for  $O^-$  as close to unity as possible, and a transport and a transport number for electronic conduction as close to zero as possible. Zirconia-based electrolytes are suitable for SOFCs because they exhibit pure anionic conductivity over a wide range of  $O_2$  partial pressures ( $1$  to  $10^{-20}$  atmospheres). The other cell components should permit only electronic conduction,<sup>37</sup> and interdiffusion of ionic species in these components at  $1000^\circ C$  ( $1832^\circ F$ ) should not have a major effect on their electronic conductivity. Other severe restrictions placed on the cell components are that they must be stable in the gaseous environments in the cell and that they must be capable of withstanding thermal cycling. The materials listed in Table 8-1 appear to have the properties for meeting these requirements.

The resistivities of typical cell components at  $1000^\circ C$  ( $1832^\circ F$ ) under fuel cell gaseous environments are (6): 10 ohm cm (ionic) for the electrolyte (8-10 mol%  $Y_2O_3$  doped  $ZrO_2$ ), 1 ohm cm (electronic) for the cell interconnection (doped  $LaCrO_3$ ), 0.01 ohm cm (electronic) for the cathode (doped  $LaMnO_3$ ), and  $3 \times 10^{-6}$  ohm cm (electronic) for the anode (Ni/ $ZrO_2$  cermet).<sup>38</sup> It is apparent that the solid oxide electrolyte is the least conductive of the cell components, followed by the cell interconnection. Furthermore, an operating temperature of about  $1000^\circ C$  ( $1832^\circ F$ ) is necessary if the ionic conductivity of the solid electrolyte [i.e.,  $0.02 \text{ ohm}^{-1}\text{cm}^{-1}$  at  $800^\circ C$  ( $1472^\circ F$ ) and  $0.1 \text{ ohm}^{-1}\text{cm}^{-1}$  at  $1000^\circ C$  ( $1832^\circ F$ )] is to be within even an order of magnitude of that of aqueous electrolytes. The solid electrolyte in SOFCs must be only about 25-50  $\mu m$  thick if its ohmic loss at  $1000^\circ C$  ( $1832^\circ F$ ) is to be comparable to that of the electrolyte in PAFCs (8). Fortunately, thin electrolyte structures of about 40  $\mu m$  thickness can be fabricated by EVD, as well as by tape casting and other ceramic processing techniques.

---

<sup>37</sup>. Mixed conducting (i.e., electronic and ionic) materials for anodes may be advantageous if  $H_2$  oxidation can occur over the entire surface of the electrode to enhance current production, instead of only in the region of the three-phase interface (gas/solid electrolyte/electrode). Similarly, mixed conductors also may be advantageous for cathodes.

<sup>38</sup>. The cermet becomes an electronic conductor at Ni contents of  $>30 \text{ vol\%}$  (1).

The successful operation of SOFCs requires individual cell components that are thermally compatible so that stable interfaces are established at 1000°C (1832°F), i.e., thermal expansion coefficients for cell components must be closely matched to reduce stresses arising from differential thermal expansion between components. Fortunately, the electrolyte, interconnection, and cathode listed in Table 8-1 have reasonably close thermal expansion coefficients [i.e.,  $\sim 10^{-5}$  cm/cm°C from room temperature to 1000°C (1832°F)]. An anode made of 100 mol% nickel would have excellent electrical conductivity. However, the thermal expansion coefficient of 100 mol% nickel would be 50% greater than the ceramic electrolyte, or the cathode tube, which causes a thermal mismatch. This thermal mismatch has been resolved by mixing ceramic powders with Ni or NiO. The trade-off of the amount of Ni (to achieve high conductivity) and amount of ceramic (to better match the other component thermal coefficients of expansion) is Ni/YSZ: 30/70, by volume (1).

A configuration for electrically connecting tubular cells to form a stack is described in Section 8.1.2 under sealless tubular configuration (Figure 8-6). The cells are connected in a series-parallel array by nickel felt strips that are exposed to the reducing fuel gas. In this arrangement, the nickel felt strips and cell interconnections extend the length of the cell. Because the current flows in the circumferential direction of the electrodes, a relatively large ohmic loss exists, which places an upper limit on the tube diameter.

### 8.1.2 Cell Configuration Options

As with the other cell types, it is necessary to stack SOFCs to increase the voltage and power being produced. Because there are no liquid components, the SOFC can be cast into flexible shapes (Figure 8-1).

In the early 1960s, experimental SOFCs with a planar geometry were evaluated, but this geometry presented a problem for building cell stacks because of difficulties with fabricating large flat, thin cells and obtaining adequate gas seals.<sup>39</sup> A tubular configuration (i.e., cylindrical design) adopted for SOFCs, appeared to alleviate the problems with gas seals and thin layer structure fabrication. An early tubular design is illustrated in the schematic representation of the cross section of a SOFC stack (Figure 8-3). Overlapping components (i.e., electrodes, electrolyte, cell interconnection) in thin layers (10-50  $\mu\text{m}$ ) are deposited on a porous support tube of calcia-stabilized zirconia; fabrication of the fuel cell stack is described by Isenberg (4) and Sverdrup et al. (8). In this tubular design, individual fuel cells are arranged in bands along the support tube and are connected in series by a ceramic interconnect material. Another variation of an early tubular design is referred to as a "bell and spigot" configuration (see Figure 8-4), which consists of short, cylindrical electrolyte segments shaped so that they can be fitted one into the other and connected to form a long tube by bell-and-spigot joints (9,10). A less complex variation of this design used a series of interconnected cones. The sealless tubular design, however, is the most advanced among the several SOFC configuration concepts.

***Sealless Tubular Configuration:*** The most developed solid oxide fuel cell is the Siemens Westinghouse tubular cell. This approach results in eliminating seal problems between adjacent cells. A schematic representation of the cross section of the present Siemens Westinghouse

---

<sup>39</sup>. Recently, the planar structures using bipolar current collection have received more consideration for SOFCs because of new gas sealing and fabrication techniques.

tubular design<sup>40</sup> for a SOFC and its gas manifold is presented in Figure 8-5 and Figure 8-6, respectively. In this design, the cathode is formed by extrusion. Then, the electrolyte and the cell interconnection are deposited by EVD and plasma spraying, respectively, on the cathode, which provides a mechanically strong structure for the thin cell components. The anode is sequentially formed on the electrolyte layer by slurry deposition. A major advantage of this design over earlier designs is that relatively large single tubular cells can be constructed in which the successive active layers can be deposited without chemical or material interference with previously deposited layers. The support tube is closed at one end. The tubular approach with one closed end eliminates gas seals between cells. The manifolding of the oxidant and fuel gases for this tubular cell is illustrated in Figure 8-6. The oxidant gas is introduced via a central Al<sub>2</sub>O<sub>3</sub> injector tube, and the fuel gas is supplied to the exterior of the closed-end tube. In this arrangement, the Al<sub>2</sub>O<sub>3</sub> tube extends to the proximity of the closed end of the tube, and the oxidant flows back past the cathode surface to the open end. The fuel gas flows past the anode on the exterior of the cell and in a parallel direction (coflow) to the oxidant gas. The spent gases are exhausted into a common plenum where the remaining active gases react and the generated heat serves to preheat the incoming oxidant stream and/or drive an expander. One attractive feature of this arrangement is that it eliminates the need for leak-free gas manifolding of the fuel and oxidant streams. However, the sealless tubular design results in a relatively long current path around the circumference of the cell to the interconnect, limiting performance (Figure 8-7). Siemens Westinghouse has increased the length of the cell from 30 to 150 cm.

***Bipolar (Flat Plate) Configuration:*** A bipolar or flat plate structure (Figure 8-1), which is the common configuration for cell stacks in PAFCs and MCFCs, permits a simple series electrical connection between cells without the need for external cell interconnections such as those used with the tubular configuration shown in Figure 8-1 and Figure 8-6. Perpendicular current collection in a cell stack with a bipolar design should have a lower ohmic polarization than the tubular configuration, and overall stack performance should be improved. However, gas leaks in a SOFC of bipolar configuration with compressive seals are difficult to prevent, and thermal stresses at the interfaces between dissimilar materials must be accommodated to prevent mechanical degradation of cell components. Planar electrodes and solid electrolyte structures were proposed for use in high temperature fuel cells and electrolysis cells by Hsu and co-workers (11,12) in the mid-1970s. Later, Hsu (13,14) developed bipolar structures for SOFCs, which are reported to have the following attractive features: 1) high power density, 2) structural ruggedness, 3) concealed electrodes, 4) ease of heat removal, and 5) low-stress assembly.

---

<sup>40</sup>. The present tubular design is about 150 cm length and 1.27 cm diameter. These cells produce about 35 W each; thus, about 28 cells are required to generate 1 kW.

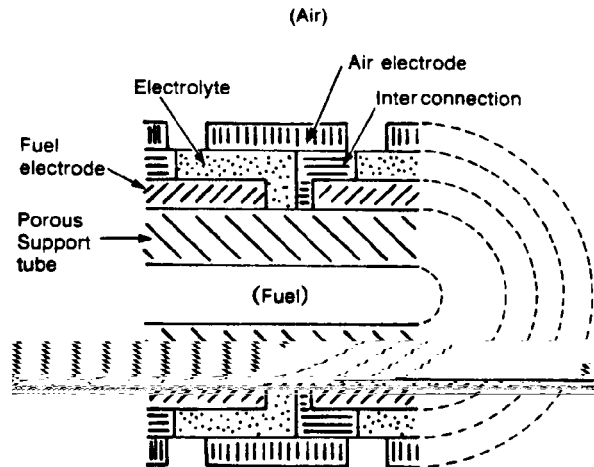


**Figure 8-3 Cross Section (in the Axial Direction of the +) of an Early Tubular Configuration for SOFCs [(8), Figure 2, p. 256]**

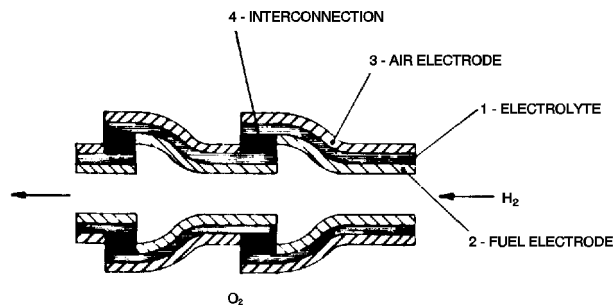


**Figure 8-4 Cross Section (in the Axial Direction of the Series-Connected Cells) of an Early "Bell and Spigot" Configuration for SOFCs [(15), Figure 24, p. 332]**

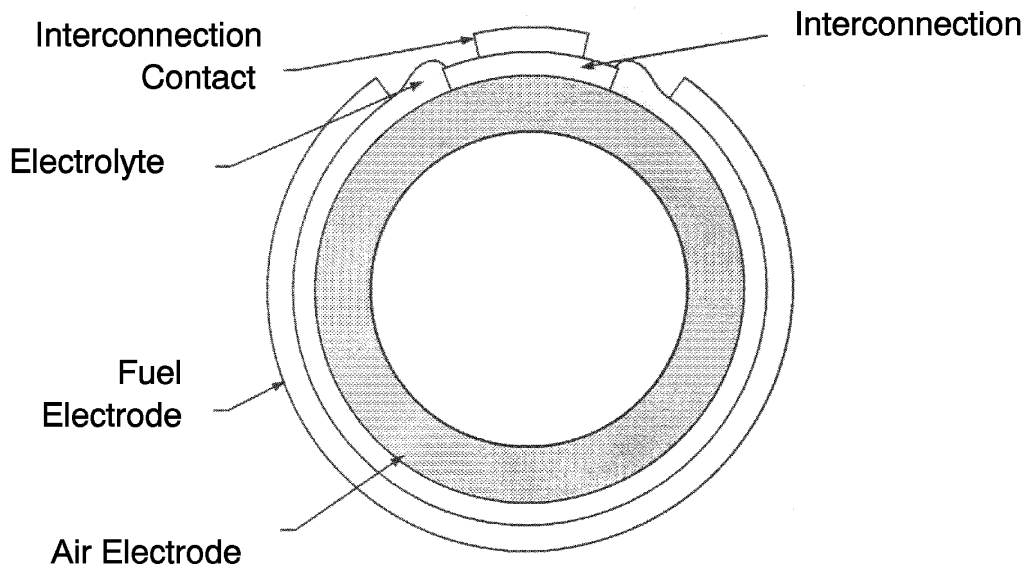


Figure 8-5 Cross Section of Present Tubular Configuration for SOFCs (2)

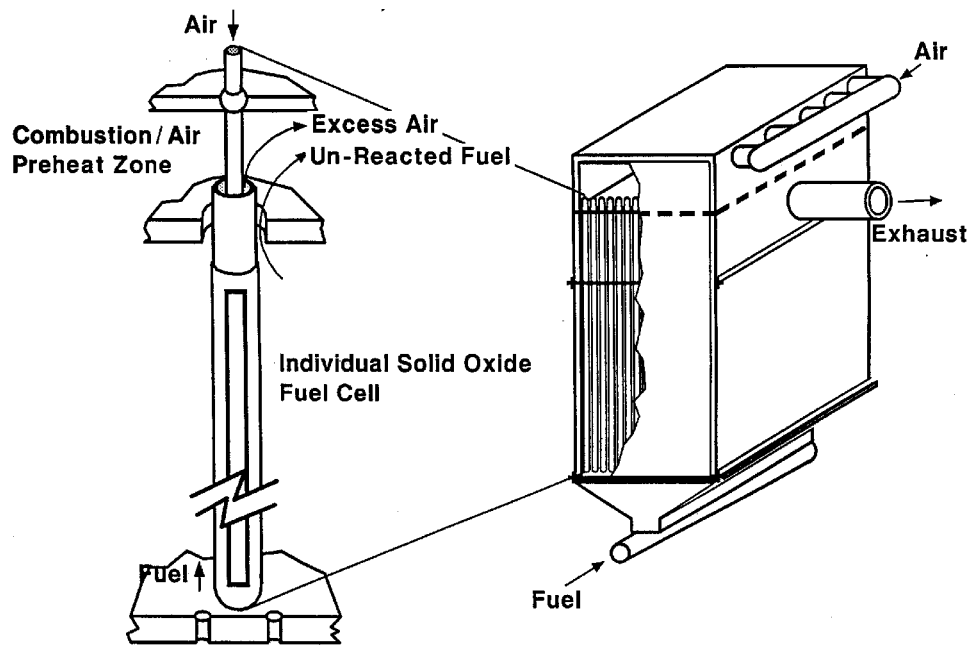
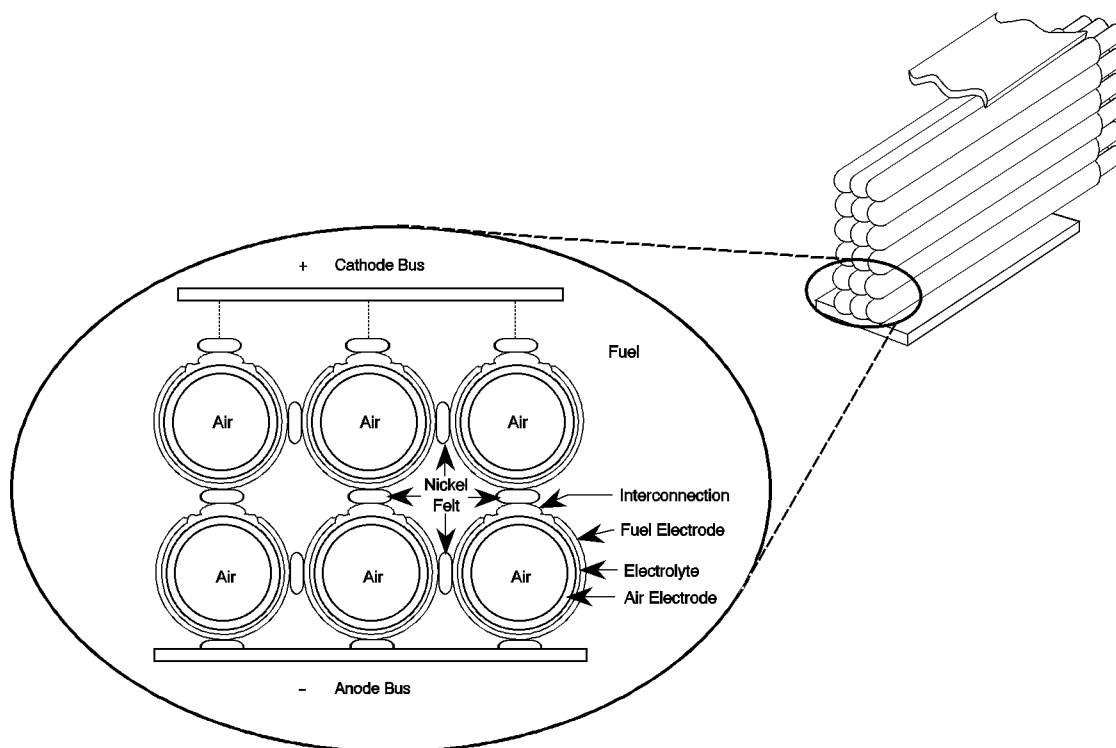


Figure 8-6 Gas-Manifold Design for a Tubular SOFC (2)



**Figure 8-7 Cell-to-Cell Connections Among Tubular SOFCs (2)**

Solid electrolyte structures of yttria-stabilized  $ZrO_2$  of up to 10 cm diameter and 0.25 mm thickness with better than 0.025 mm flatness have been fabricated (14). The interconnect, having ribs on both sides, forms gas flow channels and serves as a bipolar gas separator contacting the anode and cathode of adjoining cells. The flat plate design offers improved power density relative to the tubular and segmented cell-in-series designs but requires high temperature gas seals at the edges of the plates. Compressive seals have been proposed; however, the unforgiving nature of a compressive seal can lead to a nonuniform stress distribution on the ceramic and cracking of the layers. Further, seals may limit the height of a cell stack. There is a higher probability for mismatches in tolerances (creating unacceptable stress levels) in taller stacks. Fabrication and assembly appear to be simpler for the flat plate design as compared with the other designs. The electrolyte and interconnect layers are made by tape casting. The electrodes are applied by the slurry method, by screen printing, or by plasma spraying. Fuel cell stacks are formed by stacking up layers much like other fuel cell technologies (16). Tests of single cells and two cell stacks of SOFCs with a planar configuration (5 cm diameter) have demonstrated power densities up to  $0.12 \text{ W/cm}^2$ . One major technical difficulty with these structures is their brittleness in tension; the tensile strength is only about 20% of their compressive strength. However, the two cell stack was able to withstand five thermal cycles without suffering detectable physical damage, and adequate gas sealing between cells was reported. Developers at Tokyo Gas have reported a  $400 \text{ cm}^2$  and a ten cell stack of small 5 cm x 5 cm cells (17). The successful demonstration of larger multicell stacks has yet to be performed.

### 8.1.3 Development Components

Materials and design approaches have been developed so that SOFC technology, particularly the Siemens Westinghouse tubular cell configuration, is technically feasible. However, the application of the materials used in the non-restrained tubular cell to the restrained alternative planar configurations results in excessive mechanical stresses. Moreover, the present approaches exhibit lower than desired performance (higher operating costs) and difficult designs and fabrication (higher capital costs). Cost reduction of cell components and simplification of the manufacturing are an important focus of ongoing development. The major issue for improving SOFC technology is to develop materials that sustain good performance while withstanding the high operating temperature presently used (1000°C). Related critical issues are as follows:

1) the present materials and relevant designs used in the SOFC must operate at high temperature to obtain performance due to their intrinsic high resistivity, 2) there are high mechanical stresses in planar designs arising from differential thermal expansion coefficients of adjacent component materials, 3) there are interfacial reactions among adjacent components caused by the high sintering temperatures needed to obtain high density, which alter component design integrity, and 4) high temperatures are required in the fabrication of ceramic components, which adds production complexity, hence cost. Raw material costs are \$7/kW to \$15/kW, but manufacturing drives this to \$700/kW for the stack (16, 18,19). Research, as summarized below, is being performed to address these and other issues to bring SOFC technology into the competitive range. Research is proceeding to address material and design improvements that allow operation within the high temperature environment (1000°C) of the existing state-of-the-art components.

Development work for cells operating at 1000°C is focused on increasing the mechanical toughness of the cell materials to alleviate the impact of thermal mismatch and to develop techniques that will decrease interfacial changes of the various material layers during thin film cell fabrication. Interfacial issues among cell components include diffusion, volatilization, and segregation of trace constituents. For example,  $\text{La}_2\text{Zr}_2\text{O}_7$  and  $\text{SrZrO}_3$  may form at the cathode/electrolyte interface, and Sr and Mn ions diffuse across the interface at temperatures as low as 800°C for up to 400 hours (20).

Approaches to resolving the mismatch caused by different component materials' thermal expansion coefficient include increasing the fracture toughness of the electrolyte, controlling the electrolyte processing faults, varying the component thickness, and adding minor constituents to alter the anode properties.

The electrolyte of choice at present is yttria, fully stabilized  $\text{ZrO}_2$ . Researchers are investigating partially stabilized  $\text{ZrO}_2$  and adding  $\text{Al}_2\text{O}_3$  to fully yttria stabilized  $\text{ZrO}_2$  to strengthen the electrolyte matrix. Yamamoto et al. (21) have investigated the tetragonal phase (TZP) of zirconia to strengthen the electrolyte structure so that it can be made thinner to obtain lower resistivity. This increased strength is needed for self-supporting planar cells. An increase in bending strength of 1200 MPa was observed in the TZP material compared to 300 MPa for cubic zirconia stabilized with > 7.5 mol%  $\text{Y}_2\text{O}_3$ . The TZP was stabilized by taking advantage of fine particle technology and minor doping of  $\text{Y}_2\text{O}_3$ . Resistivity increased slightly.

The air electrode material typically has been constructed using high purity component oxides such as  $\text{La}_2\text{O}_3$  and  $\text{MnO}_2$ . Over 70% cost reduction of the air electrode raw materials is possible

if mixed lanthanides are used instead of pure lanthanum. The performance of cells using mixed lanthanides has been shown to be only 8% lower than for cells using pure lanthanum. Further adjustments in composition are expected to result in performance equivalent to high purity electrode material (22).

It has been observed that solid oxide fuel cell voltage losses are dominated by ohmic polarization and that the most significant contribution to the ohmic polarization is the interfacial resistance between the anode and the electrolyte (23). This interfacial resistance is dependent on nickel distribution in the anode. A process has been developed, PMSS (pyrolysis of metallic soap slurry), where NiO particles are surrounded by thin films or fine precipitates of yttria stabilized zirconia (YSZ) to improve nickel dispersion to strengthen adhesion of the anode to the YSZ electrolyte. This may help relieve the mismatch in thermal expansion between the anode and the electrolyte.

Researchers have surmised that there would be a reduction in interfacial activity among adjacent components if the interconnect could be sintered to a high density at temperatures below 1550° (24,25). Either chemical or physical sintering aids could be used. One approach is to use synthesized submicrometer, active powders. The use of these powders causes a depleting or enriching of the rare earth substitution cation with La or Y on one component while holding Cr concentrations constant on the other. This, in turn, alters the sintering temperature. Results show that high densities might be achievable at temperatures of 1400°C and below (25).

Alternative lower cost fabrication methods to sintering and electrochemical vapor deposition (EVD) are receiving more attention. These methods include plasma spraying and chemical vapor deposition (CVD). Many development projects are being conducted in fabrication techniques. Examples of some of the work follow.

Investigations were conducted to determine whether jet vapor deposition (JVD) could be substituted for EVD, which is capital intensive. JVD is a thin film technique in which sonic gas jets in a low vacuum fast flow serve as deposition sources. Results showed that the YSZ films can be made dense and pinhole free; they seal highly porous electrode surfaces and are gas tight. Conductivity needs to be improved, which should be obtainable. The ultimate goal will be to fabricate thin film SOFCs, both electrolyte and the electrodes, in an unbroken sequence of JVD steps. This would also allow the use of alternate metal cathode, such as Ag thin films (19).

Because of a number of conditions that can be set independently, plasma spray techniques may make it attractive to fabricate dense, gas tight, or porous layers with conditions where one layer's application does not affect the preceding layer (26). The Electrotechnical Laboratory in Japan has demonstrated applying a YSZ on a substrate using a laser plasma spray approach. The sprayed material maintained identical crystalline structure during the process. Because a high melting point material was coated on a low melting point material, this method offers the potential for multilayer coating (27). Work at Siemens Westinghouse with plasma spraying also has yielded promising results. Deposition of a Ni-YSZ slurry over the YSZ electrolyte followed by sintering has yielded fuel electrodes that are equivalent in conductivity to electrodes fabricated by a total EVD process. Cells fabricated with only one EVD step (plasma sprayed interconnection, EVD electrolyte, and sintered fuel electrode) will replace current cells (22).



## 8.2 Performance<sup>41</sup>

The thermodynamic efficiency of SOFCs at open circuit voltage is lower than that of MCFCs and PAFCs, which utilize H<sub>2</sub> and O<sub>2</sub>, because of the lower  $\Delta G$ <sup>42</sup> at higher temperatures (see discussion in Section 2). However, as mentioned in Section 2, the higher operating temperature of SOFCs is beneficial in reducing polarization.

The voltage losses in SOFCs are governed by ohmic losses in the cell components. The contribution to ohmic polarization (iR) in a tubular cell<sup>43</sup> is 45% from cathode, 18% from the anode, 12% from the electrolyte, and 25% from the interconnect, when these components have thickness (mm) of 2.2, 0.1, 0.04 and 0.085, respectively, and specific resistivities (ohm cm) at 1000°C of 0.013,  $3 \times 10^{-6}$ , 10, and 1, respectively. The cathode iR dominates the total ohmic loss despite the higher specific resistivities of the electrolyte and cell interconnection because of the short conduction path through these components and the long current path in the plane of the cathode.

### 8.2.1 Effect of Pressure

SOFCs, like PAFCs and MCFCs, show an enhanced performance by increasing cell pressure. The following equation approximates the effect of pressure on cell performance at 1000°C (1832°F):

$$\Delta V_p(\text{mV}) = 59 \log \frac{P_2}{P_1} \quad (8-8)$$

where  $P_1$  and  $P_2$  are different cell pressures. The above correlation was based on the assumption that overpotentials are predominately affected by gas pressures and that these overpotentials decrease with increased pressure.

Siemens Westinghouse, in conjunction with Ontario Hydro Technologies, tested AES cells at pressures up to 15 atmospheres on both hydrogen and natural gas (22). Figure 8-8 illustrates the performance at various pressures:

---

<sup>41</sup>. This section provides practical information that may be used for estimating the relative performance of SOFCs based on various operating parameters at this time. The SOFCs being developed have unique designs, are constructed of varying materials, and are fabricated by differing techniques. SOFCs, particularly the flat plate types, will undergo considerable development in materials, design, and fabrication techniques. As SOFC technology progresses, it will mature towards more standardized cells as has happened with PAFCs and MCFCs that are closer to conformity. The process is expected to result in an evolution of the performance trends depicted here.

<sup>42</sup>.  $\Delta G$  decreases from 54.617 kcal/mole at 27°C to 43.3 kcal/mole at 927°C, whereas  $\Delta H$  is nearly constant over this temperature range (39).

<sup>43</sup>. A uniform current distribution through the electrolyte is assumed.

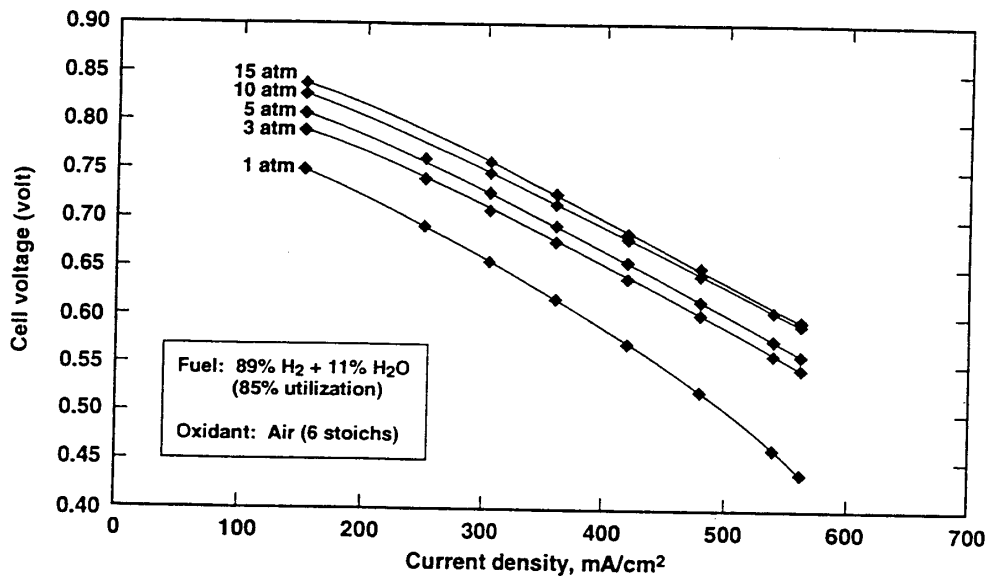


Figure 8-8 Effect of Pressure on AES Cell Performance at 1000°C  
[(22) 2.2 cm diameter, 150 cm active length]

### 8.2.2 Effect of Temperature

The dependence of SOFC performance on temperature is illustrated in Figure 8-9 for a two cell stack using air (low utilization) and a fuel of 67% H<sub>2</sub>/22% CO/11% H<sub>2</sub>O (low utilization). The sharp decrease in cell voltage as a function of current density at 800°C (1472°F) is a manifestation of the high ohmic polarization (i.e., low ionic conductivity) of the solid electrolyte at this temperature. The ohmic polarization decreases as the operating temperature increases to 1050°C (1922°F), and correspondingly, the current density at a given cell voltage increases. The data in Figure 5-10 show a larger decrease in cell voltage with decreasing temperature between 800 and 900°C (1472 to 1652°F) than that between 900 and 1000°C (1652 to 1832°F), at constant current density. This and other data suggest that the voltage gain with respect to temperature is a strong function of temperature and current density. One reference (28) postulates the voltage gain as

$$\Delta V_T(\text{mV}) = 1.3(T_2 - T_1)(^\circ\text{C}) \quad (8-9)$$

for a cell operating at 1000°C, 160 mA/cm<sup>2</sup> and a fuel composition of 67% H<sub>2</sub>/22% CO/11% H<sub>2</sub>O. In light of the strong functionality with respect to current density, it might be more appropriate to describe the voltage gain with the following relationship:

$$\Delta V_T(\text{mV}) = K(T_2 - T_1)(^\circ\text{C}) * J \quad (8-10)$$

where J is the current density in mA/cm<sup>2</sup>.

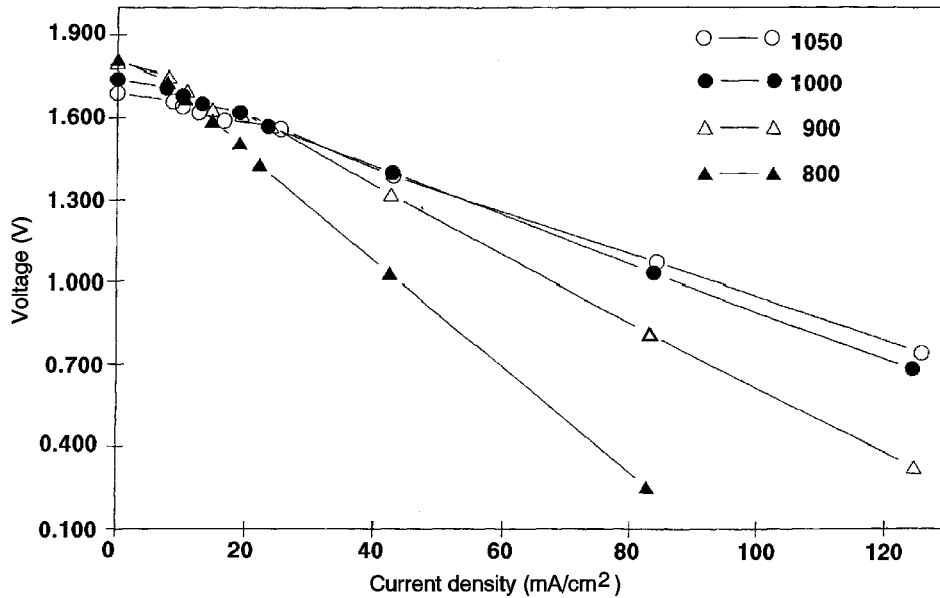


Figure 8-9 Two Cell Stack Performance with 67% H<sub>2</sub> + 22% CO + 11% H<sub>2</sub>O/Air (29)

the following values of K have been deduced from several references that utilized a fuel composition of 67% H<sub>2</sub>/22% CO/11% H<sub>2</sub>O, and an air oxidant.

Table 8-2 K Values for  $\Delta V_T$

K	Temperature (°C)	Ref.
0.008	~1000	28
0.006	1000 - 1050	29
0.014	900 - 1000	
0.068	800 - 900	
0.003	900 - 1000	30
0.009	800 - 900	

As can be seen, there is a reasonably large range in the value of K between these references. As the SOFC technology matures, these differences may reconcile to a more cohesive set of values. In the interim, the following single average combination of the above K values may help the reader if no specific information is available.

$$\Delta V_T(\text{mV}) = 0.008(T_2 - T_1)(^\circ\text{C}) * J(\text{mA}/\text{cm}^2) \quad 900^\circ\text{C} \leq T \leq 1050^\circ\text{C} \quad (8-11)$$

Equation (8-11) is for a fuel composed of 67% H<sub>2</sub>/22% CO/11% H<sub>2</sub>O. Experiments using different fuel combinations, such as 80% H<sub>2</sub>/20% CO<sub>2</sub> (30) and 97% H<sub>2</sub>/3% H<sub>2</sub>O (31,29), suggest that these correlations may not be valid for other fuels. Figure 8-10 presents a set of performance curves for a fuel of 97% H<sub>2</sub>/3% H<sub>2</sub>O at various temperatures. Voltage actually increases with decreasing temperature for current densities below approximately 65 mA/cm<sup>2</sup>. Other data (32) show that this inverse relationship can extend to current densities as high as 200 mA/cm<sup>2</sup>.

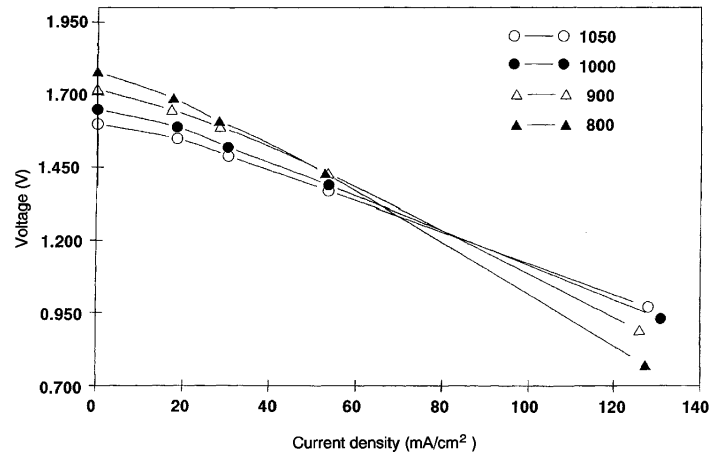


**Figure 8-10 Two Cell Stack Performance with 97% H<sub>2</sub> and 3% H<sub>2</sub>O/Air (28)**

### 8.2.3 Effect of Reactant Gas Composition and Utilization

Because SOFCs operate at high temperature, they are capable of internally reforming fuel gases (i.e., CH<sub>4</sub> and other light hydrocarbons) without the use of a specific reforming catalyst (i.e., anode itself is sufficient), and this attractive feature of high temperature operation of SOFCs has recently been experimentally verified. Another important aspect of SOFCs is that recycle of CO<sub>2</sub> from the spent fuel stream to the inlet oxidant, as required by MCFCs, is not necessary because SOFCs utilize only O<sub>2</sub> at the cathode.

**Oxidant:** The performance of SOFCs, like that of other fuel cells, improves with pure O<sub>2</sub> rather than air as the oxidant. With a fuel of 67% H<sub>2</sub>/22% CO/11% H<sub>2</sub>O at 85% utilization, the cell voltage at 1000°C shows an improvement with pure O<sub>2</sub> over that obtained with air (see Figure 5-12). In the figure, the experimental data are extrapolated by a dashed line to the theoretical Nernst potential for the inlet gas compositions. At a target current density of 160 mA/cm<sup>2</sup> for the tubular SOFC operating on the above mentioned fuel gas, a difference in cell voltage of about 55 mV is obtained. The difference in cell voltage with pure O<sub>2</sub> and air increases as the current density increases, which suggests that concentration polarization plays a role during O<sub>2</sub> reduction in air.

Based on the Nernst equation, the theoretical voltage gain due to a change in oxidant utilization at  $T = 1000^\circ\text{C}$  is

$$\Delta V_{\text{Cathode}} = 63 \log \frac{(\bar{P}_{\text{O}_2})_2}{(\bar{P}_{\text{O}_2})_1} \quad (8-12)$$

where  $\bar{P}_{\text{O}_2}$  is the average partial pressure of  $\text{O}_2$  in the system. Data (28) suggest that a more accurate depiction of voltage gain is described by

$$\Delta V_{\text{Cathode}} = 92 \log \frac{(\bar{P}_{\text{O}_2})_2}{(\bar{P}_{\text{O}_2})_1} \quad (8-13)$$

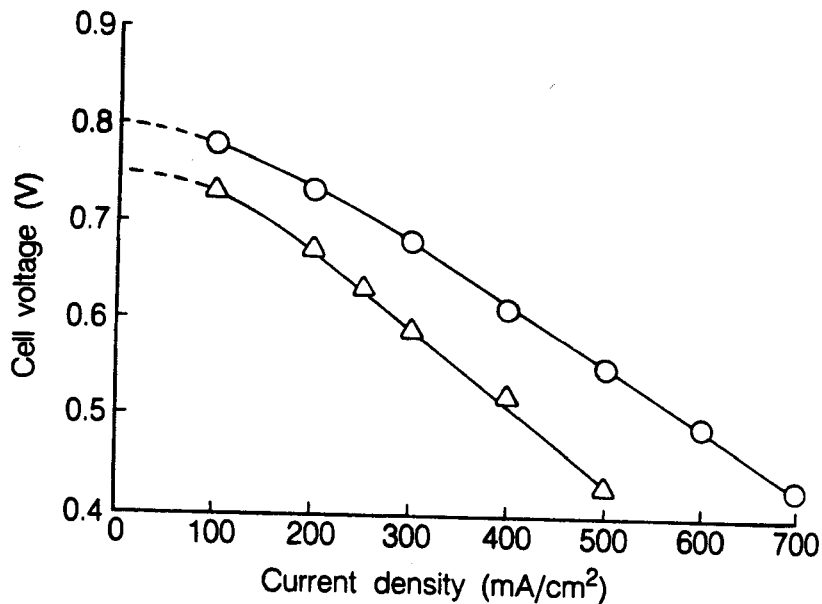


**Figure 8-17 Cell Performance at 1000°C with Pure Oxygen (o) and Air (Δ) Both at 25% Utilization (Fuel (67%  $\text{H}_2$ /22%  $\text{CO}$ /11% $\text{H}_2\text{O}$ ) Utilization is 85%) (30)**

**Fuel:** The influence of fuel gas composition on the theoretical open circuit potential of SOFCs is illustrated in Figure 8-12, following the discussion by Sverdrup, et al. (8). The oxygen/carbon (O/C) atom ratio and hydrogen/carbon (H/C) atom ratio, which define the fuel composition, are plotted as a function of the theoretical open circuit potential at 1000°C. If hydrogen is absent from the fuel gas,  $\text{H/C} = 0$ . For pure  $\text{CO}$ ,  $\text{O/C} = 1$ ; for pure  $\text{CO}_2$ ,  $\text{O/C} = 2$ . The data in the figure

show that the theoretical potential decreases from about 1 V to about 0.6 V as the amount of O<sub>2</sub> increases, and the fuel gas composition changes from CO to CO<sub>2</sub>. The presence of hydrogen in the fuel produces two results: (a) the potential is higher, and (b) the O/C ratio corresponding to complete oxidation extends to higher values. These effects occur because the equilibrium composition obtained by the water gas shift reaction in gases containing hydrogen (H<sub>2</sub>O) and carbon (CO) produces H<sub>2</sub>, but this reaction is not favored at higher temperatures (see Appendix 11.1). In addition, the theoretical potential for the H<sub>2</sub>/O<sub>2</sub> reaction exceeds that for the CO/O<sub>2</sub> reaction at temperatures about 800°C; consequently, the addition of hydrogen to the fuel gas will yield a higher open circuit potential in SOFCs. Based on the Nernst equation, the theoretical voltage gain due to a change in fuel utilization at T = 1000°C is

$$\Delta V_{\text{Anode}} = 126 \log \frac{(\bar{P}_{\text{H}_2} / \bar{P}_{\text{H}_2\text{O}})_2}{(\bar{P}_{\text{H}_2} / \bar{P}_{\text{H}_2\text{O}})_1} \quad (8-14)$$

where  $\bar{P}_{\text{H}_2}$  and  $\bar{P}_{\text{H}_2\text{O}}$  are the average partial pressures of H<sub>2</sub> and H<sub>2</sub>O in the system.

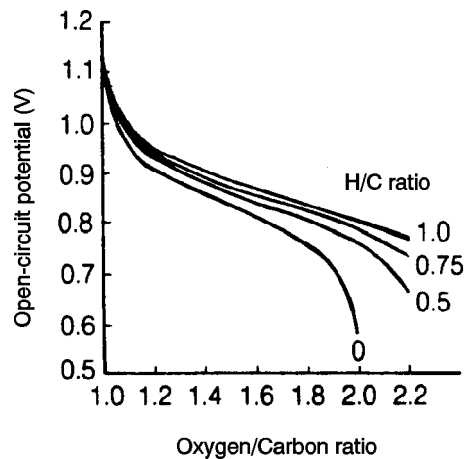


**Figure 8-12 Influence of Gas Composition of the Theoretical Open-Circuit Potential of SOFC at 1000°C [(8) Figure 3, p. 258]**

The fuel gas composition also has a major effect on the cell voltage of SOFCs. The performance data (33) obtained from a 15 cell stack (1.7 cm<sup>2</sup> active electrode area per cell) of the tubular configuration (see Figure 8-1) at 1000°C illustrate the effect of fuel gas composition. With air as the oxidant and fuels of composition 97% H<sub>2</sub>/3% H<sub>2</sub>O, 97% CO/3% H<sub>2</sub>O, and 1.5% H<sub>2</sub>/3% CO/75.5% CO<sub>2</sub>/20% H<sub>2</sub>O, the current densities achieved at 80% voltage efficiency were ~220, ~170, and ~100 mA/cm<sup>2</sup>, respectively. The reasonably close agreement in the current densities obtained with fuels of composition 97% H<sub>2</sub>/3% H<sub>2</sub>O and 97% CO/3% H<sub>2</sub>O indicates that CO is a useful fuel for SOFCs. However, with fuel gases that have only a low concentration of H<sub>2</sub> and

CO (i.e., 1.5% H<sub>2</sub>/3% CO/75.5% CO<sub>2</sub>/20% H<sub>2</sub>O), concentration polarization becomes significant and the performance is lower.

A reference fuel gas utilized in experimental SOFCs has had a composition 67% H<sub>2</sub>/22% CO/11% H<sub>2</sub>O. With this fuel (85% utilization) and air as the oxidant (25% utilization), individual cells (~1.5 cm diameter, 30 cm length and ~110 cm<sup>2</sup> active surface area) have delivered a peak power of 22 W (34). Figure 8-13 (30) shows the change in the cell voltage with fuel utilization for a SOFC that operates on this reference fuel and pure O<sub>2</sub> or air as oxidant (25% utilization). The cell voltage decreases with an increase in the fuel utilization at constant current density. Insufficient data are available in the figure to determine whether the temperature has a significant effect on the change in cell voltage with utilization. However, the data do suggest that a larger voltage decrease occurs at 1000°C than at 800 or 900°C. Based on this and other data (27,34), the voltage gain at T = 1000°C and with air is defined by Equation (8-15):

$$\Delta V_{\text{Anode}} = 172 \log \frac{(\bar{P}_{\text{H}_2} / \bar{P}_{\text{H}_2\text{O}})_2}{(\bar{P}_{\text{H}_2} / \bar{P}_{\text{H}_2\text{O}})_1} \quad (8-15)$$

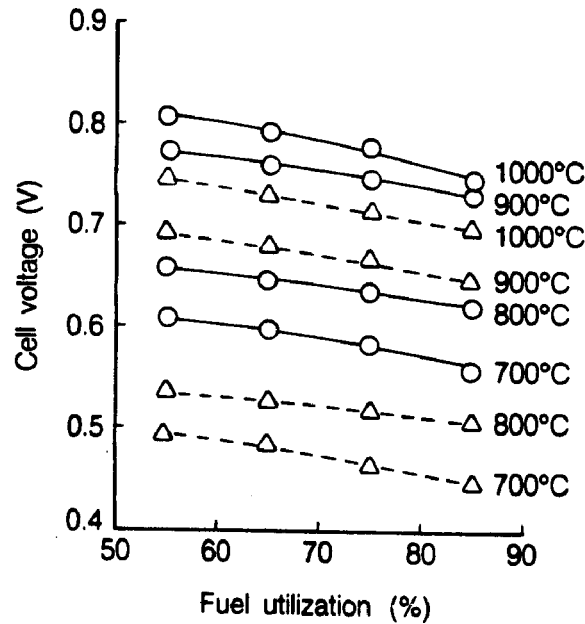


**Figure 8-13 Variation in Cell Voltage as a Function of Fuel Utilization and Temperature (Oxidant (o - Pure O<sub>2</sub>; Δ - Air) Utilization is 25%. Currently Density is 160 mA/cm<sup>2</sup> at 800, 900 and 1000°C and 79 mA/cm<sup>2</sup> at 700°C) (30)**

#### 8.2.4 Effect of Impurities

Hydrogen sulfide (H<sub>2</sub>S), hydrogen chloride (HCl) and ammonia (NH<sub>3</sub>) are impurities typically found in coal gas. Some of these substances may be harmful to the performance of SOFCs. Recent experiments (35) have used a simulated oxygen-blown coal gas containing 37.2% CO/34.1% H<sub>2</sub>/0.3% CH<sub>4</sub> /14.4% CO<sub>2</sub>/13.2% H<sub>2</sub>O/0.8% N<sub>2</sub>. These experiments have shown no

degradation due to the presence of 5000 ppm NH<sub>3</sub>. An impurity level of 1 ppm HCl also has shown no detectable degradation. H<sub>2</sub>S levels of 1 ppm result in an immediate performance drop, but this loss soon stabilizes into a normal linear degradation. Figure 8-14 shows the performance of the experimental cell over time. Additional experiments have shown that removing H<sub>2</sub>S from the fuel stream returns the cell to nearly its original level. It has also been found that maintaining an impurity level of 5000 ppm NH<sub>3</sub> and 1 ppm HCl, but decreasing the H<sub>2</sub>S level to 0.1 ppm, eliminates any detrimental effect due to the presence of sulfur, even though, as mentioned above, 1 ppm H<sub>2</sub>S causes virtually no degradation in the tubular 1,000°C cell.

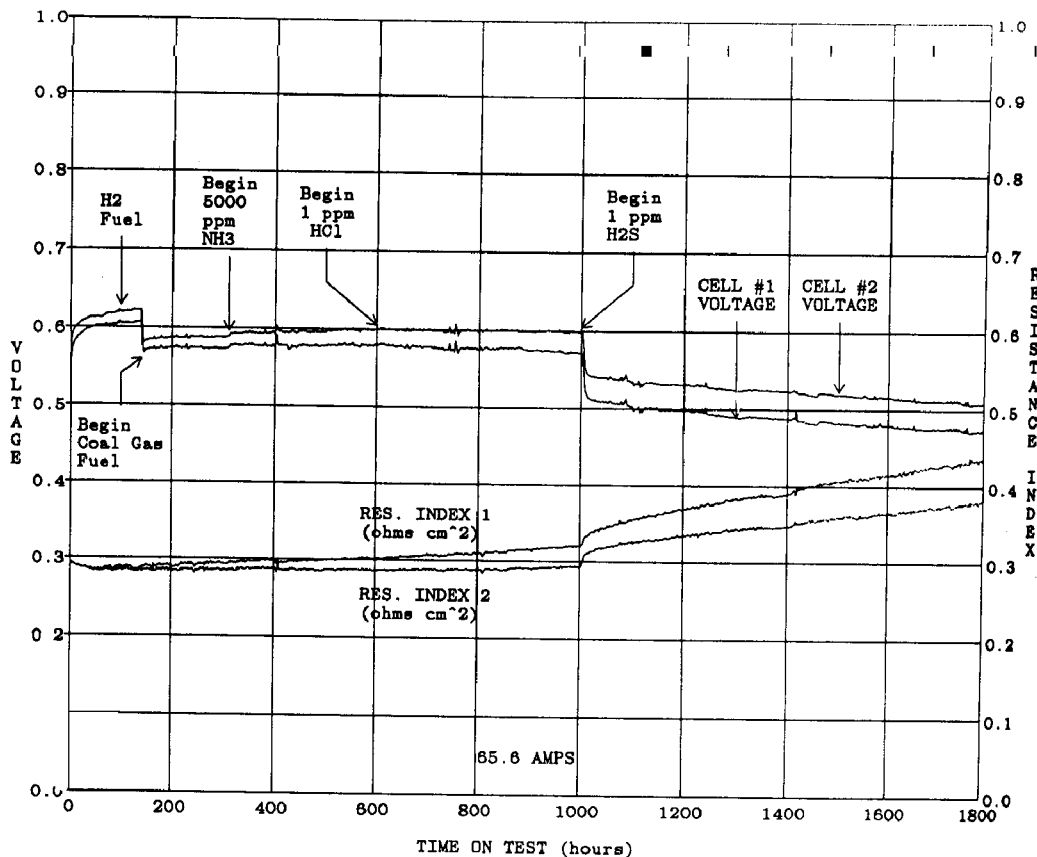


**Figure 8-14 SOFC Performance at 1000°C and 350 mA/cm<sup>2</sup>, 85% Fuel Utilization and 25% Air Utilization (Fuel = Simulated Air-Blown Coal Gas Containing 5000 ppm NH<sub>3</sub>, 1 ppm HCl and 1 ppm H<sub>2</sub>S) (35)**

In addition, silicon (Si), which also can be found in coal gas, has been studied (35) as a contaminant. It is believed to accumulate on the fuel electrode in the form of silica (SiO<sub>2</sub>). The deposition of the Si throughout the cell has been found to be enhanced by high (~50%) H<sub>2</sub>O content in the fuel. Si is transported by the following reaction:





As the CH<sub>4</sub> component of the fuel reforms to CO and H<sub>2</sub>, H<sub>2</sub>O is consumed. This favors the reversal of Equation (8-16), which allows SiO<sub>2</sub> to be deposited downstream, possibly on exposed nickel surfaces. Oxygen-blown coal gas, however, has an H<sub>2</sub>O content of only ~13%, and this is not expected to allow for significant Si transport.

### 8.2.5 Effects of Current Density

The voltage level of a SOFC is reduced by ohmic, activation, and concentration losses, which increase with increasing current density. The magnitude of this loss is described by the following equation that was developed from information in the literature (36,29,37,38,39,40):

$$\Delta V_j(\text{mV}) = -0.73\Delta J \quad (T = 1000^\circ\text{C}) \quad (8-17)$$

where J is the current density (mA/cm<sup>2</sup>) at which the cell is operating. The latest AES cells by Siemens Westinghouse exhibit the following performance:

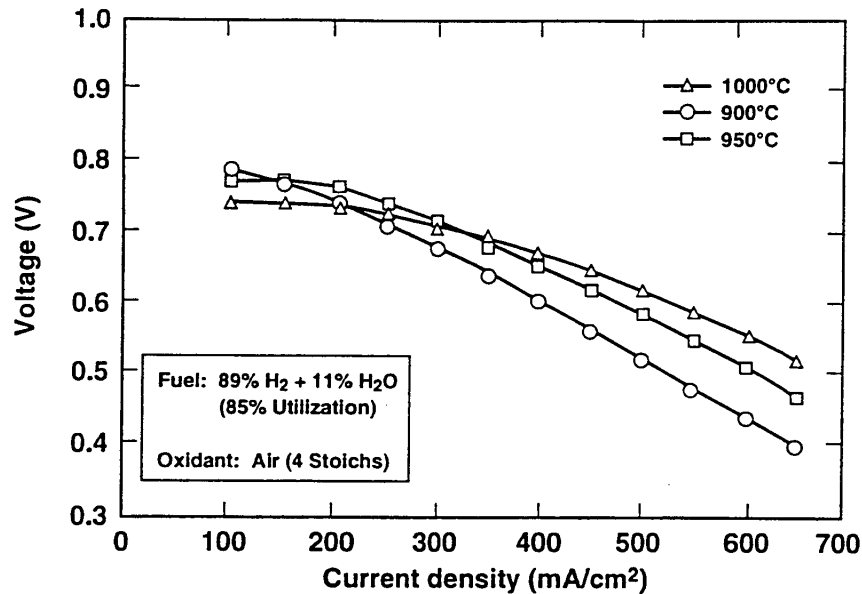


Figure 8-15 Voltage-Current Characteristics of an AES Cell (1.56 cm Diameter, 50 cm Active Length)

### 8.2.6 Effects of Cell Life

The endurance of the cell stack is of primary concern for SOFCs. As SOFC technology has continued to approach commercialization, research in this area has increased and improvements made. The Siemens Westinghouse state-of-the-art tubular design has been validated by continuous electrical testing of over 69,000 hours with less than 0.5% voltage degradation per 1,000 hours of operation. This tubular design is based on the early calcia-stabilized zirconia porous support tube (PST). In the current technology, the PST has been eliminated and replaced by a doped lanthanum manganite air electrode tube. These air electrode supported (AES) cells have shown a power density increase of approximately 33% over the previous design. Siemens

Westinghouse AES cells have shown less than 0.2 % voltage degradation per 1000 hours in a 25 kW stack operated for over 13,000 hours (22).

### 8.3 Summary Of Equations For SOFC<sup>41</sup>

The preceding sections provide parametric performance based on various referenced data at different operating conditions. It is suggested that the following set of equations could be used for performance adjustments unless the reader prefers other data or correlations.

<u>Parameter</u>	<u>Equation</u>	<u>Comments</u>
Pressure	$\Delta V_p(\text{mV}) = 59 \log \frac{P_2}{P_1}$	1 atm $\leq$ P $\leq$ 10 atm (8-8)
Temperature <sup>44</sup>	$\Delta V_T(\text{mV}) = 0.008(T_2 - T_1)(^\circ\text{C}) * J$	900°C $\leq$ T $\leq$ 1050°C (8-11)
Oxidant	$\Delta V_{\text{Cathode}}(\text{mV}) = 92 \log \frac{(\bar{P}_{\text{O}_2})_2}{(\bar{P}_{\text{O}_2})_1}$	$0.16 \leq \frac{\bar{P}_{\text{O}_2}}{\bar{P}_{\text{Total}}} \leq 0.20$ 18 (8-13)
Fuel	$\Delta V_{\text{Anode}} = 172 \log \frac{(\bar{P}_{\text{H}_2} / \bar{P}_{\text{H}_2\text{O}})_2}{(\bar{P}_{\text{H}_2} / \bar{P}_{\text{H}_2\text{O}})_1}$	$0.9 \leq \bar{P}_{\text{H}_2} / \bar{P}_{\text{H}_2\text{O}} \leq 6.9$ T = 1000°C, with air (8-15)
Current Density	$\Delta V_J(\text{mV}) = -0.73\Delta J$	50 < J < 400 mA/cm <sup>2</sup> (8-17) P = 1 atm., T = 1000°C

### 8.4 References

1. N.Q. Minh, "Ceramic Fuel Cells," *J. Am. Ceram. Soc.*, p. 76 [3]563-88, 1993.
2. Courtesy of Siemens Westinghouse.
3. T.H. Etsell, S.N. Flengas, *J. Electrochem. Soc.*, p. 118, 1890 (1971).
4. A.O. Isenberg, in Proceedings of the Symposium on Electrode Materials and Processes for Energy Conversion and Storage, edited by J.D.E. McIntyre, S. Srinivasan and F.G. Will, The Electrochemical Society, Inc., Pennington, NJ, 1977, p. 682.
5. A.O. Isenberg, in Proceedings of the Symposium on Electrode Materials and Processes for Energy Conversion and Storage, edited by J.D.E. McIntyre, S. Srinivasan and F.G. Will, The Electrochemical Society, Inc., Pennington, NJ, 1977, p. 572.
6. D.C. Fee, S.A. Zwick, J.P. Ackerman, in Proceedings of the Conference on High Temperature Solid Oxide Electrolytes, held at Brookhaven National Laboratory, August 16-17, 1983, BNL 51728, compiled by F.J. Salzano, October 1983, p. 29.
7. D.W. Dees, T.D. Claar, T.E. Easler, D.C. Fee, F.C. Mrazek, *J. Electrochem. Soc.*, p. 134, 2141, 1987.
8. E.F. Sverdrup, C.J. Warde, A.D. Glasser, in *From Electrocatalysis to Fuel Cells*, Edited by G. Sandstede, University of Washington Press, Seattle, WA, 1972, p. 255.

<sup>44</sup>. Where J = mA/cm<sup>2</sup>, for fuel composition of 67% H<sub>2</sub>/22% CO/11% H<sub>2</sub>O

9. D.H. Archer, L. Elikan, R.L. Zahradnik, in *Hydrocarbon Fuel Cell Technology*, Edited by B.S. Baker, Academic Press, New York, NY, 1965, p. 51.
10. D.H. Archer, J.J. Alles, W.A. English, L. Elikan, E.F. Sverdrup, R.L. Zahradnik, in *Fuel Cell Systems, Advances in Chemistry Series 47*, edited by R.F. Gould, American Chemical Society, Washington, DC, 1965, p. 332.
11. M.S.S. Hsu, W.E. Morrow, J.B. Goodenough, in Proceedings of the 10th Intersociety Energy Conversion Engineering Conference, The Institute of Electrical and Electronics Engineering, Inc., New York, NY, 1975, p. 555.
12. M.S.S. Hsu, T.B. Reed, in Proceedings of the 11th Intersociety Energy Conversion Engineering Conference, American Institute of Chemical Engineers, New York, NY, 1976, p. 1.
13. M. Hsu, "Zirconia Fuel Cell Power System," 1985 Fuel Cell Seminar Abstracts, 1985 Fuel Cell Seminar, Tucson, AZ, May 19-22, 1985.
14. M. Hsu, "Zirconia Fuel Cell Power System Planar Stack Development," Fuel Cell Abstracts, 1986 Fuel Cell Seminar, Tucson, AZ, October 26-29, 1986.
15. *Fuel Cells*, DOE/METC-86/0241, Technology Status report, Morgentown Energy Technology Center, Morgantown, WV, 1986.
16. N.Q. Minh, "High-Temperature Fuel Cells, Part 2: The Solid Oxide Cell," *ChemTech*, Vol. 21, February, 1991.
17. Y. Jatsuzaki, et al., "High Power Density SOFC Development at Tokyo Gas," Fuel Cell Program and Abstracts, 1992 Fuel Cell Seminar, Tucson, Arizona, November 29 - December 2, 1992.
18. K. Krist, "Gas Research Institute's Fundamental Research on Intermediate-Temperature Planar Solid Oxide Fuel Cells," in Fuel Cell Program and Abstracts, 1992 Fuel Cell Seminar, Tucson, AZ, November 29 - December 2, 1992.
19. B.L. Halpern, J.W. Golz, Y. Di, "Jet Vapor Deposition of Thin Films for Solid Oxide and Other Fuel Cell Applications," in Proceedings of the Fourth Annual Fuel Cells Contractors Review Meeting, U.S. DOE/METC, July, 1992.
20. H.U. Anderson, M.M. Nasrallah, "Characterization of Oxides for Electrical Delivery Systems," An EPRI/GRI Fuel Cell Workshop on Fuel Cell Technology Research and Development, New Orleans, LA, April 13-14, 1993.
21. O. Yamamoto, et al., "Zirconia Based Solid Ion Conductors," The International Fuel Cell Conference Proceedings, NEDO/MITI, Tokyo, Japan, 1992.
22. S.C. Singhal, "Recent Progress in Tubular Solid Oxide Fuel Cell Technology," Proceedings of the Fifth International Symposium on Solid Oxide Fuel Cells (SOFC-V), The Electrochemical Society, Inc., Pennington, NJ, 1997.
23. Y. Matsuzaki, et al., "High Power Density SOFC Development at Tokyo Gas," Fuel Cell Program and Abstracts, 1992 Fuel Cell Seminar, Tucson, AZ, November 29 - December 2, 1992.
24. C. Bagger, "Improved Production Methods for YSZ Electrolyte and Ni-YSZ Anode for SOFC," Fuel Cell Program and Abstracts, 1992 Fuel Cell Seminar, Tucson, AZ, November 29 - December 2, 1992.
25. J.L. Bates, "Alternative Materials for Solid Oxide Fuel Cells: Factors Affecting Air-Sintering of Chromite Interconnections," Proceedings of the Fourth Annual Fuel Cells Contractors Review Meeting, U.S. DOE/METC, July, 1992.

26. A.R. Nicoll, G. Barbezat, A. Salito, "The Potential of Plasma Spraying for the Deposition of Coatings on SOFC Components," The International Fuel Cell Conference Proceedings, NEDO/MITI, Tokyo, Japan, 1992.
27. F. Uchiyama, et al., "ETL Multi-Layer Spray Coating for SOFC Component," The International Fuel Cell Conference Proceedings, NEDO/MITI, Tokyo, Japan, 1992.
28. H. Ide et al., "Natural Gas Reformed Fuel Cell Power Generation Systems - A Comparison of Three System Efficiencies," Proceedings of the 24th Intersociety Energy Conversion Engineering Conference, The Institute of Electrical and Electronics Engineers, Washington, D.C., 1989.
29. Data from Allied-Signal Aerospace Company, 1992.
30. C. Zeh, private communication, 2nd edition of Handbook, April 29, 1987.
31. A. Sammells, "Perovskite Electrolytes for SOFC," Proceedings of the Third Annual Fuel Cells Contractors Review Meeting, U.S. DOE/METC, p. 152, June, 1991.
32. A. Khandkar, S. Elangovan, "Planar SOFC Development Status," Proceedings of the Second Annual Fuel Cells Contractors Review Meeting, U.S. DOE/METC, p. 152, May, 1990.
33. C. J. Warde, A. O. Isenberg, J. T. Brown "High-Temperature Solid-Electrolyte Fuel-Cells Status and Programs at Westinghouse," in Program and Abstracts, ERDA/EPRI Fuel Cell Seminar, Palo Alto, CA, June 29-30 to July 1, 1976.
34. W.J. Dollard, J.T. Brown, "Overview of the Westinghouse Solid Oxide Fuel Cell Program," Fuel Cell Abstracts, 1986 Fuel Cell Seminar, Tucson, AZ, Oct. 26-29, 1986.
35. N. Maskalick, "Contaminant Effects in Solid Oxide Fuel Cells," Proceedings of the Fourth Annual Fuel Cells Contractors Review Meeting, U.S. DOE/METC, July, 1992.
36. N. Minh et al., "Monolithic Solid Oxide Fuel Cell Development: Recent Technical Progress," AlliedSignal, Fuel Cell Seminar Program and Abstracts, 1992 Fuel Cell seminar, 1992.
37. Y. Yoshida et al., "Development of Solid Oxide Fuel Cell," paper provided by Mitsubishi Heavy Industries Ltd.
38. A. Khandkar et al., "Planar SOFC Technology Status and Overview," Ceramatec, Inc., Fuel Cell Seminar Program and Abstracts, 1992 Fuel Cell Seminar, Tucson, AZ, November 29-December 2, 1992.
39. "Research and Development on Fuel Cell Power Generation Technology," FY 1990 Annual Report, NEDO, April, 1991.
40. T. Nakanishi, "Substrate Type, Planar Solid Oxide Fuel Cell," Fuji Electric, Fuel Cell Seminar Program and Abstracts, 1992 Fuel Cell Seminar, Tucson, AZ, November 29 - December 2, 1992.

---

## 9. FUEL CELL SYSTEMS

---

Although a fuel cell produces electricity, a fuel cell power system requires the integration of many components beyond the fuel cell stack itself, for the fuel cell will produce only dc power and utilize only processed fuel. Various system components are incorporated into a power system to allow operation with conventional fuels, to tie into the ac power grid, and often, to utilize rejected heat to achieve high efficiency. In a rudimentary form, fuel cell power systems consist of a fuel processor, fuel cell power section, power conditioner, and potentially a cogeneration or bottoming cycle to utilize the rejected heat. A simple schematic of these basic systems and their interconnections is presented in Figure 9-1.

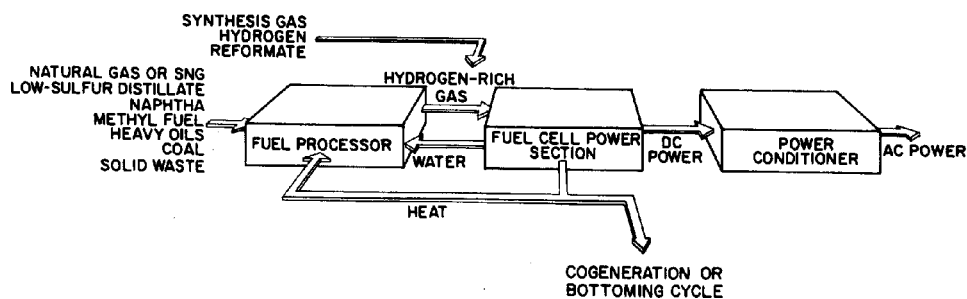


**Figure 9-1 A Rudimentary Fuel Cell Power System Schematic**

The cell and stacks that compose the power section have been discussed extensively in the previous sections of this handbook. Section 9.1 addresses system processes such as fuel processors, rejected heat utilization, the power conditioner, and equipment performance guidelines. System optimization issues are addressed in Section 9.2. System design examples for present day and future applications are presented in Sections 9.3 and 9.4 respectively. Section 9.5 discusses research and development areas that are required for the future system designs to be developed. Section 9.5 presents some advanced fuel cell network designs, and Section 9.6 introduces hybrid systems that combine fuel cells with other generating technologies in integrated systems.

## 9.1 System Processes

The design of a fuel cell system involves more than the optimizing of the fuel cell section with respect to efficiency or economics. It involves power minimizing of the cost of electricity (or product as in a cogeneration system) within the constraints of the desired application. For most applications, this requires that the fundamental processes be integrated into an efficient plant with low capital costs. Often these objectives are conflicting, so compromises, or design decisions, must be made. In addition, project-specific objectives, such as desired fuel, emission levels, potential uses of rejected heat (electricity, steam, or heat), desired output levels, volume or weight criteria (volume/kW or weight/kW), and tolerance for risk all influence the design of the fuel cell power system.

A detailed discussion of all the trade-offs and considerations of system design is outside the scope of this handbook. Nevertheless, a brief discussion of various system considerations is presented.

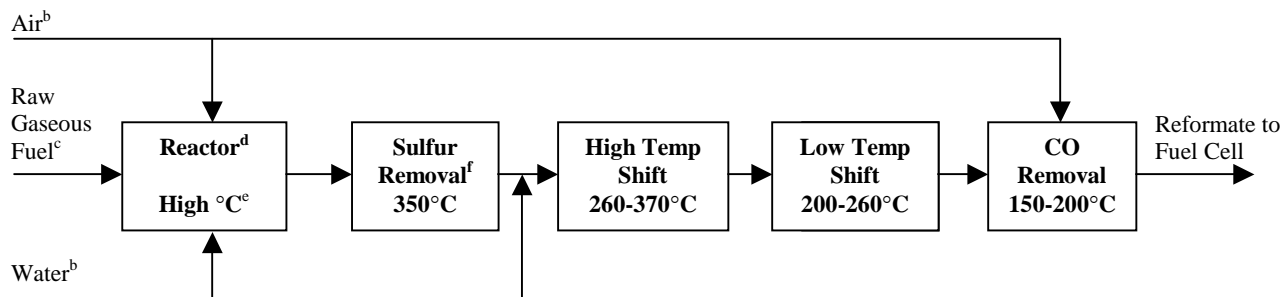
### 9.1.1 Fuel Processing

Fuel processing is defined in this Handbook as the conversion of a commercially available gas, liquid, or solid fuel (raw fuel) to a fuel gas reformat suitable for the fuel cell anode reaction. Fuel processing encompasses the cleaning and removal of harmful species in the raw fuel, the conversion of the raw fuel to the fuel gas reformat, and downstream processing to alter the fuel gas reformat according to specific fuel cell requirements. Examples of these processes are:

- Raw Fuel Cleaning – Removal of sulfur, halides, and ammonia to prevent fuel processor and fuel cell catalysts poisoning.
- Raw Fuel Conversion – Converting a hydrocarbon fuel to a hydrogen-rich gas reformat.
- Reformat Gas Alteration – Converting carbon monoxide (CO) and water (H<sub>2</sub>O) in the fuel gas reformat to hydrogen (H<sub>2</sub>) and carbon dioxide (CO<sub>2</sub>) via the water-gas shift reaction; selective oxidation to reduce CO to a few ppm; or removal of water by condensing to increase the H<sub>2</sub> concentration.

A fuel processor is defined in this Handbook as an integrated unit consisting of one or more of the above processes, as needed according to the fuel cell requirements and the raw fuel, that function together to be cost effective for the application. Figure 9-2 is a depiction of the component path needed. Cost effectiveness may include high thermal efficiency, high hydrogen yield (for some fuel cells hydrogen plus carbon monoxide yield), multi-cycling, compact, lightweight, and quick starting, depending on application. Most fuel processors make use of the chemical and heat energy left in the fuel cell effluents to provide heat energy for fuel processing that enhances system efficiency. The system section addresses using fuel cell anode effluent (residual fuel), and rejected heat from the fuel cell and other components.

**Figure 9-2  
Representative Fuel Processor Major Components<sup>a</sup> & Temperatures**



- a) - For MCFC & SOFC, no high temperature shift, low temperature shift, nor CO removal required.
  - For PAFC, no CO removal required.
  - For PEFC, all components required.
- b) Possible to use residual air, water, and heat of fuel effluent from fuel cell and other downstream components.
- c) Vaporizer required for liquid fuels.
- d) Non-catalytic POX does not require water.
- e) Temperature dependent on fuel and type of reactor.

Fuel conversion and alteration catalysts are normally susceptible to poisoning; thus the raw fuel cleaning process takes place upstream or within the fuel conversion process. The fuel conversion and reformat gas alteration processes can take place either external to the fuel cell or within the fuel cell anode compartment. The former is referred to as an external reforming fuel cell system and the latter is referred to as an internal reforming fuel cell system. Cells are being developed to directly react commercially available gas and liquid fuels but the chemically preferred reaction of present fuel cells is via a hydrogen-rich gas. This section will address external reforming fuel processors only. Capabilities of internal reforming are contained within the specific fuel cell sections. The system calculation section provides examples of heat and material balances for both externally and internally reforming approaches.

Fuel processors are being developed to allow a wide range of commercial fuels suitable for stationary, vehicle, and military applications to be used in a fuel cell system. Technology from large chemical installations has been successfully transferred to small compact fuel cell units to convert pipeline natural gas, the fuel of choice for small stationary power generators. Cost is an issue as it is with the entire fuel cell unit for widespread application. Several hundred multi-kWe commercial fuel cell units are operating, see Section 1.6. Scaling of the fuel processing technology to larger power plants using pipeline gas will lower the specific cost of the fuel processor.

Recent fuel processor research and development has become focused on consumer vehicles and military applications. The issue with consumer vehicles is how to match a plausible commercial fuel infrastructure with the requirements of the fuel cell unit to be competitive. What fuel to use

is open to question at this time. Infrastructure economics drive the fuel of choice toward a gasoline type fuel. Environmental concerns drive the fuel of choice toward pure hydrogen. Methanol fuel processors (regarded by some as a step towards the eventual fuel) are easier to develop, hence further along in development than processors capable of converting gasoline that has high sulfur content and requires high conversion temperatures. Processors for both methanol and gasoline have been tested up to the 50 kWe level for vehicle application.

The US military has a significant fuel supply infrastructure in place. The two predominant fuel types in this infrastructure are diesel and jet fuel, a kerosene. It is highly improbable that the US military would change these fuels to accommodate fuel cells. Use of a fuel more suitable to the fuel cell would limit the technology's military use (there is R&D activity for fuel cell power packs to provide man-portable soldier power using hydrogen cartridges or other forms as well as methanol). Diesel and jet fuel are two of the most difficult conventional fuels to convert to a hydrogen-rich gas. They contain a large amount of sulfur, a catalyst poison, that requires high conversion temperature. Fuel processors that convert diesel and jet fuel to a hydrogen-rich gas are in the early stages of development. The technology has been demonstrated at a 500 W size; 50 kWe units are being developed.

This fuel processing section addresses the above issues in more detail and provides a technical description of fuel processing technology.

### ***Fuel Processing Issues***

Major issues that influence the development of a fuel processor are a) choice of commercially available fuels suitable for specific applications, b) fuel flexibility, c) fuel cell gas reformate requirements, and d) fuel cell unit size. Vaporization of heavier hydrocarbons is another issue. Heavy hydrocarbons, such as diesel, require vaporization temperatures much in excess of 350-400°C where components of these heavier fuels begin to pyrolyze and decompose.

### ***Fuel Choice and Flexibility Issues***

The fuel cell is a power generation technology that is in the early stages of its commercial use. As a result, it is paramount to target applications that have the potential for widespread use (to attract adequate development money) with the simplest technology development (to minimize development cost). There is a strong relation between applications and the infrastructure of available fuels.

Several high-value niche markets drove early fuel cell technology development. These were the use of fuel cells for on-board electric power in space vehicles and to demonstrate that fuel cells are an efficient, environmentally-friendly technology for stationary on-site commercial power.

The selected technology for on-board electric power on mid-length space vehicle missions (several days to a year), including the important man-moon mission, was the fuel cell. This is because the use of batteries for more than a couple of days proved too heavy, combustion engines and gas turbines required too heavy a fuel supply because of relatively low efficiency, and the use of a nuclear reactor was only suitable for missions of a year or more. There was a



simple choice of fuel with space fuel cells. It was hydrogen because it doesn't require a fuel processor other than storage and pressurization, is relatively lightweight when stored under pressure, and was the best fuel for the early-developed alkaline fuel cell. Fuel flexibility was not an issue.

It was logical to exploit fuel cell space development by trying to adapt it to terrestrial use. The initial terrestrial application was to increase power generation efficiency (in reaction to the oil shocks of the early 1970s) and to improve the environment by lowering fossil-fueled power generator exhaust emission. Coal was the fuel of choice at the time, but fuel cell development reasoning was that fuel cells had to be developed through a path of easier pipeline gas use prior to operating on coal-derived gas. One of the major fuel cell funders at the time was the gas industry.

Pipeline gas consists primarily of methane that is relatively easy to clean. The technology to convert methane to a H<sub>2</sub>-rich gas existed for large chemical plants. Developers had only to adapt this existing technology to small fuel cell units, not easy due to several magnitudes of scale-down. Owners of stationary power plants usually desire fuel flexibility. Fortunately, the fuel processor on these early plants could convert a light distillate, such as naphtha, with minor changes (e.g., add a vaporizer, change-out the fuel nozzles).

Once these niche markets were exploited to start fuel cells on their development path, it became apparent that, as stated above, it was necessary to target widespread potential applications while keeping technology development as simple as possible. General application areas of present interest to the fuel cell community are multi-kWe residential, commercial, and light industrial stationary power, transportation prime and auxiliary power, and military uses.

In summary, these are the applications and coupled fuel choices of interest to fuel cell technology to date:

- H<sub>2</sub> is preferable for a closed environment such as space vehicle application. There are sources of H<sub>2</sub>-rich gases, such as an off-gas at a chemical plant, that require only fuel cleaning. Fuel flexibility is not applicable in either case.
- The fuel choice for small stationary power plants is pipeline gas due to its availability for multiple commercial, light-industrial, and residential applications. Some users request that the fuel processor convert at least one additional fuel, i.e., a light distillate.
- For light vehicles, a key commercial target due to number of potential units, the fuel choice is open to question. There is a strong argument for liquid fuels due to vehicle on-board volume restrictions and infrastructure. Candidate liquid fuels for light vehicles could be available gasoline or a new gasoline, if driven by the infrastructure. Methanol may have an edge if it proves too difficult to process gasoline provided using it compares favorably on a cost and environmental basis with the present internal combustion engine (ICE) and gasoline system. Fuel flexibility in processors being developed should be considered because of the indecision on fuel type and because the public is accustomed to a selection of different octane liquid fuels and diesel.
- The present infrastructure fuel for heavy vehicles is high sulfur diesel (~300 ppm sulfur by weight) but this may change to a nearly sulfur-free diesel as proposed by the EPA (15 ppm

sulfur by weight). The fuel for this sector could also be a gasoline if such a fuel cell system can compete.

- On-board vehicle auxiliary power is increasing dramatically to satisfy consumer convenience. Fuel selection for these applications parallel light and heavy vehicle fuels, above.
- The military will continue with its fuel infrastructure of high sulfur diesel (up to 1,000 ppm sulfur by weight) and jet fuel (JP-8). Sulfur specification will remain high because the military has to consider worldwide fuel sources. High sulfur diesel and JP-8 are close in characteristics so no fuel flexibility is required. However, there is a possibility that some parts of the military or the Coast Guard (a military service within the DOT) could use fuels more compatible to the fuel cell in limited applications.
- As environmental regulation becomes more stringent for megawatt size power stations and fuel cells are scaled larger in size, there is the possibility to use the US's most plentiful, indigenous fuel, coal. The term, coal, covers a broad spectrum of solid fuels that complicate fuel processing, particularly cleanup. Fuel cells will find it difficult to compete economically with the high power density and relatively low cost gas turbine power generators in this application area. Large power station operators require an alternate fuel, usually heavy oil.
- There is the possibility of using other available fuels such as light distillates, ethanol, anaerobic digester gas, biomass, and refuse-derived fuel. However, these fuels apply to niche market applications. Fuel cell application here, if practical, will evolve from and after widespread uses. Users may require an alternate fuel, probably natural gas.

As stated earlier, fuel processing technology from large chemical installations has been successfully transferred to small compact fuel cell units to convert pipeline natural gas, the fuel of choice for small stationary power generators. The technology for converting natural gas is described later in this section.

The fuel decision that has the greatest impact on fuel processor development at this time is in the light vehicle application sector, due to the potential large number of units. Many fuel processor developers are presently focusing on the development of methanol fuel processing either as the fuel of choice or as a development step toward processing gasoline. Others consider that it is best to develop a vehicle system that uses the most environmentally attractive fuel, hydrogen. There are numerous opinions such as storage and distribution of H<sub>2</sub> on vehicles is difficult and costly, and the space required for onboard storage (while available on buses) is prohibitive for small cars. It is best to convert liquid fuels. There is no payoff by going to other methods such as liquid H<sub>2</sub>, compressed H<sub>2</sub>, or metal hydride (1).

Methanol is unquestionably the easiest of the potential fuels to convert to hydrogen for vehicle use. Methanol disassociates to carbon monoxide and hydrogen at temperatures below 400°C and can be catalytically steam reformed at 250°C or less. This provides a quick start advantage. Methanol can be converted to hydrogen with efficiencies of >90 %. But methanol is produced primarily from natural gas requiring energy and it is less attractive than gasoline on a well-to-wheels efficiency (2).

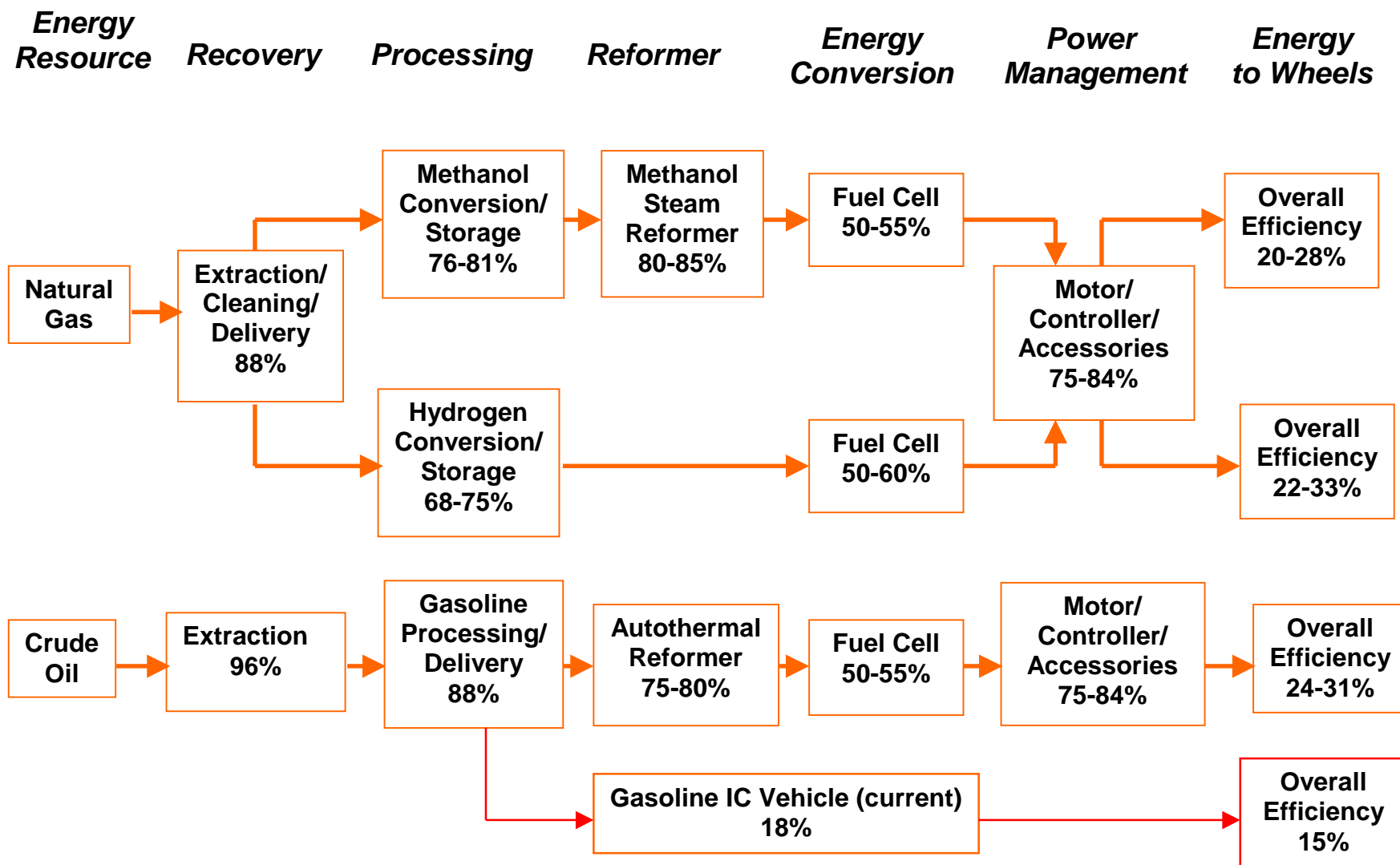
Gasoline has many advantages over methanol, but conversion to H<sub>2</sub> requires temperatures in excess of 650°C and produces greater amounts of CO, methane (CH<sub>4</sub>), and possibly coke.

Without catalyst, the conversion temperature is 1,000°C or higher. High temperatures require special materials of construction and significant preheating. Petroleum-derived fuels contain more sulfur and trace amounts of metal that could be harmful to the fuel cell. Natural gas is not good for transportation because of its low relative energy density and 700°C or higher processing temperature (3).

ExxonMobil has presented a position paper (4) for liquid fuels that addresses the pros and cons of methanol versus gasoline. Paraphrased excerpts from this are:

- Fuels that are most directly suited to the fuel cell are the most difficult and costly to produce and distribute. Gasoline and methanol are the leading candidates to power fuel cell engines. Both the gasoline and methanol fuel cell vehicles should be more fully developed prior to making a commercial decision on fuel choice.
- Due to methanol's corrosivity and its affinity for water, it cannot be readily distributed in today's fuel infrastructure. Methanol burns with a nearly invisible flame. Available luminosity additives won't reform in the low-temperature methanol steam reformers. Methanol is more acutely toxic than gasoline. Additives that are likely to be needed for safety and health reasons will impact the fuel processor's performance and cost.
- Gasoline fuel processing has the ability to utilize the existing infrastructure, a major advantage. It is inherently more flexible than the low temperature methanol processor, allowing multiple fuel use in the same system. The gasoline processor is also more tolerant of contaminants or additives contained in the fuel. Due to the higher energy density of gasoline, the gasoline system offers the potential for up to twice the vehicle range of the methanol system (editor's note - if similar conversion efficiencies are attained).
- Today's mid-sized passenger cars are about 15 to 18 % "well-to-wheels" energy efficient as indicated in Figure 9-3. Despite the increased vehicle efficiency of a methanol

Figure 9-3 “WELL-TO-WHEEL” EFFICIENCY FOR VARIOUS VEHICLE SCENARIOS



fuel cell system, the resultant "well-to-wheel" efficiency would be only 23 %, substantially lower than either gasoline hybrids or gasoline fuel cell vehicles.<sup>45</sup>

- A customized gasoline for fuel cells could offer better performance and be produced at lower cost because many of today's conventional gasoline's more expensive ingredients would not be required. Naphtha is a common refinery stream that is an inexpensive alternative to conventional gasoline. Although its octane is too low for today's ICE, naphtha is ideal for fuel cells and could be supplied to retail stations within the existing gasoline infrastructure.

### ***Fuel Cell Issues***

There are three major gas reformat requirements imposed by the various fuel cells that need addressing. These are sulfur tolerance, carbon monoxide tolerance, and carbon deposition. The activity of catalysts for steam reforming and autothermal reforming can also be affected by sulfur poisoning and coke formation. These requirements are applicable to most fuels used in fuel cell power units of present interest. There are other fuel constituents that can prove detrimental to various fuel cells. However, these appear in specific fuels and are considered beyond the scope of this general review. Examples of these are halides, hydrogen chloride, and ammonia. Finally, fuel cell power unit size is a characteristic that impacts fuel processor selection.

There are discrepancies in the amounts of harmful species tolerance that fuel cell developers establish, even for similar type fuel cells. These discrepancies are probably due to electrode design, microstructure differences, or in the way developers establish tolerance. There are some cases where the presence of certain harmful species causes immediate performance deterioration. More often, the degradation occurs over a long period of time, dependant on the developer's allowable voltage degradation rate on exposure to the specific harmful species. Here, the developer establishes an estimated cell life based on economics. The permissible amount of the harmful constituent is then determined based on its life effects.

### **Sulfur Requirements**

Present formula gasolines contain approximately 300 ppm. No. 2 fuel oil contains 2,200 to 2,600 ppm by weight of sulfur. Even pipeline gas contains sulfur-containing odorants (mercaptans, disulfides, or commercial odorants) for leak detection. Metal catalysts in the fuel reformer can be susceptible to sulfur poisoning and it is very important that sulfur in the fuel reformat be removed. Some researchers have advised limiting the sulfur content of the fuel in a stream reformer to less than 0.1 ppm, but noted the limit may be higher in an autothermal

---

<sup>45</sup>. Editor's note - The gasoline-fueled ICE well-to-wheel efficiency values apply to today's technology and are averaged over the entire driving cycle. Advanced IC engine/vehicles are more efficient over the entire operating cycle than 18 % (up to 20 some odd %). This implies that future IC engine/vehicle efficiency for light vehicles can be in excess of the 15 to 18 % quoted in the ExxonMobil paper. Vehicle miles per gallon increase when the ICE is combined with a battery in developmental vehicles with very low drag coefficients, for example the 60+ mpg for the Honda Insight, 40 to 50+ mpg for the Toyota Prius, 70+ mpg for the Ford Prodigy, and ~80 mpg for the GM Precept. The overall well-to-wheel efficiency over a standard city/highway driving cycle for a four passenger, production hybrid vehicle has been estimated to be about 25-30 %, close to a fuel cell vehicle. The fuel cells engines for lightweight vehicles are likely to be hybrids, and therefore the projected efficiencies have to be carefully considered.

reformer (5), see Argonne National Laboratory, under State-of-the-Art Components later in this section.

Sulfur poisons catalytic sites in the fuel cell also. The effect is aggravated when there are nickel or iron-containing components including catalysts that are sensitive to sulfur and noble metal catalysts, such as found in low temperature cell electrodes. Sulfur tolerances are described in the specific fuel cell sections of this handbook.<sup>46</sup> In summary, the sulfur tolerances of the cells of interest, by percent volume in the cleaned and altered fuel reformat gas to the fuel cells from published data, are:

PEFC - <1 ppm sulfur as H<sub>2</sub>S, poisoning is cumulative and not reversible

PAFC - <50 ppm sulfur as H<sub>2</sub>S + COS or <20 ppm sulfur as H<sub>2</sub>S at the anode. Poisoned anodes can be re-activated by polarization at high potentials.

MCFC - <0.5 ppm sulfur as H<sub>2</sub>S (at the cathode) equates to <10 ppm at the anode because of fuel exhaust being sent to the cathode in an MCFC system (same amount of sulfur, more gas at the cathode), poisoning is reversible.

SOFC - <1 ppm sulfur as H<sub>2</sub>S, poisoning is reversible for the tubular SOFC. H<sub>2</sub>S levels of 1 ppm result in an immediate performance drop, but this loss soon stabilizes into a normal linear degradation. Tests show that high temperature planar SOFCs with all-ceramic components can tolerate up to 3,000 ppm of sulfur. Sulfur, in H<sub>2</sub>S form, has been used as a fuel for an external reforming, all-ceramic SOFC operating at 1,000°C (6). However, developers want to bring the cell temperature down to allow less expensive metal components, primarily interconnects, and improve cycle efficiency. There is a requirement to lower sulfur significantly if metal parts are used in an SOFC. For planar SOFCs, claims for sulfur tolerance varies among the developers. The range of sulfur has been published as 10 to 35 ppm. Planar SOFC sulfur tolerance probably will be secondary to the fuel processor catalyst that, as mentioned, may be as low as 0.1 ppm.

### **Carbon Monoxide Requirements**

Carbon monoxide, a fuel in high temperature cells (MCFC and SOFC), is preferentially absorbed on noble metal catalysts that are used in low temperature cells (PAFC and PEFC) in proportion to the hydrogen to CO partial pressure ratio. A particular level of carbon monoxide yields a stable performance loss. The coverage percentage is a function of temperature and that is the sole difference between PEFC and PAFC (7). Cell limits are:

PEFC – Consensus tolerant limit is <50 ppm into the anode.

PAFC – Major US manufacturer set tolerant limit as <1.0 % into the anode.

MCFC - CO and H<sub>2</sub>O shift to H<sub>2</sub> and CO<sub>2</sub> in the cell as the H<sub>2</sub> is consumed by the cell reaction due to a favorable temperature level and catalyst.

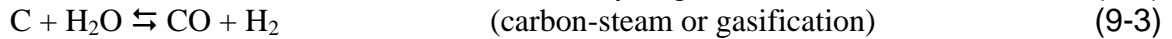
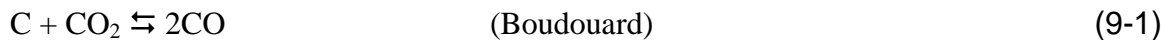
---

<sup>46</sup>. There is an ambiguity in the way sulfur is reported in the literature that has caused confusion in the amount that can be tolerated. Reports often fail to distinguish whether the sulfur is measured by weight, as it would be before vaporization of a liquid fuel, or by volume, as it would be in a gas fuel or fuel gas reformat. An approximate rule of thumb is that the amount (by volume) of sulfur in a vaporized fuel is one-tenth the amount of sulfur measured by weight in the liquid fuel. 300 ppm sulfur (by weight) in the liquid fuel equates to 30 ppm sulfur (by volume) when the fuel is converted to a gaseous reformat.

SOFC - CO can be a fuel. However, if the fuel gas contains H<sub>2</sub>O, the shift reaction (CO + H<sub>2</sub>O → H<sub>2</sub> + CO<sub>2</sub>) is chemically favored with present designs and operating conditions.

### Carbon Deposition Requirements

The processing of hydrocarbons always has the potential to form coke (soot). If the fuel processor is not properly designed or operated, coking is likely to occur (3). Carbon deposition not only represents a loss of carbon for the reaction but more importantly also results in deactivation of catalysts in the processor and the fuel cell, due to deposition at the active sites. Thermodynamic equilibrium calculations provide a first approximation of the potential for coke formation. The governing equations are:



Indications at what conditions carbon may be formed for various fuels are determined by the simultaneous solution of the above equations using their equilibrium coefficients.<sup>47</sup> No solid graphitic carbon exists at low temperatures (~600°C) in binary mixtures containing at least 2 atoms of oxygen or 4 atoms of hydrogen per atom of carbon (9).

### Fuel Cell Unit Size Requirements

There is a lower level of power output where it is no longer advantageous to incorporate a fuel processor in a fuel cell unit. The decision is also application specific. It is likely that releasing H<sub>2</sub> by chemical reaction from a solid compound when mixed with water is economical for small portable units (below 100 W). An H<sub>2</sub> storage cartridge can be replaced in seconds (10). Actual power levels where the tradeoff is likely to occur change as processing and storage technology advances. One fuel processor developer has produced a 100 W size POX methane reactor that takes up the space of a coffee can. The unit includes a reforming zone, shift reactors, and all heat exchangers. H<sub>2</sub> is 36% (assume dry) and the CO level can be reduced to 1%. The unit ran on methane, propane, and ethanol (11). Another research project is investigating methanol reformers for sub-watt fuel cell power sources for the Army.

---

<sup>47</sup>. Carbon is slightly less likely to be deposited than equilibrium coefficient calculations indicate, due to kinetics.

## ***Fuel Processing Technology Descriptions***

### **Fuel Conversion Description**

The generic term generally applied to the process of converting liquid or gaseous light hydrocarbon fuels to hydrogen and carbon monoxide is “reforming”. There are a number of methods to reform fuel. The three most commercially developed and popular methods are 1) steam reforming, 2) partial-oxidation reforming, and, 3) autothermal reforming. Each of these methods can be used to produce a fuel suitable for the fuel cell.

Steam reforming (SR) provides the highest concentration of hydrogen and can obtain a high fuel processing conversion efficiency. Partial oxidation (POX) is a fast process, good for starting, fast response, and a small reactor size. Non-catalytic POX operates at temperatures of approximately 1,400°C, but adding a catalyst (catalytic POX or CPOX) can reduce this temperature as low as 870°C. Combining steam reforming closely with CPOX is termed autothermal reforming (ATR).

### **Steam Reforming Description**

Historically, steam reforming has been the most popular method of converting light hydrocarbons to hydrogen. In the steam reforming process, the fuel is heated and vaporized, then injected with superheated steam into the reaction vessel. The steam-to-carbon molar ratio used is usually in the neighborhood of 2.5:1 but developers strive for lower ratios to improve cycle efficiency. Excess steam is used to help force the reaction to completion as well as to inhibit soot formation. Like most light hydrocarbons, heavier fuels can be reformed through high temperature reaction with steam. Steam reforming is usually carried out using nickel-based catalysts. Cobalt and noble metals are also active but more expensive. The catalytic activity depends on metal surface area. For nickel, the crystals will sinter quickly above the so-called Tamman temperature (590°C) approaching a maximum size related to the pore diameter of the support. The crystal growth results in loss of surface area and activity (12). The steam reformer can operate with (always in conjunction with fuel cells) or without a catalyst. Most commercial applications of steam reforming use a catalyst to enhance reaction rates at decreased temperatures. Lower temperatures favor high CO and hydrogen equilibrium. The reforming catalyst also promotes the competitive water-gas shift reaction. Steam reforming is endothermic thus favored by high temperatures. But it is a slow process and requires a large reactor (1). As a result, rapid start and transients cannot be achieved by steam reforming due to it inherently slower indirect heating (13). The steam reforming process suits pipeline gas and light distillate stationary fuel cell power generation well.

An intrinsic, exothermic water-gas shift reaction occurs in the steam reformer reactor. The combined reaction, steam reforming and water gas shift, is endothermic. As such, an indirect high temperature heat source is needed to operate the reactor. This heat source usually takes the shape of an immediately adjacent high temperature furnace that combusts a small portion of the raw fuel or the fuel effluent from the fuel cell. Efficiency improves by using rejected heat from other parts of the system. Note that the intrinsic water-gas shift in the reactor may not lower the



CO content to the fuel cell requirement and additional shifting and alteration will be needed for lower temperature fuel cells.

Steam reforming of higher hydrocarbons can also be used to produce methane suitable for use in high temperature internal reforming fuel cells. Steam pre-reforming of hydrocarbons, as a process step in the manufacture of hydrogen, ammonia, methanol, carbon monoxide and syngas, is an established technology. All higher hydrocarbons are converted over a nickel-based catalyst into a gas mixture containing hydrogen, methane and carbon oxides. Establishment of equilibria of the methanation and shift reactions at the process conditions determines the composition of the pre-reformed gas. By proper design of appropriate fuel processing systems, a wide variety of fuels may be converted to a reformat with higher methane. This reformat can then be used to promote internal reforming for high temperature fuel cell systems. For each type of fuel, optimum operating parameters viz. temperature, steam/carbon ratio, and the most suitable catalyst needs to be established (14).

### **Partial Oxidation Description**

As the name implies, partial oxidation, or POX, is the partial, or incomplete, combustion of a fuel. A substoichiometric amount of air, or oxygen, is used. This partial oxidation process is highly exothermic and raises the reactants to a high temperature.

The resulting high temperature reaction products, still in a reduced state, are then quenched through the introduction of superheated steam. The addition of the steam promotes the combined water-gas shift and steam reforming reactions, which further cools the gas. In most cases, and if sufficient pre-heating of the reactants is used, the overall reaction is exothermic and self-sustaining. For some applications however, particularly small-scale configurations, a catalyst can be used to increase reaction rates at lowered reaction temperatures. Again, additional, separate water-gas shift and alteration may be necessary to satisfy the fuel cell requirements.

POX reactor exit temperatures vary widely. Noncatalytic processes for gasoline reforming require temperatures in excess of 1,000°C. These temperatures require the use of special materials and significant preheating and integration of process streams. The use of a catalyst can substantially reduce the operating temperature allowing the use of more common materials such as steel. Lower temperature conversion leads to less carbon monoxide (an important consideration for low temperature fuel cells), so that the shift reactor can be smaller. Lower temperature conversion will also increase system efficiency.

For some heavy hydrocarbon fuels, typical values range from as low as 870°C for catalytic POX upwards to 1,400°C for non-catalytic POX. For sulfur-bearing diesel fuel, a catalytic POX reactor will usually operate at approximately 925°C. This relatively elevated temperature is needed to overcome catalyst degradation due to the presence of sulfur. Non-catalytic POX reactors operating at around 1,175°C on diesel fuel.

Advantages of POX that make this type fuel conversion suitable for transportation power are:

- POX does not need indirect heat transfer (across a wall) so the processor is more compact and lightweight (3).
- Contrary to widely-held opinion, POX and ATR are capable of higher reforming efficiencies than are steam reformers (15).

Partial oxidation should be reacted so that the overall reaction is exothermic, but at a low value of oxygen-to-fuel where the higher hydrogen yields and concentrations are favored.

It is a widely held opinion that POX leads to lower efficiency than steam reforming due to the POX reaction being exothermic. However, a thorough examination of the thermodynamics shows that POX and ATR have higher reforming efficiencies than steam reformers. This begs the question on why is there a need to use steam reforming or an ATR if the POX's efficiency is higher. The minimum oxygen to carbon (O/C) ratio allowable is 1 for the POX process. This generates high heat that leads to undesirable high temperatures (low H<sub>2</sub>, CO<sub>2</sub> selectivity, materials of construction constraints, etc). The steam reformer and ATR allow lower O/C ratios, keep the temperature down, and result in higher CO<sub>2</sub> and H<sub>2</sub> selectivity (more H<sub>2</sub> yield per mole of fuel). Developers chose among the processes depending on application.

### **Autothermal Reforming Description**

The coupling of SR with POX is termed autothermal reforming (ATR). The exact definition varies. Some define ATR as an SR reaction and a POX reaction that take place over microscopic distances at the same catalytic site thus avoiding complex heat exchanging (16). Others have the less restrictive definition that ATR occurs when there is no wall between a combined SR reaction and catalytic POX reaction. ATR is carried out in the presence of a catalyst that controls the reaction pathways and thereby determines the relative extents of the POX and SR reactions. The SR reaction absorbs part of the heat generated by the POX process reaction, limiting the maximum temperature in the reactor. The net result is a slightly exothermic process.

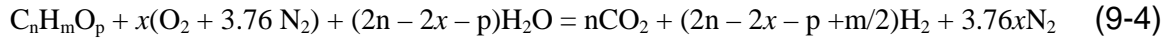
Autothermal reforming provides a fuel processor compromise that operates at a lower O/C and lower temperature than the POX; is smaller, quicker starting, and quicker responding than the SR; and results in good H<sub>2</sub> concentration and high efficiency. A catalytic POX must be used to reduce the reaction temperature to a value compatible with the SR temperature. Once started, surplus heat from other parts of the unit can be sent to the ATR to increase its efficiency.

### **Other Reforming Combinations**

There have been fuel processor configurations where a non-catalytic POX is placed in series with a steam reformer. Without catalyst, the POX reaction has to be at a higher temperature than the steam reformer reaction. These reactions have to take place in separate compartments with heat exchange and a wall between them (13). This configuration is not considered within the definition of autothermal reforming.

## Generic Fuel Conversion

Considering a spectrum of fuel conversion from steam reforming to partial oxidation should convey a basic understanding of the reforming processes. An elegant general equation published by the Argonne National Laboratory (ANL) describes fuel conversion throughout the spectrum. Autothermal reforming falls within this spectrum so that the equation encompasses processes of interest to fuel cells. The equation does not apply to complete combustion, but that conversion process is not relevant to fuel cells (15,17). The general equation is:



where  $x$  is the molar ratio of oxygen-to-fuel. This ratio is very important because it determines:

- the minimum amount of water that is required to completely convert the carbon in the fuel to carbon dioxide ( $2n - 2x - p$ ). Excess water is used in practice to insure the conversion, resulting in water in the reformat (right side of the equation). Typically, one or two moles of water for every mole of oxygen are used.
- the hydrogen yield ( $2n - 2x - p + m/2$ )
- the concentration of hydrogen in the reformat  $\{[2n - 2x - p + m/2]/[n + (2n - 2x - p + m/2) + 3.76x]$  all times 100}
- the heat of reaction  $\{\Delta H_r = n(\Delta H_{f,CO_2}) - (2n - 2x - p)\Delta H_{f,H_2O} - \Delta H_{f,fuel}\}$ .

Decreasing the oxygen-to-fuel ratio,  $x$ , results in increasing demand for water (water-to-fuel ratio), with commensurate increases in the yield and concentration of hydrogen in the reformat gas. When  $x = 0$ , the equation reduces to the strongly endothermic steam reforming reaction. The reaction becomes less endothermic with increasing oxygen. It becomes thermoneutral<sup>48</sup> at  $x = x_0$  (0.44 for natural gas). Above this point, the reaction becomes increasingly exothermic. At  $x = 1$ , the pure POX reaction, the feed contains sufficient oxygen to convert all of the carbon in the fuel to  $CO_2$ . No water needs to be added. The equation is a mix of the steam reforming reaction and the POX reaction at values of  $x$  between 0 and 1.

The general equation, above, is no longer accurate above an  $x$  of 1. Beyond  $x = [n - (p/2)] = 1$  (when  $p = 0$ ), where water is a product, the heat of reaction is determined by the phase of the product water. At still higher values, the excess oxygen oxidizes the hydrogen to produce water. Finally, at stoichiometric combustion, all carbon and hydrogen are converted to carbon dioxide and water.

Equation 9-4 depicts a total reaction where the fuel input is converted to carbon dioxide. Actually, the initial reforming step is carried out at elevated temperatures, where a mixture of carbon monoxide and carbon dioxide is formed. In the subsequent reformat conversion step, the carbon monoxide is converted via the water-gas shift to carbon dioxide: This step may not be needed for the high-temperature fuel cells.



<sup>48</sup>. The thermoneutral point (of oxygen-to-carbon ratio) is where the enthalpy of the reaction is zero, ( $\Delta H_{f,298} = 0$ ).

There may be additional, downstream inputs of water/steam and oxygen/air, for water-gas shift and selective oxidation to further reduce CO, if needed.

When the function of a fuel processor is to convert a fuel to hydrogen, the fuel conversion efficiency is

$$\text{Efficiency} = \frac{\text{Lower Heating Value of Anode Fuel(s) Produced}}{\text{Lower Heating Value of Fuel Used}} \quad (9-6)$$

The fuel conversion efficiency for methane conversion to hydrogen is 93.9% at the thermoneutral point,  $x = 0.44$  (an ATR reaction) and 91.7% at  $x = 0$  (the SR reaction). The difference is probably due to the heat of condensation of the H<sub>2</sub>O in the SR burner exhaust. The concentration of hydrogen is 53.9% at  $x = 0.44$  and 80% at  $x = 0$ .

Equation 9-4 and related heats of reaction can be manipulated to show that the maximum efficiency is a state point function, regardless of path (steam reforming, partial oxidation, or autothermal reforming), and is achieved at the thermoneutral point. In practice,  $x$  is set slightly higher than the thermoneutral point so that additional heat is generated to offset heat losses from the reformer. Table 9-1 presents efficiencies at the thermoneutral point for various hydrocarbon fuels.

### *Specific Fuel Processing*

Because the components and design of a fuel processing subsystems depend on the raw fuel type, the discussion after Table 9-1 is organized by the fuel being processed.

**Table 9-1 Calculated Thermoneutral Oxygen-to-Fuel Molar Ratios ( $x_o$ ) and Maximum Theoretical Efficiencies (at  $x_o$ ) for Common Fuels**

$C_nH_mO_p$	n	m	p	$\Delta H_{f,\text{fuel}}$ (kcal/gmol)	m/2n	$X_o,$ $\Delta H_r = 0$	Efficiency (%)
<b>Methanol</b> <b>CH<sub>3</sub>OH(l)</b>	1	4	1	-57.1	2	0.230	96.3
<b>Methane</b> <b>CH<sub>4</sub></b>	1	4	0	-17.9	2	0.443	93.9
<b>Iso-Octane</b> <b>C<sub>8</sub>H<sub>18</sub>(l)</b>	8	18	0	-62.0	1.125	2.947	91.2
<b>Gasoline</b> <b>C<sub>7.3</sub>H<sub>14.8</sub>O<sub>0.1</sub>(l)</b>	7.3	14.8	0.1	-53.0	1.014	2.613	90.8

### **Hydrogen Processing**

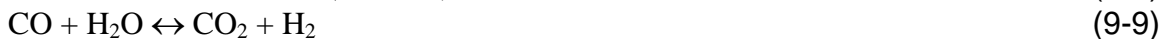
When hydrogen is supplied directly to the fuel cell, as may be the case in transportation systems, the fuel processing section is no more than a storage and delivery system. However, in most

practical applications, hydrogen needs to be generated from other fuels and processed to meet the various system requirements.

### Natural Gas Processing

The major constituents of pipeline gas are methane, ethane, propane, CO<sub>2</sub>, and, in some cases, N<sub>2</sub>. Sulfur containing odorants (mercaptans, disulfides, or commercial odorants) are added for leak detection. Because neither fuel cells nor commercial reformer catalysts are sulfur tolerant, the sulfur must be removed. This is usually accomplished with a zinc oxide sulfur polisher and the possible use of a hydrodesulfurizer, if required. The zinc oxide polisher is able to remove the mercaptans and disulfides. However, some commercial odorants, such as Pennwalt's Pennodorant 1013 or 1063, contain THT (tetrahydrothiophene), more commonly known as thiophane, and require the addition of a hydrodesulfurizer before the zinc oxide catalyst bed. The hydrodesulfurizer will, in the presence of hydrogen, convert the thiophane into H<sub>2</sub>S that is easily removed by the zinc oxide polisher. The required hydrogen is supplied by recycling a small amount of the reformed natural gas product. Although a zinc oxide reactor can operate over a wide range of temperatures, a minimum bed volume is achieved at temperatures of 350 to 400°C (660 to 750°F).

The CH<sub>4</sub> in the natural gas is usually converted to H<sub>2</sub> and CO in a SR reactor. Steam reforming reactors yield the highest percentage of hydrogen of any reformer type. The basic SR reactions for methane and a generic hydrocarbon are:



In addition to natural gas, steam reformers can be used on light hydrocarbons such as butane and propane and on naphtha with a special catalyst. Steam reforming reactions are highly endothermic and need a significant heat source. Often the residual fuel exiting the fuel cell is burned to supply this requirement. Fuels are typically reformed at temperatures of 760 to 980°C (1,400 to 1,800°F).

A typical steam reformed natural gas reformat is presented in Table 9-2.

**Table 9-2 Typical Steam Reformed Natural Gas Reformat**

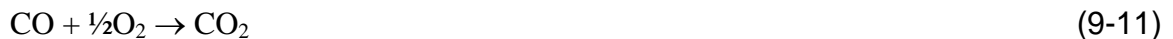
Mole Percent	Reformer Effluent	Shifted Reformat
H <sub>2</sub>	46.3	52.9
CO	7.1	0.5
CO <sub>2</sub>	6.4	13.1
CH <sub>4</sub>	2.4	2.4
N <sub>2</sub>	0.8	0.8
H <sub>2</sub> O	37.0	30.4
Total	100.0	100.0

A POX reformer also can be used for converting gaseous fuels, but does not produce as much hydrogen as the steam reformers. For example, a methane-fed POX reformer would produce only about 75% of the hydrogen (after shifting) that was produced by an SR. Therefore, partial oxidation reformers are typically used only on liquid fuels that are not well suited for steam reformers. Partial oxidation reformers rank second after steam reformers with respect to their hydrogen yield. For illustration, the overall POX reaction (exothermic) for methane is



When natural gas fuels a PAFC or a PEFC system, the reformat must be water-gas shifted because of the high CO levels in the reformat gas. A PAFC stack can tolerate about 1% CO into the cell before having an adverse effect on the cell performance due to catalyst absorption. The allowable CO level in the fuel gas for a PEFC is considerably lower. The shift conversion is often performed in two or more stages when CO levels are high. A first high-temperature stage allows high reaction rates, while a low-temperature converter allows for a higher conversion. Excess steam also is utilized to enhance the CO conversion. A single-stage shift reactor is capable of converting 80 to 95% of the CO (18). The water gas shift reaction is mildly exothermic, so multiple stage systems must have interstage heat exchangers. Feed temperatures of high- and low-temperature shift converters range from approximately 260 to 370°C (500 to 700°F) and 200 to 260°C (400 to 500°F), respectively. Hydrogen formation is enhanced by low temperatures, but is unaffected by pressure.

When used in a PEFC system, the reformat must pass through a preferential CO catalytic oxidizer, even after being shifted in a shift reactor. Typically, the PEFC can tolerate a CO level of only 50 ppm. Work is being performed to increase the CO tolerance level in PEFC. At least two competing reactions can occur in the preferential catalytic oxidizer:



The selectivity of these competing reactions depends upon the catalyst and determines the quantity of required oxygen (19).

### **Liquid Fuel Processing**

Liquid fuels such as distillate, naphtha, diesel oils, and heavy fuel oil can be reformed in partial oxidation reformers. All commercial POX reactors employ noncatalytic POX of the feed stream by oxygen in the presence of steam with reaction temperatures of approximately 1,300 to 1,500°C (2,370 to 2,730°F) (18). For illustration, the overall POX reaction for pentane is



The overall reaction is exothermic, and largely independent of pressure. The process is usually performed at 20 to 40 atmospheres to yield smaller equipment (18). A typical fuel composition for a fuel oil fed POX reformer is presented in Table 9-3. The CO contained in this reformat

may need to be converted with a shift converter or selective catalytic converter, as for the gaseous fuel case, depending upon the specific fuel cell being fed.

**Table 9-3 Typical Partial Oxidation Reformed Fuel Oil Reformate (18)**

Mole Percent (dry, basis)	Reformer Effluent
H <sub>2</sub>	48.0
CO	46.1
CO <sub>2</sub>	4.3
CH <sub>4</sub>	0.4
N <sub>2</sub>	0.3
H <sub>2</sub> S	0.9
Total	100.0

Alcohols are steam-reformed at lower temperatures (<600°C) while alkanes<sup>49</sup> and unsaturated hydrocarbons require slightly higher temperatures. Cyclic hydrocarbons and aromatics have also been reformed at relatively low temperatures, however a different mechanism appears to be responsible for their reforming. Blended fuels like gasoline and diesel, that are mixtures of a broad range of hydrocarbons, require temperatures of >700°C for complete H<sub>2</sub> production (leads to maximum hydrogen production). Methanol, one of the prime fuels being considered for transportation application, can be converted into hydrogen by steam reforming:



The equivalent overall result of these two specific reactions is:



The optimum choice of operating conditions are around a steam to methanol ratio of 1.5 and a temperature range of 250°C to 399°C. Pressure does not influence the reaction rate, but very high pressures limit the equilibrium conversion, which otherwise is better than 99% at the preferred range of 5 to 15 bars. The CU/Zn/Al and Cu/Zn/Cr based catalysts have been used in large units in industry for many years (12).

## Coal Processing

The numerous coal gasification systems available today can be reasonably classified as one of three basic types: a) moving-bed, b) fluidized-bed, and c) entrained-bed. All three of these types utilize steam, and either air or oxygen to partially oxidize coal into a gas product. The moving-bed gasifiers produce a low temperature (425 to 650°C; 800 to 1,200°F) gas containing

<sup>49</sup>. Alkanes are saturated hydrocarbons, i.e., no double carbon bonds. Examples are CH<sub>4</sub>, C<sub>2</sub>H<sub>6</sub>, C<sub>3</sub>H<sub>8</sub>, and C(n)H(2n+2). Alkenes have carbon-carbon double bonds such as ethene C<sub>2</sub>H<sub>4</sub> and C(n)H(2n).

devolatilization products such as methane and ethane, and a hydrocarbon liquid stream containing naphtha, tars, oils, and phenolics. Entrained-bed gasifiers produce a gas product at high temperature ( $>1,260^{\circ}\text{C}$ ;  $>2,300^{\circ}\text{F}$ ), which essentially eliminates the devolatilization products from the gas stream and the generation of liquid hydrocarbons. In fact, the entrained-bed gas product is composed almost entirely of hydrogen, carbon monoxide and carbon dioxide. The fluidized-bed gasifier product gas falls between these two other reactor types in composition and temperature ( $925$  to  $1,040^{\circ}\text{C}$ ;  $1,700$  to  $1,900^{\circ}\text{F}$ ).

The heat required for gasification is essentially supplied by the partial oxidation of the coal. Overall, the gasification reactions are exothermic, so waste heat boilers often are used at the gasifier effluent. The temperature, and therefore composition, of the product gas is dependent upon the amount of oxidant and steam, as well as the design of the reactor that each gasification process utilizes.

Gasifiers typically produce contaminants that need to be removed before entering the fuel cell anode. These contaminants include  $\text{H}_2\text{S}$ ,  $\text{COS}$ ,  $\text{NH}_3$ ,  $\text{HCN}$ , particulate, and tars, oils and phenols. (See Table 6-3 for the MCFC contaminant list). The contaminant levels are dependent upon both the fuel composition and the gasifier employed. There are two families of cleanup that can be utilized to remove the sulfur impurities: hot and cold gas cleanup systems. The cold gas cleanup technology is commercial, has been proven over many years, and provides the system designer with several choices. The hot gas cleanup technology is still developmental and would likely need to be joined with low temperature cleanup systems to remove the non-sulfur impurities in a fuel cell system. For example, tars, oils, phenols, and ammonia could all be removed in a low temperature water quench followed by gas reheat.

A typical cold gas cleanup process on an entrained bed gasifier would include the following subprocesses: heat exchange (steam generation and regenerative heat exchange), particulate removal (cyclones and particulate scrubbers),  $\text{COS}$  hydrolysis reactor, ammonia scrubber, acid gas ( $\text{H}_2\text{S}$ ) scrubbers (Sulfinol, SELEXOL), sulfur recovery (Claus and SCOT processes), and sulfur polishers (zinc oxide beds). All of these cleanup systems increase system complexity and cost, while decreasing efficiency and reliability. In addition, many of these systems have specific temperature requirements that necessitate the addition of several heat exchangers or direct contact coolers.

For example, a  $\text{COS}$  hydrolysis reactor needs to operate at about  $180^{\circ}\text{C}$  ( $350^{\circ}\text{F}$ ), the ammonia and acid scrubbers need to be in the vicinity of  $40^{\circ}\text{C}$  ( $100^{\circ}\text{F}$ ), while the zinc oxide polishers need to be about  $370^{\circ}\text{C}$  ( $700^{\circ}\text{F}$ ). Thus, gasification systems with cold gas cleanup often become a maze of heat exchange and cleanup systems.

Typical compositions for several oxygen-blown coal gasification products are shown in Table 9-4.

***Other Solid Fuel Processing:*** Solid fuel other than coal also can be utilized in fuel cell systems. For example, biomass and RDF (refuse-derived-fuels) can be integrated into a fuel cell system as long as the gas product is processed to meet the requirements of the fuel cell. The resulting systems would be very similar to the coal gas system with appropriate gasifying and cleanup



systems. However, because biomass gas products can be very low in sulfur, the acid cleanup systems may simply consist of large sulfur polishers.

**Table 9-4 Typical Coal Gas Compositions for Selected Oxygen-Blown Gasifiers**

Gasifier Type Manufacturer	Moving-Bed	Fluidized-Bed	Entrained-Bed			
	Lurgi (20)	Winkler	Destec	Koppers-Totzek	Texaco	Shell
Coal	Illinois No. 6	Texas Lignite	Appalachian Bit.	Illinois No. 6	Illinois No. 6	Illinois No. 6
Mole Percent						
Ar	trace	0.7	0.8	0.9	0.9	1.1
CH <sub>4</sub>	3.3	4.6	0.6	-	0.1	-
C <sub>2</sub> H <sub>4</sub>	0.1	-	-	-	-	-
C <sub>2</sub> H <sub>6</sub>	0.2	-	-	-	-	-
CO	5.8	33.1	45.2	43.8	39.6	63.1
CO <sub>2</sub>	11.8	15.5	8.0	4.6	10.8	1.5
COS	trace	-	-	0.1	-	0.1
H <sub>2</sub>	16.1	28.3	33.9	21.1	30.3	26.7
H <sub>2</sub> O	61.8	16.8	9.8	27.5	16.5	2.0
H <sub>2</sub> S	0.5	0.2	0.9	1.1	1.0	1.3
N <sub>2</sub>	0.1	0.6	0.6	0.9	0.7	4.1
NH <sub>3</sub> + HCN	<u>0.3</u>	<u>0.1</u>	<u>0.2</u>	=	=	=
Total	100.0	100.0	100.0	100.0	100.0	100.0

Reference Sources: (20,21)

Note: All gasifier effluents are based on Illinois No. 6, except the Winkler, which is based on a Texas Lignite, and the Destec, which is based on an Appalachian Bituminous.

### ***Cleaning and Removal Of Contaminants (Reformate Alteration)***

Fuel processors require the removal of impurities that degrade the fuel processor or fuel cell performance. Sulfur is the major contaminant encountered. Carbon monoxide reduction for low temperature fuel cells and avoidance of carbon deposition are also addressed in this section. A typical processing chain for a low temperature fuel cell will have a hydrodesulfurizer, a halogen guard, a zinc oxide sulfur absorber, a catalytic reformer, a high temperature shift converter, a second halogen guard, and low temperature shift converter. Figure 9-2 provides insight into these may be arranged. The function of all these components, except the reformer, is to remove impurities. For the PEFC cell, there needs to be an additional device to remove essentially all CO, such as a preferential oxidizer (22).

### **Sulfur Reduction**

There are high temperature and low temperature methods to remove sulfur from a fuel reformate stream. Low temperature cleanup, such as hydrodesulfurizing (limited to fuels with boiling end points below 205°C), is less difficult and lower in cost so should be used where possible, certainly with low temperature cells. Sulfur species in the fuel are converted to H<sub>2</sub>S, if necessary, then the H<sub>2</sub>S is trapped on zinc oxide. As previously mentioned, a minimum bed volume of the zinc oxide reactor is achieved at temperatures of 350 to 400°C. Simple

thermodynamic and economic analyses show that it is appropriate to use high temperature cleanup with high temperature cells.

There is a vast difference between removing sulfur from a gaseous fuel and a liquid fuel. The sulfur in a liquid fuel is usually removed after it is converted to a gas. This occurs in the reformer reactor so that it has to handle the sulfur either by operating at significantly high temperature, by removing the sulfur in the reforming reactor vessel, or by incorporating sulfur resistant catalysts. Sulfur resistant catalysts are being developed but none are mature enough for use. ANL for example has demonstrated that their catalyst can tolerate sulfur, but it has not been demonstrated on an engineering scale.

At least one developer is developing a liquid-phase fuel desulfurizer cartridge that will be used to remove sulfur prior to fuel vaporization. Other developers remove the sulfur immediately after vaporization and prior to the reforming. Hydrogen needs to be recirculated to the removal device to convert the sulfur species to  $H_2S$  so that it can be entrapped on zinc oxide, a complication. Zinc oxide beds are limited to operation at temperatures below  $430^\circ C$  probably because of pore plugging during sulfur removal and sintering. Thermodynamics also favors lower temperatures. At the higher temperatures, the  $H_2S$  cannot be reduced to levels low enough for shift catalyst or to reach fuel cell limits.

Sulfur content in fuel and sulfur removal processor development are in a constant stage of change and the reader is referred to the literature to assess the latest status and techniques.

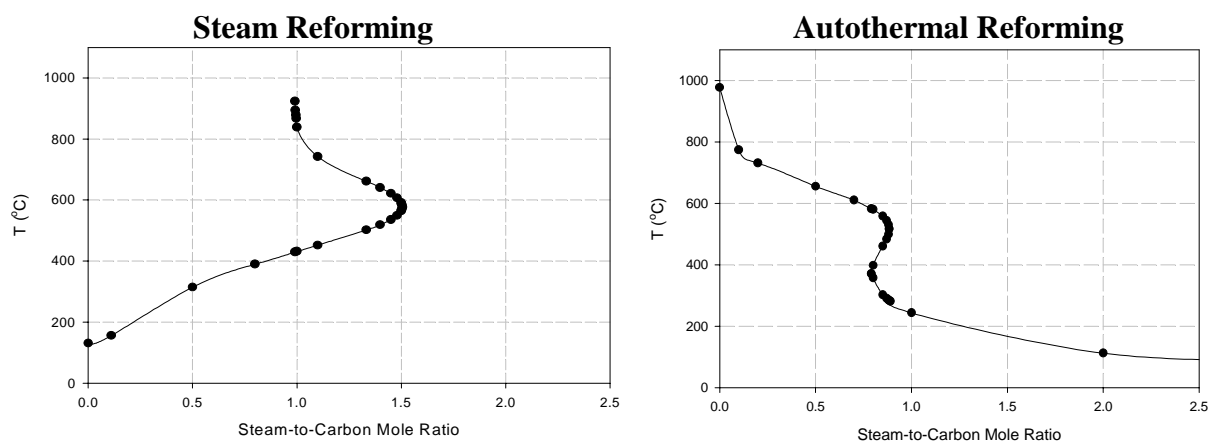
### **Carbon Monoxide Reduction**

The use of CO as a fuel in high temperature cells and water-gas shift reactions to lower carbon monoxide to conditions suitable for a PAFC have been previously described. Fuel gas reformat contains 0.5 to 1% by volume of CO even after the shift reactions. Present PEFCs operate below  $100^\circ C$ . At these temperatures, even small amounts of CO are preferentially adsorbed on the anode platinum (Pt) catalysts. This blocks access of  $H_2$  to the surface of the catalyst, degrading cell performance (23). Reformat for PEFC stacks must contain very low, (<50 ppm) CO to minimize Pt absorption to a reasonable value (allow sufficient active sites for the oxidation of  $H_2$ ). This can be achieved in two ways, by air injection into the anode at up to about 4% of the reformat feed rate or by reducing CO to the needed value prior to the cell (Even at 50 ppm, the CO effect must be mitigated by the injection of air at the anode). For the latter approach, a preferential oxidizer (PROX) is used to reduce CO prior to the cell. It has highly dispersed supported Pt or Pt-Ru (ruthenium) catalyst. Such catalysts act on the principle of selective adsorption of CO onto the active Pt or Pt-Ru (relative to  $H_2$ ), leading to CO being selectively oxidized by stoichiometric amounts of air co-fed to the catalyst bed. As the CO is oxidized, the gas temperature rises, which decreases the selectivity of CO adsorption on the catalyst and also increases the kinetics of the reverse water-gas shift reaction. In practice, the PROX process is carried out in stages to permit cooling the gas in-between the stages. The PROX is a relatively large component that operates at 100 to  $180^\circ C$  (17). Preferential gas cleanup by selective oxidation results in 0.1 to 2%  $H_2$  lost (24).

## Carbon Deposition Avoidance

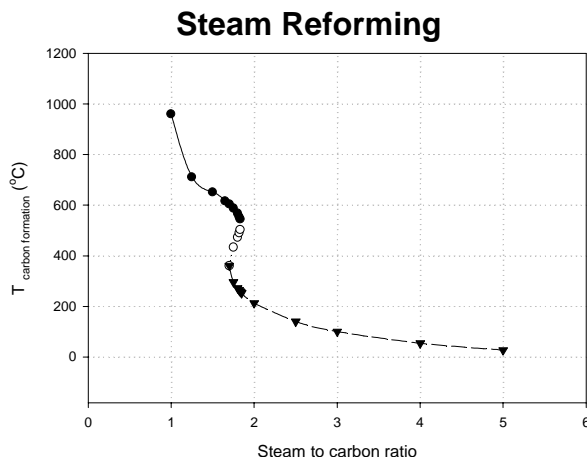
The processing of hydrocarbons always has the potential to form coke. Coke formation is influenced by the composition of the fuel, the catalyst, and the process conditions (e.g., partial pressure of steam). Coke causes the greatest problems in gas flow paths and on catalyst. Carbon deposition not only represents a loss of carbon for the reaction but more importantly also results in deactivation of the catalyst due to deposition at the active sites. Thermal cracking<sup>50</sup> in overheated preheaters and manifolds can easily form carbon. If the fuel conversion reactor is not properly designed or operated, coking is likely to occur. Thermo equilibrium calculations provide a first approximation of the potential for coke formation. Free carbon in hydrocarbon fuels forms according to the three equations, (9-1), (9-2), and 9-3). Figures 9-4 and 9-5 show the effect of increasing steam on carbon deposition for methane and octane respectively. Increasing steam, hydrogen, and carbon dioxide concentrations alleviates carbon deposition. Low contents of aromatics and alkenes<sup>5</sup> will help to maintain the activity of the catalyst (5). No carbon exists at low temperatures ( $\sim 600^{\circ}\text{C}$ ) in mixtures containing at least two atoms of oxygen and four atoms of hydrogen per atom of carbon. In these systems, all carbon is present as  $\text{CO}_2$  or  $\text{CH}_4$  (3).

**Figure 9-4 Carbon Deposition Mapping of Methane ( $\text{CH}_4$ )**  
(Carbon-Free Region to the Right of Curve)



<sup>50</sup>. Thermal cracking is the breaking of a hydrocarbon carbon-carbon bond through the free-radical mechanism. Cracking may result in the formation of lower chained hydrocarbons, the original "cracked" hydrocarbon, or further cracking of the hydrocarbon to "soot."

**Figure 9-5 Carbon Deposition Mapping of Octane (C<sub>8</sub>H<sub>18</sub>)  
(Carbon-Free Region to the Right and Above the Curve)**



Higher hydrocarbon fuels show a higher tendency for carbon formation than does methane. One method to alleviate carbon deposition problems in the fuel processor is to use special catalysts either containing alkali or based on an active magnesia support. With a highly active catalyst, the limit permitted on the final boiling point of the hydrocarbon feedstock is related mainly to the possibility of desulfurizing the feed to below 0.1 ppm, rather than to the reactivity of the hydrocarbons. With proper desulfurization, it has been possible to convert light gas oil into syngas with no trace of higher hydrocarbons in the reformat gas (12).

Coke formation resulting from the use of higher hydrocarbon fuels can also be eliminated with an adiabatic pre-reformer. The adiabatic reformer is a simple fixed bed reactor. By adiabatic pre-reforming, all higher hydrocarbons are converted at low temperature (below ~500°C) with steam into methane, hydrogen, and carbon oxides at conditions where carbon formation does not occur. If so, it is possible to use a high pre-heating temperature (650°C or above) for internal reforming in MCFC and SOFC without the risk of carbon formation. For natural gas containing only minor amounts of higher hydrocarbons, adiabatic pre-reforming at a steam to carbon ratio as low as 0.25 mole/atom has been demonstrated. For heavier feedstocks such as naphtha, operation at a steam to carbon of 1.5 is proven in industry. Pilot tests have been carried out at a steam to carbon ratio of 1.0 with reformat recycle.

Coking can be also be avoided by operating at high temperatures and at high oxygen-to-carbon ratios. For a given O/C ratio, it is preferable that the oxygen feed be in the form of water. In other words, the coking tendency is reduced at high O/C and H/C ratios. Thus, less coke is formed in the order, POX > ATR > SR (15,25).

### **Other Impurities Reduction**

Halides in fuels such as naphtha have deleterious effects on steam reforming and low temperature shift, thus halogen guards need to be included in the fuel processing.

There are many types of coal with different compositions, including harmful species. The handling of these species is addressed earlier under “Coal Processing.” One common constituent, HCl, will cause formation of stable chlorides and corrosion in a MCFC, see the section on MCFC. There has not been much work in SOFC yet on this topic. It is doubtful whether low temperature cells will be fueled by coal.

### *State-of-the-Art Components*

Developers have brought fuel processing technology to the point where conversion of all fuels of present interest to fuel cells has been demonstrated to a degree. Natural gas steam reforming is being used on commercial fuel cell units. There has been equal success with steam reforming light distillates although these fuels are not in common use. Tests have been performed on reactors and complete small fuel processors on methanol, gasoline, and diesel, all suitable for vehicle use. These tests have not advanced to operation over prolonged periods; however, there have been tests that indicate these fuels can be processed in POX and ATR reactors with high levels of sulfur. Water-gas shift and methods to lower CO even to a few ppm have been developed, but the final CO cleanup processes are in an early stage of development. All fuel processors need additional engineering development to reduce volume, weight, and cost to allow widespread fuel cell power unit use. The state-of-the-art information below is based primarily on U.S. or closely related fuel cell programs.

**Argonne National Laboratory**, (ANL) is pursuing fuel processor technology development that ranges from catalyst development, to component (CO, S cleanup, etc.) evaluations, to fuel processor hardware design, modeling, and demonstration.

ANL's reforming process is based on the autothermal reforming reaction, a choice that has been driven by the need for compact, lightweight fuel processors that can meet the rapid start and load following capabilities needed by most small fuel cell systems. ANL has developed a number of novel catalysts for the processes involved in the production of hydrogen from hydrocarbon fuels such that the reformat stream is suitable for PEFC units. For the reforming reaction, ANL has developed a family of catalysts that have proven effective for the conversion of a wide range of conventional and alternative fuels. These catalysts consist of a substrate and a promoter, where it is surmised the substrate participates in the oxidation of the carbon while the promoter dehydrogenates the hydrocarbon. Tests in micro-reactors have shown that at temperatures of less than 700°C, complete conversion with high hydrogen yields were achievable from hydrocarbon species such as methane, methanol, ethanol, 2-pentene, cyclohexane, iso-octane, hexadecane, and available fuels such as gasoline, and diesel. Long term tests (1,700 hours) with sulfur-containing (30 ppm) gasoline-type fuels have shown that the reforming catalyst is sulfur tolerant.

Recognizing that the reforming reaction is mass transport limited, the reforming catalyst has been fabricated in microchannel forms which results in significant (factor of 3-5) reduction in the size of the reformer.

Alternative water gas shift catalysts developed at ANL have shown activity comparable to commercially available shift catalysts but with the advantage that ANL's catalyst can be exposed to oxidizing/reducing environments without any loss in activity. This is very important as

commercial catalysts are active only after being reduced to the metallic state, but are pyrophoric (due to rapid reoxidation) when exposed to air.

These various catalysts have been demonstrated in engineering scale (5-10 kWe) fuel processing hardware to convert methanol, natural gas, and gasoline. These engineering scale fuel processors are designed to integrate into a single compact unit with unit operations (steam generation, air preheating, etc.) and processes (reforming, sulfur entrapment, shift reaction, etc.) that are necessary for the conversion of hydrocarbon fuels to a reformat gas stream suitable for the PEFC. For higher temperature fuel cells (e.g. SOFC) that accept carbon monoxide, these fuel processor designs can be simplified considerably leading to much more compact units.

Argonne National Laboratory, where the work is funded by the Department of Energy, will not be involved in the commercial manufacture of fuel processors, but will license its technology to fuel processor manufacturers.

**Ceramic Fuel Cells, Limited** (CFCL), Australia, is developing a pre-reformer fuel processor that will convert hydrocarbon fuels to a methane and hydrogen-rich reformat. This reformat will be internally reformed in CFCL's planar SOFCs to produce a high efficiency system. CFCL uses a two-stage approach: hydrodesulfurization to break organic compounds down to H<sub>2</sub>S and hydrocarbons coupled with a ZnO absorber bed for H<sub>2</sub>S removal, then steam reforming to produce a mixture of methane, carbon oxides and hydrogen from higher hydrocarbons (the aim is to maximize the methane content). This approach has been demonstrated with LPG in the temperature range 300-450°C to get desired fuel mixtures. Commercial pre-reforming catalysts are used and screening experiments identified two effective catalysts from two manufacturers. Another aim of the project is to use the lowest S/C ratios possible (26).

**Honeywell**, formerly AlliedSignal, is developing CPOX based fuel processors. Honeywell selected the CPOX method to develop a lightweight, compact fuel processor for its planar SOFC systems operating on the military logistic fuels, JP-8 and diesel. The processor reaction occurs at high temperatures and is fast. Residence times are a few milliseconds. Honeywell has operated a stand-alone POX fuel processor for more than 650 hours with a surrogate fuel JP-8 containing 500 ppm by weight sulfur as dibenzothiophene. The process has been optimized to produce high H<sub>2</sub> and CO yields while avoiding carbon deposition. No water was injected for control. The processor yielded 90% CO and 80% H<sub>2</sub> yield (H<sub>2</sub> produced - in mols)/(H<sub>2</sub> in the hydrocarbon fuel). The syngas consists of 19% H<sub>2</sub>, 24% CO, 1% CO<sub>2</sub>, and 56% N<sub>2</sub>, dry basis, and its product lower heating value is 70 to 80% of the fuel in. There is less than 1% hydrocarbons in the product gas. Sulfur is produced as H<sub>2</sub>S (50 ppm) and minimal SO<sub>2</sub>. The reactor was run with surrogate fuels containing 1,000 ppm by weight dibenzothiophene for over 280 hours. The Honeywell planar SOFC cells have a tolerance of 35 ppm sulfur as H<sub>2</sub>S. This corresponds to 350 ppm by weight in logistic fuels. Honeywell has operated an integrated fuel processor and planar SOFC unit for 20+ hours as of early 2000 (27).

**Hydrogen Burner Technology** (HBT) (28) was founded to bring to market reformer systems based on the principles of under-oxidized combustion (UOB™). These systems use either non-catalyzed partial oxidation reformers or catalyzed autothermal reformers. The systems for fuel cell applications include all of the components required to deliver anode-ready gas and to

combust anode-off gas. Targeted fuel cells for these processes are primarily PEFC, but also for at least one SOFC developer. All present fuel processing with diesel is now pointed toward PEFC. SOFC presents different issues that will affect the fuel processor design. HBT has produced six fuel-processing systems for fuel cell type applications. To date, four of these units have been delivered to customers for laboratory evaluation. Two of these units have an equivalent 50 kWe maximum rated capacity and two have under a 10 kWe rating. The initial two units used non-catalyzed partial oxidation and the other four used autothermal reformers. One of these will be operated on diesel in the year 2000 for a fuel cell client. The catalyst in this ATR unit is capable of operation with the sulfur in diesel (under 200 ppmw sulfur in the liquid phase). Based on this ATR technology, HBT developed a  $\leq 10$  kWe fuel processing system directed at the stationary market. The first group of twenty pre-production units is being built for evaluation by fuel cell developers during late 2000 and early 2001.

A fuel processor for PEFC application contains sulfur removal, an ATR-enhanced UOB<sup>TM</sup> reformer, advanced shift reactors, a steam generation system, a product gas cooler, a PROX system, a gas compressor, an air compressor, an anode-off gas oxidizer, and a control system. Goal efficiency (LHV H<sub>2</sub> consumed by fuel cell/LHV fuel consumed by fuel processor) is 69 to 72%. H<sub>2</sub> concentration is presently >50% (dry).

**Johnson Matthey Technology Centre (J-M)** is primarily a supplier of catalysts. However, the company has developed a modular “Hot Spot<sup>TM</sup>” fuel processor for fuel cell power units that addresses the integrated issues of catalytic reactions and thermal issues. The processor contains a POX reaction that results in net thermal energy being produced and a steam reforming process that requires input of thermal energy. The 5 kWe equivalent, prototype unit is designed so that these two opposing thermal events occur at the same discrete active catalytic site. A typical fuel processor reactor consists of four to eight canisters, that contain the catalyst, mounted on each side of a thermal block. The catalyst is mounted on a support material rather than being in a packed bed. The thermal block, where the fuel and water are vaporized, is kept at 130°C to 150°C with the heat contained within the hydrogen exiting the fuel cell. The POX and steam reforming reactions of methanol take place at 400°C to 450°C, but an imbalance has the potential to drive the temperature to 600°C. This effect is counteracted by adding more water or reducing the air feed-rate to the catalytic chamber. Development to date has been primarily with the conversion of methanol and natural gas to a hydrogen-rich reformat where essentially 97 to 98% of the CO has been converted to H<sub>2</sub> and CO<sub>2</sub>. This means that selective oxidation is needed to reduce the CO if the cell cannot tolerate it, a complication of design since it is necessary to cool the product gas for oxidation. The present reformer tolerates sulfur but converts it to H<sub>2</sub>S. This H<sub>2</sub>S has to be removed prior to selective oxidation because of the non-sulfur tolerant catalyst in that process. This produces temperature issues that must be resolved through the use of in-line components. One to three percent methane is unconverted. The processor yields a hydrogen-rich gas that has 55% H<sub>2</sub> and 2% CO (dry basis) from methanol. The CH<sub>3</sub>OH conversion is >99%. A similar processor is capable of converting >90% natural gas to 40% H<sub>2</sub> (dry basis) in the POX mode and 58% H<sub>2</sub> in the ATR mode (16,29).

It is surmised that the conversion of gasoline and diesel will result in a more complicated unit than the natural gas unit because of the more complex conversion of higher hydrocarbon fuels, greater sulfur cleaning requirements, and higher conversion temperature. J-M is beginning to

test an experimental breadboard fuel processor operating on gasoline. The unit is in a non-integrated stage (i.e., heat input for vaporization is supplied electrically, rather than by exchange from another part of the unit). It has been tested with AVCAT fuel (NATO military diesel). The specification for this fuel lists a maximum of 0.3% sulfur (by weight) in the liquid state. A 5 kW fuel processor that converts gasoline plus CO cleanup is scheduled to be delivered in September 2000. It will be incorporated with a PEFC power section that will supply auxiliary power for automobiles. J-M indicated that it intends to replace the eight canisters (used in the 5 kW methanol reformer) with two larger canisters for reduced cost.

**McDermott Technology, Inc.** (MTI), the research and development branch of McDermott International, Inc. has been developing fuel processors for the past six years. Reformers for liquid fuels such as gasoline and diesel fuel, and for natural gas have been developed. McDermott has operated non-catalytic POX reformers as large as 35 kWe and catalytic autothermal reformers as large as 30 kWe, the latter on high-sulfur marine diesel. McDermott has over 1,000 hours experience utilizing a POX reactor and about 400 hours on the autothermal unit. The longest continuous run of the autothermal reformer has been 175 hours (30,31).

McDermott is designing a 500 kWe autothermal fuel processor for diesel fuel for marine applications (PEFC) and a 50 kWe gasoline processor for automotive applications (PEFC). The gasoline processor includes a liquid-phase desulfurizer cartridge to reduce sulfur in low-sulfur gasoline to 3 ppm prior to the reforming catalyst. The reformer operates at an average temperature of 800°C. McDermott is also developing a 10 kWe natural gas fuel processor for use with a residential size PEFC system.

Nuvera Fuel Cells, a company formed in April 2000 through the merger of DeNora Fuel Cells S.p.A and Epyx Corporation, originally pursued partial oxidation technology but is now developing catalytic POX, autothermal reforming (ATR), and steam reforming. ATR is being used to convert natural gas, gasoline, and diesel to a hydrogen-rich reformat. Reforming gasoline in an ATR reactor yields 40 to 42 percent H<sub>2</sub> on a dry basis. If determined after the selective oxidation process, fuel conversion efficiency<sup>51</sup> of the fuel processor is about 85 percent. The ATR-based fuel processor consists of a reforming zone, high-temperature shift converter, desulfurization reactor, low-temperature shift converter, and a selective oxidation reactor. The ATR is also used to convert natural gas, methanol, and propane. The reactor produces a hydrogen-rich reformat with nearly no sulfur (<0.2 ppm) or carbon monoxide (<10 ppm).

The largest gasoline-fueled ATR reactor operated by Nuvera is 200 kWt. Nuvera had over 2,000 hours run time with no catalyst change while experiencing multiple start/stop conditions. The longest continuous run has been 500 hours.

---

<sup>51</sup>. Nuvera defines fuel conversion efficiency as thermal value of H<sub>2</sub> produced/thermal value of fuel fed to processor.



**Wellman CJB Ltd.** manages a European Community JOULE project named MERCATOX that has as its objective to develop a compact methanol reformer and gas clean-up unit for a PEFC passenger car. The concept is the use of compact aluminum heat exchangers comprising corrugated plates coated on one side with methanol reforming catalyst and having the combustion gas (preferably anode off-gas) on the other side (32).

### ***Research & Development Components***

There are two major areas where fuel processor developers are focusing their research and development efforts, catalyst development and process/engineering development. A smaller, long term effort on novel processing schemes is in the early stages of being investigated.

Catalyst Development (3,33,34): There is a need to develop better shift catalysts. Commercial shift catalyst are available but are based on large bed design rather than with small fuel processors needed in fuel cell units. These commercial catalysts have fixed size, high density, and are susceptible to contaminant poisoning by ingredients found in infrastructure fuels. Present catalysts are developed for process plant service where transient conditions are not a concern. Typical shift catalysts, such as copper-zinc oxide, are reduced in place and must be isolated from air. There is a need for smaller, high surface area catalyst beads on low-density monolith substrate to be developed without reducing activity. This need applies to all fuel processor catalyst, not just the shift catalysts. There is also a need to demonstrate that the low-temperature, PROX catalysts have high selectivity toward CO and long term stability under operating conditions.

**Process/Engineering Development** (15,25,34) There are numerous engineering and process issues that are being addressed by fuel processor developers. Several major issues are:

- As the size of the catalyst bed increases, the segregation within an ATR reactor bed toward over-oxidation and catalyst overheating in the front of the bed, and air starvation and carbon formation in the back end of the bed are important to consider. Maintaining a good temperature distribution in the bed, especially with a larger reactor is identified as one of the challenges facing this approach.
- Fuel processor tests have been on the order of 40 hours. There is a need is to show similar results at realistic operating conditions and further engineering development to enhance the catalyst activity and make the fuel processor lighter and smaller.
- There is a need to investigate improved and simplified fuel processor designs. Examples are combining the reformer and the desulfurizer in a single stage to reduce weight and volume, producing an integrated vaporizer design, and designing for a wide variation of fuel vaporization temperatures to allow fuel flexible operation.
- Transient issues are important in transport applications and should be addressed early by testing. The challenge is to demonstrate the operation at high sulfur content over the full operating envelope of the vehicle power unit – start-up, transients, shutdown, sulfur spikes in the fuel, etc. using the same processor.

**Novel Processing Schemes:** Various separators have been proposed to separate the hydrogen-rich fuel in the reformat for cell use or to remove harmful species. At present, the separators are expensive, brittle, require large pressure differential, and are attacked by some hydrocarbons. There is a need to develop thinner, lower pressure drop, low cost membranes that can withstand separation from their support structure under changing thermal loads. Plasma reactors offer independence of reaction chemistry and optimum operating conditions that can be maintained over a wide range of feed rates and H<sub>2</sub> composition. These processors have no catalyst and are compact. However, they are preliminary and have only been tested at a laboratory scale.

**Other:** Although not R&D, it should prove beneficial for fuel cell developers to provide species tolerance specifications to fuel processor developers established by standard definition, determination methods, and measurement procedures. This would aid the fuel processor developer to develop products compatible with various fuel cell units. Of particular importance are sulfur and CO limits.

### **9.1.2 Rejected Heat Utilization**

Rejected heat (i.e., heat not utilized in the fuel processing and fuel cell subsystems) can be used to generate hot water, steam, or additional electricity. The utilization of the rejected heat depends upon the needs of the end user as well as the specifics of the process. The higher temperature fuel cells (i.e., MCFC and SOFC) are capable of generating significant quantities of high-pressure superheated steam because of the high temperature of the rejected heat. In a large fuel cell power system, on the order of 100 to 200 MW or more, production of electricity via a steam turbine bottoming cycle may be advantageous. In pressurized fuel cell systems, it may also be advantageous to utilize a gas expander before the steam generation. Possible locations for heat recovery include the gasifier effluent, before cold gas cleanup, around the fuel cell, and the fuel cell or burner exhaust.

### **9.1.3 Power Conditioners and Grid Interconnection**

Power conditioning for a fuel cell power plant used to supply DC rated equipment includes current and voltage controls. Power conditioning for a fuel cell power plant used to supply AC rated equipment includes DC to AC inversion and current, voltage and frequency control, stepping the voltage up or down through a transformer depending on final equipment utilization voltage, and maintaining harmonics output to an acceptable level. In addition, transient response of the power conditioning equipment should be considered. For utility grid interconnection, synchronization, real power (watts) ramp rate, and VAR control must also be addressed.

In the initial phase of systems analysis, the important aspect of power conditioning is the efficiency of the power conversion and incorporation of the small power loss into the cycle efficiency. Power conditioning efficiencies typically are on the order of 94 (32) to 98%.

**Electric Power System Design:** For specific applications, fuel cells can be used to supply DC power distribution systems designed to feed DC drives such as motors or solenoids, controls, and other auxiliary system equipment. The goal of the commercial fuel cell power plant is to deliver usable AC power to an electrical distribution system. This goal is accomplished through a subsystem that has the capability to deliver the real power (watts) and reactive power (VARs) to a facility's internal power distribution system or to a utility's grid. The power conditioning

equipment a fuel cell installation has two main purposes. The first is to adapt the fuel cell output to suit the electrical requirements at the point of power delivery. The second is provide power to the fuel cell system auxiliaries and controls. The conversion of the direct current produced by the fuel cells into three-phase alternating current is accomplished by solid state inverters and if required, voltage transformers. Inverters minimize both system harmonics and radiated noise. Controls are provided to regulate the real power output by controlling both, the fuel rate and the electrical output. Electrical protection is provided so that a utility grid disturbance will not damage the fuel cell installation, while the connected power distribution system is protected by conventional equipment isolation in case of an over-current malfunction.

***Interaction with the Electrical Power Distribution System:*** The fuel cell system power plant can be used in a wide variety of applications:

- Dedicated to an isolated/remote load
- Backup power to a load normally connected to the local utility
- Operated in parallel with the local utility while supplying power to a facility's power distribution system
- Electrical power supply connected directly to the local utility
- Cogeneration (supply both electrical power and heat)

Connection to the utility grid provides many advantages to on-site power producers such as reliability improvement and increase of load factor, as well as giving the electric utilities a chance to improve the supply capability. When a fuel cell power plant is used for electric utility applications, the inverter is the interface equipment between the fuel cell and the electrical network. The inverter acts as the voltage and frequency adjuster to the final load. The interface conditions require the following characteristics for the inverter:

- Ability to synchronize to the network
- Inverter output voltage regulation typically 480 volts plus or minus 2%, three-phase. Network voltage imbalance will not be a concern while the fuel cell is connected to the grid.
- Inverter output frequency regulation typically plus or minus 0.5%
- Supply of necessary reactive power to the network within the capabilities of the inverter, adjustable between 0.8 lagging and 1.0 power factor depending on the type of inverter used and without impacting maximum kW output
- Protection against system faults
- Suppression of the ripple voltage fed back to the fuel cells

- Suppression of harmonics so that the power quality is within the IEEE 519 harmonic limits requirements
- High efficiency, high reliability, and stable operation.

Some limitations of the inverters used are:

- Transient current capability for such conditions as motor or other inrush currents
- Transient current capability to operate over current devices to clear equipment or cable faults

The response of the fuel cell to system disturbances or load swings also must be considered whether it is connected to a dedicated load or to the utility's grid. Demonstrated fuel cell power conditioning responses are (33):

- No transient overload capability beyond the kW rating of the fuel cell
- A load ramp rate of 10 kW/second when connected to the utility grid
- A load ramp rate of 0 to 100% in one cycle when operated independently of the utility grid
- A load ramp rate of 80 kW/second when operated independently of the utility grid and following the initial ramp up to full power

#### **9.1.4 System and Equipment Performance Guidelines**

In designing a system, an engineer accounts for the physical performance and limitations of equipment to be utilized in the system. For example, practical heat exchangers are limited in how close the temperature of the cold fluid can come to the temperature of the hot fluid at any point in the heat exchanger. This minimum temperature difference is known as the "approach." For a gas to gas heat exchanger, a reasonable approach design value is 100°F. An engineer who employs a gas to gas heat exchanger with only a 50°F approach will have implied the use of a very large and expensive heat exchanger, and is likely to find the process economics are not practical.

This section documents reasonable equipment performance assumptions that can be used in a first pass conceptual design effort. The reader should be aware that the list includes many assumptions and simplifications that may not be suitable for detailed design. The documentation of equipment guidelines at a significant level of detail is the subject for entire books [e.g., several excellent books have already been written concerning conceptual design and equipment performance (34,35,36)]. The list presented here simply illustrates the more important equipment performance considerations and their common performance ranges, which may be useful to the novice system designer for incorporating a level of realism. Detailed conceptual design efforts need to address many factors not addressed by the list below, such as the effects of flow rates, temperatures, pressures, corrosive elements, the impact of the equipment on the cycle itself, and, of course, the specific performance of the actual equipment.

The list of equipment performance assumptions is presented in Table 9-5.

**Table 9-5 Equipment Performance Assumptions**

Parameter	Common Range	Notes
Pump Efficiency 100 gpm 1000 gpm 10,000 gpm	10 to 90% 35 to 60% 60 to 80% 78 to 90%	Flow rate dependent. Pump efficiencies do not include the motor or driver efficiency.
Compressor Efficiency Reciprocating Industrial quality- Centrifugal High quality- Centrifugal	65 to 90% 76 to 85% 82 to 90%	Flow rate and PR dependent. Compressor efficiency only. Motor or driver efficiency not included.
Compressor Intercooling Optimal per stage pressure ratio Intercooled temperature Intercooling recommended	$PR_i = (PR_{total})^{1/n \text{ stages}}$ 130°F $PR_{total} > 5.0$	For a two-stage system, $PR_1 = PR_2$ . Assumes 100°F cooling water.
Turbine Efficiency (isentropic) Steam Turbine Gas Turbine Gas Expander	75 to 90% 80 to 90% 80 to 85%	Flow rate and condition dependent. Best to refer to a heat balance or specific model information.
Pressure Drops Heat exchanger - gas side Heat exchanger - water side Fuel cell Fuel processor Steam superheater/reheater	1-2% 5-10 psi 2% 2% 5-10%	Gas phase pressure drop. Water side pressure drop.
Temperature Approaches Gas to Gas Air to water coolers Gas to steam (superheater) Water to water Economizer Evaporator	100°F 30°F 30°F 20°F 20°F 20°F	
Heat Recovery Boiler Radiant heat loss	0.5 to 1.0%	
Fuel Cell Fuel utilization Oxidant utilization Heat loss	- -	See Technology specific sections. See Technology specific sections.
Inverter Efficiency	94 to 98%	96.5% is common for sizes ~ 1 MW.
Turbine Generator Efficiency 1 to 10 MW	96 to 98.5% 98.0%	
Transformer Loss	0.5 to 0.8%	Stepping up or down.
Motor Efficiency 1 to 10 kW 10 to 100 kW 100 to 1000 kW 1 to 10 MW	<90% 90 to 92% 92 to 95% 95 to 97%	
Auxiliary Power Steam turbine auxiliaries Gas turbine auxiliaries	0.5% 0.5%	Dependent upon auxiliary systems

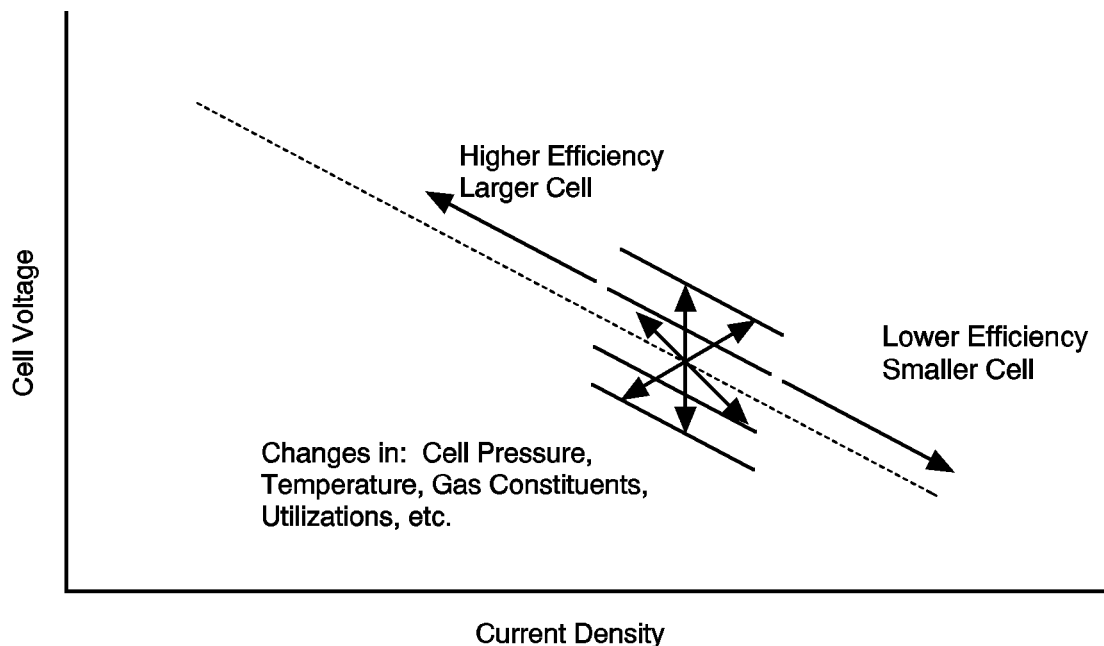
## **9.2 System Optimizations**

The design and optimization of a fuel cell power system is very complex because of the number of required systems, components, and functions. Many possible design options and trade-offs affect unit capital cost, operating cost, efficiency, parasitic power consumption, complexity, reliability, availability, fuel cell life, and operational flexibility. Although a detailed discussion of fuel cell optimization and integration is not within the scope of this section, a few of the most common system optimization areas are examined.

From Figure 9-6, it can be seen that the fuel cell itself has many trade-off options. A fundamental trade-off is determining where along the current density voltage curve the cell should operate. As the operating point moves up in voltage by moving (left) to a lower current density, the system becomes more efficient but requires a greater fuel cell area to produce the same amount of power. That is, by moving up the voltage current density line, the system will experience lower operating costs at the expense of higher capital costs. Many other parameters can be varied simultaneously to achieve the desired operating point. Some of the significant fuel cell parameters that can be varied are pressure, temperature, fuel composition and utilization, and oxidant composition and utilization. The system design team has a fair amount of freedom to manipulate design parameters until the best combination of variables is found.

### **9.2.1 Pressurization**

Fuel cell pressurization is typical of many optimization issues, in that there are many interrelated factors that can complicate the question of whether to pressurize the fuel cell. Pressurization improves process performance at the cost of providing the pressurization. Fundamentally, the question of pressurization is a trade-off between the improved performance (and/or reduced cell area) and the reduced piping volume, insulation, and heat loss compared to the increased parasitic load and capital cost of the compressor and pressure-rated equipment. However, other factors can further complicate the issue. To address this issue in more detail, pressurization for an MCFC system will be examined.



9-

**Figure 9-6 Optimization Flexibility in a Fuel Cell Power System**

In an MCFC power system, increased pressure can result in increased cathode corrosion. Cathode corrosion is related to the acidity of the cell, which increases with the partial pressure of  $\text{CO}_2$ , and therefore with the cell pressure. Such corrosion is typified by cathode dissolution and nickel precipitation, which can ultimately result in a shorted cell, causing cell failure (37). Thus, the chosen pressure of the MCFC has a direct link to the cell life, economics, and commercial viability.

Increasing the pressure in a MCFC system can also increase the likelihood of soot formation and decrease the extent of methane reforming. Both are undesirable. Furthermore, the effect of contaminants on the cell and their removal from a pressurized MCFC system have not been quantified. The increased pressure also will challenge the fuel cell seals (37).

The selection of a specific fuel cell pressure will affect numerous design parameters and considerations such as the current collector width, gas flow pattern, pressure vessel size, pipe and insulation size, blower size and design, compressor auxiliary load, and the selection of a bottoming cycle and its operating conditions.

These issues do not eliminate the possibility of a pressurized MCFC system, but they do favor the selection of more moderate pressures. For external reforming systems sized near 1 MW, the current practice is a pressurization of 3 atmospheres.

The performance of an internal reforming MCFC also would benefit from pressurization, but unfortunately, the increase is accompanied by other problems. One problem that would need to be overcome is the increased potential for poisoning the internal reforming catalyst resulting from the

increase in sulfur partial pressure. The current practice for internal reforming systems up to 3 MW is atmospheric operation.

Pressurization of an SOFC yields a smaller gain in fuel cell performance than either the MCFC or PAFC. For example, based on the pressure relationships presented earlier, changing the pressure from one to ten atmospheres would change the cell voltage by ~150, ~80, and ~60 mV for the PAFC, MCFC, and SOFC, respectively. In addition to the cell performance improvement, pressurization of SOFC systems allows the thermal energy leaving the SOFC to be recovered in a gas turbine, or gas turbine combined cycle, instead of just a steam bottoming cycle. Siemens Westinghouse is investigating the possibilities associated with pressurizing the SOFC for cycles as small as 1 to 5 MW.

Large plants benefit the most from pressurization, because of the economy of scale on equipment such as compressors, turbines, and pressure vessels. Pressurizing small systems is not practical, as the cost of the associated equipment outweighs the performance gains.

Pressurization in operating PAFC systems demonstrates the economy of scale at work. The IFC 200 kWe and the Fuji Electric 500 kWe PAFC offerings have been designed for atmospheric operation, while larger units operate at pressure. The 11 MWe plant at the Goi Thermal Power Station operated at a pressure of 8.2 atmospheres (38), while a 5 MWe PAFC unit (NEDO / PAFCTRA) operates at slightly less than 6 atmospheres (39). NEDO has three 1 MWe plants, two of which are pressurized while one is atmospheric (39).

Although it is impossible to generalize at what size a plant would benefit by pressurization, when plants increase in size to approximately 1 MW and larger, the question of pressurization should be evaluated.

### **9.2.2 Temperature**

Although the open circuit voltage decreases with increasing temperature, the performance at operating current densities increases with increasing temperature due to reduced mass transfer polarizations and ohmic losses. The increased temperature also yields higher quality rejected heat stream. An additional benefit to an increased temperature in the PAFC is an increased tolerance to CO levels, a catalyst poison. The temperatures at which the various fuel cells can operate are, however, limited by material constraints. The PAFC and MCFC are both limited by life shortening corrosion at higher temperatures. The TSOFC is limited by material property limitations. Again, the fuel cell and system designers should evaluate what compromise will work best to meet their particular requirements.

The PAFC is limited to temperatures in the neighborhood of 200°C (390°F) before corrosion and lifetime loss become significant. The MCFC is limited to a cell average temperature of approximately 650°C (1200°F) for similar reasons. Corrosion becomes significant in an MCFC when local temperatures exceed 700°C (1290°F). With a cell temperature rise on the order of 100°C (180°F), an average MCFC temperature of 650°C (1200°F) will provide the longest life, highest performance compromise. In fact, one reference (40) cites "the future target of the operating temperature must be 650°C ±30°C (1290°F ±55°F)."



The high operating temperature of the SOFC puts numerous requirements (phase and conductivity stability, chemical compatibility, and thermal expansion) on material selection and development (41). Many of these problems could be alleviated with lower operating temperatures. However, a high temperature of approximately 1000°C (1830°F), i.e., the present operating temperature, is required in order to have sufficiently high ionic conductivities with the existing materials and configurations (41).

### 9.2.3 Utilization

Both fuel and oxidant utilizations<sup>52</sup> involve trade-offs with respect to the optimum utilization for a given system. High utilizations are considered desirable (particularly in smaller systems) because they minimize the required fuel and oxidant flow, for a minimum fuel cost and compressor/blower load and size. However, utilizations that are pushed too high result in significant voltage drops. One study (42) cites that low utilizations can be advantageous in large fuel cell power cycles with efficient bottoming cycles because the low utilization improves the performance of the fuel cell and makes more heat available to the bottoming cycle. Like almost all design parameters, the selection of optimum utilizations requires an engineering trade-off that considers the specifics of each case.

**Fuel Utilization:** High fuel utilization is desirable in small power systems, because in such systems the fuel cell is usually the sole power source. However, because the complete utilization of the fuel is not practical, except for pure H<sub>2</sub> fuel, and other requirements for fuel exist, the selection of utilization represents a balance between other fuel/heat requirements and the impact of utilization on overall performance.

Natural gas systems with endothermic steam reformers often make use of the residual fuel from the anode in a reformer burner. Alternatively, the residual fuel could be combusted prior to a gas expander to boost performance. In an MCFC system, the residual fuel often is combusted to maximize the supply of CO<sub>2</sub> to the cathode while at the same time providing air preheating. In an SOFC system, the residual fuel often is combusted to provide high-temperature air preheating.

The designer has the ability to increase the overall utilization of fuel (or the oxidant) by recycling a portion of the spent stream back to the inlet. This increases the overall utilization while maintaining a lower per pass utilization of reactants within the fuel cell to ensure good cell performance. The disadvantage of recycling is the increased auxiliary power and capital cost of the high temperature recycle fan or blower.

One study by Minkov et al. (42) suggests that low fuel and oxidant utilizations yield the lowest COE in large fuel cell power systems. By varying the fuel cell utilization, the electric power generation split between the fuel cell, steam turbine, and gas turbine are changed. The low fuel utilization decreases the percentage of power from the fuel cell while increasing the fuel cell performance. The increased power output from the gas turbine and steam turbine also results in their improved performance and economy of scale. The specific analysis results depend upon the assumed stack costs. The optimal power production split between the fuel cell and the gas and steam turbines is approximately 35%, 47%, and 17% for a 575 MW MCFC power plant. The

---

<sup>52</sup>. Utilization - the amount of gases that are reacted within the fuel cell compared to that supplied.

associated fuel utilization is a relatively low 55%. It remains to be seen whether this trend will continue to hold for the improved cells that have been developed since this 1988 report was issued.

***Oxidant Utilization:*** In addition to the obvious trade-off between cell performance and compressor or blower auxiliary power, oxidant flow and utilization in the cell often are determined by other design objectives. For example, in the MCFC and SOFC cells, the oxidant flow is determined by the required cooling. This tends to yield oxidant utilizations that are fairly low (~25%). In a water-cooled PAFC, the oxidant utilization based on cell performance and a minimized auxiliary load and capital cost is in the range of 50 to 70%.

#### **9.2.4 Heat Recovery**

Although fuel cells are not heat engines, heat is still produced and must be removed in a fuel cell power system. Depending upon the size of the system, the temperature of the available heat, and the requirements of the particular site, this thermal energy can be either rejected, used to produce steam or hot water, or converted to electricity via a gas turbine or steam bottoming cycle or some combination thereof.

***Cogeneration:*** When small quantities of heat and/or low temperatures typify the waste heat, the heat is either rejected or used to produce hot water or low-pressure steam. For example, in a PAFC cycle where the fuel cell operates at approximately 205°C (400°F), the highest pressure steam that could be produced would be something less than 14 atmospheres (205 psia). This is obviously not practical for a steam turbine bottoming cycle, regardless of the quantity of heat available. At the other end of the spectrum is the TSOFC, which operates at ~1000°C (~1800°F) and often has a cell exhaust temperature of approximately 815°C (1500°F) after air preheating. Gas temperatures of this level are capable of producing steam temperatures in excess of 540°C (1000°F), which makes it more than suitable for a steam bottoming cycle. However, even in an SOFC power system, if the quantity of waste heat is relatively small, the most that would be done with the heat would be to make steam or hot water. In a study performed by Siemens Westinghouse of 50 to 2000 kW TSOFC systems, the waste heat was simply used to generate 8 atmospheres (100 psig) steam (32).

***Bottoming Cycle Options:*** Whenever significant quantities of high-temperature rejected heat are available, a bottoming cycle can add significantly to the overall electric generation efficiency. Should the heat be contained within a high-pressure gas stream, then a gas turbine potentially followed by a heat recovery steam generator and steam turbine should be considered. If the hotgas stream is at low pressure, then a steam bottoming cycle is logical.

If a steam bottoming cycle is appropriate, many design decisions need to be made, including the selection of the turbine cycle (reheat or non-reheat) and the operating conditions. Usually, steam turbines below 100 MW are non-reheat, while turbines above 150 MW are reheat turbines. This generalization is subject to a few exceptions. In fact, a small (83 MW) modern reheat steam turbine went into operation (June 1990) as a part of a gas turbine combined cycle repowering (43).

### 9.2.5 Miscellaneous

**Compressor Intercooling:** Whether a compressor should be intercooled or not depends on the trade-off between the increased efficiency of the intercooled compressor and its increased capital cost. In general, intercooling is required for large compressors with pressure ratios that exceed approximately 5:1 (44). The designer also should consider whether the heat is advantageous to the process. For example, when near the 5:1 pressure ratio, it may not be appropriate to intercool if the compressed stream will subsequently require preheating as it would with the process air stream of an MCFC or SOFC system.

**Humidification/Dehumidification:** Water often is added or removed in fuel cell systems to promote or prevent certain chemical reactions. For some reactions, excess water can help to drive the reaction, while too much requires larger equipment and can even reduce the yield of a reaction or decrease the performance of a fuel cell. Excess water often is utilized to increase the yield of reforming reactions and the water gas shift.

In a natural gas fueled PAFC, water is condensed out of the fuel stream going to the fuel cell to increase the partial pressure of hydrogen. In a coal gasification MCFC, water often is added to the fuel stream prior to the fuel cell to prevent soot formation. The addition of excess steam not only prevents the soot formation, but also causes a voltage drop of approximately 2 mV per each percentage point increase in steam content (45). The use of zinc ferrite hot gas cleanup can aggravate the soot formation problem because of the catalytic effect of the sorbent on carbon formation, and requires even higher moisture levels (46).

Maintaining the proper quantity of water within a PEFC is very important for proper operation. Too much, and the cell will flood; too little, and the cell membrane will dehydrate. Both will severely degrade cell performance. The proper balance is achieved only by considering water production, evaporation, and humidification levels of the reactant gases. Achieving the proper level of humidification is also important. With too much humidification, the reactant gases will be diluted with a corresponding drop in performance. The required humidification level is a complex function of the cell temperature, pressure, reactant feed rates, and current density. Optimum PEFC performance is achieved with a fully saturated, yet unflooded membrane (47).

### 9.2.6 Concluding Remarks on System Optimization

System design and optimization encompass many questions, issues, and trade-offs. In the process of optimizing a power plant design, the engineer will address the selection of fundamental processes, component arrangements, operating conditions, fuel cell and bottoming cycle technologies and associated power production split, system integration, and capital and life cycle costs. The design will be governed by criteria such as output, weight, fuel basis, emissions, and cost objectives. Site and application specific criteria and conditions may strongly influence the cycle design criteria and resulting design.

The objective of this system optimization discussion was not to present a detailed review of the subject of optimization, but simply to present select issues of system optimization as they apply to fuel cell power systems.

### 9.3 Fuel Cell System Designs

The following five cycles are examples of current fuel cell offerings that reflect manufacturers' anticipated commercialization plans. These cycles are based on information available in relevant literature and may differ from the ultimate size of the commercial offering.

#### 9.3.1 Natural Gas Fueled PEFC System

A natural gas PEFC power plant configuration is shown in Figure 9-7 and is a slight simplification of a cycle published in 1997 by a Ballard Researcher (48). In light of the PEFC sensitivity to CO, CO<sub>2</sub> and methane, the fuel processing represents a significant portion of the cycle. Natural gas fuel enters a fuel compressor and a fuel cleanup device. (The reference document does not describe the cleanup device, but it is assumed to be a sulfur polisher to prevent poisoning of the fuel cell catalyst.) The cleaned gas is mixed with water in a vaporizer, which evaporates the liquid water into water vapor with waste heat from the reformer. This humidified fuel is reformed in the steam reformer. Because natural gas reformat is high in CO, the reformat is sent to a shift converter and selective oxidizer to reduce the CO to 10 to 50 ppm. This hydrogen rich/carbon monoxide lean fuel is fed to the PEFC stack where it reacts electrochemically with compressed air.

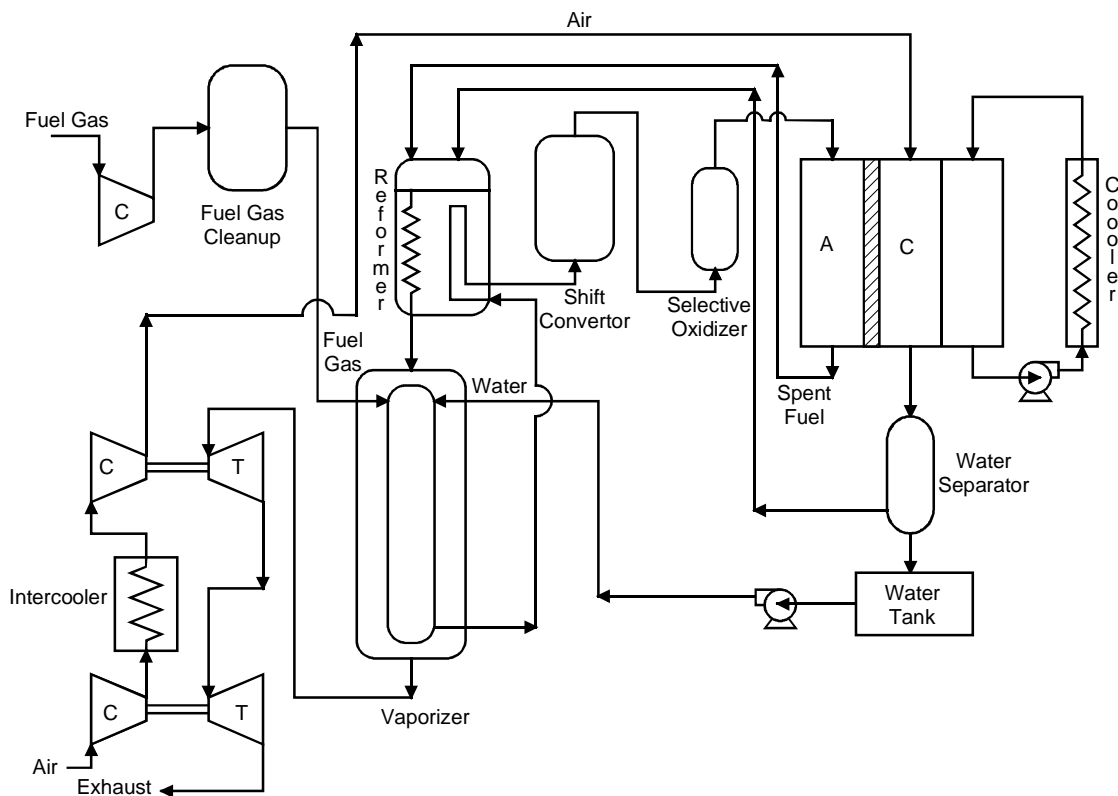


Figure 9-7 Natural Gas Fueled PEFC Power Plant

Ambient air is compressed in a turbocharger, powered by the expansion of the hot pressurized exhaust gases. Following this first compression stage, the air is intercooled by a fin fan air cooler and fed into a second turbocharger. The high-pressure air is fed directly to the PEFC

stack. The fuel cell water product is liberated to the oxidant gas stream. The spent oxidant stream exits the fuel cell where a water separator removes much of this water, which is subsequently used to humidify the fuel gas prior to the entering the reformer. The spent oxidant and fuel streams are combusted in the reformer burner to provide heat for the endothermic reforming reactions. The reformer exhaust also provides heat to the vaporizer. Finally, the residual heat and pressure of this exhaust stream are used in the turbochargers to drive the air compressor.

The fuel cell itself liberates heat that can be utilized for space heating or hot water. The reference article did not list any operating conditions of the fuel cell or of the cycle. The PEFC is assumed to operate at roughly 80°C. Another recent article (49) published by Ballard shows numerous test results that were performed at 3 to 4 atmospheres where fuel utilizations of 75 to 85% have been achieved. Performance levels for an air fed PEFC are now in the range of 180 to 250 mW/cm<sup>2</sup>. Ballard Power Systems has performed field trials of 250 kW systems with select utility partners. Commercial production of stationary power systems is anticipated for the year 2002. Similarly sized transportation cycles also are anticipated for commercial production in the same year.

### **9.3.2 Natural Gas Fueled PAFC System**

IFC has been marketing the PC25, a 200 kW atmospheric PAFC unit, since 1992. Details of this commercial cycle are proprietary and not available for publication. In order to discuss an example PAFC cycle, a pressurized (8 atm) 12 MW system will be presented (50). This cycle is very similar to the 11 MW IFC PAFC cycle that went into operation in 1991 in the Tokyo Electric Power Company system at the Goi Thermal Station, except that two performance enhancements have been incorporated. Limited data are available regarding the Goi power plant. However, it is understood that the average cell voltage is 750 mV and the fuel utilization is 80% (51). The enhanced 12 MW cycle presented here utilizes values of 760 mV and 86%. This enhanced cycle (Figure 9-8) is discussed below with selected gas compositions presented in Table 9-6.

Natural gas (stream 100) is supplied at pressure and contains sulfur odorants for leak detection. A small hydrogen-rich recycle stream (stream 117) is mixed with the natural gas to hydrolyze the sulfur compounds to facilitate sulfur removal. The fuel stream (stream 102) is heated to 299°C (570°F) before entering the sulfur removal device. Superheated steam (stream 1) is mixed with the heated fuel to provide the required moisture for the reforming and the water gas shift reactions. The humidified stream (stream 105) is heated to approximately (705°C) 1300°F before entering the reformer. The effluent fuel stream (stream 107) leaves the reformer at approximately 760°C (1400°F) and is cooled in the heat exchanger used to preheat the humidified natural gas stream. This stream (stream 108) enters the high temperature shift converter (HTSC) at approximately 360°C (680°F), while leaving (stream 109) at about 415°C (780°F). The HTSC effluent is cooled in two heat exchangers before proceeding to the low temperature shift converter. A two-stage approach is utilized, allowing the HTSC to proceed at a faster rate, while the LTSC yields higher hydrogen concentrations.

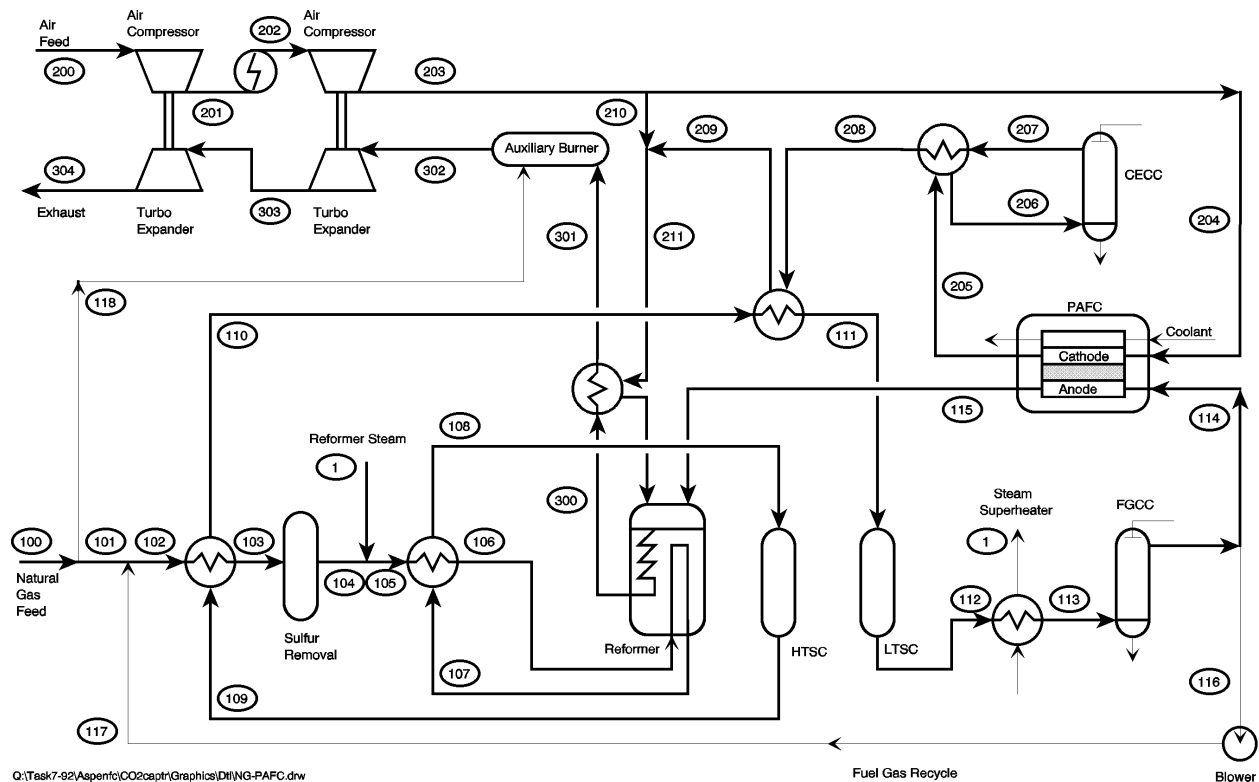


Figure 9-8 Natural Gas fueled PAFC Power System

Table 9-6 Stream Properties for the Natural Gas Fueled Pressurized PAFC

Strm No.	Description	Temp. C	Press. atm	Mole Flow Kgmol/hr	Mass Flow kg/hr	MW	Ar %	CH4 %	C2H6 %	CO %	CO2 %	H2 %	H2O %	N2 %	O2 %	Total %
1	Reformer Steam	243.3	10.00	418.8	7,545	18.02							100.0			100.0
100	NG Feed	15.6	13.61	115.1	1,997	17.34		90.0	5.0					5.0		100.0
106	Reformer Feed	712.8	9.93	562.6	9,846	17.50		18.3	1.0	trace	1.0	4.0	74.5	1.1		100.0
107	Reformer Effluent	768.3	9.59	755.9	9,846	13.03		2.4	trace	7.1	6.5	46.3	37.0	0.8		100.0
112	LTSC Effluent	260.0	8.72	755.9	9,846	13.03		2.4		0.5	13.1	52.9	30.4	0.8		100.0
114	Anode Feed	60.6	8.55	506.6	5,557	10.97		3.3		0.7	18.3	74.5	2.0	1.1		100.0
115	Anode Exhaust	207.2	7.95	181.4	4,901	27.02		9.3		1.9	51.2	28.8	5.7	3.1		100.0
118	NG to Aux Burner	15.6	13.61	1.59	27.5	17.34		90.0	5.0					5.0		100.0
200	Air Feed	15.6	1.00	1,156.5	33,362	28.85	0.9				trace		1.1	77.2	20.7	100.0
204	Cathode Feed	192.8	8.27	1,120.8	32,332	28.85	0.9				trace		1.1	77.2	20.7	100.0
205	Cathode Exhaust	207.2	8.09	1,283.4	32,987	25.70	0.8				trace		26.3	67.5	5.4	100.0
208	Cath. Gas to Heat Exch.	151.7	7.85	1,045.3	28,697	27.45	1.0				trace		9.5	82.8	6.7	100.0
209	Cath. Gas to Ref. Burner	243.9	7.81	1,045.3	28,697	27.45	1.0				trace		9.5	82.8	6.7	100.0
211	Cath. Gas to Heat Exch.	242.2	7.81	1,081.0	29,727	27.50	1.0				trace		9.2	82.6	7.1	100.0
301	Reformer Exhaust	380.6	7.71	1,234.6	34,629	28.05	0.9				9.2		15.9	72.8	1.2	100.0
302	Aux. Burner Exhaust	410.6	7.68	1,236.2	34,656	28.03	0.9				9.3		16.1	72.7	1.0	100.0
304	Exhaust	180.0	1.03	1,236.2	34,656	28.03	0.9				9.3		16.1	72.7	1.0	100.0

The LTSC effluent (stream 112) is utilized to superheat the steam required for the reformer and water gas shift reactions. The saturated steam sent to the superheater is supplied by the fuel cell water cooling circuit. The cooled stream (stream 113) is further cooled in a fuel gas contact

cooler (FGCC) to remove the excess moisture levels. This raises the partial pressure of hydrogen in the fuel before entering the fuel cell. Some of the hydrogen-rich fuel is recycled back, as mentioned previously, to the incoming natural gas, while the majority of the fuel (stream 114) proceeds to the fuel cell anode. Approximately 86% of the hydrogen in the fuel stream reacts in the fuel cell, where the hydrogen donates an electron and the resulting proton migrates to the cathode, where it reacts with oxygen in the air to form water. Key cell operating parameters are summarized in Table 9-7. The overall performance is summarized in Table 9-8. The spent fuel is combusted in the reformer burner and supplies heat for the endothermic reforming reactions.

**Table 9-7 Operating/Design Parameters for the NG fueled PAFC**

<b>Operating Parameters</b>	<b>Value</b>
Volts per Cell (V)	0.76
Current Density (mA/cm <sup>2</sup> )	320
No of stacks	12
Cell Operating Temp. (°C)	207
Cell Outlet Pressure (atm)	8.0
Overall Fuel Utilization (%)	86.2
Overall Oxidant Utilization (%)	70.0
DC to AC Inverter efficiency	97.0%
Auxiliary Load	4.2%

**Table 9-8 Performance Summary for the NG fueled PAFC**

<b>Performance Parameters</b>	<b>Value</b>
LHV Thermal Input (MW)	25.42
Gross Fuel Cell Power (MW)	
Fuel Cell DC Power	13.25
<u>Inverter Loss</u>	<u>(0.40)</u>
Fuel Cell AC Power	12.85
Auxiliary Power	0.54
Net Power	12.31
Electrical Efficiency (% LHV)	48.4
Electrical Efficiency (% HHV)	43.7
Heat Rate (Btu/kWh, LHV)	7,050

Note: The net HHV efficiency for the Goi Thermal Power Station is 41.8% (HHV) (1).

Ambient air (stream 200) is compressed in a two-stage compressor with intercooling to conditions of approximately 193°C (380°F) and 8.33 atmospheres (122.4 psia). The majority of the compressed air (stream 203) is utilized in the fuel cell cathode; however, a small amount of

air is split off (stream 210) for use in the reformer burner. The spent oxidant (stream 205) enters a recuperative heat exchange before entering a cathode exhaust contact cooler, which removes moisture to be reused in the cycle. The dehumidified stream (stream 207) is again heated, mixed with the small reformer air stream, and sent to the reformer burner (stream 211). The reformer burner exhaust (stream 300) preheats the incoming oxidant and is sent to the auxiliary burner, where a small amount of natural gas (stream 118) is introduced. The amount of natural gas required in the auxiliary burner is set so the turbine shaft work balances the work required at the compressor shaft. The cycle exhaust (stream 304) is at approximately 177°C (350°F).

Some of the saturated steam generated by the fuel cell cooling water is utilized to meet the reformer water requirements. Approximately 3,800 kg/hr (8,400 lb/hr) of 12.2 atmospheres (180 psi) saturated steam is available for other uses.

Cycle performance is summarized in Table 9-8. The overall net electric conversion efficiency is 43.7% based on HHV input, or 48.4% on LHV.

### 9.3.3 Natural Gas Fueled Internally Reformed MCFC System

Fuel Cell Energy expects to have its initial market entry MCFC power systems available in the year 2001, with mature megawatt class units projected to be available in 2004. These units will be produced in various sizes. Preliminary cycle information was received from FCE for a nominal 3 MW power plant. This cycle is presented in Figure 9-9 and is described below.

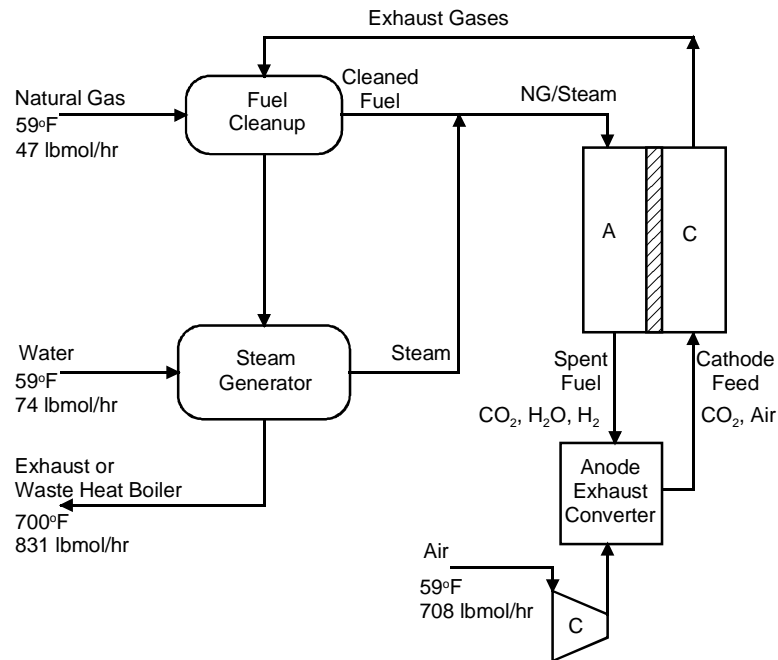


**Figure 9-9 Natural Gas Fueled MCFC Power System**



Natural gas is cleaned of its sulfur contaminants in a fuel cleanup device. Steam is added to the fuel stream prior to being fed to the internally reforming fuel cell. The fuel reacts electrochemically with the oxidant within the fuel cell to produce 3 MW of dc power.

The spent fuel is completely combusted in the anode exhaust converter. This flue gas mixture is fed directly to the fuel cell cathode. The cathode exhaust has significant usable heat, which is utilized in the fuel cleanup and in steam generation. The residual heat can be utilized to heat air, water, or steam for cogeneration applications. Design parameters for the IR-MCFC are presented in Table 9-9. Overall performance values are presented in Table 9-10.

**Table 9-9 Operating/Design Parameters for the NG Fueled IR-MCFC**

Operating Parameters	Value
Volts per Cell (V)	unknown
Current Density (mA/cm <sup>2</sup> )	unknown
Operating Temperature (°C)	unknown
Cell Outlet Pressure (atm)	1.0
Fuel Utilization (%)	78.%
Oxidant Utilization (%)	75.%
Inverter Efficiency	95.%

**Table 9-10 Overall Performance Summary for the NG Fueled IR-MCFC**

Performance Parameters	Value
LHV Thermal Input (MW)	4.8
Gross Fuel Cell Power (MW)	
Fuel Cell DC Power	3.0
<u>Inverter Loss</u>	<u>(0.15)</u>
Fuel Cell AC Power	2.85
Auxiliary Power (MW)	0.05
Net Power (MW)	2.80
Electrical Efficiency (% LHV)	58%
Heat Rate (Btu/kWh, LHV)	5,900

### 9.3.4 Natural Gas Fueled Pressurized SOFC System

This natural gas fuel cell power system is based on a pressurized TSOFC combined with a combustion turbine developed by Siemens Westinghouse<sup>53</sup> (52). Most TSOFC power plant concepts developed to date have been based on atmospheric operation. However, as shown in

<sup>53</sup>. The referenced Siemens Westinghouse publication presented the cycle concept and overall performance values. Neither specific stream information nor assumptions were presented. The stream data and assumptions presented here were developed by Parsons. The stream data were developed using an ASPEN simulation which yielded performance numbers in general agreement with the publication.

Section 8, the cell voltage increases with cell pressure. Thus, operating with an elevated pressure will yield increased power and efficiency for a given cycle. In addition, the use of a pressurized SOFC will also allow integration with a combustion turbine. The combustion turbine selected for integration by Siemens Westinghouse is the unique 1.4 MW Heron reheat combustion turbine, a proposed product of Heron (53).

A flow diagram for the natural gas fueled 4.5 MW class cascaded<sup>54</sup> TSOFC power cycle is presented in Figure 9-10. A brief process description is given below, followed by a performance summary. Selected state point values are presented in Table 9-11.

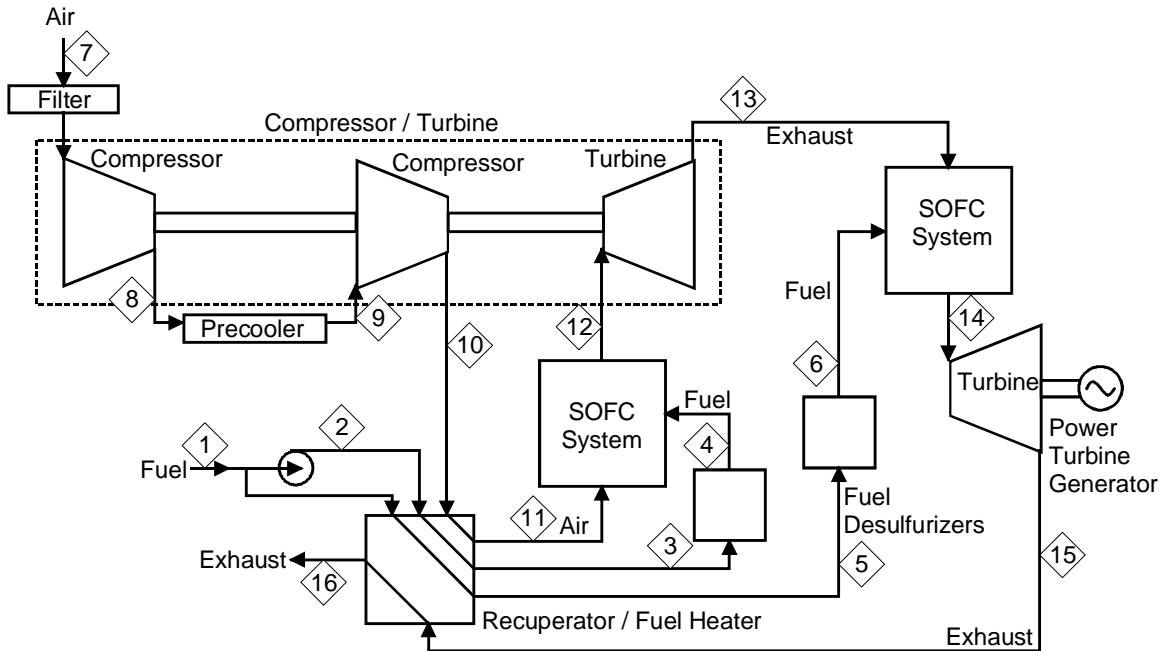


**Figure 9-10 Schematic for a 4.5 MW Pressurized SOFC**

<sup>54</sup>. The term "cascaded" fuel cells is used here to describe a fuel cell system where the exhaust of a high-pressure fuel cell is utilized as an oxidant feed stream in a low-pressure fuel cell after passing through an expander.

**Table 9-11 Stream Properties for the Natural Gas Fueled Pressurized SOFC**

Strm No.	Description	Temp C	Press. atm	Mass Flow kg/hr	Mole Flow kgmol/hr	MW	Ar %	CH4 %	CO2 %	H2O %	N2 %	O2 %	Total %
1	Fuel feed	15	8.85	508	30.9	16.44		97.4	0.4		0.9		100.0
2	Pressurized Fuel	21	9.53	508	30.9	16.44		97.4	0.4		0.9		100.0
3	Heated HP Fuel	399	9.42	508	30.9	16.44		97.4	0.4		0.9		100.0
4	Cleaned HP Fuel	399	9.32	281	17.1	16.44		97.4	0.4		0.9		100.0
5	Heated LP Fuel	399	9.42	227	13.8	16.44		97.4	0.4		0.9		100.0
6	Cleaned LP Fuel	399	3.13	227	13.8	16.44		97.4	0.4		0.9		100.0
7	Air Feed	15	0.99	18,536	642.3	28.86	0.9		trace	1.0	77.2	20.8	100.0
8	Compressed Air	135	2.97	18,536	642.3	28.86	0.9		trace	1.0	77.2	20.8	100.0
9	Intercooled Air	27	2.69	18,351	635.9	28.86	0.9		trace	1.0	77.2	20.8	100.0
10	HP Air	160	8.80	18,351	635.9	28.86	0.9		trace	1.0	77.2	20.8	100.0
11	Heated Air	555	8.66	18,167	629.5	28.86	0.9		trace	1.0	77.2	20.8	100.0
12	HP FC Exhaust	860	8.39	18,448	646.5	28.53	0.9		2.7	6.2	75.2	15.0	100.0
13	HPT Exhaust	642	3.11	18,631	653.1	28.53	0.9		2.7	6.2	75.2	15.0	100.0
14	LP FC Exhaust	874	2.83	18,859	667.0	28.28	0.9		4.7	10.2	73.7	10.6	100.0
15	LPT Exhaust	649	1.01	18,859	667.0	28.28	0.9		4.7	10.2	73.7	10.6	100.0
16	Cycle Exhaust	258	1.00	19,044	673.4	28.28	0.9		4.6	10.1	73.7	10.7	100.0

Reference Source: (30).

The natural gas feed to the cycle (stream 1) is assumed to consist of 95% CH<sub>4</sub>, 2.5% C<sub>2</sub>H<sub>6</sub>, 1% CO<sub>2</sub>, and 1.5% N<sub>2</sub> by volume along with trace levels of sulfur odorants. The odorants must be reduced to 1 ppmv before entrance into the fuel cell to prevent performance and cell life deterioration. Because the desulfurization requires elevated temperatures, the fuel (streams 3 and 5) is fed through a heat exchanger that recovers heat from the fuel cell exhaust stream (stream 15). The hot desulfurized fuel stream (stream 4) enters the anodes of the high-pressure fuel cell at approximately 399°C (750°F) and 9.3 atmospheres. The fuel entering the low-pressure fuel cell (stream 6) is approximately 399°C (750°F) and 3.1 atmospheres. Ambient air (stream 7) is compressed to 3.0 atmospheres and 135°C (275°F) (stream 8), subsequently intercooled to 27°C (81°F) (stream 9), compressed again to 8.8 atmospheres and 160°C (320°F) (stream 10), and heated to 555°C (1031°F) prior to entering the high-pressure fuel cell cathode (stream 11).

The hot desulfurized fuel and the compressed ambient air are electrochemically combined within the high-pressure fuel cell module with fuel and oxidant utilizations of 78% and 20.3%, respectively. The SOFC high-pressure module was assumed to operate at 0.63 volts per cell. The spent fuel and air effluents of the Siemens Westinghouse tubular geometry SOFC are combusted within the module to supply heat required for the endothermic reforming reaction within the pre-reformer. The majority of the reforming takes place within the tubular fuel cell itself. The heat for internal reforming is supplied by the exothermic fuel cell reaction. A gas recirculation loop provides water for the internal reforming and to prevent soot formation.

The combusted air and fuel stream (stream 12) from the high-pressure fuel cell are expanded (stream 13) in a turbine expander. The work of this turbine is used to drive the low- and high-pressure air compressors. The reduced pressure exhaust stream (stream 13) is utilized as the low-pressure fuel cell oxidant stream. Although vitiated, it still has 15% oxygen. The low-pressure TSOFC operates at 0.62 volts per cell, and fuel and air utilizations of 78 and 21.9%, respectively. The spent air and fuel effluents are combusted and sent (stream 14) to the low-pressure power turbine. The turbine generator produces approximately 1.4 MW AC. The low-pressure exhaust (stream 15) still has a temperature of 649°C (1200°F) and is utilized to

preheat the fuel and oxidant streams. The resulting cycle exhaust stream (stream 16) exits the plant stack at approximately 258°C (496°F).

Operating parameters are summarized in Table 9-12. Cycle performance is summarized in Table 9-13. The overall net electric LHV efficiency is 67%.

The high efficiency of this TSOFC/Heron combined cycle is a result of synergism that exists between the SOFC and the Heron turbine. The TSOFC is able to fully replace the gas turbine combustor. That is, the waste heat of the SOFC exhaust is able to completely eliminate the need for the gas turbine combustor at the design point. As seen in Table 9-14, the Heron combustor design temperature of roughly 860°C (1580°F) is well within the TSOFC operating temperature range. Conversely, the Heron cycle is able to act as an efficient bottoming cycle without requiring a waste heat boiler or steam turbine. In simple cycle mode, the Heron cycle has a respectable LHV net electric efficiency of 42.9%. Together, the TSOFC/Heron cycle operates at an efficient 67%. Another advantage of this cycle is the low NO<sub>x</sub> emissions, because only the spent fuel is fired at the design point. The majority of the fuel reacts within the fuel cell. Overall NO<sub>x</sub> levels of less than 4 ppmv are expected.

**Table 9-12 Operating/Design Parameters for the NG Fueled Pressurized SOFC**

Operating Parameters	HP FC	LP FC
Volts per Cell (V)	0.63*	0.62*
Current Density (mA/cm <sup>2</sup> )	NA	NA
Cell Operating Temp. (°C)	1000*	1000*
Cell Outlet Pressure (atm)	8.4*	2.9*
FC Fuel Utilization (%)	78.0*	78.0*
FC Oxidant Utilization (%)	20.3*	21.9*
DC to AC Inverter Effic. (%)	96.0	
Generator Efficiency (%)	96.0*	
Auxiliary Load (% of gross)	1.0*	

Note: \* assumed by Parsons to reasonably match the reference paper.

**Table 9-13 Overall Performance Summary for the NG Fueled Pressurized SOFC**

Performance Parameters	Value
LHV Thermal Input (MW)	6.68
Gross Fuel Cell Power (MW)	
Fuel Cell DC Power	3.22
<u>Inverter Loss</u>	<u>(0.13)</u>
Fuel Cell AC Power	3.09
Gross AC Power (MW)	
Fuel Cell AC Power	3.09
<u>Turbine Expander</u>	<u>1.40</u>
Gross AC Power	4.49
Auxiliary Power	0.04
Net Power	4.45
Electrical Efficiency (% LHV)	66.6
Electrical Efficiency (% HHV)	60.1
Heat Rate (Btu/kWh, LHV)	5,120

**Table 9-14 Heron Gas Turbine Parameters**

Performance Parameters	Value
Compressor Air Flow (kg/h)	18,540
HP Combustor Temperature (°C)	861
LP Combustor Temperature (°C)	863
Compressor Pressure Ratio	8.8:1
Power Turbine Exhaust Temp. (°C)	620

The cycle discussed here is based on a Siemens Westinghouse publication for a 4.5 MWe plant. Recent information from Siemens Westinghouse, plans for commercialization of a scaled down 1 MWe version of this dual pressure TSOFC/Heron cycle. A 1 MW cycle was not available in the literature.

### 9.3.5 Natural Gas Fueled Multi-Stage Solid State Power Plant System

The Fuel Cell system presented below is based on an innovative solid state fuel cell system developed by U.S.DOE (54). Conventional fuel cell networks, in order to effectively use the supplied fuel, often employ fuel cell modules operating in series to achieve high fuel utilization<sup>55</sup> or combust the remaining fuel for possible thermal integration such as cogeneration steam or a steam bottoming cycle. Both of these conventional approaches utilize fuel cell modules at a single state-of-the-art operating temperature. In conventional fuel cell networks, heat exchangers are utilized between the fuel cell modules to remove heat so the subsequent fuel cell can operate at the desired temperature.

In the multi-stage fuel cell, the individual stages are designed to operate at different temperatures, so that heat exchangers are not required to cool the effluent gases between stages. Each stage is designed to accommodate the next higher temperature regime. In addition, the multi-stage fuel cell concept does not attempt to maximize the fuel utilization in each stage, but allows lower utilizations in comparison to the state-of-the-art design. The number of stages and the fuel utilization per stage in the multi-stage concept is a matter of design choice and optimization. An example of the fuel utilization for a five stage concept is presented in Table 9-15.

**Table 9-15 Example Fuel Utilization in a Multi-Stage Fuel Cell Module**

Stage	Fuel Balance for 100 Units of Fuel			Fuel Utilization	
	Fuel Feed	Fuel Out	Fuel Used	per Stage	Cumulative
1	100.0	81.0	19.0	19.0 %	19.0 %
2	81.0	62.0	19.0	23.5 %	38.0 %
3	62.0	43.0	19.0	30.6 %	57.0 %
4	43.0	24.0	19.0	44.2 %	76.0 %
5	24.0	6.0	18.0	75.0 %	94.0 %
Overall	100.0	6.0	94.0		94.0 %

A flow diagram for a natural gas fueled, 4 MW class, solid state fuel cell power cycle is presented in Figure 9-11. A brief process description is given below, followed by a performance summary. Selected state point values are presented in Table 9-16.

<sup>55</sup>. Current state-of-the-art SOFCs have fuel utilizations of 75 to 85%. By utilizing a second fuel cell in series, the total utilization could be theoretically increased to 93 to 98%. Note: Two cascaded fuel cells operating with a fuel utilization of 85% will have an overall utilization of 98%.  $1-(0.15)^2 = 1-0.02 = 0.98$  or 98%.

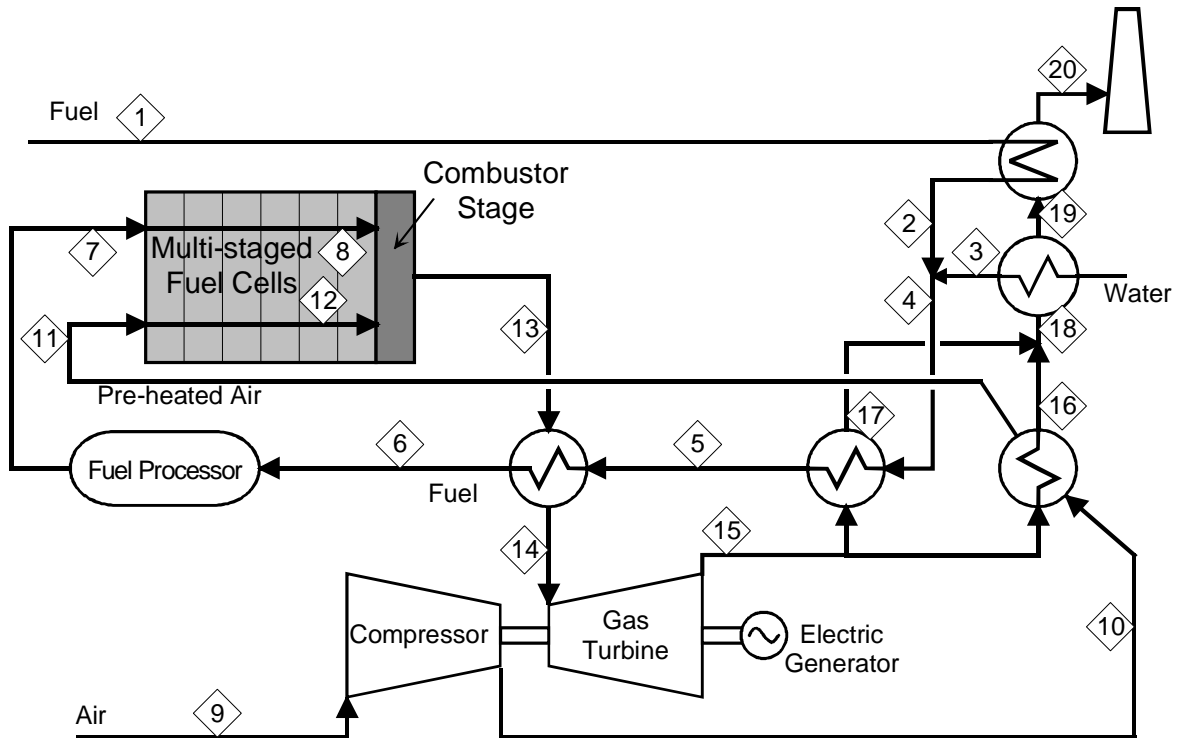


Figure 9-11 Schematic for a 4 MW Solid State Fuel Cell System

Table 9-16 Stream Properties for the Natural Gas Fueled Solid State Fuel Cell Power Plant System

Strm No.	Description	Temp. C	Press. atm	Mass Flow kg/hr	Mole Flow kgmol/hr	CH4 %	C2H6 %	C3H8+ %	CO %	CO2 %	H2 %	H2O %	N2 %	O2 %	Total %
1	Fuel feed	25	3.74	373	21.64	17.23	93.9	3.2	1.1	1.0			0.8		100
2	Heated fuel	84	3.67	373	21.64	17.23	93.9	3.2	1.1	1.0			0.8		100
3	Humidification water	275	3.93	614	34.09	18.02						100.0			100
4	Humidified fuel	192	3.67	987	55.73	17.71	36.5	1.3	0.4	0.4		61.2	0.3		100
5	Heated fuel	725	3.60	987	55.73	17.71	36.5	1.3	0.4	0.4		61.2	0.3		100
6	Heated fuel	725	3.60	987	55.73	17.71	36.5	1.3	0.4	0.4		61.2	0.3		100
7	Processed fuel	494	3.53	987	63.70	15.50	29.1	0.0	0.6	6.0	##	41.6	0.3		100
8	Spent Fuel	999	3.46	2,319	98.40	23.57	1.1		0.3	21.7	0.6	76.1	0.2		100
9	Air feed	25	1.00	7,484	259.42	28.85							79.0	21.0	100
10	Compressed air	175	3.47	7,484	259.42	28.85							79.0	21.0	100
11	Heated air	725	3.40	7,484	259.42	28.85							79.0	21.0	100
12	Spent air	999	3.33	6,149	217.69	28.25							94.1	5.9	100
13	FC exhaust	1119	3.33	8,471	315.78	26.83				7.2		24.7	65.0	3.2	100
14	Cooled exhaust	1119	3.33	8,471	315.78	26.83				7.2		24.7	65.0	3.2	100
15	Expanded exhaust	856	1.04	8,471	315.78	26.83				7.2		24.7	65.0	3.2	100
16	Cooled exhaust	328	1.02	6,438	239.99	26.83				7.2		24.7	65.0	3.2	100
17	Cooled exhaust	333	1.02	2,033	75.79	26.83				7.2		24.7	65.0	3.2	100
18	Combined exhaust	329	1.02	8,471	315.78	26.83				7.2		24.7	65.0	3.2	100
19	Cooled exhaust	152	1.01	8,471	315.78	26.83				7.2		24.7	65.0	3.2	100
20	Cycle exhaust	147	1.00	8,471	315.78	26.83				7.2		24.7	65.0	3.2	100

Reference Source: (55).

The natural gas feed to the cycle (stream 1) is typical of pipeline quality natural gas within the U.S. containing both sulfur odorants and higher hydrocarbons (C<sub>2</sub>H<sub>6</sub>, C<sub>3</sub>H<sub>8</sub>, etc.). The odorants

must be removed before entrance into the fuel cell to prevent performance and cell life deterioration. Higher hydrocarbons are assumed to be pre-reformed to hydrogen and carbon monoxide in a mild reformer<sup>56</sup> to avoid "sooting" or carbon deposition within the fuel cell. Because both the desulfurization and reforming require elevated temperatures, the fuel is fed through a series of heat exchangers that recover heat from the fuel cell exhaust stream (streams 13 to 20). Humidification steam (stream 3) is added to the fuel to provide the required moisture for the reforming and water-gas shift reactions. The heated and humidified fuel is desulfurized in a sorbent bed and partially reformed in a mild reformer catalyst bed. The balance of the reforming will occur between the stages of the multi-stage fuel cell module. The hot desulfurized and partially reformed fuel stream (stream 7) enters the fuel cell anode at approximately 500°C (930°F).

Ambient air (stream 9) is compressed to 3.5 atmospheres and 175°C (347°F) (stream 10), and subsequently heated to 500°C (932°F) prior to entering the fuel cell cathode (stream 11).

The hot processed fuel and the compressed ambient air are electrochemically combined within the fuel cell module. The fuel hydrocarbons still remaining after the mild reformer are reformed within the fuel cell. The heat required for the endothermic steam reforming reactions is supplied by the exothermic fuel cell reactions. The overall reactions are exothermic, and the fuel and oxidant temperatures rise to 999°C (1830°F) (streams 8 and 12). The fuel cell is capable of utilizing both H<sub>2</sub> and CO as fuel and has an overall fuel utilization of 94%.

The spent fuel (stream 8) and oxidant (stream 12) are combusted upon exiting the multi-stage fuel cell module. The resulting exhaust stream (stream 13) has a temperature of 1119°C (2046°F) before being cooled in a fuel heater and expanded to 1.04 atmospheres and 856°C (1573°F) (stream 15). This nearly atmospheric exhaust stream passes through several additional heat exchangers before leaving the plant stack at 147°C (300°F).

Operating parameters are summarized in Table 9-17. Cycle performance is summarized in Table 9-18. The overall net electric LHV efficiency is 80.1%.

One advantage of this concept is the elimination of heat exchangers between fuel cell modules. This will minimize the cycle complexity, cost, and losses. Another advantage of the concept is the minimization of unreacted fuel leaving the fuel cell. By having discrete fuel cell stages, each operating with its own voltage and current density, fuel utilization can be pushed to very high levels without hurting the performance of the entire module. The voltage and performance degradation resulting from the low fuel concentrations (high utilization) is isolated to the latter fuel cell stage(s) whereas a single fuel cell module, the entire fuel cell performance is degraded. Experiencing a reduced voltage, power, and efficiency level in the latter stages of a multi-stage module is acceptable because it minimizes the heat released in the combustion stage, which is largely passed to the bottoming cycle, which typically has an efficiency of roughly 40%. That is, 60% of the heat liberated to the bottoming cycle is wasted. Thus, the minimization of heat

---

<sup>56</sup>. A "mild reformer" is assumed to eliminate the higher hydrocarbons prior to entering the fuel cell to prevent sooting. This reformer is called a "mild reformer" to indicate that the reforming reactions are not pushed to completion, for it is desired that the methane be reformed in the fuel cell for better temperature management. Some of the methane, however, will be reformed with the higher hydrocarbons in the mild reformer.



passed to the bottom cycle is desirable, even at the "cost" of reduced efficiency in a fraction of the fuel cell module.

One obstacle for this concept is the uncertainty of fuel cell performance in a high utilization multi-stage concept. No testing has been performed to date utilizing a fuel cell in this manner. The exact loss of performance in the latter stages is not known. The reference document (56) for this multi-stage fuel cell concept did not attempt to specify the number of stages nor the fuel cell performance within each stage. Instead, an average fuel cell performance was assumed. This assumption may or may not represent of how a multi-stage fuel cell will perform. Additional development work of this novel and efficient concept is required.

**Table 9-17 Operating/Design Parameters for the NG fueled Multi-Stage Fuel Cell System**

Operating Parameters	Value
Volts per Cell (V)	0.800
Current Density (mA/cm <sup>2</sup> )	unspecified
Number of Stages	to be determined
Cell Operating Temperature (°C)	multiple temps (~650 to 850°C)
Cell Outlet Pressure (atm)	3.3
Overall Fuel Utilization (%)	94.0%
Overall Oxidant Utilization (%)	81.5%
Steam to Carbon Ratio	1.5:1
DC to AC Inverter efficiency	97.0%
Generator efficiency	98.0%
Fuel Cell Heat Loss (% of MW <sub>dc</sub> )	1.7%
Auxiliary Load	1.0%

**Table 9-18 Overall Performance Summary for the NG fueled Multi-Stage Fuel Cell System**

Performance Parameters	Value
LHV Thermal Input (MW)	4.950
Gross Fuel Cell Power (MW)	
Fuel Cell DC Power	3.579
<u>Inverter Loss</u>	<u>(0.108)</u>
Fuel Cell AC Power	3.471
Gross AC Power (MW)	
Fuel Cell AC Power	3.471
<u>Net Compressor/Expander</u>	<u>0.534</u>
Gross AC Power	4.005
Auxiliary Power	0.040
Net Power	3.965
Electrical Efficiency (% LHV)	80.10%
Electrical Efficiency (% HHV)	72.29%
Heat Rate (Btu/kWh, LHV)	4,260

### 9.3.6 Coal Fueled SOFC System (Vision 21)

The coal fueled solid oxide fuel cell power system presented here is based on work performed for the Department of Energy's Vision 21 Program (57) to develop of high efficiency, low emission, fuel flexible (including coal) processes. This cycle is a coal-fueled version of the Siemens Westinghouse TSOFC cycle presented in Section 9.3.5 consists of a Destec gasifier, cascaded SOFCs at two pressure levels, an integrated reheat gas turbine, and a reheat steam turbine bottoming cycle. The high-pressure portion of the cycle is designed to operate at 15 atmospheres to capitalize on a reasonable gas turbine expansion ratio and an advanced, but not unrealistic, fuel cell pressure. An operating pressure of 30 atmospheres would yield better fuel cell and gas turbine performance, but has been conservatively limited to 15 atmospheres; this is lower than the typical Destec design pressure. Higher pressure operation is feasible and would have better performance. The coal analysis is presented in Table 9-20.

A flow diagram for the coal fueled 500 MW class cascaded TSOFC power cycle is presented in Figure 9-12. A brief process description is given below, followed by a performance summary. Selected state point values are presented in Table 9-21.

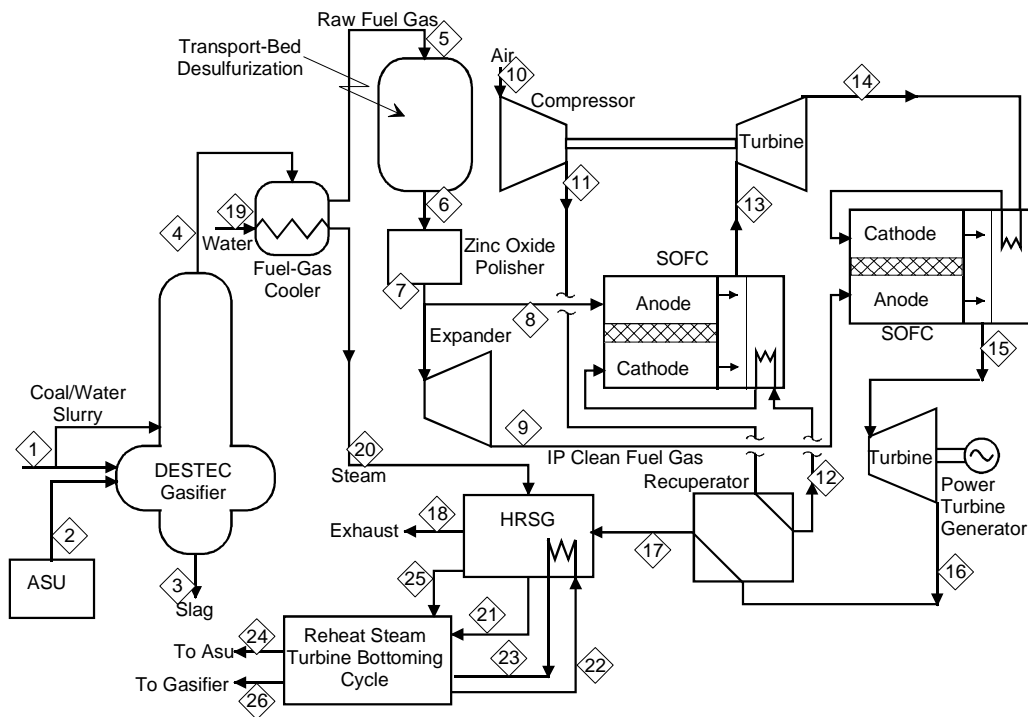


**Figure 9-12 Schematic for a 500 MW Class Coal Fueled Pressurized SOFC**

**Table 9-19 Stream Properties for the 500 MW Class Coal Gas Fueled Cascaded SOFC**

Strm No.	Description	Temp C	Press atm	Mass Flow t/h	Mole Flow kgmol/hr	MW	CH4 %	CO %	CO2 %	H2 %	H2O %	H2S %	N2+Ar %	NH3 %	O2 %	Total %
1	Coal Slurry Feed	18	23.8	151.2	-	NA										
2	ASU Oxygen	179	23.8	83.3	2,583	32.23							5.0		95.0	100.0
3	Slag Waste	93	19.1	11.6	-	NA										
4	Gasifier Effluent	1043	18.6	237.6	12,280	19.35	0.3	42.3	9.5	35.8	9.6	0.7	1.5	0.2		100.0
5	Raw Fuel Gas	593	17.6	237.6	12,280	19.35	0.3	42.3	9.5	35.8	9.6	0.7	1.5	0.2		100.0
6	Desulfurized Gas	593	16.6	236.2	12,280	19.23	0.3	42.3	9.6	35.8	10.3	trace	1.5	0.2		100.0
	Recycle to Gasifier	399	15.0	9.4	491	19.23	0.3	42.3	9.6	35.8	10.3	trace	1.5	0.2		100.0
7	Polished Gas	399	15.0	226.7	11,789	19.23	0.3	42.3	9.6	35.8	10.3	trace	1.5	0.2		100.0
8	HP Fuel Gas	399	15.0	108.8	5,659	19.23	0.3	42.3	9.6	35.8	10.3	trace	1.5	0.2		100.0
9	IP Fuel Gas	221	3.7	117.9	6,130	19.23	0.3	42.3	9.6	35.8	10.3	trace	1.5	0.2		100.0
10	Ambient Air	17	0.98	1,270.1	44,024	28.85					1.1		78.1		20.8	100.0
11	Compressed Air	409	15.1	1,146.2	39,732	28.85					1.1		78.1		20.8	100.0
12	Heated Air	579	15.0	1,146.2	39,732	28.85					1.1		78.1		20.8	100.0
13	HP SOFC Exhaust	979	14.7	1,255.1	43,181	29.07			6.9		7.1	trace	72.1	trace	13.9	100.0
14	HPT Exhaust	645	3.6	1,296.3	44,609	29.06			6.6		6.9	trace	72.3	trace	14.1	100.0
15	IP SOFC Exhaust	982	3.3	1,414.2	48,346	29.25			12.7		12.3	trace	66.9	0.1	8.0	100.0
16	IPT Exhaust	691	1.01	1,477.7	50,547	29.23			12.2		11.8	trace	67.4	0.1	8.6	100.0
17	Cooled Exhaust	573	0.99	1,477.7	50,547	29.23			12.2		11.8	trace	67.4	0.1	8.6	100.0
18	Cycle Exhaust	126	0.98	1,477.7	50,540	29.24			12.2		11.8		67.5		8.6	100.0
19	Gas Cooler Water	306	107.4	244.6	13,580	18.02					100.0					100.0
20	Gas Cooler Steam	317	107.4	244.6	13,580	18.02					100.0					100.0
21	HP Steam	538	99.6	301.4	16,730	18.02					100.0					100.0
22	Cold Reheat	359	29.3	298.4	16,563	18.02					100.0					100.0
23	Hot Reheat	538	26.4	298.4	16,563	18.02					100.0					100.0
24	ASU Steam	538	26.4	3.9	218	18.02					100.0					100.0
25	LP Steam	310	6.1	15.6	865	18.02					100.0					100.0
26	Gasifier Steam	307	5.4	32.0	1,774	18.02					100.0					100.0

Reference Source: (30)

The Destec entrained bed gasifier is fed both a coal water slurry (stream 1) and a 95% pure oxygen stream (stream 2) and operates with a cold gas conversion efficiency<sup>57</sup> of 84%. The gasifier fuel gas product (stream 4) is cooled in a radiant heater, which supplies heat to the bottoming cycle. The cooled fuel gas is cleaned (stream 6) in a hot gas desulfurizer at 593°C (1100°F) and a polisher (stream 7) at 399°C (750°F) to less than 1 ppmv of sulfur prior to entering the high-pressure fuel cell (stream 8). Part of the polished fuel is expanded to 3.7 atmospheres and 220°C (429°F) before being sent to the low-pressure fuel cell (stream 9).

Ambient air (stream 10) is compressed to 15.1 atmospheres and 409°C (275°F) (stream 11), and subsequently heated to 579°C (1075°F) prior to entering the high-pressure fuel cell cathode (stream 12).

The hot clean fuel gas and the compressed ambient air are electrochemically combined within the high-pressure fuel cell with fuel and oxidant utilizations of 90% and 24.5%, respectively. The SOFC module is set (sized) to operate at 0.69 volts per cell.<sup>58</sup> The spent fuel and air effluents of the SOFC are combusted within the module to supply heat for oxidant preheating. Unlike the natural gas case, the fuel does not require a pre-reformer with only 0.3% methane along with 36% hydrogen and 43% carbon monoxide. The carbon monoxide will be either water gas shifted to hydrogen or utilized directly within the fuel cell. A gas recirculation loop for the

<sup>57</sup>. Cold gas conversion efficiency is the ratio of the gasifier fuel gas total heating value [i.e., (heating value)(mass flow)] to that of the coal feed, [(heating value)(mass flow)].

<sup>58</sup>. Siemens Westinghouse provided TSOFC performance values for the HP and LP conditions, which Parsons incorporated into the systems analysis.

fuel cell has not been assumed, for water is not required for pre-reforming nor internal reforming.

The combusted air and fuel stream (stream 13) from the high-pressure fuel cell is expanded (stream 14) in a turbine expander. The work of this turbine is used to drive the low- and high-pressure air compressors. The reduced pressure exhaust stream (stream 14) is utilized as the low-pressure fuel cell oxidant stream. Although vitiated, it still has 14% oxygen. The low-pressure SOFC operates at 0.69 volts per cell and fuel and air utilizations of 90 and 34.7%, respectively (58). The spent air and fuel effluents are combusted and sent (stream 15) to the low-pressure power turbine. The turbine generator produces approximately 134 MWe. The low-pressure exhaust (stream 16) has a temperature of 691°C (1276°F) and is utilized to preheat the high-pressure oxidant. The resulting cooled exhaust stream (stream 17) still has a temperature of 573°C (1063°F) and is utilized to supply heat to a steam bottoming cycle.

Steam generated in the bottoming cycle is utilized in a reheat turbine to produce 118 MWe, as well as to supply the steam required by the air separation unit (ASU) and the gasifier coal slurry heater. The cycle exhaust exits the heat recovery steam generator at 126°C (259°F) and 0.98 atmospheres.

Operating parameters are summarized in Table 9-21. Cycle performance is summarized in Table 9-22. The overall cycle net HHV efficiency is 59%, and is very near the 60% Vision 21 goal.

**Table 9-20 Coal Analysis**

Coal Parameters	Value
Source	Illinois No. 6
Ultimate Analysis, (wt %, a.r.)	
Moisture	11.12
Carbon	63.75
Hydrogen	4.50
Nitrogen	1.25
Chlorine	0.29
Sulfur	2.51
Ash	9.70
<u>Oxygen (by difference)</u>	<u>6.88</u>
Total	100.00
HHV (Btu/lb)	11,666
LHV (Btu/lb)	11,129

**Table 9-21 Operating/Design Parameters for the Coal Fueled Pressurized SOFC**

Operating Parameters	HP FC	LP FC
Volts per Cell (V)	0.69	0.69
Current Density (mA/cm <sup>2</sup> )	312	200
Cell Operating Temp. (°F)	1794	1800
Cell Outlet Pressure (atm)	14.7	3.3
Overall Fuel Utilization (%)	90%	90%
Overall Oxidant Utilization (%)	18.7%	20.4%
DC to AC Inverter Efficiency	97.0%	
Generator Effic. - ST, GT	98.5%	
Generator Effic. - Expander	98.0%	
Auxiliary Load	7.2%	

**Table 9-22 Overall Performance Summary for the Coal Fueled Pressurized SOFC**

Performance Parameters	Value
LHV Thermal Input (MW)	875.8
Gross Fuel Cell Power (MW)	
Fuel Cell DC Power	310.9
<u>Inverter Loss</u>	<u>(9.3)</u>
Fuel Cell AC Power	301.6
Gross AC Power (MW)	
Fuel Cell AC Power	301.6
Combustion Turbine	133.7
Steam Turbine	118.1
<u>Fuel Expander</u>	<u>9.6</u>
Gross AC Power	562.9
Auxiliary Power	40.3
Net Power	522.6
Electrical Efficiency (% HHV)	59.7%
Electrical Efficiency (% LHV)	62.6%
Heat Rate (Btu/kWh, HHV)	5,720

This configuration has the potential to yield a very competitive cost of electricity. For example, for a fuel cell stack cost of \$300 to \$400/kW, it is estimated that the COE would range from 3.5 to 3.9 cents/kWh (Assuming 20% equity at 16.5%, 80% debt at 6.3%, and a levelized carrying charge of 0.12.)

### 9.3.7 Power Generation by Combined Fuel Cell and Gas Turbine Systems

In general, the oxidation of H<sub>2</sub>, CO, CH<sub>4</sub>, and higher hydrocarbons in fuel cells to produce power also produces reject heat. This heat arises from two sources:

- the entropy decrease,  $\Delta S$ , resulting from the overall oxidation reaction -- accompanying the usual decrease in the number of mols of gas, from reactants to products; and

- the loss in work, or a conversion of "reversible" work from the oxidation process to heat, due to irreversible processes occurring in the operation of the cell.

Heat from these two sources must be rejected from the fuel cell in order to maintain its temperature at a desired level. The heat can be removed and recovered by transferring it across a bounding surface to a heat transfer fluid, but care must be taken to maintain the cell at its desired temperature in this and adjacent regions. Alternatively, heat can be removed in one of the reactant streams passing through the cell -- most practically the air, oxidant stream.

Also in the operation of a practical fuel cell, some unburned fuel must remain in the combustion products leaving the cell in order to maintain a significant generated voltage throughout the cell.

In order to obtain the highest possible efficiency in electrical generation, both the thermal energy in the heat and the unburned fuel rejected from the cell must be recovered and converted into additional electrical energy. This can be accomplished by means of a heat engine cycle making use of a gas turbine operating in a regenerative Brayton or combined Brayton-Rankine cycle or a steam turbine operating in a Rankine cycle. The relative merits of these three heat engine cycles depend on their overall efficiencies and on the practical aspects of integration, operation, and cost of the power generation plant as a whole.

### 9.3.8 Heat and Fuel Recovery Cycles

Simple representations of three fuel cell based heat and fuel recovery cycles are shown in Figures 9-12, 9-13, and 9-16.

**Regenerative Brayton Cycle:** The regenerative Brayton cycle, Figure 9-13, shows a gas turbine compressor for the air flow to the cell. The flow then passes through a countercurrent, recuperative heat exchanger to recover heat from the combustion product gases leaving the gas turbine. The air and the fuel streams then pass into the cathode and anode compartments of the fuel cell(s). The air and fuel streams leaving the cell(s) enter the combustor where they mix and the residual fuel burns. The combustion products enter the turbine, expand, and generate additional power. The turbine exhaust gases pass through the recuperative exchanger to the stack.

The most significant variables characterizing the cycle are the fuel cell operating temperature range and the temperature and pressure at the gas turbine expander inlet. These variables are directly related to certain operating variables: the air/fuel ratio entering the fuel cell, the fraction of the fuel leaving the cell unburned, and the temperature difference between the combustion products and air at the high temperature end of the recuperative heat exchanger. The operating variables must be selected and controlled to allow effective operation of the fuel cell, combustor, and gas turbine. There may well be an optimal quantity of unburned fuel leaving the fuel cell, depending on the acceptable fuel cell operating temperature range and turbine inlet temperature.

Further insight can be gained from the idealized T - S diagram for the cycle, Figure 9-14. The compression of the air and fuel streams is represented here as a single adiabatic reversible (constant S) process in which the temperature of the gases rises above ambient. The heating of

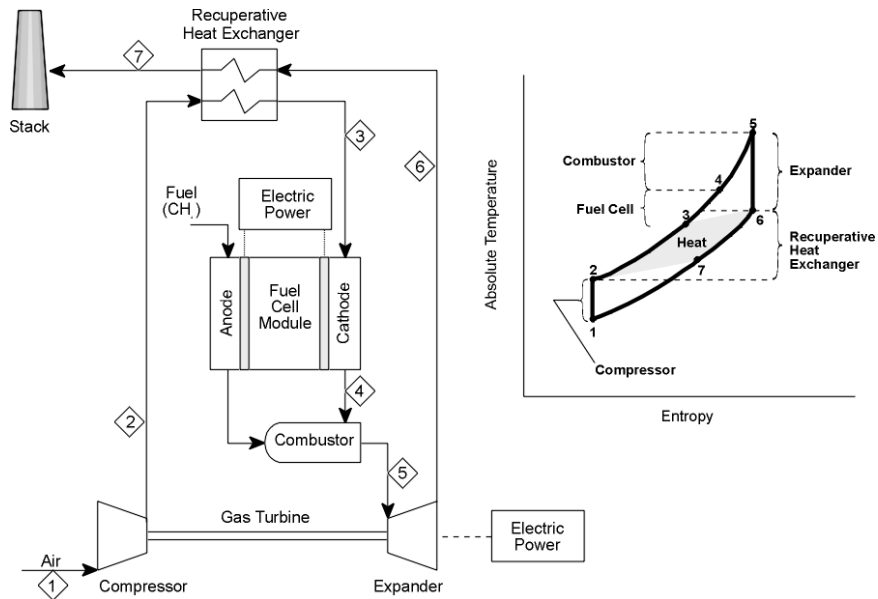


**Figure 9-13. Regenerative Brayton Cycle Fuel Cell Power System**

the air and also the fuel streams first in the recuperative exchanger, then in the fuel cell and finally in the combustor is assumed to occur along a single line of constant pressure. The subsequent expansion of the combustion gases in the turbine is also represented as an adiabatic reversible (constant  $S$ ) process in which the temperature of the gases drops to a value close to that of the gases entering the fuel cell. The pressure ratio (PR) of the turbine (and of the compressor) is therefore established by the turbine nozzle inlet temperature (NIT) and the fuel cell operating temperature. In general, the pressure ratio of a regenerative Brayton cycle is low compared with that of a combined Brayton-Rankine cycle. A low pressure ratio allows a low outlet temperature of the exhaust gases from the recuperative exchanger as heat is transferred to the air leaving the compressor (and possibly also the fuel) and consequently results in low heat rejection and a high cycle efficiency.

The practical aspects of the cycle involve the efficiencies of the gas compressors, the turbine expander, and the fuel cell; the pressure losses as the gases flow through the system; and the temperature differences and the difference in heat capacities of the streams flowing through the recuperative heat exchanger. Other aspects of the fuel cell operation must be considered in greater detail for the design and evaluation of the power system. These include the possible need for fuel reforming external to the cell and the recycle of combustion product streams to provide the steam required to carry out the reforming process, to avoid carbon deposition, and to provide  $H_2$  for effective cell operation.

**Table 9-23. Performance Calculations for a Pressurized, High Temperature Fuel Cell (SOFC) with a Regenerative Brayton Bottoming Cycle; Approach Delta T=30F**

COMPRESSOR EFF = 0.83                      n = number of moles  
 TURB EXPANDER EFF = 0.89                      Cp = specific heat  
 FUEL CELL EFF= 56.9                      Hf = heat of formation at standard conditions  
 CYCLE EFF= 82.1                      So = entropy at standard conditions

STREAM #	1	2	3	4	5	6	7	Cycle
p, PRESSURE, atm	1	1.48	1.48	1.48	1.48	1	1	
T, TEMPERATURE, K	298	337	1200	1311	1332	1216	352	
CH <sub>4</sub> , n	1	1	1	0.07	0	0	0	
CO, n								
H <sub>2</sub> , n								
CO <sub>2</sub> , n	0	0	0	0.93	1	1	1	
H <sub>2</sub> O, n	0	0	0	1.86	2	2	2	
O <sub>2</sub> , n	16.23	16.23	16.23	14.37	14.23	14.23	14.23	
N <sub>2</sub> , n	64.92	64.92	64.92	64.92	64.92	64.92	64.92	
SUM (n)	82.15	82.15	82.15	82.15	82.15	82.15	82.15	
SUM (nCp)	629.72	629.72	629.72	628.97	628.92	628.92	628.92	
SUM (nHf)	-17.9	-17.9	-17.9	-196.181	-209.6	-209.6	-209.6	
SUM (nSo)	3813.11	3813.11	3813.11	3811.99	3811.91	3811.91	3811.91	
GAMMA	1.350				1.351			
Q, HEAT, kcal/molCH <sub>4</sub>		0.0	543.5	0.0	-0.2	0.0	543.5	1086.8
W, WORK, kcal/molCH <sub>4</sub>		-24.4	0.0	109.1	0.0	72.7	0.0	157.4

The performance of a solid electrolyte fuel cell (SOFC) system (Hirschenhofer et al., 1994) operating with a regenerative Brayton bottoming cycle for heat and fuel recovery has been calculated. Table 9-23 illustrates the results. The work from the fuel cell burning CH<sub>4</sub> is assumed to be 60% the theoretical maximum; the corresponding fuel cell voltage is 0.63 volts. The efficiencies of the fuel and air compressors are 83%; and the expander of the turbine, 89%. It is assumed that the cell makes direct use of CH<sub>4</sub> fuel, or that oxidation and reforming are coincident; operation of the cell thus provides both the heat and the H<sub>2</sub>O required for CH<sub>4</sub> reforming. Pressure losses in the fuel cell, combustor, recuperative exchanger, and the ducts of the system are ignored.

The results of the performance calculations are summarized in Table 9-24. The efficiency of the overall power system, work output divided by the lower heating value (LHV) of the CH<sub>4</sub> fuel, is increased from 57% for the fuel cell alone to 82% for the overall system with a 30 F difference in the recuperative exchanger and to 76% for an 80 F difference. This regenerative Brayton cycle heat rejection and heat-fuel recovery arrangement is perhaps the simplest approach to heat recovery. It makes minimal demands on fuel cell heat removal and gas turbine arrangements, has minimal number of system components, and makes the most of the inherent high efficiency of the fuel cell.



**Table 9-24. Performance Computations for Various High Temperature Fuel Cell (SOFC) Heat Recovery Arrangements**

General Conditions

SOFC, solid oxide fuel cell  
 Operating temperature, 1700-1900 F  
 Fuel cell output: 60% of theoretical maximum from CH4 fuel  
 Gas turbine compressor, expander efficiencies: 83, 89%  
 Steam turbine efficiency: 90%

Notes

PR = pressure ratio of the gas turbine  
 NIT = nozzle inlet temperature of the turbine expander

Heat Recovery Arrangement	Work Output, %			Overall System Eff., %	Remarks
	Fuel Cell	Gas Turbine	Steam Turbine		
Regenerative Brayton Cycle	69.3	30.7	n/a	82.1	30 F Approach in Recuperative Exchanger Gas Turbine PR=1.48, NIT=1938 F
Regenerative Brayton Cycle	74.5	25.5		76.3	80 F Approach in Recuperative Exchanger Gas Turbine PR=1.35, NIT=1938 F
Combined Brayton-Rankine Cycle	75.3	10.3	14.3	75.6	Gas Turbine PR=12, NIT=2300 F Steam Turbine: 1600 psia, 1000 F, 1.5" Hg
Rankine Cycle	79.1		20.9	72.4	Steam Turbine: 1600 psia, 1000 F, 1.5" Hg

**Combined Brayton-Rankine Cycle:** The combined Brayton-Rankine cycle, Figure 9-14, again shows the gas turbine compressor for the air flow to the cell. This flow passes through a heat exchanger in direct contact with the cell; it removes the heat produced in cell operation and maintains cell operation at constant temperature. The air and fuel streams then pass into the cathode and anode compartments of the fuel cell. The separate streams leaving the cell enter the combustor and then the gas turbine. The turbine exhaust flows to the heat recovery steam generator and then to the stack. The steam produced drives the steam turbine. It is then condensed and pumped back to the steam generator.

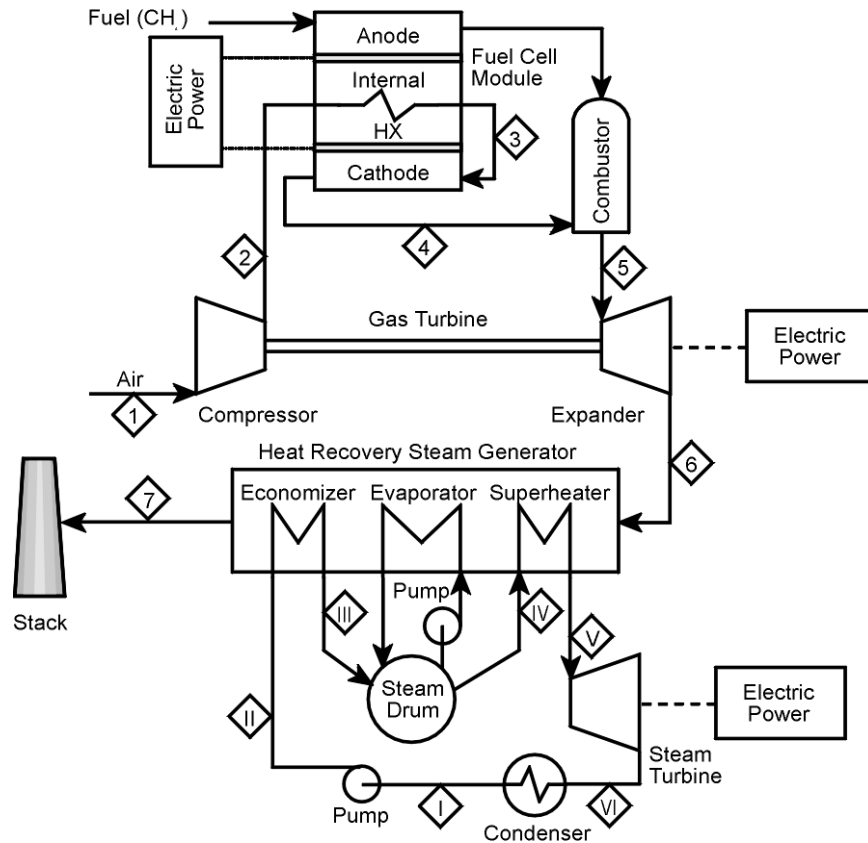


**Figure 9-14. Combined Brayton-Rankine Cycle Fuel Cell Power Generation System**

The air/fuel ratio entering the fuel cell and the fraction of the  $\text{CH}_4$  fuel consumed in the cell are selected to achieve the desired fuel cell operating temperature range and gas turbine NIT and PR. These are selected to correspond with those of a conventional, large-scale, utility gas turbine.

Further insight can be gained from an idealized T-S diagram for the cycle, Figure 9-15, in which both the Brayton and the Rankine cycles are illustrated. Both the pressure and the temperature increase during fuel and air compression in this combined cycle will be significantly greater than in the regenerative Brayton cycle described above. The heating of the air and fuel, the operation of the fuel cell, and the burning of the residual fuel are assumed to occur at constant pressure. The expansion of the combustion product gases in the gas turbine again is represented as an adiabatic, reversible (constant S) process. Next, heat is removed from these gases at nearly constant pressure in the heat recovery steam generator; and they pass out through the stack.

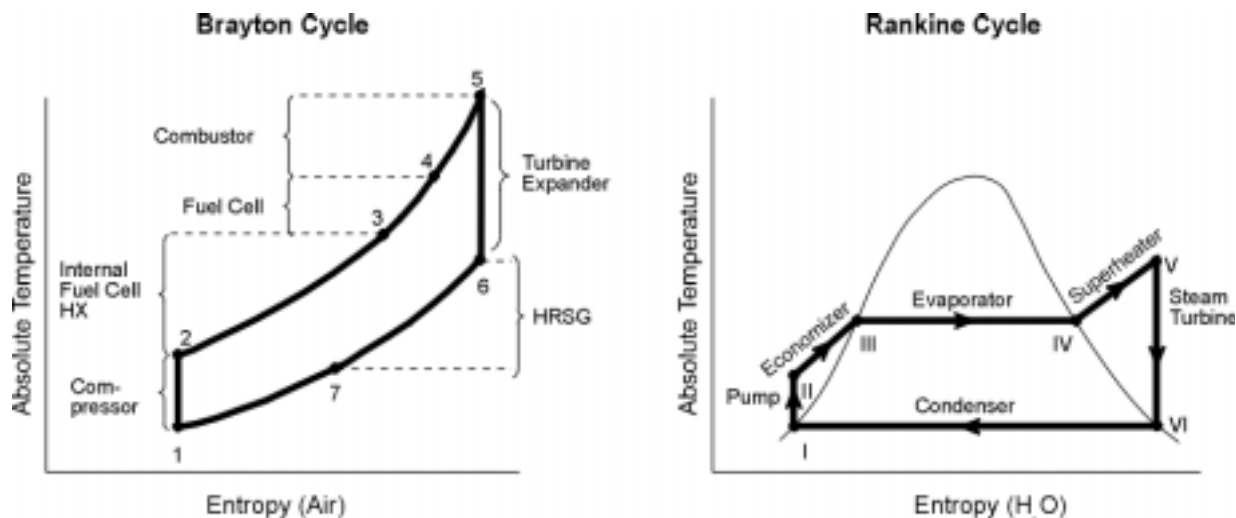


**Figure 9-15. Combined Brayton-Rankine Cycle Thermodynamics**

The Rankine cycle diagram placed adjacent the Brayton cycle in Figure 9-15 is indicated as a simple steam cycle with superheat, but no reheat and no multi-pressure steam generation. The thermodynamic advantage of the Rankine bottoming cycle is the lowered temperature of heat rejection, in the steam condenser, from the overall combined cycles.

The performance of a SOFC system with a Brayton-Rankine bottoming cycle for heat and fuel recovery has been calculated. Gas turbine compressor and expander efficiencies of 83% and 89% and a steam turbine efficiency of 90% have been assumed.

The significant operating conditions of the gas and steam turbines and the results of the computations are summarized in Table 9-24. The principal result is that the efficiency of the overall system, work output divided by the CH<sub>4</sub> LHV, is increased from 57% for the fuel cell alone to 75% for the overall system. This combined Brayton-Rankine cycle heat-fuel recovery arrangement is significantly more complex and less efficient than the simple regenerative Brayton cycle approach. It does, however, eliminate the requirement for a large, high temperature gas to gas heat exchanger.

The key link between the Brayton and the Rankine cycles is the heat recovery steam generator whose operation is illustrated by the temperature-heat (T-Q) plot in Figure 9-16. The temperatures of the gases and of the water, T, are plotted as a function of the heat, Q, transferred from the combustion product gases to the water-steam between their entrance and any point in the steam generator. The area between the temperature curves for the two flowing streams is an indication of the irreversibility, or loss in available work, resulting from the transfer of heat over a finite temperature difference. Reducing this area, moving the gas and steam curves closer, requires increased heat transfer surface area in the steam generator. Steam reheat and multi-pressure level heat recovery boilers are frequently proposed to minimize the loss in available work.

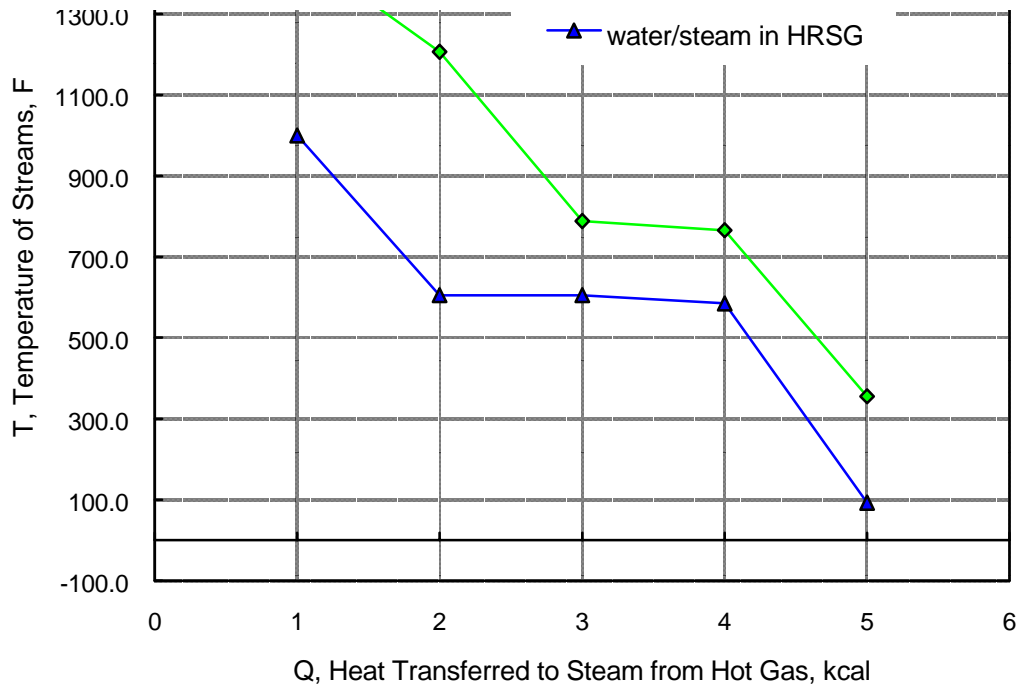
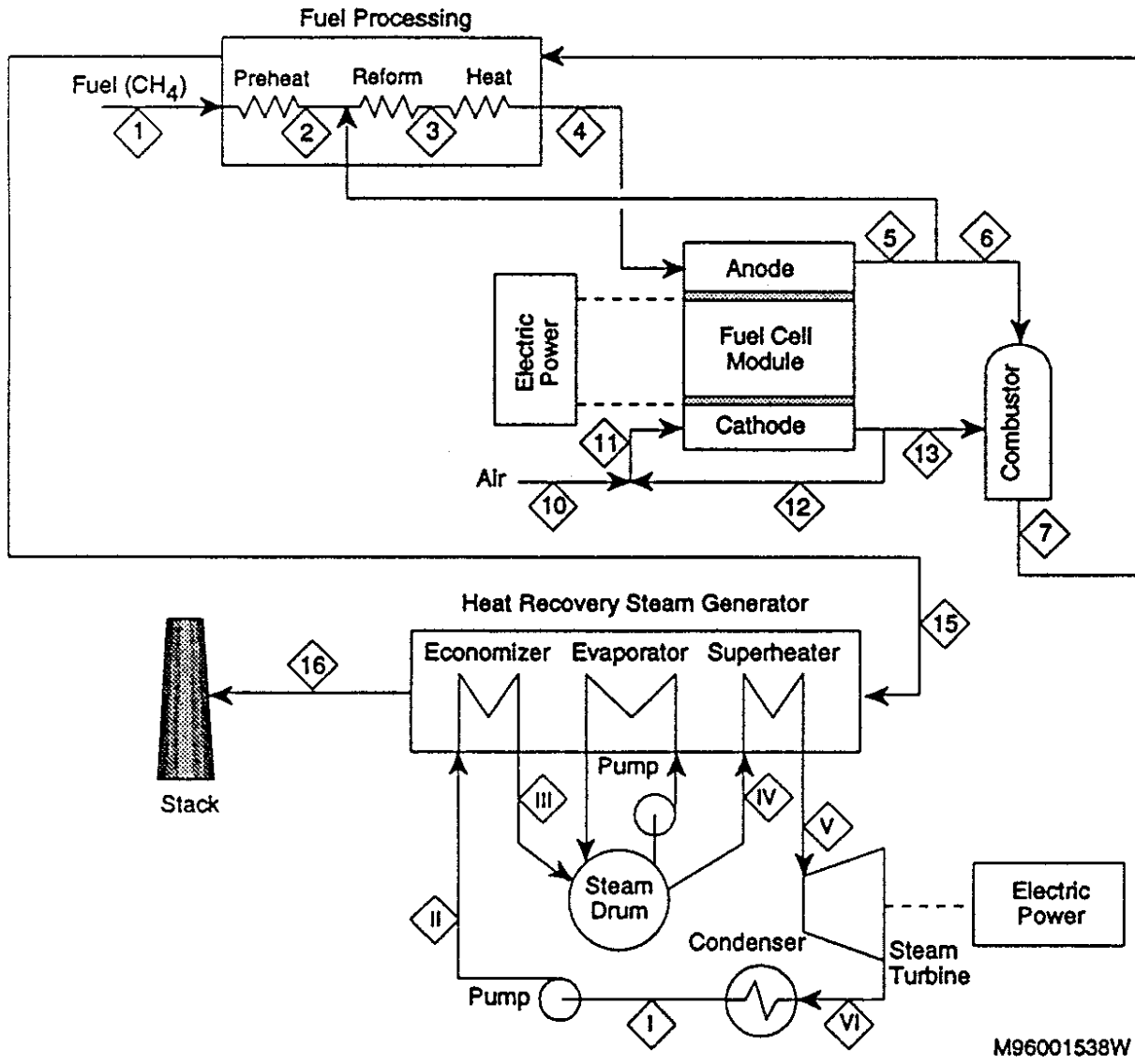


**Figure 9-16 T-Q Plot for Heat Recovery Steam Generator (Brayton-Rankine)**

**Rankine Cycle:** The fuel cell Rankine cycle arrangement in Figure 9-17 employs a heat recovery steam generator operating on the exhaust combustion product stream from the fuel cell and combustor at atmospheric pressure. This exhaust stream first provides the heat required to preheat and reform the  $\text{CH}_4$  fuel, providing  $\text{CO}$  and  $\text{H}_2$  at temperature to the fuel cell. Partially combusted fuel from the cell is recycled to provide the  $\text{H}_2\text{O}$  required for reforming the fuel. Depleted air from the cell exhaust is recycled to the air feed stream to raise its temperature to the desired value at the cell inlet. The operating conditions and the T - S diagram for the Rankine cycle are identical to those illustrated for the combined Brayton-Rankine cycle in Figure 9-15 and Table 9-24.

The results of the performance calculations for the fuel cell, Rankine cycle heat recovery system, summarized in Table 9-24, indicate that the efficiency of the overall system is increased from 57% for the fuel cell alone to 72% for the overall system. This Rankine cycle heat-fuel recovery arrangement is less complex but less efficient than the combined Brayton-Rankine cycle approach, and more complex and less efficient than the regenerative Brayton approach. It does, however, eliminate the requirement for a large, high temperature gas to gas heat exchanger. And in applications where cogeneration and the supply of heat is desired, it provides a source of steam.

The T - Q plot for the heat transfer processes involved in this fuel cell Rankine cycle arrangement is shown in Figure 9-18. Because heat is removed from the exhaust gases to heat and reform the  $\text{CH}_4$  fuel feed, the temperature of the hot gas entering the heat recovery steam generator in this



M96001538W

Figure 9-17 Fuel Cell Rankine Cycle Arrangement

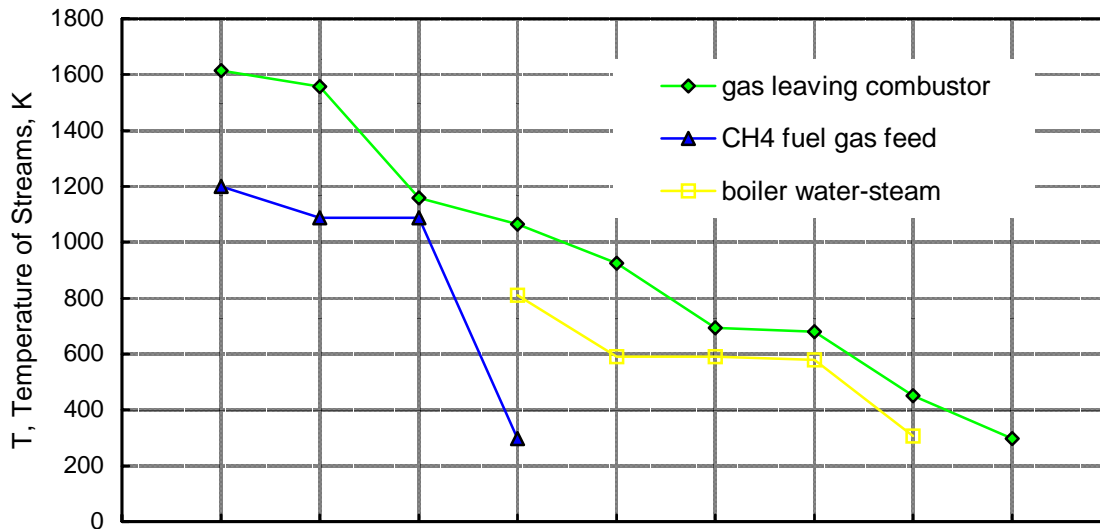


**Figure 9-18 T-Q Plot of Heat Recovery from Hot Exhaust Gas**

particular Rankine cycle fuel cell arrangement is significantly lower than in the previous combined Brayton-Rankine cycle arrangement. Increased surface area is, therefore, required in the heat recovery steam generator for this fuel cell Rankine cycle arrangement.

These three approaches to reject heat and exhaust fuel recovery with power generation apply primarily to the higher temperature, solid oxide (1800 F) and molten carbonate (1200 F), fuel cell systems operating on CH<sub>4</sub> fuel. The lower operating temperatures of the phosphoric acid (400 F) and polymer electrolyte (175 F) fuel cells severely limit the effectiveness of thermal cycle based power generation as a practical means of heat recovery.

All three of the heat recovery arrangements have calculated overall efficiencies greater than 70% as indicated in Table 9-24. None have been optimized in any sense -- in terms of efficiency, capital and operating costs, maintainability or availability. Each of the arrangements has its advantages and disadvantages. It appears, however, that the regenerative Brayton cycle has the advantage of greatest simplicity and highest potential overall efficiency over the combined Brayton-Rankine and Rankine cycle approaches.

The consideration of heat recovery and use in such fuel cell systems requires some consideration of heat generation and transfer within the cells of the system. Direct oxidation of CH<sub>4</sub> at the anode of the cell, if possible, would implement the overall process:



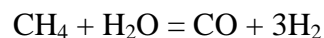
This reaction, having equal number of mols of gas reactants and products, has a negligible change in entropy and thus a negligible heat effect if carried out reversibly at constant temperature. The maximum work available from a fuel cell under these circumstances would then be approximately the enthalpy change of the reaction, i.e., the heat of combustion of the

CH<sub>4</sub>; the efficiency of the fuel cell power generation process could, therefore, approach 100%. However, work is lost and a corresponding quantity of heat is produced by irreversibilities both in fuel cell operation --

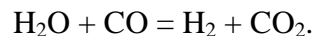
- the electrical resistance of the electrolyte to ion flow and of the electrodes, current collectors, and leads to electron flow;
- the kinetics of the processes involving reactants, ions, and electrons at the anode and cathode of the cell;
- the transport, or diffusion, of reactants within the anode and cathode chambers to the electrode;
- and also in overall system operation –
- the preheating of the air and fuel streams;
- the pretreating, or reforming, of the CH<sub>4</sub> fuel to provide more reactive H<sub>2</sub> and to prevent the deposition of carbon (C).

The heat resulting from these irreversibilities must then be removed in order to maintain the fuel cells at a desired operating temperature. Irreversibilities and the resulting quantity of heat produced can be reduced, in general, by increasing the active area of the fuel cells, heat exchangers, and fuel reformer; but increased equipment costs result.

In general, reforming of the CH<sub>4</sub> fuel with excess H<sub>2</sub>O outside the cell has been practiced both in molten carbonate and solid oxide fuel cell systems in order to produce H<sub>2</sub>, more reactive on a fuel cell anode, and to avoid the possible deposition of C. This reforming reaction



is associated with an increase in entropy and absorbs heat. Excess H<sub>2</sub>O produces additional H<sub>2</sub> and reduces the CO content of the reformed gases, which may adversely affect anode reactions, by the shift reaction



This reaction is thermally neutral. The heat absorbed in the CH<sub>4</sub> reforming reaction is released by the subsequent reaction of the H<sub>2</sub> product at the anode of the fuel cell. If, therefore, the reforming process can be carried out in close proximity to and in thermal contact with the anode process, the thermal neutrality of the overall CH<sub>4</sub> oxidation process can be approximated. And the heat removal and recovery process for the fuel cell system can deal merely with the heat produced by its operational irreversibilities.

Heat removal from fuel cells, and cell batteries, can be accomplished:

- directly through the flow of reactants to and products from them.
- indirectly through heat transfer surfaces in contact with the cell or included within a battery.

A specific fuel cell system is viewed here as having a fixed range of operating temperature between a maximum and minimum; heat must therefore be removed in such a manner to maintain the temperature within these limiting values. If heat is removed directly by reactant flows, then the quantity of flow must be adjusted so that inlet and outlet temperatures (as well as

the intermediate temperatures) of the cell and of the flow streams are within the permissible range. Practically, the air stream is adjusted to achieve this result, since the purpose of the fuel cell is to consume the fuel in the production of electrical energy. Increasing the fuel flow to remove heat from the cell increases the quantity of unburned fuel in the exhaust from the cell. If heat is removed from the fuel cell indirectly through adjacent or embedded surface, then the flow and temperature of the coolant stream can be selected somewhat independent of the cell operating temperature. But the distribution of heat transfer surface in the cell (or battery) and the rate of heat transfer across that surface must be carefully adjusted and controlled to maintain the temperature throughout the cell (or battery) within the prescribed temperature range.

The regenerative Brayton cycle, as presented, depends primarily on its fuel cell component for conversion of the fuel and thus for its overall efficiency. The gas turbine merely provides the means for recovery of the waste heat and residual fuel in the combustion product stream. The gas turbine operates, therefore, at a temperature only slightly elevated above that of the cell by the combustion of the residual fuel. The pressure ratio selected for the turbine in this regenerative cycle is determined by the ratio of the temperature of the gases leaving the auxiliary combustor to the temperature of the reactant gases entering the fuel cell. In general, for either molten carbonate or solid oxide cells, this selected pressure ratio will be less than two. The proposed method of cell cooling is air flow, which will be increased significantly, by a factor of 4-8 above that required for oxidation of the fuel. The feasibility of this cycle will depend on the availability of air compressor and turbine expander units with:

- the pressure ratio and temperature capability compatible with the fuel cell operation.
- a capacity appropriate to market applications.

The effectiveness of the regenerative Brayton cycle performance will depend on the efficiency of the fuel cell, compressor, and turbine units; the pressure loss of gases flowing through the system; the approach temperatures reached in the recuperative exchanger; and, most importantly, the cost of the overall system.

The combined Brayton-Rankine cycle depends on both the fuel cell and the gas turbine components for conversion of the fuel and thus for its overall efficiency. The extent of conversion of the fuel occurring in the fuel cell increases as the cell operating temperature and the range of coolant temperature rise increase. For this reason, the cycle as presented is based on indirect heat removal from the cell, heating the air stream temperature from the compressor outlet to the cell operating temperature. This provision maximizes the cell contribution to the energy output of the combined cycle. The PR and NIT of the turbine are those selected to match those of the current utility scale equipment -- a PR of 12 and an NIT of 2300 F -- resulting in a combined cycle efficiency of perhaps 45-50%, not considering the electrical energy output of and the fuel input to the fuel cell. The fuel combustion occurring in the combustor and overall air/fuel ratio is then determined by the combination of the cell and the turbine inlet temperatures.

The fuel cell Rankine cycle arrangement has been selected so that all fuel preheating and reforming are carried out external to the cell and air preheating is accomplished by mixing with recycled depleted air. The air feed flow is adjusted so that no heat transfer is required in the cell or from the recycled air. Consequently, the internal fuel cell structure is greatly simplified, and the requirement for a heat exchanger in the recycle air stream is eliminated.



## *Summary*

### Advantages, Disadvantages of Various Fuel Cell, Power Cycles

#### **Regenerative Brayton**

##### Advantages:

- simple cycle arrangement, minimum number of components.
- relatively low compressor and turbine pressure ratio, simple machines.
- relatively low fuel cell operating pressure, avoiding the problems caused by anode/cathode pressure differential and high pressure housing and piping.
- relatively low turbine inlet temperatures, perhaps 1950 F for solid oxide and 1450 F for molten carbonate fuel cell systems. Turbine rotor blade cooling may not be required.
- relatively simple heat removal arrangements in fuel cells, accomplished by excess air flow. No internal heat transfer surface required for heat removal.
- fuel conversion in cells maximized, taking full advantage of fuel cell efficiency.
- adaptability to small scale power generation systems.

##### Disadvantages:

- tailoring of compressor and turbine equipment to fuel cell temperature and cycle operating pressure required. (It is not clear to what extent available engine supercharging and industrial compressor and turbine equipment can be adapted to this application.)
- large gas to gas heat exchanger for high temperature heat recuperation required.
- efficiency and work output of the cycle sensitive to cell, compressor, and turbine efficiencies; pressure losses; and temperature differentials.

#### **Combined Brayton-Rankine**

##### Advantages:

- integrated plant and equipment available for adaptation to fuel cell heat recovery.
- high efficiency system for heat recovery.

##### Disadvantages:

- complex, multi component, large scale system for heat recovery.
- adaptation of existing gas turbine required to provide for air take off and return of hot depleted air and partially burned fuel.
- high pressure operation of the bulky fuel cell system required.
- precise balancing of anode and cathode pressures required to prevent rupture of fuel cell electrolyte.
- indirect heat removal required from fuel cells with compressed air, initially at low temperature, to enable significant conversion of the fuel flow in the cells.

#### **Rankine**

##### Advantages:

- ambient pressure operation within the fuel cell.
- heat recovery in a boiler, avoiding the high temperature gas to gas exchanger of a regenerative Brayton cycle.
- no gas turbine required, only fans for air and exhaust product gas flow.

- steam available for cogeneration applications requiring heat.

Disadvantages:

- inherently lower efficiency than regenerative Brayton and combined Brayton-Rankine cycles.
- requirement for cooling and feed water.
- greater complexity than regenerative Brayton cycle arrangement.

## 9.4 Fuel Cell Networks

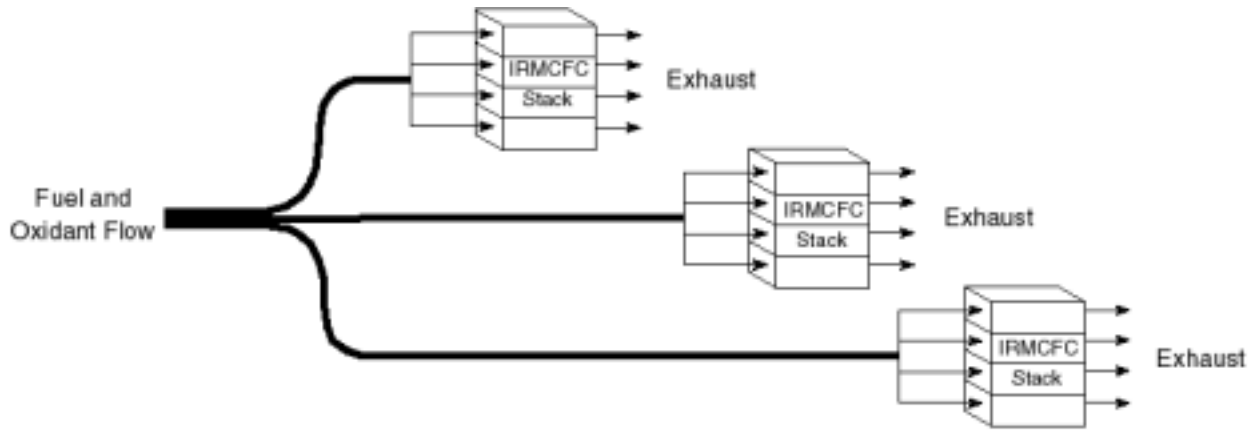
### 9.4.1 Molten Carbonate Fuel Cell Networks: Principles, Analysis and Performance

The U.S. Department of Energy's National Energy Technology Laboratory (NETL) sponsors the research and development of engineered systems which utilize domestic fuel supplies while achieving high efficiency, economy and environmental performance. One of the most promising electric power generation systems currently being sponsored by NETL is the molten carbonate fuel cell (MCFC).

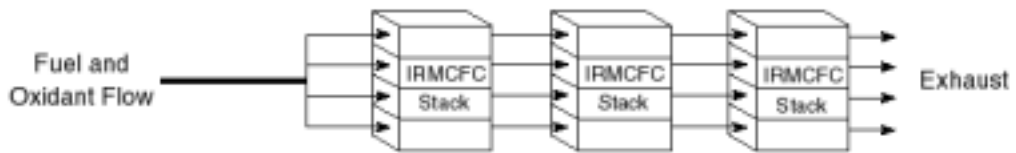
NETL looked at improving upon conventional MCFC system designs, in which multiple stacks are typically arranged in parallel with regard to the flow of reactant streams. As illustrated in Figure 9-19a, the initial oxidant and fuel feeds are divided into equal streams which flow in parallel through the fuel cell stacks.

In an improved design, called an MCFC network, reactant streams are ducted such that they are fed and recycled among multiple MCFC stacks in series. Figure 9-19b illustrates how the reactant streams in a fuel cell network flow in series from stack to stack. By networking fuel cell stacks, increased efficiency, improved thermal balance, and higher total reactant utilizations can be achieved. Networking also allows reactant streams to be conditioned at different stages of utilization. Between stacks, heat can be removed, streams can be mixed, and additional streams can be injected.

**Stacks in series approach reversibility.** MCFC stack networks produce more power than conventional configurations because they more closely approximate a reversible process. To illustrate this fact, consider Figure 9-20, which compares the maximum power that could be generated by three different MCFC systems having identical feed stream compositions<sup>1</sup>.



(a) Parallel Flow of Reactant Streams Through Stacks



(b) Series Flow of Reactant Streams Through Stacks

M92002265

**Figure 9-19 MCFC System Designs**

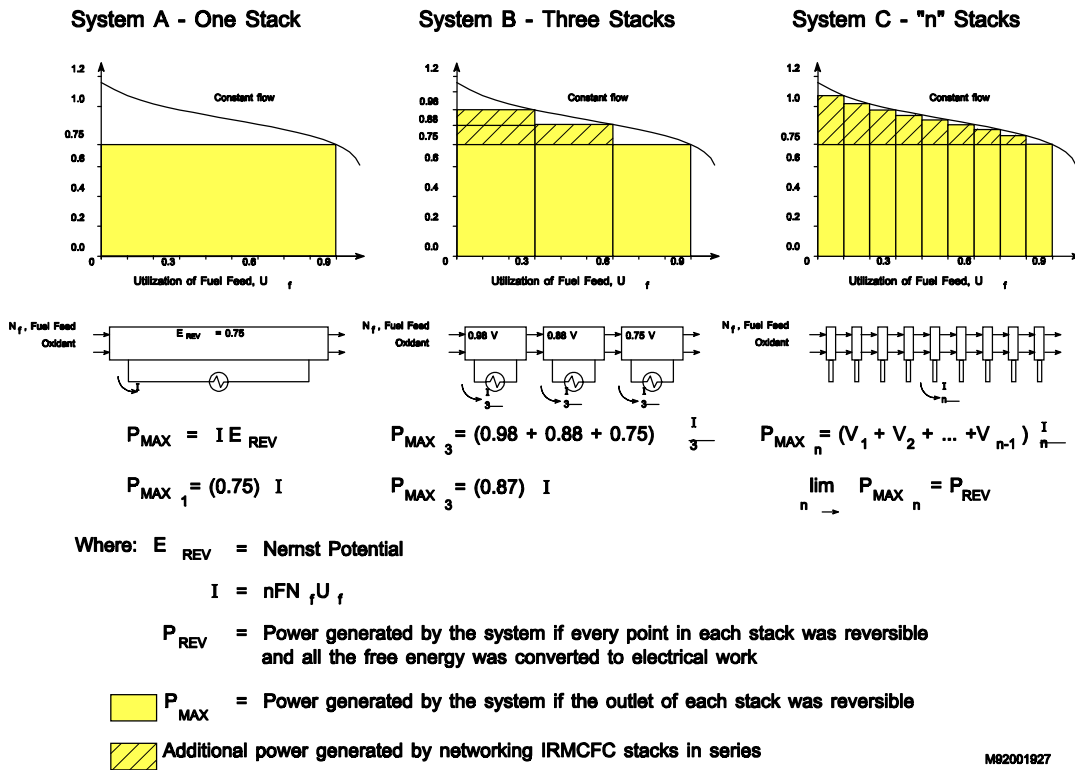


**Figure 9-20 Stacks in Series Approach Reversibility**

A graph of Nernst potential versus fuel utilization for the given feed stream compositions (60) was duplicated three times in Figure 9-20. The Nernst potential is the voltage which drives reversible electrode reactions. This reversible voltage, generated by the overall cell reaction, is a function of the local temperature, pressure, and reactant concentrations. As reactants are utilized, their concentrations change. Since Nernst potential is dependent upon the concentrations of reactants, it varies with the degree of utilization.

Fuel utilization is directly proportional to the charge transferred across the electrolyte. Therefore, the shaded areas of the graphs represent power -- the product of voltage and current. If reversibility is assumed at the outlet of each stack, no voltage losses are deducted from the Nernst potential. Therefore, each shaded area represents the maximum power, which each cell could generate.

System A in Figure 9-20 is composed of a single stack. Three stacks are arranged in series in system B. System C features many, or "n," stacks configured in series. In all three systems, the voltage of each stack corresponds to reactant concentrations at its outlet.

For comparison, each system is assumed to have the same total stack membrane area. That is, the area of each stack in system B is one third the area of the stack in system A. Similarly, the

area of each stack in system C is one "nth" the area of the single stack in system A. For simplicity, each stack is considered to contain only one cell.

Since each system achieves the same total fuel utilization (90%) across the same total area, each stack has the same average current density. Irreversible voltage loss is mainly a function of current density and stack temperature. Since these parameters are equivalent in each stack, it is assumed that the Nernst potential of each stack would be reduced by the same amount.

In system A, 90% of the fuel is utilized in a single stack, and all the current is generated at a single voltage. The power that this system can achieve is represented by the graph's shaded region.

In system B, three stacks in series each utilize 30% of the fuel. The current generated by each stack in system B is one third of the current generated in system A. Each stack in system B produces a different voltage. At the exit of the first stack, a high Nernst potential is generated because 70% of the fuel is still unburned. Likewise, at the exit of the second stack, 40% of the fuel remains unburned, generating another improved Nernst potential. Only ten percent of the fuel remains at the exit of the third stack, yielding the same Nernst potential that the single stack in system A produced. The three stack network can produce more power because two-thirds of the total charge is transferred at increased voltages. Comparing the shaded areas of the graphs illustrates the additional power that can be produced by arranging stacks in series.

In system C, many stacks are connected in series. Very small currents are generated at still higher voltages. As the number of stacks in series is increased, the maximum achievable power quickly approaches the power which a reversible system would generate, i.e. complete conversion of the available free energy. (A reversible system is reversible at every point in each stack, not just at the stack outlets.) The shaded area in the graph nearly fills the entire area under the curve - the reversible power.

Each system in Figure 9-19 converts an equivalent amount of free energy (90% fuel utilization) into heat and electrical work. The key difference, however, is that the systems with MCFC stacks networked in series transfer charge at higher voltages, thus converting more of the free energy directly into electrical work, and less into heat. As the number of stacks in series is increased, a reversible process is approached which would convert all the free energy into work and none into heat. Although heat that is produced from free energy can be reconverted into electrical work (e.g. via a steam turbine), an MCFC stack's direct conversion of free energy is intrinsically more efficient. Therefore, networking MCFC stacks in series results in more efficient power production even when waste heat is recovered.

Although each stack added to a series network would improve the system's efficiency, the incremental benefit obtained with each additional stack diminishes. A finite number of stacks could adequately, but not exactly, approach a reversible process. In a practical network, the number of stacks would be limited by economic, space, and design constraints.

In a similar study, Liebhafsky and Cairns (31) compared two arrangements of tubular, calcia-stabilized solid oxide fuel cells. In one arrangement, hydrogen and air were supplied to a single,

30-cm cell. In the other arrangement, the same cell was segmented into three, 10-cm cells which were ducted such that the same reactant streams flowed through them in series. Each arrangement had a total fuel utilization of 90% and each cell had the same average current density. Each cell in the series arrangement accomplished one-third of the total fuel utilization. Calculations showed that the series arrangement produced 5% more power than the single cell, and that further sectioning would produce greater improvements. It was concluded that the increase in irreversibility associated with changes in gas composition has nothing to do with electrode kinetics, but is rooted in the Nernst equation.

#### **9.4.2 MCFC Network**

When designing an MCFC power system, several requirements must be met. An MCFC system must properly condition both the fuel and oxidant gas streams. Methane must be reformed into the more reactive hydrogen and carbon monoxide. Carbon deposition, which can plug gas passages in the anode gas chamber, must be prevented. To supply the flow of carbonate ions, the air oxidant must be enriched with carbon dioxide. Both oxidant and fuel feed streams must be heated to their proper inlet temperatures. Each MCFC stack must be operated within an acceptable temperature range. Excess heat generated by the MCFC stacks must be recovered and efficiently utilized.

Figure 9-21 shows an MCFC network. The arrangement of stacks in series, as well as a unique recycle scheme, allows an MCFC network to meet all the requirements of an MCFC power system, while achieving high efficiency.

#### **9.4.3 Recycle Scheme**

In the network's recycle scheme, a portion of the spent fuel (Stream 5) and oxidant (Stream 4) is mixed and burned. The products of combustion (Stream 3) are then recycled through the cathode in order to provide the necessary carbon dioxide to the stacks. This eliminates the need for an external source of pure carbon dioxide. The cathode-cathode recycle (Stream 4) is large enough to cool the stacks, transferring excess energy to the heat recovery boilers. During the transfer of heat, enough energy is left in the oxidant recycle to heat the fresh air feed to the designated cathode inlet temperature. A second portion of the spent fuel (Stream 1) is recycled through the anode to provide enough steam to prevent carbon deposition and internally reform methane. This eliminates the need for steam to be supplied from another source. The anode-anode recycle also heats the fresh fuel feed to the designated anode inlet temperature.

#### **9.4.4 Reactant Conditioning Between Stacks in Series**

When MCFC stacks are networked in series, reactant streams can be conditioned between the stacks -- at different stages of utilization. The composition of reactant streams can be optimized between stacks by injecting a reactant stream (see Figure 9-19) or by mixing the existing reactant streams.

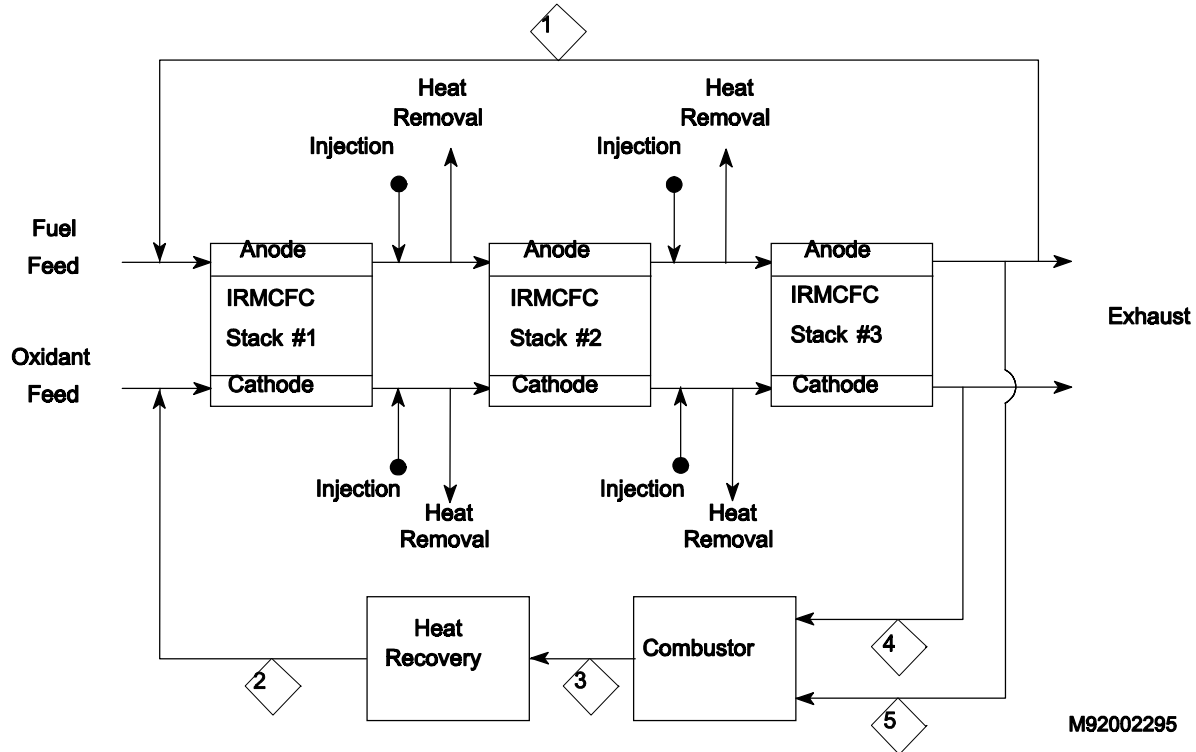


**Figure 9-21 MCFC Network**

Between stacks networked in series, heat can be removed from the reactant streams to assist in controlling stack temperatures. The heat in a network reactant stream can be transferred to a cooler process stream in a heat exchanger or hot and cold reactant streams can be mixed directly. The recovered heat may be utilized in a combined cycle or for cogeneration.

Methane can be injected into fuel streams between stacks networked in series. Since the reforming of methane into hydrogen is endothermic, its careful distribution among stacks in series is expected to improve the thermal balance of the system by allowing waste heat to be more evenly consumed throughout the total utilization of reactants. Improved thermal balance should allow stacks to be operated nearer their maximum temperature, reducing ohmic voltage losses. However, injecting portions of the fuel feed between stacks in series decreases the Nernst potential of every stack except the last one, since less fuel passes through each stack. (The amount of fuel which passes through the last stack does not change.) Optimizing the system requires an evaluation of the point at which the benefits of improved thermal balance outweigh the reduction in Nernst potential associated with such fuel redistribution.

### 9.4.5 Higher Total Reactant Utilization

The optimum total reactant utilization of stacks networked in series is higher than that of conventional, parallel stacks. Conventional designs avoid high utilization, because that would result in low voltages. In conventional configurations, the total utilization of reactants is accomplished in one stack. Therefore, when high utilizations are attempted, the low voltage which is generated adversely affects the total power production. In networks, however, the

utilization of reactants is accomplished incrementally, and the low voltage associated with high utilization is restricted to stacks which produce only a portion of the total power.

Manifolding problems can further limit the practical reactant utilization of conventional MCFC systems. Ideally, fuel and oxidant streams are distributed equally among individual cells in a stack. Today's manifolds, however, have not been able to achieve this, and cells are typically supplied with unequal reactant flows. This causes the composition of outlet reactant streams to be variable among the cells. At high utilizations, this variability leads to a significant reduction in stack voltage. Therefore, conventional systems avoid such high utilizations. However, when stacks are networked in series, reactant streams can be thoroughly mixed between cells. This reduces the variability in reactant composition and helps to minimize the stack voltage loss.

Another study (32) maximized the efficiency of conventional and series-connected fuel cell systems by optimizing cell voltage and current density. The study found that the optimum fuel utilization in the series-connected system was higher than that in the conventional system. Most importantly, the higher fuel utilization and lower current density of the series-connected system combined to give more efficient performance than the conventional system.

#### **9.4.6 Disadvantages of MCFC Networks**

For recycling to improve the performance of an MCFC network, it must provide benefits that outweigh its inherent disadvantages. If carbon dioxide is not separated from the anode-anode recycle, the concentration of carbon dioxide in the anode is increased. This reduces the Nernst potential. The Nernst potential is similarly reduced by the anode-cathode recycle if steam is not condensed out, since recycled steam dilutes reactant concentrations in the oxidant. In addition, part of the power generated by the network is consumed by the equipment necessary to circulate the recycle streams. Such circulation equipment, along with the additional ducting required by recycling, also increases the capital cost of the MCFC network.

Given the same initial feed streams, the flowrate of reactants through stacks networked in series is much larger than the flowrate of reactants through stacks in a conventional system.

Conventional fuel cell systems divide the initial feed streams among many stacks arranged in parallel. However, the initial feed streams in an MCFC network are not divided, but fed directly into the first of a series of many stacks. Perhaps the greatest disadvantage of MCFC networks is that this increased flowrate creates larger pressure drops.

Another potential disadvantage of an MCFC network is the interdependence of the stacks in series. A problem with one stack could alter the performance of succeeding stacks. Furthermore, bypassing or isolating a problematic stack in a network could be a difficult control process. In the conventional parallel configuration, stack performance is not so interrelated.

#### **9.4.7 Comparison of Performance**

Two ASPEN (Advanced System for Process Engineering, public version) simulations compare the performance of conventional and networked fuel cell systems having identical recycle schemes and steam bottoming cycles. Each simulated system was composed of three MCFC stacks operating at the same temperature and pressure. The Nernst potential of each MCFC in both systems was reduced by 0.3 volts due to activation, concentration and ohmic voltage



polarizations. (This is a conservative estimate, representing a much higher outlet voltage polarization than would be expected.) Simple, single-pressure steam cycles produce secondary power.

When the total fuel utilization of each system was optimized for maximum efficiency, the efficiency of the fuel cell stacks networked in series was nearly 10% greater than that of the stacks arranged in parallel (44.9% vs. 35.4%, LHV). When the power generated by each system's steam bottoming cycle was considered in addition to its fuel cell power, the gap in efficiency narrowed to 5.5%. The efficiency of the total networked system is 56.8%, while that of the total conventional system was 51.3%.

The fuel cell network which was simulated was not fully optimized. Optimization of flow geometry, operating pressure, stack fuel utilization and current, reactant conditioning, and other parameters would be expected to yield further significant increases in total system efficiency.

#### **9.4.8 Conclusions**

Key to the concept of networking is the arrangement of multiple fuel cell stacks relative to the flow of reactant streams. Conventional fuel cells systems have been designed such that reactant streams flow in parallel through fuel cell stacks. In a fuel cell network, however, reactant streams are ducted such that they are fed and recycled through stacks in series.

Arranging fuel cell stacks in series offers several advantages over conventional fuel cell systems. Stacks networked in series more closely approach a reversible process, which increases the system efficiency. Higher total reactant utilizations can be achieved by stacks networked in series. Placing stacks in series also allows reactant streams to be conditioned at different stages of utilization. Between stacks, heat can be consumed or removed, (methane injection, heat exchange) which improves the thermal balance of the system. The composition of streams can be adjusted between stacks by mixing exhaust streams or by injecting reactant streams.

Computer simulations have demonstrated that a combined cycle system with MCFC stacks networked in series is significantly more efficient than an identical system with MCFC stacks configured in parallel.

### **9.5 Hybrids**

This section present hybrids for generating electricity or for providing power in automotive vehicles. Hybrid systems that incorporate gas turbines build upon the outstanding performance of the fuel cell by utilizing the exhausted fuel cell heat. Hybrid electric vehicles utilize fuel cells to provide electric power to augment or replace exiting power sources. These systems are highly efficient and deliver superior environmental performance. Presented below is a general discussion of hybrid technology as well as specific initiatives in the gas turbine / fuel cell and electric power hybrid vehicle areas.

#### **9.5.1 Technology**

Advanced power generation cycles that combine high-temperature fuel cells and gas turbines, reciprocating engines, or another fuel cell are the hybrid power plants of the future. These conceptual systems have the potential to achieve efficiencies greater than 70 % and be

commercially ready by the year 2010 or sooner. The hybrid fuel cell/turbine (FC/T) power plant will combine a high-temperature, conventional molten carbonate fuel cell (MCFC) or a solid oxide fuel cell (SOFC) with a low-pressure-ratio gas turbine, air compressor, combustor, and in some cases, a metallic heat exchanger (66). The synergistic effects of the hybrid fuel cell/turbine technology will also provide the benefits of reduced greenhouse gas emissions. Nitrous (NO<sub>x</sub>) emissions will be an order of magnitude below those of non-fuel cell power plants and carbon monoxide emissions will be less than 2 parts per million (ppm) (67). There will also be a substantial reduction in the amount of carbon dioxide produced compared to conventional power plants.

The hybrid system is key to the Department of Energy’s Vision 21 plants. The Vision 21 program has set power plant goals of achieving efficiencies greater than 75 % (LHV) for natural gas. The higher efficiencies play a key role in reducing emissions, another target in Vision 21 plants. As a comparison, conventional coal-burning power plants are typically 35 % efficient and natural gas fired plants are now 40 to 50 % efficient. Figure 9-22 shows the estimated efficiency ranges of current and future power generation systems.

The combination of the fuel cell and turbine operates by using the rejected thermal energy and residual fuel from a fuel cell to drive the gas turbine. The fuel cell exhaust gases are mixed and burned, raising the turbine inlet temperature while replacing the conventional combustor of the gas turbine. Use of a recuperator, a metallic gas-to-gas heat exchanger, transfers heat from the gas turbine exhaust to the fuel and air used in the fuel cell. Figure 9-23 illustrates an example of a proposed fuel cell/turbine system.

There can be many different cycle configurations for the hybrid fuel cell/ turbine plant. In the topping mode described above, the fuel cell serves as the combustor for the gas turbine while the

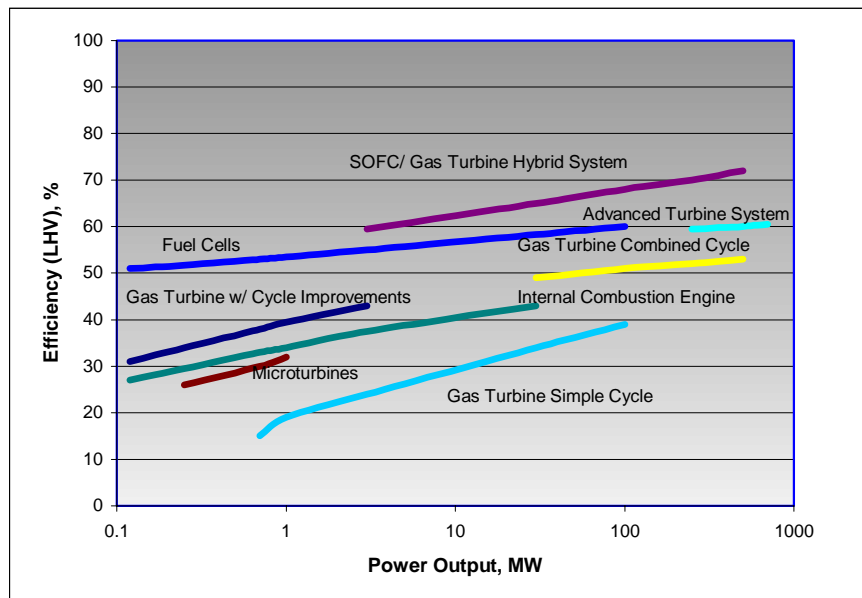


**Figure 9-22 Estimated performance of Power Generation Systems**

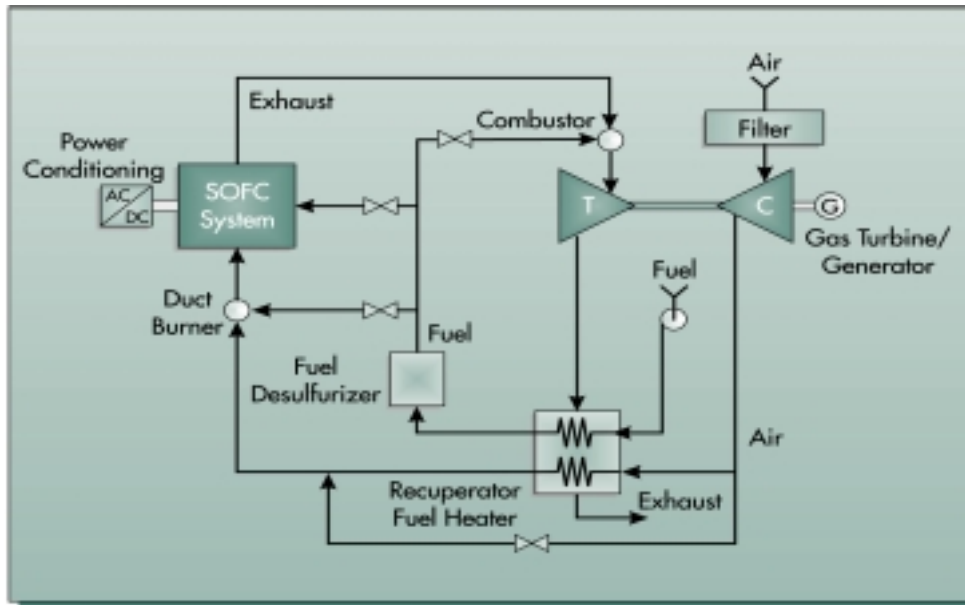


**Figure 9-23 Diagram of a proposed Siemens-Westinghouse hybrid system**  
*(Taken from DOE Project Fact Sheet – Fuel Cell/ ATS Hybrid Systems)*

gas turbine is the balance-of-plant for the fuel cell, with some generation. In the bottoming mode, the fuel cell uses the gas turbine exhaust as air supply while the gas turbine is the balance of plant. In indirect systems, high temperature heat exchangers are used (68).

The hybrid plants are projected to cost 25 % below comparably sized fuel cells, (69) and be capable of producing electricity at costs of 10 to 20 % below today's conventional plants (66). Operation of the plant is almost totally automatic. Therefore, it can be monitored and managed remotely with the possibility of controlling hundreds of the power plants from a single location (67).

Initial systems will be less than 20 MW, with typical system sizes of 1-10 MW. Future systems, in the megawatt class size, will boost efficiency even further by combining two solid oxide fuel cell modules with more advanced gas turbines and introducing sophisticated cooling and heating procedures. Another possibility of a hybrid power plant is to combine a solid oxide fuel cell with a proton exchange membrane (PEM) fuel cell. The SOFC would produce both electric power and hydrogen. This hydrogen would then be utilized by the PEM to generate more electric power (67).

## 9.5.2 Projects

In 1997, a Program Research and Development Announcement (PRDA) was issued by the Department of Energy for conceptual feasibility studies of high-efficiency fossil power plants (HEFPPs). The terms of the conceptual power plant must be less than 20 MW in size, operate on

natural gas and contain a high-temperature fuel cell. By late 1998, DOE awarded contracts to determine the feasibility of the highly efficient hybrid power plants.

FCE, of Danbury, CT, teamed with Allison Engine Company to evaluate a carbonate fuel cell combined with a gas turbine and a steam turbine generator. The system was operated at ambient pressure. The net power of the hybrid system was 20.6 MW and the NO<sub>x</sub> levels were less than 1 ppm. The process showed a 65 % efficiency with off-the-shelf turbomachinery and 72 % efficiency with cycle specific machinery. The COE is predicted to be comparable to present day alternatives.

Siemens-Westinghouse Power Corporation, of Pittsburgh, PA, with a subcontract to Allison Engine Company, evaluated a pressurized solid oxide fuel cell coupled with conventional gas turbine technology without a steam plant. The system was operated at a pressure of 7 atm. The fuel cell generated 16 MW of power and the gas turbine generated 4 MW of power. The process showed 67 % efficiency as developed. An efficiency of 70 % is deemed achievable with improvement in component design. The COE is predicted to be comparable to present day alternatives. NO<sub>x</sub> levels were less than 1 ppm.

McDermott Technology, Inc., of Alliance, OH, developed a conceptual design of a high efficiency power plant system that joins planar solid oxide fuel cell technology with micro-turbine technology in a combined cycle. The system was operated at atmospheric conditions. The power plant had a combined cycle output of 700 kW with the turbine supplying 70 kW. The results indicate 70 % efficiency is possible and the COE is comparable to present day alternatives.

Siemens-Westinghouse Power Corporation, Pittsburgh, PA, and Solar Turbines developed a conceptual design of an economically and technically feasible 20-MW, 70-% efficient natural gas-fueled power system that employs solid oxide fuel cells operating at elevated pressure in conjunction with an Advanced Turbine System gas turbine. The fuel cell, operated at 9 atm pressure, generated 11 MW of power. Two Solar Mercury 50 gas turbines were used to generate 9 MW of power. The results of the study indicated a system efficiency near 60 %. A low COE relative to conventional power generation is predicted.

In March of 1999, FCE, of Danbury, CT, with Allison Engine Company, Indianapolis, IN, and Capstone Turbine Corp., Woodland Hills, CA. was awarded a project under the Vision 21 program to create a fuel cell/turbine system that provides efficiencies and emissions targets that meet or exceed stringent Vision 21 goals. The 3-year program will include four steps:

1. Development of a high-utilization fuel cell,
2. Development of key system components,
3. Tests of the fuel cell/hybrid system would be performed to assess integration and system operation of an existing 250-kilowatt fuel cell stack with a commercially available micro-turbine, and
4. Preparation of a conceptual design of a 40 MW ultra-high efficiency power plant.

A unique feature of the proposed system will allow the fuel cell and turbine modules to operate at independent pressures. The fuel cell will be operated at ambient pressure. This can increase

the fuel cell stack life and save on piping and vessel costs. The turbine can then be operated at its optimum pressure ratio.

Countries around the world are developing interest in the high-efficiency hybrid cycles. A 320 kW hybrid (SOFC and gas turbine) plant will enter service in Germany in 2001, operated by a consortium under the leadership of RWE Energie AG. This will be followed in 2002 by the first 1 MW plant, which will be operated by Energie Baden-Wurttemberg AG (EnBW), Electricite de France (EDF), Gaz de France, and Austria's TIWAG (68).

Another project under development at the NETL is an advanced power plant system that combines a multistaged fuel cell with an extremely efficient turbine. Preliminary estimates show efficiencies greater than 80% (LHV). Studies showed that natural gas to electricity LHV efficiencies could break through an 80% barrier, while remaining cost competitive for a 4-MW solid oxide plant (tubular or planar). The Advanced Fuel Cell concept directly coincides with the long-term goals of the 21<sup>st</sup> Century Fuel Cell Program. These include system costs of \$400/kW and efficiencies of 70-80 percent or more (LHV to AC electricity), with fuel flexibility and a stack-life of 40,000 hours. They are intended for commercial application in 2015, maintaining ultra-low emissions.

### **9.5.3 World's First Hybrid Project**

Siemens-Westinghouse Power Corporation of Pittsburgh, PA developed and fabricated the first advanced power plant to combine a solid oxide fuel cell and a gas turbine. The microturbine generator was manufactured by Northern Research and Engineering Corporation of Woburn, Mass. The factory acceptance test was completed in April 2000. Southern California Edison will operate the new hybrid plant at The National Fuel Cell Research Center at the University of California-Irvine. A year of testing in a commercial setting will be performed at this site. The system cycle is expected to generate electric power at 55 % efficiency.

The pressurized system will generate 220 kilowatts of power and be operated at 3 atm of pressure. The fuel cell is made up of 1152 individual tubular ceramic cells and generates about 200 kilowatts of electricity. The microturbine generator will produce an additional 20 kilowatts of electricity at full power. No sulfur dioxide pollutants will be released into the air. Nitrogen oxide emissions are likely to be less than 1 ppm.

A 320-kilowatt hybrid system is also in the planning stages. An initial commercial offering of a one MW fuel cell-microturbine power plant in late 2002 will be the end results of this Department of Energy/Siemens Westinghouse partnership program (70).

### **9.5.4 Hybrid Electric Vehicles (HEV)**

Hybrid Electric Vehicles (HEVs) typically combine the conventional internal combustion engine of the automobile with an energy storage device, such as a battery. However, there are many different arrangements for the HEV. The key components to an HEV are the energy storage system (batteries, ultracapacitors, and flywheels), the power unit (spark ignition engines, compression ignition direct injection engines, gas turbines and fuel cells) and the vehicle propulsion system (electric motor). The benefits of HEVs, much like the hybrid power plants, are increased efficiency and lower emissions.

Fuel cell hybrid cars are not a new concept. In the early 1970s, K. Kordesch modified a 1961 Austin A-40 two-door, four-passenger sedan to an air-hydrogen fuel cell/battery hybrid car (71). This vehicle used a 6-kW alkaline fuel cell in conjunction with lead acid batteries, and operated on hydrogen carried in compressed gas cylinders mounted on the roof. The car was operated on public roads for three years and about 21,000 km.

In 1994 and 1995, H-Power (Belleville, New Jersey) headed a team that built three PAFC/battery hybrid transit buses(72,73). These 9 meter (30 foot), 25 seat (with space for two wheel chairs) buses used a 50 kW fuel cell and a 100 kW, 180 amp-hour nickel cadmium battery.

Recently, the major activity in transportation fuel cell development has focused on the PEFC. In 1993, Ballard Power Systems (Burnaby, British Columbia, Canada) demonstrated a 10 m (32 foot) light-duty transit bus with a 120 kW fuel cell system, followed by a 200 kW, 12 meter (40 foot) heavy-duty transit bus in 1995 (74). These buses use no traction batteries. They operate on compressed hydrogen as the on-board fuel. In 1997, Ballard provided 205 kW (275 HP) PEFC units for a small fleet of hydrogen-fueled, full-size transit buses for demonstrations in Chicago, Illinois, and Vancouver, British Columbia. Working in collaboration with Ballard, Daimler-Benz built a series of PEFC-powered vehicles, ranging from passenger cars to buses (75). The first such vehicles were hydrogen-fueled. A methanol-fueled PEFC A-class car unveiled by Daimler-Benz in 1997 has a 640 km (400 mile) range. Plans are to offer a commercial vehicle by 2004. A hydrogen-fueled (metal hydride for hydrogen storage), fuel cell/battery hybrid passenger car was built by Toyota in 1996, followed in 1997 by a methanol-fueled car built on the same RAV4 platform (76).

Other major automobile manufacturers, including General Motors, Volkswagen, Volvo, Honda, DaimlerChrysler, Nissan, and Ford, also have announced plans to build prototype polymer electrolyte fuel cell vehicles operating on hydrogen, methanol, or gasoline (77). Honda's FCX, a fuel cell prototype sedan, includes both hydrogen- and methanol-based systems. Honda hopes to have this car on the road by 2003. The GM Precept will use a hydrogen hydride storage system to help it to attain a 108 miles per gallon gasoline equivalent (78).

The Department of Energy's Transportation Fuel Cell program is a collaboration between government and industry that supports the Partnership for a New Generation of Vehicles. Domestic automakers, fuel cell developers, national labs, universities, component suppliers and the fuel industry have created a Fuel Cell Alliance. This alliance helps in collaborating government sponsored research and development within the auto industry. Some of the goals of the program include developing fuel cell stack systems that are greater than 57 % efficient at 25 % peak power, more than 100 times cleaner than EPA Tier 2 emissions, and capable of operating on hydrogen or hydrogen-rich fuel from gasoline, methanol, ethanol and natural gas. By 2004, the program hopes to have fuel cell power systems that are reliable, safe and cost competitive with internal combustion engines (79).

California has started a Fuel Cell Partnership with oil companies, automakers and fuel cell companies. They hope to have 50 fuel cell vehicles, both passenger cars and transit buses, on the

road by 2003. The goals of the program include demonstrating vehicle performance, identifying fuel infrastructure issues and addressing commercialization challenges (80).

DOD is interested in new or novel advanced power and propulsion systems that will reduce fuel consumption, improve performance, extend vehicle range, reduce emissions, and reduce support costs. The Navy and Army are considering hybrids for ships, land vehicles, helicopters, and battlefield power requirements.

In 1997, the Office of Naval Research (ONR) initiated an advanced development program to demonstrate a ship service fuel cell (SSFC) power generation module. During Phase 1, competitive conceptual designs of 2.5 MW SSFC were prepared, along with critical component demonstrations. Phase 2 of the development program, scheduled for completion in 2002, will result in a nominal 500 kW fuel cell ship service generator demonstration module to be constructed and tested in a laboratory setting. The baseline concept is fueled by logistic fuel which is reformed in an adiabatic reformer designed and built by International Fuel Cells. Downstream of the reformer is a series of components that remove CO and H<sub>2</sub>S before the gas is sent to the fuel cell. The spent fuel and air are mixed and burned to drive a turbocompressor and recover compression work.<sup>59</sup>

The Army has two programs that are looking at hybrids using fuel cells. In 1999, the Land Warrior Operational Combat System was approved. The goal is to develop a portable hybrid fuel cell system that weighs less than one kilogram and meets the power demand of the Land Warrior Power requirements. The second program is the Future Combat System. This program plans to develop technologies and systems for a lightweight, overwhelming lethal, strategically deployable, self-sustaining combat systems.<sup>60</sup>

## 9.6 References

1. Impact of Catalysis on Clean Energy in Road Transportation," P.G. Gray and J.C. Frost Johnson Matthey, Energy&Fuels, Vol. 12, No. 6, pp. 1121 - 1129, 1998.
2. Private communication with Argonne National Laboratory, Argonne IL, August 2000.
3. "Fuel Processing for Fuel Cell Power Systems," S. Ahmed, R. Kumar, and M. Krumpelt, ANL, Fuel Cells Bulletin, Elsevier Scientific, Ltd., ISSN 1464-2859, No. 12, September 1999.
4. "Fuel Choices for Fuel Cell Powered Vehicles," J. Holmes, statement before Subcommittee on Energy and Environment of the Committee on Science, U.S. House of Representatives, on behalf of The American Petroleum Institute, Exxon Corporation, October 5, 1999.
5. Private communication with Forschungszentrum Jillich, Rilich, Germany, July 2000.
6. Private communication with Ceramatec, Salt Lake City, UT, April 2000.
7. Private communications with IFC, South Windsor, CT, September 2000.
8. "Program Overview," P. Devlin, DOE-OTT and R. Sutton, ANL, DOE Fuels for Fuel Cell Program, 2000.
9. "Synthetic Fuels," Probstein and Hicks, McGraw-Hill Book Company, 1982.

---

<sup>59</sup> R.M. Privette, et al., "2.5 MW PEM Fuel Cell System for Navy Ship Service Power," paper presented at the 1999 Review Conference on Fuel Cell Technology, Chicago, Illinois, August 3-5, 1999.

<sup>60</sup> J.C. Stephens, K. Gardner, and R. Jacobs, "US Army CECOM Fuel Cell Program," presented at the World Association for Case Method Research and Application, Lucerne, Switzerland, January 5-7, 2000.

10. "Portable Self-Sufficient 12 Volt PEFC Power Source with Integrated Chemical Hydrogen Generator," U. Bossel, Pg. 742, Fuel Cell Seminar Abstracts, Courtesy Associates, Inc., November 1998.
11. "Fuel Processing Technology for Premium Power Fuel Cell Systems," J.C. Cross et al., Epyx/ADL, Pg. 749, Fuel Cell Seminar Abstracts, Courtesy Associates, Inc., November 1998.
12. "Fuel Processing for High Efficiency Fuel Cell Systems," J.R. Rostrup-Nielsen, L.J. Christiansen, and K. Aasberg-Petersen, Haldor Topsoe A/S, Grove III Fuel Cell Symposium, September 1993.
13. "Compact Fuel Processor for Fuel Cell-Powered Vehicles," T.J. Flynn, R. Privette et al., McDermott Technology, Inc. and Catalytical Advanced Technologies, Paper 1999-01-0536, Society of Automotive Engineers, Inc., 1999.
14. "Steam pre-reforming of propane to a methane-rich fuel for internal reforming in solid oxide fuel cells," K. Ahmed and K. 176ger, Ceramic Fuel Cells Ltd., 4th EUROSOFC, Lucerne/Switzerland July 2000
15. "Gasoline to Hydrogen - A New Route for Fuel Cells," ANL, Electric & Hybrid Vehicle Technology of'97,1997.
16. Private communication with Johnson Matthey Technology Centre, Reading, England, February 2000. 17. "Catalytic Partial Oxidation Reforming of Hydrocarbon Fuels," S. Ahmed, et al., ANL, Pg. 242, Fuel Cell Seminar Abstracts, Courtesy Associates, Inc., November 1998.
18. Chemical Process Industries, fourth edition, R. Shreve and J. Brink, McGraw-Hill, 1977.
19. "General Progress in the Research of Solid Polymer, Fuel Cell Technology at Ballard," D. Wilkinson, and A. Steck, 1997 Proceedings of the Second International Symposium on New Materials for Fuel Cells and Modern Battery Systems, Montreal, Quebec Canada, July 1997.
20. Coal Gasification Systems: A Guide to Status, Applications and Economics, prepared by Synthetic Fuels Associates, Inc., EPRI AP-3109, Project 2207, Final Report; June 1983.
21. Coal Gasification Guidebook: Status, Applications and Technologies, EPRI TR- 102034, December 1993.
22. "Fuel Cell Handbook," J. Appleby and F. Foulkes, Texas A&M University, Van Nostrand Reinhold, New York (out of print), republished by Krieger Publishing Co., Melbome, FL, 1989.
23. "Removal of CO from Reformate for PEFC Application," S. Lee, R. Kumar, M. Krumpelt, ANL, Pg. 578, Fuel Cell Seminar Abstracts, Courtesy Associates, Inc., November 1998.
24. "Development of an Integrated Reformer/Fuel Cell Power System for Petroleum and Alcohol-Fueled Vehicles, Part I - Brassboard Demonstration," W. Mitchell, Epyx, Pg. 230, Fuel Cell Seminar Abstracts, Courtesy Associates, Inc., November 1998.
25. "Preliminary Assessment of Planar Solid Oxide Fuel Cells for Transportation Power Applications," J. Hirschenhofer and J. White, Parsons Corporation, for ANUDOE, to be published, October 2000.
26. Personal communication with Ceramic Fuel Cells Ltd., August 2000.
27. "High-performance, reduced-temperature SOFC technology," N. Q. Minh, et al., Honeywell, Fuel Cell Bulletin, March 1999.
28. "Fuel Processing and Electrodes for Low-Temperature Fuel Cell Systems," J.C. Frost, Johnson- Matthey Technology Centre, Reading, England, European Fuel Cell News, April 1999.



29. "Advances in Fuel Processing for PEFC Systems for Transport," R. Dams, P. Hayter, and S. Moore, Wellman CJB Ltd., Pg. 238, Fuel Cell Seminar Abstracts, Courtesy Associates, Inc., November 1998.
30. "Catalytic Reforming of Gasoline and Diesel Fuel," C. Pereira, R. Wilkenhoener, S. Ahmed, and M. Krumpelt, ANL, AIChE Spring 2000 Meeting, March 2000.
31. "Fuel-Flexible Fuel Processor," J. Cuzens, J. Mauzey, and R. Woods, Hydrogen Burner Technology, Pg. 234 Fuel Cell Seminar Abstracts, Courtesy Associates, Inc., November 1998.
32. R. Shreve and J. Brink, *Chemical Process Industries*, fourth edition, McGraw-Hill, 1977.
33. *Coal Gasification Systems: A Guide to Status, Applications and Economics*, prepared by Synthetic Fuels Associates, Inc., EPRI AP-3109, Project 2207, Final Report, June 1983.
34. *Coal Gasification Guidebook: Status, Applications and Technologies*, EPRI TR-102034, December 1993.
35. W.L. Lundberg, "Solid Oxide Fuel Cell Cogeneration System Conceptual Design," prepared by Westinghouse for Gas Research Institute, Report No. GRI-89-0162, July 1989.
36. PC-25 Capability, Communication with ONSI Corporation, September 1998.
37. James M. Douglas, *Conceptual Design of Chemical Processes*, McGraw-Hill, Inc., New York, NY, 1988.
38. Max S. Peters, and Klaus D. Timmerhaus, *Plant Design and Economics for Chemical Engineers*, 3<sup>rd</sup> Edition, McGraw-Hill, Inc., New York, NY, 1980.
39. Warren L. McCabe, Julian C. Smith, Peter Harriot, *Unit Operations of Chemical Engineering*, 4<sup>th</sup> Edition, 1985.
40. M.C. Williams, and T.J. George, "Research Issues in Molten Carbonate Fuel Cells: Pressurization," *presented at the 1992 IECEC*, Vol. 3, pp. 263-267.
41. "Overview of 11 MW Fuel Cell Power Plant," non-published information from Tokyo Electric Power Company, September 1989.
42. T. Koshimizu, et al., "Development of 5000 kW and 1000 kW PAFC Plants," *presented at the JASME-ASME Joint Conference (ICOPE-93)*, Tokyo, September 1993.
43. T. Okado, et al., "Study of Temperature Control in Indirect Internal Reforming MCFC Stack," presented at 25th IECEC, pp. 207-212, 1990.
44. N.Q. Minh, "High-Temperature Fuel Cells, Part 2: The Solid Oxide Cell," *Chemtech*, Vol. 21, February 1991.
45. V. Minkov, et al., "Topping Cycle Fuel Cells Effective Combined with Turbines," *Power Engineering*, July 1988, pp. 35-39. "Design and Economics of Large Fuel Cell Power Plants," presented at 1986 Fuel Cell Seminar, Tucson, AZ, p 255.
46. F.G. Baily, "Steam Turbines for Advanced Combined Cycles," *presented at the 35th GE Turbine State-of-the-Art Technology Seminar*, 1991.
47. M.S. Peters, and K.D. Timmerhaus, *Plant Design and Economics for Chemical Engineers*, Third Edition, McGraw-Hill, 1980.
48. M. Farooque, "Development of Internal Reforming Carbonate Fuel Cell Stack Technology," Performed under Contract No. DE-AC21-87MC23274, DOE/MC/23374-2941, October 1990.
49. M. Farooque, et al., "Comparative Assessment of Coal-Fueled Carbonate Fuel Cell and Competing Technologies," *presented at the 25th IECEC*, Vol. 3, pp.193-200, 1990.
50. Dawn M. Bernardi, "Water-Balance Calculations for Solid-Polymer-Electrolyte Fuel Cells," *Journal of Electrochemical Society*, Vol. 137, No. 11, November 1990.

51. David P. Wilkinson, (Ballard Power Systems) and David Thompsett (Johnson Matthey Technology Centre), "Materials and Approaches for CO and CO<sub>2</sub> Tolerance for Polymer Electrolyte Membrane Fuel Cells," *presented at the 1997 Proceedings of the Second International Symposium on New Materials for Fuel Cells and Modern Battery Systems*, Montreal, Quebec, Canada, July 6-10, 1997.
52. David P. Wilkinson, and Alfred E. Steck, "General Progress in the Research of Solid Polymer Fuel Cell Technology at Ballard," *presented at the 1997 Proceedings of the Second International Symposium on New Materials for Fuel Cells and Modern Battery Systems*, Montreal, Quebec Canada, July 6-10, 1997.
53. Thomas L. Buchanan, John H. Hirschenhofer, David B. Stauffer, and Jay S. White, "Carbon Dioxide Capture in Fuel Cell Power Systems," September 1994, G/C Report 2981.
54. "Overview of 11 MW Fuel Cell Power Plant," Non-published information from Tokyo Electric Power Company, September 1989.
55. F. P. Bevc, W. L. Lundberg and D. M. Bachovchin, "Solid Oxide Fuel Cell Combined Cycles," ASME Paper 96-GT-447, *presented at International Gas Turbine and Aeroengine Congress & Exhibition*, Birmingham, UK, June 1996.
56. R. Hendricks, "Heron Turbine Prototype Test Results," 20<sup>th</sup> International Congress on Combustion Engines, International Council on Combustion Engines (CIMAC), London, 1993.
57. T.J. George, K.D Lyons, and R. James III, "Multistaged Oxide Fuel Cell Power Plant Concept," May 1998.
58. Fax Transmittal from J. Hirschenhofer of Parsons Energy & Chemicals Group to Tom George of USDOE/FETC, dated August 26, 1998, Re: Aspen Analysis Results of the Multistaged SOFC Concept.
59. Parsons Energy & Chemical, work for the U.S. DOE, Spring 1998.
60. Appleby, A.J.; Foulkes F.R. *Fuel Cell Handbook*; Van Nostrand Reinhold: New York, 1989.
61. Liebhafsky, H.A.; Cairns, E.J. *Fuel Cells and Fuel Batteries*; John Wiley & Sons: New York, 1968.
62. Shah V.B. ASPEN Models for Solid Oxide Fuel Cell, Molten Carbonate Fuel Cell and Phosphoric Acid Fuel Cell; Prepared by EG&G Washington Analytical Services Center for the Morgantown Energy Technology Center under Contract No. DE-AC21-85MC21353, 1988.
64. Walhood, D.G.; Ferguson J.R. The Optimum Voltage-Current Operation of Single and Series Connected Fuel Cells; In *Proceedings of the International Symposium of the European Communities*: Luxembourg, 1992, 2d. ed., pp 289-296.
65. Wimer, J.G.; Williams, M.C.; Archer, D.H.; Osterle, J.F. Networking Electrochemical Membrane Separation Devices:
66. Theory and Application; Paper presented at the 1992 AIChE Annual Meeting: Miami Beach, FL, 1-6 November, 1992.
67. "Developing Power Systems for the 21<sup>st</sup> Century – Fuel Cell/ATS Hybrid Systems," U.S. Dept. of Energy, National Energy Technology Center & Office of Industrial Technologies, Project facts for Advanced Clean/ Efficient Power Systems, PS031.1099.
68. U. Eberl, "Fuel Cells and Gas Turbines: A Marriage of Efficiency," *Research and Innovation*, January 2000.

69. R. Gemmen, et al, "Technical Development Issues and Dynamic Modeling of Gas Turbine and Fuel Cell Hybrid Systems," *Proceedings of the 1999 Review Conference on Fuel Cell Technology*, August 1999.
70. "Fuel Cells- Opening New Frontiers in Power Generation," U.S. Department of Energy, Office of Fossil Energy, National Energy Technology Center, November 1999.
71. DOE Techline Press Release, "Department of Energy Announces World's First "Hybrid" Fuel Cell-Turbine," April 2000.
72. "Auto Show Attendees get a Glimpse of Future Concept Cars," *Alternative Fuel News*, Vol.4 No.1, US Department of Energy, Office of Energy Efficiency and Renewable Energy.
73. K.V. Kordesh, "City Car with H<sub>2</sub>-Air Fuel Cell and Lead Battery," *6<sup>th</sup> Intersociety Energy Conversion Engineering Conference*, SAE Paper No. 719015, 1971.
74. A. Kaufman, "Phosphoric Acid Fuel Cell Bus Development," *Proceedings of the Annual Automotive Technology Development Contractors' Coordination Meeting*, Dearborn, MI, October 1994, SAE Proceedings Volume P-289, pp. 289-293, 1995.
75. R.R. Wimmer, "Fuel Cell Transit Bus Testing & Development at Georgetown University," *Proceedings of the Thirty Second Intersociety Energy Conversion Engineering Conference*, July 1997, Honolulu, HI, pp. 825-830.
76. N.C. Otto, P.F. Howard, "Transportation Engine Commercialization at Ballard Power Systems," *Program and Abstracts 1996 Fuel Cell Seminar*, November 1996, Orlando, FL, pp.559-562.
77. F. Panik, "Fuel Cells for Vehicle Applications in Cars – Bringing the Future Closer," *J. Power Sources*, 71, pp.36-38, 1998.
78. S. Kawatsu, "Advanced PEFC Development for Fuel Cell Powered Vehicles," *J. Power Sources*, 71, pp. 150-155, 1998.
79. *Fuel Cell Technology: Powering the Future*, Electric Line, November/December 1996.
80. J. Milliken, "The DOE Transportation Fuel Cell Program: Recent Accomplishments and Future Plans," U.S. Dept. of Energy, Office of Transportation Technologies. "Questions and Answers – California Fuel Cell Partnership," [www.drivingthefuture.org](http://www.drivingthefuture.org).

---

## 10. SAMPLE CALCULATIONS

---

This section presents sample calculations to aid the reader in understanding the calculations behind the development of a fuel cell power system. The sample calculations are arranged topically with unit operations in Section 10.1, system issues in Section 10.2, supporting calculations in Section 10.3, and cost calculations in Section 10.4. A list of conversion factors common to fuel cell systems analysis is presented in Section 10.5 and a sample automotive design calculation is presented in Section 10.6.

### 10.1 Unit Operations

The following examples are presented for individual unit operations found within a fuel cell system. Unit operations are the individual building blocks found within a complex chemical system. By analyzing example problems for the unit operation, one can learn about the underlying scientific principles and engineering calculation methods that can be applied to various systems. This approach will provide the reader with a better understanding of these fuel cell power system building blocks as well as the interactions between the unit operations. For example, the desired power output from the fuel cell unit operation will determine the fuel flow requirement of the fuel processor.

This section starts by examining the fuel cell unit operation, and continues on to the fuel processors and power conditioners. Other more common unit operations, such as pumps and heat exchangers, will be left to the reader to investigate with the help of standard engineering handbooks.

#### 10.1.1 Fuel Cell Calculations

##### **Example 10-1 Fuel Flow Rate for 1 Ampere of Current (Conversion Factor Derivation)**

What hydrogen flow rate is required to generate 1.0 ampere of current in a fuel cell? (This exercise will generate a very useful conversion factor for subsequent calculations.)

##### ***Solution:***

For every molecule of hydrogen ( $H_2$ ) that reacts within a fuel cell, two electrons are liberated at the fuel cell anode. This is most easily seen in the PAFC and PEFC because of the simplicity of the anode (fuel) reaction, although the rule of two electrons per diatomic hydrogen molecule ( $H_2$ ) holds true for all fuel cell types. The solution also requires knowledge of the definition of an ampere (A) and an equivalence of electrons.<sup>61</sup>

---

<sup>61</sup> One equivalence of electrons is 1 g mol of electrons or  $6.022 \times 10^{23}$  electrons (Avagadro's number). This quantity of electrons has the charge of 96,487 coulombs (C) (Faraday's constant). Thus, the charge of a single



(PAFC & PEFC anode reaction)

$$n_{\text{H}_2} = (1.0 \text{ A}) \left( \frac{1 \text{ coulomb / sec}}{1 \text{ A}} \right) \left( \frac{1 \text{ equivalence of e}^-}{96,487 \text{ coulombs}} \right) \left( \frac{1 \text{ g mol H}_2}{2 \text{ equiv. of e}^-} \right) \left( \frac{3600 \text{ sec}}{1 \text{ hr}} \right) = 0.018655 \frac{\text{g mol}}{\text{hr}} \text{ H}_2 \text{ per } 1.0 \text{ A}$$

$$m_{\text{H}_2} = \left( 0.018655 \frac{\text{g mol}}{\text{hr}} \text{ H}_2 \text{ per A} \right) \left( \frac{2.0158 \text{ g}}{1 \text{ g mol H}_2} \right) \left( \frac{1 \text{ kg}}{1000 \text{ g}} \right) = 37.605 \times 10^{-6} \frac{\text{kg H}_2}{\text{A}} \text{ or } 0.037605 \frac{\text{kg H}_2}{\text{kA}}$$

The result of this calculation, 0.037605 kg H<sub>2</sub> per kA (0.08291 lb H<sub>2</sub> per kA), is a convenient factor that is often utilized in determining how much fuel must be consumed to supply a desired fuel cell power output as illustrated below.

### Example 10-2 Required Fuel Flow Rate for 1 MW Fuel Cell

A 1.0 MW<sub>DC</sub> fuel cell stack is operated with a cell voltage of 700 mV on pure hydrogen with a fuel utilization, U<sub>f</sub> of 80%. (a) How much hydrogen will be consumed in lb/hr? (b) What is the required fuel flow rate? (c) What is the required air flow rate for a 25% oxidant utilization, U<sub>ox</sub>?

#### **Solution:**

(a) We shall simplify the solution of this problem by artificially assuming that the individual fuel cells are arranged in parallel. That is, the fuel cell module voltage is the same as the cell voltage, and the fuel cell module current is equal to the current of an individual fuel cell times the number of fuel cells.

Recalling that power is the product of the voltage and current,

$$\text{Power (P)} = I \times V$$

Therefore, the current through the fuel cells can be calculated as

$$I = \frac{P}{V} = \left( \frac{1.0 \text{ MW}}{0.7 \text{ V}} \right) \left( \frac{10^6 \text{ W}}{1 \text{ MW}} \right) \left( \frac{1 \text{ VA}}{1 \text{ W}} \right) \left( \frac{1 \text{ kA}}{1000 \text{ A}} \right) = 1429 \text{ kA}$$

The quantity of hydrogen consumed within the fuel cell is

---

electron is  $1.602 \times 10^{-19}$  C. One (1) ampere of current is defined as 1 C/sec.

$$m_{\text{H}_2, \text{consumed}} = (1429 \text{ kA}) \left( \frac{0.08291 \text{ lb H}_2}{\text{kA}} \right) = 118.4 \frac{\text{lb H}_2}{\text{hr}}$$

Note that had we skipped the simplifying assumption that the fuel cells were arranged in parallel, we would have calculated the same hydrogen mass flow answer with a few extra steps. For example, if the fuel cell stacks were composed of 500 cells, then the stack voltage would have been 350 volts [(500 cells)(0.7 v/cell)], and the stack current would have been 2.858 kA [1429 kA / 500 cells]. Because this stack current passes through the 500 cells arranged in series, the hydrogen consumption is calculated as:

$$m_{\text{H}_2, \text{consumed}} = (2.858 \text{ kA}) \left( \frac{0.08291 \text{ lb H}_2}{\text{kA}} \right) (500 \text{ cells}) = 118.4 \frac{\text{lb H}_2}{\text{hr}}$$

Thus, the reader may find it more expedient and less error prone to make the parallel arrangement assumption when determining the mass flow requirement of hydrogen, in spite of the actual arrangement.

(b) Per equation 8-14, the utilization of fuel in a PAFC is defined as

$$U_f = \frac{H_{2, \text{consumed}}}{H_{2, \text{in}}}$$

Therefore the required fuel flow rate can be calculated as

$$H_{2, \text{in}} = \frac{H_{2, \text{consumed}}}{U_f} = \frac{118.4 \frac{\text{lb H}_2}{\text{h}}}{80 \%} = 148.0 \frac{\text{lb H}_2}{\text{h}}$$

(c) To determine the air supply requirement, we first observe that the stoichiometric<sup>62</sup> ratio of hydrogen to oxygen is 2 to 1 for H<sub>2</sub>O. Thus, the moles of oxygen required for the fuel cell reaction are determined by

$$n_{\text{O}_2, \text{ consumed}} = \left( 118.4 \frac{\text{lb H}_2}{\text{h}} \right) \left( \frac{1 \text{ lb mol H}_2}{2.0158 \text{ lb H}_2} \right) \left( \frac{1 \text{ lb mol O}_2}{2 \text{ lb mol H}_2} \right) = 29.38 \frac{\text{lb mol O}_2}{\text{h}}$$

If a 25% utilization is required, then the air feed must contain four times the oxygen that is consumed,

$$n_{\text{O}_2, \text{ supplied}} = \left( 29.38 \frac{\text{lb mol O}_2 \text{ consumed}}{\text{h}} \right) \left( \frac{1 \text{ lb mol O}_2 \text{ supplied}}{0.25 \text{ lb mol O}_2 \text{ consumed}} \right) = 118.5 \frac{\text{lb mol O}_2}{\text{h}}$$

Because dry air contains 21% O<sub>2</sub> by volume, or by mole percent, the required mass flow rate of dry air is,

$$m_{\text{air, supplied}} = \left( 118.5 \frac{\text{lb mol O}_2 \text{ supplied}}{\text{h}} \right) \left( \frac{1 \text{ lb mol air}}{0.21 \text{ lb mol O}_2} \right) \left( \frac{29.0 \text{ lb dry air}}{1 \text{ lb mol of air}} \right) = 16,400 \frac{\text{lb dry air}}{\text{h}}$$

### Example 10-3 PAFC Effluent Composition

A PAFC, operating on reformed natural gas (900 lb/hr) and air, has a fuel and oxidant utilization of 86% and 70% respectively. With the fuel and oxidant composition and molecular weights listed below, (a) How much hydrogen will be consumed in lb mol/hr? (b) How much oxygen is consumed in lb mol/hr? (c) What is the required air flow rate in lb mol/hr and lb/hr? (d) How much water is generated? (e) What is the composition of the effluent (spent) fuel and air streams in mol %?

---

<sup>62</sup> The stoichiometric ratio is the ratio of atoms in a given molecule.

Fuel Data	mol %
CH <sub>4</sub>	4.0
CO	0.4
CO <sub>2</sub>	17.6
H <sub>2</sub>	75.0
<u>H<sub>2</sub>O</u>	<u>3.0</u>
Total	100.0
MW	10.55

Air Data	mol %, dry	mol %, wet
H <sub>2</sub> O	0.00	1.00
N <sub>2</sub>	79.00	78.21
<u>O<sub>2</sub></u>	<u>21.00</u>	<u>20.79</u>
Total	100.00	100.00
MW	28.85	28.74

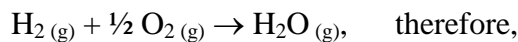
**Solution:**

(a) Before determining the lb mol/hr of hydrogen, we will first determine the molar fuel flow.

$$n_{\text{fuel, supplied}} = \left( 900 \frac{\text{lb fuel}}{\text{h}} \right) \left( \frac{1 \text{ lb mol fuel}}{10.55 \text{ lb fuel}} \right) = 85.29 \frac{\text{lb mol fuel}}{\text{h}} ; \text{ thus}$$

$$n_{\text{H}_2 \text{ consumed}} = \left( 85.29 \frac{\text{lb mol fuel}}{\text{h}} \right) \left( \frac{75 \text{ lb mol H}_2}{100 \text{ lb mol fuel}} \right) \left( \frac{86 \text{ lb mol H}_2 \text{ consumed}}{100 \text{ lb mol H}_2 \text{ supplied}} \right) = 55.01 \frac{\text{lb mol H}_2}{\text{h}}$$

(b) To determine how much oxygen is consumed, it is useful to note the overall fuel cell reaction



$$n_{\text{O}_2, \text{ consumed}} = \left( 55.01 \frac{\text{lb mol H}_2}{\text{h}} \right) \left( \frac{\frac{1}{2} \text{ lb mol O}_2}{1 \text{ lb mol H}_2} \right) = 27.51 \frac{\text{lb mol O}_2}{\text{h}}$$

(c) The required air flow will be determined on a wet air basis, thus

$$n_{\text{air, required}} = \left( 27.51 \frac{\text{lb mol O}_2}{\text{h}} \right) \left( \frac{100 \text{ lb mol O}_2 \text{ supplied}}{70 \text{ lb mol O}_2 \text{ consumed}} \right) \left( \frac{100 \text{ lb mol wet air}}{20.79 \text{ lb mol O}_2} \right) = 189.01 \frac{\text{lb mol wet air}}{\text{h}}$$

$$m_{\text{air, required}} = \left( 189.01 \frac{\text{lb mol wet air}}{\text{h}} \right) \left( \frac{28.74 \text{ lb wet air}}{1 \text{ lb mol wet air}} \right) = 5,433 \frac{\text{lb wet air}}{\text{h}}$$



(d) Per the overall fuel cell reaction above, the water generated is equal to the moles of hydrogen consumed,

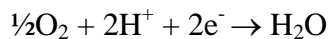
$$n_{\text{H}_2\text{O generated}} = n_{\text{H}_2 \text{ consumed}} = 55.01 \frac{\text{lb mol H}_2}{\text{h}}$$

(e) The composition of the fuel is developed in the table below, by working from the left to right. The composition is determined by converting the composition to moles, accounting for the fuel cell reaction, and converting back to the desired units, mol %. (Note: mol % is essentially equivalent to volume % for low pressure gases.)

<b>Spent Fuel Effluent Calculation</b>					
	mol %	lb mol/hr			mol %
<b>Gas</b>	<b>FC inlet</b>	<b>FC inlet</b>	<b>FC reaction</b>	<b>FC outlet</b>	<b>FC outlet</b>
CH <sub>4</sub>	4.0	3.41		3.41	11.27
CO	0.4	0.34		0.34	1.13
CO <sub>2</sub>	17.6	15.01		15.01	49.58
H <sub>2</sub>	75.0	63.97	-55.01	8.96	29.58
<u>H<sub>2</sub>O</u>	<u>3.0</u>	<u>2.56</u>		<u>2.56</u>	<u>8.45</u>
<b>Total</b>	<b>100.0</b>	<b>85.29</b>	<b>-55.01</b>	<b>30.28</b>	<b>100.00</b>

In the PAFC, only the moles of hydrogen change on the anode (fuel) side of the fuel cell. The other fuel gas constituents simply pass through to the anode exit. These inert gases act to dilute the hydrogen, and as such will lower the cell voltage. Thus, it is always desirable to minimize these diluents as much as possible. For example, to reform natural gas, significant quantities of steam are typically added to maximize the reforming reactions. The wet reformer effluent would commonly have a water composition of 30 to 50%. The reformat gas utilized in this example has been “dried” to only 3% moisture via condensation in a contact cooler.

The spent oxidant composition is calculated in a similar manner. We note that in both the PAFC and PEFC the water is generated on the cathode (air) side. This can be seen from the cathode reaction listed below and the following table listing the fuel cell reaction quantities.



(PAFC & PEFC cathode reaction)

**Spent Air Effluent Calculation**

Gas	mol %	lb mol/hr			mol %
	FC inlet	FC inlet	FC reaction	FC outlet	FC outlet
H <sub>2</sub> O	1.00	1.89	55.01	56.90	26.28
N <sub>2</sub>	78.21	147.82		147.82	58.27
O <sub>2</sub>	<u>20.79</u>	<u>39.30</u>	<u>-27.51</u>	<u>11.79</u>	<u>5.44</u>
<b>Total</b>	<b>100.00</b>	<b>189.01</b>	<b>27.51</b>	<b>216.51</b>	<b>100.00</b>

**Example 10-4 MCFC Effluent Composition - Ignoring the Water Gas Shift Reaction**

An MCFC operating on 1000 lb/hr of fuel gas and a 70% air/30% CO<sub>2</sub> oxidant has a fuel and oxidant utilization of 75% and 50% respectively. With the fuel and oxidant composition and molecular weights listed below, (a) How much hydrogen will be consumed in lb mol/hr? (b) How much oxygen is consumed in lb mol/hr? (c) What are the required air and oxidant flow rates in lb mol/hr? (d) How much CO<sub>2</sub> is transferred from the cathode to the anode? (e) What is the composition of the effluent (spent) fuel and oxidant streams in mol % (ignoring the water gas shift equilibrium)?

Fuel Data	mol %
CH <sub>4</sub>	0.0
CO	0.0
CO <sub>2</sub>	20.0
H <sub>2</sub>	80.0
<u>H<sub>2</sub>O</u>	<u>0.0</u>
Total	100.0
MW	10.42

Oxidant Data	Air	Air + CO <sub>2</sub>
	mol %, wet	mol %, wet
CO <sub>2</sub>	0.00	30.00
H <sub>2</sub> O	1.00	0.70
N <sub>2</sub>	78.21	54.75
<u>O<sub>2</sub></u>	<u>20.79</u>	<u>14.55</u>
Total	100.00	100.00
MW	28.74	33.32

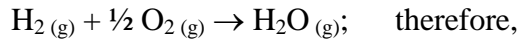
**Solution:**

(a) Before determining the lb mol/hr of hydrogen, we will first determine the molar fuel flow.

$$n_{\text{fuel, supplied}} = \left( 1000 \frac{\text{lb fuel}}{\text{h}} \right) \left( \frac{1 \text{ lb mol fuel}}{10.42 \text{ lb fuel}} \right) = 96.02 \frac{\text{lb mol fuel}}{\text{h}} ; \text{ thus}$$

$$n_{\text{H}_2 \text{ consumed}} = \left( 96.02 \frac{\text{lb mol fuel}}{\text{h}} \right) \left( \frac{80 \text{ lb mol H}_2}{100 \text{ lb mol fuel}} \right) \left( \frac{75 \text{ lb mol H}_2 \text{ consumed}}{100 \text{ lb mol H}_2 \text{ supplied}} \right) = 57.61 \frac{\text{lb mol H}_2}{\text{h}}$$

(b) To determine how much oxygen is consumed, it is useful to note the overall fuel cell reaction,



$$n_{\text{O}_2, \text{ consumed}} = \left( 57.61 \frac{\text{lb mol H}_2}{\text{h}} \right) \left( \frac{\frac{1}{2} \text{ lb mol O}_2}{1 \text{ lb mol H}_2} \right) = 28.81 \frac{\text{lb mol O}_2}{\text{h}}$$

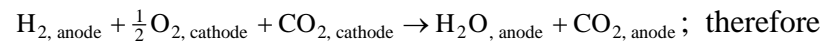
(c) The required air flow will be determined on a wet air basis; thus

$$n_{\text{air, required}} = \left( 28.81 \frac{\text{lb mol O}_2}{\text{h}} \right) \left( \frac{100 \text{ lb mol O}_2 \text{ supplied}}{50 \text{ lb mol O}_2 \text{ consumed}} \right) \left( \frac{100 \text{ lb mol wet air}}{20.79 \text{ lb mol O}_2} \right) = 277.11 \frac{\text{lb mol wet air}}{\text{h}}$$

The oxidant flow rate will be calculated knowing that air is 70% of the total oxidant flow.

$$n_{\text{oxidant, required}} = \left( 277.11 \frac{\text{lb mol wet air}}{\text{h}} \right) \left( \frac{100 \text{ lb mol oxidant}}{70 \text{ lb mol wet air}} \right) = 395.86 \frac{\text{lb mol oxidant}}{\text{h}}$$

(d) Per the overall fuel cell reaction presented below, the quantity of CO<sub>2</sub> transferred from the cathode to the anode side of the fuel cell equals the moles of hydrogen consumed,



$$n_{\text{CO}_2 \text{ transferred}} = n_{\text{H}_2 \text{ consumed}} = 57.61 \frac{\text{lb mol H}_2}{\text{h}}$$

(e) The composition of the fuel effluent is developed in the table below, by working from the left to right. The composition is determined by converting the composition to moles, accounting for the fuel cell reaction, and converting back to the desired units, mol %.

### Spent Fuel Effluent Calculation

Gas	mol %		lb mol/hr			mol %	
	FC inlet	FC inlet	FC reaction	FC outlet	FC outlet	FC outlet	
CH <sub>4</sub>	0.0	0.00		0.00	0.00		
CO	0.0	0.00		0.00	0.00	0.00	
CO <sub>2</sub>	20.0	19.20	57.61	76.82	50.00		
H <sub>2</sub>	80.0	76.82	-57.61	19.20	12.50		
H <sub>2</sub> O	<u>0.0</u>	<u>0.00</u>	<u>57.61</u>	<u>57.61</u>	<u>37.50</u>		
<b>Total</b>	<b>100.0</b>	<b>96.02</b>	<b>-57.61</b>	<b>153.63</b>	<b>100.00</b>		

The spent oxidant composition is calculated in a similar manner. We note that in the MCFC, both oxygen and carbon dioxide are consumed on the cathode (air) side. This can be seen from the cathode reaction listed below and the following table listing the fuel cell reaction quantities.



### Spent Oxidant Effluent Calculation

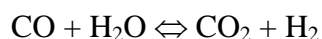
Gas	mol %		lb mol/hr			mol %	
	FC inlet	FC inlet	FC reaction	FC outlet	FC outlet	FC outlet	
CO <sub>2</sub>	30.00	83.13	-57.61	25.52	13.38		
H <sub>2</sub> O	0.70	1.94		1.94	1.02		
N <sub>2</sub>	54.70	151.71		151.71	79.56		
O <sub>2</sub>	<u>14.6</u>	<u>40.33</u>	<u>-28.81</u>	<u>11.52</u>	<u>6.04</u>		
<b>Total</b>	<b>100.00</b>	<b>277.11</b>	<b>-86.42</b>	<b>190.69</b>	<b>100.00</b>		

### Example 10-5 MCFC Effluent Composition - Accounting for the Water Gas Shift Reaction

For the above example, determine the composition of the effluent (spent) fuel stream in mol % including the effect of the water gas shift equilibrium. Assume an effluent temperature of 1200°F.

**Solution:**

The solution to this problem picks up where we left off in Example 10-4 above. For convenience, the water gas shift reaction is presented below:



The double headed arrow is used in the field of chemistry to indicate that a reaction is an equilibrium reaction. That is, the reaction does not proceed completely to the left or to the right.

Instead, the reaction proceeds to an equilibrium point, where both “products” and “reactants” remain. The equilibrium composition is dependent upon both the initial composition and final temperature. Fortunately, the equilibrium concentrations can be determined by a temperature dependent equilibrium constant, K, and the following equation.

$$K = \frac{[\text{CO}_2][\text{H}_2]}{[\text{CO}][\text{H}_2\text{O}]}$$

At 1200°F, the equilibrium constant is 1.967<sup>63</sup>. A check of the compositions from the preceding example shows that those concentration levels are not in equilibrium.

$$\frac{[\text{CO}_2][\text{H}_2]}{[\text{CO}][\text{H}_2\text{O}]} = \frac{[0.50][0.125]}{[0.0][0.375]} = \infty \neq 1.967$$

Because the numerator contains the products of the reaction and the denominator contains the reactants, it is clear that the reaction needs to proceed more towards the reactants. We shall equilibrate this equation, by introducing a variable x, to represent the extent of the reaction to proceed to the right and rewriting the equilibrium equation as:

$$K = \frac{[\text{CO}_2][\text{H}_2]}{[\text{CO}][\text{H}_2\text{O}]} = \frac{[0.50 + x][0.125 + x]}{[0.0 - x][0.375 - x]} = 1.967$$

This can be solved by trial and error or algebraically. First, we’ll demonstrate the trial and error solution, by guessing that x is -0.1. That is, the reaction should “move” to the left as written (more CO and H<sub>2</sub>O). This yields the following:

$$K = \frac{[\text{CO}_2][\text{H}_2]}{[\text{CO}][\text{H}_2\text{O}]} = \frac{[0.50 + (-0.1)][0.125 + (-0.1)]}{[0.0 - (-0.1)][0.375 - (-0.1)]} = \frac{[0.40][0.025]}{[0.1][0.475]} = 0.210$$

---

<sup>63</sup> Equilibrium constants can be calculated from fundamental chemical data such as Gibbs free energy, or can be determined from temperature dependent tables or charts for common reactions. One such table has been published by Girdler Catalysts (1). The following algorithm fits this temperature dependent data to within 5% for 800 to 1800°F, or within 1% for 1000 to 1450°F:  $K_p = e^{(4.276/T - 3.961)}$ .  $K_p(1200^\circ\text{F}$  or  $922\text{K})$  equals 1.967.

The value of x of -0.1 was in the right direction, but apparently too large. We shall now guess x is -0.05.

$$K = \frac{[\text{CO}_2][\text{H}_2]}{[\text{CO}][\text{H}_2\text{O}]} = \frac{[0.50 + -0.05][0.125 + -0.05]}{[0.0 - -0.05][0.375 - -0.05]} = \frac{[0.45][0.075]}{[0.05][0.425]} = 1.588$$

We could continue this simple trial and error procedure until we guessed that x is -0.0445, which yields:

$$K = \frac{[\text{CO}_2][\text{H}_2]}{[\text{CO}][\text{H}_2\text{O}]} = \frac{[0.50 + -0.0445][0.125 + -0.0445]}{[0.0 - -0.0445][0.375 - -0.0445]} = \frac{[0.4555][0.0805]}{[0.0445][0.4195]} = 1.964$$

These concentrations are now in equilibrium. The following table summarizes the effect of accounting for the water gas shift equilibrium.

<b>Spent Fuel Effluent Calculation</b>					
	mol %	lb mol/hr, assuming 100 lb mol/hr basis			mol %
<b>Gas</b>	<b>FC outlet w/o shift.</b>	<b>FC outlet w/o shift</b>	<b>effect of shift rxn</b>	<b>FC outlet in shift equil.</b>	<b>FC outlet in shift equil.</b>
CO	0.00	0.00	4.45	4.45	4.45
CO <sub>2</sub>	50.00	50.00	-4.45	45.55	45.55
H <sub>2</sub>	12.50	12.50	-4.45	8.05	8.05
H <sub>2</sub> O	<u>37.50</u>	<u>37.50</u>	<u>4.45</u>	<u>41.95</u>	<u>41.95</u>
<b>Total</b>	<b>100.0</b>	<b>100.00</b>	<b>0.00</b>	<b>100.00</b>	<b>100.00</b>

Alternately, one could have solved this problem algebraically as follows:

$$K = \frac{[\text{CO}_2 + x][\text{H}_2 + x]}{[\text{CO} - x][\text{H}_2\text{O} - x]}, \text{ can be written as}$$

$$K[\text{CO} - x][\text{H}_2\text{O} - x] = [\text{CO}_2 + x][\text{H}_2 + x], \text{ which can be expanded as}$$

$K \{x^2 - ([CO] + [H_2O])x + [CO][H_2O]\} = x^2 + ([CO_2] + [H_2])x + [CO_2][H_2]$ , which can be combined to

$$\underbrace{(1 - K)x^2}_a + \underbrace{\{[CO_2] + [H_2] + K([CO] + [H_2O])\}x}_b + \underbrace{\{[CO_2][H_2] - [CO][H_2O]K\}}_c = 0$$

This is in the standard quadratic form of:

$$ax^2 + bx + c = 0$$

which can be solved by the quadratic formula:

$$x = \frac{-b \pm \sqrt{b^2 - 4ac}}{2a}$$

Substituting the appropriate values for K and the concentrations yields two roots of -0.0445 and 1.454. We throw out the larger root because it is a nonsensical root. This larger root “wants to” react more CO and H<sub>2</sub>O than are initially present. When using the quadratic formula, the user will throw out all roots greater than 1 or less than -1. The remaining root of -0.0445 is precisely what was developed by our previous trial and error exercise.

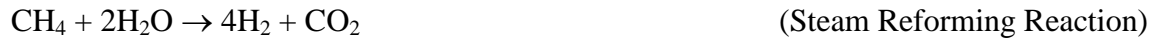
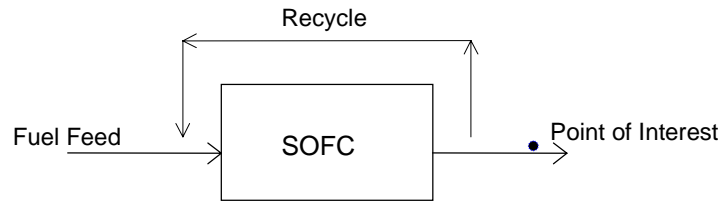
### **Example 10-6 SOFC Effluent Composition - Accounting for Shift and Reforming Reactions**

An SOFC is operating on 100 % methane (CH<sub>4</sub>) and a fuel utilization of 85%. (a) What is the composition of the effluent (spent) fuel in mol %? Assume that the methane is completely reformed within the fuel cell, and the moisture required for reforming is supplied by internal recirculation.

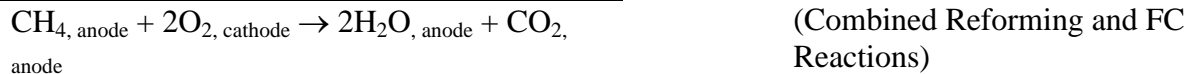
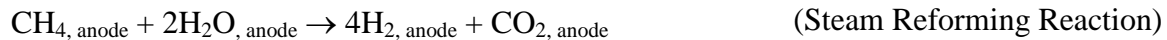
#### ***Solution:***

- (a) There are many different ways to approach this problem, some of which may seem rather complex because of the simultaneous reactions (fuel cell, reforming and water gas shift reactions) and the recycle stream supplying moisture required for the reforming reaction. We shall simplify the solution to this problem by focusing on the fuel cell exit condition. Because we have drawn the box of interest at a point after the recycle, this will allow us to ignore the recycle stream and to deal with the reactions in steps and not simultaneously.

First, we shall write the relevant reactions:



Next we shall combine the reforming reaction and the fuel cell reaction into an overall reaction for that portion of the fuel that is utilized within the fuel cell (i.e., 85%). The combined reaction is developed by adding the steam reforming reaction to 4 times the fuel cell reaction. The factor of four allows the hydrogen molecules to drop out of the resulting equation because it is fully utilized.



For the 15% of the fuel that is not utilized in the cell reaction we shall simply employ the reforming reaction. To the resulting gas composition, we will then impose the water gas shift equilibrium.

For ease of calculation, we shall assume a 100 lb/hr basis for the methane.

$$n_{\text{fuel, supplied}} = \left(100 \frac{\text{lb CH}_4}{\text{h}}\right) \left(\frac{1 \text{ lb mol CH}_4}{16.043 \text{ lb CH}_4}\right) = 6.23 \frac{\text{lb mol CH}_4}{\text{h}},$$

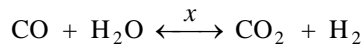
Thus, 85%, or 5.30 lb mol CH<sub>4</sub> /h, will be reformed and consumed by the fuel cell. The remainder will be reformed but not consumed by the fuel cell reaction. We will summarize these changes in the following table.



### Spent Fuel Effluent Calculation

Gas	mol %		lb mol/hr			mol %	
	FC inlet	FC inlet	Ref / FC rxn	Reforming	FC outlet	FC outlet	
CH <sub>4</sub>	100.0	6.23	-5.30	-0.93	0.00	0.00	0.00
CO	0.0	0.00	0.00	0.00	0.00	0.00	0.00
CO <sub>2</sub>	0.0	0.00	5.30	0.93	6.23	33.33	33.33
H <sub>2</sub>	0.0	0.00	0.00	3.74	3.74	20.00	20.00
H <sub>2</sub> O	0.0	0.00	10.60	-1.87	8.73	46.67	46.67
<b>Total</b>	<b>100.0</b>	<b>6.23</b>	<b>10.60</b>	<b>1.87</b>	<b>18.70</b>	<b>100.00</b>	<b>100.00</b>

Now, we have created an artificial solution that reflects only two out of three reactions. We shall now apply the water gas shift reaction to determine the true exit composition. We shall apply the quadratic equation listed in Example 10-5 to determine how far the reaction will proceed, where  $x$  is the extent of the reaction in the forward direction as written.



$$x = \frac{-b \pm \sqrt{b^2 - 4ac}}{2a}$$

$$a = (1 - K) = (1 - 0.574) = 0.426$$

$$b = \{[\text{CO}_2] + [\text{H}_2] + K([\text{CO}] + [\text{H}_2\text{O}])\} = 0.3333 + 0.2000 + 0.574*(0.00 + 0.4667) = .8012$$

$$c = \{[\text{CO}_2][\text{H}_2] - [\text{CO}][\text{H}_2\text{O}]K\} = (0.3333)(0.20) - (0.00)(0.4667)(0.574) = 0.0666$$

$$x = \frac{-b \pm \sqrt{b^2 - 4ac}}{2a} = \frac{-0.8012 \pm \sqrt{(0.8012)^2 - 4(0.426)(0.0666)}}{2(0.426)} = -0.0873 \text{ and } -1.794$$

Again we throw out the value greater than 1, or less than -1, leaving -0.0873. The following table summarizes the effect of accounting for the water gas shift equilibrium.

### Spent Fuel Effluent Calculation

Gas	mol %		lb mol/hr, assuming 100 lb mol/hr basis		mol %	
	FC outlet w/o shift.	FC outlet w/o shift	Effect of shift rxn	FC outlet in shift equil.	FC outlet in shift equil.	
CO	0.00	0.00	-(-8.73)	8.73	8.73	
CO <sub>2</sub>	33.33	33.33	-(-8.73)	24.61	24.61	
H <sub>2</sub>	20.00	20.00	-8.73	11.27	11.27	
H <sub>2</sub> O	<u>46.67</u>	<u>46.67</u>	-8.73	<u>55.39</u>	<u>55.39</u>	
<b>Total</b>	<b>100.00</b>	<b>100.00</b>	<b>0.00</b>	<b>100.00</b>	<b>100.00</b>	

#### Example 10-7 Generic Fuel Cell - Determine the Required Cell Area, and Number of Stacks

Given a desired output of 2.0 MW<sub>DC</sub>, and the desired operating point of 600 mV and 400 mA/cm<sup>2</sup>, (a) How much fuel cell area is needed? (b) Assuming a cell area of 1.00 m<sup>2</sup> per cell and 280 cells per stack, how many stacks are needed for this 2.0 MW unit?

**Solution:**

(a) Recalling again that power is the product of the voltage and current, we first determine the total current for fuel cell as

$$I = \frac{P}{V} = \left( \frac{2.0 \text{ MW}}{0.600 \text{ V}} \right) \left( \frac{10^6 \text{ W}}{1 \text{ MW}} \right) \left( \frac{1 \text{ VA}}{1 \text{ W}} \right) \left( \frac{1 \text{ kA}}{1000 \text{ A}} \right) = 3,333 \text{ kA}$$

Because each individual fuel cell will operate at 400 mA/cm<sup>2</sup>, we determine the total area required as,

$$\text{Area} = \frac{I}{\text{Current Density}} = \left( \frac{3,333 \text{ kA}}{400 \text{ mA} / \text{cm}^2} \right) \left( \frac{1000 \text{ mA}}{1 \text{ A}} \right) \left( \frac{1000 \text{ A}}{1 \text{ kA}} \right) = 8,333,333 \text{ cm}^2$$

b) The number of required stacks and cells are calculated simply as

$$\text{No. of Cells} = \frac{(8,333,333 \text{ cm}^2)}{(1 \text{ m}^2 \text{ per cell})} \left( \frac{1 \text{ m}^2}{10,000 \text{ cm}^2} \right) = 833 \text{ cells}$$

$$\text{No. of Stacks} = \frac{(833 \text{ cells})}{(280 \text{ cells per stack})} = 2.98 \text{ stacks} \cong 3 \text{ stacks}$$

## 10.1.2 Fuel Processing Calculations

### Example 10-8 Methane Reforming - Determine the Reformate Composition

Given a steam reformer operating at 1400°F, 3 atmospheres, pure methane feed stock, and a steam to carbon ratio of 2 (2 lb mol H<sub>2</sub>O to 1 lb mol CH<sub>4</sub>), (a) List the relevant reactions, (b) Determine the equilibrium concentration assuming the effluent exits the reactor in equilibrium at 1400°F (c) Determine the heats of reaction for the reformer's reactions. (d) Determine the reformer's heat requirement assuming the feed stocks are preheated to 1400°F. (e) Considering LeChâtelier's principle, indicate whether the reforming reaction will be enhanced or hindered by an elevated operating temperature (f) Considering LeChâtelier's principle, indicate whether excess steam will tend to promote or prevent the reforming reaction.

#### *Solution:*

(a) The relevant reactions for the steam reformer are presented below:



A third relevant reaction is also presented below. However, this reaction is simply a combination of the other two. Of the three reactions, any two can be utilized as an independent set of reactions for analysis, and should be chosen for the user's convenience. Here we have chosen the steam reforming and the shift reactions.



- (b) The determination of the equilibrium concentrations is a rather involved problem, requiring significant background in chemical thermodynamics, and therefore will not be solved here. One aspect that makes this problem more difficult than Example 10-6, which accounted for the steam reforming reaction within the fuel cell, is that we cannot assume the reforming reactions will proceed to completion as we did in the former example. In Example 10-6, hydrogen is consumed within the fuel cell thus driving the reforming reaction to completion. Without being able to assume the reforming reaction goes to completion, we must simultaneously solve two independent equilibrium reactions. The solution to this problem is most easily accomplished with chemical process simulation programs using a technique known as the minimization of Gibbs free energy. To solve this problem by hand, however, is a arduous, time-consuming task.

For interest, an ASPEN™ computer solution of this problem is given below:

	Inlet Composition (lb mols/hr)	Effluent Composition (lb mols/hr)	Effluent Composition (mol fraction)
CH <sub>4</sub>	100	11.7441	2.47
CO	0	64.7756	13.59
CO <sub>2</sub>	0	23.4801	4.93
H <sub>2</sub>	0	288.2478	60.49
H <sub>2</sub> O	200	88.2639	18.52
Total	300	476.5115	100.00

- (c) This problem is rather time-consuming to solve without a computer program and will therefore be left to the ambitious reader to solve<sup>64</sup> from thermodynamic fundamentals. As an alternative, the reader may have access to tables that list heat of reaction information for important reactions. The following temperature dependent heats of reaction values were found for the water gas shift and reforming reactions in the Girdler tables (1).



Note: a positive heat of reaction is endothermic (heat must be added to maintain a constant temperature), while a negative heat of reaction is exothermic (heat is given off).

<sup>64</sup> The reader can refer to Reference 2, Example 4-8 for the solution of a related problem.

(d) With knowledge of the equilibrium concentration and the heat of reactions, we can easily calculate the heat requirement for the reformer. Knowing that for each lb mol of CH<sub>4</sub> feed, 88.3% [(100-11.7)/100= 88.3%] of the CH<sub>4</sub> was reformed, and 26.6% [23.5/88.3= 26.6%] of the formed carbon monoxide shifts to carbon dioxide, then the overall heat generation for each lb mol of methane feed can be developed from

$$(1 \text{ lbmol CH}_4) \left( \frac{88.3\% \text{ CH}_4 \text{ reacted}}{100\% \text{ CH}_4 \text{ feed}} \right) \left( 97,741 \frac{\text{Btu}}{\text{lbmol reformed CH}_4} \right) = 86,300 \frac{\text{Btu}}{\text{lbmol CH}_4 \text{ feed}}$$

$$(1 \text{ lbmol CH}_4) \left( \frac{88.3\% \text{ CH}_4 \text{ rxt.}}{100\% \text{ CH}_4 \text{ feed}} \right) \left( \frac{1 \text{ lbmol CO}}{\text{lbmol CH}_4 \text{ rxt.}} \right) \left( \frac{26.6\% \text{ CO shifts}}{\text{lbmol CO Feed}} \right) \left( \frac{-13,982 \text{ Btu}}{\text{lbmol CO rxn}} \right) = -3,300 \frac{\text{Btu}}{\text{lbmol CH}_4 \text{ feed}}$$

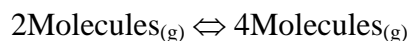
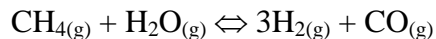
Therefore the heat requirement for the reformer is 83,000 Btu/lb mol of CH<sub>4</sub> fed to the reformer. Because this value is positive, the overall reaction is endothermic and heat must be supplied.

(e) LeChâtelier's principle simply states that "*if a stress is applied to a system at equilibrium, then the system readjusts, if possible, to reduce the stress*" (3). The power of this simple principle is illustrated by the insight that it provides in many situations where little is known. In our reforming example, we can learn from LeChâtelier's principle whether higher or lower temperatures will promote the reforming reaction just by knowing that the reaction is endothermic. To facilitate the application of principle, we shall write the endothermic reforming reaction with a heat term on the left side of the equation.



Now if we consider that raising the temperature of the system is the applied stress, then the stress will be relieved by the reaction when the reaction proceeds forward. Therefore, we can conclude that the reforming reaction is thermodynamically favored by high temperatures.

(f) To solve this application of LeChâtelier's principle, we shall write the reforming reaction in terms of the number of gaseous molecules on the left and right sides.



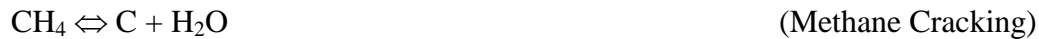
Now if we imagine a reforming system at equilibrium, and increase the pressure (the applied stress), then the reaction will try to proceed in a direction that will reduce the pressure (stress). Because a reduction in the number of molecules in a system will reduce the stress, an elevated pressure will tend to inhibit the reforming reaction. (Note: reforming systems often operate at moderate pressures, for operation at pressure will reduce the equipment size and cost. To compensate for this elevated pressure, the designer may be required to raise the temperature.)

### Example 10-9 Methane Reforming - Carbon Deposition

Given the problem above, (a) list three potential coking (carbon deposition, or sooting) reactions, (b) considering LeChâtelier's principle, indicate whether excess steam will tend to promote or inhibit the coking reactions, (c) determine the minimum steam to methane ratio required in order to prevent coking based on a thermodynamic analysis, and (d) determine the minimum steam to methane ratio to prevent coking considering the chemical kinetics of the relevant reactions.

#### *Solution:*

(a) Three of the most common/important carbon deposition equations are presented below.



(b) Considering LeChâtelier's principle, the addition of steam will clearly inhibit the formation of soot for the methane cracking and CO reduction reactions. (The introduction of excess steam will encourage the reaction to proceed towards the reactants, i.e., away from the products of which water is one.) Excess steam does not have a direct effect on the Boudouard coking reaction except that the presence of steam will dilute the reactant and product concentrations. When the Boudouard coking reaction proceeds towards the left, the concentration of CO will increase faster than the concentration of CO<sub>2</sub>. Thus, dilution steam will cause the Boudouard coking reaction to proceed toward the left. Clearly, the addition of steam is quite useful at preventing sooting from ruining the expensive catalysts that are utilized in reformers and fuel cell systems. Too much steam, however, will simply add an unnecessary operating cost.

(c) The determination of the minimum steam to carbon ratio that will inhibit carbon deposition is of interest to the fuel cell system designer, but it is, however, beyond the scope of this handbook. The interested reader is referred to references (4), (5), and (6).

(d) A steam quantity that will preclude the formation of soot based upon a thermodynamic analysis will indeed prevent soot from forming. However, it may not be necessary to add as much steam as is implied by thermodynamics. Although soot formation may be thermodynamically favored under certain conditions, the kinetics of the reaction can be so slow that sooting will not be a problem. Thus, the determination of sooting on a kinetic basis is of significant interest. The solution to this problem is, however, beyond the scope of this handbook, so the interested reader is referred to reference (6). When temperatures drop to about 750°C, kinetic limitations preclude sooting (7). However, above this point, the composition and temperature together determine whether sooting is kinetically precluded. Typically, steam reformers have operated with steam to carbon ratios of 2 to 3 depending on the operating conditions in order to provide an adequate safety margin. An example calculation presented in Reference 6, however, reveals that conditions requiring a steam to carbon ratio of 1.6 on a thermodynamic basis can actually support a steam to carbon ratio of 1.2 on a kinetic basis.

### 10.1.3 Power Conditioners

#### Example 10-10 Conversion between DC and AC Power

Given a desired output of 1.0 MW<sub>AC</sub>, and an inverter efficiency of 96.5%, what DC output level is required from the fuel cell stack?

**Solution:**

(a) The required DC power output level is found simply as the quotient of AC power and the inverter efficiency as demonstrated below.

$$MW_{DC} = (1.0 MW_{AC}) \left( \frac{1 MW_{DC}}{96.5\% MW_{AC}} \right) = 1.036 MW_{DC}$$

### 10.1.4 Others

Numerous other unit operations and subsystems can be found in fuel cell systems. It is not however the intent of this handbook to review all of these operations and subsystems that are well documented in many other references [e.g., (2,8,9,10)]. For convenience, the unit operations that are commonly found within fuel cell power system are listed below:

- heat exchangers
- pumps
- compressors
- expanders
- intercoolers
- direct contact coolers
- gasification
- gas clean up

## 10.2 System Issues

This section covers system issues such as HHV, LHV, and cogeneration efficiency calculations, heat rate calculations, and cogeneration steam duty calculations.

### 10.2.1 Efficiency Calculations

#### Example 10-11 LHV, HHV Efficiency and Heat Rate Calculations

Given a 2.0 MW<sub>AC</sub> fuel cell cycle operating on 700 lb/hr of methane, what is (a) the HHV<sup>65</sup> thermal input of the methane gas, (b) the LHV thermal input, (c) the HHV electric efficiency, (d) the LHV electric efficiency, and (e) the HHV Heat Rate? Assume the higher and lower heating value of methane as 23,881 and 21,526 Btu/lb respectively.

**Solution:**

(a) The HHV thermal input of the methane gas is

$$\text{HHV Thermal Input} = (700 \text{ lb/h CH}_4) \left( \frac{23,881 \text{ Btu, HHV}}{1 \text{ lb CH}_4} \right) \left( \frac{1 \text{ MMBtu}}{10^6 \text{ Btu}} \right) = 16.716 \text{ MMBtu/h, or}$$

$$\text{HHV Thermal Input} = (16.716 \text{ MMBtu/h}) \left( \frac{1 \text{ MW}}{3.412 \text{ MMBtu}} \right) = 4.899 \text{ MW}_t$$

(b) The LHV thermal input of the methane gas is

$$\text{HHV Thermal Input} = (700 \text{ lb/h CH}_4) \left( \frac{21,526 \text{ Btu, HHV}}{1 \text{ lb CH}_4} \right) \left( \frac{1 \text{ MMBtu}}{10^6 \text{ Btu}} \right) = 15.068 \text{ MMBtu/h, or}$$

$$\text{HHV Thermal Input} = (15.068 \text{ MMBtu/h}) \left( \frac{1 \text{ MW}}{3.412 \text{ MMBtu}} \right) = 4.416 \text{ MW}_t$$

---

<sup>65</sup> Heating values are expressed as higher or lower heating values (HHV or LHV). Both higher and lower heating values represent the amount of heat released during combustion. The difference between the HHV and LHV is simply whether the product water is in the liquid phase (HHV), or the gaseous phase (LHV). Because the evaporation of water consumes energy, the LHV is always less than the HHV.



(c) The HHV electrical efficiency is

$$\text{Electrical Efficiency (HHV)} = \left( \frac{\text{Output}}{\text{Input, HHV}} \right) = \left( \frac{2.0 \text{ MWac}}{4.899 \text{ MWt, HHV}} \right) = 40.8\% \text{ HHV}$$

(d) The LHV electrical efficiency is

$$\text{Electrical Efficiency (LHV)} = \left( \frac{\text{Output}}{\text{Input, LHV}} \right) = \left( \frac{2.0 \text{ MWac}}{4.416 \text{ MWt, LHV}} \right) = 45.3\% \text{ LHV}$$

Note: *Because a fuel's LHV is less than its HHV value, the LHV efficiency will always be higher than the HHV efficiency.*

(e) Heat rate is the amount of heat (Btu/h) required to produce a kW of electricity. Alternatively it can be thought of as an inverse efficiency. Because 1 kW is equivalent to 3,412 Btu/h, a heat rate of 3,412 Btu/kWh represents an efficiency of 100%. Note that as the efficiency goes up, the heat rate goes down. The HHV heat rate for this example can be calculated easily from either the HHV efficiency or the thermal input. Both methods are demonstrated below:

$$\text{Heat Rate (HHV)} = \left( \frac{3412 \text{ Btu/kWh}}{\text{Efficiency, HHV}} \right) = \left( \frac{3412 \text{ Btu/kWh}}{40.8\%} \right) = 8,360 \frac{\text{Btu}}{\text{kWh}} (\text{HHV}), \text{ or alternatively,}$$

$$\text{Heat Rate (HHV)} = \left( \frac{\text{Input, HHV}}{\text{Output}} \right) = \left( \frac{16,717,000 \text{ Btu/h}}{2,000 \text{ kW}} \right) = 8,360 \frac{\text{Btu}}{\text{kWh}} (\text{HHV}).$$

Note: The LHV to HHV ratio of 90% for methane (21,526/23,881 = 90.%) is typical of that for natural gas, while this ratio is roughly 94% for fuel oils. Common coals typically have a LHV to HHV ratio of 92 to 96% depending upon the hydrogen and moisture content<sup>66</sup>. Typically, gas turbine based cycles are presented on an LHV basis. Conventional power plants, such as coal-, oil-, and gas-fired steam generator/steam turbine cycles are presented on an HHV basis within the U.S, and on an LHV basis in the rest of the world.

---

<sup>66</sup> The difference between the LHV and HHV heating values can be estimated by (1055 Btu/lb)\*w, where w is the lbs moisture after combustion per lb of fuel. Thus, w can be determined from the fuel's hydrogen and moisture content by w= moisture + 18/2 \* hydrogen. [e.g., for a fuel with 10% moisture and 4% hydrogen, the LHV to HHV difference is 485 Btu/lb, [i.e., 1055\*(.10+.04\*9)=485.]

### Example 10-12 Efficiency of a Cogeneration Fuel Cell System

Given the system described in Example 10-11, what is (a) the combined heat and power efficiency assuming that cycle produces 2 tons/hr of 150 psia/400°F steam? Assume a feedwater temperature of 60°F.

#### **Solution:**

- (a) Before calculating the cogeneration efficiency, we first need to determine the heat duty associated with the steam production. This requires knowledge of the steam and feed water enthalpies, which we can find in the ASME Steam Tables (11) as indicated below:

	Temperature (°F)	Pressure (psia)	Enthalpy (Btu/lb)
Steam	400	150	1219.1
Feedwater	60	180	28.6

The steam heat duty is calculated as

$$\text{Heat Duty} = (\text{mass flow})(\text{Change in enthalpy}) = (4000 \text{ lb/h})(1219.1 - 28.6 \text{ Btu/lb}) \left( \frac{1 \text{ MMBtu}}{10^6 \text{ Btu}} \right) = 4.762 \text{ MMBtu/h}$$

Alternatively, this heat duty can be expressed as 1.396 MW<sub>t</sub>, [4.762 / 3.412 = 1.396 MW]. Thus, the combined heat and power efficiency is calculated as

$$\text{Combined Heat \& Electrical Efficiency (HHV)} = \left( \frac{\text{Output}}{\text{Input, HHV}} \right) = \left( \frac{2.00 \text{ MW}_{AC} + 1.40 \text{ MW}_t}{4.899 \text{ MW}_t, \text{ HHV}} \right) = 69.4\% \text{ HHV}$$

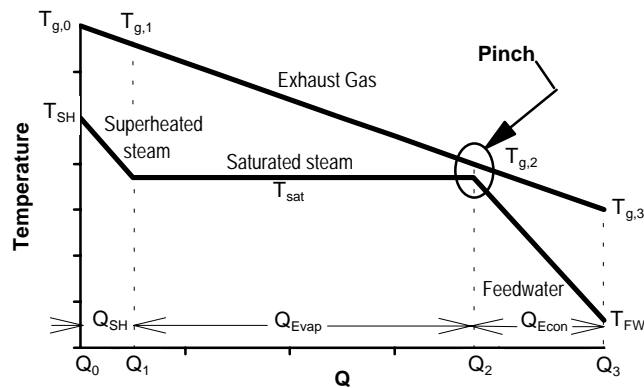
## 10.2.2 Thermodynamic Considerations

### Example 10-13 Production of Cogeneration Steam in a Heat Recovery Boiler (HRB)

Given 10,000 lb/hr of 700°F cycle exhaust gas passing through a heat recovery boiler (HRB) (a) How much 150 psia, 400°F steam can be produced? (b) How much heat is transferred from the gas to the steam? (c) What is the exhaust temperature of the gas leaving the HRB? and (d) Sketch the T-Q (temperature-heat) diagram for the HRB. Assume a gas side mean heat capacity of 0.25 Btu/lb, °F, an evaporator pinch temperature of 30°F, a feedwater temperature of 60°F, and an evaporator drum pressure of 180 psia to allow for pressure losses.

**Solution:**

- (a) We shall develop our solution strategy by examining a typical HRB T-Q diagram presented below. From this diagram we observe that the pinch point, the minimum temperature differential between the gas and saturated steam, limits the steam production. If we were to try to produce more steam, the lower steam line would be stretched to the right until it "bumped" into the hot gas line. At the point of contact, both the hot gas and saturated steam would be at the same temperature. This is thermodynamically impossible, because heat will only "flow" from a higher temperature to a lower one. In practice, the temperature approach at the pinch point is kept large enough (15 to 40°F) to prevent an unusually large and expensive evaporator. Because the pinch limits the steam production, we can use the heat available in the gas down to the pinch point to determine how much steam can be produced.



The governing equations for the heat available in the gas down to the pinch point ( $T_{g,0}$  to  $T_{g,2}$ ), and the corresponding heat absorbed by the superheated and saturated steam are presented below.

$$Q_{SH + Evap}^{gas} = (m_{gas})(C_p)(T_{g,0} - T_{g,2})$$

$$Q_{SH + Evap}^{steam} = (m_{steam})(h_{superheated} - h_f), \text{ and}$$

$$Q_{SH + Evap}^{gas} = Q_{SH + Evap}^{steam}$$

We can calculate  $Q_{SH + Evap}^{gas}$  if we determine the steam saturation temperature from the steam tables. By using the ASME steam tables (11), we can determine the saturation temperature and enthalpies of interest as

$$h_{steam} (150 \text{ psia}, 400 \text{ }^\circ\text{F}) = 1219.1 \text{ Btu/lb}$$

$$h_g (180 \text{ psia}, \text{ saturated steam}) = 1196.9 \text{ Btu/lb}$$

$$h_f (180 \text{ psia}, \text{ saturated water}) = 346.2 \text{ Btu/lb}$$

$$T_{sat} (180 \text{ psia}, \text{ saturated steam/water}) = 373.1^\circ\text{F}$$

$$h_{feedwater} (60 \text{ }^\circ\text{F}) = 28.6 \text{ Btu/lb}$$

Thus, we can solve for  $Q_{SH + Evap}^{gas}$ , by allowing the gas side pinch temperature to be equal to the saturation temperature of  $373.1^\circ\text{F}$  plus the desired approach temperature of  $30^\circ\text{F}$  for a value of  $403.1^\circ\text{F}$ . Thus,

$$Q_{SH + Evap}^{gas} = \left( 10,000 \frac{\text{lb}}{\text{hr}} \right) \left( 0.25 \frac{\text{Btu}}{\text{lb}, \text{ }^\circ\text{F}} \right) (700 - 403.1 \text{ }^\circ\text{F}) = 842,000 \frac{\text{Btu}}{\text{hr}}$$

By substituting this heat value into the steam side equation, we can solve directly for the steam mass flow rate by

$$m_{steam} = \frac{Q_{SH + Evap}^{steam}}{(h_{superheated} - h_f)} = \frac{742,000 \frac{\text{Btu}}{\text{hr}}}{\left( 1219.1 - 346.2 \frac{\text{Btu}}{\text{lb}} \right)} = 850 \frac{\text{lb}}{\text{hr}}$$

(b) Now that we know the water/steam mass flow, we can easily determine the HRB heat duty by the following equation.

$$Q_{Total}^{steam} = (m_{steam})(h_{superheated} - h_{feedwater}) = \left( 850 \frac{\text{lb}}{\text{hr}} \right) (1219.1 - 28.6 \frac{\text{Btu}}{\text{lb}}) = 1,012,000 \frac{\text{Btu}}{\text{hr}}$$

(c) The gas temperature leaving the HRB ( $T_{\text{gas},3}$ ) is now easily calculated, because the total heat transferred to the steam is equivalent to that lost by the gas stream.

$$Q_{\text{Total}}^{\text{gas}} = (m_{\text{gas}})(C_p)(T_{\text{gas},0} - T_{\text{gas},3}) \quad \text{Thus,}$$

$$1,012,000 \frac{\text{Btu}}{\text{hr}} = \left(10,000 \frac{\text{lb gas}}{\text{hr}}\right) \left(0.25 \frac{\text{Btu}}{\text{lb, }^\circ\text{F}}\right) (700 \text{ F} - T_{\text{g},3})$$

Solving for  $T_{\text{gas},3}$ , we find that  $T_{\text{gas},3}$  is 295°F.

(d) Because we assumed a constant mean  $C_p$  for the exhaust gas over the temperature range of interest, we can simply draw a straight line from 700°F to 295°F, with the 295°F corresponding to a transferred quantity of heat of 1.01 MMBtu/hr. To draw the water line, we will need to determine the heat absorbed by the superheater, the evaporator, and the economizer. These heats are determined by the following equations.

$$Q_{\text{SH}}^{\text{steam}} = (m_{\text{steam}})(h_{\text{superheated}} - h_g)$$

$$Q_{\text{Evap}}^{\text{steam}} = (m_{\text{steam}})(h_g - h_f)$$

$$Q_{\text{Econ}}^{\text{water}} = (m_{\text{water}})(h_f - h_{\text{feedwater}})$$

Substituting the known flow and enthalpy data allows us to solve for these three quantities as

$$Q_{\text{SH}}^{\text{steam}} = \left(850 \frac{\text{lb}}{\text{h}}\right) \left(1219.1 - 1196.9 \frac{\text{Btu}}{\text{lb}}\right) = \left(850 \frac{\text{lb}}{\text{h}}\right) \left(22.2 \frac{\text{Btu}}{\text{lb}}\right) = 18,900 \frac{\text{Btu}}{\text{h}}$$

$$Q_{\text{Evap}}^{\text{steam}} = \left(850 \frac{\text{lb}}{\text{h}}\right) \left(1196.9 - 346.2 \frac{\text{Btu}}{\text{lb}}\right) = \left(850 \frac{\text{lb}}{\text{h}}\right) \left(850.7 \frac{\text{Btu}}{\text{lb}}\right) = 723,100 \frac{\text{Btu}}{\text{h}}$$

$$Q_{\text{Econ}}^{\text{water}} = \left(850 \frac{\text{lb}}{\text{h}}\right) \left(346.2 - 28.6 \frac{\text{Btu}}{\text{lb}}\right) = \left(850 \frac{\text{lb}}{\text{h}}\right) \left(317.6 \frac{\text{Btu}}{\text{lb}}\right) = 270,000 \frac{\text{Btu}}{\text{h}}$$

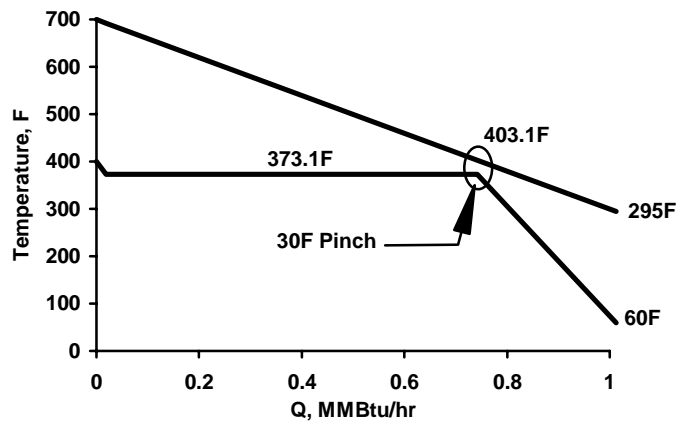
Using these values to develop cumulative heat transfer quantities, we calculate the following;

$$Q_1 = Q_{SH}^{steam} = 18,900 \frac{\text{Btu}}{\text{h}} = 0.019 \frac{\text{MMBtu}}{\text{h}} \text{ at } 373.1^\circ \text{F}$$

$$Q_2 = Q_1 + Q_{Evap}^{steam} = 18,900 + 723,100 \frac{\text{Btu}}{\text{h}} = 742,000 \frac{\text{Btu}}{\text{h}} = 0.742 \frac{\text{MMBtu}}{\text{h}} \text{ at } 373.1^\circ \text{F}$$

$$Q_3 = Q_2 + Q_{economizer}^{water} = 742,000 + 270,000 \frac{\text{Btu}}{\text{h}} = 1,012,000 \frac{\text{Btu}}{\text{h}} = 1.012 \frac{\text{MMBtu}}{\text{h}} \text{ at } 60^\circ \text{F}$$

Plotting these points on the chart below, we yield the following T-Q diagram.



### 10.3 Supporting Calculations

#### Example 10-14 Molecular Weight Calculation for Air

Assuming that dry air is composed of 79%  $\text{N}_2$  and 21%  $\text{O}_2$ , what is the molecular weight of air?

**Solution:**

- (a) Atomic weights for elements that are common to fuel cell systems are presented in Table 10-1.

**Table 10-1 Common Atomic Elements and Weights**

Atomic Species		Atomic Weights
Argon,	Ar	39.948
Carbon,	C	12.011
Hydrogen,	H	1.0079
Nitrogen,	N	14.0067
Oxygen,	O	15.9994
Sulfur,	S	32.06

The molecular weight for diatomic (2 atoms per molecule) nitrogen and oxygen is simply twice their atomic weight. Thus, the molecular weights for N<sub>2</sub> and O<sub>2</sub> are 28.01 and 32.00.

Now because atmospheric air is a low pressure gas (< 10 atm), we can assume that it will behave as an ideal gas and that its mole % is equivalent to its volume %. We also shall simplify our solution by assuming a calculation basis of 100 lb mols of air. With these assumption, the molecular weight of air is developed in the following table by working from left to right.

**Molecular Weight Calculation for Dry Air**

Gas	mol %	100 lb mol/hr basis			MW lb/lb mol
		lb mol	MW	lbs	
N <sub>2</sub>	79.00	79.00	28.01	2212.8	
O <sub>2</sub>	<u>21.00</u>	<u>21.00</u>	32.00	<u>672.0</u>	
<b>Total</b>	<b>100.00</b>	<b>100.00</b>		<b>2884.8</b>	<b>28.85</b>

Thus, the molecular weight of dry air is 28.85 lb/lb mol (28.85 g/g mol) as presented previously in Example 10-3.

**Example 10-15 Molecular Weight, Density and Heating Value Calculations**

Given the natural gas composition presented below, what is (a) the molecular weight, (b) the higher heating value in Btu/ft<sup>3</sup>? (c) the density of the gas in lb/ft<sup>3</sup> at 1 atm and 60°F? (d) the higher heating value in Btu/lb, and (e) the lower heating value in Btu/ft<sup>3</sup>?

Fuel Constituent	mol %
CH <sub>4</sub>	4.0
CO	0.4
CO <sub>2</sub>	17.6
H <sub>2</sub>	75.0
<u>H<sub>2</sub>O</u>	<u>3.0</u>
Total	100.0

**Solution:**

- (a) Before determining the molecular weight of the natural gas mixture, we shall develop the molecular weights of each of the gas constituents in the following table.

Fuel Constituent	MW Derivation	MW
CH <sub>4</sub>	$(12.01) + 4*(1.008) = 16.04$	16.04
CO	$(12.01) + 1*(16.00) = 28.01$	28.01
CO <sub>2</sub>	$(12.01) + 2*(16.00) = 44.01$	44.01
H <sub>2</sub>	$2*(1.008) = 2.016$	2.016
H <sub>2</sub> O	$2*(1.008) + 1*(16.00) = 18.02$	18.02

Thus, the molecular weight for the gas mixture is calculated below by utilizing a 100 lb mol basis:

Fuel Constituents	mol %	100 lb mol basis			1 lb mol
		lb mols	MW (lb/lb mol)	Weight (lb)	MW (lb/lb mol)
CH <sub>4</sub>	4.0	4.0	16.04	64.16	
CO	0.4	0.4	28.01	11.20	
CO <sub>2</sub>	17.6	17.6	44.01	774.58	
H <sub>2</sub>	75.0	75.0	2.016	151.20	
H <sub>2</sub> O	<u>3.0</u>	<u>3.0</u>	18.02	<u>55.06</u>	
Total	100.0	100.0		1056.2	10.56

- b) The higher heating value of the natural gas can be reasonably predicted from the composition. The following table presents the higher heating value for many common fuel gas constituents.



**Table 10-2 HHV Contribution of Common Gas Constituents**

Gas	Higher Heating Value	
	Btu/lb	Btu/ft <sup>3</sup>
H <sub>2</sub>	60,991	325
CO	4,323	321
CH <sub>4</sub>	23,896	1014
C <sub>2</sub> H <sub>6</sub>	22,282	1789
C <sub>3</sub> H <sub>8</sub>	22,282	2573
C <sub>4</sub> H <sub>10</sub>	21,441	3392
H <sub>2</sub> O, CO <sub>2</sub> , N <sub>2</sub> , O <sub>2</sub>	0	0

Reference (12)

HHV (Btu/ft<sup>3</sup>) are for 1 atm, and 60°F.

Using these HHV contributions, the gas composition, and the ideal gas law assumption where we equate % moles with % volume, we calculate the overall HHV by utilizing a basis of 100 ft<sup>3</sup> in the following table by working from left to right.

Fuel Constituents	mol %	100 ft <sup>3</sup> Basis			1 ft <sup>3</sup> Basis
		Volume (ft <sup>3</sup> )	HHV (Btu/ft <sup>3</sup> )	Heat Input (Btu)	HHV (Btu/ft <sup>3</sup> )
CH <sub>4</sub>	4.0	4.0	1014	4056.	
CO	0.4	0.4	321	128.	
CO <sub>2</sub>	17.6	17.6	0	0	
H <sub>2</sub>	75.0	75.0	325	24,375.	
H <sub>2</sub> O	<u>3.0</u>	<u>3.0</u>	0	<u>0.</u>	
Total	100.0	100.0		28,559.	285.6

Thus, the higher heating value for the specified natural gas composition is 285.6 Btu/ft<sup>3</sup>.

(c) The density of any ideal gas can be calculated by modifying the ideal gas law, presented below:

$$PV = nRT$$

Because density is simply the mass of a substance divided by its volume, we shall multiply both sides of the ideal gas equation by the molecular weight, MW, of the gas mixture. We recall that the moles of a substance, n, times its molecular weight equal its mass.

$$PV(MW) = n(MW)RT$$

$$PV(MW) = (\text{mass})RT$$

Rearranging this equation so that we have mass divided by volume, we can derive an ideal gas law equation that will allow us to calculate density of any ideal gas, given the temperature, pressure and MW, per

$$\text{density} = \frac{\text{mass}}{\text{volume}} = \frac{P(MW)}{RT}$$

The selection of the ideal gas constant, R, in convenient units, such as (atm, ft<sup>3</sup>)/(lb mol, R) will simplify the density calculation in units of lbs per ft<sup>3</sup>

$$\text{density} = \frac{P(MW)}{RT} = \frac{(1 \text{ atm})(10.56 \frac{\text{lb}}{\text{lbmol}})}{(0.7302 \frac{\text{atm} \cdot \text{ft}^3}{\text{lbmol} \cdot \text{R}})(60 + 460 \text{ R})} = 0.02781 \frac{\text{lb}}{\text{ft}^3}, \text{ (at 1 atm, 60}^\circ\text{F)}$$

(d) The HHV in Btu/lb can be calculated from the HHV in Btu/ft<sup>3</sup> and the density per

$$\text{HHV} = \left( 285.6 \frac{\text{Btu}}{\text{ft}^3} \right) \left( \frac{\text{ft}^3}{0.02781 \text{ lb}} \right) = 10,270. \frac{\text{Btu}}{\text{lb}}$$

(e) The LHV can be calculated by recalling that the fundamental difference between HHV and LHV values is the state of the product water. That is, HHV values are based on a liquid water product, while LHV values are based on a gaseous water product. Because energy is consumed to evaporate liquid water into gaseous water, LHV values are always lower than HHV values. [To convert liquid water to water vapor at 1 atm, and 60°F, requires approximately 1050 Btu/lb, or 50 Btu/ft<sup>3</sup>.] For a given gas mixture, the quantitative difference between the HHV and LHV is, obviously, a function of how much water is produced by the given fuel. So the first step in converting the HHV to LHV is the determination of the amount of water produced by the fuel. This is done in the table below.

Fuel Constituents	mol %	Basis: 1.0 ft <sup>3</sup> of Natural Gas			
		Fuel Gas Volume (ft <sup>3</sup> )	Stoichiometric Factor <sup>67</sup> for Gas to H <sub>2</sub> O	Water Volume (ft <sup>3</sup> )	LHV to HHV Adjustment (Btu/ft <sup>3</sup> )
CH <sub>4</sub>	4.0	0.04	2.0	0.08	2.0
CO	0.4	0.004	0.0	0.00	0.0
CO <sub>2</sub>	17.6	0.176	0.0	0.00	0.0
H <sub>2</sub>	75.0	0.75	1.0	0.75	37.5
H <sub>2</sub> O	<u>3.0</u>	<u>0.03</u>	0.0	<u>0.00</u>	<u>0.0</u>
Total	100.0	1.00		.83	39.5.

Thus, the LHV can be estimated from the HHV of 285.6 Btu/ft<sup>3</sup> as 246.1 Btu/ft<sup>3</sup> (285.6 - 39.5 = 246.1 Btu/ft<sup>3</sup>).

### Example 10-16 Heat Capacity

Given a 100 lb mol/hr flow of pure methane at near atmospheric conditions, what is (a) the heat capacity for methane at 77°F (25°C) and 752°F (400°C) in Btu/lb mol, °F, (b) the mean heat capacity for methane between 77 and 752°F, (c) the heat required to raise the 100 lb mol/hr flow from 77 to 752°F in Btu's and (d) the heat capacity for a gas mixture of 98% methane and 2% water?

#### **Solution:**

(a) Heat capacities of real gases ( $C_p$ ) at low pressure are accurately approximated by the ideal gas heat capacities ( $C_p^\circ$ ). Published ideal gas heat capacity correlations are smoothed algorithm of experimental data based on sophisticated theoretical and numerical techniques. Many different coefficients and forms of heat capacity correlations can be found in the literature. Scientists and engineers who require correlations relating heat capacity, enthalpy and entropy together with a high level of precision often utilize data found in the JANAF<sup>68</sup> tables (8) or NASA publications (e.g., 9, 10). For this example, we will utilize correlations that are well respected, yet simple enough for hand calculations. A short list of ideal gas law heat capacity coefficients is presented below for the following form of  $C_p^\circ$ :

<sup>67</sup> The stoichiometric factor is the number of water molecules produced per fuel molecule in complete combustion. For example, for CH<sub>4</sub>, which combusts to 2 H<sub>2</sub>O, the stoichiometric factor is two.

<sup>68</sup> Thermochemical data were originally developed by the US Joint Army, Navy, Air Force (JANAF). Today this information is simply known as the JANAF tables.

$$C_p^0 = a + bT + cT^2$$

where  $C_p^0$  [=] (cal/ g mol, °C) or (Btu/ lb mol, °F)

and T [=] K, for 298 K to 1500 K (25°C to 1227°C, or 77°F to 2240°F)

**Table 10-3 Ideal Gas Heat Capacity Coefficients for Common Fuel Cell Gases**

Fuel Constituent		a	$bx10^3$	$cx10^6$
<b>Organic Gases (16)</b>				
Methane	CH <sub>4</sub>	3.381	18.044	-4.300
Ethane	C <sub>2</sub> H <sub>6</sub>	2.247	38.201	-11.049
n-Propane	C <sub>3</sub> H <sub>8</sub>	2.410	57.195	-17.533
n-Butane	C <sub>4</sub> H <sub>10</sub>	3.844	73.350	-22.655
<b>Inorganic Gases (17)</b>				
Carbon monoxide	CO	6.420	1.665	-0.196
Carbon dioxide	CO <sub>2</sub>	6.214	10.396	-3.545
Hydrogen	H <sub>2</sub>	6.9469	-0.1999	0.4808
Nitrogen	N <sub>2</sub>	6.524	1.250	-0.001
Oxygen	O <sub>2</sub>	6.148	3.102	-0.923
Water	H <sub>2</sub> O	7.256	2.298	0.283

Thus the heat capacity of methane at 77°F (25°C, or 298 K) is calculated as

$$C_p^0(T) = 3.381 + 18.044 \times 10^{-3} T - 4.300 \times 10^{-6} T^2$$

$$C_p^0(298K) = 3.381 + 18.044 \times 10^{-3} (298 K) - 4.300 \times 10^{-6} (298 K)^2$$

$$C_p^0(298K) = 3.381 + 5.3771 - 0.3819 = 8.376 \text{ Btu/lb mol, } ^\circ\text{F}$$

The heat capacity for methane at 752°F (400 °C or 673 K) is calculated as

$$C_p^0(673K) = 3.381 + 18.044 \times 10^{-3} (673 K) - 4.300 \times 10^{-6} (673 K)^2$$

$$C_p^0(673K) = 3.381 + 12.1436 - 1.9476 = 13.577 \text{ Btu/lb mol, } ^\circ\text{F}$$

- (b) As can be seen from part (a) above, there is considerable change in the heat capacities with temperatures. For this reason, a single heat capacity value is used to calculate heats over only small temperature ranges. To calculate the sensible heat over a larger temperature range, mean heat capacities often are used. A mean heat capacity can be found from charts or can be integrated from the  $C_p^\circ$  correlations. We shall demonstrate the integration method.

$$C_{p, \text{mean}}^\circ(T_1, T_2) = \frac{\int_{T_1}^{T_2} C_p^\circ(T) dT}{T_2 - T_1}$$

$$C_{p, \text{mean}}^\circ(T_1, T_2) = \frac{\int_{T_1}^{T_2} (3.381 + 18.044 \times 10^{-3} T - 4.300 \times 10^{-6} T^2) dT}{T_2 - T_1}$$

$$C_{p, \text{mean}}^\circ(T_1, T_2) = \frac{\left[ 3.381T + (1/2)(18.044 \times 10^{-3})T^2 - (1/3)(4.300 \times 10^{-6})T^3 \right]_{T_1=298 \text{ K}}^{T_2=673 \text{ K}}}{T_2 - T_1}$$

$$C_{p, \text{mean}}^\circ(T_1, T_2) = \frac{\left[ 3.381(673 - 298) + (1/2)(18.044 \times 10^{-3})(673^2 - 298^2) - (1/3)(4.300 \times 10^{-6})(673^3 - 298^3) \right]}{(673 - 298)}$$

$$C_{p, \text{mean}}^\circ(T_1 = 673\text{K}, T_2 = 298) = \frac{[1267.9 + 3285.1 - 399.0]}{375} = \frac{4154.0}{375} = 11.077 \text{ Btu / lb mol, } ^\circ\text{F}$$

- (c) The heat required to raise the gas from one temperature,  $T_1$ , to another,  $T_2$ , knowing the mean  $C_p^\circ$  is simply

$$Q = (C_{p, \text{mean}}^\circ)(T_2 - T_1), \text{ thus}$$

$$Q = (11.077 \text{ Btu / lbmol, } ^\circ\text{F})(752 - 77^\circ\text{F}) = 7,480 \text{ Btu / lbmol}$$

Thus, 100 lb mol/hr of pure methane would require 748,000 Btu/hr to heat it from 77°F to 752°F (25°C to 400°C).

- (d) The gas mixture problem is identical in nature to the pure methane problem just completed, because both a gas mixture and a pure gas, at low pressure, can be approximated as ideal gases. Heat capacities for the individual gases are simply averaged on a molar, or volume basis. Going through a similar calculation for water, we find a mean  $C_p^\circ$  of 8.44 Btu/lb mol,  $^\circ\text{F}$ . Thus, we can easily develop the composite mean  $C_p^\circ$  by determining the molar average as illustrated below:

$$C_{p, \text{mean, mixture}}^\circ = y_A C_{p, \text{mean, A}}^\circ + y_B C_{p, \text{mean, B}}^\circ$$

Where  $y_i$  is the molar, or volume fraction, of species  $i$ .

$$C_{p, \text{mean, mixture}}^\circ = (0.98)(11.077) + (0.02)(8.44) = 11.02 \text{ Btu/lb mol, } ^\circ\text{F}$$

## 10.4 Cost Calculations

This section presents information on developing the Cost of Electricity (COE), as well as information for the development of capital costs.

### 10.4.1 Cost of Electricity

Three major contributors are considered in the computation of the COE for a fuel cell power plant: 1) capital cost, 2) fuel cost and 3) operation and maintenance costs. The cost of electricity (\$/MWh) can be calculated using these parameters as follows:

$$\text{COE} = \frac{0.125\text{CC}}{H} + \frac{3.412 \text{FC}}{\varepsilon_s} + \frac{\text{O\&M}}{H}$$

where 0.125 is a capital recovery rate (excluding taxes and insurance), CC is the capital cost (\$/kW), FC is the fuel cost (\$/10<sup>6</sup> Btu), 3.412 is the theoretical heat rate for 100% efficiency (3412 Btu/kWh) divided by 1000 for units consistency,  $\varepsilon_s$  is the fractional efficiency, H is the annual operating hours divided by 1000, and O&M is the operating and maintenance cost (\$/kW-yr total, including fixed and variable costs).

#### Example 10-17 Cost of Electricity

Given a capital cost of \$1000/kW, a fuel cost of \$2 per MMBtu, a net plant efficiency of 40%, 6000 operating hours, and a total O&M cost of \$20/kW-yr, what is the estimated cost of electricity?

**Solution:**

$$\text{COE} = \frac{(0.125)(1000)}{6} + \frac{(3.412)(2)}{0.40} + \frac{(20)}{6}$$

$$\text{COE} = 20.8 + 17.1 + 3.3 = \$41.2/\text{MWh, or 4.1 cents/kWh}$$

### 10.4.2 Capital Cost Development

There is a need for an easily understood, flexible, and reasonably accurate methodology for rapidly estimating the cost of conceptual fuel cell power plants.

One method proposed for estimating the cost of fuel cell power plants is to calculate distributive (bulk) costs as a function of the equipment cost using established factors based on conventional generating technologies. When applied in such a way as to compensate for the differences associated with a fuel cell plant, this approach can yield reasonable results. NETL has elected, based on the international prominence of the Association for the Advancement of Cost Engineering (AACE), to utilize this approach in estimating the costs for fuel cell/turbine power plant systems currently under study.

The factors currently being used by NETL are listed in Table 10-4. These factors apply to processes operating at temperatures in excess of 400 °F at pressures of under 150 psig, and are taken from the AACE Recommended Practice No. 16R-90, *Conducting Technical and Economic Evaluations in the Process and Utility Industries*.

**Table 10-4 Distributive Estimating Factors**

<b>Area</b>	<b>Material</b>	<b>Labor</b>
Foundations	0.06	1.33
Structural Steel	0.05	0.50
Buildings	0.03	1.00
Insulation	0.02	1.50
Instruments	0.07	0.75
Electrical	0.06	0.40
Piping	0.40	0.50
Painting	0.005	3.00
Misc.	0.04	0.80

The suggested bulk material factors are applied to direct equipment costs, whereas the bulk labor factors apply to the corresponding bulk material item. Because the distributive factors are based on larger scale field built plants, FETC applies an additional factory fabrication adjustment to reflect a more modular construction approach requiring less field fabrication as would likely be the case with smaller plant configurations. This approach is illustrated in reference (18).

NETL's choice to use the approach discussed above does not preclude the use of alternate methodologies. One such alternate methodology, currently in the early stages of development, is based on the premise that fuel cell plant costs could ultimately be more accurately estimated using factors developed specifically for fuel cell applications, rather than factors based on conventional generating technologies. An overview of this approach along with a "first cut" at developing new fuel cell specific factors is presented in reference (19). Fuel cell specific factors developed to date are based on limited data and should be considered highly preliminary. Continued refinement will be required as additional fuel cell plant costing information becomes available.

## 10.5 Common Conversion Factors

The following is a tabulation of conversion factors common to fuel cell analysis.

To Convert From	To	Multiply by	To Convert From	To	Multiply by
A (amperes)	Faradays/sec	1.0363E-05	Joule (J)	V coulomb	1
A/ft <sup>2</sup>	mA/cm <sup>2</sup>	1.0764	KA	kg H2/h	0.037605
atm	kg/cm <sup>2</sup>	1.0332	KA	lb H2/h	0.082906
atm	lb/in <sup>2</sup>	14.696	KA	lb mol H2/h	0.041128
atm	bar	1.01325	kg	lb	2.2046
atm	Pa	101,325	kg/cm <sup>2</sup>	lb/in <sup>2</sup>	14.223
Avagadro's number	particles/g mol	6.0220E+23	kg H2/hr	KA	24.314
bar	atm	0.98692	Kcal	Btu	3.9686
bar	lb/in <sup>2</sup>	14.504	kPa	lb/in <sup>2</sup>	0.14504
bar	kg/cm <sup>2</sup>	1.0197	kW	Btu/h	3412.1
bar	N-m <sup>2</sup>	100,000	kW	kcal/s	0.23885
bar	Pa	100,000	kW	hp	1.3410
Btu	cal	251.98	lb	grams	453.59
Btu	ft-lb	778.17	lb	kg	0.45359
Btu	J (Joules)	1055.1	lb H2/hr	KA	12.062
Btu	kWh	2.9307E-04	lb mol H2/hr	KA	24.314
Btu/hr	W	0.29307	lb/in <sup>2</sup>	kg/cm <sup>2</sup>	0.070307
Btu/lb, °F	cal/g, °C	1.0000	lb/in <sup>2</sup>	Pa	6894.7
°C	°F	°C*(9/5)+32	l (liter)	m <sup>3</sup>	1.0000E-03
°C	K	°C+273.16	m (meter)	ft	3.2808
cal	J	4.1868	m (meter)	in	39.370
cm	ft	0.032808	m <sup>2</sup>	ft <sup>2</sup>	10.764
cm	in	0.39370	m <sup>3</sup>	ft <sup>3</sup>	35.315
°F	°C	°F-32*(5/9)	m <sup>3</sup>	gal	264.17



To Convert From	To	Multiply by	To Convert From	To	Multiply by
Faradays	C (coulombs)	96,487	mA/cm <sup>2</sup>	A/ft <sup>2</sup>	0.92903
Faradays/sec	A	96,487	MMBtu/h	MW	0.29307
ft	m	0.30480	MW	MMBtu/h	3.4121
ft	cm	30.480	Pa	lb/in <sup>2</sup>	1.4504E-04
ft <sup>2</sup>	cm <sup>2</sup>	929.03	R (gas constant)	atm, ft <sup>3</sup> /lbmol, R	0.73024
ft <sup>2</sup>	m <sup>2</sup>	0.092903	R (gas constant)	Btu/lb mol, R	1.9859
ft <sup>3</sup>	liters	28.317	R (gas constant)	cal/g mol, K	1.9857
ft <sup>3</sup>	m <sup>3</sup>	0.028317	R (gas constant)	ft, lbf/lb mol, R	1545.3
ft <sup>3</sup>	gal	7.4805	R (gas constant)	J/g mol, K	8.3144126
gal	liters	3.7854	R (gas constant)	l, atm/g mol, K	0.082057
grams (g)	lb	2.2046E-03	tonne	kg	1000.0
hp	ft-lb/s	550.00	tonne	lb	2204.6
horsepower (hp)	kW	0.74570	Watts	Btu/h	3.4121
hp	W	745.70	Watts	hp	1.3410E-03

## 10.6 Automotive Design Calculations

The total power, P, needed from a vehicle's power system must be sufficient for vehicle acceleration, aerodynamic drag losses, rolling resistance, changes in elevation, and auxiliary power for vehicle accessories (20,21). These power terms are, respectively:

$$P = (mav + 0.5 \cdot C_D A_F v^3 + mgC_{RV} + mgv \cdot \sin(\&)) / \$ + P_{aux}$$

Where P = total power (W)

m = vehicle mass (kg)

a = vehicle acceleration (m/sec<sup>2</sup>)

v = vehicle velocity (m/sec)

$\rho$  = air density (kg/m<sup>3</sup>)

C<sub>D</sub> = aerodynamic drag coefficient

A<sub>F</sub> = vehicle area normal to direction of travel (m<sup>2</sup>)

g = gravitation constant (9.8 m/sec<sup>2</sup>)

C<sub>R</sub> = coefficient of rolling resistance

& = inclined angle of road (radians)

\$ = efficiency of motor, controller, and gearing

P<sub>aux</sub> = auxiliary power for lights, radio, wipers, air conditioner, cigarette lighter, etc. (W)

The power system may consist of the fuel cell plus peak power storage device(s). Criteria established by the Partnership for a New Generation of Vehicles (PNGV) specify that:

- The fuel cell system (without peak power device) must provide enough power to sustain a speed of 55 mph (24.58 m/sec) on a 6.5 % grade, and
- The output of the fuel cell system plus peak power device must allow acceleration for high speed passing of 3 mph/sec (1.34 m/sec<sup>2</sup>) at 65 mph (29.05 m/sec)

These values are computed for a conventional mid-size passenger vehicle using the following assumptions:

$$m = 1360 \text{ kg (vehicle weight)} + 272 \text{ kg (weight of passengers plus cargo)}$$

$$\rho = 1.29 \text{ kg/m}^3 \text{ (at standard temperature and pressure)}$$

$$C_D = 0.3$$

$$A_F = 2.0 \text{ m}^2$$

$$g = 9.8 \text{ m/sec}^2$$

$$C_R = 0.0085$$

$$\phi = 0.77$$

$$P_{\text{aux}} = 400 \text{ W (= 400 kg-m}^2\text{/sec}^3\text{)}$$

Plugging these values into the equation above, the minimum power needed by the fuel cell alone to sustain 24.58 m/sec on a 6.5 % grade (0.0649 radians) is:

$$P_S = ((0.5)(1.29)(0.3)(2.0)(24.58)^3 + (1632)(9.8)(0.0085)(24.58) + (1632)(9.8)(24.58)\sin(0.0649))/0.77 + 400$$

$$P_S = 45,339 \text{ kg-m}^2\text{/sec}^3 = 4.53 \text{ kW}$$

The minimum power needed by the power system to accelerate on a level road at 1.34 m/sec<sup>2</sup> at 29.05 m/sec is:

$$P_A = (1632)(1.34)(29.05) + (0.5)(1.29)(0.3)(2.0)(29.05)^3 + (1632)(9.8)(0.0085)(29.05)/0.77 + 400$$

$$P_A = 100,355 \text{ kg-m}^2\text{/sec}^3 = 10.03 \text{ kW}$$

## 10.7 References

1. "Physical and Thermodynamic Properties of Elements and Compounds," Girdler Catalysts, Chemetron Corporation, Catalysts Division.
2. J. M. Smith, H. C. Van Ness, Introduction to Chemical Engineering Thermodynamics, Third Edition, McGraw-Hill, 1975.
3. Chemistry: Principles and Applications, M.J. Sienko, R.A. Plane, McGraw-Hill, New York, NY, 1979.
4. D.B. Stauffer, J.S. White, J.H. Hirschenhofer, "An ASPEN/SP MCFC Performance User Block," DOE Contract DE-AC21-89-MC25177, Task 7, July 1991.
5. D.B. Stauffer, R.R. Engleman Jr., J.S. White, J.H. Hirschenhofer, "An ASPEN/SP SOFC Performance User Block," DOE Contract DE-AC21-88-FE-61684, Task 14, September 1993.

6. E.S. Wagner, G.F. Froment, "Steam Reforming Analyzed," *Hydrocarbon Processing*, July 1992, pp. 69 -77.
7. Fuel Cell Systems, Edited by L.J. M. Blomen, M.N. Mugerwa, Plenum Press, New York, NY, 1993.
8. W.L. McCabe, J.C. Smith, P. Harriot, Unit Operations of Chemical Engineering, 4<sup>th</sup> Edition, 1985.
9. Chemical Engineers' Handbook, Edited by R.H. Perry, D. Green, 6<sup>th</sup> Edition, McGraw-Hill, 1984
10. M.S. Peters, K.D. Timmerhaus, Plant Design and Economics for Chemical Engineers, 3<sup>rd</sup> Edition, McGraw-Hill, Inc., New York, NY, 1980.
11. C.A. Meyers, R.B. McClintok, G.J. Silverstri, R.C. Spencer, Jr., 1967 ASME Steam Tables, New York, 1967.
12. Combustion, Fossil Power: A Reference Book on Fuel Burning and Steam Generation, 4<sup>th</sup> Edition, edited by J.G. Singer, P.E., Combustion Engineering, 1991.
13. M.W. Chase, Jr. et al., JANAF Thermochemical Tables, Third Edition, American Chemical Society and the American Institute for Physics, Journal of Physical and Chemical Reference Data Volume 14, 1985, Supplement 1.
14. B.J. McBride, "Coefficients for Calculating Thermodynamic and Transport Properties of Individual Species," NASA Technical Memorandum 4513, October 1993.
15. B.J. McBride, "Thermodynamic Data for Fifty Reference Elements," NASA Technical Paper 3287, January 1993.
16. H.M. Spencer, *Ind. Eng. Chem.*, 40:2152 (1948), as presented in Introduction to Chemical Engineering Thermodynamics, Third Edition, J.M. Smith and H.C. Van Ness, McGraw-Hill, 1975.
17. H.M. Spencer, *J. Amer. Chem. Soc.*, 67: 1858, (1945), as presented in Fuel Cells A Handbook, Revision 3, J. Hirschenhofer, D. Stauffer, R. Engleman, DOE/METC-94/1006, January 1994.
18. T.J. George, R. "RJ" James III, K. D. Lyons, "Multi-Staged Fuel Cell Power Plant (Targeting 80% Lower Heating Value Efficiency)," *Power Generation International 1998 Conference*, December 9-11, 1998, Orange County Convention Center, Orlando, Florida.
19. L.L. Pinkerton, "Express Method for Estimating the Cost of Fuel Cell Plants," *1998 Fuel Cell Seminar*, November 16-19, 1998, Palm Springs Convention Center, Palm Springs, California.
20. Ogden, J.M., Steinbugler, M.M., and Kreutz, T.G. 1999. "A Comparison of Hydrogen, Methanol, and Gasoline as Fuels for Fuel Cell Vehicles: Implications for Vehicle Design and Infrastructure Development." *Journal of Power Sources*, 79 (1999) 143-168.
21. Hauer, K.H., Friedmann, D.J., Moore, R.M., Ramaswamy, S., Eggert, A., and Badranarayanan, P. March 6-9, 2000. "Dynamic Response of an Indirect-Methanol Fuel Cell Vehicle." *Fuel Cell Power for Transportation 2000*. Society of Automotive Engineers World Congress, Detroit, Michigan.

---

## 11. APPENDIX

---

### 11.1 Equilibrium Constants

Figure 11-1 presents the temperature dependence of the equilibrium constants for the water gas shift reaction,



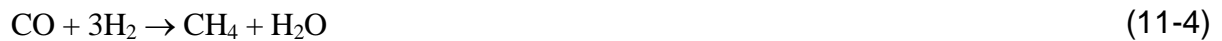
the carbon deposition (Boudouard reaction) reaction,



the methane decomposition reaction,



and the methane formation reaction,



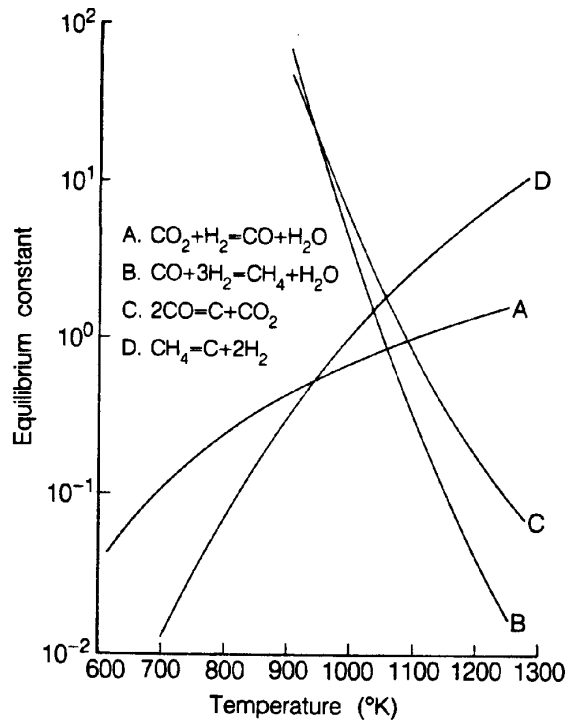


**Figure 11-1 Equilibrium Constants (Partial Pressures in MPa) for (a) Water Gas Shift, (b) Methane Formation, (c) Carbon Deposition (Boudouard Reaction), and (d) Methane Decomposition (J.R. Rostrup-Nielsen, in *Catalysis Science and Technology*, Edited by J.R. Anderson and M. Boudart, Springer-Verlag, Berlin GDR, p.1, 1984.)**

## 11.2 Contaminants from Coal Gasification

A list of contaminant levels that result from various coal gasification processes is presented in Table 11-1. The contaminant levels obtained after a first stage of hot gas cleanup with zinc ferrite also are listed.

**Table11-1 Typical Contaminant Levels Obtained from Selected Coal Gasification Processes**

Parameters	Coal Gasification Process		
	LURGI Fixed Bed	METC (raw gas) Fixed Bed	Cleaned Gas
Max. Product Temp. (EC)	750	1300	<800
Gasification	O <sub>2</sub> blown	Air blown	Regenerative
Pressure (psi)	435	220	150
Product Gas (EC)	600	650	<700
Methane (vol%)	11	3.5	3.5
Coal type	Sub-bitum. Navajo	Sub-bitum. New Mexico	(Humidified Output)
Particulates (g/l)	0.016	0.058	0.01 est.
Sulfur (ppm) (Total H <sub>2</sub> S, COS, CS <sub>2</sub> , mercaptans)	2,000	5,300	<10
NH <sub>3</sub> (vol%)	0.4	0.44	0.25
Trace metals (ppm)			
As	2	NS <sup>a</sup>	NS
Pb	0.8	2	1.7
Hg	0.4	NS	NS
Zn	0.4	NS	140
Halogens (ppm)	200	700	500
Hydrocarbons (vol%)			
C <sub>2</sub> H <sub>6</sub>	1	NS	NS
C <sub>2</sub> H <sub>4</sub>	1	0.3	NS
C <sub>2</sub> H <sub>2</sub>	1	NS	NS
Oil tar	0.09	NS	NS

a - Not specified

Source: A. Pigeaud, Progress Report prepared by Energy Research Corporation for U.S. Department of Energy, Morgantown, WV, Contract No. DC-AC21-84MC21154, June 1987.

### 11.3 Selected Major Fuel Cell References, 1993 to Present

#### Books on Fuel Cells:

1. A.J. Appleby, F.R. Foulkes, *Fuel Cell Handbook*, Van Norstand Reinhold, New York, N.Y., 1989. Republished by Krieger Publishing Company, Melborne, FL, 1993.
2. L.J. Blomen, M.N. Mugerwa, editors, *Fuel Cell Systems*, ISBN 0-306-44158-6, Plenum Press, New York, N.Y., 1993.
3. K. Kordesch, G. Simander, *Fuel Cells and Their Applications*, VCH Publishers, New York, N.Y., 1996.
4. S. Gottesfeld, T.A. Zawodzinski, "Polymer Electrolyte Fuel Cells," *Advances in Electrochemical Science and Engineering, Volume 5*, edited by R.C. Alkire, et al., Wiley-VCH, 1998.

#### Proceedings and Abstracts from Major U.S. Fuel Cell Conferences:

1. *Fuel Cell Seminar, Programs and Abstracts*, Fuel Cell Seminars, sponsored by Fuel Cell Seminar Organizing Committee. Meetings held every two years at U.S. locations, Courtesy Associates, Inc., Washington, D.C.:

November /December 1994 - San Diego, Calif.

November 1996 - Orlando, Fl.

2. *Proceedings of the Annual Fuel Cells Review Meeting*. Meetings held annually at the U.S. DOE Morgantown Energy Research Center, Morgantown, W.V., until 1998, then at U.S. locations:

DOE/METC-94/1010, August 1994

DOE/METC-95/1020, August 1995

DOE/METC CD-ROM, August 1996

DOE/METC CD-ROM, August 1997

Joint DOE/EPRI/GRI Workshop on Fuel Cell Technology, May 1998, San Francisco, Calif., (Abstracts, issuance of final proceedings on CD-ROM expected in early 1999).

3. *EPRI/GRI Fuel Cell Workshop on Technology Research and Proceedings*, Cosponsored by EPRI and GRI, Proceedings by EPRI, Palo Alto, Calif., March 1994.

March 1994, Atlanta, Georgia

April 1995, Irvine, Calif.

April 1996, Temple, Arizona

In 1997, the EPRI/GRI Workshop joined with the DOE Annual Fuel Cells Contractors Meeting. See Item 2 for information in 1997 and 1998.

4. J.R. Selman, et al., ed. *Carbonate Fuel Cell Technology IV*, Proceedings Vol. 97-4, Montreal, Canada, The Electrochemical Society, Inc., Pennington, N.J., 1997.
5. S.C. Singhal, et al., *Proceedings at the Fourth International Symposium on Solid Oxide Fuel Cells*, Proceedings Vol. 95-1, Yokohama, Japan, The Electrochemical Society, Inc., Pennington, N.J., 1995.
6. S.C. Singhal, et al., *Proceedings of the Fifth International Symposium on Solid Oxide Fuel Cells*, Proceedings Vol. 97-40, Aachen, Germany, The Electrochemical Society, Inc., Pennington, N.J., 1997.
7. A.R. Landgrebe, S. Gottesfeld, First International Symposium on Proton Conducting Membrane Fuel Cells, Chicago, IL, Proceedings Vol. 95-23, The Electrochemical Society, Inc., Pennington, N.J., 1995.
8. *Proceedings of the Workshop on Very High Efficiency Fuel Cell/Gas Turbine Power Cycles*, edited by M.C. Williams, C.M. Zeh, U.S. DOE Federal Energy Technology Center, Morgantown, W.V., October 1995.
9. *Proceedings of the National Hydrogen Association Meetings*, National Hydrogen Association, usually in Alexandria, VA., annually in Spring.
10. *Proceedings of the Intersociety Energy Conversion Engineering Conference*. Sponsorship of meeting rotates among seven technical societies. Meetings are held annually (usually in August) in different cities of the United States:
  - 29<sup>th</sup> - Part 2, Sponsor - American Institute of Aeronautics and Astronautics, Monterey, Calif, August 1994.
  - 30<sup>th</sup> - Volume 3, Sponsor - American Society of Mechanical Engineers, Orlando, FL, August 1995.
  - 31<sup>st</sup> - Volume 2, Sponsor - Institute of Electrical and Electronics Engineers, Washington, D.C., August 1996.
  - 32<sup>nd</sup> - Sponsor - American Institute of Chemical Engineers, Honolulu, Hawaii, July/August 1997.
  - 33<sup>rd</sup> - CD-ROM, Sponsor - American Nuclear Society, Colorado Springs, Colo., August 1998.
11. Proceedings of the 58<sup>th</sup> American Power Conference, Volume 58-1, Sponsored by Illinois Institute of Technology, Chicago, IL., 1996.
12. Proceedings of U.S. Russian Workshop on Fuel Cell Technologies, Sandia National Laboratories, Albuquerque, N.M., September 1995.



## Other Important Annual Information on Fuel Cells:

1. U.S. DOE, *Fuel Cell Program Plans*, published each Fiscal Year by U.S. Department of Energy, Assistant Secretary of Fossil Energy:  
  
1994 - DOE/FE-0311P  
1995 - DOE/FE-0335  
1996 - DOE/FE-0350
2. NEDO, *Research and Development on Fuel Cell Power Generation Technology*, published yearly by the New Energy and Industrial Technology Development Organization, Tokyo, Japan.
3. *Fuel Cell RD&D in Japan*, Published annually by the Fuel Cell Development Information Center c/o The Institute of Applied Energy, Tokyo, Japan, usually in August.
4. *Proceedings of the Grove Anniversary Fuel Cell Symposium*, London, UK, September 1995, Journal of Power Sources, Elsevier Sequoia Science, The Netherlands, January 1995.
5. *Proceedings of the Grove Anniversary Fuel Cell Symposium*, London, UK, September 1997, Journal of Power Sources, Elsevier Sequoia Science, The Netherlands, January 1997.
6. U. Bossel, editor, *Proceedings of the European Solid Oxide Fuel Cell Forums*, European Fuel Cell Group and IEA Advanced Fuel Cell Programme, 1994, 1996, 1998.

## Selected Fuel Cell Related URLs:

DOE National Energy Technology Laboratory	<a href="http://www.netl.doe.gov">www.netl.doe.gov</a>
DOE Fossil Energy	<a href="http://www.fe.gov">www.fe.gov</a>
DOE R&D Project Summaries	<a href="http://www.doe.gov/rnd/dbhome">www.doe.gov/rnd/dbhome</a>
Department of Defense	<a href="http://www.dodfuelcell.com">www.dodfuelcell.com</a>
Argonne National Labs	<a href="http://www.anl.gov">www.anl.gov</a>
Sandia National Labs	<a href="http://www.sandia.gov">www.sandia.gov</a>
Oak Ridge National Labs	<a href="http://www.ornl.gov">www.ornl.gov</a>
Los Alamos National Labs	<a href="http://www.lanl.gov">www.lanl.gov</a>
National Fuel Cell Research Center	<a href="http://www.Nfrcr.uci.edu">www.Nfrcr.uci.edu</a>
Fuel Cell 2000	<a href="http://www.fuelcells.org">www.fuelcells.org</a>
US Car	<a href="http://www.uscar.org">www.uscar.org</a>
Partnership for a New Generation of Vehicles	<a href="http://www.ta.doc.gov/pngv">www.ta.doc.gov/pngv</a>
Electric Power Research Institute	<a href="http://www.epri.com">www.epri.com</a>
Gas Research Institute	<a href="http://www.gri.org">www.gri.org</a>
NEDO (Japan)	<a href="http://www.nedo.go.jp/nedo-info">www.nedo.go.jp/nedo-info</a>
Honeywell	<a href="http://www.honeywell.com">www.honeywell.com</a>
Ballard Power Systems	<a href="http://www.ballard.com">www.ballard.com</a>
ElectroChem, Inc.	<a href="http://www.fuelcell.com">www.fuelcell.com</a>
Energy Partners	<a href="http://www.gate.net/~hz-ep">www.gate.net/~hz-ep</a>
Fuel Cell Energy	<a href="http://www.fce.com">www.fce.com</a>

H-Power, Inc.  
International Fuel Cells  
Plug Power L.L.C.  
Siemens Westinghouse S&T Center

[www.hpower.com](http://www.hpower.com)  
[www.hamilton-standard.com/ifc-onsi](http://www.hamilton-standard.com/ifc-onsi)  
[www.plugpower.com](http://www.plugpower.com)  
[www.stc.westinghouse.com](http://www.stc.westinghouse.com)

## 11.4 List of Symbols

### Abbreviations:

®	registered
A.R.	as received
ABS	acrylonitril-butadiene-styrene
AES	air electrode supported
AFC	alkaline fuel cell
APU	auxiliary power unit
ASF	amps/ft <sup>2</sup>
ASR	area-specific resistance
ASU	air separation unit
CC	capital cost
COE	cost of electricity
CVD	chemical vapor deposition
DIR	direct internal reforming
DOE	Department of Energy
EMF	electromotive force
EVD	electrochemical vapor deposition
FC	fuel cost
FCE	Fuel Cell Energy
FEP	fluoro-ethylene-propylene
FETC	Federal Energy Technology Center
HHV	higher heating value
HR	heat rate
IIR	indirect internal reforming
iR	ohmic loss
J-M	Johnson Matthey Technology Center
LHV	lower heating value
MCFC	molten carbonate fuel cell
NETL	National Energy Technology Laboratory
O&M	operating and maintenance costs
ODS	oxide dispersion strengthened anode
OS/IES	on-site/integrated energy systems
PAFC	phosphoric acid fuel cell
PC	phthalocyanines
PEFC	polymer electrolyte fuel cell
PMSS	pyrolysis of metallic soap slurry
PR	pressure ratio
Pt	platinum
PTFE	polytetrafluoroethylene

RDF	refuse derived fuel
SOFC	solid oxide fuel cell
TAA	tetraazaannulenes
TBA	tetrabutyl ammonium
TFMSA	trifluoromethane sulfonic acid
THT	tetrahydrothiophene (thiophane)
TMPP	tetramethoxyphenylporphyrins
TPP	tetraphenylporphyrins
TZP	tetragonal phase
™	trade mark
U.S.	United States of America
WSF	watts/ft <sup>2</sup>
YSZ	yittria stabilized zirconia

### Letter Symbols:

$\Delta E$	potential difference
$\Delta G$	Gibbs free energy
$\Delta H_c$	heat available from combustion of fuel gas
$\Delta H_r$	enthalpy of reaction
$\Delta S_r$	entropy of reaction
$\Delta V$	voltage difference
$\langle D \rangle$	equilibrium pore size
a	$(-2.3RT/\alpha nF) \log i_o$
a	coefficient
AC	alternating current
b	$2.3RT/\alpha nF$
b	coefficient
b	Tafel slope
Btu	British Thermal Unit
c	coefficient
$C_B$	bulk concentration
$C_p$	heat capacity
$C_s$	surface concentration
D	diffusion coefficient
D	pore diameter
dBA	average decibels
DC	direct current
e <sup>-</sup>	electron
E	equilibrium (reversible) potential
E°	standard potential
E <sub>a</sub>	activation energy
F	Faraday's constant
f	gas flow rate
hrs	hours
I	current

$i$	current density
$i_L$	limiting current density
$i_o$	exchange current density
$J$	current density
$K$	equilibrium constant
$k(T)$	constant, function of temperature
$kW$	kilowatt
$lb$	pound
$MM$	million
$mol$	mole
$MW$	megawatt (1000 kW)
$MWhr$	megawatt-hour
$n$	number of electrons participating in a reaction
$n_{max}$	maximum stoichiometric value
$P$	pressure
$P_i$	partial pressure
$ppm$	parts per million
$P_T$	total pressure
$R$	cell resistance
$R$	universal gas constant
$t$	electrolyte thickness
$T$	temperature
$U$	utilization
$V$	cell voltage
$v$	rate at which reactant species are consumed
$V$	volume
$V_c$	voltage of single cell
$vol$	volume
$W_{el}$	maximum electrical work
$wt$	weight
$X$	mole fraction
$yr$	year

### Greek Letter Symbols:

$\alpha$	transfer coefficient
$\beta$	hydrogen utilization
$\Gamma$	mole fraction
$\gamma$	interfacial surface tension
$\gamma$	oxidant utilization
$\delta$	diffusion layer thickness
$\eta_{act}$	activation polarization
$\eta_{conc}$	concentration polarization
$\eta_{ohm}$	ohmic polarization
$\theta$	electrolyte contact angle
$\theta_{CO}$	CO coverage

## Subscripts:

a	anode
c	cathode
e	electrolyte
f	fuel
i	species
in	cell inlet
out	cell outlet
ox	oxygen or oxidant
p	pressure
t	temperature

## 11.5 Fuel Cell Related Codes and Standards

### 11.5.1 Introduction

The rapid development and application of fuel cells throughout the world has created the need for fuel cell technology related codes and standards. Several organizations and committees are currently working on the development of codes and standards related to fuel cells.

According to the National Fire Protection Agency (NFPA) Regulations Governing Committee Projects, codes and standards are defined as follows:

**Code:** A standard that is an extensive compilation of provisions covering broad subject matter or that is suitable for adoption into law independently of other codes and standards.

**Standard:** A document, the main text of which contains only mandatory provisions using the word "shall" to indicate requirements and which is in a form generally suitable for mandatory reference by another standard or code or for adoption into law. Non-mandatory provisions shall be located in an appendix, footnote, or fine-printnote and are not to be considered a part of the requirements of a standard.

This section provides a brief overview of the existing and developing codes and standards related to fuel cell technologies. The discussion focuses on participating organizations, specific codes and standards and more generally applied codes and standards (e.g., the Uniform Building Code) that apply to system installation.

### 11.5.2 Organizations

Below is a listing and brief description of organizations involved in the development of codes and standards pertaining to fuel cell technology.

**American National Standards Institute (ANSI):** ANSI has served in its capacity as administrator and coordinator of the United States private sector voluntary standardization system for 80 years. The Institute is a private, nonprofit membership organization supported by a diverse constituency of private and public sector organizations. ANSI Z21.83 has been published and provides a means of testing and certifying the safety of stationary fuel cell power plants having a capacity of less than 1 MW.

***American Society of Mechanical Engineers (ASME):*** ASME is an international engineering society that conducts one of the world's largest technical publishing operations. ASME International is a nonprofit educational and technical organization serving a worldwide membership. Its mission is to promote and enhance the technical competency and professional well being of engineers through programs and activities in mechanical engineering. To this end, ASME has developed the Boiler and Pressure Vessel Code which is referenced as part of the AGA certification. Additionally, ASME is working on a fuel cell standard, ASME PTC 50, which will address fuel cell performance. Publication of this standard is not expected until 2002.

***Institute of Electrical and Electronics Engineers (IEEE):*** The mission of IEEE is to advance global prosperity by promoting the engineering process of creating, developing, integrating, sharing and applying knowledge about electrical and information technologies. IEEE Standards Coordinating Committee 21 (SCC21) oversees the development of standards in the area of fuel cells, photovoltaics, distributed generation, and energy storage. SCC21 coordinates efforts in these fields among the various IEEE societies and other appropriate organizations to insure that all standards are consistent and properly reflect the views of all applicable disciplines. Working Group 1547 - Standard for Distributed Resources Interconnected with Electric Power Systems - establishes criteria and requirements for interconnection by distributed resources with electric power systems. The purpose is to provide a uniform standard for interconnection of distributed resources with electric power systems and requirements relevant to the performance, operation, testing, safety considerations, and maintenance of the interconnection.

***International Electrotechnical Commission (IEC):*** The IEC is the world organization that prepares and publishes international standards for all electrical, electronic and related technologies. The membership consists of more than 50 participating countries, including all the world's major trading nations and a growing number of industrializing countries. The IEC's mission is to promote, through its members, international cooperation on all questions of electrotechnical standardization and related matters, such as the assessment of conformity to standards, in the fields of electricity, electronics and related technologies. The IEC charter embraces all electrotechnologies including electronics, magnetics and electromagnetics, electroacoustics, telecommunication, and energy production and distribution, as well as associated general disciplines such as terminology and symbols, measurement and performance, dependability, design and development, safety and the environment.

***The National Fire Protection Association (NFPA):*** NFPA is non-profit organization that publishes the National Electrical Code<sup>®</sup>, the Life Safety Code<sup>®</sup>, the Fire Prevention Code<sup>™</sup>, the National Fuel Gas Code<sup>®</sup>, and the National Fire Alarm Code<sup>®</sup>. The mission of NFPA is to reduce the worldwide burden of fire and other hazards on the quality of life by providing and advocating scientifically based consensus codes and standards, research, training, and education. NFPA is developing a fuel cell specific code, NFPA 853, which will cover the installation of stationary fuel cells of at least 50 kW output. Publication is expected to occur in 2000.

***Society of Automotive Engineers (SAE):*** SAE is a resource for technical information and expertise used in designing, building, maintaining, and operating self-propelled vehicles for use on land, sea, in air or in space. Comprised of nearly 80,000 engineers, business executives, educators, and students from more than 97 countries, the network of members share information

and exchange ideas for advancing the engineering of mobility systems. Technical committees write more new aerospace and automotive engineering standards than any other standards-writing organization in the world. In late 1999, a Fuel Cell Standards Forum was created to establish standards and test procedures for fuel cell powered vehicles. It will address the safety, performance, reliability and recyclability of fuel cell systems in vehicles with an emphasis on efficiency and environmental impact.

**Underwriters Laboratories Inc. (UL):** UL is an independent, not-for-profit product safety testing and certification organization. UL has tested products for public safety for more than a century with more than 14 billion UL Marks applied to products worldwide. UL has developed a standard for inverters that can be applied to fuel cells.

### 11.5.3 Codes & Standards

A summary of existing and pending fuel cell related codes and standards is presented in Table 11-2. More detailed descriptions are provided subsequently based on their specific area of application.

**Table 11-2 Summary of Related Codes and Standards**

<b>CODE/STANDARD</b>	<b>ORGANIZATION</b>	<b>SUMMARY</b>
1. PTC 50	ASME	<i>Performance Test Code</i> - Will provide test procedures, methods and definitions for the performance characterization of fuel cell power systems.
2. IEEE SCC 21	IEEE	<i>Standards coordinating committee</i> - fuel cells, photovoltaics, dispersed generation and energy storage
3. IEEE P1547	IEEE	<i>DG Interconnection Standard</i> - Establishes criteria and requirements for interconnection of distributed resources with electric power systems
4. ANSI Z21.83-1998	ANSI	<i>Product Standard</i> – Provides detailed test and examination criteria for fuel cell power plants that make use of natural and liquefied petroleum gases.
5. NFPA 853	NFPA	<i>Installation Standard</i> - applies to installation of stationary fuel cell power plants.
6. NEC/NFPA 70 Article 690,691 & 705	NFPA	690 – Solar Photovoltaic Systems 691 – Fuel Cells 705 – Interconnected Power Production Sources
7. IEEE SCC 36	IEEE	<i>Standards Coordinating Committee</i> - pertains to utility communications
8. UL 1741	UL	<i>Electric Inverters</i> – Standard for testing, listing and safety certification for Inverters
9. SAE Standards Forum	SAE	<i>Vehicle Standards</i> – in the early stages of developing standards for safety, performance, reliability and recyclability. Also establish testing procedures.
10. IEC TC 105	IEC	<i>Technical Committee 105</i> - to expand the scope of ANSI Z21.83 for international basis and additional fuel cell technologies.

## **Codes and Standards for Fuel Cell Manufacturers**

**ANSI Z21.83:** American National Standard - Fuel Cell Power Plants provides a means of testing and certifying the safety of stationary fuel cell power plants with a nominal electric capacity not exceeding 1.0 MW. This standard is intended for applications other than residential when installed outdoors and operated on a gaseous hydrocarbon as the reactant. The current version of the standard is based on two specific fuel cell technologies and is being revised to take into consideration the characteristics of additional fuel cell power plant technologies. This standard has been adopted by many state and local regulatory authorities. The revised version of the standard is expected to be approved in 2001.

**ASME PTC 50:** ASME Performance Test Code 50 - Fuel Cell Power Systems provides test procedures, methods and definitions for the performance characterization of fuel cell power systems. The code specifies the methods and procedures for conducting and reporting fuel cell system ratings. Specific methods of testing, instrumentation, techniques, calculations and reporting are presented. This standard is currently being drafted and is expected to be approved and published in 2002.

**IEC TC 105:** The International Electrotechnical Committee has established a Technical Committee charged with the preparation of an international standards regarding fuel cell technologies for all fuel cell applications including stationary power plants, transportation propulsion systems, transportation auxiliary power units and portable power generation systems. The committee was established in 2000 and plans to have the standards approved and published in 2004.

**IEEE SCC21/P1547:** The Institute of Electrical and Electronic Engineers has established a Standards Coordinating Committee (SCC 21) chartered with the development of a standard for the interconnection of distributed resources. This standard focuses on electrical interface standards for the application of distributed generation technologies described as fuel cells, photovoltaics, dispersed generation and energy storage. The resulting standard will be IEEE P1547 which will establish criteria and requirements for the interconnection of distributed resources with electric power systems. This standard is currently under development and is expected to be approved by IEEE and published in 2001.

**IEEE SCC 36:** Reviews, recommends and solicits the development of standards relevant to the gas, water, and electric utility industries on a worldwide basis with respect to utility communication architecture. This SCC coordinates standards-development activities with other relevant IEEE groups and sponsors standards-development activities that are appropriate to the needs of the utility industry.

**UL 1741:** Underwriters Laboratory 1741 is a standard for the testing, listing and safety certification for electric inverters. This standard is for static inverters and charge controllers for use in photovoltaic power systems, but may be used for fuel cells.



## **Codes and Standards for the Installation of Fuel Cells**

**NFPA 853:** National Fire Protection Association 853 - Standard for Fuel Cell Power Plants provides a standard for the design, construction and installation of stationary packaged, self contained and field constructed fuel cell power plants with a capacity greater than 50 kW. This standard has been approved and will be published during the summer of 2000.

**NFPA 70:** National Fire Protection Association 70 is also known as the National Electric Code (NEC). Revisions and addendum's to the code are currently being developed that specifically address fuel cells. Article 690 - Solar Photovoltaic Systems has been targeted for revision to include fuel cells and alternate energy sources systems. This proposal is not expected to be approved since the technological and operational differences between fuel cells and photovoltaic systems is considerable. A new article, currently identified as Article 691, has been proposed and applies to fuel cells for buildings or residential dwellings. This standard addresses the electrical interface between the fuel cell system and a building's electrical distribution panel. The fuel cell specific standard is not likely to be identified as Article 691 and is expected to be approved and published in 2001. NFPA Article 705 - Interconnected Electrical Power Production Sources is also being revised to address fuel cell power sources.

## **Codes and Standards for Fuel Cell Vehicles**

SAE has established a Fuel Cells Standard Forum that is chartered with the establishment of standards and test procedures for fuel cell powered vehicles. The committee was established in 1999. The standards will cover the safety, performance, reliability and recyclability of fuel cell systems in vehicles with emphasis on efficiency and environmental impact. The standards will also establish test procedures for uniformity in test results for the vehicle/systems/components performance, and define interface requirements of the systems to the vehicle. Task Groups have been formed in the areas of safety, performance, reliability, emissions, recyclability, interface and miscellaneous.

### **11.5.4 Application Permits**

The installation of fuel stationary fuel cells requires adherence to a variety of building codes. A few of the major codes are summarized below.

**Uniform Building Code:** The Uniform Building Code (UBC) is the most widely adopted model building code in the world and is a proven document meeting the needs of government units charged with enforcement of building regulation. Published triennially, the UBC provides complete regulations covering all major aspects of building design and construction relating to fire and life safety and structural safety. The requirements reflect the latest technological advances in the building and fire and life-safety industry.

**Uniform Mechanical Code:** Provides a complete set of requirements for the design, construction, installation and maintenance of heating, ventilating, cooling and refrigeration systems, incinerators, and other heat-producing appliances.

**Uniform Plumbing Code:** Published by the International Association of Plumbing and Mechanical Officials (IAPMO), the Uniform Plumbing Code covers all aspects of plumbing, including requirements for plumbing materials and IAPMO installation standards.

**National Electric Code:** The National Electrical Code (NFPA 70) provides "practical safeguarding of persons and property from hazards arising from the use of electricity." More specifically, the National Electric Code covers the installation of electric conductors and equipment in public and private buildings or other structures (including mobile homes, recreational vehicles, and floating buildings), industrial substations, and other premises (such as yards, carnivals, and parking lots). The National Electric Code also covers installations of optical fiber cable. Wiring, general electrical equipment, the use of electricity in specific occupancies (from aircraft hangars to health care facilities), and equipment (ranging from elevators to hot tubs) are covered, as well as special conditions (emergency and stand-by power, or conditions requiring more than 600 volts, for example) and communication systems.

**National Fire Code:** The National Fire Code consists of approximately 300 codes and standards as published by the National Fire Protection Association (NFPA). These codes address the practices to reduce the burden of fire on the quality of life by advocating scientifically based consensus codes and standards, research and education for fire and related safety issues. The most widely applied codes are:

- (1.) NFPA 70 – National Electric Code
- (2.) NFPA 101 – Life Safety Code
- (3.) NFPA 30 – Flammable and Combustible Liquids Code
- (4.) NFPA 13 – Standard for the Installation and Maintenance of Automatic Fire Sprinkler Systems

## **11.6 Fuel Cell Field Sites Data**

This section of the handbook contains field site information. Most of the worldwide summaries were extracted from an IEA paper. Information on the U.S. Department of Defense (DoD) Fuel Cell Demonstration was taken from the following web site: [www.dodfuelcell.com](http://www.dodfuelcell.com). Finally, Fuel Cell Energy, IFC, and Siemens Westinghouse provided information on their field sites. The IFC PAFC summary includes a number of projects reported by DoD. In the DoD demonstration program, a total of 30 PAFC units were installed at DoD sites across the United States. These were model B and C PC-25 units.

### **11.6.1 Worldwide Sites**

Worldwide information reported in this handbook is for stationary application of fuel cells in different countries. Data on PEFC, PAFC, AFC, MCFC, and SOFC has been collected. Most of the data reported is as of April 1999. The main worldwide projects are summarized below:

### **11.6.2 PEFC**

Canada: Ballard 250 kWe stationary prototypes are developed by Ballard Generation Systems. The first prototype operating is in Vancouver, Canada. Ballard delivered a second 250-kilowatt PEM fuel cell power system to Cinergy Technology. This is the first field trial unit built by Ballard. The unit runs on natural gas, and was commissioned in 1999 at the Naval Surface Warfare Center in Crane, Indiana. A third unit in Berlin, Germany at Bewag Treptow Heating Plant started operating the second half of 1999. Two other prototypes are scheduled to be tested, one at EBM headquarters, Basel, Switzerland and the other at NNT Research Laboratory, Tokyo, Japan. The unit at EBM Headquarters is currently being commissioned and the unit at NNT Research Laboratory is currently being shipped to site, installation planned for September 2,000.

Japan: 2 and 30 kWe PEFC pilot plants have been promoted in Japan as a part of New Sunshine Program. The 2 kWe plant is for residential use and will be developed by Sanyo Electric. The plant is scheduled for testing in 2000.

United States: Plug Power is developing a 7 kWe fuel cell system for residential applications. They have tested their system on hydrogen and are planning market introduction of several models which could use hydrogen, propane, or natural gas.

### **11.6.3 PAFC**

Europe: The Energetic Utility of Milan, the National Agency for Energy, New Technology and Environment (ENEA), and Ansaider Ricerche designed, built, and tested 1.3 MWe PAFC system in Milan. The powerplant had an actual capacity of 930 kW and an energy efficiency of 38% (LHV). It has operated for over 5,000 hours.

Japan: Fuji Electric has developed a 100 kWe on-site system. To date, they have tested a 50 kW power plant using innovative cell design that improves electrolyte management. They tested this stack (154 cells) for about 2,000. They have tested 65, 50 kWe units for a total cumulative operating time of over 1 million hours. They have tested 3, 500 kWe units for a total of 43,437 hours. Their latest design, FP100E, has been shown to have a net AC efficiency of 40.2% (LHV).

Mitsubishi Electric has developed a 200 kWe class on-site powerplant. To date, 11 units are being operated in the field with applications ranging from an electric utility to a brewery factory. Four of the units have operated more than 2,000 hours.

### **11.6.4 AFC**

United Kingdom: ZeTek Power, an UK based company with plants in the US and Europe, is developing Alkaline fuel cells. They are putting AFCs in fleet vehicles and boats in Europe. AFCs are getting greater than 50% efficiency over most of the power curve (5-95%). Capital cost for the AFC stack is \$300/kWe, and approximately \$700 for the system.

### **11.6.5 MCFC**

Japan: As part of the New Sunshine Program, 200 and 1,000 kWe test facilities are planned in Japan. This plan is promoted collectively by 10 electric power companies, 3 gas companies, Central Research Institute of Electric Power Industry, 7 manufacturers, and 2 research

associations. The 1,000 kWe is located in Kawagoe, and the 200 kWe is located in Amagasaki. Both units are scheduled to begin operations in the first half of 1999.

Europe: Italy and Spain have been working on research and development of MCFC systems as a collaborative project called MOLCARE program. The project has a budget of 10 billion pesetas (35% by Spain and 65% by Italy). They have partnered with industry to develop and conduct a 1,000-hour test on a 100 kWe unit.

The European Direct Fuel Cell Consortium carries out the largest European program for the commercialization of MCFC. They are developing an innovative direct fuel cell process which is internally reformed and operates on humidified hydrocarbon fuels. They have successfully tested a 292 cell, 155 kW stack (60% of maximum power).

United States: Fuel Cell Energy is developing an externally manifolded internally reformed MCFC and has constructed a 17 MWe/year cell manufacturing plant. They have also constructed a 400 kWe test facility. They have successfully completed the manufacture and test of 16 stack (4 modules), 2 MWe test in Santa Clara, California, for 4,000 hours. Details on Fuel Cell Energy field site are found in Table 11-5.

### **11.6.6 SOFC**

Japan: The Kansai Electric Company has tested a four-cell article and accumulated 10,529 hours of operation at high current densities and completed 101 thermal cycles. Tokyo Gas started research and development of a planar SOFC in 1993. They conducted a 1.7 kW module test with stable performance.

Australia: Ceramic Fuel Cells Limited was demonstrated a 5 kWe laboratory prototype fuel cell system in 1997. Their system has thin sheet steel components as interconnects in a planar fuel cell design. They are currently scaling up to a 25 kWe pre-commercial stack module.

Canada: Ontario Hydro has tested a single Siemens-Westinghouse cell for 1725 hours. Over 1425 of the hours were at elevated pressure of 5 atm.

Europe: The ELSAM/EDB project for a 100 kWe Siemens-Westinghouse SOFC field unit has operated from January 1998. The unit will operate until January 2000 with a total of 17,500 test hours according to the plan.

Spain: A consortium called SEGE is developing an intermediate temperature planar fuel cell.

United States: Siemens-Westinghouse projects on SOFC include a 250 kWe tubular prototype at the Irvine University campus (California), that will be operated by Southern California Edison Company. It is pressurized to 3.5 bar and thus is expected to give 200 kWe; a coupled microturbine gives an additional 50 kWe. They have operated a tubular SOFC at pressures up to 15 atm.

### **11.6.7 DoD Field Sites**

DoD's Climate Change Fuel Cell program included purchasing and installing 30 ONSI PC25 200 kWe PAFC at DoD installations in addition to providing rebates of \$1,000/kW (up to 1/3 of the installed cost). There are many factors that determine the availability and efficiency of individual units; maintenance programs and application are two of many possible factors. The summary table, Table 11-2, does provide information on operating hours, efficiency, and availability. Logging onto can access additional information on individual units: [www.dodfuelcell.com](http://www.dodfuelcell.com).

### **11.6.8 IFC Field Units**

IFC provided DOE with information on their 59 fuel cell unit operating in North America. This information is provided in Table 11-4. As mention before, several of these units are operating on DoD field site and are report on Table 11-3.

### **11.6.9 Fuel Cell Energy**

Fuel Cell Energy provided DOE with information on their fuel cell field units. This information is provided in Table 11-5.

### **11.6.10 Siemens Westinghouse**

Siemens Westinghouse provided DOE with information on their fuel cell field units. This information is provided in Table 11-6.

**Table 11-3 DoD Field Site**

SITE NAME	SERVICE	<b>Through December 31, 1999</b>					
		START DATE	OPER. HOURS	MWHRs OUTPUT	AVG kWe	ELEC. EFF.	AVAIL.
<b>MODEL B UNITS</b>							
Naval Station Newport	Navy	1/23/95	35,884	5,484.999	152.9	30.2%	82.0%
U.S. Army Soldier Systems Center	Army	1/27/95	32,475	5,411.324	166.6	30.9%	74.3%
US Military Academy	Army	11/17/95	28,534	4,777.548	167.4	31.6%	78.3%
934 <sup>th</sup> Airlift Wing	Air Force	2/1/95	26,174	4,210.264	160.9	29.0%	60.9%
Picatinny Arsenal	Army	10/11/95	25,194	4,368.716	173.4	31.4%	67.5%
Naval Hospital	Marines	10/6/95	25,161	4,131.284	164.2	32.6%	67.6%
MCB Camp Pendleton							
Naval Hospital	Marines	6/20/95	20,905	3,392.946	162.3	31.5%	52.2%
MCAGCC Twentynine Palms							
Nellis AFB	Air Force	9/23/95	16,687	2,845.942	170.5	29.6%	44.0%
Watervliet Arsenal	Army	10/29/97	16,236	2,527.312	155.7	32.5%	85.1%
Fort Eustis	Army	9/12/95	14,292	2,626.718	183.8	32.3%	37.4%
Kirtland AFB	Air Force	7/20/95	14,136	2,084.220	147.4	31.2%	35.8%
Naval Oceanographic Office	Navy	10/7/97	12,427	2,154.166	173.3	35.9%	62.9%
Pine Bluff Arsenal	Army	10/21/97	9,099	1,689.116	185.6	34.0%	47.2%
CBC Port Hueneme	Navy	9/18/97	6,828	1,340.970	196.4	36.4%	33.9%
<b>B's TOTAL/AVG:</b>			284,039	47,045.525	165.6	31.5%	59.2%
<b>MODEL C UNITS*</b>							
911 <sup>th</sup> Airlift Wing	Air Force	12/18/96	22,410	3,979.615	177.6		85.3%
Naval Hospital	Navy	3/18/97	19,726	3,662.949	185.7		80.9%
NAS Jacksonville							
NAS Fallon	Navy	3/30/97	19,485	3,348.443	171.8		78.2%
Subase New London	Navy	9/30/97	18,164	3,355.269	184.7		92.1%
Fort Richardson	Army	12/17/96	17,680	3,176.828	179.7		65.5%
Little Rock AFB	Air Force	8/17/97	17,515	3,264.199	186.4		88.8%
Westover AFB	Air Force	9/19/97	17,396	3,438.906	197.7		87.1%
Barksdale AFB	Air Force	7/24/97	17,138	3,311.453	193.2		80.1%
Fort Huachuca	Army	7/28/97	16,288	3,112.414	191.1		77.3%
Laughlin AFB	Air Force	9/16/97	14,910	2,901.040	194.6		74.7%
US Naval Academy	Navy	9/22/97	14,886	2,183.549	146.7		75.4%
Edwards AFB	Air Force	7/5/97	14,483	2,796.847	193.1		63.7%
Fort Bliss	Army	10/10/97	13,839	2,397.983	173.3		71.0%
Davis-Monthan AFB	Air Force	10/14/97	13,780	2,599.937	188.7		69.7%
NDCEE	Other	8/14/97	9,337	1,145.801	122.7		43.8%
<b>C's TOTAL/AVG:</b>			247,044	44,675.235	180.8		75.6%
<b>B+C TOTAL/AVG:</b>			531,084	91,720.759	172.7	N/A	67.7%

\* Model C units do not have natural gas or electrical efficiency data.

**Disclaimer**

Electrical efficiency calculations include fuel cell idle time (such as when the fuel cell is awaiting the return to operation of the utility grid, etc.). If values were adjusted for idle time, fuel cell electrical efficiencies would be higher. ONSI fuel cells passed DoD Fuel Cell Program electrical efficiency criteria during unit acceptance tests (range = 33.5% to 37.2%, Higher Heating Value).

Availability values are not adjusted for times when the fuel cell was down for extended periods unrelated to typical fuel cell operation (delays in maintenance personnel response, site operating conditions, etc.). Adjusting for these times would result in higher availability values.

**Table 11-4 IFC Field Units**

PC25 C Fuel  
Cell Power  
Plant (Run  
hours, etc. as  
of 8/4/00)

North America						
	<u>Status</u>	<u>Country/State</u>	<u>Site</u>	<u>Start Date</u>	<u>Load hrs</u>	<u>MW-hrs</u>
1	Active	SOUTH WINDSOR, CT	PROTOTYPE FOR R&D	N/A	N/A	N/A
2	Active	DEL RIO, TX	HOSPITAL	9/6/97	20,143	3,743.4
3	Active	LITTLE ROCK, AR	HOSPITAL	10/6/97	21,408	3,872.6
4	Active	SHREVEPORT, LA	HOSPITAL	7/18/97	19,577	3,786.3
5	Active	GROTON, CT	CENTRAL BOILER PLANT	9/27/97	23,175	4,044.2
6	Active	ANNAPOLIS, MD	DORMITORY	9/20/97	20,274	2,945.9
7	Active	STATEN ISLAND, NY	CHEMICAL PLANT	8/22/96	27,412	4,940.3
8	Active	ANCHORAGE, AK	YMCA	11/18/96	21,589	3,572.0
9	Active	JACKSONVILLE, FL	HOSPITAL	3/17/97	24,396	4,580.2
10	Active	EL PASO, TX	LAUNDRY	10/7/97	16,775	2,870.1
11	Active	STATEN ISLAND, NY	CHEMICAL PLANT	8/27/96	29,333	5,342.8
12	Active	PITTSBURGH, PA	CENTRAL BOILER PLANT	12/16/96	28,105	4,988.9
13	Active	SYRACUSE, NY	SCHOOL	1/22/97	27,222	2,802.1
14	Active	CAPE COD, MA	COLLEGE	3/31/99	10,995	2,016.5
15	Active	OMAHA, NE	BANK	3/25/99	11,084	1,569.1
16	Active	YONKERS, NY	ANAEROBIC DIGESTER GAS	4/8/97	18,321	2,349.2
17	Active	OMAHA, NE	BANK	3/24/99	11,030	1,565.1
18	Active	ANCHORAGE, AK	ARMORY BUILDING	12/24/96	9,046	1,739.4
19	Active	ANCHORAGE, AK	ARMORY BUILDING	12/11/96	22,321	4,061.2
20	Active	DEER ISLAND, MA	ANAEROBIC DIGESTER GAS	9/4/97	2,760	395.7
21	Being Installed	ANN ARBOR, MI	RESEARCH LAB		0	0.0
22	Active	FALLON, NV	GALLEY BUILDING	2/28/97	25,781	4,211.7
23	Active	OMAHA, NE	BANK	3/24/99	10,648	1,521.4
24	Active	SPOKANE, WA	HOTEL	6/11/97	22,680	4,370.4
25	Active	CHICOPEE, MA	CENTRAL BOILER PLANT	9/15/97	22,230	4,393.4
26	Active	TUCSON, AZ	CENTRAL BOILER PLANT	10/18/97	20,577	3,644.0
27	Active	ROSAMOND, CA	CENTRAL BOILER PLANT	6/19/97	19,325	3,367.7
28	Active	SIERRA VISTA, AZ	BARRACKS	7/28/97	20,812	3,893.1
29	Will be restarted Fall '00	JOHNSTOWN, PA	OFFICE/RESEARCH LAB	7/28/97	9,637	1,180.7
30	Active	HARTFORD, CT	OFFICE BUILDING	6/18/97	26,023	4,800.7
31	Active	WINDSOR LOCKS, CT	DATA CENTER	12/19/97	19,634	2,135.2



32	Active	MERIDAN, CT	OFFICE BUILDING	9/21/97	20,987	3,991.5
33	Being Installed	ALCORN STATE, MS	UNIVERSITY		0	0.0
34	Active	BRAINTREE, MA	LANDFILL	9/10/99	5,211	906.2
35	Being Installed	BRONX, NY	HOSPITAL		0	0.0
36	Active	SOUTH WINDSOR, CT	INDUSTRIAL SPACE HEATING	3/9/98	19,689	3,771.9
37	Active	PORTLAND, OR	WASTE WATER TREATMENT PLANT	5/21/99	7,259	1,051.5
38	Active	OMAHA, NE	BANK	3/25/99	11,068	1,570.6
39	Owner sold property; being relocated	HARVEY, LA	COMMERCIAL FACILITY	3/13/99	6,823	1,185.1
40	Active	HOUSTON, TX	MANUFACTURING	5/12/98	17,871	1,847.8
41	Not Yet Installed	NY, USA	TBD		0	0.0
42	Active	GULFPORT, MI	DINING FACILITY	5/13/99	7,775	1,504.3
43	Not Yet Installed	NJ, USA	COLLEGE		0	0.0
44	Active	NEW YORK, NY	SKYSCRAPER OFFICE BUILDING	12/15/99	5,220	920.5
45	Active	NEW YORK, NY	SKYSCRAPER OFFICE BUILDING	12/16/99	5,553	1,039.2
46	Active	RAMAPO, NJ	COLLEGE	3/29/00	2,448	429.1
47	Active	NEW YORK, NY	POLICE STATION	4/17/99	11,108	231.1
48	Active	MESA, AZ	MUNICIPAL BUILDING	4/29/00	2,192	410.2
49	Active	ANCHORAGE, AK	POST OFFICE DISTRIBUTION CENTER	6/28/00	3,396	475.2
50	Active	ANCHORAGE, AK	POST OFFICE DISTRIBUTION CENTER	6/28/00	3,329	518.0
51	Active	ANCHORAGE, AK	POST OFFICE DISTRIBUTION CENTER	6/28/00	3,939	612.0
52	Active	ANCHORAGE, AK	POST OFFICE DISTRIBUTION CENTER	6/28/00	4,123	614.1
53	Active	ANCHORAGE, AK	POST OFFICE DISTRIBUTION CENTER	6/28/00	3,563	531.4
54	Active	CALABASAS, CA	ANAEROBIC DIGESTER GAS	12/15/99	6,613	953.9
55	Active	CALABASAS, CA	ANAEROBIC DIGESTER GAS	12/15/99	8,322	1,216.0
56	Active	JOHNSTOWN, PA	RESEARCH LAB	1/6/00	3,655	497.9
57	Active	SOUTH KINGSTOWN, RI	HOSPITAL	10/18/99	6,532	1,032.4
58	Active	SYRACUSE, NY	HIGH SCHOOL	2/4/00	4,427	803.0
59	Active	BELLAIR, TX	INDUSTRIAL BUILDING	5/24/00	1,867	364.7

**Table 11-5 Fuel Cell Energy Field Sites**

Fuel Cell Type	Location	Status	Start Date	Operating Hours	MWhrs Output	Size, kw Design	Actual*	Eff. %	Avail. %
Direct Fuel Cell	Santa Clara, CA	Completed	3/1996	5,800	2,570	1,800	1,930	44	99**
Direct Fuel Cell	Danbury, CT	Completed	2/1999	11,800	1,906	250	263	45	93
Direct Fuel Cell	Bielefeld, Germany	Continuing	11/1999	4,300+	500+	250	225	45	90

\*Maximum attained

\*\* BOP Availability

**Table 11-6 Siemens Westinghouse SOFC Field Units**

Year	Customer	Size, kWe	Fuel	Cell Type	Cell Length (cm)	Operating Hours	Cell Number	MWH (DC)	Operating Hours
1986	TVA	0.4	H2+CO	TK-PST	30.0	1,760	24	0.5	1,760
1987	Osaka Gas	3.0	H2+CO	TK-PST	36.0	3,012	144	6	3,012
1987	Osaka Gas	3.0	H2+CO	TK-PST	36.0	3,683	144	7	3,683
1987	Tokyo Gas	3.0	H2+CO	TK-PST	36.0	4,882	144	10	4,882
1992	JGU-1	20.0	PNG	TK-PST	50.0	817	576	11	817
1992	Utilities-A	20.0	PNG	TK-PST	50.0	2,601	576	36	2,601
1992	Utilities-B1	20.0	PNG	TK-PST	50.0	1,579	576	26	1,579
1993	Utilities-B2	20.0	PNG	TK-PST	50.0	7,064	576	108	7,064
1994	SCE-1	20.0	PNG	TK-PST	50.0	6,015	576	99	6,015
1995	SCE-2	27.0	PNG/DF-JP-8	AES	50.0	5,582	576	118	5,582
1995	JGU-2	25.0	PNG	AES	50.0	13,194	576	282	13,194
1998	SCE-2/NFCRC	27.0	PNG	AES	50.0	3,394+	576	73+	3,800+
1997	EDB/ELS AM-1	100.0	PNG	AES	150.0	4,035	1152	471	4,035
1999	EDB/ELS AM-2	100.0	PNG	AES	150.0	10,085+	1152	1,153+	10,400+
2000	SCE	200.0	PNG	AES	150.0	263+	1152	25+	254

PND = Pipeline Natural Gas

TK-PST = Thick Wall Porous Support Tube

TN-PST = Thin Wall Porous Support Tube

AES = Air Electrode Support

+ = Testing Continues

## 11.7 Thermal-Hydraulic Model of a Monolithic Solid Oxide Fuel Cell

A mathematical model has been developed to simulate the electrochemistry and thermal hydraulics in a cross-flow monolithic or planar solid oxide fuel cell (SOFC).<sup>69</sup> The fuel cell stack consists of repeat cell units with alternating layers of anode, electrolyte, cathode, and interconnect. In the cross-flow designs, the fuel gas flow channels in the anode are orthogonal to the air flow channels in the cathode. Dividing a single cell layer into a number of nodes, the model sets up the heat and mass transfer equations for each node in the cell layer. Using a specified cell voltage and averaged thermal and compositional conditions at each node, the model calculates the Nernst potential and the resultant current, heat generation, and heat removal rates at each node. These calculations yield the temperature, the fuel and oxidant compositions, and species partial pressure matrices for the entire cell. The simulation also provides related performance data for the fuel cell stack, such as the energy conversion efficiency, fuel utilization, and power density. The model can be used to analyze the performance of hydrogen/air SOFCs as well as reformat/air SOFCs fueled with fuel gases other than hydrogen, such as coal gas or synthesis gas.

The model can be used to examine the effects of changing one or more of the various design and operating variables, and to evaluate the potential benefits that can be obtained with fabrication improvements and/or technology development. In the design phase, the model can be used to determine the size of the stack that would be required to obtain a desired rated power, and to make design decisions regarding structure-specific parameters, such as the thicknesses of the anode, electrolyte, cathode, and interconnect layers and dimensions of the flow channels for the air and fuel gas flow fields. The model may also be used to determine *a priori* the effects of altering process variables, such as flow rates and feed conditions, for a particular SOFC stack.

The model, TFLOW, is available for licensing from Argonne National Laboratory. Please contact: Dr. Romesh Kumar, Argonne National Laboratory, Argonne, IL 60439. Tel. 630-252-4342.

## 11.8 References

1. M. Glass, *Fuel Cell Codes and Standards Summit III Summary*, April 5-7, 1999, Pacific Northwest Labs.
2. ASME, *Object & Scope for the Proposed Code on Fuel Cell Power Systems*, August, 2000, <http://www.asme.org>.
3. IEEE, *Distributed Resources and Electrical Power Systems Interconnection Working Group - Meeting Minutes*, June 7-8, 2000, <http://grouper.ieee.org>.
4. SAE, *SAE Initiates Activities in Area of Fuel Cells*, August, 1999, <http://www.sae.org>.
5. UL, *Standard for Safety for Static Inverters and Charge Controllers for Use in Photovoltaic Power Systems*, 2000, <http://ulstandardsinfonet.ul.com>.
6. National Evaluation Service, *National Evaluation Protocol for Stationary Fuel Cell Power Plant*, June 5, 2000, <http://www.nateval.org>.

---

<sup>69</sup> S. Ahmed, C. McPheeters, and R. Kumar, "Thermal-Hydraulic Model of a Monolithic Solid Oxide Fuel Cell," *J. Electrochem. Soc.*, **138**(9), 2712–2718 (1991).

7. International Electrotechnical Commission, IEC TC 105 Strategic Policy Statement, March, 2000, CA/1719A/R, <http://www.iec.ch>.
8. R. Bielen, *Telephone Contact*, August 9, 2000, NFPA.
9. S. Kazubski, *Telephone Contact*, August 14, 2000, CSA International.
10. D. Conover, *Telephone Contact*, August 9, 2000, National Evaluation Service.

---

## 12. INDEX

---

- acid, xii, 1-3, 1-4, 1-7, 1-12, 1-25, 3-1, 3-4, 3-7, 5-2, 5-4, 5-5, 5-9, 5-10, 6-7, 9-82, 11-8
- activation losses, 2-16
- alkali, 1-4, 6-5, 6-7, 6-10, 6-26, 6-27
- alkaline, 1-3, 1-4, 1-7, 1-12, 1-25, 9-82, 11-7
- AlliedSignal, 8-24, 11-6
- anode, 1-1, 1-2, 1-4, 1-5, 1-11, 1-12, 2-1, 2-2, 2-3, 2-7, 2-8, 2-13, 2-14, 3-1, 3-2, 3-4, 3-5, 3-6, 3-8, 3-11, 3-12, 5-1, 5-2, 5-7, 5-8, 5-9, 5-11, 5-13, 5-14, 5-15, 5-18, 6-1, 6-2, 6-3, 6-4, 6-5, 6-6, 6-8, 6-9, 6-14, 6-15, 6-16, 6-17, 6-18, 6-19, 6-21, 6-22, 6-24, 6-26, 6-27, 6-28, 6-29, 6-30, 6-35, 8-2, 8-4, 8-5, 8-6, 8-7, 8-10, 8-11, 8-12, 8-13, 8-16, 9-37, 9-43, 9-45, 9-52, 10-1, 10-2, 10-6, 10-7, 10-8, 10-13, 11-10
- anodic, 2-2, 2-13, 5-14, 5-17, 6-26
- Ansaldo, 1-14, 6-1
- applications, 1-2, 1-3, 1-9, 1-11, 1-12, 1-13, 1-14, 1-15, 1-26, 2-19, 3-1, 3-3, 3-6, 3-10, 3-11, 3-12, 5-5, 9-1, 9-2, 9-30, 9-31, 9-45, 10-37
- availability, xii, 1-10, 1-15, 9-34
- balance, 1-2, 1-4, 2-2, 2-16, 2-17, 3-2, 6-2, 9-33, 9-37, 9-39, 9-52
- Ballard Power Systems, 1-16, 1-25, 1-26, 1-37, 3-3, 3-15, 9-41, 9-82, 9-86, 11-6
- bio-fuel, 1-12
- bipolar, 3-3, 3-8, 5-3, 6-8, 8-6, 8-7, 8-10
- bottoming cycle, 8-1, 9-1, 9-30, 9-35, 9-36, 9-37, 9-38, 9-39, 9-48, 9-50, 9-52, 9-54, 9-55, 9-56
- Brandstofel Nederland, 6-1
- Cairns, 2-15, 2-26, 5-22, 6-39
- carbon, 1-7, 2-2, 2-12, 3-4, 3-5, 3-7, 5-2, 5-7, 5-8, 5-9, 6-14, 6-15, 6-17, 6-31, 8-17, 9-39, 9-40, 9-52, 9-55, 10-9, 10-16, 10-18, 10-19, 10-20, 11-1
- carbon black, 1-7, 5-2, 5-7, 5-8, 5-9
- carbon monoxide, 2-2, 3-5, 9-40, 9-52, 9-55, 10-18
- Carnot, 2-19
- catalyst, 1-2, 1-5, 1-12, 2-1, 2-2, 2-17, 3-1, 3-3, 3-4, 3-5, 3-6, 3-8, 5-2, 5-7, 5-8, 5-9, 5-11, 6-26, 6-29, 6-30, 8-16, 9-35, 9-36, 9-52
- catalysts loading, 1-4
- cathode, 1-1, 1-2, 1-4, 1-12, 1-13, 2-1, 2-3, 2-7, 2-8, 2-13, 2-14, 2-15, 2-16, 3-1, 3-2, 3-4, 3-6, 3-7, 3-10, 5-2, 5-5, 5-7, 5-9, 5-10, 5-12, 5-15, 5-18, 6-1, 6-2, 6-3, 6-4, 6-5, 6-6, 6-8, 6-10, 6-11, 6-12, 6-14, 6-16, 6-18, 6-19, 6-20, 6-21, 6-22, 6-26, 6-27, 6-35, 8-2, 8-5, 8-6, 8-7, 8-10, 8-11, 8-12, 8-13, 8-16, 9-35, 9-37, 9-43, 9-45, 9-47, 9-52, 9-55, 10-6, 10-7, 10-8, 10-9, 10-13, 11-10
- cathode dissolution, 6-10, 9-35
- cation, 3-1, 8-12
- Ceramtec, 1-20, 8-24
- ceramic, 1-4, 1-13, 6-6, 6-9, 8-1, 8-5, 8-6, 8-10, 8-11
- cermet, 1-4, 8-5
- characteristics, 1-1, 1-9, 1-10, 1-13, 1-16, 1-19, 2-2, 2-9, 3-2, 3-7, 6-35, 9-31
- chemisorption, 3-2, 3-10
- cleanup, 1-20, 5-8, 6-9, 6-11, 6-24, 6-25, 9-30, 9-39, 9-40, 9-45, 11-2
- coal gasification, 6-23, 9-39, 11-2
- coflow, 2-14, 8-7
- cogeneration, 1-9, 1-11, 1-12, 1-13, 1-15, 5-1, 8-1, 9-1, 9-2, 9-45, 9-50, 10-21, 10-23
- coking, 10-19
- commercialization, 1-18, 3-13, 5-1, 6-28, 8-21, 9-40, 9-49
- concentration losses, 2-16, 5-17, 6-28, 8-21
- contaminants, 1-9, 1-20, 3-5, 5-8, 5-11, 6-11, 6-12, 6-23, 6-24, 6-28, 9-35, 9-45
- cooling, 1-15, 3-3, 3-5, 3-6, 5-4, 9-33, 9-38, 9-42, 9-44
- corrosion, 1-1, 1-3, 1-13, 2-12, 2-19, 3-1, 5-2, 5-3, 5-7, 5-9, 5-11, 6-2, 6-3, 6-6, 6-8, 6-19, 6-27, 8-1, 9-35, 9-36
- cost of electricity, 9-2, 9-57, 10-35, 11-7
- counterflow, 2-14
- creepage, 6-3
- crossflow, 2-14
- crossover, 3-12, 6-11
- current density, 2-5, 2-9, 2-10, 2-16, 2-18, 2-23, 3-2, 3-6, 5-5, 5-10, 5-12, 5-17, 6-6, 6-13, 6-16, 6-18, 6-19, 6-26, 6-28, 6-33, 6-34, 8-14, 8-16, 8-19, 8-21, 9-34, 9-39, 9-52, 11-9
- Daimler-Benz, 1-26, 9-82
- degradation, 1-1, 1-3, 3-11, 5-3, 5-6, 5-7, 5-8, 5-11, 5-18, 6-23, 6-28, 8-7, 8-20, 8-21, 9-52
- demonstration, 1-16, 5-2, 8-10
- desulfurization, 6-25, 9-47, 9-52
- dielectric, 5-4
- digester, xii
- diluent, 1-12, 5-17
- direct internal reforming, 6-29, 11-7
- doping, 8-11
- Dow Chemical, 3-4, 3-7
- drag, 3-2
- DuPont, 3-4, 3-7

efficiency, xii, 1-5, 1-9, 1-12, 1-13, 1-14, 1-15, 1-16, 1-18, 1-20, 2-9, 2-10, 2-12, 2-17, 2-18, 2-19, 3-2, 3-10, 3-11, 6-9, 6-11, 6-15, 6-24, 8-13, 9-1, 9-2, 9-30, 9-32, 9-33, 9-34, 9-38, 9-39, 9-43, 9-44, 9-46, 9-48, 9-52, 9-53, 9-54, 9-55, 9-56, 10-20, 10-21, 10-22, 10-23, 10-35  
 electrocatalyst, 1-4, 1-7, 2-12, 3-4, 3-11, 5-2, 5-5  
 electrochemical performance, 1-2  
 electrochemical vapor deposition (EVD), 8-12  
 electrode degradation, 2-12  
 electrodes, 1-1, 1-2, 1-3, 1-6, 1-7, 1-13, 2-6, 2-7, 2-14, 3-1, 3-2, 3-4, 3-5, 3-7, 3-8, 3-9, 3-12, 5-2, 5-8, 5-9, 5-14, 5-16, 5-17, 6-2, 6-3, 6-4, 6-9, 6-10, 8-6, 8-7, 8-10, 8-12  
 emissions, xii, 1-9, 1-20, 1-25, 9-39, 9-48  
 endothermic, 1-5, 3-2, 6-17, 6-29, 6-30, 9-37, 9-41, 9-43, 9-47, 9-52, 10-17, 10-18  
 equilibria, 6-21  
 equilibrium, 1-7, 2-2, 2-3, 2-5, 2-13, 2-15, 2-16, 2-25, 6-2, 6-3, 6-15, 6-17, 6-18, 6-19, 6-21, 6-22, 6-26, 6-30, 8-18, 10-7, 10-9, 10-10, 10-11, 10-13, 10-14, 10-16, 10-17, 10-18, 10-19, 11-1, 11-8, 11-9  
 Europe, xii, 1-25, 6-1  
 exchange current, 2-6, 2-23, 2-25, 5-10, 11-9  
 exothermic, 1-5, 3-10, 6-17, 6-29, 6-30, 9-47, 9-52, 10-17  
 external, 1-1, 1-3, 1-5, 1-12, 2-2, 3-1, 3-3, 6-11, 6-29, 6-30, 8-7, 9-35  
 Faraday, 2-19, 6-35, 10-1, 11-8  
 flat plate, 1-7, 1-13, 5-5, 8-7, 8-10, 8-13  
 flooded, 1-3, 1-6, 6-2  
 Foulkes, 1-2, 1-35, 2-26, 11-4  
 fuel, xii, xiii, 1-1, 1-2, 1-3, 1-4, 1-6, 1-7, 1-8, 1-9, 1-10, 1-11, 1-12, 1-13, 1-14, 1-15, 1-16, 1-18, 1-19, 1-20, 1-21, 1-25, 1-26, 1-35, 2-1, 2-2, 2-3, 2-4, 2-5, 2-6, 2-7, 2-8, 2-9, 2-11, 2-12, 2-13, 2-14, 2-15, 2-16, 2-17, 2-18, 2-19, 2-20, 2-22, 2-23, 3-1, 3-2, 3-3, 3-5, 3-6, 3-8, 3-11, 3-12, 3-13, 5-1, 5-2, 5-3, 5-7, 5-8, 5-9, 5-10, 5-13, 5-14, 5-15, 5-17, 5-18, 6-4, 6-6, 6-8, 6-9, 6-11, 6-15, 6-16, 6-17, 6-18, 6-21, 6-22, 6-23, 6-24, 6-25, 6-26, 6-27, 6-28, 6-29, 6-30, 6-31, 6-33, 8-1, 8-2, 8-5, 8-6, 8-7, 8-10, 8-12, 8-14, 8-15, 8-16, 8-17, 8-18, 8-19, 8-20, 8-21, 8-22, 9-1, 9-2, 9-30, 9-31, 9-32, 9-34, 9-35, 9-36, 9-37, 9-38, 9-39, 9-40, 9-41, 9-42, 9-43, 9-44, 9-45, 9-46, 9-47, 9-48, 9-50, 9-51, 9-52, 9-53, 9-54, 9-55, 9-56, 9-57, 9-82, 10-1, 10-2, 10-3, 10-4, 10-5, 10-6, 10-7, 10-8, 10-9, 10-12, 10-13, 10-15, 10-17, 10-19, 10-20, 10-21, 10-22, 10-27, 10-29, 10-31, 10-32, 10-35, 10-36, 10-37, 11-7, 11-8, 11-10  
 fuel cell stacks, 1-16, 10-3  
 fuel electrode, 8-12, 8-20  
 fuels, 1-1, 1-9, 1-12, 1-19, 1-25, 2-1, 2-2, 2-18, 3-5, 3-11, 5-13, 6-2, 6-15, 6-16, 6-27, 6-29, 8-2, 8-16, 8-18, 9-1  
 Fuji Electric Corporation, 5-1  
 gas turbine, 1-9, 1-12, 1-18, 9-36, 9-37, 9-38, 9-48, 9-54, 10-22  
 gasification, 10-20  
 gasified coal, 6-15  
 gasifiers, 1-20, 5-15  
 Germany, 1-36, 5-21, 11-5  
 Gibbs Free Energy, 2-3, 2-19  
 Girdler, 10-10, 10-17, 10-39  
 graphite, 3-5, 3-8, 5-2, 5-3, 5-4  
 Grove, 11-6  
 Grubbs, 3-1  
 Halides, 6-24, 6-27, 6-40  
 harmonics, 9-30, 9-31, 9-32  
 heat exchanger, 9-32, 9-41, 9-47, 9-50, 9-52, 10-1, 10-20  
 heat rate, 6-2, 10-21, 10-22, 10-35, 11-7  
 heat removal, 5-4, 8-7  
 heat transfer, 3-5, 6-12, 10-26  
 higher heating value, 2-18, 10-28, 10-29, 10-30, 11-7  
 Hitachi, 6-1, 6-37  
 hybrid, 1-18, 1-25, 1-26, 9-82  
 hydrogen, 1-2, 1-3, 1-4, 1-5, 1-8, 1-11, 1-15, 1-19, 1-25, 1-26, 1-35, 2-2, 2-3, 2-4, 2-7, 2-13, 2-18, 3-1, 3-2, 3-5, 3-8, 3-13, 5-8, 5-13, 6-29, 6-30, 8-2, 8-13, 8-17, 8-19, 9-39, 9-40, 9-41, 9-43, 9-52, 9-55, 9-82, 10-1, 10-2, 10-3, 10-4, 10-5, 10-6, 10-7, 10-8, 10-13, 10-17, 10-22, 11-9  
 impurities, 2-9, 3-6, 5-9, 5-14, 5-15, 8-19  
 indirect internal reforming, 6-29, 11-7  
 interconnect, 1-3, 1-7, 8-4, 8-6, 8-7, 8-10, 8-12, 8-13  
 interconnections, 8-6, 8-7, 9-1  
 intercooled, 9-39, 9-40, 9-47  
 interfacial reactions, 8-11  
 internal, 1-3, 1-5, 1-11, 2-2, 2-16, 3-10, 6-11, 6-29, 6-30, 8-1, 9-31, 9-35, 9-47, 9-56, 10-12  
 internal manifolding, 6-11  
 internal reforming, 1-3, 1-5, 1-11, 2-2, 6-29, 6-30, 8-1, 9-35, 9-47, 9-56  
 International Fuel Cells Corporation (IFC), 1-14  
 inverter, 9-31, 10-20  
 ionic species, 8-5  
 ionomer, 3-8  
 JANAF, 2-17, 2-21, 2-26, 10-32, 10-40  
 Japan, 1-14, 1-15, 1-25, 5-1, 5-21, 5-22, 6-1, 6-29, 6-37, 6-38, 8-12, 8-23, 8-24, 11-5, 11-6  
 Johnson Matthey, 3-12, 5-7, 9-86  
 kinetics, 1-3, 1-11, 1-13, 2-5, 2-16, 2-24, 5-11, 6-10, 8-1, 10-19, 10-20  
 life, xii, 1-1, 1-3, 1-7, 1-12, 1-15, 2-9, 2-11, 3-1, 3-3, 3-4, 5-1, 5-3, 5-4, 5-5, 5-7, 5-8, 5-9, 5-18, 6-2, 6-9, 6-10, 6-11, 6-19, 6-24, 9-34, 9-35, 9-36, 9-39, 9-47, 9-52  
 logistic fuel, xii, 1-19, 1-20  
 loss, 2-5, 2-6, 2-12, 2-13, 2-15, 2-16, 2-17, 2-18, 2-19, 3-8, 3-10, 3-11, 5-8, 5-9, 5-12, 5-14, 5-15, 5-17, 5-18, 6-8, 6-9, 6-10, 6-11, 6-15, 6-19, 6-20, 6-23, 6-27, 6-28, 8-13, 8-20, 8-21, 9-30, 9-33, 9-34, 9-36, 9-53  
 lower heating value, 1-9, 10-21, 10-28, 11-7  
 management, 1-3, 1-4, 1-11, 2-11, 3-2, 3-3, 3-5, 3-8, 6-2, 6-3, 6-30, 8-1, 9-52  
 manifold, 1-3, 5-4, 6-11, 8-7  
 manufacturing, 1-14, 1-16, 3-4, 3-7, 8-11  
 M-C Power, 1-21, 6-1, 6-38  
 mechanical stress, 8-11  
 membrane, 1-3, 1-11, 1-12, 2-11, 3-1, 3-2, 3-4, 3-5, 3-6, 3-7, 3-8, 3-9, 3-10, 9-39  
 membranes, 3-3, 3-4, 3-6, 3-7, 3-8  
 methanation, 3-5, 6-14, 6-17  
 methane (CH<sub>4</sub>), 8-2, 10-12  
 methanol, 1-8, 1-25, 1-26, 3-1, 3-8, 3-11, 3-12, 3-13  
 migration, 5-9, 6-3  
 Mitsubishi Electric Corporation, 5-1, 5-7, 6-1  
 Mitsubishi Heavy Industries, 8-24

molten carbonate, xii, 1-3, 1-7, 6-2, 6-3, 6-4, 6-6, 6-7, 6-8, 6-27, 6-29, 11-7

multi-stage, 9-50, 9-52, 9-53

Nafion, 3-4, 3-7, 3-8, 3-9

Nafion membranes, 3-4, 3-7, 3-9

natural gas, xii, 1-5, 1-8, 1-12, 1-13, 1-15, 1-16, 1-18, 1-20, 1-25, 1-35, 2-18, 3-1, 3-8, 5-13, 6-9, 6-11, 6-18, 6-30, 8-13, 9-39, 9-40, 9-41, 9-43, 9-44, 9-45, 9-46, 9-47, 9-50, 9-51, 9-55, 10-4, 10-6, 10-22, 10-28, 10-29, 10-30

Nernst, 2-2, 2-3, 2-12, 2-14, 2-15, 2-22, 2-23, 2-25, 3-10, 5-12, 6-14, 6-18, 6-22, 8-2, 8-16, 8-17, 8-18

nitrogen compounds, 5-17

odorants, 9-41, 9-47, 9-51

ohmic, 2-5, 2-6, 2-8, 2-11, 2-16, 2-23, 3-10, 3-11, 5-9, 5-10, 5-11, 5-17, 6-6, 6-11, 6-19, 6-28, 8-5, 8-6, 8-7, 8-12, 8-13, 8-14, 8-21, 9-36, 11-7, 11-9

ohmic loss, 2-6, 2-16, 5-10, 5-11, 6-6, 6-11, 8-5, 8-6, 8-13, 9-36, 11-7

ohmic polarization, 2-5, 2-8, 2-23, 6-6, 6-19, 8-7, 8-12, 8-13, 8-14, 11-9

ohmic resistance, 2-11, 3-10, 6-6

ONSI, 1-21, 1-36, 9-85, 11-7

overpotential, 2-5, 5-12, 5-14, 6-10

overvoltage, 2-5

oxidant, 1-1, 1-2, 1-3, 1-7, 2-12, 2-13, 2-14, 2-15, 2-16, 2-17, 5-4, 5-9, 5-10, 5-12, 5-13, 5-14, 5-17, 5-18, 6-12, 6-15, 6-17, 6-18, 6-19, 6-20, 6-21, 6-22, 6-23, 6-24, 8-5, 8-7, 8-15, 8-16, 8-17, 8-18, 8-19, 9-34, 9-37, 9-38, 9-41, 9-44, 9-45, 9-46, 9-47, 9-52, 9-55, 9-56, 10-2, 10-4, 10-6, 10-7, 10-8, 10-9, 11-9, 11-10

oxidation, 1-2, 1-7, 2-2, 2-3, 2-4, 2-13, 3-1, 3-5, 3-8, 3-12, 5-11, 5-14, 5-16, 6-1, 6-4, 6-29, 6-30, 8-2, 8-5, 8-18

oxygen, 1-1, 1-2, 1-4, 1-8, 1-11, 1-12, 2-1, 2-2, 2-3, 2-17, 2-18, 3-1, 3-6, 3-8, 3-10, 5-9, 5-10, 5-11, 5-14, 8-1, 8-17, 9-43, 9-47, 9-55, 9-56, 10-4, 10-5, 10-7, 10-8, 10-9, 10-28, 11-10

phosphoric acid, xii, 1-3, 1-4, 5-1, 5-4, 5-7, 5-8, 5-9, 6-2, 11-7

planar, 1-20, 8-6, 8-10, 8-11

poison, 1-4, 1-12

polarization, 1-6, 2-5, 2-6, 2-7, 2-8, 2-11, 2-23, 2-24, 2-25, 3-10, 5-9, 5-10, 5-11, 5-12, 5-14, 5-15, 6-9, 6-18, 6-19, 6-20, 6-22, 8-12, 8-13, 8-14, 8-16, 8-19, 11-9

polymer, xii, 1-3, 1-25, 1-26, 3-1, 3-2, 3-3, 3-4, 3-6, 3-12, 9-82, 11-7

porous electrodes, 1-3, 1-7, 3-1, 5-2, 5-3, 6-2, 6-3

potential, 1-11, 1-20, 2-1, 2-2, 2-3, 2-5, 2-6, 2-7, 2-9, 2-11, 2-14, 2-15, 2-19, 2-20, 2-22, 2-23, 2-25, 3-2, 3-10, 3-12, 5-2, 5-10, 5-11, 5-12, 5-17, 6-2, 6-3, 6-8, 6-11, 6-14, 6-15, 6-17, 6-18, 6-21, 6-22, 6-26, 6-28, 8-12, 8-16, 8-17, 9-2, 9-35, 9-57, 10-19, 11-8

power conditioning, 1-8, 9-30, 9-31, 9-32

pressure, 1-3, 1-4, 1-5, 1-8, 1-11, 1-12, 1-15, 1-35, 2-1, 2-3, 2-4, 2-8, 2-9, 2-11, 2-12, 2-14, 2-15, 2-18, 2-19, 2-20, 2-21, 3-2, 3-3, 3-5, 3-6, 3-9, 3-10, 3-11, 5-2, 5-6, 5-9, 5-10, 5-12, 5-13, 5-14, 5-15, 5-18, 6-7, 6-9, 6-10, 6-12, 6-14, 6-15, 6-16, 6-18, 6-19, 6-24, 6-27, 6-30, 6-35, 8-13, 8-17, 9-33, 9-34, 9-35, 9-36, 9-38, 9-39, 9-41, 9-43, 9-46, 9-47, 9-49, 9-54, 9-56, 10-6, 10-19, 10-23, 10-28, 10-31, 10-32, 10-35, 11-9, 11-10

pressurization, 2-12, 3-6, 5-8, 5-10, 9-34, 9-35, 9-36

processing, 1-8, 1-20, 3-5, 6-6, 8-5, 8-11, 9-30, 9-40

production, 1-1, 1-16, 3-1, 3-2, 8-3, 8-5, 8-11, 9-30, 9-37, 9-39, 9-41, 10-23, 10-24

ramp, 1-15, 9-30, 9-32

reactants, 1-1, 1-2, 1-3, 1-6, 1-8, 2-3, 2-5, 2-6, 2-9, 2-12, 2-16, 2-19, 2-21, 2-22, 3-5, 6-12, 6-14, 6-15, 9-37, 10-10, 10-19

recrystallization, 2-12

reformate, 3-8, 3-11, 6-30, 9-40, 10-6

reformer, 1-5, 1-19, 1-35, 3-13, 6-29, 9-37, 9-40, 9-41, 9-42, 9-44, 9-52, 10-6, 10-16, 10-18

reservoir, 5-5

resistivity, 1-13, 3-6, 6-11, 8-11

sealless tubular, 8-6, 8-7

seals, 2-12, 5-5, 8-6, 8-7, 8-10, 9-35

separator plate, 1-7

shift, 2-2, 2-7, 2-13, 2-14, 2-15, 2-16, 3-5, 3-8, 5-8, 5-13, 6-1, 6-15, 6-17, 6-18, 6-19, 6-21, 6-25, 6-26, 6-30, 8-2, 8-18, 9-39, 9-40, 9-41, 9-42, 9-52, 10-7, 10-9, 10-11, 10-12, 10-13, 10-14, 10-15, 10-16, 10-17, 11-1

Siemens Westinghouse, xiii, 1-18, 1-20, 1-21, 8-1, 8-4, 8-6, 8-11, 8-12, 8-13, 8-21, 8-22, 9-36, 9-38, 9-45, 9-47, 9-49, 9-54, 9-55, 11-7

sintering, 2-12, 5-11, 6-9, 8-3, 8-4, 8-5, 8-11, 8-12

siting, 1-14

solid oxide, xii, 1-3, 1-7, 8-5, 8-6, 8-12, 9-54, 11-8

sorbent, 9-39, 9-52

space, 1-2, 1-11, 1-13, 1-15, 1-25, 1-26, 3-4, 5-8, 9-41, 9-82

stability, 1-4, 1-12, 2-8, 3-4, 5-1, 5-3, 5-7, 6-2, 6-6, 6-9, 8-3, 9-37

stack, 1-7, 1-16, 1-19, 1-20, 2-9, 3-1, 3-3, 3-4, 3-5, 3-6, 3-9, 5-3, 5-4, 5-5, 5-6, 5-7, 5-10, 5-18, 6-4, 6-6, 6-9, 6-11, 6-12, 6-13, 6-16, 6-19, 6-20, 6-23, 6-28, 6-30, 6-35, 8-6, 8-7, 8-10, 8-11, 8-14, 8-18, 8-21, 9-1, 9-37, 9-40, 9-41, 9-48, 9-52, 9-57, 10-2, 10-3, 10-15, 10-20

stacking, 1-16, 8-10

stationary, 1-13, 1-14, 1-16, 1-20, 1-21, 2-9, 3-1, 3-10, 5-1, 9-41

steam reforming, 2-2, 5-13, 6-21, 6-29, 6-30, 8-2, 9-52, 10-13, 10-16, 10-17

steam turbine, 1-12, 9-30, 9-37, 9-38, 9-48, 9-54, 10-22

structure, 1-1, 1-2, 1-6, 1-7, 3-2, 3-4, 3-8, 5-2, 5-4, 6-2, 6-4, 6-6, 6-8, 6-9, 6-10, 6-11, 6-27, 8-4, 8-5, 8-6, 8-7, 8-11, 8-12

sulfonic, 1-3, 3-1, 3-4, 3-7, 11-8

sulfur, 5-14, 5-15, 5-17, 6-9, 6-24, 6-26, 6-27, 6-28, 8-20, 9-36, 9-40, 9-41, 9-45, 9-47, 9-51, 9-55

system efficiency, 1-5, 1-9, 1-12, 2-9, 2-19, 6-9

Tafel, 2-5, 2-23, 2-24, 11-8

tape casting, 6-6, 8-5, 8-10

temperature, 1-3, 1-4, 1-5, 1-7, 1-8, 1-9, 1-10, 1-11, 1-12, 1-13, 1-14, 2-1, 2-2, 2-3, 2-4, 2-8, 2-9, 2-11, 2-15, 2-17, 2-19, 2-20, 2-22, 2-23, 2-25, 3-1, 3-2, 3-5, 3-9, 3-10, 3-11, 5-2, 5-3, 5-8, 5-9, 5-10, 5-11, 5-14, 5-15, 5-17, 6-2, 6-7, 6-8, 6-9, 6-11, 6-12, 6-16, 6-17, 6-18, 6-19, 6-22, 6-24, 6-29, 6-30, 8-1, 8-2, 8-3, 8-4, 8-5, 8-6, 8-7, 8-10, 8-11, 8-12, 8-13, 8-14, 8-16, 8-19, 9-30, 9-32, 9-33, 9-34, 9-36, 9-37, 9-38, 9-39, 9-41, 9-47, 9-48, 9-50, 9-52, 9-56, 10-9, 10-10, 10-16, 10-17, 10-18, 10-19, 10-20, 10-23, 10-24, 10-25, 10-26, 10-31, 10-34, 11-1, 11-9, 11-10

thermal stress, 8-7

thermodynamic, 2-1, 2-4, 6-2, 8-13, 10-17, 10-19, 10-20

three phase interface, 1-2, 5-3  
Tokyo Electric Power, 5-5, 5-6, 5-21, 9-41, 9-85, 9-86  
Toshiba Corporation, 1-14, 5-1, 6-1  
UltraFuelCell, 9-50, 9-51, 9-53  
vehicle, xii, 1-11, 1-25, 1-26, 2-9, 3-12, 9-82  
voltage, 1-7, 2-2, 2-3, 2-4, 2-5, 2-7, 2-8, 2-9, 2-10, 2-11, 2-12, 2-14, 2-15, 2-16, 2-18, 2-23, 3-10, 3-11, 5-2, 5-4, 5-8, 5-10, 5-11, 5-12, 5-14, 5-17, 6-4, 6-6, 6-11, 6-12, 6-13, 6-15, 6-16, 6-17, 6-18, 6-19, 6-20, 6-23, 6-26, 6-27,

6-28, 6-33, 6-35, 8-6, 8-12, 8-13, 8-14, 8-16, 8-17, 8-18, 8-19, 8-21, 9-30, 9-31, 9-34, 9-36, 9-37, 9-39, 9-41, 9-46, 9-52, 10-2, 10-3, 10-6, 10-15, 11-8, 11-9  
voltage efficiency, 8-18  
Westinghouse, 1-36, 5-22, 8-1, 8-4, 8-6, 8-22, 8-24, 9-46, 9-49, 9-85  
yttria, 8-5, 8-11, 8-12  
zirconia, 8-5, 8-6, 8-11, 8-12, 8-21, 11-8